

Z. Czernicki
A. Baethmann
U. Ito
Y. Katayama
T. Kuroiwa
D. Mendelow
Editors

Brain Edema XIV



 SpringerWienNewYork

Acta Neurochirurgica
Supplementum

Editor: H.-J. Steiger

Brain Edema XIV

Edited by

Z. Czernicki, A. Baethmann, U. Ito, Y. Katayama,
T. Kuroiwa, D. Mendelow

Acta Neurochirurgica

Supplementum 106

SpringerWienNewYork

Editors

Zbigniew Czernicki
PAN Warszawa
Medical Research Center
Department of Neurosurgery
Ceglowska St. 80
01-809 Warszawa
Poland
zczernicki@cmdik.pan.pl

Umeo Ito
Musashino Red Cross Hospital
Department of Neurosurgery
1-26-1 Kyonan-cho
Musashino City, Tokyo
180 Japan
umeo-ito@po.ujnet.or.jp

Toshihiko Kuroiwa
Medical Research Institute
Department of Neuropathology
1-5-45 Yushima
Tokyo
Bunkyo-ku
113-8510 Japan
t.kuroiwa.upat@mri.tmd.ac.jp

Alexander Baethmann
Universitätsklinikum München
Klinikum Großhadern
Inst. Chirurgische Forschung
Marchioninstr. 15
81377 München
Germany
baethman@icf.med.uni-muenchen.de

Yoichi Katayama
Nihon University
School of Medicine
Department of Neurological Surgery
30-1 Oyaguchikami-machi
Tokyo
Itabashi-ku
173-8610 Japan
ykatayam@med.nihon-u.ac.jp

David Mendelow
Newcastle General Hospital
Department of Neurosurgery
Westgate Road
Newcastle upon Tyne
United Kingdom NE4 6BE
a.d.mendelow@ncl.ac.uk

This work is subject to copyright.

All rights are reserved, whether the whole or part of the material is concerned, specifically those of translation, reprinting, re-use of illustrations, broadcasting, reproduction by photocopying machines or similar means, and storage in data banks.

Product Liability: The publisher can give no guarantee for all the information contained in this book. This does also refer to information about drug dosage and application thereof. In every individual case the respective user must check its accuracy by consulting other pharmaceutical literature.

The use of registered names, trademarks, etc. in this publication does not imply, even in the absence of a specific statement, that such names are exempt from the relevant protective laws and regulations and therefore free for general use.

© 2010 Springer-Verlag/Wien
Printed in Germany

SpringerWienNewYork is part of
Springer Science+Business Media
springer.at

Typesetting: SPI, Pondicherry, India

Printed on acid-free and chlorine-free bleached paper
SPIN: 12231874

With 32 (partly coloured) Figures

Library of Congress Control Number: 2009927241

ISSN 0065-1419
ISBN 978-3-211-98758-2
DOI 10.1007/978-3-211-98811-4
SpringerWienNewYork

e-ISBN 978-3-211-98811-4

Preface

The XIV International Symposium on Brain Edema and Brain Tissue Injury took place in Warsaw, Poland, on 11–14 June 2008.

Two prominent members of the International Society for Brain Edema: Dr. Igor Klatzo and Dr. Julien Hoff have passed away after the last 2005 Symposium in Ann Arbor, USA. Dr. Igor Klatzo was actually the founder of the Society, and the Advisory Board decided to commemorate Dr. Igor Klatzo by introducing a lecture named after him to be given at the Symposium. Prof. Dr. Hans-Jürgen Reulen has been honored to give the first Igor Klatzo lecture entitled “*Bulk Flow and Diffusion revisited, and Clinical Applications*”.

This volume contains 65 out of the 104 papers presented at the Symposium as lectures or posters. The topics of the Symposium were similar to those discussed at the previous ones. Many discussions focused on clinical work especially diagnosis, subarachnoid hemorrhage, hydrocephalus, and traumatic brain injury. Diagnosis and therapy, including surgical methods, have also been verified. Much attention was drawn to the application of decompressive craniectomy in the treatment of posttraumatic intracranial hypertension.

The pathomechanisms of brain edema and tissue injury studied in experimental models have been also presented.

The Symposium was completed by a session on Nanoparticles organized by Dr. Hari Shanker Sharma. This new topic was presented at the Brain Edema Symposium for the first time. The impact of the nanoparticles on the blood–brain barrier and brain edema as well as the possibility of use of nanoparticles in cases of spinal cord damage have been discussed.

The Advisory Board and the Organizing Committee would like to thank the authors for their co-operation and the Springer Verlag for the willingness to publish the Symposium’s materials in line with our tradition to date.

We would like to announce that the XV International Symposium on Brain Edema and Brain Tissue Injury will be held in Kawaguchi-Lake, Yamanashi, Japan in 2011 under the chair of Prof. Dr. Yoichi Katayama.

Zbigniew Czernicki and Editors

Contents

Part I Igor Klatzo Lecture

- Bulk Flow and Diffusion Revisited, and Clinical Applications**..... 3
Hans-J. Reulen

Part II Ischemia and the Blood-Brain Barrier Disorders

- Experimental Cerebral Ischemia: The Contribution
of the Bethesda Group** 17
Toshihiko Kuroiwa

- Past and Recent BBB Studies with Particular Emphasis
on Changes in Ischemic Brain Edema** 21
Maria Spatz

- Increase in Activity of Neutrophils and Proinflammatory
Mediators in Rats Following Acute and Prolonged
Focal Cerebral Ischemia and Reperfusion** 29
Stanisław Hendryk, Zenon Czuba, Halina Jędrzejewska-Szypułka,
Piotr Bażowski, Hanna Doleżych, and Wojciech Król

- Factors in Creepy Delayed Neuronal Death
in Hippocampus Following Brain Ischemia–Reperfusion
Injury with Long-Term Survival** 37
Ryszard Pluta, Sławomir Januszewski, Mirosław Jabłoński,
and Marzena Ułamek

- Endogenous Pituitary Adenylate Cyclase Activating
Polypeptide Is Involved in Suppression of Edema
in the Ischemic Brain** 43
Tomoya Nakamachi, Hirokazu Ohtaki, Sachiko Yofu,
Kenji Dohi, Jun Watanabe, Hiroyoshi Mori, Atsushi Sato,
Hitoshi Hashimoto, Norihito Shintani, Akemichi Baba,
and Seiji Shioda

- Reduced Matrix Metalloproteinase-9 Activity
and Cell Death After Global Ischemia in the Brain
Preconditioned with Hyperbaric Oxygen** 47
Robert P. Ostrowski, Vikram Jadhav, Wanqiu Chen,
and John H. Zhang

Radiation Exposure Prior to Ischemia Decreases Lesion Volume, Brain Edema and Cell Death	51
E. Titova, A. Adami, R. Ostrowski, S. L alas, R. Vlkolinsky, J.H. Zhang, G. Nelson, and A. Obenaus	
Effects of VEGF Administration or Neutralization on the BBB of Developing Rat Brain	55
N. Ortuzar, E.G. Argandoña, H. Bengoetxea, O. Leis, S. Bulnes, and J.V. Lafuente	
Alterations in Blood–Brain Barrier Function and Brain Pathology by Morphine in the Rat. Neuroprotective Effects of Antioxidant H-290/51	61
Hari Shanker Sharma, Per-Ove Sjöquist, and Syed F. Ali	
Part III Hydrocephalus	
Clinical Proof of the Importance of Compliance for Hydrocephalus Pathophysiology	69
Michael Kiefer and Regina Eymann	
An Algorithm to Assess the Rehabilitation Potential in Patients with Chronic Hydrocephalus	75
Michael Kiefer and Regina Eymann	
What Can Be Found Inside Shunt Catheters	81
Z. Czernicki, R. Strzałkowski, N. Walasek, and B. Gajkowska	
Glue Instead of Stitches: A Minor Change of the Operative Technique with a Serious Impact on the Shunt Infection Rate	87
Regina Eymann and Michael Kiefer	
Animal Experiments to Evaluate Complications of Foreign Materials on Silicone with Shunt Catheters: Preliminary Results	91
Regina Eymann, Ullrich Meier, and Michael Kiefer	
Huge Thrombosis as a Consequence of VA-Shunts	95
Michael Kiefer and Regina Eymann	
Does Idiopathic Normal Pressure Hydrocephalus Always Mean a Poor Prognosis?	101
Michael Kiefer, Ulrich Meier, and Regina Eymann	
Gravitational Shunt Complications After a Five-Year Follow-Up	107
Michael Kiefer and Regina Eymann	
Is It Possible to Minimize Overdrainage Complications with Gravitational Units in Patients with Idiopathic Normal Pressure Hydrocephalus? Protocol of the Randomized Controlled SVASONA Trial (ISRCTN51046698)	113
J. Lemcke, U. Meier, C. Müller, M. Fritsch, R. Eymann, M. Kiefer, U. Kehler, N. Langer, V. Rohde, H-Ch. Ludwig, F. Weber, V. Remenez, M. Schuhmann, and D. Stengel	

Early Shunting Using the Parallel Shunt System in Hemorrhagic Hydrocephalus: In Vitro Testing of Handling, Technical Complications and Clogging Rate	117
F. Al-Zain, U. Meier, and J. Lemcke	
Intracranial Irregularities Beside Hydrocephalus in H-Tx Rats	121
Michael Kiefer, Guenther Schneider, and Regina Eymann	
Co-morbidity as a Predictor of Outcome in Patients with Idiopathic Normal-Pressure Hydrocephalus	127
Ullrich Meier and Johannes Lemcke	
Part IV Subarachnoid Hemorrhage and Intracerebral Hemorrhage	
Effects of Magnesium Sulfate Infusion on Cerebral Perfusion in Patients After Aneurysmal SAH	133
George Kwok-Chu Wong, Rachael Kwok, Karen Tang, David Yeung, Anil Ahuja, Ann Dorothy King, and Wai-Sang Poon	
Timing of Serum Active MMP-9 and MMP-2 Levels in Acute and Subacute Phases After Spontaneous Intracerebral Hemorrhage	137
Massimiliano Castellazzi, Carmine Tamborino, Giuseppe De Santis, Francesco Garofano, Angelica Lupato, Vania Ramponi, Alessandro Trentini, Ilaria Casetta, Tiziana Bellini, and Enrico Fainardi	
Timing of Serum Soluble HLA-G Levels in Acute and Subacute Phases After Spontaneous Intracerebral Hemorrhage	141
Enrico Fainardi, Roberta Rizzo, Angelica Lupato, Vania Ramponi, Giuseppe De Santis, Francesco Garofano, Marina Stignani, Carmine Tamborino, Massimiliano Castellazzi, Ilaria Casetta, and Olavio Roberto Baricordi	
Minocycline Attenuates Brain Edema, Brain Atrophy and Neurological Deficits After Intracerebral Hemorrhage	147
J. Wu, S. Yang, Y. Hua, W. Liu, R. F. Keep, and G. Xi	
Myocardial Dysfunction in Subarachnoid Hemorrhage: Prognostication by Echo Cardiography and Cardiac Enzymes. A Prospective Study	151
Prasad Vannemreddy, Prasanna Venkatesh, Kumar Dinesh, Pratap Reddy, and Anil Nanda	
The Effects of Tetrahydrobiopterin on Intracerebral Hemorrhage-Induced Brain Injury in Mice	155
Reiko Tsuchiyama, Takumi Sozen, Elena Titova, John H. Zhang, and Jiping Tang	
Estrogen Reduces Iron-Mediated Brain Edema and Neuronal Death	159
Y. Gu, G. Xi, W. Liu, R. F. Keep, and Y. Hua	

Part V Imaging and Diagnosis

Improving Diagnostic Value of CT Examinations in Hyperacute Ischemic Stroke	165
A. Przelaskowski, J. Walecki, K. Sklinda, and G. Ostrek	
Pattern Recognition Methods in ¹H MRS Monitoring In Vivo of Normal Appearing Cerebellar Tissue After Treatment of Posterior Fossa Tumors	171
Łukasz Boguszewicz, Sławomir Blamek, and Maria Sokół	
Metabolic Changes in Rat Brain Following Intracerebroventricular Injections of Streptozotocin: A Model of Sporadic Alzheimer's Disease	177
M. Labak, T. Foniok, D. Kirk, D. Rushforth, B. Tomanek, A. Jasiński, and P. Grieb	
MR Spectroscopic Evaluation of Brain Tissue Damage After Treatment for Pediatric Brain Tumors	183
Sławomir Blamek, Dawid Larysz, Kornelia Ficek, Maria Sokół, Leszek Miszczyk, and Rafał Tarnawski	
The Incidence of Imaging Abnormalities after Stereotactic Radiosurgery for Cerebral Arteriovenous and Cavernous Malformations	187
Sławomir Blamek, Marek Boba, Dawid Larysz, Adam Rudnik, Kornelia Ficek, Bartosz Eksner, Leszek Miszczyk, and Rafał Tarnawski	
Magnetic Resonance Spectroscopic Evaluation of Brain Tissue Metabolism After Irradiation for Pediatric Brain Tumors in Long-Term Survivors: A Report of Two Cases	191
Sławomir Blamek, Jerzy Wydmański, Maria Sokół, Łukasz Matulewicz, and Łukasz Boguszewicz	
Evaluation of the Late Effects of CNS Prophylactic Treatment in Childhood Acute Lymphoblastic Leukemia (ALL) Using Magnetic Resonance Spectroscopy	195
Kornelia Ficek, Sławomir Blamek, Dorota Syguła, Leszek Miszczyk, Danuta Sońta-Jakimczyk, and Rafał Tarnawski	
A Non-invasive Assessment of Intracranial Volume Reserve by Measuring Cerebrospinal Fluid Volume with the Aid of CT Imaging	199
Mariusz Glowacki, Karol Budohoski, Piotr Marszałek, Jerzy Walecki, and Zbigniew Czernicki	
Is Neuroradiological Imaging Sufficient for Exclusion of Intracranial Hypertension in Children? Intracranial Hypertension Syndrome Without Evident Radiological Symptoms	203
Dawid Larysz, Patrycja Larysz, Andrzej Klimczak, and Marek Mander	
Part VI Trauma and Brain Tissue Injury	
Substance P Immunoreactivity Increases Following Human Traumatic Brain Injury	211
Andrew C. Zacest, Robert Vink, Jim Manavis, Ghafar T. Sarvestani, and Peter C. Blumbergs	

Hyperbaric Oxygen Preconditioning Reduces Postoperative Brain Edema and Improves Neurological Outcomes After Surgical Brain Injury	217
Vikram Jadhav, Robert P. Ostrowski, Wenni Tong, Brenden Matus, Connie Chang, and John H. Zhang	
Following Brain Trauma, Copeptin, a Stable Peptide Derived from the AVP Precursor, Does Not Reflect Osmoregulation but Correlates with Injury Severity	221
A. Kleindienst, G. Brabant, N.G. Morgenthaler, K.C. Dixit, H. Parsch, and M. Buchfelder	
The Effects of Selective Brain Hypothermia and Decompressive Craniectomy on Brain Edema After Closed Head Injury in Mice	225
Jacek Szczygielski, Angelika E. Mautes, Karsten Schwerdtfeger, and Wolf-Ingo Steudel	
Outcome of Patients with Severe Head Injury After Decompressive Craniectomy	231
J. Lemcke, S. Ahmadi, and U. Meier	
Assessing the Neurological Outcome of Traumatic Acute Subdural Hematoma Patients with and without Primary Decompressive Craniectomies	235
George Kwok-Chu Wong, Yuk-Wah Hung, Charing Chong, Janice Yeung, Stephanie Chi-Ping Ng, Tim Rainer, and Wai-Sang Poon	
Changes in the Blood–CSF Barrier in Experimental Traumatic Brain Injury	239
Mounir N. Ghabriel, Irena M. Zdziarski, Chris Leigh, and Robert Vink	
Dynamics of S100B Release into Serum and Cerebrospinal Fluid Following Acute Brain Injury	247
A. Kleindienst, S. Meissner, I.Y. Eyupoglu, H. Parsch, C. Schmidt, and M. Buchfelder	
Ultrastructural and Immunochemical Studies of Glial Scar Formation in Diabetic Rats	251
Malgorzata Frontczak-Baniewicz, Lidia Struzynska, Jaroslaw Andrychowski, Jolanta Opertowska, Dorota Sulejczak, and Michal Walski	
Significance of Monitoring the Initial Intracranial Pressure on Hematoma Irrigation with Trephination Therapy for Acute Subdural Hematomas in Critical Conditions	257
Naoki Otani, Yoshio Takasato, Hiroyuki Masaoka, Takanori Hayakawa, Yoshikazu Yoshino, Hiroshi Yatsushige, Hiroki Miyawaki, Kyoko Sumiyoshi, Takashi Sugawara, Aoyagi Chikashi, Satoru Takeuchi, and Go Suzuki	

Surgical Outcome Following a Decompressive Craniectomy for Acute Epidural Hematoma Patients Presenting with Associated Massive Brain Swelling	261
Naoki Otani, Yoshio Takasato, Hiroyuki Masaoka, Takanori Hayakawa, Yoshikazu Yoshino, Hiroshi Yatsushige, Hiroki Miyawaki, Kyoko Sumiyoshi, Takashi Sugawara, Aoyagi Chikashi, Satoru Takeuchi, and Go Suzuki	
Prognosis for Severe Traumatic Brain Injury Patients Treated with Bilateral Decompressive Craniectomy	265
Hiroshi Yatsushige, Yoshio Takasato, Hiroyuki Masaoka, Takanori Hayakawa, Naoki Otani, Yoshikazu Yoshino, Kyoko Sumiyoshi, Takashi Sugawara, Hiroki Miyawaki, Chikashi Aoyagi, Satoru Takeuchi, and Go Suzuki	
Posterior Fossa Brain Tissue Injury: Developmental, Neuropsychological, and Neurological Consequences of Brain Tumors in Children	271
Dawid Larysz, Slawomir Blamek, Patrycja Larysz, Katarzyna Pietras, and Marek Mandera	
Part VII Tumor	
The Role of eNOS in Vascular Permeability in ENU-Induced Gliomas	277
S. Bulnes, E.G. Argandoña, H. Bengoetxea, O. Leis, N. Ortuzar, and J.V. Lafuente	
Potential Role of CT Perfusion Parameters in the Identification of Solitary Intra-axial Brain Tumor Grading	283
Enrico Fainardi, Francesco Di Biase, Massimo Borrelli, Andrea Saletti, Michele Cavallo, Silvio Sarubbo, Stefano Ceruti, Riccardo Tamarozzi, and Arturo Chierгато	
Part VIII Treatment	
Neuromodulation with Pleiotropic and Multimodal Drugs – Future Approaches to Treatment of Neurological Disorders	291
Dafin F. Muresanu	
Selected Combination of Neurotrophins Potentiate Neuroprotection and Functional Recovery Following Spinal Cord Injury in the Rat	295
Hari Shanker Sharma	
Antibodies to Dynorphin A (1–17) Attenuate Closed Head Injury Induced Blood–Brain Barrier Disruption, Brain Edema Formation and Brain Pathology in the Rat	301
H.S. Sharma, R. Patnaik, S. Patnaik, A. Sharma, S. Mohanty, and P. Vannemreddy	
Serine Protease Inhibitor Attenuates Intracerebral Hemorrhage-Induced Brain Injury and Edema Formation in Rat	307
Takehiro Nakamura, Yasuhiro Kuroda, Naohisa Hosomi, Naohiko Okabe, Nobuyuki Kawai, Takashi Tamiya, Guohua Xi, Richard F. Keep, and Toshifumi Itano	

State-of-the-Art management and Monitoring of Brain Edema and Intracranial Hypertension in Fulminant Hepatic Failure. A Proposed Algorithm	311
Jaime Gasco, Leonardo Rangel-Castilla, Brodus Franklin, Philip G. Thomas, and Joel Patterson	
Novel Free Radical Monitoring in Patients with a Neurological Emergency Diseases	315
Kenji Dohi, Kazue Satoh, Tomoya Nakamachi, Hirokazu Ohtaki, Sachiko Yofu, Shunsuke Nakamura, Seiji Shioda, and Tohru Aruga	
Cerebrolysin Attenuates Blood–Brain Barrier and Brain Pathology Following Whole Body Hyperthermia in the Rat	321
Hari Shanker Sharma, Sibilla Zimmermann-Meinzingen, Aruna Sharma, and Conrad E. Johanson	
Chronic Hypertension Aggravates Heat Stress-Induced Brain Damage: Possible Neuroprotection by Cerebrolysin	327
Dafin Fior Muresanu, Sibilla Zimmermann-Meinzingen, and Hari Shanker Sharma	
Part IX Nanoparticles and Brain Edema	
Carbon Nanotubes in Neuroscience	337
Erik B. Malarkey and Vladimir Parpura	
Nanowired-Drug Delivery Enhances Neuroprotective Efficacy of Compounds and Reduces Spinal Cord Edema Formation and Improves Functional Outcome Following Spinal Cord Injury in the Rat	343
Hari Shanker Sharma, Syed F. Ali, Z. Ryan Tian, R. Patnaik, S. Patnaik, Aruna Sharma, Arne Boman, Per Lek, Elisabeth Seifert, and Torbjörn Lundstedt	
A New Antioxidant Compound H-290/51 Attenuates Nanoparticle Induced Neurotoxicity and Enhances Neurorepair in Hyperthermia	351
Hari Shanker Sharma, Aruna Sharma, Saber Hussain, John Schlager, Per-Ove Sjöquist, and Daffin Muresanu	
Influence of Nanoparticles on Blood–Brain Barrier Permeability and Brain Edema Formation in Rats	359
Hari Shanker Sharma, Saber Hussain, John Schlager, Syed F. Ali, and Aruna Sharma	
Author Index	365
Subject Index	397

Part I
Igor Klatzo Lecture

Bulk Flow and Diffusion Revisited, and Clinical Applications

Hans-J. Reulen

Abstract The first Klatzo-Lecture pays homage to an exceptional academician, scientist and teacher. The author spent nearly 1 year in Klatzo's laboratory at the NHI in Bethesda, and the first part of results presented here originate directly from this collaboration. It was shown that following cortical injury, movement of edema fluid into the tissue occurs by bulk flow, and that the driving force is a small tissue pressure gradient. Resolution of edema fluid is achieved by clearance into the ventricular and subarachnoid CSF, is enhanced in the presence of pressure gradients and is supported by re-absorption into capillaries. Using appropriate techniques, the formation rate as well as clearance of edema into CSF and tissue resorption could be determined in human brain metastases and malignant gliomas.

Three examples of clinical applications based on the discussed mechanisms are presented:

- a. *Fluorescence-guided surgery* of gliomas is based on the accumulation of 5-ALA in tumour cells; there being enzymatically converted to PP-IX, a compound with deep red fluorescence. This fluorescence is used for the more accurate surgical removal of gliomas.
- b. *Radioimmunotherapy* of gliomas uses an anti-tenascin antibody, coupled with a nuclide, administered postoperatively into the tumour cavity, from where it diffuses into tissue, couples to the receptor at the glioma cells. Then the isotope destroys the tumour cells.
- c. *Convection-enhanced delivery* is based on the interstitial infusion of an appropriate cytotoxic drug into the white matter at low pressure. Thus, the method employs bulk flow, distributes a drug in a larger tissue volume and eventually achieves drug concentrations greater than systemic levels.

Experimental studies and clinical results are presented for all three clinical applications.

H.-J. Reulen (✉)
Maximilians University Munich,
Kastellstr. 581247, München, Germany
e-mail: hjreulen@gmx.de

I am very grateful to Z. Czernicki and the organizing group for being offered the great honour of presenting the first **Igor Klatzo** Lecture. In this report first previous results of bulk flow and diffusion in the development and resolution of brain edema will be revisited, then some recent examples will be shown as to how this knowledge of diffusion and bulk flow can be transferred into clinical applications.

A great part of the work on bulk flow and diffusion was done during a stay in I. Klatzo's laboratory in Bethesda in 1973/1974 (Fig. 1). Since then a long collaboration developed with I. Klatzo and M. Spatz. Due to given limits, I will concentrate on the studies of our group. Unfortunately it will not be possible to mention all the important groups who have contributed by essential studies.

Keywords Brain edema • diffusion • bulk flow • resolution • fluorescence-guided surgery • glioblastomas • malignant gliomas • radioimmunotherapy • tenascin • antibody • convection-enhanced transport

Part I. Bulk Flow and Diffusion in Vasogenic Brain Edema

Spreading of Edema

During the stay at Klatzo's laboratory an attempt was made to characterize the mechanisms responsible for the spreading and resolution of edema fluid in cold-induced vasogenic edema. The two possible mechanisms to distinguish were diffusion and bulk flow. The cold-induced edema model was used in cats, where distances of various tracers given at the same time and travelling with edema fluid could be measured, simultaneously the water content in consecutive tissue blocks and tissue pressure (16) at various distances from the injury (17). Figure 2 shows the linear distances travelled within 6 h by C-14 sucrose, Fluorescein-labelled albumin (FLA) and Evans-Blue-albumin, three substances



Fig. 1 Igor Klatzo, Maria Spatz and colleagues in Bethesda

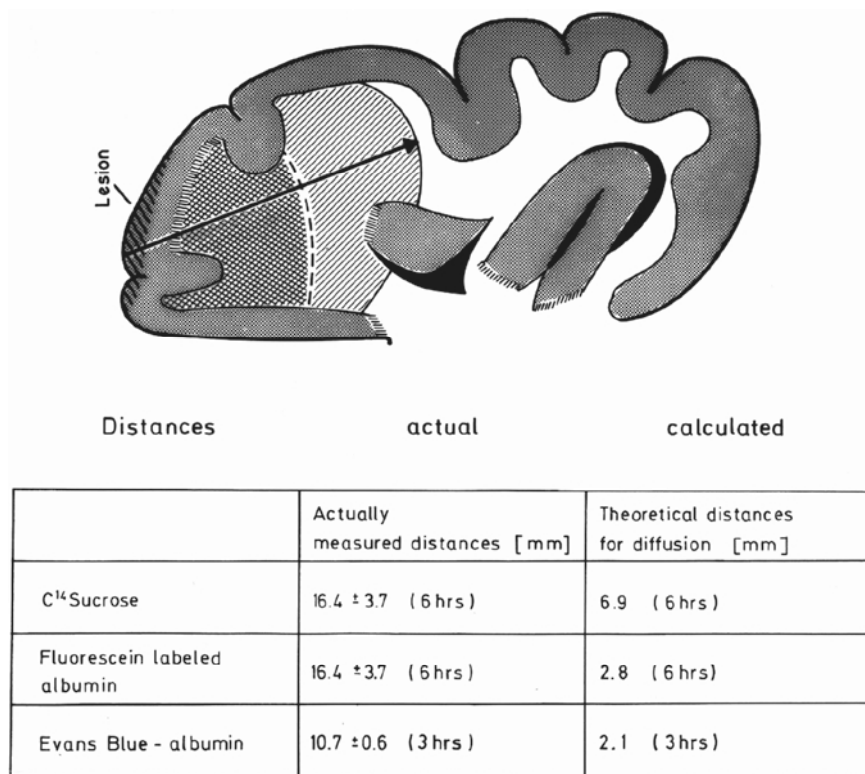


Fig. 2 Distances various substances travelled in edema vs. calculated theoretical distances for diffusion in white matter

with highly different diffusion coefficients. The theoretical distances for diffusion were calculated using the mathematical model of Patlak and Fenstermacher (2,13,16) and the respective diffusion coefficients, and they were significantly shorter than the distances actually travelled.

This fact and the finding that C-14 sucrose and FLA, despite their highly different diffusion coefficients, travelled the same distance, strongly supported bulk flow as the prevailing mechanism. Similar results were obtained by Bruce et al. (3).

A second finding of the study was the existence of a tissue pressure gradient between edematous and normal white matter, and this pressure gradient was shown to be the driving force for the propagation of edema fluid (17). In 2000 the existence of a tissue pressure gradient had also been shown to exist in experimental peritumoural edema (14, 15).

Resolution of Edema Fluid

How is edema fluid removed from the tissue? It was tempting to hypothesize that such hydrostatic pressure gradients between the edematous brain and the CSF could be the driving force for the movement of edema fluid into the CSF. This theory was examined in cold-induced edema. Immediately after lesion production Evans blue, I-131-labelled albumin and C-14 sucrose were administered i.v. About 40 h later, the time when edema had expanded and reached the ventricular wall, the animals were re-anaesthetized and a ventriculo-cisternal perfusion was installed. This allowed determination of the appearance and wash-out of the labelled markers in the cisternal outflow (Fig. 3). Simultaneously a certain amount of markers as well as edema were removed from the edematous tissue close to the ventricle (18,19).

In the following study the clearance of edema into the ventricle was measured quantitatively by labelling edema fluid with an extracellular marker, sodiumthiosulfate S 35. Edema clearance amounted to 0.8–1.4 ml/day. If this value was recalculated

for the human brain on a weight basis, the corresponding edema clearance would be about 30–60 ml/day (21,22).

The question remained whether and to what extent clearance of edema fluid occurred through the cortex and pial lining into the subarachnoid CSF? This question was examined by Uhl et al. (23) using the infusion edema model of Marmarou (9,11). Ventriculo-cisternal perfusion was combined with a closed cranial window perfusion technique, which allowed determining the arrival of labelled edema fluid in the ventricle and the subarachnoid CSF (Fig. 4). Clearance of edema

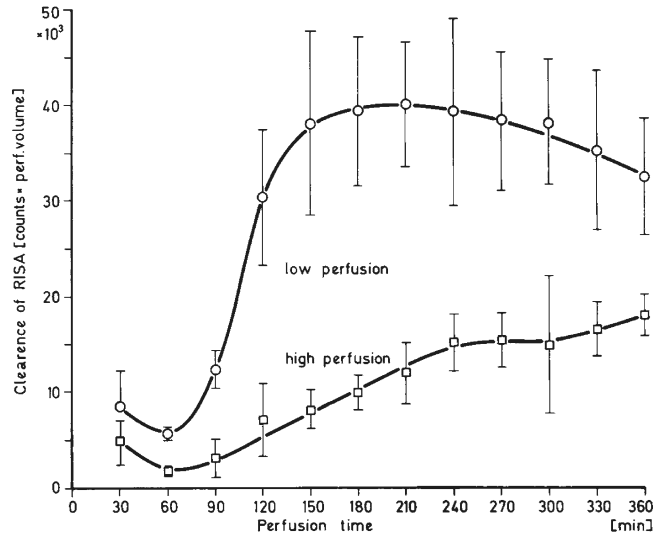


Fig. 3 Appearance of RISA and C-14 sucrose in cisternal outflow during low- and high-pressure ventriculo-cisternal perfusion

Edema Clearance into Ventricle and SAS

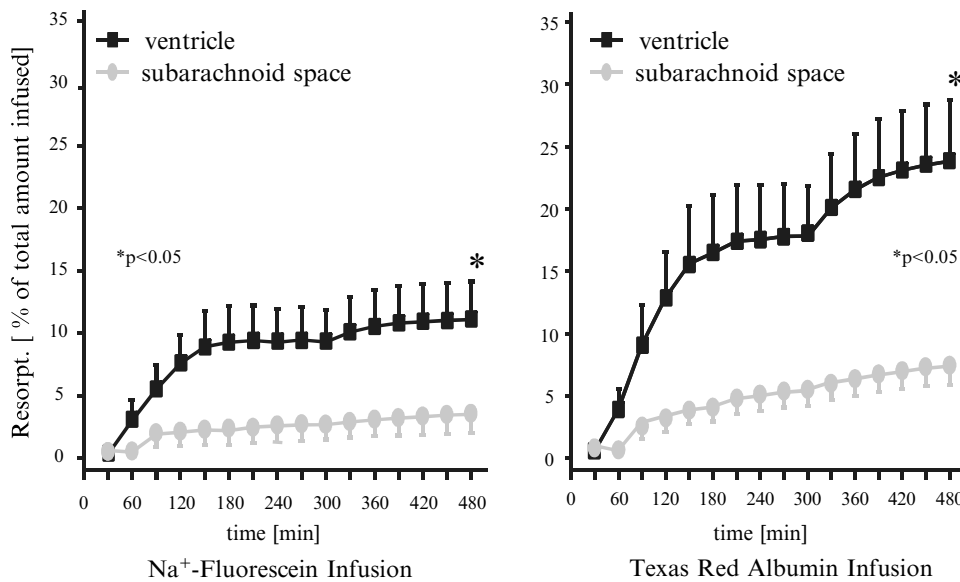


Fig. 4 Appearance of sodium-fluorescein and Texas-red albumin in cisternal outflow and subarachnoid CSF after simultaneous ventriculo-cisternal perfusion and supracortical perfusion with closed-window-technique

fluid into the subarachnoid space occurred in a significantly smaller amount as compared to drainage into the ventricular system (23).

These data together with results of Marmarou (9–11), Bruce (3) and others (2,13) justify the conclusion that resolution of edema fluid is achieved by clearance into CSF, is enhanced in the presence of pressure gradients and is supported by re-absorption into capillaries. It seems conceivable that resolution by bulk flow prevails as long as pressure gradients exist. If they dissipate, the remaining edema would have to be removed by diffusion and re-absorption mechanisms. Basic studies on the roles of diffusion, convection and capillary transporters in solute removal from extracellular space of the brain were reported by Groothuis et al. (37).

Clinical Studies in Peritumoural Edema

The important question was whether the experimental results were applicable to human brain edema? Brain tumours continuously produce edema fluid, and since the edema volume remains constant during at least several days, production must be balanced with resolution. Would it be possible to measure edema production and resorption non-invasively in patients?

In order to study this question U. Ito joined our group in Berne in 1986 for some months. First we could demonstrate, by measuring the Hounsfield-units in CT-scans, that in brain tumours – metastases and gliomas – the distribution of edema or the water content were comparable to cold-induced edema (6,20) (Fig. 5). Ito et al. developed a method that

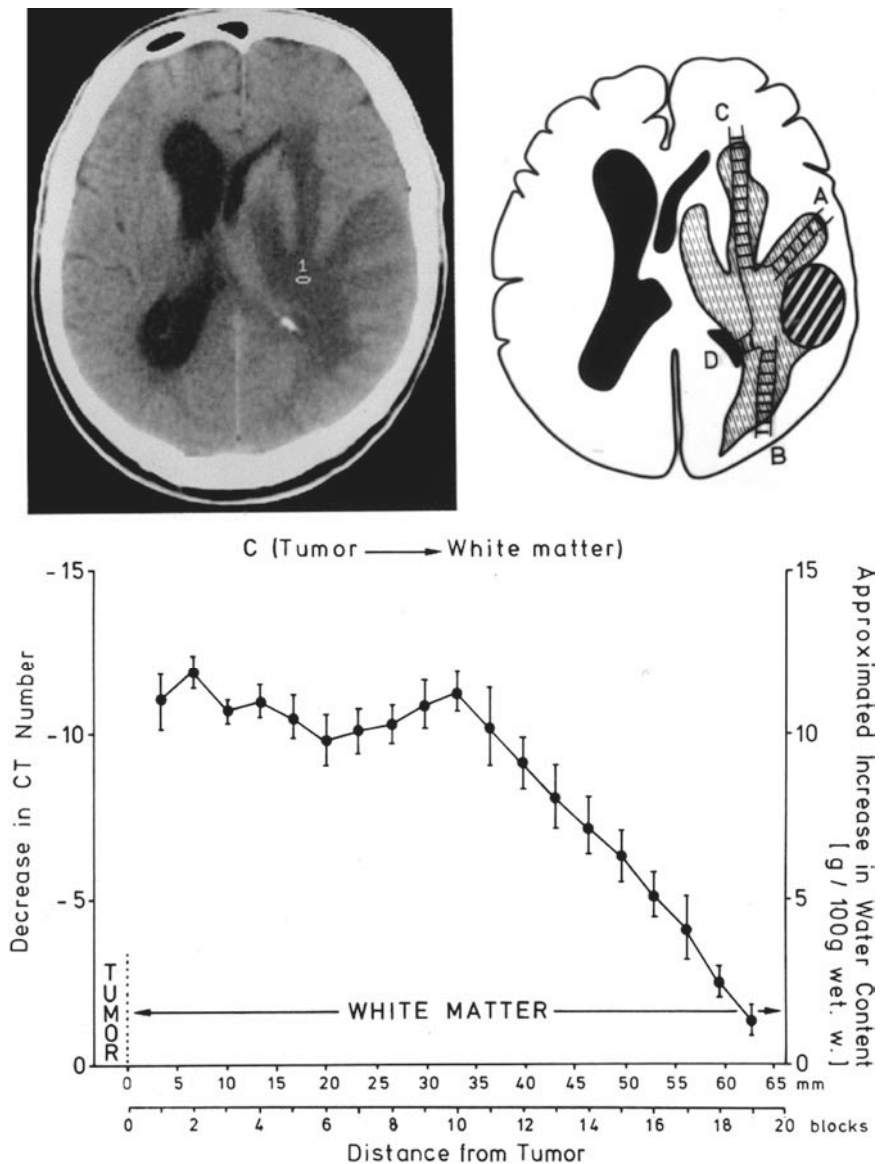


Fig. 5 Decrease in CT-numbers in white matter (in direction C) in a malignant glioma

allowed measuring the production rate of edema fluid in such tumours (7,8). Contrast medium was infused during 90 min and CT-scans were taken before, 1.5, 3, 6 and 9 h after the start of infusion. The area of contrast enhancement was measured planimetrically at all time intervals, thus allowing determination of the increase in volume of the contrast enhanced area, and then to calculate the radial propagation of edema in the tissue, which amounted on average to 1.5 mm/h (5,7,8).

The amount of newly formed edema fluid V_e can be calculated by using the assumption that the ECR in the edema area amounts to 25–30% (4) and concentration of the contrast medium in the newly formed edema fluid is similar to that in the plasma. The values for V_e in a group of malignant gliomas and metastases are between 0.2 and 3.2 ml/h, or 4 and 75 ml/day, respectively (5,7,8). Edema fluid production was dependant on the volume of the tumour (7) (Fig. 6).

Edema resolution may occur within the tissue via reabsorption into blood or by drainage into the ventricular or subarachnoidal CSF. The average rate of resolution of edema fluid during the passage through 1 cm³ tissue was determined to be about 0.009 to +0.03 ml/h (5,7). By using a theoretical

mathematical convection/diffusion model, a value of 0.003 ml/min/cm³ was found by Nagashima et al. (12).

Taken together, these data allow estimating the edema fluid turnover as a dynamic situation. The first example shows a small metastasis with a small peritumoural edema (Fig. 7). Edema production rate in the tumour was determined as 3.4 ml/day; the edematous tissue volume was 35 ml and in this case tissue resorption was 3.36 ml/day. Thus the amount of fluid cleared into the CSF was negligible. In a second case – a large metastasis – the production rate of edema was 48 ml/day, tissue resorption in the edematous tissue volume was 8.6 ml/day and the rest, ca. 39 ml, was drained into the CSF.

Finally, using the mathematical model of fluid transport in brain tissue developed by Patlak and Fenstermacher (13) and by determining the distribution profiles of a tracer (Telebrix 30), it was definitely shown that movement of edema fluid in human brain tumours follows bulk flow and cannot be explained solely by diffusion (1).

As a clinician I was always interested in transferring the results from our experimental studies into clinical application. The modern term for this is translational research. I will now present three examples of clinical applications of the discussed mechanisms.

Edema Formation and Tumor Volume
Edema formation rate (ml/h)

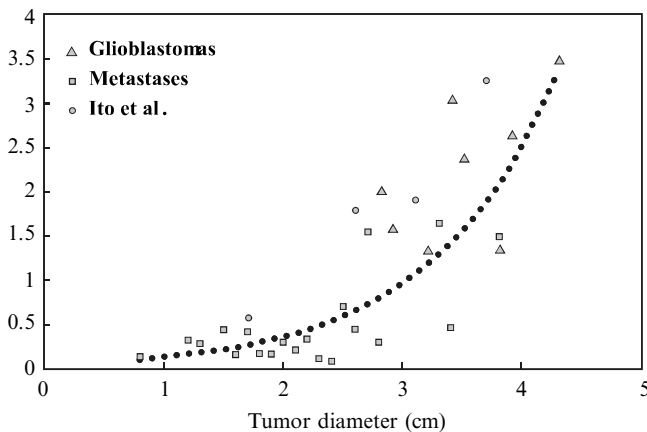


Fig. 6 Edema fluid formation in relation to tumor diameter in gliomas and metastases

Part II. Clinical Applications of Bulk Flow and Diffusion Mechanisms

Fluorescence-Guided Surgery of Malignant Gliomas

One of the dreams of neurosurgeons was to contrast intraoperatively malignant gliomas to be able to remove such tumours with more accuracy. Previous approaches using i.v. administered fluorescent markers like Fluorescein or Photofrin II were hampered by the fact that these substances distribute in the ECS of tumour and migrate with bulk flow out into the surrounding brain tissue (24). Thus the risk exists that during



Edema Fluid Turnover in metastases

	Small Metastasis	Large Metastasis
Tumor volume	3 ml	30 ml
Edema tissue volume	35 ml	90 ml
Edema production rate	3.4 ml/day	48 ml/day
Tissue resorption (0.004 ml/h/cm ³)	3.36 ml/day	8.6 ml/day
Ventricular clearance	0 ml/day	39 ml/day

Fig. 7 Edema fluid production and resolution in 2 examples of brain metastasis. CT of a small metastasis without contact to the ventricles

Principle of fluorescence-accumulation in malignant gliomas after administration of 5-ALA

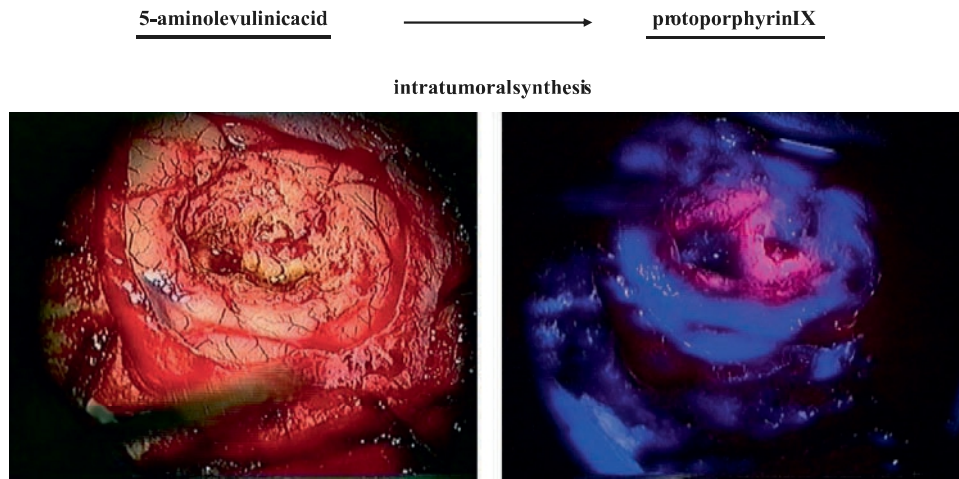


Fig. 8 Principle of fluorescence-accumulation in malignant gliomas after administration of 5-ALA

surgery not only the tumour is removed, but also peritumourally stained but normal tissue. In this situation bulk flow is of disadvantage and this method, therefore, was abandoned.

In 1994 we became aware of a substance – 5-aminolevulinic acid (5-ALA) – which at that time had already been in use for the visualisation of bladder tumours. 5-ALA is a naturally occurring precursor in the heme biosynthesis and has the property to accumulate specifically in tumour cells, there being enzymatically converted to PP-IX, a compound with deep red fluorescence (Fig. 8). No uptake occurs in normal tissue (25,26). Stummer et al. could demonstrate in the rat C6-glioma model that glioma cells strongly accumulate ALA, and this uptake was selective for glioma tissue. By using violet-blue light and adequate filters the tumour can be visualized and clearly distinguished from surrounding tissue (25). Together with engineers from Zeiss (Oberkochen/Germany) a fluorescence kit for the neurosurgical microscope was developed, which permitted switching from conventional white light to violet-blue excitation light (25). A phase I/II clinical trial with 52 patients proved a high sensitivity and specificity of fluorescence detection, respectively detection of glioma tissue (26). Eventually a randomised controlled multicenter Phase III trial was organized with 19 neurosurgical centers participating (supported by medac, Wedel/Germany), comparing resection of malignant gliomas under conventional white light with resection under fluorescence conditions (27).

Results

Patients with primary malignant gliomas were randomized to either the white light group with conventional microsurgery

or to the ALA-group using fluorescence guidance. In both groups surgery was followed by conventional radiotherapy. Randomization considered the important prognostic factors age and KPS, eloquent or non-eloquent location and surgeon, so that both study arms were well balanced with regard to these factors (27).

The first end-point was to determine the number of patients in each study arm with residual contrast enhancement on early postoperative MRI. In the control-group, early postoperative MRI was devoid of residual tumour in 35% of cases. In contrast, in the ALA-group, 65% of the patients had complete resections of contrast-enhancing tumour. This difference is highly significant. The result shows that with this technique a significantly larger group of patients can be completely resected.

The second end-point was the progression-free survival at 6 months postoperatively. Figure 9 shows the Kaplan-Meier curve of patients in the WL-arm, based on MRI data. Only 21% of patients survived and remained free of progression 6 months after surgery. The curve corresponds well to historical data of previous studies. In the ALA-group the fraction of patients surviving without progression at 6 months was doubled to 42% and this difference was highly significant.

Our results can be used to examine another long-standing and important question: Does the extent of surgery influence survival in patients with malignant gliomas? Previous retrospective studies seem to support the hypothesis that complete resection translates into longer survival, but due to the retrospective nature of these studies, the evidence-grade remained low. The present study allows examining this question on the basis of prospective randomized data. For this purpose patients from both study-arms who had complete resections

according to postoperative MRI were compared with patients with residual tumour.

Median length of survival from time of surgery was 12 months in patients with residual contrast enhancing tumour and 17.2 months in patients without residual tumour. This difference in a uni- and multivariate analysis is statistically highly significant (28). The difference is as large as or even larger than any effect of additional therapies known so far.

In 2007 EMEA, the “European FDA” officially licensed this technique for clinical use.

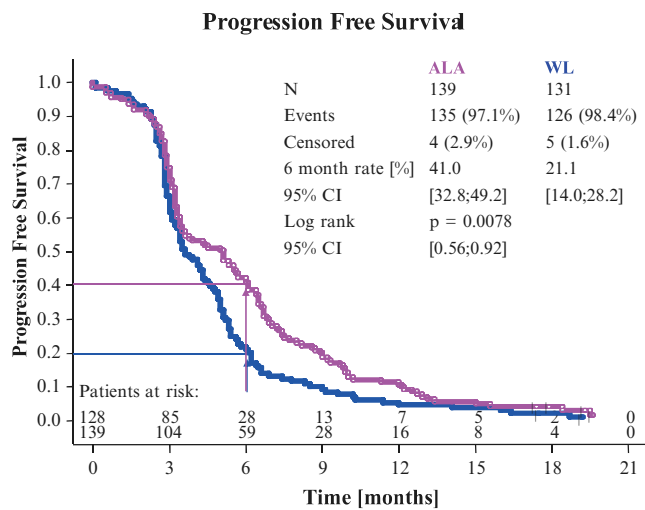


Fig. 9 Kaplan–Meier curve of progression-free survival in white-light (control) group and the 5-ALA-group

Intracavitary Radioimmunotherapy

The problem in malignant gliomas is that tumour cell infiltration can extend well beyond the surgical site into normal brain parenchyma, and this is the reason for local recurrences. The blood-brain barrier prevents an effective systemic drug delivery in the treatment of brain tumours (37). However, direct application of a drug into the postoperative resection cavity is an interesting alternative, ensures higher concentrations of the drug at its destination and reduces the risks of systemic therapy. This method is based on *diffusion*, or a concentration gradient of the agent from the cavity to the tissue, respectively, and is only influenced by the molecular weight of the agent.

The basic idea of radioimmunotherapy in human glioblastomas takes advantage of the fact that a distinct antigen-tenascin is expressed by the matrix of gliomas in a significantly higher amount than by normal brain tissue. A tenascin antibody is labelled with a suitable isotope and the antibody-isotope-complex is applied via an Ommaya-reservoir into the postoperative resection cavity (34). The antibody-isotope-complex travels through the tissue, couples to tumour cells, and the isotope then selectively destroys the tumour cells (Fig. 10). The main question is how far the targeted antibody can penetrate into the tissue by means of diffusion? For an optimal effect the targeted antibody should be able to reach tumour cells that have migrated some distance from the tumour margin. This question was examined in a C6-glioma model in rats together with the department of Nuclear medicine at Munich University.

Method: Intracavitary Radioimmunotherapy

- Implantation of the Ommaya-Reservoir
- Application of antibody-nuclide-complex
- Migration into the tissue (diffusion)
- Binding to glioma cells
- Destruction of glioma cell

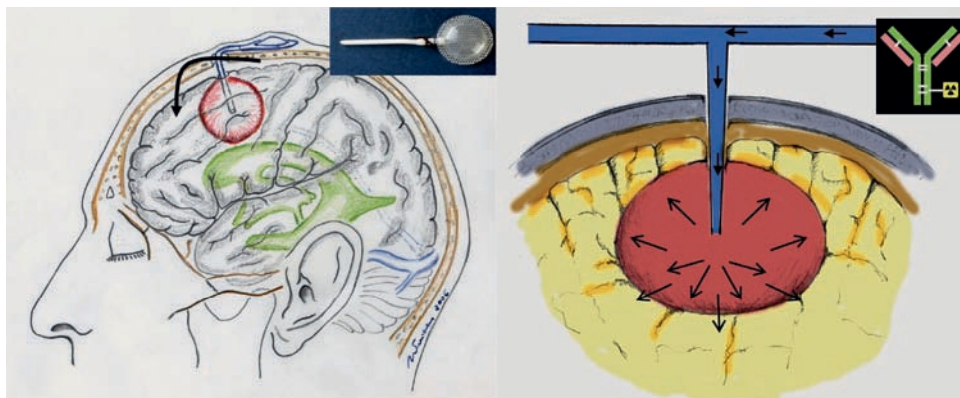


Fig. 10 Technique of application of the TN-antibody-nuclide-complex via an Ommaya-reservoir into the postoperative resection cavity

Experimental Studies

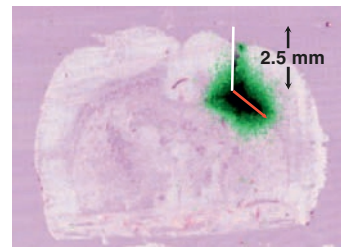
I-125-labelled antibody was infused via a stereotactically placed needle into the intact tumour, and the spreading of the isotope was measured autoradiographically at 6, 24 and 48 h (30,32). The autoradiographs were matched with the corresponding HE-stained images from frozen sections by means of computer-assisted image analysis. The distances travelled by the isotope increased from 6 to 24 h and were unchanged after 48 h. In order to reduce the large molecular weight of the antibody, the experiment was repeated with fragments of the antibody (Fab's), again labelled with I-125. The mean migration distance of the labelled Fab's was significantly prolonged at 6 and 24 h (Fig. 11). The longest distance measured after 24 h was 6.7 mm in the rat brain, and from our experience in human tumours this may correspond to 1.5–2.5 cm. In order to simulate the clinical situation, the experiment was repeated after surgical removal of the tumour and successive application of the antibody-isotope-complex into the tumour cavity. Now the driving force is diffusion and the distances reached at the same time periods are significantly shorter.

Clinical Studies

Intracavitary radioimmunotherapy has been under clinical testing in a few centres since the beginning of the 1990s (29,34). In 1994, we adopted a technique used by Riva et al. (34,35), where a tenascin antibody, labelled with I-131 or Yttrium-90 was applied via an Ommaya-reservoir into the tumour-cavity

of resected malignant gliomas. Tenascin-expression was tested in the tumour specimens and prior to treatment a PET-scan with a test dose of technetium-99, injected into the Ommaya-reservoir, was obtained to exclude leakage of the system and to measure the volume of the tumour cavity. Treatment is repeated three times in intervals of 7 weeks with a dose of 50, 40 and 30 mCi (31,33). Meanwhile more than 50 patients have been treated in a phase II-study. In general, the treatment is well tolerated and Fig. 12 shows the survival time of this patient cohort. As compared to a

Migration of Antibody and Fab

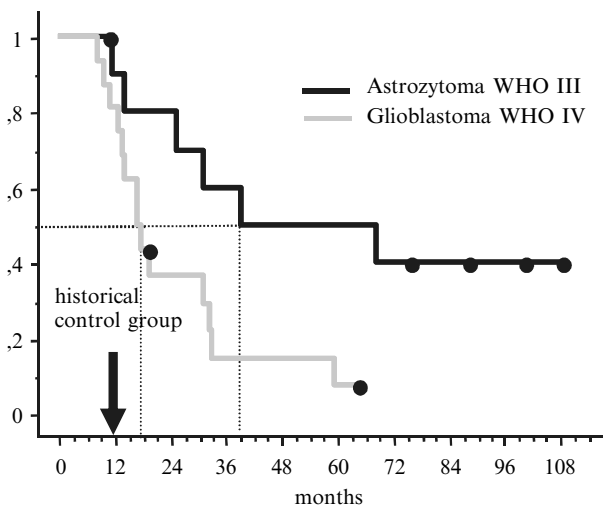


	Labelled Antibody	Labelled Fab-Fragment
Intact tumour	4.1 ± 1.9 mm	6.7 ± 1.1 mm
Subtotally resected tumour	3.0 ± 0.4 mm	3.4 ± 0.3 mm

Fig. 11 Migration distances (mm) at 24 h after injection of I-125-labelled antibodies and Fab-fragments into intact or subtotally resected C6-gliomas in rats. Autoradiography with the tumor (black) and the migrated antibody (green)

Survival Time after RIT

Cesena-Munich-group (n=27 patients)



Munich-group (n=23 patients) with protocol modifications

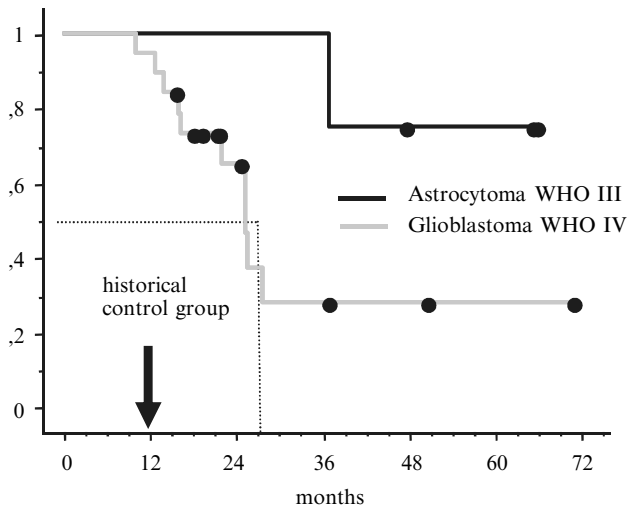


Fig. 12 Survival time of two patient cohorts with glioblastoma WHO grade IV and astrocytoma WHO grade III following intracavitary radioimmunotherapy

historical group of glioblastoma patients, the median survival time in glioblastomas is 25 months, and for anaplastic astrocytomas 5-year survival is 77% approximately. This prolongation in survival time is highly significant for both glioblastomas and anaplastic astrocytomas.

In order to further improve this technique a different isotope – Rhenium-188 – was used, which has a significantly shorter half-life time of 17 h (instead of 6 days with J-131), a higher average β -energy and an increased penetration depth as compared to I-131. Presently a Phase-I dose-escalation study is being performed to determine the most effective dose. The next step will be to use a smaller single-chain antibody, as in the experimental studies. With these two improvements we hope to advance further this already very effective approach.

Since pure diffusion does not result in appropriate distribution of the therapeutic agent in cases with large edema or extensive cell infiltration, respectively, distribution can be facilitated by another new technique.

Convection-Enhanced Delivery

This method is based on the direct intraparenchymal infusion of targeted molecules and was developed by Oldfield et al. in the early 1990s (36), based on previous studies of Marmarou and his group (11). This microinfusion delivery technique became known as convection-enhanced delivery (CED) (36,38,39). After stereotactic insertion of one to three catheters, interstitial infusion into the white matter is generated by a syringe pump at a low pressure of 10–18 mmHg. Thus, the method employs *bulk flow* and may account for 7–10 mm propagation per hour in linear distance, distributes a drug in a larger tissue volume and eventually achieves drug concentrations greater than systemic levels (36,38).

Clinical Trials in Human Malignant Gliomas

After demonstration of the efficacy in a mouse glioma model (38) by intratumoural infusion of targeted toxins, several clinical Phase I/II studies were performed and showed the practicability of the technique (40,41). In clinical application the principal idea is that the solid tumour is the target for surgery, while the infiltrative component is the target of CED.

The Munich Neurosurgical Clinic participates in the IL13 phase III trial. The human Interleukin-13 (IL13) receptor is expressed at high density on malignant glioma cells and is used as carrier ligand for a cytotoxin, Pseudomonas exotoxin A. This complex is administered via two to three catheters with a total flow rate of 0.75 ml/h for 96 h, thus delivering a maximum total volume of 72 ml. Results will probably be available in 2009.

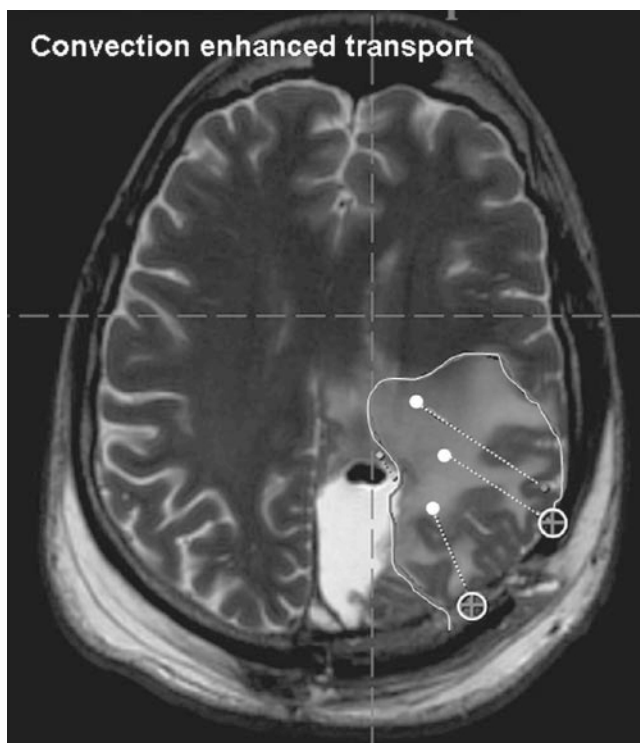


Fig. 13 Example of modelling infusion in three geometries with the aid of a mathematical planning system. Catheters (*white*) are positioned according to the distribution of the hyperintense signal in the T2-weighted MR-images

An improvement of the method is the modelling of infusion in three geometries (Fig. 13) with the aid of a mathematical planning system and positioning of the catheters according to the distribution of the hyperintense signal in T2-weighted images. This ensures precise drug delivery to the desired location at relatively uniform concentrations (39,41,42). An advantage of convection-enhanced delivery is the possibility to use MRI imaging to visualize real-time drug distribution during infusion by adding Gadolinium as surrogate tracer. Such real-time monitoring is a new component for obtaining optimal treatment results in humans.

While the efficacy of the various infused agents remains to be determined, early evidence from these clinical trials suggests that convection can be used safely for drug delivery while at the same time overcoming many problems associated with other drug delivery techniques used for tumour therapy.

Conclusion

The intention of this report was to revisit bulk flow and diffusion and to demonstrate some recent clinical applications of these two mechanisms, lessons that were learned through the basic studies in brain edema. It is the privilege and the

task of clinicians to translate basic findings into new treatment strategies. I am happy and proud to be offered the honour of giving this lecture as a tribute to my mentor and friend Igor Klatzo.

Conflict of interest statement We declare that we have no conflict of interest.

References

Bulk Flow and Diffusion in BE

1. Aaslid R, Gröger U, Patlak CS, Fenstermacher JD, Huber P, Reulen H-J (1990) Fluid flow rates in human peritumoral edema. *Acta Neurochir Suppl* 51:152–154
2. Blasberg RG, Gazendam I, Patlak CS, Fenstermacher JP (1980) Quantitative autoradiographic studies of brain edema. In: Cervos-Navarro I, Ferszt R (eds) *Brain edema, pathology and therapy*. Raven-Press, New York
3. Bruce DA, Ter Weeme C, Kaiser G (1976) The dynamics of small and large molecules in the extracellular space and CSF following cold injury of the cortex. In: Pappius HM, Feindel W (eds) *Dynamics of brain edema*. Springer, Berlin/Heidelberg/New York, pp 95–97
4. Fenske A, Samii M, Reulen H-J, Hey O (1973) Extracellular space and electrolyte distribution in cortex and white matter of dog brain in cold-induced brain edema. *Acta Neurochir* 28:81–94
5. Gröger U, Huber P, Reulen H-J (1994) Formation and resolution of human peritumoral brain edema. *Acta Neurochir Suppl* 60:373–374
6. Ito U, Reulen H-J, Huber P (1986) Spatial and quantitative distribution of human peritumoral brain edema in computerized tomography. *Acta Neurochir* 81:53–60
7. Ito U, Tomita H, Tone O, Shishido T, Hayashi H (1990) Formation and resolution of white matter edema in various types of brain tumors. *Acta Neurochir Suppl* 51:149–151
8. Ito U, Tomita H, Tone O, Masaoka H, Tominaga B (1994) Peritumoral edema in meningioma: a contrast enhanced study. *Acta Neurochir Suppl* 60:361–364
9. Marmarou A, Shapiro K, Poll W, et al. (1976) Studies on kinetics of fluid movements within brain tissue. In: *Intracranial pressure III*. Springer, Berlin/Heidelberg/New York, pp 1–4
10. Marmarou A, Shulman K, Shapiro K, Poell W (1976) Dynamics of Brain Edema. In: Pappius HM, Feindel W (eds) *The time course of brain tissue pressure and local CBF in vasogenic edema*. Springer, Berlin/Heidelberg/New York
11. Marmarou A, Nakamura T, Tanak K, Hochwald GM (1984) The time course and distribution of water in the resolution phase of infusion edema. In: *Brain edema*. Plenum, New York, pp 37–44
12. Nagashima T, Tamaki N, Takada M, Tada Y (1994) Formation and resolution of brain edema associated with brain tumors. A comprehensive theoretical model and clinical analysis. *Acta Neurochir Suppl* 60:165–167
13. Nakagawa H, Groothuis DR, Owens ES, Fenstermacher JD, Patlak CS, Blasberg RG (1987) Dexamethasone effects on I-125 albumin distribution in experimental RG-2 gliomas and adjacent brain. *J Cereb Blood Flow Metab* 7:687–701
14. Navalitloha Y, Schwartz ES, Groothuis EN, Allen CV, Levy RM, Groothuis DR (2000) Therapeutic implications of tumor interstitial fluid pressure in subcutaneous RG-2 tumors. *Neuro-Oncol* 8(3):227–233

15. Okada Y, Hoehn-Berlage M, Bockhorst K, Tolxdorff T, Hossmann K-A (1990) Magnetic resonance imaging and regional biochemical analysis of experimental brain tumors in cats. *Acta Neurochir Suppl* 51:129–130
16. Reulen H-J, Kreysch HG (1973) Measurement of brain tissue pressure in cold-induced brain edema. *Acta Neurochir* 29:29–40
17. Reulen H-J, Graham R, Spatz M, Klatzo I (1977) Role of pressure gradients and bulk flow in dynamics of vasogenic brain edema. *J Neurosurg* 46:24–35
18. Reulen H-J, Tsuyumu M, Tack A, Fenske A, Prioleau GR (1978) Clearance of edema fluid into cerebrospinal fluid. A mechanism for resolution of vasogenic brain edema. *J Neurosurg* 48:754–764
19. Reulen H-J, Tsuyumu M (1981) Pathophysiology of formation and resolution of vasogenic brain edema. In: M. de Vlieger, S. deLange, JWF Beks (eds) *Brain edema*. Wiley, New York, pp 31–47
20. Reulen H-J, Graber S, Huber P, Ito U (1988) Factors affecting the extension of peritumoral brain edema. A CT-study. *Acta Neurochir* 95:19–24
21. Tsuyumu M, Reulen H-J, Prioleau GR (1981) Dynamics of formation and resolution of vasogenic brain edema. I. Measurement of edema clearance into ventricular CSF. *Acta Neurochir* 57:1–13
22. Tsuyumu M, Reulen H-J, Inaba Y (1985) II. Dynamics of fluid movement through brain parenchyma and into the CSF in vasogenic edema. In: Inaba Y (ed) *Brain edema*. Springer, Berlin/Heidelberg, pp 99–107
23. Uhl E, Wrba E, Nehring V, Chang RCC, Baethmann A, Reulen H-J (1999) Technical note: a new model for quantitative analysis of brain edema resolution into the ventricles and the subarachnoid space. *Acta Neurochir* 141:89–92

Fluorescence-Guided Surgery

24. Stummer W, Goetz C, Hassan A, Heimann A, Kempfski O (1993) Kinetics of photofrin II in perifocal brain edema. *Neurosurgery* 33:1075–1082
25. Stummer W, Stocker S, Wagner S, Stepp H, Fritsch C, Goetz C, Goetz A, Kieffmann R, Reulen H-J (1998) Intraoperative detection of malignant gliomas by 5-aminolevulinic acid-induced porphyrin fluorescence. *Neurosurgery* 42:518–526
26. Stummer W, Nowotny A, Stepp H, Goetz C, Bise K, Reulen H-J (2000) Fluorescence-guided resection of glioblastoma multiforme by using 5-aminolevulinic acid-induced porphyrins: a prospective study in 52 consecutive patients. *J Neurosurg* 93:1003–1013
27. Stummer W, Pichlmeier U, Meinel T, Wiestler OD, Zanella F, Reulen H.-J, and the german glioma study group (2006) Fluorescence-guided surgery with 5-ALA for resection of malignant glioma: a randomised controlled multicentre phase III-trial. *Lancet Oncol* 7:392–401
28. Stummer W, Reulen H-J, Meinel T, Pichlmeier U, Tonn J-C, Rohde V, Opperl F, Turowski B, Woiciechowsky C, Franz K, Pietsch T, and the ALA-Glioma Study Group. (2008) Extent of resection and survival in glioblastoma multiforme – identification of and adjustment for bias. *Neurosurgery* 62:564–56

Radioimmunotherapy

29. Bigner DD, Brown MT, Friedman AH, Coleman RE, Akabani G, Friedman HS, Thorstad WL, McLendon RE, Bigner SH, Zhao XG, Pegram CN, Wikstrand CJ, Herndon JE, Vick NA, Paleologos N, Cokgor I, Provenzale CJ, Zalutsky MR (1998) Iodine-131-labeled

- antitnascein monoclonal antibody 81C6 treatment of patients with recurrent malignant gliomas: phase I trial results. *J Clin Oncol* 16:2202–2212
30. Gildehaus F-J, Rachinger W, Decker M, Stocker S, Goetz C, Poepperl G, Tatsch K, Reulen H-J (2003) Migration properties of a radiolabelled intact antibody and Fab-fragment after locoregional application in C6-glioma of the rat. *J Nucl Med* 44 (suppl):36
 31. Goetz C, Riva P, Tatsch K, Gildehaus F-J (2003) Radioimmunotherapy in selected patients with malignant gliomas, survival time and side-effects. *J Neurooncol* 62:321–328
 32. Goetz C, Rachinger W, Decker M, Gildehaus F-G, Stocker S, Jung G, Tatsch K, Tonn J-C, Reulen H-J (2005) Distribution of labelled anti-tenascin antibodies and fragments after injection into intact or partly resected C6 gliomas in rats. *Cancer Immunol Immunother* 54:337–344
 33. Poepperl G, Goetz C, Gildehaus F-J, Reulen H-J, Hahn K, Tatsch K (2002) Initial experience with locoregional immunotherapy using 131I-labeled monoclonal antibodies against tenascin (BC-4) for treatment of glioma WHO grade III and IV. *Nuklearmedizin* 41:120–128
 34. Riva P, Franceschi G, Arista A, Frattarelli M, Riva N, Cremonini AM, Giuliani G, Casi M (1997) Local application of radiolabeled monoclonal antibodies in the treatment of high grade malignant gliomas: a six-year experience. *Cancer* 80:2733–2742
 35. Riva P, Franceschi G, Frattarelli M, Riva N, Casi M, Santimaria M, Adamo M (2000) Role of nuclear medicine in the treatment of malignant gliomas: The locoregional radioimmunotherapy approach. *Eur J Nucl Med* 27:601–609
 36. Bobo RH, Laske DW, Akbasack A, Morrison PF, Dedrick RL, Oldfield EH (1994) Convection enhanced delivery of macromolecules in the brain. *Proc Natl Acad Sci USA* 91:2076–2080
 37. Groothuis DR (2000) The BBB and blood-tumor barrier: a review of strategies for increasing drug delivery. *Neuro-Oncol* 2:45–59
 38. Hall WA, Rustamzadeh E, Asher AL (2003) Convection-enhanced delivery in clinical trials. *Neurosurg Focus* 14(2):e2
 39. Nguyen TT, Pannu YS, Sung C, Dedrick RL, Walbridge S, Brechbiel MW, Garmestani K, Beitzel M, Yordanov AT, Oldfield EH (2003) Convective distribution of macromolecules in the primate brain demonstrated using computerized tomography and magnetic resonance imaging. *J Neurosurg* 98:584–590
 40. Saito R, Bringas JR, Panner A, Tamas M, Pieper RO, Berger M, Bankiewicz KS (2004) Convection-enhanced delivery of tumor necrosis factor-related apoptosis-inducing ligand with systemic administration of temozolomide prolongs survival in an intracranial glioblastoma xenograft model. *Cancer Res* 64:6858–6862
 41. Sampson JH, Raghavan R, Provenzale JM, Croteau D, Reardon DA, Coleman RE, Rodríguez Ponce I, Pastan I, Puri RK, Pedain C (2007) Induction of hyperintense signal on T2-weighted MR images correlates with infusion distribution from intracerebral convection-enhanced delivery of a tumor-targeted cytotoxin. *Am J Roentgenol* 188(3):703–709
 42. Smith JS, Humphrey JAC (2006) Modeling convection enhanced delivery in brain: fluid and mass transport analyses. 9th AIAA/ASME joint thermophysics and heat transfer conference, 5–8 June, 2006, San Francisco, CA

Convection Enhanced Delivery

Part II
Ischemia and the Blood-Brain Barrier Disorders

Experimental Cerebral Ischemia: The Contribution of the Bethesda Group

Toshihiko Kuroiwa

Abstract Igor Klatzo started his research on cerebral ischemia at the NIH in the 1960s. The mechanism that produces the blood-brain barrier change after ischemia was a focus of interest in Klatzo's experiments, which used larger mammals. Studies using Mongolian gerbils, started by U. Ito, resulted in several important findings, including observation of the maturation phenomenon in 1975. Using newly developed ischemia models, the mechanism of postischemic neuronal/tissue injury was extensively studied. The cumulative effect was observed after repetitive cerebral ischemia. The protective mechanism of cortical spreading depression after global ischemia was investigated. Projects including in vitro studies of human brain endothelial cells and mucosal tolerance to E-selectin were performed in the Stroke branch after Klatzo retired from the NIH. Klatzo published a biography of Cecil and Oskar Vogt after retirement. He passed away in May 2007 in Gaithersburg, Maryland a few months after he completed the first part of his autobiography.

Keywords Igor Klatzo • experimental cerebral ischemia • NIH

Igor Klatzo started his research on cerebral ischemia in the 1960s at the NIH. In the first series of studies, postischemic blood-brain barrier (BBB) changes as well as clinicopathological changes were the foci of interest. The first paper in this series of studies using larger mammals was published in 1970 in the first issue of *Stroke* journal (2), followed by reports on the ultra-structural changes and hemodynamic aspects of postischemic BBB changes (13). Biphasic opening of the BBB during the postischemic phase was reported in 1985 (10).

Research studies using Mongolian gerbils were started with U. Ito in the 1970s. Approximately one third of the gerbils developed ischemic symptoms such as circling hemiparesis and seizure after the occlusion of the unilateral

common carotid artery (12). By selecting these symptom-positive animals (which will develop infarction), it is possible to have animals with a homogeneous intensity of tissue injury. In this series of investigations, the slow appearance of neuronal necrosis in the H2 (CA1) sector was observed. Shorter ischemic insults resulted in delayed appearances of necrosis (3). Blood-brain barrier disruption was also delayed as a result of milder ischemic insult (4). This facet of the response was named the 'maturation phenomenon'. Energy failure after a short period ischemia also developed slowly over a few days of postischemia, with a tendency to be delayed in the areas suffering milder ischemic insults (11).

In Klatzo's laboratory, several new animal models of cerebral ischemia have been developed and extensively tested. Studies using these new models of ischemia resulted in many interesting observations; after repetitive ischemic insults, a pronounced cumulative effect on brain edema and tissue injury was observed. The effect was most evident after 1 h interval ischemia, i.e. repetitive ischemia during the period of marked postischemic hypoperfusion (15). A model of complete global ischemia in a rat by Korpatchev (9) was introduced to Klatzo's laboratory in the 1980s (6). This model is characterized by complete circulatory arrest, and it is much closer to clinical cardiac arrest than was previously employed in animal models. Postresuscitation pathophysiology was extensively investigated using this model. The protective effect of spreading depression was observed on the postischemic neurons (5).

Klatzo organized the first brain edema symposium with Franz Seitelberger from the University of Vienna Neurological Institute in 1965, and the proceedings were published by Springer Verlag (7) (Fig. 1). The succeeding international brain edema symposia were organized every 3 years in the USA, Europe, and Asia in rotation. Researchers who once worked in Klatzo's laboratory organized most of the symposia. During Klatzo's appointment at the Laboratory of Neuropathology and Neuroanatomical Sciences NINDS NIH, many researchers, including many neurosurgeons from Japan, visited his laboratory from all over the world.

T. Kuroiwa (✉)
Laboratory of Clinical Medicine, Namegata District General Hospital,
98-8 Inoue Fujii, Namegata, Ibaraki 311-3516, Japan
e-mail: tkuroiwa-nsu@umin.ac.jp

BRAIN EDEMA

*Proceedings of the Symposium
September 11-13, 1965, Vienna*

Edited by

Igor Klatzo

National Institute of Neurological Diseases and Blindness
National Institutes of Health
Bethesda, Maryland, U.S.A.

and

Franz Seitelberger

Neurologisches Institut der Universität Wien, Austria



SPRINGER-VERLAG • WIEN • NEW YORK • 1967

Fig. 1 Inside cover of the proceedings of the First brain edema symposium. The symposium was organized by Klatzo and Seitelberger in 1965 in Vienna. The proceedings of the conference were published by Springer in 1967

After Klatzo retired from NIH, important projects including in vitro study of human brain endothelial cell (1) and mucosal tolerance have been performed. Hallenbeck succeeded Klatzo's at NINDS, NIH, and continued his project on the mucosal tolerance to E-selectin (14). The project is very interesting from a clinical point of view, and it has resulted in important publications.

After retirement from the NIH in 1993, Klatzo focused his academic activity on writing a biography on Cecil and Oskar Vogt, the men who proposed the pathoclinic theory, and founders of the Brain Research Institute in Neustadt, Germany, where Klatzo started his academic career. The book was published by Springer Verlag in 2002 (8).

After publishing the biography, Klatzo started writing his autobiography. In October 9, 2006, he arranged a party in the Blue Ridge Mountains Virginia to celebrate his 90th birthday. His former collaborators, family members and friends gathered to celebrate the occasion. Several months after the party, his health conditions declined. He returned home and passed away on May 5, 2007 in Gaithersburg Maryland (Fig. 2).

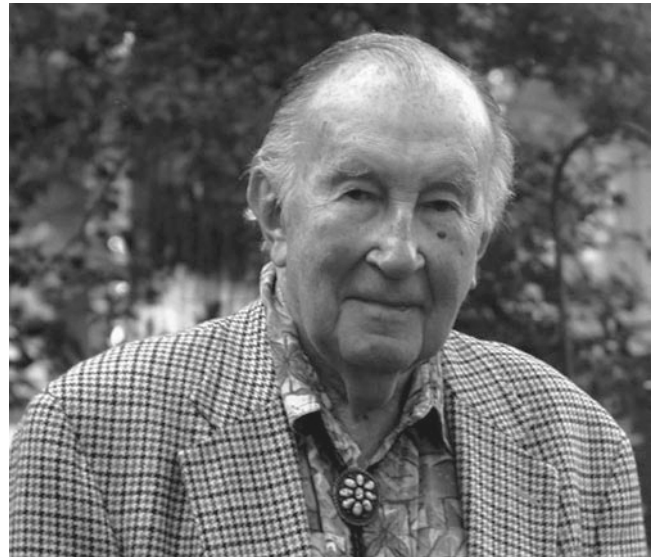


Fig. 2 Dr. Igor Klatzo in November 2005 in Virginia

Conflict of interest statement We declare that we have no conflict of interest.

References

1. Bacic F, Uematsu S, McCarron RM, Spatz M (1991) Dopaminergic receptors linked to adenylyl cyclase in human cerebrovascular endothelium. *J Neurochem* 57:1774-1780
2. Crowell RM, Olsson Y, Klatzo I, Ommaya A (1970) Temporary occlusion of the middle cerebral artery in the monkey: clinical and pathological observations. *Stroke* Nov-Dec 1(6):439-448
3. Ito U, Spatz M, Walker JT Jr, Klatzo I (1975) Experimental cerebral ischemia in Mongolian gerbils. I. Light microscopic observations. *Acta Neuropathol* 32:209-223
4. Ito U, Go KG, Walker JT Jr, Spatz M, Klatzo I (1976) Experimental cerebral ischemia in Mongolian gerbils. III. Behaviour of the blood-brain barrier. *Acta Neuropathol* 34:1-6
5. Kawahara N, Ruetzler CA, Klatzo I (1995) Protective effect of spreading depression against neuronal damage following cardiac arrest cerebral ischaemia. *Neurol Res* 17:9-16
6. Kawai K, Nitecka L, Ruetzler CA, Nagashima G, Joó F, Mies G, Nowak TS Jr, Saito N, Lohr JM, Klatzo I (1992) Global cerebral ischemia associated with cardiac arrest in the rat. I. Dynamics of early neuronal changes. *J Cereb Blood Flow Metab* 12:238-249
7. Klatzo I, Seitelberger F (eds) (1967) *Brain edema*. Springer, New York, Berlin, Heidelberg
8. Klatzo I (2002) Cécile and Oskar Vogt: the visionaries of modern neuroscience. *Acta Neurochir Suppl* 80:1-130
9. Korpatchev WG, Lysenkov SP, Thieliz PS (1982) Modeling clinical death and postresuscitation disease in rats (Russian). *Patol Fiziol Eksp Ter* 3:78-80
10. Kuroiwa T, Ting P, Martinez H, Klatzo I (1985) The biphasic opening of the blood-brain barrier to proteins following temporary middle cerebral artery occlusion. *Acta Neuropathol* 68:122-129
11. Kuroiwa T, Mies G, Hermann D, Hakamata Y, Hanyu S, Ito U (2000) Regional differences in the rate of energy impairment after threshold level ischemia for induction of cerebral infarction in gerbils. *Acta Neuropathol* 100:587-594

12. Ohno K, Ito U, Inaba Y (1984) Regional cerebral blood flow and stroke index after left carotid artery ligation in the conscious gerbil. *Brain Res* 297:151–157
13. Olsson Y, Crowell RM, Klatzo I (1971) The blood–brain barrier to protein tracers in focal cerebral ischemia and infarction caused by occlusion of the middle cerebral artery. *Acta Neuropathol* 18: 89–102
14. Takeda H, Spatz M, Ruetzler C, McCarron R, Becker K, Hallenbeck J (2002) Induction of mucosal tolerance to E-selectin prevents ischemic and hemorrhagic stroke in spontaneously hypertensive genetically stroke-prone rats. *Stroke* 33:2156–2163
15. Tomida S, Nowak TS Jr, Vass K, Lohr JM, Klatzo I (1987) Experimental model for repetitive ischemic attacks in the gerbil: the cumulative effect of repeated ischemic insults. *J Cereb Blood Flow Metab* 7:773–782

Past and Recent BBB Studies with Particular Emphasis on Changes in Ischemic Brain Edema

Dedicated to the memory of Dr. Igor Klatzo

Maria Spatz

Abstract The blood-brain barrier (BBB) functions to protect the environment of the brain through endothelial cells and their interactions with other cells and components of the cerebral vasculature and the brain parenchyma. Alterations in the BBB as a result of injuries (i.e., brain ischemia and traumatic brain injury) play a crucial role in the pathophysiological response.

The following is a brief review of the BBB and the mechanisms by which its cellular elements participate in barrier disruptions such as those associated with ischemia and resulting brain edema formation.

Keywords Blood-brain barrier (BBB) • neurovascular unit • ischemia • brain edema

Introduction

The blood brain barrier (BBB) is a physical and metabolic barrier between systemic blood circulation and the central nervous system (CNS). This concept originated over a hundred years ago when Paul Erlich and subsequently E. E. Goldman published studies demonstrating a limited penetration of certain substances (i.e., dyes) from blood to brain and from brain to blood (see review 21). Present notion about the CNS includes other barriers (i.e., blood-cerebrospinal fluid (BCSF) and blood-retinal barrier (BRB)). The morphologic localization of the barriers was advanced by light microscopy and electron microscopy using contrast media (i.e., horseradish peroxidase, etc.). The capillary endothelium in the brain and retina was

demonstrated at the site of the BBB and BRB, whereas the choroid plexus represents the site of BCSF. Many additional studies showed that the passage of substances through the BBB depends on the size and lipid solubility. It has also been demonstrated that non-diffusible polar substances (such as nutrients) require specific transporters to cross this barrier. These transporters were characterized as facilitated or active (energy-linked to ATP) transporters dependent on the given substance's intrinsic requirement namely its downhill or uphill concentration gradient. In addition, both in vivo and in situ studies showed the existence of a metabolic barrier (i.e., enzymatic) provided by endothelial cells that limits the passage of molecules from blood to brain and brain to blood. These observations were reinforced and advanced by the ability to separate the capillaries and microvessels from the rest of the brain parenchyma as well as the subsequent culturing of endothelial cells and other brain cells. It became evident that the cerebrovascular tree represents a separate and distinct biochemically active compartment. Moreover, the understanding of the BBB has been increased by the recently acquired molecular insight into its structural components. This function has been attributed to the endothelial cells, the main constituent of the BBB. Thus, these cells originally thought of as physical barrier were shown to have a variety of biological activities that were responsible for BBB properties and could be influenced by other cells. This brings us to take into consideration the likely contribution of cells adjacent to the endothelium and broadens the previous supposition regarding the just endothelial cells as BBB and to redefine it as the so-called Neurovascular Unit (NVU).

The great numbers of past and recent reviews of these barriers (1, 5, 17–19, 21, 23, 26) provide the basis for this communication. However, this report will present an abrogated review of the BBB. It will focus on past as well as the latest available studies that are relevant to the understanding of processes involved in the development and progression of ischemic brain edema.

M. Spatz (✉)
Stroke Branch, NINDS National Institutes of Health,
Bethesda, MD, 20892, USA
e-mails: maria.spatz@med.navy.mil; spatzm@ninds.nih.gov

The Current View of the BBB

The Cellular Components of the BBB

Morphological and functional characteristics of the BBB reside in the capillary and microvascular endothelium (including venules and arterioles), pericytes, astrocytes and neurons, which are collectively designated as the NVU (Fig. 1a). In the last decade the identification and demonstration of subcellular components of the capillary and microvascular endothelium as well as the surrounding cells expanded our comprehension of the BBB. Particularly the emerging knowledge indicating that the functional role of maintaining the BBB integrity is not limited to endothelial tight junctions; luminal and basement membrane along with the extracellular matrix (ECM) are also involved. In general, there is a functional interplay among all the cellular elements of the NVU that is responsible for the homeostasis of the brain environment. Under physiological conditions the BBB safeguards a constant supply of nutrients (i.e., oxygen, glucose and other substances) for the brain and steers inflammatory responses to the changes in the neighborhood.

Endothelium Endothelial cells (EC) of the BBB differ from the endothelial cells from the rest of the body by the presence of extensive tight junctions, a great number of mitochondria, an absence of fenestration and sparse pinocytotic vesicular transport. The tight junctions limit the flux of hydrophilic molecules across BBB while lipophilic substances (i.e., oxygen and CO₂) freely diffuse through the plasma membrane along their concentration gradient. Brain endothelial cells produce agents and factors as well as express various receptors that may be involved in autocrine and paracrine regulation of the microvascular function of the brain. In general, the substances (e.g., prostacyclin, nitric oxide (NO), and adenosine) produced by these cells are considered to be cytoprotective. However, several other agents that are formed in endothelial cells (i.e., endothelin-1 (ET-1), angiotensin II, thromboxane, leukotrienes, platelet-activating factor, and superoxide radicals) impair perfusion, alter BBB permeability and/or mediate cellular injury when released in excess. Many of these substances which modulate the secretory functions and reactivity of the vascular endothelium can also be released from adjacent cellular elements including other vascular cells, circulating blood cells and brain cells.

Tight Junctions The junctional complexes of endothelial plasma membranes consist of tight and adherent junctions (TJ and AJ, respectively) (Fig. 1b). The TJ are composed of three integral membrane proteins, namely claudins, occludins and junctional adhesion molecules as well as cytoplasmic accessory molecules (i.e. ZO1, ZO2, ZO3, cingulin and others). The cytoplasmic protein links the

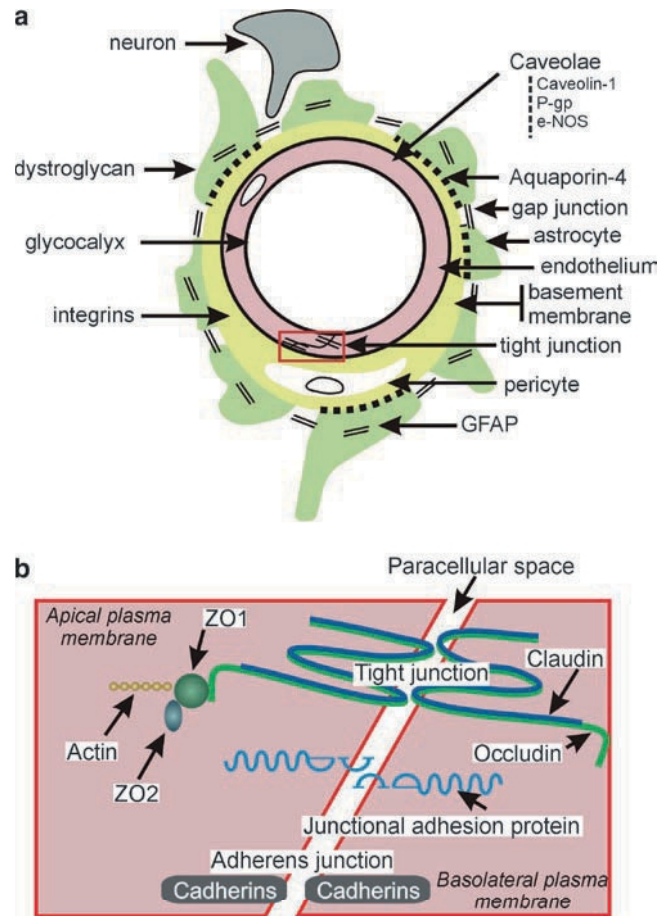


Fig. 1 Blood-brain barrier and tight junctions. (a) Cross section displaying schematically the localization of cellular and subcellular components of the NVU (b) Schematic representation of proteins associated with tight junctions (modified from Ballabh et al. (2004) (1)).

membrane protein to actin, the primary cytoskeleton protein that maintains the structural functional integrity of EC.

Claudin 1, 2 and 3 (among about 20 known members of this family) are 22-kDa phosphoproteins. They represent the main components of TJ and are localized exclusively at TJ. Claudins bind homotypically to other claudins on adjacent EC to form a primary seal. The carboxyl terminal of claudins binds to cytoplasmic proteins such as ZO-1, ZO2 and ZO3.

Occludin, a 65-kDa phosphoprotein, has four transmembrane domains, with two cytoplasmic domains (a long COOH-terminal and a short NH₂-terminal). The cytoplasmic domain of occludin is directly associated with ZO proteins. The two extracellular loops of occludins and claudins originating from neighboring cells form the 'paracellular' barrier of TJ. Occludin appears to be a regulatory protein that can alter paracellular permeability. Occludin phosphorylation occurs at serine and threonine residues that control the intracellular distribution of this TJ junction protein and subsequent barrier properties. The decreased phosphorylation status of occludin (by inhibition of protein kinase C) correlates

with a rapid fall in transendothelial resistance. On the other hand, TJ phosphorylation is associated with increased BBB permeability, which is induced by vascular endothelial growth factor (VEGF); a similar observation has been made with monocyte chemotactic protein (MCP-1).

Junctional adhesion molecules (JAM) is a 40 kDa protein belonging to the immunoglobulin superfamily that binds directly to ZO-1. It has a single transmembraneous domain and the extracellular part has two immunoglobulin groups that are formed by disulfide bonds. JAM-1 and -2 but not JAM-3 exist in brain blood vessels. JAM-1 localizes with actin at the cell-to-cell contacts and is involved in cell-to-cell adhesions. JAMs are also expressed by circulating blood cells (i.e., monocytes, neutrophils, subsets of lymphocytes and platelets). Although their function is not clear, they are reportedly (in vitro studies) involved in transmigration of monocytes through EC.

Cytoplasmic accessory proteins include zonula occludens proteins (ZO-1, -2 and -3), cingulin, and others. The zonula occludens proteins have similar amino acid sequences and belong to the family of proteins known as membrane associated guanylate kinase-like proteins (MAGUL). They function as protein binding molecules and play a role in organizing proteins at the plasma membrane. Many signaling pathways and proteins have been implicated in regulating the tight junction assembly (i.e., Ca^{2+} , protein kinase A and C, G-protein, calmodulin, cAMP, and phospholipase). In addition, small G-proteins and GTPase have been suggested to play a regulatory role of the structure and function of tight junction.

Adherens junction (AJ) consists of membrane protein, cadherin, which joins to the actin cytoskeleton via intermediary proteins known as catenins to form adhesive contact between cells. AJ are known to interact with ZO-1 and catenins and influence the TJ assembly.

Endothelial Membranes

Both luminal and basal membranes are known to be sites of enzyme receptors and transporters. The advance of specific immuno-markers and the ability to separate these membranes enable better localization of their components.

Examples of Luminal Membrane Constituents at the BBB

Glycocalyx is a negatively charged surface coating the luminal EC membrane and consisting of proteoglycans, glycosaminoglycan and adsorbed plasma proteins. It participates in maintaining vascular permeability. It contains many enzymes that might be involved in vasoactive processes (i.e., extracellular superoxide dismutase (SOD) that converts oxygen radicals

to H_2O_2) and is bound to heparin sulfate proteoglycans within glycocalyx. Damage leads to a pro-oxidant state (i.e., ischemia and/or trauma) and the shearing of the glycocalyx permitting attachment of leukocytes (i.e., inflammation).

Among molecules involved in transcytoplasmic route for blood borne proteins are clathrin and caveolae (23). The former takes part in receptor-mediated endocytoses and the latter represents clathrin-independent endocytotic pathway.

Caveolae and Caveolin The caveolae consist of microdomains of invaginations in plasma membranes that are involved in receptor-mediated uptake and regulation of many dynamic events (i.e., signal transduction, cell growth, apoptosis and lipid metabolism). Their functional activities are due to caveolins, a family of integral membrane proteins (isoforms 1, 2 and 3). In the brain, caveolin-1 expression was demonstrated on endothelial cells, pericytes and perivascular astrocytes, while caveolin-3 was muscle specific. The expression of caveolin was co-localized with endothelial nitric oxide synthase (eNOS) and plasma glycoprotein (P-gp) in the endothelial caveolae (8). Reports also indicate that caveolin-1 has the ability to negatively regulate NO production and proangiogenic factors (7). Caveolin deficiency increases cerebral ischemic injury as demonstrated in caveolin-1 knockout mice, which also showed increased levels of eNOS and apoptosis along with cerebral volume of infarction (7). Studies in vitro also demonstrated that caveolin-1 regulates expression of tight junction-associated protein, occludin (20).

P-glycoprotein (P-gp) is a major representative of the ATP-dependent efflux transport family and multidrug resistant-associated proteins (MRP). Cationic and zwitterionic compounds are preferentially transported by the P-gp whereas ionic compounds are transported by MRP. The disputed localization of P-gp was recently clarified by demonstration of its expression on capillary endothelial cells comprising the BBB as well as pericytes and astrocytes; this transporter was colocalized with caveolin 1. P-gp expression was demonstrated along the nuclear envelope in caveolae, cytoplasmic vesicles of the Golgi's complex and endoplasmic reticulum. Increased intestinal expression of P-gp reduces the absorption of drugs and it has been suggested that P-gp on EC comprising the BBB might likewise regulate drug transport processes in CNS at both cellular and subcellular levels. The interaction of caveolin and P-gp also negatively affects the function of P-gp; a reduced interplay between the two proteins separately increases the transport activity of P-gp.

Examples of Basement Membrane Components at the BBB

The role of the basement membrane is multifold in that it includes maintenance of capillary and microvascular

morphology, cell adhesion interactions and prevention of vascular plasma protein leakage. It is constructed from extracellular matrix proteins (i.e., collagen type 4, laminin) and is regulated by matrix metalloproteinases (MMP) and plasma.

Matrix metalloproteinases (MMP) are members of zinc-dependent endopeptidases that are active at neutral pH and are inhibited by proteins known as tissue inhibitors of metalloproteinases (TIMPs) (18, 19). The blocking activity of TIMPs occurs through high affinity noncovalent binding to MMP catalytic domains. Both MMPs and TIMPs are implicated in many pathological processes (i.e., ischemia and trauma). They are also important in recovery by facilitating angiogenesis and neurogenesis.

Extracellular matrix (ECM) of basal laminin separates the endothelium from the astrocyte. It provides an anchor for the EC through interactions of laminin, collagen type 4, fibronectin and other matrix proteins with endothelial integrin receptors. The capillary endothelial cells, microvascular smooth muscle cells and pericytes with surrounding astrocytes cooperate to generate and maintain the basal laminal membrane and the unique function of endothelial cells (4, 13).

Matrix adhesion receptors such as integrins and dystrophin represent two types of ECM receptor families that are associated with the microvasculature in the CNS. Both are present on the opposite side of endothelium and astrocytes (4, 13). Their position contributes to endothelial cell matrix adhesions and maintenance of the connection of the astrocytic endfeet to the abluminal endothelial surface. Selective integrins are also expressed on neurons, microglia and oligodendroglia.

Integrins are cell surface transmembranous, noncovalently linked, α/β heterodimers that recognize specific matrix ligands. Functionally they connect the matrix with the cytoskeleton and are implicated in regulating cellular responses by transmitting extracellular stimuli to intracellular signals and generating increased receptor specificity.

The dystroglycan is a single α - β heterodimeric transmembranous receptor that forms a physical link between the intracellular cytoskeleton and the ECM. α -dystrophin of the extracellular glycosylated subunit binds to ECM proteins laminin, perlecan and agrin. The intracellular carboxy-terminus of β -dystrophin binds to cytoskeleton proteins (dystrophin and utrobin). The 'dystroglycan complex' shares laminin as a ligand with a number of integrin receptors (including $\alpha/\beta 1$, $\alpha 3/\beta$, $\alpha 6/\beta 1$ and $\alpha 6/\beta 4$).

Cell Components of the BBB

Smooth Muscle These cells surround the endothelium of arterioles showing tight junction morphology. They are known to play a role in the regulation of cerebral blood flow (CBF). However, to the best of our knowledge, the full and distinct

contribution of smooth muscle (vascular mural cells) to the BBB is unknown. Most of the information regarding the presence of various receptors that could be or are involved in regulating the microvascular tone and/or CBF (i.e., adrenergic, prostaglandins, NPY and ET-1) was obtained from in situ or in vivo microvascular studies. Therefore it is worthwhile mentioning that in the mid-1980s our comparative studies of separately cultured endothelial cells, smooth muscle and glial cells derived from rat brain clearly demonstrated distinct differences in the reaction of these cells to vasoactive factors, etc. (i.e., cAMP, vasoactive peptides, and 5-HT). For example, the stimulation of 6-keto-PGF 1α synthesis by adrenergic agonists was seen in EC but not in smooth muscle. On the other hand, angiotensin-1 and -2, as well as bradykinin, markedly enhanced the 6-keto-PGF 1α in smooth muscle but had less effect on glia and little or no effect on EC (27). These studies suggested that EC and glia cells provide protection of the smooth muscle against the exposure to substances which could contribute to the dysfunction of CBF and alter BBB integrity.

Pericytes These cells are localized within the basal membrane of the capillaries and microvessels opposite the luminal face of the astrocytic endfeet. Pericytes have been implicated in providing structural support and vasodynamic capacity to the vessels (5). The emerging observation suggests that these cells regulate endothelial proliferation, migration, differentiation, and vascular branching. In vitro studies also suggest that pericytes can stimulate the astrocyte evoked BBB 'tightness' and in this way may contribute to the BBB integrity.

Astrocytes The astrocytic endfeet envelop the capillary and microvascular endothelial basement membrane. In this way, astrocytes provide a linkage between the endothelium and neurons. The astrocyte-endothelium interactions induce and modulate the development of BBB and its distinct phenotype. Reports indicate that both the physical proximity and substances released from the astrocyte may influence the integrity of BBB permeability.

The recent demonstrations of aquaporins (AQPs) (11, 16) are of special interest due to their localization and co-localization with BBB-related factors (i.e., P-gp) as well as connection to ECM and inwardly rectifying potassium channels (i.e., Kir4.1). Moreover, keeping in mind the above mentioned endothelial co-localization of caveolin-1 expression with those of P-gp and eNOS, this strongly suggests an intricate functional relationship between the endothelial cells and astrocytes. AQPs are a family of water-selective channels that provide a major pathway for osmotically driven water transport through cell membranes and in the choroid plexus. Aquaporin 4 is expressed in foot processes of astrocytes and ependymocytes facing capillaries and CSF interfaces. AQP 9 is localized in tanycytes and astrocytic processes (and more recently in neurons). The perivascular astrocytic endfeet containing AQP4 is connected to the dystrophin-dystroglycan complex mediating

the contact to ECM-laminin. Anchoring the AQP4 to cell membrane and the localization of astrocytic foot processes occurs through binding to α -syntrophin, a member of the protein dystrophin protein complex.

Neurons The innervation of brain vasculature or microvasculature and its influence on BBB was disputable even though anatomical and physiological observations were indicative of such a possibility. However, biochemical and immunocytochemical demonstration of microvascular, endothelial and/or astrocytic innervation as well as evidence of functional receptors provides support for neurogenic regulation of the BBB.

Pathophysiology

Brain edema accompanies many diseases of the CNS (i.e., ischemia (stroke) and trauma). Originally, Klatzo classified brain edema into two categories: cytotoxic brain edema (BE) and vasogenic edema (VE), which has been helpful in evaluating the brain damage and treatment (9). Brain edema (in which the BBB remains intact) is due to derangements in cellular metabolism from malfunction of the sodium and potassium pumps in the cell membrane and is characterized by: (a) an increase of intracellular sodium and water; (b) Na⁺/K⁺-ATPase failure; (c) uptake of osmotically active solution and the edema fluid rich in electrolytes; and (d) cell swelling with decreased interstitial space. Vasogenic edema is due to a breakdown of endothelial tight junctions and is characterized by: (a) an increase BBB permeability; (b) edema fluid rich in protein; and (c) increase in interstitial fluid without cell swelling. However, in most cases ischemia leads to so-called mixed edema, which expresses components of both BE and VE, and depends on the severity and duration of the insult.

Cerebral ischemia (stroke) and trauma are among many CNS diseases manifested by altered BBB integrity and formation of edema. The variety of ischemic models performed in different animal species provided disputable but valuable observations. It concerns the time course of increased BBB permeability and mechanism (vesicular and/or alteration of tight junction) that are responsible for it. However, the restricted space for this report does not permit discussion of all aspects, including BCSF involvement. Nevertheless, few of the past studies are noteworthy to mention since their results contribute to the understanding of this topic (21) and references. Firstly, the alteration of BBB to proteins depended on the duration of ischemic insult and its appearance was inversely proportionate to the time of re-established blood circulation. The observed increase in BBB permeability (to Evans blue complex or horse radish peroxidase (HRP)) was seen early (within 30 min of reperfusion) after 6 h brain

injury and even later after 1 h brain ischemia (after 3 h of reperfusion). It was manifested by endothelial vesicles of various sizes and progressive presence of HRP in neuropil including swelling astrocytic processes (25). The absence of this marker was conspicuous in the tight junction. Thus, the observed changes suggested an altered BBB permeability due to increased vesicular transport that was also inducible in normal animals by injection of 5-HT. Secondly, the biphasic increment of water content in the brain was observed in the same gerbil model of unilateral ischemia (1 h) with various times of re-circulation (up to 20 h). The initial increase in water content (first phase) preceded the augmented BBB permeability to small and large molecules (i.e., sucrose, Evans blue complex, RISA, radioactive dextran). Thus, the first increment in brain water content was observed prior to the increase of small molecular markers, whereas, the brain swelling (second phase) corresponded to the increased passage of radiolabeled large molecular markers. Thirdly, in addition, the inhibition of the observed increases of radiolabeled 2-deoxyglucose (2-DG) uptake in the presence of unlabeled 2-DG was incomplete suggesting BBB dysfunction of glucose analog transport. It should be added that brain ischemia or anoxia per se reduces the brain uptake of glucose or glucose analog (21, 22). These observations were confirmed by in vitro studies in microvessels isolated from ischemic brains. A similar reduction of 2-DG uptake into isolated microvessels exposed to anoxia was completely reversed by replacement of nitrogen by oxygen or prevented by the addition of free-fatty acid albumin (22). This protection was partially or fully abated by individually and mixed saturated and unsaturated fatty acids to the incubation medium. It is suggestive of albumin preventing shedding of the membrane glycocalyx layer (21). Taken together these studies (ex-vivo and in vitro) implicated ischemic and anoxic microvascular membrane changes with affects on the uptake of glucose analog (caused by free-fatty acid). This supposition is supported by the observed ability of arachidonic acid (AA) to modify the endothelial membrane "fluidity" without altering the permeability of the cultured EC (24). However the exposure of these cells to both AA and H₂O₂ altered the EC permeability (preventable by catalase) to a greater extent than by AA alone, as evidenced by greater formation of lipid peroxidation (malondialdehyde (MDA) assay).

Interestingly, an increase in caveolin-1 and -2 expression prior to that of occludin and claudin 5 in association with fibronectin, a known marker of BBB damage, was seen in microvessels after cold injury (14). These observations support the previous reports demonstrating an increased ischemic vesicular BBB transport and/or "open" tight junction which most likely depended on duration and the model of brain injury. The above noted fibronectin extravasation is in agreement with the reported ischemic reduction of other matrix ligands (i.e., laminin-1, collagen-4) within basal

membrane (4, 13). The time-dependent events correlate well with simultaneous generation of matrix proteases (i.e., MMP-2 and MMP-9) as well as their activators urokinase, in microvessels and neurons within the region of injury (13, 18, 19). The role of ECM components in ischemia/reperfusion was strengthened by concomitant findings of increased BBB permeability and MMP-2 levels which were blocked with MMP inhibitors. Furthermore, this supposition was confirmed in MMP-9 knock-out mice. In addition, ischemia reduced the expression of dystroglycan on microvessels as well as dystroglycan and integrin $\alpha 6/\beta 4$ expression on the astrocytic endfeet, both in vivo and in vitro studies. These changes corresponded to the separation of astrocytes from the vascular matrix and to early cell swelling following MCA occlusion (3, 4).

The knowledge of astrocytic role in development of cytotoxic or vasogenic edema has been advanced by studying AQP4 null mice (1,3,11,16). As previously mentioned, AQP4 controls water fluxes into and out of the brain. The induction of hyponatremia in AQP4-null mice by intraperitoneal injection of water reduced mortality which was associated with decreased BBB permeability to water and reduced water flow. These animals also protected the cytotoxic edema in other models. Dystrophin-deficient mice have normal levels of AQP4 mRNA but their protein expression is mislocated rendering similar features to AQP4-deficient mice showing delayed onset of cellular edema. Deletion of α -syntrophin or other components of dystrophin complex leads also to mislocation and unstable AQP4 protein expression. Reports indicate that α -null mice were also protected from cytotoxic edema induced by focal ischemia. On the other hand, the observed AQP4 deletion aggravates vasogenic edema induced by freeze injury or tumor implantation. In addition, an increase of AQP4 expression in astrocytes corresponded with maximum brain swelling induced by focal ischemia (3). In patients with middle cerebral artery occlusion, a single nucleotide polymorphism at 3'end of AQP4 was found to be associated with severe brain edema (10).

Actually, the post-ischemic hypoperfusion (reduce CBF) greatly contributes to the ischemic events leading to the development of BBB dysfunction and brain edema. It has been shown that all of the above mentioned endothelial functions are involved in this process. Presently, there is no doubt that the mechanism responsible for the noted ischemic and traumatic sequela is multifactorial and primarily involves the endothelium (as schematically illustrated in Fig. 2). Free radical species formation during ischemic hypoperfusion are one of the first among many factors (mediators or modulators) produced by endothelium and other brain and blood cells that were implicated in alterations of BBB permeability and edema formation. It is not surprising since tissue damage in the brain or other organs leads to the formation of free radical species (H_2O_2 , $\cdot OH$, $\cdot O^-$), release of fatty acids from phos-

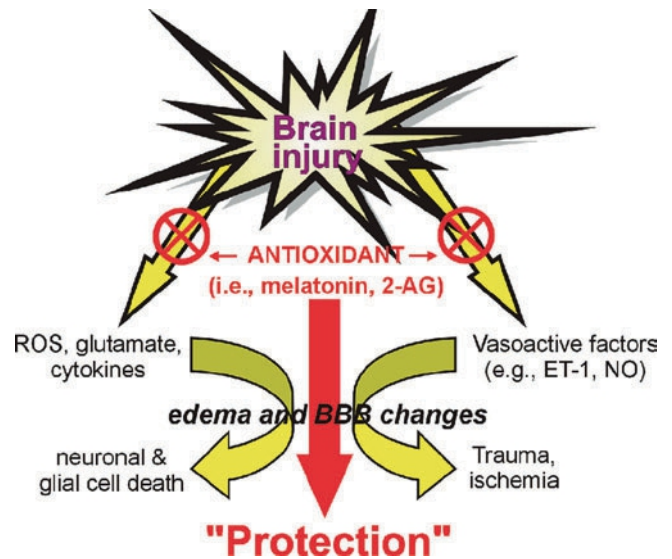


Fig. 2 Proposed mechanism of antioxidant protection of brain injury.

pholipids, and lipid peroxidation of cellular membranes (6). The same processes have also been implicated in altering the BBB permeability and the development of brain edema (12). The involvement of free radical species in ischemic reduction of CBF, alteration of BBB permeability, and formation of edema was substantiated by anti-oxidant therapy (i.e., nitroxide, melatonin). In addition, 2-arachinonylglycerol (2-AG), which reduced traumatic and ischemic tissue damage (BBB permeability and edema) was mediated through CB1 receptors and was shown to have antioxidant properties (15). Taking into consideration the endothelial in vitro functional characteristics, we investigated the endothelium and its ability to influence the microvascular activity implicated in the regulation and dysregulation of vascular tone, CBF and BBB permeability (12 and unpublished observation). These studies demonstrated that the altered cellular permeability, increased calcium mobilization, activated phosphorylation of 44/42 kinase, and cytoskeleton arrangements (actin and vimentin) induced by H_2O_2 were all decreased or abolished by antioxidants (same as described above). The results of this study are in agreement with our previous investigations regarding interactions between ET-1 and NO or 2-AG and their signal transduction pathways, and further demonstrate that the endothelium has the capacity to respond to various endogenous and exogenous mediators (2). Such endothelial reactivity is important for interconnective processes with other vascular and brain cells that affect the BBB and CBF.

Taken together the findings described in this review indicate that ischemic processes leading to changes of the BBB permeability and formation of edema involve all the cellular and subcellular components of the NVU. In spite of the abundance of available data, it is still not clear which of the factors initiate the cascade of events.

Nevertheless, it is suggestive that the functional endothelial alteration of the luminal membrane, induced by ischemic “stress” and the release of blood-born mediators, occur prior to all the subsequent sequela.

Conflict of interest statement We declare that we have no conflict of interest.

Acknowledgement The author is extremely grateful to Dr. Ye Chen, Dr. T. Tomori, Dr. K. Teranishi for their technical support and special thanks to Dr. R. McCarron for editorial assistance.

References

- Ballabh P, Braun A, Nedergaard M (2004) The blood-brain barrier: an overview: structure, regulation, and clinical implications. *Neurobiol Dis* 16:1–13
- Chen Y, McCarron RM, Ohara Y, Bembry J, Azzam N, Lenz FA, Shohami E, Mechoulam R, Spatz M (2000) Human brain capillary endothelium: 2-arachidonoglycerol (endocannabinoid) interacts with endothelin-1. *Cir Res* 87(4):323–327
- de Castro Ribeiro M, Hirt L, Bogousslavsky J, Regli L, Badaut J (2006) Time course of aquaporin expression after transient focal cerebral ischemia in mice. *J Neurosci Res* 83:1231–1240
- del Zoppo GJ, Milner R (2006) Integrin-matrix interactions in the cerebral microvasculature. *Art Thro Vasc Biol* 26(9):1966–1975
- Dore-Duffy P (2008) Pericytes: pluripotent cells of the blood brain barrier. *Curr Pharm Des* 14(16):1581–1593
- Heo JH, Han SW, Lee SK (2005) Free radicals as triggers of brain edema formation after stroke. *Free Rad Bio Med* 39:51–70
- Jasmine JF, Malhotra S, Dhallu MS, Mercier I, Rosenbaum DM, Lisanti MP (2007) Caveolin-1 deficiency increases cerebral ischemic injury. *Circ Res J* 100:721–729
- Jodoin J, Demeule M, Fenart L, Cecchelli R, Farmer S, Linton KJ, Higgins CF, Béliveau R (2003) P-glycoprotein in blood-brain barrier endothelial cells: interaction and oligomerization with caveolins. *J Neurochem* 87:1010–1023
- Klatzo I (1987) Blood-brain barrier and ischaemic brain oedema. *Z Kardiol* 76(4):67–69
- Kleffner I, Bungeoth M, Schiffbauer H, Schäbitz WR, Ringelstein EB, Kühlenbäumer G (2008) The role of aquaporin-4 polymorphisms in the development of brain edema after middle cerebral artery occlusion. *Stroke* 39:1333–1335
- Lehmann GL, Gradilone SA, Marinelli RA (2004) Aquaporin water channels in central nervous system. *Curr Neurovasc Res* 1:293–303
- McCarron RM, Shohami E, Panikashvili D, Chen Y, Golech S, Strasser A, Mechoulam R, Spatz M (2003) Antioxidant properties of the vasoactive endocannabinoid, 2-arachidonoyl glycerol (2-AG). *Acta Neurochir Suppl* 86:271–275
- Milner R, Hung S, Wang X, Spatz M, Del Zoppo GJ (2008) The rapid decrease in astrocyte-associated dystroglycan expression by focal cerebral ischemia is protease-dependent. *J Cereb Blood Flow Metab* 28:812–823
- Nag S, Venugopalan R, Stewart DJ (2007) Increased caveolin-1 expression precedes decreased expression of occluding and claudin-5 during blood-brain barrier breakdown. *Acta Neuropathol* 114:459–469
- Panikashvili D, Simeonidou C, Ben-Shabat S, Hanus L, Breuer A, Mechoulam R, Shohami E (2001) An endogenous cannabinoid (2-AG) is neuroprotective after brain injury. *Nature* 413:527–531
- Papadopoulos MC, Verkman AS (2007) Aquaporin-4 and brain edema. *Pediatr Nephrol* 22:778–784
- Persidsky Y, Ramirez SH, Haorah J, Kanmogne GD (2006) Blood-brain barrier: structural components and function under physiological and pathologic conditions. *J Neuroimm Phar* 1:223–236
- Rosell A, Lo EH (2008) Multiphasic roles for matrix metalloproteinases after stroke. *Curr Opin Pharmacol* 8:82–89
- Rosenberg GA, Yang Y (2007) Vasogenic edema due to tight junction disruption by matrix metalloproteinases in cerebral ischemia. *Neurosurg Focus* 15:22:E4
- Song L, Ge S, Pachter JS (2007) Caveolin-1 regulates expression of junction-associated proteins in brain microvascular endothelial cells. *Blood* 109:1515–1523
- Spatz M (1984) Attenuated blood-brain barrier. In: Lajtha A (ed) *Handbook of neurochemistry*, vol 7. Plenum, New York, pp 501–543
- Spatz M, Micic D, Mrsulja BB, Klatzo I (1978) Cerebral microvessels as mediators of cerebral transport. *Adv Neurol* 20:189–196
- Uemo M (2007) Molecular anatomy of the brain endothelial barrier: an overview of the distributional features. *Curr Med Chem* 14:1199–1206
- Villacara A, Spatz M, Dodson RF, Corn C, Bembry J (1989) Effect of arachidonic acid on cultured cerebrovascular endothelium: permeability, lipid peroxidation and membrane “fluidity”. *Acta Neuropathol* 78:310–316
- Westergaard E, Go G, Klatzo I, Spatz M (1976) Increased permeability of cerebral vessels to horseradish peroxidase induced by ischemia in Mongolian Gerbils. *Acta Neuropathol* 35:307–325
- Wolburg H, Lippoldt A (2002) Tight junctions of the blood-brain barrier: development, composition and regulation. *Vas Pharm* 38:323–337
- Wroblewska B, Kempinski O, Merkel N, Bembry J, Spatz M (1988) Effect of vasoactive peptides on prostacyclin formation in cerebrovascular cellular elements and glia. A comparative study. *Neurochem Int* 12:1–4

Increase in Activity of Neutrophils and Proinflammatory Mediators in Rats Following Acute and Prolonged Focal Cerebral Ischemia and Reperfusion

Stanisław Hendryk, Zenon Czuba, Halina Jędrzejewska-Szypułka, Piotr Bażowski, Hanna Doleżych, and Wojciech Król

Abstract

Purpose It has been proposed that the immune system is activated during ischemic cerebral events and that brain damage caused by ischemia is increased by this immune activity. Neutrophils (PMNs) are one of the first factors in the chain of reactions of the immune system during focal cerebral ischemia. Experimental and clinical studies have emphasized the important role of proinflammatory cytokines such as interleukin-1 β (IL-1 β) and tumor necrosis factor (TNF α), in addition to vasoactive peptide and endothelin-1 (ET-1), in the formation of cerebral ischemia.

Material and Methods The experiments were carried out using Wistar rats that were divided into four groups: three experimental groups (acute and prolonged focal cerebral ischemia and following reperfusion) and one control group (*sham*). Focal cerebral ischemia was induced by the intraluminal surgical suture method. The oxidative activity of PMNs was measured after stimulation with phorbol myristate acetate, a protein kinase C activator (luminol enhanced chemiluminescence). The concentration of IL-1 β and TNF α in rat lymphocyte culture after stimulation with CSF was determined using commercial ELISA kits. The plasma concentration of ET-1 was determined using commercial kits with the RIA method.

Results We confirmed a statistically significant increase in the oxidative activity of PMNs in rats with acute focal cerebral ischemia ($p < 0.00001$), prolonged ischemia ($p < 0.001$) and reperfusion ($p < 0.05$). An increase in IL-1 β and TNF α in lym-

phocytes following CSF stimulation was observed in the group with prolonged ischemia and in the group with reperfusion after transient ischemia ($p < 0.05$ for both). An increase in plasma ET-1 concentration was observed with acute and prolonged focal cerebral ischemia ($p < 0.05$ and $p < 0.01$, respectively).

Conclusions Our results show that acute and prolonged focal cerebral ischemia and reperfusion induce statistically significant increases in the oxidative activity of PMNs. The concentration of proinflammatory mediators (IL-1 β , TNF α) as well as ET-1 is also increased, indicating the important role of immune reactions in the development of damage to the brain following ischemia.

Keywords Focal cerebral ischemia–reperfusion • neutrophils • proinflammatory mediators

Introduction

Interleukin-1 (IL-1) is a key mediator of inflammation during cerebral ischemia, but its precise mechanisms of action remain unclear (42). It is known that free radicals and inflammatory mediators are involved in transient focal cerebral ischemia, and Khan et al. (29) demonstrated that administration of N-acetylcysteine even after the onset of ischemia protected the brain from free radical injury, apoptosis, and inflammation by reducing the expression of proinflammatory cytokines such as TNF α and IL-1 β , in addition to inducible nitric oxide synthase (iNOS). S-nitrosoglutathione GSNO reduced the expression of TNF α , IL-1 β and iNOS, inhibited activation of microglia/macrophages (ED1, CD11-b), and downregulated the expression of leukocyte function-associated antigen-1 and intercellular adhesion molecule-1 (ICAM-1) in the ischemic brain (30). Jatana et al. (27) demonstrated the neuroprotective potential of 5-lipoxygenase (5-LOX) inhibition via downregulation of NF- κ B in a rat model of experimental stroke. NF- κ B is an important transcription factor that

S. Hendryk (✉), P. Bażowski, and H. Doleżych
Department of Neurosurgery, Medical University of Silesia, Katowice,
Medyków 14 street, 40-752, Katowice, Poland
e-mail: stanhendryk@interia.pl

Z. Czuba and W. Król
Department of Microbiology and Immunology in Zabrze, Medical
University of Silesia, Jordana 19 street, 41-808 Zabrze-Rokitnica, Poland

H. Jędrzejewska-Szypułka
Department of Physiology, Medical University of Silesia, Katowice,
Medyków 18 street, 40-752, Katowice, Poland

plays a crucial role in mediating the inflammatory response to proinflammatory cytokines and reactive oxygen species (ROS) in animal models of experimental stroke (13,45). Potential therapeutic targets include iNOS, cyclooxygenase-2 (COX-2), NF- κ B and 5-LOX (19,25,52). Toll-like receptor 4 (TLR4) is a signaling receptor in innate immunity that is a part of specific immunological response to systemic bacterial infection and cerebral injury. TLR4-deficient mice have minor infarctions and a smaller inflammatory response following ischemic brain damage. These data demonstrate that TLR4 signaling and innate immunity are involved in brain damage and the inflammation triggered by ischemic injury (10). The role of adhesion molecules in the evolution of secondary injury following cerebral ischemia is very important (48). Inflammation plays an important role in the pathogenesis of neurodegenerative diseases including ischemia. The differential gene induction profile following ischemia suggests that activation of inflammatory processes might contribute to secondary brain damage in ischemic tissues. On the other hand, inflammation may also trigger processes that mediate neural regeneration after ischemic injury (34).

Materials and Methods

Animals

Male Wistar rats weighing 220–250 g were used in this study after the researchers received permission from the Local Ethical Committee for Animal Research (LECAR protocol No17/01 and No 41/02). All of the experiments were carried out between 2 p.m. and 4 p.m. on animals that were anesthetized intraperitoneally with pentobarbital sodium (50 mg/kg body weight) in experiments where cytokines were measured, and with xylazine (10 mg/kg) and ketamine hydrochloride (100 mg/kg) in all other experiments.

Experimental Protocols

The animals were divided into four groups to study the oxidative activity of PMNs, the plasma concentration of ET-1 and levels of IL-1 β and TNF α in lymphocyte culture (eight rats per group). In the next experiments, we used the following groups: MCAO 80' (acute MCAO for 80 min), MCAO 24h (prolonged MCAO for 24h), MCAO-R (reperfusion after 80 min of MCAO) and control (*sham*) (animals underwent all procedures except MCAO).

Evoking Focal Cerebral Ischemia and Reperfusion

Rats were subjected to middle cerebral artery occlusion (MCAO) as described by Koizumi et al. and modified by Takano et al. (31,49). The external carotid artery (ECA) was isolated and ligated. 4-0-monofilament nylon suture was inserted through the ECA into the internal carotid artery until mild resistance was felt to occlude the MCA. For rats in the group with ischemia–reperfusion, the monofilament was withdrawn to establish reperfusion after 80 min. Sham-operated rats underwent a similar procedure: the filament was advanced along the ICA and then immediately withdrawn.

Cannulation of the Cisterna Magna (CM)

Cannulation of the brain CM was performed according to the technique described by Solomon RA et al. (47), with a slight modification introduced by the author as described previously (28). The cannula was used for aspiration of 50 μ L of CSF, which was later used for stimulation of lymphocytes.

Measurement of the Oxidative Activity of PMNs by Chemiluminescence In Vitro

Samples of blood (1.0 mL) were collected from the venous plexus of the rat orbit and placed into tubes containing HBSS (1.0 mL) with heparin (20 IU). The PMNs were isolated with a two-step gradient of histopaques (1.077 and 1.119 g mL⁻¹), then washed and suspended in HBSS without phenol red. During the procedures with the PMNs, the viability of cells was controlled by staining dead cells with trypan blue solution. Chemiluminescent reactions were initiated by dispensing aliquots of solutions of luminol (5.6×10^{-6} M – final concentration) to PMNs (5.0×10^5) in HBSS, and the emitted light was recorded. After 5 min, PMA (phorbol myristate acetate – Sigma, MO, USA), a protein kinase C activator (50), was added to a final concentration of 1.6×10^{-7} M. The final sample volume was 1 mL in a 3.5 mL polystyrene test tube. The light was then recorded (counted per min, continuously for 15 min). The intensity of the chemiluminescence was determined by calculating the area under the curve (integral chemiluminescence). The chemiluminescence of the PMNs was measured with a luminometer using the single photon technique, as previously described Król et al. (32), with a low noise-count-rate photomultiplier (9514S, EMI, Middlesex, UK).

Measurement of the Plasma ET-1 Level

Samples of 1 mL of blood were collected from the venous plexus of the orbit, added to the probes with EDTA ($1 \text{ mg} \times \text{mL}^{-1}$) and aprotinin ($500 \text{ KIU} \times \text{mL}^{-1}$). They were immediately chilled to $+4^\circ\text{C}$, centrifuged at $300 \times g$ and stored at -70°C for further use. The concentrations of the ET-1 were measured using RIA method with a commercially available rat Endothelin-1 kit (Peninsula; Tracer 125J ET-1 (Rat)) according to the manufacturer's instructions.

Lymphocyte Culture and IL-1 β and TNF α Measurement

Samples of blood (1.0 mL) were collected from the venous plexus of the orbit and placed into tubes containing HBSS (1.0 mL) with heparin (20 IU). Lymphocytes were isolated using a two-step gradient with the histopaques method (1.077 and 1.119 mL^{-1}), then cultured in RPMI 1640 medium with 10% fetal calf serum (FCS), $50 \text{ }\mu\text{mol/mL}$ β -mercaptomethanol, 2 mL L-glutamine, 100 mg/mL penicillin and 100 mg/mL streptomycin. The lymphocytes were cultured for 24 h at 37°C in 24 point palettes NUNC. The concentration of lymphocytes in one sample was 1 million/mL. Lymphocytes were stimulated with rat CSF (10% vol.), and after the CSF was centrifuged ($700 \times g$), the concentration of IL-1 β and TNF α was measured in the supernatant using ELISA kits (commercial kits for measurement rat's IL-1 β (RLB00) and TNF α (RTA00) – R&D Systems; Minneapolis, MN, USA) according to the manufacturer's instructions.

Statistical Analysis

Statistical analysis was performed using Statistica 6.0 software. The average values \pm SD were calculated. Parametric data were analyzed using the Student's *t* test for single comparisons and the U Mann-Whitney nonparametric test for unpaired variables. *p* values less than 0.05 were considered significant.

Results

The Oxidative Activity of PMNs

In order to determine the effects of ischemic and ischemic-reperfusion brain damage on stimulation of systemic inflammatory responses, we investigated the oxygenic activity of

PMNs with chemiluminescence methods. Changes in the chemiluminescence of PMNs are shown in Fig. 1. A statistically significant increase in the activity PMNs was observed in rats with acute (MCAO 80' – $p < 0.00001$) and prolonged (MCAO 24h – $p < 0.001$) focal cerebral ischemia and in the group with reperfusion (MCAO-R – $p < 0.05$) compared with the control group (*sham*). Statistically significant differences in the oxidative activity of PMNs were also observed in the MCAO 80', MCAO 24h and MCAO-R groups. The level of chemiluminescence was the highest in rats with acute focal ischemia (MCAO80') compared to the MCAO 24h and MCAO-R groups ($p < 0.05$ and $p < 0.05$, respectively).

Plasma Concentration of ET-1

The greatest increase in plasma ET-1 level occurred in the group with prolonged focal ischemia, while a smaller increase was observed in the MCAO 80' group compared to the control group (*sham*) ($p < 0.01$ and $p < 0.05$, respectively) (Fig. 2). Changes in the plasma ET-1 level were also observed in rats with ischemia-reperfusion, but the results were not statistically significant. The same difference in plasma ET-1 level was observed in the MCAO 80' group compared to the MCAO 24h group ($p < 0.05$) and in the MCAO 24h compared to the MCAO-R group ($p < 0.05$).

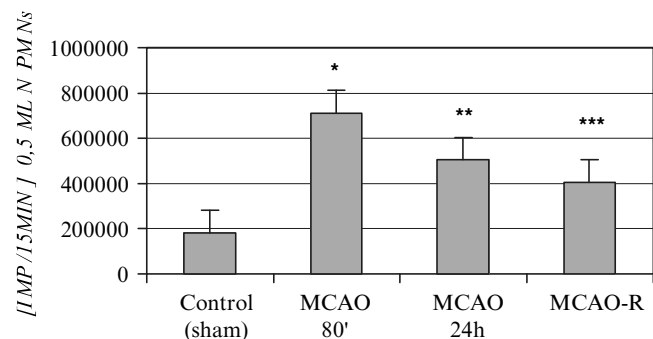


Fig. 1 PMN chemiluminescence in rats with acute and prolonged focal cerebral ischemia and after reperfusion (chemiluminescence of PMNs was measured every 15 min). * $p < 0.00001$, ** $p < 0.001$, *** $p < 0.05$ when compared with the control group (*sham*). The differences between groups were: MCAO80' and MCAO24h ($p < 0.05$); MCAO24h and MCAO-R ($p < 0.05$). In groups were: MCAO80' compared with MCAO24h ($p < 0.05$); and MCAO24h compared with MCAO-R ($p < 0.05$). Data are expressed as mean \pm SD of $n = 8$ observations

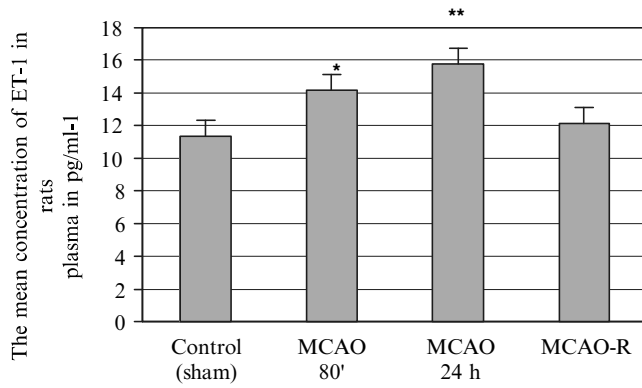


Fig. 2 The plasma concentration of ET-1 following acute and prolonged focal cerebral ischemia and after reperfusion (in pg/mL^{-1}). * $p < 0.05$ when comparing the MCAO 80' group with the control group (*sham*), and ** $p < 0.01$ when comparing the MCAO 24h group with the control group (*sham*). The same difference in the plasma levels of ET-1 was observed in MCAO 80' group compared with the MCAO 24h group ($p < 0.05$), and in the MCAO 24h compared with the MCAO-R group ($p < 0.05$). Data are expressed as mean \pm SD for $n = 8$ observations.

Expression of Proinflammatory Cytokines in Lymphocytes After Stimulation with CSF

We found increased expression of IL-1 β after acute and prolonged focal brain ischemia and after reperfusion in rat lymphocytes stimulated with CSF (Fig. 3). A statistically significant increase in the level of IL-1 β was observed in the MCAO 24 h group and in the ischemic-reperfusion group MCAO-R compared with the control group (*sham*). The increase in IL-1 β expression was greatest in the ischemic-reperfusion group, while it was similar in the MCAO 24h and MCAO-R groups ($p < 0.05$ and $p < 0.05$, respectively). Changes in TNF α expression in the lymphocytes were observed in rats after focal brain ischemia and after reperfusion, but the pattern of changes was different when compared with the IL-1 β group. In the acute focal brain ischemia group (MCAO 80'), we observed decreased expression of TNF α in lymphocytes ($p < 0.05$), while in the groups with prolonged focal cerebral ischemia (MCAO 24h) and ischemia-reperfusion (MCAO-R), there were increased levels of TNF α compared with the control group (*sham*) ($p < 0.05$ and $p < 0.05$, respectively) (Fig. 4).

Discussion

Cerebral ischemia causes changes in blood cell activities and induces the release of proinflammatory mediators, and PMNs play an important role in the intensification of brain damage in areas of focal cerebral ischemia. There is evidence that PMNs contribute to ischemic brain damage (3,6,12,14,15,56),

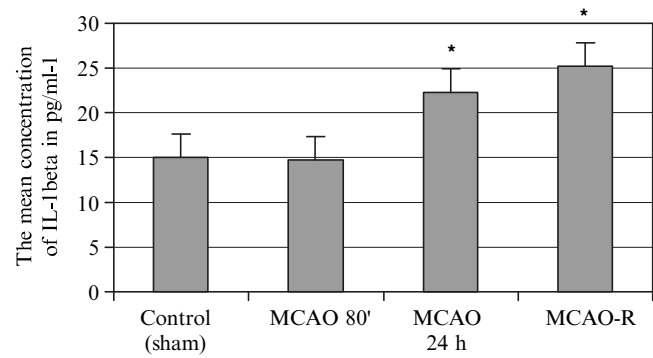


Fig. 3 Expression of IL-1 β in lymphocytes after stimulation with rat CSF following acute, prolonged focal MCA cerebral ischemia and reperfusion (in pg/mL). The IL-1 β level was increased in prolonged (* $p < 0.05$) focal cerebral ischemia and after reperfusion (* $p < 0.05$) compared to the control group (*sham*). Data are expressed as mean \pm SD for $n=8$ observations

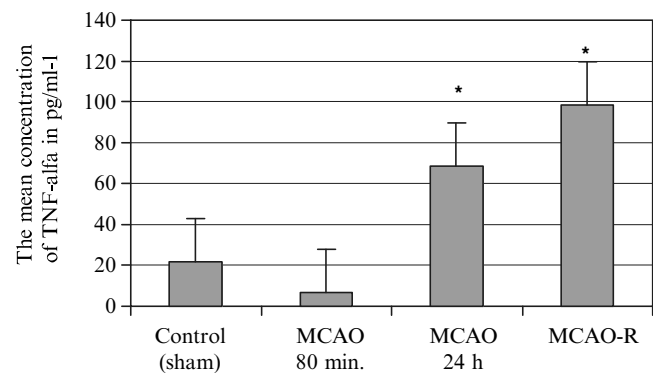


Fig. 4 Expression of TNF α in lymphocytes after stimulation with rat CSF following acute, prolonged focal MCA cerebral ischemia and reperfusion (in pg/mL^{-1}). In the acute focal brain ischemia group (MCAO 80'), we observed decreased expression of TNF α in lymphocytes ($p < 0.05$). The levels of TNF α were increased in prolonged focal cerebral ischemia and after reperfusion (* $p < 0.05$, respectively) when compared with the control group (*sham*). Data are expressed as mean \pm SD for $n = 8$ observations

although there are also opposing reports (21,38). We found an increase in PMN activity in rats with acute or prolonged focal cerebral ischemia and in rats with reperfusion. This increase was higher in rats with prolonged ischemia or with ischemia-reperfusion. The invasion of PMNs into ischemic brain tissue contributes to the exacerbation of tissue injury in stroke. Zaremba et al. (57) found that CXC chemokines have the amino acid sequence glutamic acid-leucine-arginine (ELR motif) close to the N terminus, which specifically act on PMNs. Recent studies have shown that monocyte chemoattractant protein-1 (CCL2) and its receptor (CCR2) might play important roles in regulating blood-brain barrier (BBB) permeability. Dimitrijevic et al. (16) found that CCR2(-/-) mice had reduced infarct size and significantly reduced BBB permeability, as well as reduced brain edema

in the affected ischemic hemisphere compared to CCR2(+/-) mice. This reduction in injury was associated with reduced infiltration of PMNs and reduced levels of inflammatory cytokines during reperfusion. The cytokine-induced neutrophil chemoattractant (CINC) may play an important role in PMN infiltration into ischemic lesions and in brain edema formation following ischemia–reperfusion injury (53). Yamasaki et al. (55) found that invasion of PMNs into the cerebral parenchyma was an important step in rat cerebral ischemia–reperfusion injury, with production of chemotactic factors and CINC preceding PMN invasion.

ET-1 plays an important role in the development of focal cerebral ischemia and is regarded one of the essential causative factors in prolonged vasospasm and brain ischemia after aneurysmal subarachnoid hemorrhage. Recent studies have suggested that endothelins might be important mediators of leukocyte activation in stroke. In the present study, we found the greatest increase in ET-1 plasma levels in the group with prolonged focal ischemia, while a smaller increase was observed in rats with acute focal brain ischemia. Changes in the plasma ET-1 level were also observed in rats with ischemia–reperfusion, but these changes were not statistically significant. Endothelins mediate leukocyte activation in ischemic stroke, and administration of the endothelin A receptor antagonist, BSF-208075, during reperfusion reduces post-ischemic leukocyte activation and has a neuroprotective effect (23).

It is known that cerebral ischemia stimulates the production of IL-1 β in the brain (7,20). We found increased IL-1 β expression in rats with prolonged focal brain ischemia. An increase in the levels of IL-1 β was also observed in rats in the ischemia–reperfusion group. McColl et al. (37) found that systemic IL-1 β changes led to the deterioration of acute brain injury by exacerbating the mobilization and infiltration of PMNs into the ischemic brain. IL-1 β potentiated post-ischemic PMNs and the accumulation of PMNs in cerebral cortex prior to changes in brain damage. PMNs might promote the conversion of vulnerable yet viable cortical tissue to infarction through obstruction or thrombosis of microvasculature (44,58), production of ROS causing oxidative stress (2) and release of matrix metalloproteinases that degrade components of the vascular basement membrane and extracellular matrix (4,22). Cytokines play key roles influencing the immune, endocrine and central nervous systems (24). It has been suggested that IL-1 is a potent inflammatory mediator that is synthesized and secreted into the brain parenchyma. Thus, it appears that IL-1 β plays an important role in ischemic brain damage following reperfusion (54). IL-1 is an important mediator of acute brain injury (1) and a key regulator of inflammation during the host defense response. It has been shown that proinflammatory interleukins can intensify the cascade of biochemical changes in ischemic brain damage (24).

Clinical findings also lend support to the idea that IL-1 β -induced potentiation of PMN mobilization contributes to poorer outcomes in stroke patients with preexisting systemic inflammation. Activation and migration of PMNs are regulated by CXC chemokines, small peptides that bind G-protein-coupled receptors on the PMN surface, stimulating their discharge from bone marrow and directing their local movement to sites of injury and/or infection (5,9). IL-1 β stimulates the peripheral immune system and causes greater production of interleukins and TNF α , which may in turn exacerbate brain injury (7). An increase in serum TNF α could be explained as part of the acute phase response in stroke patients (26). In this study, we found decreased expression of TNF α in lymphocytes during the first period of acute focal brain ischemia and increased expression of TNF α in rats with prolonged focal cerebral ischemia or ischemia–reperfusion.

Stroke elicits a systemic acute phase response and is associated with increased levels of circulating cytokines, acute phase reactants, PMNs and total leukocyte counts, which correlate with poor clinical outcomes (18,41,43,46,51). PMN mobilization and cortical PMN infiltration were aggravated by IL-1 prior to changes in ischemic damage (37). McColl et al. (37) first demonstrated that IL-1 had pathological effects similar to LPS, acting via the induction of neutrophil-selective CXC chemokines and neutrophil-dependent mechanism. LPS induces the synthesis and release of multiple inflammatory mediators via TLR activation. Peripheral IL-1 challenge is a similar stimulus to LPS, further supporting the idea that IL-1 is the key mediator of LPS in this brain injury paradigm (35,36,40). Cerebral ischemia evokes a strong inflammatory response characterized by the activation and release of cytokines, chemokines, adhesion molecules and proteolytic enzymes that exacerbate tissue damage (10). This inflammatory response is associated with activation of inflammatory-related gene expression (17,59). TLR4 is involved in the inflammatory response, suggesting effects of innate immunity on inflammation and damage in the brain after stroke (11). Caso et al. (11) first reported a direct effect of TLR4 signaling in brain injury and inflammation caused by stroke. Their data confirmed that innate immunity participated in brain damage following stroke and that TLR4 signaling was implicated in ischemic brain damage via the expression of iNOS, COX-2, interferon-regulatory factor 1 (IRF-1) and matrix metalloproteinase-9 (MMP9). TLRs activate NF- κ B signaling pathways that lead to the transcription of many proinflammatory genes and enzymes such as iNOS (39). TLR4 is expressed in microglia and astrocytes after MCAO, in agreement with previous data showing that it is expressed in microglia (33) and astrocytes (8) following inflammatory stimuli. It is not known, however, how ischemia activates TLRs. Innate immune responses are largely mediated by leukocytes such as PMNs, macrophages and

dendritic cells. Acute but transient elevation in chemokine levels initially mobilizes PMNs from bone marrow; then, rapidly declining chemokine levels facilitate the detection of local tissue chemokine gradients required for PMNs extravasation (37). There is currently no support for an integral role of IL-1 and PMN mobilization in mediating the deleterious effects of a systemic inflammatory challenge on acute ischemic brain damage (37).

Conclusion

Our results demonstrate that acute and prolonged focal cerebral ischemia as well as reperfusion induce a statistically significant increase in the oxidative activity of PMNs. Proinflammatory mediators (IL-1 β , TNF α) and plasma ET-1 levels were also increased, indicating the important role of immune reactions in the development of damage to the brain following ischemia and reperfusion. In this systemic inflammatory reaction and PMN mobilization, IL-1 plays an integral role in mediating the deleterious effects via the synthesis and release of multiple inflammatory mediators, perhaps through TLR activation.

Conflict of interest statement We declare that we have no conflict of interest.

Acknowledgements This work was supported by a research grant from the Medical University of Silesia, Poland, NN-2-161/03.

References

- Allan SM, Tyrrell PJ, Rothwell NJ (2005) Interleukin-1 and neuronal injury. *Nat Rev Immunol* 5:629–640
- Aizawa H, Makita Y, Sumitomo K, Aburakawa Y, Katayama T, Nakatani-Enomoto S, Suzuki Y, Fujiwara K, Enomoto H, Kuroda K, Kimura T, Yahara O, Koyama S, Maruyama J, Nakamura M, Hasebe N, Kikuchi K (2006) Edaravone diminishes free radicals from circulating neutrophils in patients with ischemic brain attack. *Intern Med* 45:1–4
- Arumugam TV, Salter JW, Chidlow JH, Ballantyne CM, Kevil CG, Granger DN (2004) Contributions of LFA-1 and Mac-1 to brain injury and microvascular dysfunction induced by transient middle cerebral artery occlusion. *Am J Physiol* 287:H2555–H2560
- Asahi M, Wang X, Mori T, Sumii T, Jung JC, Moskowitz MA, Fini ME, Lo EH (2001) Effects of matrix metalloproteinase-9 gene knock-out on the proteolysis of blood–brain barrier and white matter components after cerebral ischemia. *J Neurosci* 21:7724–7732
- Baggiolini M (1998) Chemokines and leukocyte traffic. *Nature* 392:565–568
- Beray-Berthat V, Croci N, Plotkine M, Margaill I (2003) Polymorphonuclear neutrophils contribute to infarction and oxidative stress in the cortex but not in the striatum after ischemia–reperfusion in rats. *Brain Res* 987:32–38
- Betz AL, Schielke GP, Yang G-Y (1996) Interleukin-1 in Cerebral Ischemia. *Keio J Med* 45(3):230–238
- Bowman CC, Rasley A, Tranguch SL, Marriott I (2003) Cultured astrocytes express toll-like receptors for bacterial products. *Glia* 43:281–291
- Campbell SJ, Perry VH, Pitossi FJ, Butchart AG, Chertoff M, Waters S, Dempster R, Anthony DC (2005) Central nervous system injury triggers hepatic CC and CXC chemokine expression that is associated with leukocyte mobilization and recruitment to both the central nervous system and the liver. *Am J Pathol* 166:1487–1497
- Caso JR, Pradillo JM, Hutrado O, Lorenzo P, Moro MA, Lizasoain I (2007) Toll-like receptor 4 is involved in brain damage and inflammation after experimental stroke. *Circulation* 115:1599–1608
- Caso JR, Pradillo JM, Hutrado O, Leza JC, Moro MA, Lizasoain I (2008) Toll-like receptor 4 is involved in subacute stress-induced neuroinflammation and in the worsening of experimental stroke. *Stroke* 39:1314–1320
- Chen H, Chopp M, Zhang RL, Bodzin G, Chen Q, Rusche JR, Todd RF III (1994) Anti-CD11b monoclonal antibody reduces ischemic cell damage after transient focal cerebral ischemia in rat. *Ann Neurol* 35:458–463
- Christman JW, Blackwell TS, Juurlink BH (2000) Redox regulation of nuclear factor kappa B: therapeutic potential for attenuating inflammatory responses. *Brain Pathol* 10:153–162
- Connolly ES Jr, Winfree CJ, Springer TA, Naka Y, Liao H, Yan SD, Stern DM, Solomon RA, Gutierrez-Ramos JC, Pinsky DJ (1996) Cerebral protection in homozygous null ICAM-1 mice after middle cerebral artery occlusion. Role of neutrophil adhesion in the pathogenesis of stroke. *J Clin Invest* 97:209–216
- Dawson DA, Ruetzler CA, Carlos TM, Kochanek PM, Hallenbeck JM (1996) Polymorphonuclear leukocytes and microcirculatory perfusion in acute stroke in the SHR. *Keio J Med* 45:248–252
- Dimitrijevic OB, Stamatovic SM, Keep RF, Andjelkovic AV (2007) Absence of the chemokine receptor CCR2 protects against cerebral ischemia/reperfusion injury in mice. *Stroke* 38:1345–1353
- Emsley HC, Tyrrell PJ (2002) Inflammation and infection in clinical stroke. *J Cereb Blood Flow Metab* 22:1399–1419
- Emsley HC, Smith CJ, Gavin CM, Georgiou RF, Vail A, Barberan EM, Hallenbeck JM, del Zoppo GJ, Rothwell NJ, Tyrrell PJ, Hopkins SJ (2003) An early and sustained peripheral inflammatory response in acute ischaemic stroke: relationships with infection and atherosclerosis. *J Neuroimmunol* 139:93–101
- Fagan SC, Hess DC, Hohnadel EJ, Pollock DM, Ergul A (2004) Targets for vascular protection after acute ischemic stroke. *Stroke* 35:2220–2225
- Fassbender K, Rossol S, Kammer T, Daffertshofer M, Wirth S, Dollman M, Hennerici M (1994) Proinflammatory cytokines in serum of patients with acute cerebral ischemia: kinetics of secretion and relation to the extent of brain damage and outcome of disease. *J Neurol Sci* 122:135–139
- Fassbender K, Ragoschke A, Kuhl S, Szabo K, Fatar M, Back W, Bertsch T, Kreisel S, Hennerici M (2002) Inflammatory leukocyte infiltration in focal cerebral ischemia: unrelated to infarct size. *Cerebrovasc Dis* 13:198–203
- Gidday JM, Gasche YG, Copin JC, Shah AR, Perez RS, Shapiro SD, Chan PH, Park TS (2005) Leukocyte-derived matrix metalloproteinase-9 mediates blood–brain barrier breakdown and is proinflammatory after transient focal cerebral ischemia. *Am J Physiol* 289:H558–H568
- Hauck EF, Hoffmann JF, Heimann A, Kempinski O (2007) Endothelin A receptor antagonist BSF-208075 causes immune modulation and neuroprotection after stroke in gerbils. *Brain Res* 1157:138–145
- Hendryk S, Jarzab B, Josko J (2004) Increase of the IL-1 beta and IL-6 levels in CSF in patients with vasospasm following aneurysmal SAH. *Neuro Endocrinol Lett* 25:141–147

25. Iadecola C, Zhang F, Xu S, Casey R, Ross ME (1995) Inducible nitric oxide synthase gene expression in brain following cerebral ischemia. *J Cereb Blood Flow Metab* 15:378–84
26. Intiso D, Zarrelli MM, Lagioia G, DiRienzo F, Checchia De Ambrosio C, Simone P, Tonali P, Cioffi Dagger RP (2004) Tumor necrosis factor alpha serum levels and inflammatory response in acute ischemic stroke patients. *Neurol Sci* 24:390–396
27. Jatana M, Giri S, Ansari MA, Elango C, Singh AK, Singh I, Khan M (2006) Inhibition of NF-kappaB activation by 5-lipoxygenase inhibitors protects brain against injury in a rat model of focal cerebral ischemia. *J Neuroinflammation* 3:12
28. Joško J, Hendryk S, Jędrzejowska-Szypułka H, Gwóźdź B, Herman ZS, Łątka D, Kopeć N (1996) The secretion of atrial natriuretic peptide (ANP) following subarachnoid hemorrhage (SAH) in spontaneously hypertensive rats (SHR). *J Physiol Pharmacol* 47:641–648
29. Khan M, Sekhon B, Jatana M, Giri S, Gilg AG, Sekhon C, Singh I, Singh AK (2004) Administration of N-acetylcysteine after focal cerebral ischemia protects brain and reduces inflammation in a rat model of experimental stroke. *J Neurosci Res* 76(4):519–527
30. Khan M, Sekhon B, Giri S, Jatana M, Gilg AG, Ayasolla K, Elango SAK, Singh I (2005) S-Nitrosoglutathione reduces inflammation and protects brain against focal cerebral ischemia in a rat model of experimental stroke. *J Cereb Blood Flow Metab* 25:177–192
31. Koizumi J, Yoshida Y, Nakazawa T, Ooneda G (1986) Experimental studies of ischemic brain edema. 1. A new experimental model of cerebral embolism in rats in which recirculation can be introduced in the ischemic area. *Jpn J Stroke* 8:1–8
32. Król W, Czuba Z, Scheller S, Gabrys J, Grabiec S, Shani J (1990) Anti-oxidant property of ethanolic extract of propolis (EEP) as evaluated by inhibiting the chemiluminescence oxidation of luminol. *Biochem Int* 21:593–597
33. Lehnardt S, Lachance C, Patrizi S, Lefebvre S, Follett PL, Jensen FE, Rosenberg PA, Volpe JJ, Vartanian T (2002) The toll-like receptor TLR4 is necessary for lipopolysaccharide-induced oligodendrocyte injury in the CNS. *J Neurosci* 22:2478–2486
34. Liao SL, Chen WY, Paung SL, Kuo JS, Chen CJ (2001) Association of immune responses and ischemic brain infarction in rat. *Neuroreport* 12:1943–1947
35. Long NC, Otterness I, Kunkel SL, Vander AJ, Kluger MJ (1990) Roles of interleukin 1 beta and tumor necrosis factor in lipopolysaccharide fever in rats. *Am J Physiol* 259:R724–R728
36. Luheshi G, Miller AJ, Brouwer S, Dascombe MJ, Rothwell NJ, Hopkins SJ (1996) Interleukin-1 receptor antagonist inhibits endotoxin fever and systemic interleukin-6 induction in the rat. *Am J Physiol* 270:E91–E95
37. McColl BW, Rothwell NJ, Allan SM (2007) Systemic inflammatory stimulus potentiates the acute phase and CXC chemokine responses to experimental stroke and exacerbates brain damage via interleukin-1 and neutrophil-dependent mechanisms. *J Neurosci* 27:4403–4412
38. Maier CM, Hsieh L, Yu F, Bracci P, Chan PH (2004) Matrix metalloproteinase-9 and myeloperoxidase expression: quantitative analysis by antigen immunohistochemistry in a model of transient focal cerebral ischemia. *Stroke* 35:1169–1174
39. Medzhitov R, Preston-Hurlburt P, Janeway CA Jr (1997) A human homologue of the Drosophila Toll protein signals activation of adaptive immunity. *Nature* 388:39–97
40. Miller AJ, Hopkins SJ, Luheshi GN (1997) Sites of action of IL-1 in the development of fever and cytokine responses to tissue inflammation in the rat. *Br J Pharmacol* 120:1274–1279
41. Muir KW, Weir CJ, Alwan W, Squire IB, Lees KR (1999) C-reactive protein and outcome after ischemic stroke. *Stroke* 30:981–985
42. Parry-Jones AR, Lämätäinen T, Kauppinen RA, Gröhn OH, Rothwell NJ (2006) The effect of Interleukin-1 on local brain temperature during focal cerebral ischemia in the rat; A ¹H magnetic resonance spectroscopic imaging study. *Proc Int Soc Magn Reson Med* 14:1452
43. Rallidis LS, Vikelis M, Panagiotakos DB, Rizos I, Zolindaki MG, Kaliva K, Kremastinos DT (2006) Inflammatory markers and in-hospital mortality in acute ischaemic stroke. *Atherosclerosis* 189:193–197
44. Ritter LS, Orozco JA, Coull BM, McDonagh PF, Rosenblum WI (2000) Leukocyte accumulation and hemodynamic changes in the cerebral microcirculation during early reperfusion after stroke. *Stroke* 31:1153–1161
45. Schneider A, Martin-Villalba A, Weih F, Vogel J, Wirth T, Schwaninger M (1999) NF-kappaB is activated and promotes cell death in focal cerebral ischemia. *Nat Med* 5:554–559
46. Smith CJ, Emsley HC, Gavin CM, Georgiou RF, Vail A, Barberan EM, del Zoppo GJ, Hallenbeck JM, Rothwell NJ, Hopkins SJ, Tyrrell PJ (2004) Peak plasma interleukin-6 and other peripheral markers of inflammation in the first week of ischaemic stroke correlate with brain infarct volume, stroke severity and long-term outcome. *BMC Neurol* 4:2
47. Solomon RA, Antunes JL, Chen RYZ, Bland L, Chien S (1985) Decrease in cerebral blood flow in rats after experimental subarachnoid hemorrhage: a new animal model. *Stroke* 16:58–64
48. Soriano SG, Piva S (2008) Central nervous system inflammation. *Eur L Anaesthesiol Suppl* 42:154–159
49. Takano K, Tatsumak T, Bergmann AG, Gibson DG III, Fisher M (1997) Reproducibility and reliability of middle cerebral artery occlusion using a silicone-coated suture (Koizumi) in rats. *J Neurol Sci* 153:8–11
50. Tauber AI, Brettler DB, Kennington EA, Blumberg PM (1982) Relation of human neutrophil phorbol ester receptor occupancy and NADPH-oxidase activity. *Blood* 60:333–339
51. Waje-Andreassen U, Krakenes J, Ulvestad E, Thomassen L, Myhr KM, Aarseth J, Vedeler CA (2005) IL-6: an early marker for outcome in acute ischemic stroke. *Acta Neurol Scand* 111:360–365
52. Willmot M, Gibson C, Gray L, Murphy S, Bath P (2005) Nitric oxide synthase inhibitors in experimental ischemic stroke and their effects on infarct size and cerebral blood flow: a systematic review. *Free Radic Biol Med* 39:412–425
53. Yamasaki Y, Matsuo Y, Matsuura N, Onodera H, Itoyama Y, Kogure K (1995) Transient increase of cytokine-induced neutrophil chemoattractant, a member of the interleukin-8 family, in ischemic brain areas after focal ischemia in rats. *Stroke* 26:318–322; discussion 322–323
54. Yamasaki Y, Matsuura N, Shozuhara H, Onodera H, Itoyama Y, Kogure K (1995) Interleukin-1 as a pathogenetic mediator of ischemic brain damage in rats. *Stroke* 26:676–680; discussion 681; Comment in: *Stroke* 1995 26:1729
55. Yamasaki Y, Matsuo Y, Zagorski J, Matsuura N, Onodera H, Itoyama Y, Kogure K (1997) New therapeutic possibility of blocking cytokine-induced neutrophil chemoattractant on transient ischemic brain damage in rats. *Brain Res* 759:103–111
56. Yenari MA, Kunis D, Sun GH, Onley D, Watson L, Turner S, Whitaker S, Steinberg GK (1998) Hu23F2G, an antibody recognizing the leukocyte CD11/CD18 integrin, reduces injury in a rabbit model of transient focal cerebral ischemia. *Exp Neurol* 153:223–233
57. Zaremba J, Skrobański P, Losy J (2006) The level of chemokine CXCL5 in the cerebrospinal fluid is increased during the first 24 hours of ischaemic stroke and correlates with the size of early brain damage. *Folia Morphol (Warsz)* 65:1–5
58. del Zoppo GJ, Schmid-Schonbein GW, Mori E, Copeland BR, Chang CM (1991) Polymorphonuclear leukocytes occlude capillaries following middle cerebral artery occlusion and reperfusion in baboons. *Stroke* 22:1276–1283
59. del Zoppo G, Ginis I, Hallenbeck JM, Iadecola C, Wang X, Feuerstein GZ (2000) Inflammation and stroke: putative role for cytokines, adhesion molecules and iNOS in brain response to ischemia. *Brain Pathol* 10:95–112

Factors in Creepy Delayed Neuronal Death in Hippocampus Following Brain Ischemia–Reperfusion Injury with Long-Term Survival

Ryszard Pluta, Sławomir Januszewski, Mirosław Jabłoński, and Marzena Ułamek

Abstract Brain ischemia is well known for its ability to compromise the function of the blood–brain barrier. We assessed blood–brain barrier integrity by examining the leakage of horseradish peroxidase (HRP) and different fragments of amyloid precursor protein from the vascular network into hippocampal parenchyma in rats exposed to brain ischemia with long-term survival. The areas of blood–brain barrier leakage were associated with increased staining of HRP and C-terminal of amyloid precursor protein/ β -amyloid peptide in perivascular space suggesting, respectively, an additional response to ischemia and neuronal death. These results suggest that the events associated with delayed neuronal death in hippocampus compromise blood–brain barrier function. Additionally, these data suggest that the leakage of cytotoxic amyloid precursor protein parts in the CA1 and other sectors of hippocampus may play a role in the development of creepy delayed neuronal death after the ischemia–reperfusion injury. These findings also suggest that the blood–brain barrier vessels along the hippocampal fissure especially in the medial part of the hippocampus are more vulnerable to ischemic episodes than those in other hippocampal areas.

Keywords Brain ischemia • blood–brain barrier • delayed neuronal death • hippocampus • β -amyloid peptide • amyloid precursor protein • Alzheimer disease

Introduction

Pyramidal neurons in the hippocampus CA1 area are very sensitive for brain ischemia–reperfusion and Alzheimer disease insults. About one-third of the ischemic brains due to *cardiac arrest* in rats did not show complete disappearance of CA1 area of hippocampus during 7–14 days following injury (13, 19). They probably developed complete pathology of CA1 area in long-term survival times (13). Brain ischemia and Alzheimer disease are neurodegenerative disorders that affect cognition, behavior and function. Ongoing research in ischemia–reperfusion brain provides increasing evidence that ischemic injury plays an important intimate role in the etiology of Alzheimer disease, and ischemia is a potential target for Alzheimer disease therapy (16, 17). The importance of ischemic injury in the development of Alzheimer disease has been highlighted by an increasing number of scientists (16 see for references). However mainstream Alzheimer's disease investigators have largely ignored these important information which may critically influence the development of Alzheimer disease. Actually pathological mechanisms of Alzheimer disease are related by most researchers to the toxic effects of oligomeric β -amyloid peptide, which is accumulated in intra- and extracellular space as unknown phenomenon (3). The prevalence of both types of dementia increases significantly with age. The memory deficit in both diseases is a direct effect of hippocampal neuronal cells loss and a disruption of neuronal cobweb.

The relationship between the extravasations of serum born β -amyloid peptide into the brain parenchyma and the dynamics of its deposition has recently been established in pathology and neuronal dysfunction associated with Alzheimer disease (12, 14, 15, 17). It should be clarified whether the blood–brain barrier (BBB) changes with leakage of some fragments of amyloid precursor protein (APP) from serum contribute to the vulnerability of the pyramidal neurons to ischemic episodes in the hippocampus with long-term survival (6 months). Based on this information active, slowly progressing subsequent processes will be identified that regulate life and death decisions in chronic ischemically

R. Pluta (✉), S. Januszewski, and M. Ułamek
Laboratory of Ischemic and Neurodegenerative Brain Research,
Department of Neurodegenerative Disorders,
Medical Research Centre, Polish Academy of Sciences,
Pawinskiego 5 Street, Warsaw 02-106, Poland
e-mail: pluta@cmdik.pan.pl

M. Jabłoński
Department of Orthopedic and Rehabilitation, Skubiszewski Medical
University of Lublin, Jaczewskiego 8 Street, Lublin 20-954, Poland

damaged neurons in hippocampus, thus providing better insight into the molecular mechanisms of creeping delayed neuronal death and subsequent neurodegenerative process. The relationships among ischemic delayed neuronal death and late barrier leakage have never been formally tested. In the present investigation differences in the blood–brain barrier leakage for toxic and nontoxic molecules will be presented. We will study the integrity of the late blood–brain barrier function in ischemic hippocampus by examining the staining reaction for horseradish peroxidase (HRP) and different parts of amyloid precursor protein in perivascular space with a light microscope.

Materials and Methods

Using female Wistar rats ($n = 15$, 3 months old, 150–180 g body weight) blood–brain barrier (14) and amyloid precursor protein (10) and neuronal changes (13) were studied by light microscope following 10 min brain ischemia (9) with 6 months' survival. As controls sham-operated animals ($n = 6$) were sacrificed in due time. Rats were perfusion fixed for these investigations. HRP introduced i.v. and circulated for 30 min was used as an indicator of blood–brain barrier changes (14). Five hemispheres of brains were cut at 50 μm slices in the coronal plane by a vibratome for HRP staining. Next, after putting slices on microscope slides, they were investigated. Paraffin sections from 5 brains were selected for amyloid precursor protein immunohistochemistry (10) and sections from all brains for neuronal structural observations (13). Control brains went through the same procedures as ischemic ones. Control studies for amyloid precursor protein additionally included omission of the primary antibodies (10).

Results

Immunoreactivity for HRP in Hippocampus

In ischemic hippocampus sites of extravasated horseradish peroxidase were noted. Studies on vibratome sections commonly revealed mild, diffuse, random, focal and spotty staining around BBB neurovessels (Fig. 1a). Some BBB vessels also displayed HRP staining on the microvessel wall. The BBB permeability was restricted to vessels' branching and bifurcation. These BBB abnormalities dominated in CA1 and CA4 areas and gyrus dentate of ischemic hippocampus. Control rat brains showed no HRP leakage (Fig. 1b).

Immunoreactivity for APP in Hippocampus

After ischemic hippocampus injury rats revealed intense perivascular staining for the C-terminal of APP (Fig. 1c) and the β -amyloid peptide. Multiple and abundant C-terminal of APP and β -amyloid peptide deposits embraced and/or adjoined the blood–brain barrier neurovessels, spreading multifocally outward into the adjacent parenchyma (Fig. 1c). Blood–brain barrier neurovessel lumens such as the inner and outer sides of microvessel walls were labeled, too. C-terminal of APP/ β -amyloid peptide immunoreactivity inside BBB microvessels with a halo of staining around them suggested diffusion of these parts of APP out of the vascular network (12). In any case, the halo of C-terminal of APP/ β -amyloid peptide staining in the hippocampus surrounding BBB microvessels (Fig. 1c) suggests that these proteins cross the neurovessel wall (12). Deposits inside and around BBB vessels dominated in CA1 and CA4 areas and gyrus dentate of the hippocampus (Fig. 1c). Perivascular deposits of C-terminal of APP/ β -amyloid peptide were more intense, but they took the same form as extravasated horseradish peroxidase in ischemic hippocampus. Control brains showed no APP staining inside and around BBB vessels (Fig. 1d).

Neuronal Pathology in Hippocampus

At 6 months following ischemia, localized in CA1 area, complete loss of pyramidal neurons was observed in 93% of investigated brains (Fig. 2b). At 7% of brains we noted incomplete neuronal loss, which was superimposed with degenerating neurons. Additionally different types of neurodegeneration in other sectors of hippocampus were noted. The first one took the form of acute, and the second chronic neuronal cell degeneration, but they appeared in those sectors of hippocampus that were not involved in early pathology such as the CA2, CA3 and CA4 areas and gyrus dentate (Fig. 2c). At these sectors neuron loss was superimposed with degenerating ones which at that time became even more intense and diffuse (Fig. 2c). In all sectors following ischemia naked astrocytic nuclei and glial nodules replaced disappearing neuronal cells. Hypertrophic and proliferating astrocytes were localized in sectors of complete, severe and mild neuron loss. Gross and microscopic neuropathological examinations performed at that time revealed mild atrophic features of hippocampus and other parts of brain. In control rat brains we did not observe pathology in pyramidal neurons of hippocampus (Fig. 2a)

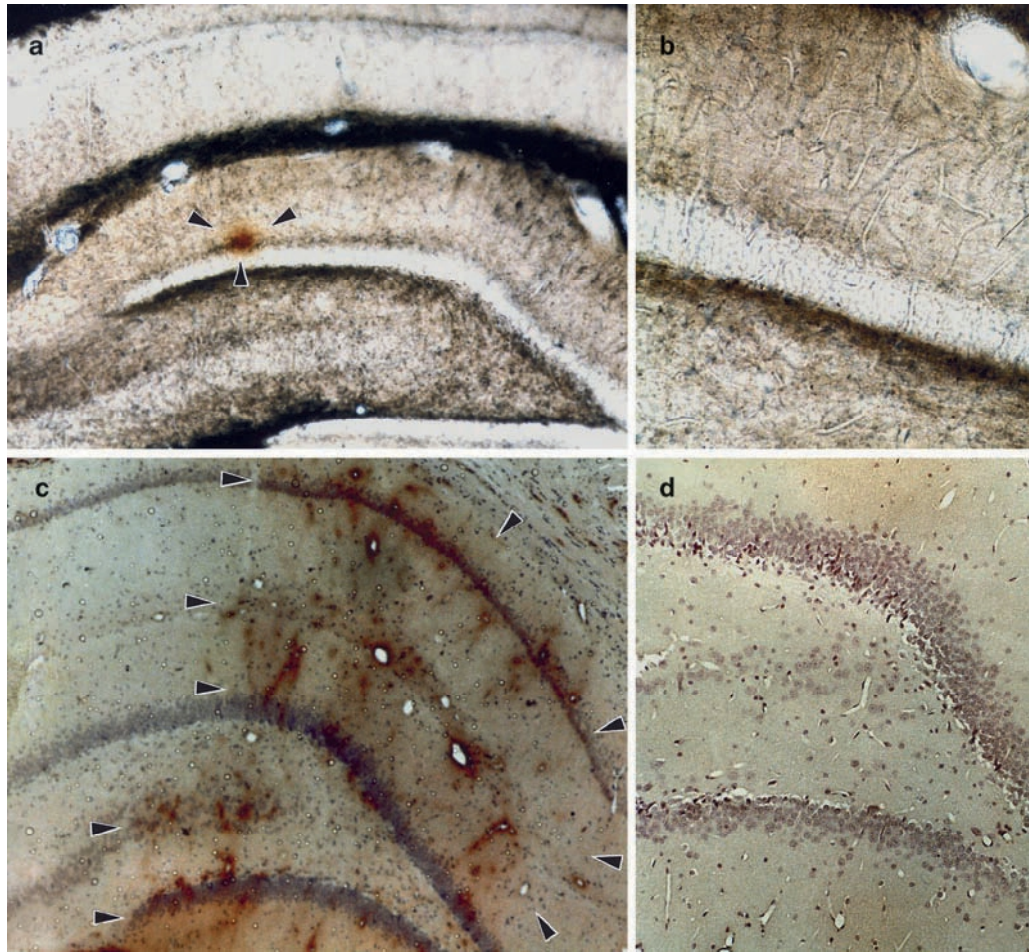


Fig. 1 Vibratome sections stained for horseradish peroxidase in ischemic hippocampus (*arrowheads*) (x40) (a) and in control hippocampus (x100) (b). Staining for C-terminal of amyloid precursor protein in ischemic hippocampus (between *arrowheads*) (x35) (c) and in control hippocampus (x100) (d).

Discussion

These results represent the first evaluation of blood–brain barrier leakage after ischemic-reperfusion hippocampal injury in rats with long-term survival. This study showed that creepy delayed neuronal death in hippocampus is associated with leakage of cytotoxic fragments of amyloid precursor protein across BBB (15) (Fig. 3), especially in the medial part of this structure (23). These data were confirmed using macro- (HRP) and micromolecular tracers (β -amyloid peptide) (14). The leakage seen was long-lived because it was still present 6 months after ischemia and was associated with continuous neuronal death and increased number of activated glial cells in all sectors of hippocampus. Taken together, this study suggests that ischemia-induced creepy delayed neuronal death by three main mechanisms: (1) immediate ischemic neuronal loss, (2) influence of β -amyloid peptide on ischemic pyrami-

dal neurons, (3) influence of β -amyloid peptide on ischemic pyramidal neurites by retrograde neuronal degeneration and all of these pathways were associated with long-term dysfunction of blood–brain barrier (Fig. 3). We would like to point out that following brain ischemia–reperfusion injury is developing creepy delayed neuronal death in all areas of hippocampus with final dementia (Fig. 3). It was recognized by us that neuropathological mechanisms in pyramidal neurons in hippocampus continue well beyond the acute stages (13).

Some studies suggest that blood–brain barrier function returns to normal activity within 14 days even after the severest injury (2, 20). It therefore appeared that factors other than only primarily ischemic were responsible for the long-lived blood–brain barrier dysfunction. The apparent insufficiency observed in the blood–brain barrier could result from some different mechanisms. These include temporal stop of microcirculation during recirculation due to platelet

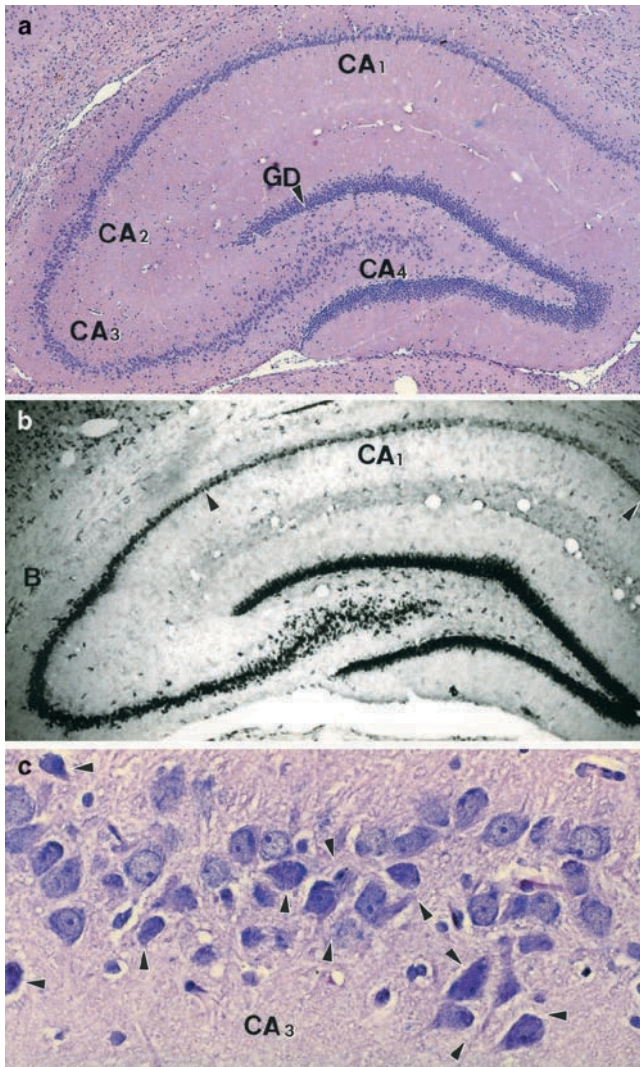


Fig. 2 Neuronal damage in ischemic hippocampus. (a) Well preserved pyramidal neurons in control hippocampus in CA1, CA2, CA3 and CA4 areas and gyrus dentate (GD) (x35). (b) Complete disappearance of pyramidal neurons in CA1 sector of hippocampus following ischemia (between arrowheads) (x40). (c) Acute and chronic neuronal damage in ischemic hippocampus in area CA3 (between arrowheads and single arrowheads) (x400). Staining H&E

aggregation (11), neovascularization that often leaks during development/formation (22), increased transcytosis (18) and dysfunction in astrocyte activity responsible for tight junctions (1). Additionally, some studies have shown that neuroinflammation is able to change normal blood–brain barrier function (8). Initially, it was suggested that only microvascular inflammogens were involved in the breakdown of blood–brain barrier. More recently it has become clear that neuroinflammation on the abluminal side of the blood–brain barrier is also able to damage the barrier (7). In addition many factors thought to be involved in the inflammation underlying Alzheimer disease may also influence blood–brain barrier activity. β -amyloid peptide was presented

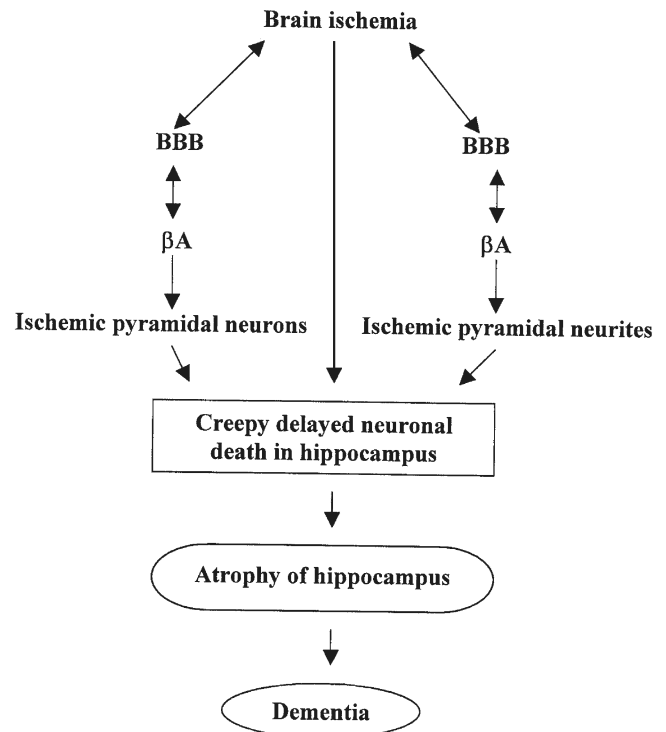


Fig. 3 Three main pathways in the development of creepy delayed neuronal death and atrophy in hippocampus and finally dementia. BBB – blood–brain–barrier, β A– β -amyloid peptide

to break down blood–brain barrier (5). Claudio (3) showed ultrastructural changes in the blood–brain barrier and collagen accumulation in areas of brain cell loss from patients with Alzheimer disease that are also observed in experimental ischemic animals with damaged blood–brain barrier (6, 11). It is possible that brain ischemia induces on the parenchyma side neuroinflammation sustain disruption of blood–brain barrier function in our study. In our experiments it was radical disruption of blood–brain barrier because we observed in leaking areas diffuse leakage and edema (15). Probably ischemia increases the toxicity of β -amyloid peptide (Fig. 3). Other possibility that ischemia increases the vulnerability of pyramidal neurons to toxicity of β -amyloid peptide (Fig. 3).

We believe that blood born β -amyloid peptide recognizes and destroys myelin sheaths and the underlying axons in hippocampus (21). Activated macrophages synthesize and secrete cytokines that damage oligodendrocytes causing interference with myelination. Disruption of the blood–brain barrier is one of the initial key steps in hippocampal white matter pathology (15, 17) that follows massive demyelination and retrograde neuronal death and finally complete disappearance of CA1 sector and some other areas in hippocampus. If creepy delayed neuronal degeneration is associated with long-lived abnormalities of blood–brain barrier function, then those sectors of the hippocampus/brain would be exposed to longer and higher quantities of vascular neurotoxins like

e.g. β -amyloid peptide that could contribute to further progression of neurodegenerative processes (16). Next, if the barrier is damaged, it is also possible that inflammogens and immune mediators from vascular network play an important role in the neuropathogenesis of ischemia- and Alzheimer-type dementia as we proposed earlier (16). Finally, repairing of disrupted barrier would offer a new strategy in the therapy of ischemic and Alzheimer dementia (4, 17).

The fundamental message of this study is that probably the neuropathology seen in ischemic hippocampus is a creepy process from initial ischemic neuronal changes to the well-established extravasations of C-terminal of APP/ β -amyloid peptide, across ischemic blood-brain barrier, culminating in the formation of amyloid plaques and dystrophic neuritis, and finally ends in full-blown Alzheimer disease.

Conflict of interest statement We declare that we have no conflict of interest.

Acknowledgements The work was supported by funds from the Polish Ministry of Science and Higher Education (2007-2100-Cost/253/2006) and European Union (Cost Action B-30) and Medical Research Centre.

References

- Ballabh P, Braun A, Nedergaard M (2004) The blood-brain barrier: an overview structure, regulation, and clinical implications. *Neurobiol Dis* 16:1–13
- Borlongan CV, Lind JG, Dillon-Carter O, Yu G, Hadman M, Cheng C, Carroll J, Hess DC (2004) Bone marrow grafts restore cerebral blood flow and blood brain barrier in stroke rats. *Brain Res* 1010:108–116
- Claudio L (1996) Ultrastructural features of the blood-brain barrier in biopsy tissue from Alzheimer's disease patients. *Acta Neuropathol* 91:6–14
- Dickstein DL, Biron KE, Ujiie M, Pfeifer CG, Jeffries AR, Jefferies WA (2006) A β peptide immunization restores blood-brain barrier integrity in Alzheimer disease. *FASEB J* 20:426–433
- Farkas IG, Czigner A, Farkas E, Dobo E, Soos K, Penke B, Endresz V, Mihaly A (2003) Beta-amyloid peptide-induced blood-brain barrier disruption facilitates T-cell entry into the rat brain. *Acta Histochem* 1005:115–125
- Ishimaru H, Ishikawa K, Haga S, Shoji M, Ohe Y, Haga C, Sasaki A, Takahashi A, Maruyama Y (1996) Accumulation of apolipoprotein E and β -amyloid-like protein in a trace of the hippocampal CA1 pyramidal cell layer after ischaemic delayed neuronal death. *NeuroReport* 7:3063–3067
- Minagar A, Alexander JS (2003) Blood-brain barrier disruption in multiple sclerosis. *Mult Scler* 9:540–549
- Nimmo AJ, Cernak I, Heath DL, Hu X, Bennett CJ, Vink R (2004) Neurogenic inflammation is associated with development of edema and functional deficits following traumatic brain injury in rats. *Neuropeptides* 38:40–47
- Pluta R, Lossinsky AS, Mossakowski MJ, Faso L, Wisniewski HM (1991) Reassessment of new model of complete cerebral ischemia in rats. Method of induction of clinical death, pathophysiology and cerebrovascular pathology. *Acta Neuropathol* 83:1–11
- Pluta R, Kida E, Lossinsky AS, Golabek AA, Mossakowski MJ, Wisniewski HM (1994) Complete cerebral ischemia with short-term survival in rats induced by cardiac arrest. I. Extracellular accumulation of Alzheimer's β -amyloid protein precursor in the brain. *Brain Res* 649:323–328
- Pluta R, Lossinsky AS, Walski M, Wisniewski HM, Mossakowski MJ (1994) Platelet occlusion phenomenon after short- and long-term survival following complete cerebral ischemia in rats produced by cardiac arrest. *J Brain Res* 35:463–471
- Pluta R, Barcikowska M, Misicka A, Lipkowski AW, Spisacka S, Januszewski S (1999) Ischemic rats as a model in the study of the neurobiological role of human β -amyloid peptide. Time-dependent disappearing diffuse amyloid plaques in brain. *NeuroReport* 10:3615–3619
- Pluta R (2002) Glial expression of the β -amyloid peptide in cardiac arrest. *J Neurol Sci* 203–204:277–280
- Pluta R (2005) Pathological opening of the blood-brain barrier to horseradish peroxidase and amyloid precursor protein following ischemia-reperfusion brain injury. *Chemotherapy* 51:223–226
- Pluta R, Ułamek M, Januszewski S (2006) Micro-blood-brain barrier openings and cytotoxic fragments of amyloid precursor protein accumulation in white matter after ischemic brain injury in long-lived rats. *Acta Neurochir (Suppl)* 96:267–271
- Pluta R (2007) Ischemia-reperfusion pathways in Alzheimer's disease. Nova Science, New York
- Pluta R (2007) Role of ischemic blood-brain barrier on amyloid plaques development in Alzheimer's disease brain. *Curr Neurovasc Res* 4:121–129
- Predescu D, Vogel SM, Malik AB (2004) Functional and morphological studies of protein transcytosis in continuous endothelia. *Am J Physiol Lung Cell Mol Physiol* 287:L895–L901
- Sadowski M, Wisniewski HM, Jakubowska-Sadowska K, Tarnawski M, Lazarewicz JW, Mossakowski MJ (1999) Pattern of neuronal loss in the rat hippocampus following experimental cardiac arrest-induced ischemia. *J Neurol Sci* 168:13–20
- Schnell L, Fearn S, Klassen H, Schwab ME, Perry VH (1999) Acute inflammatory responses to mechanical lesions in the CNS: differences between brain and spinal cord. *Eur J Neurosci* 11:3648–3658
- Wagner KR, Dean C, Beiler S, Bryan DW, Packard BA, Smulian AG, Linke MJ, de Courten-Myers GM (2005) Plasma infusions into porcine cerebral white matter induce early edema, oxidative stress, pro-inflammatory cytokine gene expression and DNA fragmentation: Implications for white matter injury with increased blood-brain barrier permeability. *Curr Neurovasc Res* 2:149–155
- Wang Y, Kilic E, Kilic U, Weber B, Bassetti CL, Marti HH, Hermann DM (2005) VEGF overexpression induces post-ischemic neuroprotection, but facilitates haemodynamic steal phenomena. *Brain* 128:52–63
- Yakota M, Saido TC, Tani E, Yamaura I, Minami N (1996) Cytotoxic fragment of amyloid precursor protein accumulates in hippocampus after global forebrain ischemia. *J Cereb Blood Flow Metab* 16:1219–1223

Endogenous Pituitary Adenylate Cyclase Activating Polypeptide Is Involved in Suppression of Edema in the Ischemic Brain

Tomoya Nakamachi, Hirokazu Ohtaki, Sachiko Yofu, Kenji Dohi, Jun Watanabe, Hiroyoshi Mori, Atsushi Sato, Hitoshi Hashimoto, Norihito Shintani, Akemichi Baba, and Seiji Shioda

Abstract Pituitary adenylate cyclase activating polypeptide is a pleiotropic neuropeptide. We previously showed that heterozygous PACAP gene knockout (PACAP^{+/-}) mice had larger infarct volumes and worse neurological scores after middle cerebral artery occlusion (MCAO). However, the relationship between endogenous PACAP levels and edema in the ischemic brain has not yet been evaluated. In this study, the formation of edema in the ischemic brain as well as cerebral blood flow was compared between PACAP^{+/-} and wild-type (PACAP^{+/+}) mice. The amount of brain edema was calculated by subtracting the contralateral volume from the ipsilateral volume 24 h after permanent MCAO. PACAP^{+/-} mice showed significantly greater brain edema than PACAP^{+/+} mice. To investigate the effects of endogenous PACAP on blood flow during ischemia, cerebral blood flow in the ipsilateral and the contralateral cortices was compared between PACAP^{+/-} and PACAP^{+/+} mice for 25 min after ischemia. With a two-dimensional laser Doppler perfusion imaging system, the blood flow in the ipsilateral and contralateral cortices was shown to be similar in PACAP^{+/-} and PACAP^{+/+} mice during ischemia. These results suggest that endogenous PACAP suppresses the formation of edema in the ischemic brain.

Keywords PACAP • brain edema • stroke • neural peptides • mouse • knockout • cerebral blood flow

S. Shioda (✉), T. Nakamachi, H. Ohtaki, S. Yofu,
K. Dohi, J. Watanabe, H. Mori, A. Sato, H. Hashimoto,
N. Shintani and A. Baba
Department of Anatomy, Showa University School of Medicine,
Shinagawa-Ku, Tokyo 142-8555, Japan,
e-mail: shioda@med.showa-u.ac.jp

K. Dohi
Department of Emergency and Critical Care Medicine, Showa
University School of Medicine, Shinagawa-Ku, Tokyo 142-8555,
Japan

N. Shintani
Laboratory of Molecular Neuropharmacology, Graduate School of
Pharmaceutical Sciences, Osaka University, Osaka 565-0871, Japan

Introduction

Pituitary adenylate cyclase activating polypeptide (PACAP) was isolated from ovine hypothalamus based on its ability to stimulate the accumulation of cAMP in rat pituitary cell cultures (1,6). PACAP has been shown to have pleiotropic functions in the central nervous system such as neurotransmission, neuroprotection and regulation of neural development (12,16). The neuroprotective effects of PACAP occurred at very low concentrations with intracerebroventricular (icv) or intravenous (iv) infusion after global or focal ischemia (10,15). We have previously shown that heterozygous PACAP gene knockout (PACAP^{+/-}) mice exhibit greater infarct volumes than wild-type (PACAP^{+/+}) mice after middle cerebral artery occlusion (MCAO) (9). Another group has since shown similar results using PACAP-deficient mice (3). These reports imply that endogenous PACAP is a potent neuroprotectant in the brain. However, the function of endogenous PACAP during the formation of edema in the ischemic brain has not yet been thoroughly examined. Moreover, the regulatory effects of endogenous PACAP on cerebral blood flow (CBF) during ischemia are unknown. In this study, we examined the effects of endogenous PACAP on the formation of brain edema and CBF after ischemia using PACAP^{+/-} mice.

Materials and Methods

Animals

All experimental procedures involving animals were approved by the Institutional Animal Care and Use Committee of Showa University (07035,08117). The PACAP null (C57/B6J) mouse has been described previously (9). Because PACAP null mice have a high rate of lethality 1 to 2 weeks after birth (4), experiments were performed only on heterozygous PACAP knockout mice (PACAP^{+/-}) and wild-type (PACAP^{+/+}) mice.

Permanent Cerebral Ischemia Model

Mice were anesthetized with 2.0% sevoflurane in N_2O/O_2 , and then subjected to permanent MCAO (pMCAO) via the intraluminal filament technique with a monofilament nylon suture. The right common carotid artery, external carotid artery (ECA), internal carotid artery, and pterygopalatine artery were exposed and the distal part of the ECA was occluded. Then, a 7-0 round tip nylon filament was introduced into the ICA from the ECA, advanced 8 to 10 mm distal to the carotid bifurcation and the MCA was occluded. After ligation of the filament to the ECA, the incision was sutured. At 24 h after ischemia, mortality and the volume of brain edema were evaluated.

Calculation of Brain Swelling

The animals were decapitated and the brain was sliced into four 2 mm coronal sections using a mouse brain matrix. The brain slices were photographed on the anterior surface of each section with a scale bar. The areas of the brain sections were measured using NIH image software. The volume of brain edema (mm^3) was determined by subtracting the volume of the non-ischemic (contralateral) hemisphere from the volume of the ischemic (ipsilateral) hemisphere.

Measurement of Cerebral Blood Flow

Cerebral blood flow (CBF) was measured with a two-dimensional laser Doppler perfusion imaging system (PeriScan PIM2; Perimed AB, Järfälla, Sweden). Mice were

anesthetized with pentobarbital and fixed to a mat with surgical tape. After incision of the head skin, the skull was exposed. The probe (0.1 mm in width) was set 15 mm anterior to the bregma, and a 20×22 mm area was scanned using the high-resolution mode. The mean value of four sites (0.1 mm^2 each) on the ipsilateral and contralateral regions of the skull on brain cortex was calculated as the CBF. The scan was performed three times before ischemia, and the mean value for the cortical region was calculated as the pre-ischemic CBF. Within 30 min after the first scan, the pMCAO was applied as described above. Blood flow was measured every 2.5 min during pMCAO until 25 min after ischemia. Blood flow values are expressed as a percentage of the baseline (pre-ischemic) CBF values.

Results

The mortality and brain swelling of PACAP^{+/-} and PACAP^{+/+} mice were evaluated 24 h after pMCAO. The mortality of the PACAP^{+/-} mice (9/24, 37.5%) was higher than that of the PACAP^{+/+} mice (3/18, 16.7%) (Fig. 1a). Swelling of the ischemic brain was assessed by subtracting the contralateral volume from the ipsilateral volume. The contralateral volumes of the PACAP^{+/+} and PACAP^{+/-} mice were 143.7 ± 1.6 and $145.3 \pm 1.3 \text{ mm}^3$, respectively, while the ipsilateral volumes of PACAP^{+/+} and PACAP^{+/-} mice were $162.7 \pm 2.2 \text{ mm}^3$ and $170.7 \pm 2.4 \text{ mm}^3$, respectively. The swelling volume of the PACAP^{+/-} mice ($25.4 \pm 1.8 \text{ mm}^3$) was significantly greater than that of the PACAP^{+/+} mice ($19.1 \pm 2.2 \text{ mm}^3$) (Fig. 1b).

We subsequently checked the CBF using a laser Doppler perfusion imaging system to compare the CBF during ischemia between PACAP^{+/-} and PACAP^{+/+} mice. When CBF

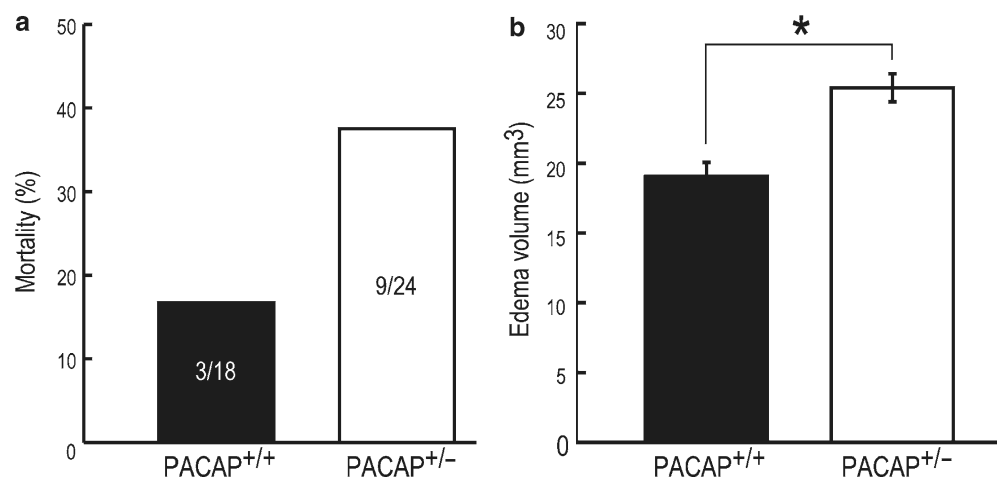
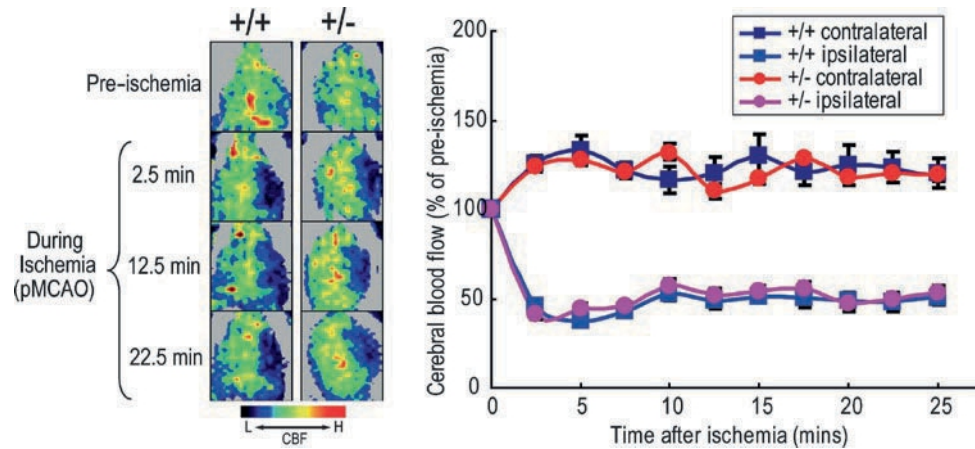


Fig. 1 Mortality (a) and the volume of brain edema (b) in PACAP^{+/+} and PACAP^{+/-} mice 24 h after pMCAO. The volume of brain edema volume is expressed as the mean \pm SE ($n = 15$). * $P < 0.05$ (unpaired Student's t -test)

Fig. 2 Cerebral blood flow (CBF) during pMCAO in PACAP^{+/+} and PACAP^{+/-} mice. The left panel shows the typical pattern of CBF. Regions of high (red) to low (blue) blood flow are displayed. The right graph shows the changes of CBF on the ipsilateral and contralateral sides of the cortical region based on pre-ischemic values (n = 5)



before ischemia was set to 100%, the CBF at 2.5 min after ischemia on the contralateral side of the PACAP^{+/+} mice was $125.5 \pm 4.2\%$ and for the PACAP^{+/-} mice, it was $123.9 \pm 4.2\%$, while the CBF on the ipsilateral side of the PACAP^{+/+} mice was $46.2 \pm 3.0\%$ and for the PACAP^{+/-} mice, it was $41.0 \pm 2.7\%$ (Fig. 2). The CBF 25 min after ischemia on the contralateral side of the PACAP^{+/+} mice was $120.1 \pm 8.3\%$ and for the PACAP^{+/-} mice, it was $119.8 \pm 2.8\%$, while the CBF on the ipsilateral side of the PACAP^{+/+} mice was $50.3 \pm 4.1\%$ and for the PACAP^{+/-} mice, it was $53.6 \pm 3.4\%$. These reductions of CBF during ischemia did not differ significantly between PACAP^{+/-} and PACAP^{+/+} mice (Fig. 2).

Discussion

Brain edema is known to be the major factor associated with mortality and morbidity in stroke patients. In this study, mortality and brain swelling were shown to be worse in PACAP^{+/-} mice. We previously reported that PACAP^{+/-} mice had greater infarct volumes and worse neurological scores than wild-type mice (9). The current results demonstrate that endogenous PACAP suppresses other ischemic insults such as brain edema in addition to infarct volume. The CBF during ischemia was compared between PACAP^{+/-} and PACAP^{+/+} mice because iv infusion of PACAP at a high concentration (5×10^{-8} mol/kg) decreased the blood pressure and regional CBF (8). The changes of CBF between PACAP^{+/-} and PACAP^{+/+} mice during ischemia did not differ. This suggests that endogenous PACAP has a neuroprotective role as well as anti-edema potential without having any adverse effect on CBF.

Brain edema is the result of perturbed water homeostasis and involves swelling of astrocytes (5). The aquaporin-4 (AQP4) water-selective channel plays a key role in the main-

tenance of brain water homeostasis, which implies that it is involved in the formation of edema in the brain. AQP4 is expressed at high levels in astrocytes and its expression increases in reactive astrocytes during an acute brain injury (2,11,14). We have reported that the PACAP-specific receptor (PAC₁-R) is expressed in astrocytes and that PAC₁-R immunoreactivity is increased in reactive astrocytes in vivo after a stab wound (7,13). These results suggest that PACAP regulates the activation of astrocytes and AQP4 expression during brain injury.

In conclusion, our results suggest that endogenous PACAP plays an important role in the regulation of brain water homeostasis and has a potent anti-edema role during ischemic stroke. Further studies are required to evaluate the relationship between the formation of brain edema and PACAP levels during ischemic stroke.

Conflict of interest statement We declare that we have no conflict of interest.

Acknowledgments We thank Dr. Jerome L. Maderdrut (Tulane University) for his editorial assistance. This work was supported in part by a Showa University Grant-in-Aid for Innovative Collaborative Research Projects and a Special Research Grant-in-Aid for Development of Characteristic Education from the Ministry of Education, Culture, Sports, Science, and Technology (T.N. and S.S.) and Research on Health Sciences focusing on Drug Innovation from The Japan Health Sciences Foundation (S.S.).

References

1. Arimura A, Shioda S (1995) Pituitary adenylate cyclase activating polypeptide (PACAP) and its receptors: neuroendocrine and endocrine interaction. *Front Neuroendocrinol* 16:53–88
2. Badaut J, Brunet JF, Grollmund L, Hamou MF, Magistretti PJ, Villemure JG, Regli L (2003) Aquaporin 1 and aquaporin 4 expression in human brain after subarachnoid hemorrhage and in peritumoral tissue. *Acta Neurochir Suppl* 86:495–498

3. Chen Y, Samal B, Hamelink CR, Xiang CC, Chen Y, Chen M, Vaudry D, Brownstein MJ, Hallenbeck JM, Eiden LE (2006) Neuroprotection by endogenous and exogenous PACAP following stroke. *Regul Pept* 137:4–19
4. Hashimoto H, Shintani N, Tanaka K, Mori W, Hirose M, Matsuda T, Sakaue M, Miyazaki J, Niwa H, Tashiro F, Yamamoto K, Koga K, Tomimoto S, Kunugi A, Suetake S, Baba A (2001) Altered psychomotor behaviors in mice lacking pituitary adenylate cyclase-activating polypeptide (PACAP). *Proc Natl Acad Sci U S A* 98:13355–13360
5. Kimelberg HK (2004) Water homeostasis in the brain: basic concepts. *Neuroscience* 129:851–860
6. Miyata A, Arimura A, Dahl RR, Minamino N, Uehara A, Jiang L, Culler MD, Coy DH (1989) Isolation of a novel 38 residue-hypothalamic polypeptide which stimulates adenylate cyclase in pituitary cells. *Biochem Biophys Res Commun* 164:567–574
7. Nakamachi T, Ohtaki H, Yofu S, Dohi K, Watanabe J, Hayashi D, Matsuno R, Nonaka N, Itabashi K, Shioda S (2008) Pituitary adenylate cyclase-activating polypeptide (PACAP) type 1 receptor (PAC1R) co-localizes with activity-dependent neuroprotective protein (ADNP) in the mouse brains. *Regul Pept* 145:88–95
8. Ohtaki H, Dohi K, Yofu S, Nakamachi T, Kudo Y, Endo S, Aruga T, Goto N, Watanabe J, Kikuyama S, Shioda S (2004) Effect of pituitary adenylate cyclase-activating polypeptide 38 (PACAP38) on tissue oxygen content-treatment in central nervous system of mice. *Regul Pept* 123:61–67
9. Ohtaki H, Nakamachi T, Dohi K, Aizawa Y, Takaki A, Hodoyama K, Yofu S, Hashimoto H, Shintani N, Baba A, Kopf M, Iwakura Y, Matsuda K, Arimura A, Shioda S (2006) Pituitary adenylate cyclase-activating polypeptide (PACAP) decreases ischemic neuronal cell death in association with IL-6. *Proc Natl Acad Sci USA* 103:7488–7493
10. Reglodi D, Somogyvari-Vigh A, Vigh S, Kozicz T, Arimura A (2000) Delayed systemic administration of PACAP38 is neuroprotective in transient middle cerebral artery occlusion in the rat. *Stroke* 31:1411–1417
11. Saadoun S, Papadopoulos MC, Watanabe H, Yan D, Manley GT, Verkman AS (2005) Involvement of aquaporin-4 in astroglial cell migration and glial scar formation. *J Cell Sci* 118:5691–5698
12. Shioda S, Ohtaki H, Nakamachi T, Dohi K, Watanabe J, Nakajo S, Arata S, Kitamura S, Okuda H, Takenoya F, Kitamura Y (2006) Pleiotropic functions of PACAP in the CNS: neuroprotection and neurodevelopment. *Ann NY Acad Sci* 1070:550–560
13. Suzuki R, Arata S, Nakajo S, Ikenaka K, Kikuyama S, Shioda S (2003) Expression of the receptor for pituitary adenylate cyclase-activating polypeptide (PAC1-R) in reactive astrocytes. *Brain Res Mol Brain Res* 115:10–20
14. Suzuki R, Okuda M, Asai J, Nagashima G, Itokawa H, Matsunaga A, Fujimoto T, Suzuki T (2006) Astrocytes co-express aquaporin-1, -4, and vascular endothelial growth factor in brain edema tissue associated with brain contusion. *Acta Neurochir Suppl* 96:398–401
15. Uchida D, Arimura A, Somogyvari-Vigh A, Shioda S, Banks WA (1996) Prevention of ischemia-induced death of hippocampal neurons by pituitary adenylate cyclase activating polypeptide. *Brain Res* 736:280–286
16. Watanabe J, Nakamachi T, Matsuno R, Hayashi D, Nakamura M, Kikuyama S, Nakajo S, Shioda S (2007) Localization, characterization and function of pituitary adenylate cyclase-activating polypeptide during brain development. *Peptides* 28:1713–1719

Reduced Matrix Metalloproteinase-9 Activity and Cell Death After Global Ischemia in the Brain Preconditioned with Hyperbaric Oxygen

Robert P. Ostrowski, Vikram Jadhav, Wanqiu Chen, and John H. Zhang

Abstract Matrix metalloproteinase-9 (MMP-9) plays a deleterious role in cell death after global cerebral ischemia. Preconditioning with hyperbaric oxygen (HBO-PC) reduces neuronal damage in the post-ischemic brain; however, its effect on ischemia-induced increase in MMP-9 activity and expression remains unexplored.

We investigated effects of HBO-PC on alterations in MMP-9 activity/tissue expression accompanying neuronal death after transient global cerebral ischemia.

Male SD rats (300–350 g), were allocated either to non-ischemic (naive control or sham-operated) or ischemic (four-vessel occlusion, 4VO; 10 min) groups that were HBO-preconditioned (2.5 ATA, 1 h daily for 5 days; the last session 24 h before ischemia) or not. Neurobehavioral deficits were assessed prior to collection of brain tissue for gel zymography (MMP-9) and histology (MMP-9 immunofluorescence, TUNEL) at 0 (without ischemia), 6, 24, 72 h and 7 days after 4VO.

Both, MMP-9 levels and cell death increased in the hippocampus at 72 h after 4VO. HBO-PC suppressed post-ischemic MMP-9 activity and CA1 cell damage, and improved functional performance. The increase in MMP-9 immunoreactivity in the brain was also detected after HBO-PC alone. HBO-PC suppresses MMP-9 activity and expression in the postischemic hippocampus. The mechanism of HBO preconditioning may depend on the induction of MMP-9 in the preischemic phase and may be in part mediated by exhaustion of MMP-9 stores in cerebral tissues.

Keywords Matrix metalloproteinase-9 • global cerebral ischemia • hyperbaric oxygen preconditioning • cell death

J.H. Zhang (✉)

Department of Physiology and Pharmacology, Department of Neurosurgery, Department of Anesthesiology, Linda University School of Medicine, Risley Hall, Room 219, Loma Linda, CA, 92350, USA
e-mail: johnzhang3910@yahoo.com

R.P. Ostrowski, V. Jadhav, and W. Chen
Department of Physiology and Pharmacology, Linda University School of Medicine, Risley Hall, Room 219, Loma Linda, CA 92350, USA

Introduction

The occlusion of four major vessels supplying the rat brain creates a model of global cerebral ischemia that may occur during major cardiovascular procedures, in liver transplant recipients and, to the extreme, during cardiac arrest, experienced by more than a thousand Americans daily (8). Ischemia-induced increase in MMP-9-mediated proteolysis may cause apoptotic neuronal death by hampering survival signals from extracellular matrix to cell interior and by degrading the matrix itself (11). Preconditioning with hyperbaric oxygen (HBO-PC) has been shown to protect against ischemic cell death; while HBO post-treatment following major cerebral ischemia may reduce MMP-9-mediated damage to the proteins forming neurovascular matrix (6,7). Therefore, the positive effects of HBO-PC may be through a reduction of ischemic MMP-9 activation, although it has yet to be examined (4). The aim of this study was to investigate the effects of preconditioning with hyperbaric oxygen on alterations in MMP-9 activity/tissue expression underlying neuronal death in the rat model of global ischemic stroke. We hypothesized that HBO-PC will decrease ischemic activation of MMP-9 and, thereby, reduce the extent of neuronal death after transient global cerebral ischemia.

Material and Methods

All experimental procedures were approved by Animal Care and Use Committee at Loma Linda University. Global cerebral ischemia was induced by bilateral occlusion of the common carotid and vertebral arteries for 10 min, as was described in detail elsewhere (9).

The surgeries were performed under Ketamine (100 mg/kg b.w.) and Xylazine (10 mg/kg b.w.) anesthesia (i.p) (9). A total of 103 male Sprague Dawley rats (300–350 g) (Harlan, Indianapolis, IN) were divided into sham surgery group, 4VO-untreated group (4VO), and HBO-PC+4VO group preconditioned with hyperbaric oxygen once daily (1 h, 2.5 ATA,

100% oxygen) for 5 consecutive days. The last HBO session was administered 24 h prior to the induction of ischemia (i.e. prior to "0" time point). At "0" time point (a group of rats preconditioned with HBO w/o ischemia) or at 6, 24, 72 h and 7 days after ischemia (preconditioned or not) rats were examined for neurobehavioral deficits and euthanized. The brains were collected for histology (MMP-9 immunofluorescence, Nissl staining and TUNEL) and gel zymography – for measurements of MMP activity (10). The immunofluorescent staining was used to evaluate immunoreactivity of MMP-9 in the brain. Terminal deoxynucleotidyl transferase-mediated dUTP nick end labeling (TUNEL) was performed with a kit (Roche, IN) in brain samples at 72 h after 4VO (2).

Results

All but two (in the untreated 4VO group) operated animals survived till the time of euthanization. The untreated rats performed worse in T-maze, as compared with HBO preconditioned rats on day 3 after ischemia (* $p < 0.05$ vs. Sham, # $p < 0.05$ vs. 4VO; ANOVA) (Fig. 1). MMP-9 activity in ischemic brains significantly increased as compared to sham group at 72 h after 4VO (* $p < 0.05$ vs Sham, ANOVA) (Fig. 2). Intergroup comparison (Holm–Sidak method) revealed a significant decrease in MMP-9 activity in brain samples from the HBO-preconditioned rats (# $p < 0.05$ vs 4VO). MMP-9 immunoreactivity increased in the postischemic hippocampus (Fig. 3c), where as HBO-PC reduced MMP-9 tissue expression 72 h after ischemia (Fig. 3d). At the same

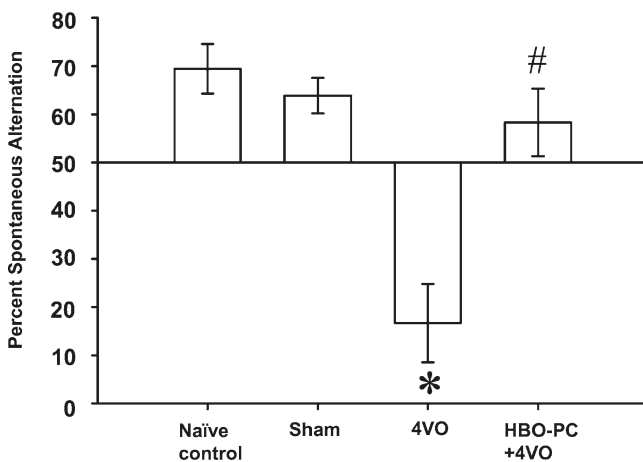


Fig. 1 The performance of rats in T-maze was tested at 72 h after global cerebral ischemia, in blinded fashion. Briefly, rats were placed in the maze stem and allowed to explore for 1 min. Then ten trials for spontaneous alternation of maze arms were done over 20 min. The results were expressed as percent of spontaneous alternation with respect to 50% reference (0% = no alternation, 100% = alternation at each trial). HBO-PC nearly reversed deterioration in T-maze performance caused by ischemia (* $p < 0.05$ vs. Sham; # $p < 0.05$ HBO-PC + 4VO vs. 4VO; $n = 4$ per each group)

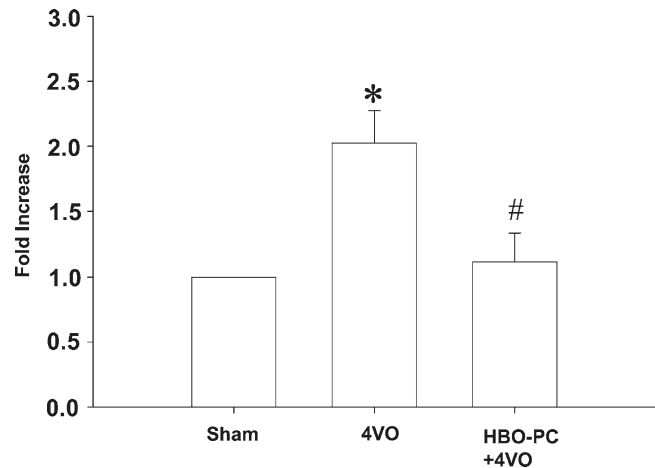


Fig. 2 Gel zymography was used to detect alterations in MMP-9 activity in the hippocampus. Whole cell protein extracts, 60 μ g per well, were separated in 10% Tris-glycine gel with 0.1% gelatin as substrate (Bio-Rad). After renaturation the gel was developed at 37°C for 48 h, stained with 0.5% Coomassie Blue R-250 for 60 min., and then destained. HBO-PC suppressed MMP-9 activity at 72 h after ischemia (* $p < 0.05$ vs. Sham; # $p < 0.05$ HBO-PC + 4VO vs. 4VO; $n = 4$ per each group)

time point we observed TUNEL positive cells in the CA1 region of the hippocampus (Fig. 3e). HBO-PC reduced abundance of cells with DNA strand breaks (Fig. 3f). The light microscope observations revealed a substantial amelioration in neuronal damage in the HBO-PC group at day 7 after ischemia (Fig. 3h). Of note, HBO-PC alone, without subsequent ischemia, caused increased MMP-9 immunoreactivity in CA1 (Fig. 3b).

Discussion

In our study, the increase in MMP-9 tissue expression and activity occurred in parallel with delayed cell death after ischemia. Previous studies indicated that MMP-9 plays a major role in the degradation of the extracellular matrix protein laminin, which may contribute to the postischemic cell death (11). The fact that HBO-PC reduces brain MMP-9 activity and tissue expression, concomitant with amelioration of cell death after global cerebral ischemia, appears to be the most significant finding of this study. As of yet, only HBO post-treatment has been shown to reduce MMP-9 levels and damage to the components of extracellular matrix (6). The increase in tissue expression of MMP-9 caused by HBO-PC observed in this study opens the possibility of exhaustion of brain MMP-9 stores for a preconditioning mechanism. Such exhaustion would lead to decreased MMP-9 release following brain ischemia (3). In these settings, reduced MMP-9 activity in the HBO-PC group would merely reflect a depletion of MMP-9 stores in the brain. However, we believe that other preconditioning mechanisms should also be taken into

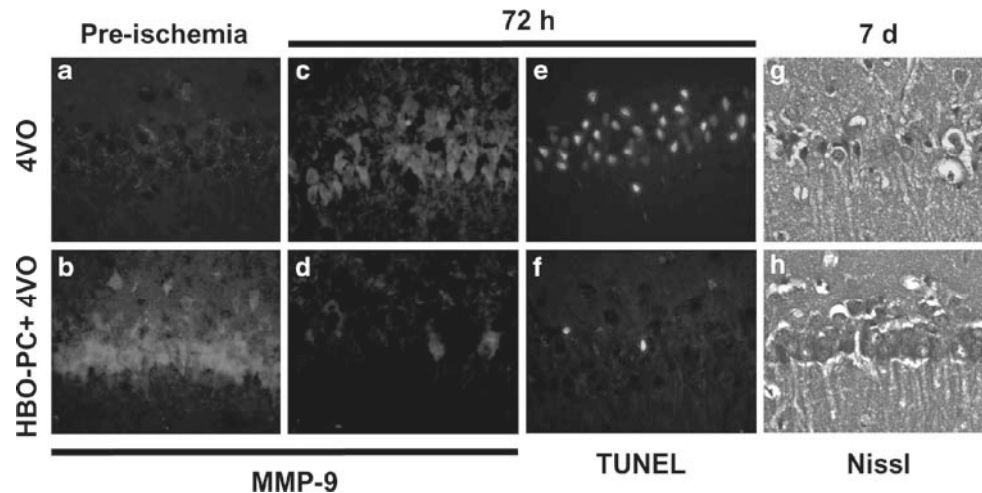


Fig. 3 HBO-PC reduced MMP-9 immunoreactivity (d) and apoptotic changes (f) on day 3, and diminished neuronal loss (h) on day 7 following ischemia. TUNEL and MMP-9 immunofluorescent labeling were performed in formalin-fixed brain sections. The rabbit anti-

MMP-9 antibody diluted 1:100 (Chemicon, CA) and Texas Red-conjugated secondary antibody (1:200; Jackson Labs) were used. TUNEL and Nissl staining were done with routinely used methods.

consideration. As demonstrated in our recent study, HBO preconditioning induced HIF-1 α , a known mediator of ischemic tolerance in the brain (5). Tissue inhibitor of metalloproteinases-1 (TIMP-1), a HIF-1 target gene, can irreversibly inactivate MMP-9 (1). Further studies are needed to determine if HBO-PC works by inducing TIMP-1 and thereby ameliorating cell death through blockade of MMP-9, following global cerebral ischemia. In summary, we observed that HBO-PC induced MMP-9 in cerebral tissues before brain insult and led to decreased MMP-9 levels following brain ischemia. Concomitantly, HBO-PC suppressed cell death in the postischemic hippocampus. The mechanism of HBO-PC-induced ischemic tolerance may depend on the reduction of MMP-9 and may be related in part to the exhaustion of MMP-9 stores in the brain.

Conflict of interest statement We declare that we have no conflict of interest.

References

- Gomez DE, Alonso DF, Yoshiji H, Thorgeirsson UP (1997) Tissue inhibitors of metalloproteinases: structure, regulation and biological functions. *Eur J Cell Biol* 74:111–122
- Kofler J, Hattori K, Sawada M, DeVries AC, Martin LJ, Hurn PD, Traystman RJ (2004) Histopathological and behavioral characterization of a novel model of cardiac arrest and cardiopulmonary resuscitation in mice. *J Neurosci Methods* 136:33–44
- Lalu MM, Csonka C, Giricz Z, Csont T, Schulz R, Ferdinandy P (2002) Preconditioning decreases ischemia/reperfusion-induced release and activation of matrix metalloproteinase-2. *Biochem Biophys Res Commun* 296:937–941
- Ostrowski RP, Graupner G, Titova E, Zhang J, Chiu J, Dach N, Corleone D, Tang J, Zhang JH (2008) The hyperbaric oxygen preconditioning-induced brain protection is mediated by a reduction of early apoptosis after transient global cerebral ischemia. *Neurobiol Dis* 29:1–13
- Peng Z, Ren P, Kang Z, Du J, Lian Q, Liu Y, Zhang JH, Sun X (2008) Up-regulated HIF-1 α is involved in the hypoxic tolerance induced by hyperbaric oxygen preconditioning. *Brain Res* 1212:71–78
- Veltkamp R, Bieber K, Wagner S, Beynon C, Siebing DA, Veltkamp C, Schwaninger M, Marti HH (2006) Hyperbaric oxygen reduces basal lamina degradation after transient focal cerebral ischemia in rats. *Brain Res* 1076:231–237
- Wada K, Miyazawa T, Nomura N, Tsuzuki N, Nawashiro H, Shima K (2001) Preferential conditions for and possible mechanisms of induction of ischemic tolerance by repeated hyperbaric oxygenation in gerbil hippocampus. *Neurosurgery* 49:160–166
- Xiao F, Arnold TC, Zhang S, Brown C, Alexander JS, Carden DL, Conrad SA (2004) Cerebral cortical aquaporin-4 expression in brain edema following cardiac arrest in rats. *Acad Emerg Med* 11:1001–1007
- Yamaguchi M, Calvert JW, Kusaka G, Zhang JH (2005) One-stage anterior approach for four-vessel occlusion in rat. *Stroke* 36:2212–2214
- Yatsushige H, Ostrowski RP, Tsubokawa T, Colohan A, Zhang JH (2007) Role of c-Jun N-terminal kinase in early brain injury after subarachnoid hemorrhage. *J Neurosci Res* 85:1436–1448
- Zalewska T, Ziemka-Nalecz M, Sarnowska A, Domanska-Janik K (2003) Transient forebrain ischemia modulates signal transduction from extracellular matrix in gerbil hippocampus. *Brain Res* 977:62–69

Radiation Exposure Prior to Ischemia Decreases Lesion Volume, Brain Edema and Cell Death

E. Titova, A. Adami, R. Ostrowski, S. Lalas, R. Vlkolinsky, J.H. Zhang, G. Nelson, and A. Obenaus

Abstract

Purpose To investigate the neuronal response to ischemic injury following exposure to whole brain proton irradiation.

Methods Brain only proton irradiation (8 Gy, 250 MeV) was performed ten days prior to middle cerebral artery occlusion (MCAO) in 1 year old male Sprague Dawley rats. MCAO was induced in two animal groups: proton irradiated (MCAO + Rad) and MCAO only. Magnetic resonance imaging (MRI) and quantitative analysis were performed prior to and 2 days after irradiation, and then 2, 14 and 28 days after MCAO. After the last imaging time point animals were sacrificed and TUNEL staining was performed on 4% paraformaldehyde – fixed brain sections.

Results Neuroimaging demonstrated a reduction in ischemic lesion volume in the MCAO + Rad group compared with MCAO alone. Neurological deficits did not differ between ischemia groups. Interestingly, there was a 34% decrease in the number of TUNEL-positive cells in MCAO + Rad brains compared to MCAO alone.

Conclusion Our results suggest that radiation treatment reduces brain edema, ischemic lesion volume and perischemic apoptosis. The underlying mechanisms are currently

unknown and additional studies will elucidate the significance of these results.

Keywords Cerebral ischemia • MRI • MCAO • proton • radiation • stroke

Introduction

Radiation has been shown to alter normal brain physiology, including brain microcirculation (8). Radiation-induced damage results in pathological modification of blood vessels, cortical atrophy, cerebral white matter necrosis and fibrosis, and delayed (months to years) neurological deficits (19).

However, radiation is used clinically for treatment of brain cancers and arteriovenous malformations (AVM) (6, 18). Modern radiotherapy techniques allow minimal damage to surrounding tissues thus improving patient survival and outcomes (12). Yet, more attention is needed to evaluate long-term treatment-related morbidity. Radiotherapy accelerates cerebral vascular atherosclerosis (5), seriously impairs cognitive functions (3, 10, 13), and leads to increased risk of stroke even many years after the initial therapy (12). Child cancer survivors who had undergone radiotherapy are at significantly increased risk for adverse cardio- and cerebrovascular effects (11). The risk of developing stroke, along with increased risk of vasculopathy, ‘blood clots’ and ‘angina-like symptoms’, is more than 40 times greater among childhood brain-tumor survivors than sibling controls (1).

While high doses of radiation are known to exert pro-inflammatory effects, low doses have been shown to have an anti-inflammatory effects (15). Inflammation significantly contributes to the acute brain damage and subsequent tissue loss caused by ischemia/reperfusion (17). We hypothesized that a moderate dose of proton radiation may have beneficial effects on post-ischemic brain injury. The mechanisms underlying the neurorepair process after combined radiation and ischemic injury are unknown and knowledge of these

A. Obenaus (✉)

Radiation Medicine, Radiobiology Program, Loma Linda University, 11175 Campus Street, Chan Shun Pavilion, A-1010, Loma Linda, CA 92350, USA
e-mail: aobenaus@llu.edu

E. Titova, A. Adami, S. Lalas and R. Vlkolinsky
Department of Radiation Medicine, Loma Linda University, 11175 Campus Street, Chan Shun Pavilion, A-1010, Loma Linda, CA 92350, USA

R. Ostrowski
Department of Physiology and Pharmacology, Linda University School of Medicine, Risley Hall, Room 219, Loma Linda, CA 92350, USA

J.H. Zhang
Department of Physiology and Pharmacology,
Department of Neurosurgery, Department of
Anesthesiology, Linda University School of Medicine,
Risley Hall, Room 219, Loma Linda, CA 92350, USA

mechanisms may improve therapeutic approaches in patients exposed to radiation and at risk of stroke.

Methods

A total of 10 male, 1 year old Sprague Dawley rats (530–550 g; Harlan, Indianapolis, IN, USA) were divided into MCAO and MCAO + Rad groups ($n = 5$ in each group). Animals were housed under 12:12 h light/dark cycle with access to water and food ad libitum. All procedures were approved by the Animal Care and Use Committee at Loma Linda University (LLU).

In the MCAO + Rad group brain only irradiation was performed at 10 days (Day -10) before middle cerebral artery occlusion (MCAO) (Day -0). Irradiation was performed at the LLU Proton Treatment Facility with accelerated protons (8 Gy, 250 MeV; 5.8 Gy/min; collimated, brain only). The focal ischemic insult was induced by 50 min MCAO using an intraluminal thread technique (7). Neurological tests were performed at 1, 2, 14 and 28 days after ischemia induction by a blinded investigator using an 18-point neurological scoring system (4) (minimum neurological score was 3 and the maximum in healthy animals was 18).

MRI data were collected prior to irradiation and 2 days after irradiation (Day -8), and after MCAO induction (2, 14, 28 days). MR data was obtained using a Bruker 4.7T and analyzed as previously described (2). 3D volumes and ROI analysis for T2WI were obtained and summarized.

After the final imaging time point animals were intracardially perfused with ice-cold 0.12 M Millonig's phosphate buffer, pH 7.3 (1 mL/1 g body weight) and fixed in 4% paraformaldehyde (Electron Microscopy Science, Hatfield, PA). Brains were cut coronally (30 μ m) through the ischemic core (based on MRI) on a cryostat.

Terminal deoxynucleotidyl transferase-mediated dUTP nick end labeling (TUNEL) was performed on coronal sections from each animal at the level corresponding to the peri-ischemic region (approximately 1 mm from ischemic core) by using in situ Cell Death Detection Kit, Fluorescein, according to the manufacturer's instructions (Roche Indianapolis, IN) (9).

Data are expressed as the mean \pm SEM. Statistical significance ($p < 0.05$) was tested by a Student's t-test or ANOVA followed by Bonferroni post hoc comparisons.

Results

Neurological Function

MCAO resulted in significant neurological deficits in both animal groups compared to pre-ischemia. However, there were no significant differences in neurological deficits

detected between MCAO and MCAO + Rad groups at all time points after ischemia induction.

MRI

Neuroimaging (T2WI) of the ischemic tissue demonstrated that whole brain radiation exposure of MCAO + Rad animals resulted in a significant reduction of the ischemic lesion volume ($*p < 0.05$ vs MCAO, ANOVA) (Fig. 1a, b). T2 values (indicative of brain water content) in MCAO and MCAO + Rad groups were significantly increased within the lesion volume in both groups after MCAO induction compared to pre-stroke values.

TUNEL Staining

Quantification of the number of TUNEL positive cells detected a 33.7% decrease in the peri-ischemic area (1 mm

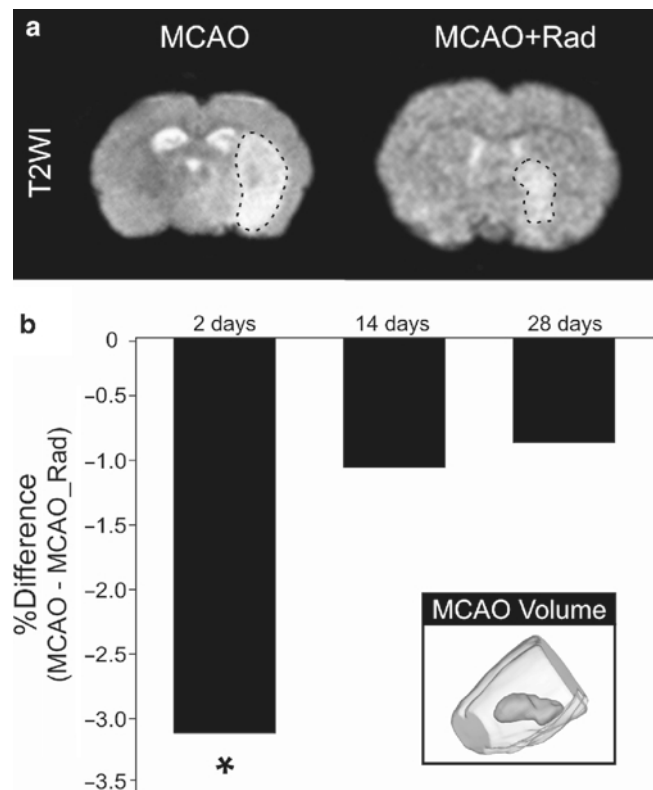


Fig. 1 Neuroimaging after MCAO induction. (a) Lesion volume from MRI (T2WI) was markedly reduced in the MCAO + Rad compared with the MCAO-only group (dotted line indicates ischemic area). (b) The percentage difference between ischemic lesion volume in MCAO animals versus MCAO + Rad animals determined at 2, 14 and 28 days was significantly reduced at 2 days ($*p < 0.01$, ANOVA). Inset: A 3D MR reconstruction of T2WI from which lesion volumes were derived

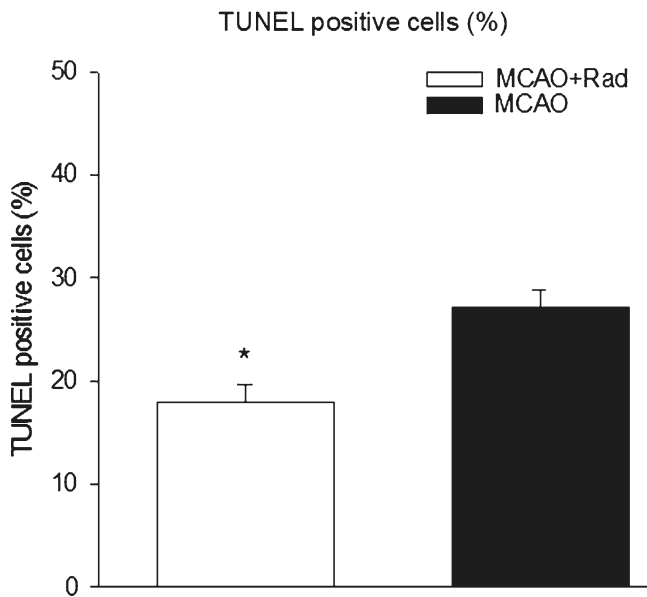


Fig. 2 TUNEL positive cells within the peri-ischemic region. The percentage of TUNEL positive cells detected in the peri-ischemic area was significantly reduced in MCAO + Rad compared with MCAO only animals (* $p < 0.001$ vs MCAO, t-test)

from core of ischemia) in MCAO + Rad animals compared with MCAO ($p < 0.05$ vs MCAO, t-test) (Fig. 2).

Discussion

Radiation treatment has a long clinical history but the biological effects of this treatment are still debated. Radiation is an effective treatment modality for tumors, angiomas, arteriovenous malformations or therapy of resistant pain syndromes such as trigeminal neuralgia (14, 16). Radiation is considered the first line of defence against some tumor types but there is no unanimous opinion about potential adverse effects of treatment including consideration of long-term outcomes.

The model presented in our study was designed to investigate the effects of combined radiation and ischemic injury, similar to that which might be encountered in the clinical population. We observed reduced lesion volume as well as decreased TUNEL positive cells in radiation treated animals, indicating that apoptotic cell death was significantly reduced in ischemic animals exposed to radiation.

Our results suggest that radiation exposure modified outcomes of experimental ischemic stroke similar to that seen in the human patient population. We present data from a relatively short time period after radiation (38 days) and ischemia (28 days). Long-term studies are needed to understand outcomes and underlying mechanisms of presumed neuroprotection.

Conflict of interest statement We declare that we have no conflict of interest.

References

1. Anderson NE (2003) Late complications in childhood central nervous system tumour survivors. *Curr Opin Neurol* 16:677–683
2. Belayev L, Obenaus A, Zhao W, Saul I, Busto R, Wu C, Vignatelli A, Lin B, Ginsberg MD (2007) Experimental intracerebral hematoma in the rat: characterization by sequential magnetic resonance imaging, behavior, and histopathology. Effect of albumin therapy. *Brain Res* 1157:146–155
3. Correa DD, Maron L, Harder H, Klein M, Armstrong CL, Calabrese P, Bromberg JE, Abrey LE, Batchelor TT, Schiff D (2007) Cognitive functions in primary central nervous system lymphoma: literature review and assessment guidelines. *Ann Oncol* 18:1145–1151
4. Garcia JH, Wagner S, Liu KF, Hu XJ (1995) Neurological deficit and extent of neuronal necrosis attributable to middle cerebral artery occlusion in rats. Statistical validation. *Stroke* 26:627–634
5. Hayward RH (1972) Arteriosclerosis induced by radiation. *Surg Clin North Am* 52:359–366
6. Levegrun S, Hof H, Essig M, Schlegel W, Debus J (2004) Radiation-induced changes of brain tissue after radiosurgery in patients with arteriovenous malformations: correlation with dose distribution parameters. *Int J Radiat Oncol Biol Phys* 59:796–808
7. Longa EZ, Weinstein PR, Carlson S, Cummins R (1989) Reversible middle cerebral artery occlusion without craniectomy in rats. *Stroke* 20:84–91
8. Lyubimova N, Hopewell JW (2004) Experimental evidence to support the hypothesis that damage to vascular endothelium plays the primary role in the development of late radiation-induced CNS injury. *Br J Radiol* 77:488–492
9. Matchett GA, Calinisan JB, Matchett GC, Martin RD, Zhang JH (2007) The effect of granulocyte-colony stimulating factor in global cerebral ischemia in rats. *Brain Res* 1136:200–207
10. Mulhern RK, Merchant TE, Gajjar A, Reddick WE, Kun LE (2004) Late neurocognitive sequelae in survivors of brain tumours in childhood. *Lancet Oncol* 5:399–408
11. Ness KK, Gurney JG (2007) Adverse late effects of childhood cancer and its treatment on health and performance. *Annu Rev Public Health* 28:279–302
12. Oeffinger KC, Nathan PC, Kremer LC (2008) Challenges after curative treatment for childhood cancer and long-term follow up of survivors. *Pediatr Clin North Am* 55:251–273, xiii
13. Pearlstein RD, Whitten C, Haerich P (2006) Assessing neurocognitive dysfunction in cranial radiotherapy: can cognitive event-related potentials help? *Technol Cancer Res Treat* 5:109–125
14. Rahimi-Movaghar V, Flickinger JC (2006) Principles and practice of gamma knife radiosurgery: a review. *East Afr Med J* 83:393–400
15. Rodel F, Keilholz L, Herrmann M, Sauer R, Hildebrandt G (2007) Radiobiological mechanisms in inflammatory diseases of low-dose radiation therapy. *Int J Radiat Biol* 83:357–366
16. Sperduto PW (2003) A review of stereotactic radiosurgery in the management of brain metastases. *Technol Cancer Res Treat* 2:105–110
17. Turner R, Vink R (2007) Inhibition of neurogenic inflammation as a novel treatment for ischemic stroke. *Timely Top Med Cardiovasc Dis* 11:E24
18. Ulitovskii DA, Ulitovskaia II (1979) [Reaction of the brain to local irradiation with protons]. *Zh Nevropatol Psikiatr Im S S Korsakova* 79:1522–1530
19. Wakisaka S, O'Neill RR, Kemper TL, Verrelli DM, Caveness WF (1979) Delayed brain damage in adult monkeys from radiation in the therapeutic range. *Radiat Res* 80:277–291

Effects of VEGF Administration or Neutralization on the BBB of Developing Rat Brain

N. Ortuzar, E.G. Argandoña, H. Bengoetxea, O. Leis, S. Bulnes, and J.V. Lafuente

Abstract We investigated the effects of exogenous Vascular Endothelial Growth Factor VEGF combined with an enriched environment on BBB integrity after a minimal trauma induced during the first days of the critical visual period in rats, when peak levels of endogenous VEGF secretion are reached. VEGF was administered using osmotic mini-pumps placed in middle cortical layers of P18 Long-Evans rats. Tissue changes were evaluated using conventional histology. BBB integrity was shown by immunohistochemistry techniques for EBA and GluT-1. Mini-pump implantation produced a wider cavity in anti-VEGF infused rats. In VEGF-infused rats there was a damaged region around the cannula that was smaller in rats raised in an enriched environment (EE). The administration of VEGF induced a high concentration of plasma proteins in the neuropil around the point of cannula placement and a high inflammatory reaction. VEGF-infused rats raised in an EE showed a lower degree of extravasation and better tissue preservation. Anti-VEGF administration produced a lower protein expression profile and more widespread deterioration of tissue. Double immunofluorescence for EBA and GluT-1 showed that the administration of VEGF preserves the tissue, which remains present but not fully functional. In contrast, a combination of VEGF administration and an EE partially protects the functionally damaged tissue with a higher preservation of BBB integrity.

Keywords Blood–brain barrier • endothelial barrier antigen • glucose transporter • vascular endothelial growth factor • visual cortex • enriched environment

J.V. Lafuente (✉)
Clinical and Experimental Neuroscience Laboratory,
Department of Neuroscience, University of Basque Country,
Leioa, Spain
e-mail: josevicente.lafuente@ehu.es

N. Ortuzar, E.G. Argandoña, H. Bengoetxea, O. Leis, and S. Bulnes
Department of Neuroscience, LaNCE; Clinical and Experimental
Neuroscience Laboratory, University of Basque Country, Leioa, Spain

Introduction

Postnatal development of the visual cortex is modulated by experience. Experience-mediated changes produce an increase in neuronal activity, which in turn leads to adaptive changes in the vascular network (4). Most of these occur during the critical period. In the rat visual system, this period is between the third and fifth postnatal weeks (7). Previous research has reported the effects of visual experience on the cortex vasculature (1,2) and the increase of several factors such as nerve growth factor (NGF), brain-derived neurotrophic factor (BDNF), or neurotrophin-3 (NT-3) related to an enriched environment (EE) (8,17).

Vascular Endothelial Growth Factor (VEGF) plays a major role in angiogenesis and vascular permeability, inducing leakage in the blood–brain barrier (BBB) (12,20). In pathological situations, VEGF has also shown strong neuroprotective and neurotrophic properties (19). The main human isoform is VEGF₁₆₅; the rodent isoform of VEGF is one amino acid shorter.

Among BBB markers, Endothelial Barrier Antigen (EBA) is a rat-specific protein that is only expressed in brain microvessels of the mature, intact and fully functional BBB (2,15). The EBA is a late-phase BBB maturation marker, whereas glucose transporter 1 (GluT-1), which is also located in the endothelial plasma membrane of brain microvessels, is a marker for the early phase (18). GluT-1 has been shown to remain immunopositive even when pathological alterations of the barrier promote changes in EBA expression (2).

The aim of this research was to investigate the effects of intracortical infusion and neutralization of VEGF on BBB integrity after light trauma induced by the implantation of an osmotic mini-pump during the first days of the critical visual period in rats. This study also compares EBA expression in rats raised under standard conditions and in an enriched environment in order to evaluate the influence of outside experiences during the critical period. EBA expression could be related to maturation of the BBB. An enriched environment was taken into consideration because of its neuroprotective effects in several brain pathologies (14).

Materials and Methods

Animals and Surgical Procedures

Experiments were performed on Long-Evans rats (Charles River) close to the beginning of the critical period (P18). Animals were anesthetized with avertin (1 ml/100 g) and a sagittal incision was made midway between the eyes. First, the skin was retracted and then the periosteum. A subcutaneous pocket was made in the animal's back, into which the osmotic mini-pump was placed (Mod. 1007 D, Alzet). The infusion kit (Mod. Alzet Brain Infusion Kit III, Alzet) was fixed with cyanoacrylate to the skull. The cannula was implanted 1 mm lateral to lambda in left visual cortex and positioned in middle cortical layers. VEGF (Santa Cruz Biotechnology) was administered (25 ng/ml at a delivery rate of 0.5 μ l/h in ten animals (five rats raised in standard conditions and five rats in an enriched environment) (Fig. 1).

Total operating time was approximately 25 min. After surgery, food and water were provided ad libitum. Mini-pumps were left in position for one week. All animal experiments were performed in accordance with the European Community Council Directive of 24 November 1986 (86/609/EEC).

The following groups were used:

- Rats raised in a standard laboratory cage with 12 h light/dark cycle.
- Rats raised in an enriched environment (EE), in a large cage (720 \times 550 \times 300 mm) with 12 h light/dark cycle and furnished with colorful toys and differently shaped objects (shelters, tunnels) that were changed every 2 days.

To study the effects of endogenous VEGF inhibition, we administered anti-VEGF (25 μ g/ml; Santa Cruz Biotechnology) to another five rats. Untreated rats were used as control.

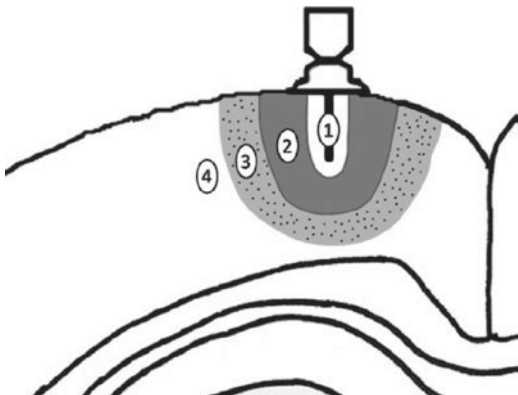


Fig. 1 Schematic representation of mini-pump implantation. (1) Cavity around the cannula. (2) Surrounded concentrically by a damaged region and a transitional penumbra-like region (3). (4) Undamaged tissue

Fixation and Tissue Processing

Rats were anaesthetized with 6% chloral hydrate. After anesthesia, the cannula was removed and the animals were transcardially perfused with a 4% paraformaldehyde fixative solution. Following perfusion, brains were removed and stored overnight at 4°C in fresh fixative solution. The next day, a thick block of occipital cortex containing the visual area including the cannula placement was coronally cut with a Rodent Brain Matrix (Electron Microscopic Sciences), rinsed in cold PBS for 4 h and embedded in paraffin. The paraffin block was serially cut with a microtome into 4 μ m slices and mounted on slides coated with APES (3-aminopropyltriethoxylane).

Immunohistochemistry

Paraffin sections were immunostained for Endothelial Barrier Antigen (EBA; Sternberger Monoclonals, 1:2,000). Parallel slices were stained with Haematoxylin-Eosin to identify the damage around the cannula. Paraffin was removed from the tissue by xylene immersion and the tissue was rehydrated. Endogenous peroxidase activity was blocked with 4% H_2O_2 /methanol for 20 min. Sections were kept in a Tris buffer at pH 7.4, and then incubated for 30 min at 37°C in Trypsin 0.1% $CaCl_2$ for antigen retrieval. Sections were incubated overnight with primary antibody. Biotinylated secondary antibody was used and revealed by ABC complex (Elite ABC, Vector Laboratories) using diaminobenzidine (DAB 0.25 mg/ml) as a chromogen. Sections were lightly counterstained with haematoxylin and finally dehydrated and covered. Some sections were used to co-localize Glucose Transporter 1 (GluT-1) and EBA antigens. These sections were incubated overnight with the aforesaid EBA primary antibody and with GluT-1 (Millipore, 1:1,000). Afterwards the following fluorochrome-conjugated secondary antibodies were used: goat anti-mouse Alexa Fluor[®] 488 and goat anti-rabbit Alexa Fluor[®] 568 (Invitrogen, 1:400). For all methods, negative controls in which the primary antibodies were omitted were included in each staining run. Images were acquired for confocal fluorescence microscopy with an Olympus Fluoview FV500 confocal microscope using sequential acquisition to avoid overlapping of fluorescent emission spectra.

Histopathological Analysis

A qualitative histopathological analysis was performed on paraffin sections. The extension of the cavity and the general tissue damage was evaluated on sections stained with

haematoxylin-eosin. The integrity of the BBB was evaluated with EBA and GluT-1 immunohistochemistry.

Results

Mini-pump implantation produced a cavity around the cannula that was surrounded concentrically by a damaged region and a transitional penumbra-like region (see schematic in Fig. 1). The cavity produced in anti-VEGF infused rats was wider than in VEGF-infused rats. In VEGF-infused rats there was a damaged region around the edge of the infusion track which appeared to be smaller in rats raised in an EE. In contrast, this region seemed to have disappeared with anti-VEGF treatment, where we found a clearly defined border.

The damaged region was present in VEGF-infused rats but not in the rest of the experimental groups. In addition, the penumbra-like transitional area was wider in VEGF-infused

rats than in anti-VEGF rats, while the combination of VEGF infusion and an EE showed a narrower transitional area.

Our results also showed that the administration of VEGF induced a high concentration of plasma proteins in the neuropil around the point of cannula placement, as well as a high inflammatory reaction. By contrast, the administration of VEGF carried out in rats raised in an EE induced a lower degree of extravasation and the tissue was better preserved. The neutralization of VEGF administration produced a lower protein expression and a wider deterioration of tissue integrity than was shown with VEGF administration.

Double immunofluorescence (Fig. 2) showed that EBA expression remained absent near the point of cannula placement both in anti-VEGF infused (2b) and VEGF-infused (2f) rats. In addition, in VEGF-infused rats reared in an EE we observed an obvious positivity for EBA near the point of cannula placement (2j), which indicated that the damaged region was diminished. GluT-1 positivity was detected in all experimental groups (2c, 2g, 2k). Whereas positive vessels

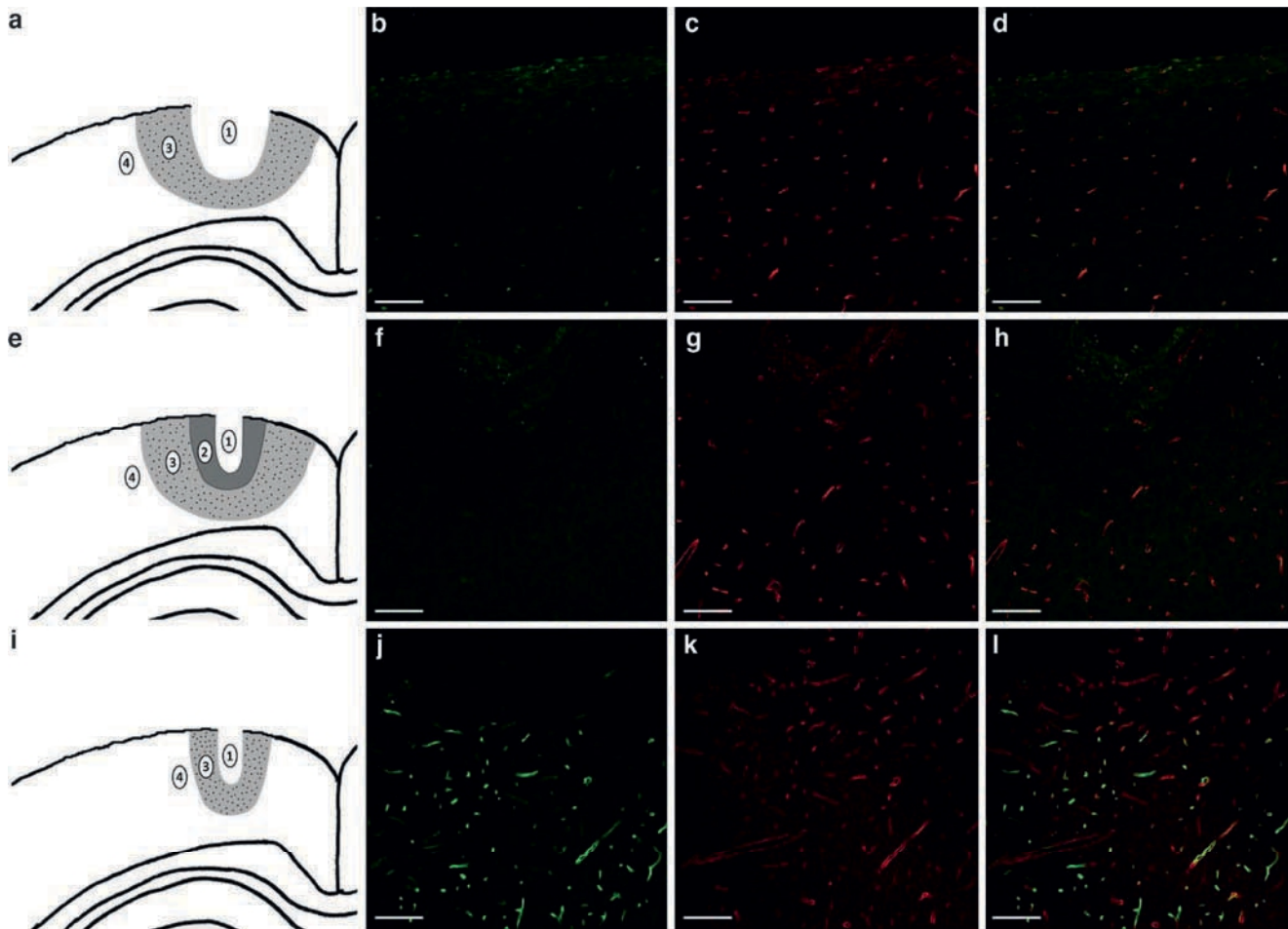


Fig. 2 Anti-VEGF infused rats (a), VEGF-infused rats (e) and VEGF-infused rats reared in an EE (i). Confocal images of immunofluorescence for EBA (b, f, j) and GluT-1 (c, g, k). Double immunolabeling for EBA and GluT-1 (d, h, l). Scale bar = 100 μ m

were close to the cavity in VEGF-EE rats and in anti-VEGF infused rats, a negative area was found in VEGF-infused rats that corresponded geographically to the damaged region found surrounding the lesion with conventional histology.

Discussion

Our results suggest that VEGF administration induces an increase in permeability but paradoxically some degree of BBB integrity is maintained. In addition, we observed a significant difference between rats raised in standard conditions and rats raised in an enriched environment. Although in both cases VEGF induced an increase of permeability, protein expression was lower in EE rats and the tissue preservation was better. The results suggest that the increase of permeability induced by VEGF can be considered as a physiological BBB opening which acts as a protective factor against necrosis of the tissue. This fact is supported by the positivity of GluT-1, which accompanies the increase in vascular permeability indicated by high protein presence in the neuropil of VEGF-infused animals.

The synergistic effects of an EE and VEGF administration could be explained by the fact that when endogenous VEGF is neutralized, the damaged area is lost; in contrast, VEGF infusion helps to preserve this area, although with a restriction of functionality reflected by the loss of barrier markers. When an EE is combined with VEGF treatment, the surrounding tissue remains functional, and acquires the characteristics of the transitional tissue, recovering a physiological pattern closer to that of the cavity.

Some authors have studied the post-traumatic effects of VEGF administration and inhibition in adults, where only a negligible level of endogenous VEGF secretion remains (21), reporting that VEGF plays an important role as an endogenous cytoprotective molecule. The authors maintain that VEGF induces both BBB permeability and inflammation on a dose-dependent basis (6).

Previous studies have posited the EBA as a specific marker for the BBB in rats, linking its expression with the functionality of the barrier (13), since a decrease in EBA positivity has been reported in pathological conditions where the administration of an anti-EBA antibody resulted in increased permeability of brain microvessels (9). Nevertheless, most of this research has been performed in adults, at an age in which under normal conditions physiological VEGF levels are quite low. In addition, our previous research showed that at the beginning of the critical period, a significant percentage of cortical vessels have a BBB that does not seem to be fully mature, as 27% of brain capillaries lack EBA positivity (2).

We also examined the expression of another component of the BBB, the Glucose transporter GluT-1, which has been

shown to remain even when pathological alterations of the barrier promote changes in EBA expression (2).

Despite the general belief that the young brain is more resilient to injury than the adult brain, lesions at early ages often produce more severe effects than equivalent lesions in adults, or evolve in a completely different way (16). Clinical experience suggests that injury to the immature brain can result in abnormal development and long-standing neurobehavioral impairment (10), even if there is little evidence of morphological damage (11).

The combination of an enriched environment and VEGF infusion shows a better recovery of the tissue surrounding the lesion. An enriched environment has been proposed for treatment of several types of brain damage because among other effects, its angiogenic and anti-apoptotic effects could tip the balance for the insulted cells in the transitional penumbra area towards survival instead of towards death. Another fact that could contribute to neuroprotection is the acceleration of cortical maturation induced by an EE (3,5). A higher degree of maturation could diminish the spread of brain edema, minimizing the consequences of the injury.

Blocking VEGF induces a lower degree of barrier opening that could be considered a break of the barrier structure, with more deleterious consequences for the surrounding tissue. Notably, this opening is necessary in order to maintain the physiological function of the cortex. Our results also show that the behavior of the repair mechanisms observed is quite similar to that in adults. Further studies should focus on the functional consequences of brain injury in the visual cortex at the beginning of the critical period and the potential role of VEGF in recovery from injury in immature brains.

Conflict of interest statement We declare that we have no conflict of interest.

Acknowledgements This work was financially supported by 9/212.327-15887 (University of the Basque Country), IT/460/07 and SAIOTEK (Basque Government).

N. Ortuzar is supported by a scholarship from the University of the Basque Country.

Confocal microscopy analysis was performed at the "Servicio de Microscopía Analítica y de Alta Resolución en Biomedicina" (High Resolution Analytical Microscopy Service for Biomedicine) at the University of the Basque Country.

References

1. Argandoña EG, Lafuente JV (2000) Influence of visual experience deprivation on the postnatal development of the microvascular bed in layer IV of the rat visual cortex. *Brain Res* 855(1):137–142
2. Argandoña EG, Bengoetxea H, Lafuente JV (2005) Lack of experience-mediated differences in the immunohistochemical expression of blood–brain barrier markers (EBA and GluT-1) during the postnatal development of the rat visual cortex. *Brain Res Dev Brain Res* 156(2):158–166

3. Bengoetxea H, Argandoña EG, Lafuente JV (2008) Effects of visual experience on vascular endothelial growth factor expression during the postnatal development of the rat visual cortex. *Cereb Cortex* 18(7):1630–1639
4. Busija DW (1994) Cerebral circulation of the fetus and newborn. In: Bevan RD, Bevan JA (eds) *The human brain circulation*. Humana, Totowa, NJ, pp 259–270
5. Cancedda L, Putignano E, Sale A, Viegi A, Berardi N, Maffei L (2004) Acceleration of visual system development by environmental enrichment. *J Neurosci* 8:52–61
6. Croll SD, Ransohoff RM, Cai N, Zhang Q, Martin FJ, Wei T et al (2004) VEGF-mediated inflammation precedes angiogenesis in adult brain. *Exp Neurol* 187(2):388–402
7. Fagiolini M, Pizzorusso T, Berardi N, Domenici L, Maffei L (1994) Functional postnatal development of the rat primary visual cortex and the role of visual experience: dark rearing and monocular deprivation. *Vision Res* 34(6):709–720
8. Franklin TB, Murphy JA, Myers TL, Clarke DB, Currie RW (2006) Enriched environment during adolescence changes brain-derived neurotrophic factor and Trk levels in the rat visual system but does not offer neuroprotection to retinal ganglion cells following axotomy. *Brain Res* 20:1–11
9. Ghabriel MN, Zhu C, Leigh C (2002) Electron microscope study of blood–brain barrier opening induced by immunological targeting of the endothelial barrier antigen. *Brain Res* 934(2):140–151
10. Giza CC, Griesbach GS, Hovda DA (2005) Experience-dependent behavioral plasticity is disturbed following traumatic injury to the immature brain. *Behav Brain Res* 157(1):11–22
11. Gurkoff GG, Giza CC, Hovda DA (2006) Lateral fluid percussion injury in the developing rat causes an acute, mild behavioral dysfunction in the absence of significant cell death. *Brain Res* 1077(1):24–36
12. Lafuente JV, Argandoña EG, Mitre B (2005) VEGFR-2 expression in brain injury: its distribution related to brain–blood barrier markers. *J Neural Transm* 113(4):487–496
13. Lin BW, Ginsberg MD (2000) Quantitative assessment of the normal cerebral microvasculature by endothelial barrier antigen (EBA) immunohistochemistry: application to focal cerebral ischemia. *Brain Res* 865(2):237–244
14. Olsson IAS, Dahlborn K (2002) Improving housing conditions for laboratory mice: a review of “environmental enrichment”. *Lab Anim* 36:243–270
15. Orte C, Lawrenson JG, Finn TM, Reid AR, Allt G (1999) A comparison of blood–brain barrier and blood–nerve barrier endothelial cell markers. *Anat Embryol (Berl)* 199(6):509–517
16. Payne BR, Lomber SG (2002) Plasticity of the visual cortex after injury: what’s different about the young brain? *Neuroscientist* 8(2):174–185
17. Pham TM, Winblad B, Granholm AC, Mohammed AH (2002) Environmental influences on brain neurotrophins in rats. *Pharmacol Biochem Behav* 73:167–175
18. Rahner-Welsch S, Vogel J, Kuschinsky W (1995) Regional congruence and divergence of glucose transporters (GluT1) and capillaries in rat brains. *J Cereb Blood Flow Metab* 15:681–686
19. Rosenstein JM, Krum JM (2004) New roles for VEGF in nervous tissue—beyond blood vessels. *Exp Neurol* 187:246–253
20. Schoch HJ, Fischer S, Marti HH (2002) Hypoxia induced vascular endothelial growth factor expression causes vascular leakage in the brain. *Brain* 125:2549–2557
21. Skold MK, Risling M, Holmin S (2006) Inhibition of vascular endothelial growth factor receptor 2 activity in experimental brain contusions aggravates injury outcome and leads to early increased neuronal and glial degeneration. *Eur J Neurosci* 23(1): 21–34

Alterations in Blood–Brain Barrier Function and Brain Pathology by Morphine in the Rat. Neuroprotective Effects of Antioxidant H-290/51

Hari Shanker Sharma, Per-Ove Sjöquist, and Syed F. Ali

Abstract The possibility that stress associated with morphine administration or withdrawal will influence the blood–brain barrier (BBB) dysfunction, brain edema formation and brain pathology was examined in a rat model. Repeated daily administration of morphine (10 mg/kg, i.p.) resulted in drug dependence in rats on the 6th day and onwards. The BBB permeability to Evans blue albumin (EBA) and radioiodine [¹³¹I]iodine did not alter during morphine dependence up to the 12th day. On the other hand, spontaneous withdrawal of morphine on day 1 resulted in profound stress symptoms and breakdown of the BBB to protein tracers in several brain regions. This increase in BBB to protein tracers was most pronounced on the 2nd day of morphine withdrawal. These rats also exhibited marked brain edema and abnormal neuronal and glial cell responses. Pretreatment with an antioxidant H-290/51 markedly attenuated the BBB dysfunction, brain edema formation and brain pathology during morphine withdrawal phases. These observations suggest that psychostimulants and associated oxidative stress are capable to induce brain pathology through modifying the BBB function.

Keywords Morphine withdrawal • brain edema • blood–brain barrier • oxidative stress • H-290/51 • glial fibrillary acidic protein • neuronal damage • neuroprotection

H.S. Sharma (✉)

Laboratory of Cerebrovascular Research, Department of Surgical Science, Anesthesiology and Intensive Care Medicine, University Hospital, Frödingsgatan 12:28, Uppsala, SE-75421, Sweden and Neurochemistry Laboratory, Division of Neurotoxicology, National Centre for Toxicological Research/FDA, Jefferson, AR, USA
e-mail: Sharma@surgsci.uu.se

P.-O. Sjöquist

Department of Integrative Pharmacology, Astra-Zeneca Mölndal, Mölndal, Sweden

S.F. Ali

Neurochemistry Laboratory, Division of Neurotoxicology, National Centre for Toxicological Research/FDA, Jefferson, AR, USA

Introduction

Psychostimulants such as morphine and methamphetamine induce profound hyperthermia and brain dysfunction (11, 13, 15, 19). However, their role in blood–brain barrier (BBB) disruption, brain edema formation and brain pathology is still unclear. Experiments carried out in our laboratory show that methamphetamine-induced hyperthermia appears to be crucial in BBB breakdown to protein tracers and brain dysfunction (6, 19). Since morphine is a well-known hyperthermic agent that also induces dependence, thus withdrawal of morphine results in profound stress symptoms (see 11, 16, 19). Previous reports from our laboratory have shown that the state of BBB permeability in morphine induced dependence and withdrawal is compromised (13, 15, 18, 19). However, the detailed mechanisms of BBB dysfunction in morphine dependence or during withdrawal are not known. Since breakdown of the BBB function is associated with brain edema formation and cell injury (16), the possibility exists that morphine dependence and withdrawal response will induce brain pathology via opening of the BBB permeability.

There is reason to believe that psychostimulants including morphine may alter the oxidative balance in the brain causing generation of free radicals and lipid peroxidation (9). Thus, it is likely that increased oxidative stress may lead to BBB dysfunction and brain edema formation leading to cell injury (15, 22). To test this hypothesis, in the present investigation, we used a potent inhibitor of lipid peroxidation, H-290/51 (23) in morphine dependent rats and during various phases of morphine withdrawal, and examined the BBB breakdown, edema formation and cell injury. Our results show that oxidative stress significantly contribute to morphine induced BBB dysfunction, brain edema formation and brain pathology.

Materials and Methods

Animals

Experiments were carried out on inbred Male Charles Foster rats (200–250 g) housed at controlled ambient temperature ($21 \pm 1^\circ\text{C}$) with 12 h light and 12 h dark schedule. Food and water were supplied ad libitum before the experiments.

Morphine Administration and Development of Dependence

Morphine Sulphate (Sigma Chemical Co., USA, 10 mg/kg, s.c.) was administered once daily at 8:00 a.m. for 12 days to induce morphine dependence (see 19). These animals developed profound tolerance from the 4th day and onwards (11, 19, 22).

Morphine Withdrawal

On day 12, morphine administration was stopped and the animals were observed for the development of spontaneous withdrawal symptoms, which normally occurred 12 h and onwards from cessation of morphine administration (18, 19). These animals were observed for withdrawal symptoms 24 and 48 h after termination of morphine administration (18, 22).

Treatment with H-290/51

In a separate group of rats, H-290/51 (Astra-Zeneca, Mölndal, Sweden) was administered (50 mg/kg, p.o.) in morphine dependent rats on day 12, and in another group of rats, the compound was administered on day 1 or day 2 of morphine withdrawal (see Tables 1 and 2) (22).

Physiological Variables

Mean arterial blood pressure (MABP), heart rate, respiration, arterial pH and blood gases were determined using standard procedures as described earlier (13).

Blood–Brain Barrier Permeability and Brain Edema Formation

The blood–brain barrier (BBB) permeability to Evans blue albumin and ^{131}I iodine was examined as described earlier (13). The brain water content was used to calculate edema formation and volume swelling (20).

Brain Pathology

Paraffin embedded brain tissues were used to evaluate neural changes using Haematoxylin and Eosin or Nissl staining and glial changes using immunohistochemistry of glial fibrillary acidic protein (GFAP) on 3 μm thick paraffin sections (20–22).

Table 1 Effect of H-290/51 on morphine dependence and withdrawal on stress symptoms

Parameters	Control	H-290/51		Morphine dependence		Morphine withdrawal		
		+Control	12th day	H-290/51	24 h	H-290/51	48 h	H-290/51
				+12th day		+24 h		+48 h
Stress symptoms	n = 6	n = 6	n = 12	n = 6	n = 14	n = 6	n = 16	n = 5
Wet-shakes	Nil	Nil	Nil	Nil	8 \pm 3	2 \pm 2#	6 \pm 2	2 \pm 2#
Piloerection	Nil	Nil	Nil	Nil	+++++	+++	++++	+++
Writhing	Nil	Nil	Nil	Nil	+++++	+++	++++	+++
Teeth chattering	Nil	Nil	Nil	Nil	+++++	+++	+++++	+++
Diarrhoea	Nil	Nil	Nil	Nil	+++++	+++	+++	+++
Aggressive behaviour	Nil	Nil	?	Nil	+++++	+++	+++++	+++
Microhaemorrhages in stomach	Nil	Nil	12 \pm 8	4 \pm 2#	68 \pm 18 ^a	60 \pm 12	85 \pm 14 ^a	80 \pm 12

Values are mean \pm SD; a = Many microhaemorrhages; # = significantly different ($P < 0.05$) from Morphine withdrawal 24 h; +++ = mild, ++++ = moderate, +++++ = severe, ? = unclear, Nil = absent.

Table 2 Effect of H-290/51 on Morphine withdrawal symptoms and brain pathology

Type of experiment	Stress symptoms			Physiological variables				Blood brain barrier permeability			Brain edema	
	Heart rate (beats/min)	Respiration (cycle/min)	Rectal (T°C)	MABP (torr)	Arterial pH	PaO ₂ (torr)	PaCO ₂ (torr)	Evans blue		Brain water %	%f	
								mg%	¹²⁵ Iodine %			
Control	280 ± 12	76 ± 6	37.61 ± 0.42	110 ± 8	7.38 ± 0.02	81.56 ± 0.23	34.62 ± 0.34	0.24 ± 0.08	0.34 ± 0.06	75.43 ± 0.21		
H-290/51	278 ± 10	74 ± 8	37.40 ± 0.21	108 ± 6	7.38 ± 0.04	81.34 ± 0.18	34.45 ± 0.28	0.26 ± 0.08	0.38 ± 0.07	75.44 ± 0.28	-	
MD 12	338 ± 10**	86 ± 7**	38.4 ± 0.31	148 ± 5**	7.36 ± 0.05	78.34 ± 1.34	33.10 ± 0.43	0.14 ± 0.05*	0.20 ± 0.06*	74.87 ± 0.12*	-2	
H-290/51+MD 12	300 ± 12*	80 ± 6*	38.05 ± 0.21	124 ± 6*	7.35 ± 0.04	79.34 ± 0.23	33.78 ± 0.28	0.20 ± 0.04	0.28 ± 0.10	75.13 ± 0.21	-	
MW 1	310 ± 8*	94 ± 4**	40.23 ± 0.18**	128 ± 6**	7.36 ± 0.08	82.45 ± 0.34**	31.54 ± 1.24*	0.75 ± 0.10**	0.89 ± 0.08**	76.23 ± 0.21*	+3	
H-290/51+MW1	300 ± 8*	90 ± 2**	39.45 ± 0.21**	120 ± 6	7.35 ± 0.08	81.89 ± 0.43	32.45 ± 0.21	0.48 ± 0.08**	0.56 ± 0.10**	75.89 ± 0.18**	<+1	
MW2	308 ± 7*	92 ± 5**	39.28 ± 0.11**	146 ± 9**	7.34 ± 0.05	82.67 ± 0.31**	32.06 ± 0.84	0.89 ± 0.11**	0.97 ± 0.08**	76.73 ± 0.22*	+5	
H-290/51+MW2	300 ± 6*	89 ± 7*	39.05 ± 0.08*	140 ± 8*	7.34 ± 0.08	82.05 ± 0.43	32.89 ± 0.98	0.56 ± 0.08**	0.64 ± 0.07**	75.88 ± 0.34**	<+2	

Values are mean ± SD of five to six rats at each observation points. * = P < 0.05, ** P < 0.01 from control, # P < 0.05, ## P < 0.01 from MW group respectively. ANOVA followed by Dunnet's test for multiple group comparison from one control. MD = Morphine dependent day 12; MW = Morphine withdrawal day 12; MW = morphine withdrawal day 1, day 2, % f = volume swelling, i.e., ≈ 1% increase in brain water will approximately show 4% increase in volume swelling (see Sharma et al., 2004 (19)).

Statistical Analysis

ANOVA followed by Dunnet's test was used to evaluate statistical significance of the data obtained from one control group. A p-value <0.05 was considered significant.

Results

Effect of H-290/51 on Morphine Withdrawal Symptoms and Physiological Variable

Morphine administration resulted in dependence from the 4th day and onwards (Sharma et al. 2004 (19)). On day 12, the morphine dependent animals showed a pronounced increase in heart rate, respiration, body temperature and MABP (control group) (Table 2). Pretreatment with H-290/51 markedly attenuated these changes (Table 2) in the morphine dependent animals; however, the compound was unable to restore these physiological values as seen in control group (Table 2). At postmortem, the microhaemorrhages in the stomach wall in H-290/51 treated morphine dependent animals were considerably reduced compared to the untreated morphine dependent rats (Table 1).

Morphine withdrawal further aggravated these physiological variables and body temperature changes on day 1 and 2 (Table 2) that was considerably attenuated by H-290/51 treatment. Likewise, the behavioral changes seen on day 1 and day 2 of morphine withdrawal (Table 1) were also considerably reduced by prior treatment with H-290/51 (Table 1).

Effect of H-290/51 on Morphine Withdrawal Induced Blood–Brain Barrier Permeability

Morphine dependence in rats significantly reduced the Evans blue and radioiodine permeability in the brain compared to control group (Table 2). Pretreatment with H-290/51 markedly restored the BBB function to these tracers to near normal values (Table 2).

On the other hand, morphine withdrawal markedly increased the penetration of these protein tracers into the brain on day 1 that was further aggravated on day 2 of morphine withdrawal (Table 2): Pretreatment with H-290/51 significantly attenuated the leakage of tracers across the BBB on day 1 or 2 following withdrawal (Table 2): However the BBB permeability to Evans blue and radioiodine remained higher from the control groups in H-290/51 treated morphine withdrawal rats (Table 2).

Effect of H-290/51 on Morphine Withdrawal Induced Brain Edema Formation

The brain water content was significantly reduced in morphine dependent rats on day 12 compared to the control rats. This reduction in brain water content was partially restored by pretreatment with H-290/51.

However, morphine withdrawal resulted in a progressive increase in brain water content on day 1 and 2 compared to control groups (Table 2) that was significantly reduced by pretreatment with H.290/51 (see Table 2). However, the brain water content still remained higher than in the control group following morphine withdrawal in H-290/51 treated groups (Table 2).

Effect of H-290/51 on Morphine Withdrawal Induced Cell Changes

Pronounced neuronal and glial cell changes are seen in morphine dependent rats on day 12 compared to the control group (Fig. 1). These cell changes and astrocytic reactions were much more pronounced following morphine withdrawal on day 1, which was further aggravated on day 2 (Fig. 1). Pretreatment with H-.290/51 significantly reduced these cell changes either caused by morphine dependence or withdrawal (results not shown).

Discussion

The present results are the first to show that morphine withdrawal is associated with brain edema formation and pretreatment with the potent antioxidant compound H-290/51 is antiedematous in nature. This indicates that psychostimulants induce oxidative stress that could be instrumental in brain edema formation and subsequent brain pathology.

Morphine is well known to induce proinflammatory cytokines including interleukin-1b, interleukin-6 and tumor necrosis factor- α via acting through micro-receptors in the brain and spinal cord (4, 5, 7). An increased concentration of these cytokines in the CNS following morphine treatment may act to inhibit the analgesic effects of the opioid causing dependence (3). Furthermore, these cytokines may exert their cytotoxic effects to induce neurotoxicity (7, 8). It appears that stress caused by morphine withdrawal may further augment the release of these cytokines leading to enhanced neurotoxicity (1). Thus, the neuronal and glial cell changes seen during morphine dependence are further aggravated following morphine withdrawal which is in line with this

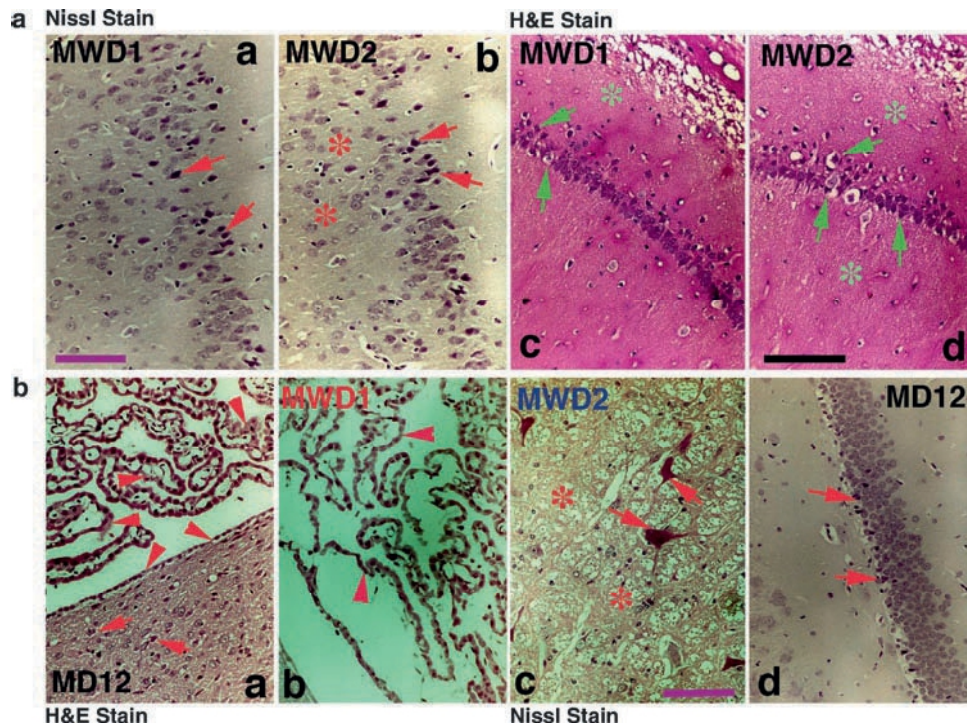


Fig. 1 Structural changes in the brain at light microscopy in rats following morphine dependence (day 12; MD12) and after its spontaneous withdrawal. (A) Nissl stained paraffin sections (3 μm thick) from rat brain passing through piriform area (-3.70 mm from bregma) shows marked selective nerve cell damage following 1 day after morphine withdrawal (MWD1; *arrows*, **a**). The magnitude and intensity of nerve cell damage appear to be increased following second day of morphine withdrawal (MWD2; *arrows*, **b**). Haematoxylin and eosin (H&E) stained 3 μm thick paraffin sections passing through hippocampus (-3.25 mm from bregma) showing CA-1 subfield from rats following morphine withdrawal (day 1, **c** and day 2, **d**). Specific cell damage (*arrows*) is clearly visible in the hippocampal CA-1 layer. Sponginess and edema (*) are clearly evident. The magnitude of cell damage is much more intensified on the second day of morphine withdrawal. (B) Structural changes in the choroid plexus of right lateral cerebral

ventricle from one morphine dependent (MD 12, **a**) and one morphine withdrawal rat (MWD1, **b**). Paraffin sections passing through right lateral ventricle (-0.83 mm from bregma) shows degeneration of choroid plexus epithelial cells and the ependymal cell lining (*arrow heads*, **a**). The degenerating changes in the choroid plexus are much more marked in rats subjected to spontaneous morphine withdrawal following 1 day (MWD1, **b**) indicating breakdown of the blood–CSF barrier (for details see text). Paraffin section passing through the mesencephalic reticular nucleus (-7.10 mm from bregma) show many damaged nerve cells (H&E stain, *arrows*), sponginess and edema (*) on the second day of spontaneous morphine withdrawal in dependent rats (MWD2, **c**). In morphine dependent rats on the day 12 (MD 12, **d**) damage to hippocampal dentate granule cells (-4.20 mm from bregma) are clearly visible (Nissl stain, *arrows*). Bars: A = 25 μm ; B = 30 μm (modified after 19)

hypothesis. Since oxidative stress alone could result in the release of cytokines (1, 19, 22), blockade of lipid peroxidation in morphine dependent animals or during the spontaneous withdrawal phase is likely to reduce the cytokines neurotoxicity. Our results with H-290/51 are in agreement with this idea. Thus, pretreatment with a potent antioxidant compound H-290/51 (15, 22) significantly attenuated morphine-induced neurotoxicity during morphine dependence as well as following morphine withdrawal (Table 2).

Alteration in fluid microenvironment of the brain and an enhanced passage of protein tracers across the BBB would lead to brain edema formation (10–12). Water transport across the cerebral microvessels from blood to brain will lead to brain swelling and from brain to blood will induce brain shrinkage (2, 19). In both cases the BBB is compromised. Thus, morphine treatment leading to dependence resulted in a decrease in the BBB function leading to slight reduction in brain water

content (13, 19, 22). On the other hand, morphine withdrawal resulted in profound increase in the BBB permeability to protein tracers and led to marled accumulation of brain water content (see 19). Interestingly during these two opposite phases, neurotoxicity was evident in both neuronal and in glial cells. Degeneration of choroid plexuses seen during morphine dependence and withdrawal phases is in agreement with this hypothesis (14, 17). Obviously, degeneration of choroid epithelial cells will affect the transport of tracers and substances between blood and CSF and vice versa (14). Similar mechanisms may also exist in brain endothelial cells, a subject that is currently being investigated in our laboratory.

Pretreatment with H-290/51 markedly restored the BBB function and brain water during morphine dependent animals suggest that oxidative stress caused by morphine dependence is influencing the BBB function and brain shrinkage (15, 21). On the other hand, significant decrease in BBB permeability

and brain edema was achieved by H-290/51 during morphine withdrawal phase and suggests that oxidative stress plays an important role in withdrawal stress induced BBB breakdown and brain edema formation (see 6, 13, 18, 19). Obviously, leakage of tracers across the BBB, i.e., from blood to brain or from brain to blood will alter brain fluid microenvironment and induce neurotoxicity. Partial restoration of BBB dysfunction by drugs, e.g., antioxidant H-290/51 will thus enhance neuroprotection.

Taken together our results are the first to show that morphine dependence and withdrawal phases are associated with brain shrinkage and swelling, respectively, that could lead to brain pathology. Furthermore, oxidative stress appears to play important roles in psychostimulant dependence and withdrawal. Thus, antioxidant compounds, e.g., H-290/51 may have pronounced neuroprotective efficacy that could be of immense clinical value in future.

Conflict of interest statement The authors have no conflict of interest with any agencies mentioned below.

Acknowledgments This study was supported by grants from Swedish Medical Research Council (2710 HSS), Astra-Zeneca, Mölndal (HSS), Sweden, The University Grants Commission (HSS), New Delhi, India, Indian Council of Medical Research (HSS), New Delhi, Govt. of India, Alexander von Humboldt Foundation (HSS), Bonn, Germany. The skillful technical assistance of Kärstin Flink, Ingamari Olsson, Gunilla Tibling and Gunilla Järild and secretarial assistance of Angela Jan and Aruna Sharma are highly appreciated.

References

- Crapo JD (2003) Oxidative stress as an initiator of cytokine release and cell damage. *Eur Respir J Suppl Sep*; 44:4s–6s. Review
- Elliott KAC, Jasper H (1949) Measurement of experimentally induced brain swelling and shrinkage. *Am J Physiol* 157:122–129
- Gul H, Yildiz O, Dogrul A, Yesilyurt O, Isimer A (2000) The interaction between IL-1beta and morphine: possible mechanism of the deficiency of morphine-induced analgesia in diabetic mice. *Pain Dec* 15; 89(1):39–45
- Hook MA, Liu GT, Washburn SN, Ferguson AR, Bopp AC, Huie JR, Grau JW (2007) The impact of morphine after a spinal cord injury. *Behav Brain Res* 179(2):281–293
- Johnston IN, Milligan ED, Wieseler-Frank J, Frank MG, Zapata V, Campisi J, Langer S, Martin D, Green P, Fleshner M, Leinwand L, Maier SF, Watkins LR (2004) A role for proinflammatory cytokines and fractalkine in analgesia, tolerance, and subsequent pain facilitation induced by chronic intrathecal morphine. *J Neurosci Aug* 18; 24(33):7353–7365
- Kiyatkin EA, Brown PL, Sharma HS (2007) Brain edema and breakdown of the blood–brain barrier during methamphetamine intoxication: critical role of brain hyperthermia. *Eur J Neurosci Sep*; 26(5):1242–1253
- Maier SF, Watkins LR (2004) A role for proinflammatory cytokines and fractalkine in analgesia, tolerance, and subsequent pain facilitation induced by chronic intrathecal morphine. *J Neurosci Aug* 18; 24(33):7353–7365
- Merrill JE, Benveniste EN (1996) Cytokines in inflammatory brain lesions: helpful and harmful. *Trends Neurosci Aug*; 19(8):331–338. Review
- Pérez-Casanova A, Noel RJ Jr, Rivera-Amill V, Husain K, Kumar A (2007) Morphine-mediated deterioration of oxidative stress leads to rapid disease progression in SIV/SHIV-infected macaques. *AIDS Res Hum Retroviruses Aug*; 23(8):1004–1007
- Rapoport SI (1976) *Blood–brain barrier in physiology and medicine*. Raven, New York
- Sharma HS (2004) Blood–brain and spinal cord barriers in stress. In: Sharma HS, Westman J (eds) *The blood–spinal cord and brain barriers in health and disease*. Elsevier Academic, San Diego, pp 231–298
- Sharma HS (2007) Neurobiology of hyperthermia. *Prog Brain Res* 162:1–617
- Sharma HS, Ali SF (2006) Alterations in blood–brain barrier function by morphine and methamphetamine. *Ann N Y Acad Sci Aug* 1074:198–224
- Sharma HS, Johanson CE (2007) Blood–cerebrospinal fluid barrier in hyperthermia. *Prog Brain Res* 162:459–478. Review
- Sharma HS, Sjöquist PO (2002) A new antioxidant compound H-290/51 modulates glutamate and GABA immunoreactivity in the rat spinal cord following trauma. *Amino Acids* 23(1–3):261–272
- Sharma HS, Westman J (2004) *The blood–spinal cord and brain barriers in health and disease*. Elsevier/Academic, San Diego, pp 1–617 (release date: Nov. 9, 2003)
- Sharma HS, Duncan JA, Johanson CE (2006) Whole-body hyperthermia in the rat disrupts the blood–cerebrospinal fluid barrier and induces brain edema. *Acta Neurochir Suppl* 96:426–431
- Sharma HS, Lundstedt T, Boman A, Lek P, Seifert E, Wiklund L, Ali SF (2006) A potent serotonin-modulating compound AP-267 attenuates morphine withdrawal-induced blood–brain barrier dysfunction in rats. *Ann N Y Acad Sci Aug* 1074:482–496
- Sharma HS, Patnaik R, Ray AK, Dey PK (2004) Blood–central nervous system barriers in morphine dependence and withdrawal. In: Sharma HS, Westman J (eds) *The blood–spinal cord and brain barriers in health and disease*. Elsevier Academic, San Diego, pp 299–328
- Sharma HS, Westman J, Nyberg F (1998) Pathophysiology of brain edema and cell changes following hyperthermic brain injury. *Prog Brain Res* 115:351–412. Review
- Sharma HS, Westman J, Alm P, Sjöquist PO, Cervós-Navarro J, Nyberg F (1997) Involvement of nitric oxide in the pathophysiology of acute heat stress in the rat. Influence of a new antioxidant compound H-290/51. *Ann N Y Acad Sci Mar* 15; 813:581–590
- Sharma HS, Sjöquist PO, Ali SF (2007) Drugs of abuse-induced hyperthermia, blood–brain barrier dysfunction and neurotoxicity: neuroprotective effects of a new antioxidant compound H-290/51. *Curr Pharm Des* 13(18):1903–1923. Review
- Westerlund C, Ostlund-Lindqvist AM, Sainsbury M, Shertzer HG, Sjöquist PO (1996) Characterization of novel indenoindoles. Part I. Structure–activity relationships in different model systems of lipid peroxidation. *Biochem Pharmacol May* 17; 51(10):1397–1402

Part III
Hydrocephalus

Clinical Proof of the Importance of Compliance for Hydrocephalus Pathophysiology

Michael Kiefer and Regina Eymann

Abstract

Introduction Recently decreased compliance is discussed as an initially disturbed CSF hydrodynamic parameter in hydrocephalus.

Materials and Methods In 180 patients with suspected chronic hydrocephalus we performed a dynamic infusion test, which was not used for shunt indication. Shunt indication was based on long-term ICP monitoring. Follow-up was 4.6 ± 1.8 years. Statistics: Spearman-, Kruskal–Wallis-, Wilcoxon-U-test.

Results Resistance to outflow (Rout) and Pressure Volume Index (PVI) alone provide positive predictive values (PPV) and sensitivity, which might be sufficient in daily practice, while negative predictive values (NPV) and specificity are weak. With an intelligent combined algorithm of Rout and PVI at a critical value of ROF of $13 \text{ mm Hg/ml} \times \text{min}$ and 30 ml, a clearly improved outcome prediction is possible.

Conclusion These clinical results support recent opinions concerning the meaning of Compliance and Rout in hydrocephalus patho-physiology.

Keywords Hydrocephalus • shunt • outcome • normal pressure hydrocephalus • iNPH • resistance to outflow • Rout • Compliance • PVI • CSF hydrodynamics

Introduction

Since the introduction of tests to measure cerebrospinal fluid (CSF) hydrodynamics (e.g. Resistance to outflow (Rout), Compliance (C) and Pressure Volume Index (PVI)) in the past

M. Kiefer (✉)

Department of Neurosurgery, Saarland University Medical School, Kirrberger Street, Building: 90.1, Homburg-Saar 66421, Germany
e-mail: Michael.Kiefer@uks.eu

R. Eymann

Department of Neurosurgery, Medical School, Saarland University, Kirrberger Street, Building 90, Homburg-Saar, Saarland 66421, Germany

decades, the value of hydrodynamics for the outcome prediction of potential shunt candidates, especially when suffering from idiopathic normal pressure hydrocephalus (i-NPH), has been controversially discussed (6–9, 11, 15, 19, 20). In communicating hydrocephalus with defective CSF absorption, as supposed underlying pathology, only Rout and not Compliance or PVI has been studied routinely in the past.

Some milestone contributions with modern flow-sensitive techniques of magnetic resonance imaging (MRI) have proposed a quite different hydrocephalus pathophysiology, with decreased compliance as the initial disturbed hydrodynamic parameter, interpreting Rout elevation solely as an epiphenomenon (1–3, 12). Against the background of this convincing, revolutionary new understanding of hydrocephalus, a clarification of the value of compliance or PVI for shunt indication was lacking. In this prospective study we aimed to perform a comparative analysis of the value of all available hydrodynamic parameters for selecting shunt responders.

Materials and Methods

Patients, Indication Policy, Follow-Up and Documentation

In a total of 180 patients with suspected chronic hydrocephalus, intracranial pressure (ICP) was measured for 48 hours using an intraventricular Spiegelberg III probe connected to a personal computer with specific software for ICP analysis (14). Furthermore, directly after the Spiegelberg III probe insertion, CSF dynamics were measured using the hydrodynamic model of the Dynamic infusion test (16). Shunt indication was based on long-term (overnight) monitoring of ICP. The hydrodynamic study was performed independently from the results of overnight monitoring. Furthermore the team that performed the infusion study had no knowledge of the results of overnight monitoring and had no influence on the decision whether shunting was performed in the studied patients or not.

Shunting was indicated in all patients with basal mean ICP > 20 mm Hg. Furthermore, all patients who presented with a minimum of 50% B-wave activity during the entire monitoring time were considered as shunt candidates if during 20% of the monitored time the B-wave amplitude exceeded 10 mm Hg. Patients who were not selected for shunting according to this protocol were excluded from the study, leaving a total of 126 patients for the analysis. We analyzed the CSF dynamics in excluded patients: if Rout exceeded 13 mm Hg / ml × min, they were shunted but excluded from the study. Eighty-four (56 ♂, 28 ♀) patients suffered from iNPH, secondary normal pressure hydrocephalus was diagnosed in 11 patients (5 ♂, 5 ♀) and 31 (12 ♂, 19 ♀) had other forms of chronic hydrocephalus. To be included in the study, patients had to present at least 2 symptoms of Hakim's triad and/or signs of intracranial pressure (ICP) elevation (e.g. headache, papilla prominence with visual disturbances etc.), while *ventricular wide had to exceed an Evans Index* of 0.3. Clinical state and state of comorbidity were meticulously assessed preoperatively, and for any documentation we used our clinical grading (KI) and the Recovery-Index (RI) (17). Patients were termed "shunt responder" if RI was ≥ 3 at the time of the last follow-up examination. Follow-up examinations included cerebral computertomography (CCT) and meticulous clinical examination. They were performed 2 and 12 months and thereafter annually after shunting. The minimal follow-up was for 1 year and the average follow-up was for 4.6 ± 1.8 years (range: 1–11 years).

Shunt Hardware

All patients were provided with ventriculo-peritoneal (VP) adjustable or non-adjustable gravitational shunts. We used the Aesculap-Miethke Shunt Assistant (Miethke KG, Potsdam, Germany) combined with adjustable Aesculap-Miethke PRO-GAV valve in 20 patients and combined with the adjustable Codman-Hakim (Codman, Johnson and Johnson, Boston, MA, USA) valve in 36 patients with an initial setting of the adjustable valves between 50 and 120 mm H₂O. The Aesculap-Miethke Dual-Switch valve (Miethke KG, Potsdam, Germany) and the Aesculap-Miethke Gravity-Assisted-Valve were used in 43 and 27 patients, respectively.

Statistics

Mann–Whitney U, Spearman, Kruskal–Wallis, ANOVA and χ^2 -tests at a significance level of $p < 0.05$ were used.

Results

The overall shunt response rate was 84%. Patients with iNPH performed slightly worse compared with other chronic hydrocephalus forms (non-iNPH), with response rates of 81% and 92%, respectively. An excellent, good, fair, transient and poor outcome was found in iNPH and non-iNPH in 43%, 23%, 10%, 4%, 15% and in 52%, 21%, 14%, 0%, 8% of cases, respectively. However, neither when comparing the outcome of iNPH and non-iNPH using the Recovery Index nor when dichotomizing (Responder vs. Non-Responder) did these outcome differences between both compared types of hydrocephalus reach significance ($p = 0.072$, $p = 0.189$).

Predictive Value Confined to Rout Exclusively

The dynamic infusion test provides ICP dependent Rout values. The following analyses deal with average Rout values, which were calculated for all ICP values between resting and highest ICP. The overall average Rout was 20 ± 8 mm Hg/ml × min. In iNPH, sNPH and all other chronic hydrocephalus forms, Rout did not differ widely, with values of 22 ± 8 mm Hg/ml × min, 17 ± 4 mm Hg/ml × min and 23 ± 9 mm Hg/ml × min, respectively ($p = 0.141$). Despite a certain trend, Rout did not increase clearly with age ($p = 0.186$). A tendency of higher Recovery Index, as a measure of clinical benefit, was obvious at higher Rout values but significant better correlations were not found when comparing thresholds of 13 mm Hg/ml × min and 18 mm Hg/ml × min respectively ($p = 0.815$, $p = 0.923$). However, when dichotomizing the clinical results and comparing shunt responder vs. non-responder, $\text{Rout} > 13$ mm Hg/ml × min and $\text{Rout} > 18$ mm Hg/ml × min significantly correlated with outcome ($p < 0.000$, $p = 0.05$). We also tried to find whether median, lowest, or highest values; or the range between lowest and highest Rout values correlated more stringently. None of the computed correlations reached improved accuracy of outcome prediction than the average Rout values used. Given the option that the dynamic infusion test provides CSF hydrodynamic data for any ICP value between resting (P0) and highest ICP during the infusion test, we tried to find an ICP range (low ICP range: P0–20 mm Hg, medium ICP range: 20–30 mm Hg, high ICP range: >30 mm Hg) which might be more relevant for outcome prediction, but again, the precision of outcome prediction could not be increased in this way compared to that for the average Rout value of a given patient. Overall, 89 patients had $\text{Rout} > 13$ mm Hg/ml × min, while the threshold of 18 mm Hg/ml × min was exceeded in only 63 patients, leaving at least 30% and 50% patients, who would have been not shunted according to

Table 1 Values indicating the quality of Pressure Volume Index (PVI) and Resistance to outcome (Rout) or a combined regard of both (with logical “AND” or “OR” combination) for predicting outcome after hydrocephalus shunting at different thresholds (PPV = positive predictive value, NPV = negative predictive value). For reasons of clarity, not all examined combinations at any threshold are illustrated

Thresholds/algorithm	Accuracy (%)	Sensitivity (%)	Specificity (%)	PPV (%)	NPV (%)
PVI < 22 ml (n = 81)	67	70	56	85	33
PVI < 30 ml (n = 107)	79	90	35	84	47
Rout > 13 mm Hg/ml × min (n = 89)	75	86	59	84	54
Rout > 18 mm Hg/ml × min (n = 24)	59	59	59	60	57
PVI < 30 ml AND Rout > 13 mm Hg/ml × min (n = 81)	75	74	49	96	36
PVI < 30 ml OR Rout > 13 mm Hg/ml × min (n = 115)	93	96	74	95	78

these results (Table 1). Of those patients, who would have been not shunted if Rout had been chosen for shunt indication, 46% (threshold Rout > 18 mm Hg/ml × min) and 43% (threshold Rout > 13 mm Hg/ml × min) responded to shunting with the given indication protocol, respectively (indicates the low negative predictive value of Rout).

Predictive Value Confined to PVI Exclusively

Similar as for Rout, we initially examined the average values of all measured PVI values between P0 and the highest reached ICP during the infusion test. The lowest and highest measured average PVI were 5 and 49 ml, respectively. On average, all patients had a mildly decreased PVI (20 ± 9 ml), which significantly increased with age ($p = 0.012$). In contrast, the PVI values between the different types of hydrocephalus (iNPH: 19 ± 7 ml; sNPH: 21 ± 9 ml; others: 23 ± 12 ml) were quite similar ($p = 0.255$). The dynamic infusion test is the only available CSF hydrodynamic test where the computation of PVI is independent of ICP. We found a striking decrease of PVI with increasing ICP ($p < 0.00038$) and a logarithmic approximation was most suitable. Despite PVI tending to become lower with increasing Rout, both CSF hydrodynamic values did not correlate ($p = 0.178$).

Recovery Index and PVI did not correlate ($p = 0.860$), but after dichotomizing the clinical outcome (Responder vs. Non-Responder) the shunt responder rate was clearly higher in patients with PVI below both examined thresholds (<22, <30 ml) than in patients with higher PVI levels ($p = 0.042$, $p = 0.014$).

Overall, at a critical level of 30 and 22 ml, 19 and 45 patients would have not been shunted if PVI alone would have been used for shunt indication. Yet 52% and 67%, of these patients, who would have been not shunted if PVI would have been used for shunt indication presented with substantial clinical benefit (Table 1).

Predictive Value of Combined Consideration of Both CSF Hydrodynamic Parameters

These figures clearly demonstrate that a non-negligible number of patients, who might have benefited from shunting, would be lost using solely Rout or PVI for shunt candidate selection. We accordingly analyzed whether a combined consideration of both hydrodynamic parameters provides a more precise outcome prediction. At different critical values (Rout > 13 or >18 mm Hg/ml × min, PVI < 22 or <30 ml), all given combinations have been calculated for their predictive potency using logical “AND” and logical “OR” combinations. Rout at a critical value of >13 mm Hg/ml × min and PVI at a critical value <30 ml, together with a logical “OR” combination, clearly provides the best outcome prediction (Table 1). Out of all combinations, this was the only one with an accuracy >90% at excellent sensitivity, with PPV and NPV each exceeding 90%; only specificity was a bit lower.

Discussion

Recently flow-sensitive sequences of MRI have provided new in vivo findings of intracranial CSF flow dynamics in hydrocephalic patients, which gave reason for a new hypothesis of hydrocephalus pathophysiology (1–3, 12). In brief, the key issues of this new hypothesis are as follows: at reduced **craniospinal compliance** the systolic capacitive “storage of blood” in the large arteries of the Circulus Willisii is hindered and the phenomenon known as the “Windkessel” effect does not function properly. *We, however, propose to consider arterial atherosclerosis, which is prevalent in more than 50% of patients shunted for iNPH (4), as an additional scenario impairing the Windkessel effect, but necessitating non-lowered cranio-spinal Compliance (C) initially.* One consequence of the impaired Windkessel effect is a lack of diastolic blood flow and subsequent cerebral ischemia. More importantly however, systolic blood pressure peaks are not dampened

but transferred to the cerebral capillaries; on the one hand affecting the balance of pre- and postcapillary fluid exchange between parenchyma and vessels and on the other hand inducing stronger brain pulsation. The role of CSF absorption in cerebral tissue has been widely debated, especially in hydrocephalus. Given that the pia and ependyma do not hinder free fluid exchange between brain and surrounding CSF spaces, elevated intracapillary pressure increases fluid secretion but reduces fluid reabsorption. The latter must increase R_{out} , which must not against this background be the primarily disturbed CSF hydrodynamic parameter. The amplified pulsating brain hits incompressible CSF on its inner and outer surface, which, at the given frequency of pulsation, cannot be compensated for by CSF evasion. Pascal's and Laplace's laws explain that the inner (periventricular) brain surface is exposed to higher forces than the outer brain surface. In this way, even in communicating hydrocephalus, brain destruction must be more distinct periventricularly. Moreover the intraluminal pressure of superficial in contrast to deep brain veins is closely coupled to ICP and craniospinal compliance. This damps the consequences of amplified brain pulsation (brain destruction) because compliance of the outer brain parenchyma increases in this way. In contrast, the periventricular brain areas become destructed significantly because the periventricular compliance decreases strikingly due to the fact that the lacking coupling of its venous intraluminal pressure to ICP effectuating that inner brain veins are squeezed out with increased ICP. Yet intraparenchymal veins' dimension strikingly affect local compliance.

The weaknesses of R_{out} and many other ancillary tests used for shunt indication were typically its low NPV and its low specificity, and their meaning for shunt indication is accordingly a matter of ongoing debate (5, 6, 8, 9, 11, 13, 15, 19, 20). Supposing that the hypothesis of the role of compliance for hydrocephalus pathophysiology holds true, outcome prediction should benefit from additional attention to compliance / PVI. However, regarding Table 1, PVI alone does not allow a more precise outcome prediction and exhibits similar weakness as R_{out} with low specificity and low

NPV. However, when regarding either $R_{out} > 13 \text{ mm Hg/ml} \times \text{min}$ "OR" $PVI < 30 \text{ ml}$ as predictors, the predictive value of CSF hydrodynamics become significantly better (Fig. 1) with accuracy, sensitivity and PPV $> 90\%$, together with specificity and NPV at 74% and 78%, respectively.

We have stressed that hydrocephalus due to Windkessel impairment can occur without lowered cranio-spinal compliance due to atherosclerosis, especially when regarding the coincidence of iNPH and subcortical atherosclerotic encephalopathy (SAE) (4, 5, 18). Windkessel impairment alone is sufficient to elevate R_{out} in this way. Furthermore, it must be kept in mind that hydrocephalus itself, but especially the high prevalence of Alzheimer's disease (AD) and/or SAE in chronic hydrocephalus (4), induces brain involution with a concomitant increase of compliance and PVI. Therefore, it is not reasonable to assume that chronic hydrocephalic patients must present with pathologically low compliance always, but that even normal compliance can be pathological in chronic hydrocephalus. Accordingly, we found the best predictive power when using a PVI threshold of 30 ml.

During early stage hydrocephalus, PVI can be reduced significantly even before a significant increase of R_{out} can be measured. In our cohort, patients with this constellation were 92% successfully shunted. These patients would have been lost when using R_{out} alone for shunt indication. The vast majority of patients (63%) however had, as predicted by the model, elevated R_{out} and $PVI < 30 \text{ ml}$ at an excellent shunt response rate of 98%. The third group, whose outcome (shunt response rate: 8%) also fit excellently to the proposed model, consisted of patients with $PVI > 30 \text{ ml}$ and low R_{out} . SAE or AD were probably chiefly responsible for their worsening with hydrocephalus playing a subordinated role, if at all. Most difficulties from the perspective of outcome prediction exist in patients with elevated R_{out} , but high PVI ($> 30 \text{ ml}$). The high compliance points at substantial brain involution which may be a consequence of AD, SAE or extremely long persistent hydrocephalus, while R_{out} elevation may be maintained by arterial arteriosclerosis only. Any of these preconditions indicates worse

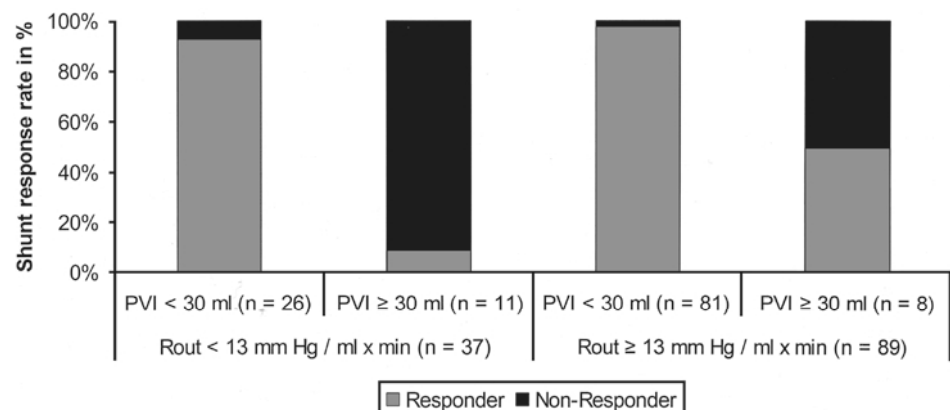


Fig. 1 Shunt response rate depends on measured PVI and R_{out} at the most promising thresholds

prognosis for shunt success; yet half of these patients experienced clinical improvement after shunting leaving some question with regard on the supposed pathophysiological model.

From our perspective, our clinical data substantiates the concept of compliance reduction in hydrocephalus pathophysiology. It has to be emphasized, however, that compliance reduction may be present exclusively during very early stages of hydrocephalus evolution. Compliance increase is an inescapable consequence of persisting hydrocephalus or may come from concomitant atrophic brain diseases (4). Further-more, the proposed model should also consider Windkessel breakdown independent of cranio-spinal compliance reduction due to arterial arteriosclerosis.

Our comparatively high shunt response rate, especially in iNPH (5, 13, 21), does not advocate the superiority of long-term ICP monitoring and B-wave analysis even if, as in this study, automated B-wave detection may be helpful (14). Rather, our strict preselection according to the patients' clinical state and comorbidity (18) and the fact that our complication rate decreased dramatically with the usage of gravitational shunt (17, 21) and antibiotic impregnated shunt catheters (10) in these fragile patients may be responsible for our, – compared with the literature, – high shunt responder rate.

Conclusion

Outcome prediction in chronic hydrocephalus can be significantly improved when considering both compliance and Rout. This may substantiate an important role of initially decreased compliance during hydrocephalus evolution. Further studies with a larger number of patients with critical CSF hydrodynamic pattern of $R_{out} < 13 \text{ mm Hg/ml} \times \text{min}$ and $PVI < 30 \text{ ml}$ or $R_{out} > 13 \text{ mm Hg/ml} \times \text{min}$ and $PVI > 30 \text{ ml}$ will be necessary for sufficient scientific rigor.

Conflict of interest statement Dr.Kiefer has received some honoraria from Aesculap-Miethke and Codman to speak about hydrocephalus. Issues of this study were not involved.

References

- Bateman GA (2000) Vascular compliance in normal pressure hydrocephalus. *Am J Neuroradiol* 21:1574–1585
- Bateman GA (2002) Pulse-wave encephalopathy: a comparative study of the hydrodynamics of leukoaraiosis and normal pressure hydrocephalus. *Neuroradiology* 44:740–748
- Bateman GA, Levi CR, Schofield P, Wang Y, Lovett EC (2008) The venous manifestations of pulse wave encephalopathy: windkessel dysfunction in normal aging and senile dementia. *Neuroradiology* 50(6):491–497
- Bech-Azeddine R, Høgh P, Juhler M, Gjerris F, Waldemar G (2007) Idiopathic normal pressure hydrocephalus: clinical comorbidity correlated with cerebral biopsy findings and outcome of cerebrospinal fluid shunting. *J Neurol Neurosurg Psychiatry* 78:157–161
- Boon AJ, Tans JTT, Delwel EJ, Egeler-Peerdeman SM, Hanlo PW, Wurzer HAL, Hermans J (1999) Dutch normal-pressure hydrocephalus study: the role of cerebrovascular disease. *J Neurosurg* 90:221–226
- Borgesen SE, Gjerris F (1982) The predictive value of conductance to outflow of CSF in normal pressure hydrocephalus. *Brain* 105:65–86
- Bret P, Chazal J (1990) L'hydrocéphalie chronique de l'adult. *Neurochirurgie (Suppl)* 36:1–159
- Costabile G, Probst C (1993) Hydrocephalus – analysis of 480 infusion tests. In: Avezaat CJJ, van Eijndhoven JHM, Maas AIR, Tans JTT (eds) *Intracranial Pressure VIII*. Springer, Berlin, Heidelberg, New York, pp 805–810
- Delwel EJ, De Jong DA, Avezaat CJJ (1993) The relative prognostic value of CSF outflow resistance measurement in shunting for normal pressure hydrocephalus. In: Avezaat CJJ, van Eijndhoven JHM, Maas AIR, Tans JTT (eds) *Intracranial pressure VIII*. Springer, Berlin, Heidelberg, New York:816–820
- Eymann R, Chehab S, Strowitzki M, Steudel WI, Kiefer M (2008) Clinical and economical consequences of antibiotic impregnated shunt catheters. *J Neurosurg* 1(6):444–450
- Gjerris F, Borgesen SE (1992) Current concepts of measurement of cerebrospinal fluid absorption and biomechanics of hydrocephalus. In: Symon L, Calliauw L, Cohadon F, Lobo J, Loew F, Nornes H, Pásztor E, Pickard JD, Strong AJ, Yasargil MG (eds) *Advances and Technical Standards in Neurosurgery, Volume 19*. Springer, Wien-New York, pp 145–177
- Greitz D (2004) Radiological assessment of hydrocephalus: new theories and implications for therapy. *Neurosurg Rev* 27:145–165
- Hebb AO, Cusimano MD (2001) Idiopathic normal pressure hydrocephalus: a systematic review of diagnosis and outcome. *Neurosurgery* 49:1166–1186
- Jetzki S, Kiefer M, Eymann R, Walter M, Leonhardt S (2007) Analysis of pulse waves in intracranial pressure. *Conf Proc IEEE Eng Med Biol Soc* 2007:2863–2866
- Kahlon B, Sundbarg G, Rehnrcrona S (2002) Comparison between the lumbar infusion test and CSF tap tests to predict outcome after shunt surgery in suspected normal pressure hydrocephalus. *J Neurol Neurosurg Psychiatry* 73:721–726
- Kiefer M, Eymann R, Steudel WI (2000) The dynamic infusion test in rats. *Childs Nerv Syst* 16:451–456
- Kiefer M, Eymann R, Meier U (2002) Five years experience with gravitational shunts in chronic hydrocephalus of adults. *Acta Neurochir (Wien)* 144:755–767
- Kiefer M, Eymann R, Steudel WI (2006) Outcome predictors for normal-pressure hydrocephalus. *Acta Neurochir Suppl* 96:364–367
- Kosteljanetz M, Westergaard L, Kaalund J, Nehen AM (1989) The significance of outflow resistance measurements in the prediction of outcome after CSF-shunting in patients with normal pressure hydrocephalus. In: Hoff JT, Betz AL (eds) *Intracranial pressure VII*. Springer, Berlin, Heidelberg, New York, pp 383–385
- Malm J, Kristensen B, Karlsson T, Fagerlund M, Elfverson J, Ekstedt J (1995) The predictive value of cerebrospinal fluid dynamic tests in patients with idiopathic adult hydrocephalus syndrome. *Arch Neurol* 52:783–789
- Meier U, Kiefer M, Neumann U, Lemcke J (2006) On the optimal opening pressure of hydrostatic valves in cases of idiopathic normal-pressure hydrocephalus: a prospective randomized study with 123 patients. *Acta Neurochir Suppl* 96:358–363

An Algorithm to Assess the Rehabilitation Potential in Patients with Chronic Hydrocephalus

Michael Kiefer and Regina Eymann

Abstract

Objective In clinical practice, it is often necessary to judge the probability of clinical benefit of invasive ancillary tests given to patients with chronic hydrocephalus before they are performed. The aim of the current study was to establish a screening tool for such prediction.

Material and Methods A total of 125 patients with chronic hydrocephalus were assessed using a clinical (HHS) and comorbidity (CMI) grading. These patients were shunted and followed-up for at least one year. The statistical tools of ANOVA, CHI-squared, Spearman, Kuskal–Wallis, and Wilcoxon-U-Test were applied.

Results The variables discovered to be of use in prediction were age ($p=0.02$), anamnesis duration ($p=0.04$), CMI ($p<0.000$) and HHS ($p=0.001$). A decision tree using solely HHS and CMI was established allowing outcome prediction of sufficient power. Interestingly, in patients who had favourable preconditions, older age impeded not a favourable prognosis.

Conclusion With our proposed decision tree, a minimum of data allow a clinician to sufficiently judge whether shunting will be of benefit to a patient, which may help to decide whether invasive ancillary tests are justified.

Keywords Hydrocephalus • iNPH • shunt • outcome • comorbidity • clinical state • age

Introduction

Patients suffering from chronic hydrocephalus such as idiopathic normal pressure hydrocephalus (iNPH) typically ask for the chance to benefit from shunting before agreeing to the ancillary invasive tests that may be necessary for shunt indication in some. Yet a precise predictions of the patient's rehabilitation potency might be impossible without invasive measures. With this background the therapist's challenge is to find a balance between the risks of ancillary tests on the one hand and on the other hand a reliable answer on the patient's question of his/her individual capacity for rehabilitation after shunting. All invasive measures (e.g., tap tests and CSF-hydrodynamic tests) have non-negligible complication rates. Recently, a 3.6% infection rate and even one fatal case in 419 patients who underwent prolonged tap tests were reported (9). Other invasive tests such as CSF hydrodynamic tests, long-term ICP monitoring or simple diagnostic lumbar punctures have some complicated risks too (1, 20). The appraisal of shunt success solely by clinical symptoms typically allows correct predictions in about 50% of patients yet (16). Therefore, we aimed to establish an algorithm that allows a more precise outcome prediction from the assessment of clinical symptoms alone without the need of invasive measures.

Material and Methods

A total of 125 adult patients suffering from iNPH ($n=87$; mean age 67 ± 16 years), secondary normal pressure hydrocephalus (sNPH) ($n=15$; mean age 63 ± 18 years), and non-communicating hydrocephalus ($n=23$; mean age 49 ± 14 years) were studied for at least one year after shunting. Patients with sNPH whose hydrocephalus related symptoms dominated were excluded from the study. Similarly, patients with tumor-associated, non-communicating hydrocephalus were excluded. Shunt indication was based on CSF hydrodynamic

M. Kiefer (✉) and R. Eymann
Department of Neurosurgery, Saarland University Medical School,
Kirrberger Street, Building: 90.1, Homburg-Saar 66421, Germany
e-mail: Michael.Kiefer@uks.eu

R. Eymann
Department of Neurosurgery, Medical School, Saarland University,
Kirrberger Street, Building 90, Homburg-Saar, Saarland 66421,
Germany

studies and B-wave analysis. B-wave patterns were considered as pathological if B-waves occurred minimally during 50% of the total monitoring time (between 48 and 72 h) and if B-waves had large amplitudes (>10 mm Hg) during 20% of the monitored period. The cutoff level for pathological resistance to outflow (Rout) to indicate shunting was 13 mm Hg/ml×min. Patients fulfilling minimally one criterion (increased Rout or pathological B-wave pattern) were shunted using adjustable or non-adjustable gravitational shunts. For clinical documentation, we used our modified clinical grading (HHS), Recovery-Index (RI) and Co-Morbidity-Index (CMI) (11). Patients were regarded as shunt responders if RI≥3 and/or if (provided given handicap preoperatively) they improved by 2 points or more in the “gait/balance” area of HHS postoperatively. To rule out primary or secondary underdrainage, we used the protocol proposed in the international guidelines (12), with the exception that our first step of the workflow is an “acetazolamide” test (6). If patients improved with acetazolamide, they were diagnosed as underdrained, and shunt revision was performed. Shunt revision due to underdrainage or other hydraulic mismanagement was not an exclusion criterion, but the clinical state at least one year after successful shunt revision was used for analysis. Only when underdrainage was definitively excluded as the reason for lacking improvement after shunting, the patients were considered “non-responders”. Clinical state evaluation and imaging were performed preoperatively, 3 and 12 months postoperatively, and annually thereafter. Patients lacking follow-up for longer than 14 months were excluded as well as patients who refused check-up and patients who had shunt-infections (because shunt infection may affect the patient outcome by itself). In this cohort, the average follow-up was 2.9 ± 1.6 years (range: 1–4 years). The clinical state of the patients at that point in time was considered as the last data point used in this analysis.

The statistics that were employed to evaluate the clinical data included the Mann–Whitney U, Spearman, Kruskal–Wallis, ANOVA and χ^2 -tests at a significance level of $p < 0.05$.

Results

The overall shunt responder rate was 79%. Clear differences between the responder rates of iNPH, sNPH and non-communicating hydrocephalus patients (77%, 83% and 87%, respectively) were not evident. The symptoms of Hakim’s triad that improved included gait/balance disturbance with an overall improvement rate of 78%, followed by a 63% improvement rate of mental disturbance and a 59% improvement rate of incontinence (Fig. 1). While there were no differences in the improvement rates of gait/balance, mental disturbances and incontinence between the examined three hydrocephalus etiologies, the overall improvement rate of gait/balance was clearly better than incontinence and mental impairment recovery ($p < 0.00035$; $p = 0.031$). Interestingly, the preoperative preconditions (age, anamnesis duration, HHS, CMI) of all three examined hydrocephalus etiologies did not differ significantly, which might explain why clinical outcome differences could not be found between the different etiologies. Overall, older age, longer anamnesis, worse CMI or worse HHS worsened the patient outcome significantly ($p = 0.026$, $p = 0.021$, $p < 0.000$, and $p = 0.002$). In this analysis, we specifically analyzed the predictive value of gait/balance disturbances. A weak correlation was found between the preoperatively assigned “raw” points for gait/balance disturbances with RI or shunt responder rate ($p = 0.046$ and $p = 0.042$). However there was a strong correlation between the quotient of points assigned for gait/balance disturbances and the sum of points

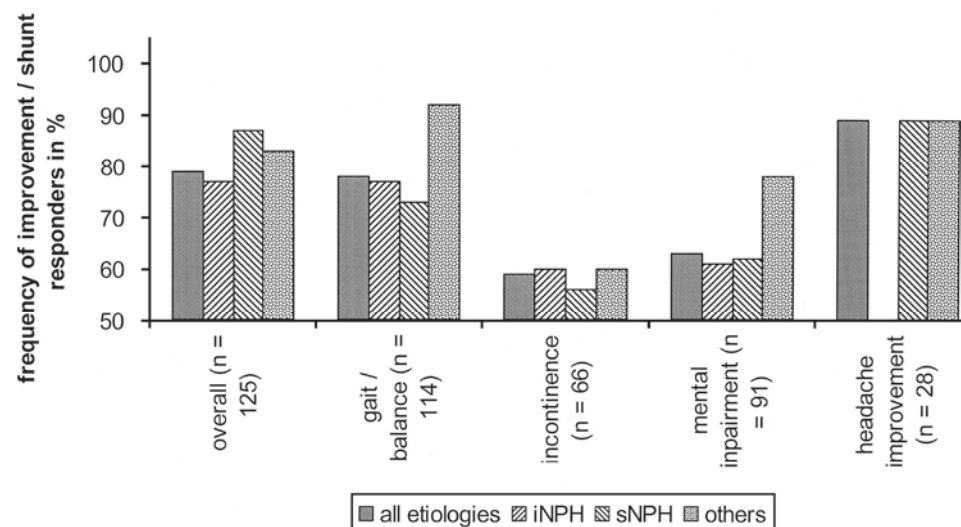


Fig. 1 Overall improvement separated based upon the symptoms of all patients and separated based on the studied hydrocephalus etiologies

evaluated in all five items of HHS grading compared with RI or shunt responder rate ($p=0.001$ and $p<0.000$). We named this quotient the “predictive value of gait” (PVG). We analyzed whether these influencing values (age, anamnesis duration, CMI, HHS, PVG) are independent outcome predictors and found that only CMI and PVG were independent outcome predictors ($p<0.000$ for both). The independent outcome prediction of HHS was still significant but at a weak level ($p=0.048$). Accordingly, it was only reasonable to look for thresholds in these three outcome predictors that might serve to separate favourable (responder) and unfavourable (non-responder) outcomes. The critical values for CMI, HHS and

PVG were found to be 3 points, 5 points and 0.5 points, respectively. Patients with higher CMI, HHS or lower PVG values had worse outcomes (Fig. 2; $p<0.000$, $p=0.008$, and $p<0.000$). Based upon this evaluation, it was possible to establish a decision algorithm (Fig. 3). This decision tree had very accurate prediction of shunt responders. Given a patient with low CMI and low HHS for whom the product of both does not exceed 11 with a clinical state that is dominated by gait/balance disturbances and an according $PVG \geq 0.5$, his or her shunt success rate will be about 97%, and the accuracy of this statement is about 92%. If the patient’s product of CMI and HHS values exceeds 11, while his or her CMI is >3 points,

Fig. 2 Shunt responder rates at given clinical states graded with HHS and CMI. It is obvious that worse preconditions have lower shunt responder rates

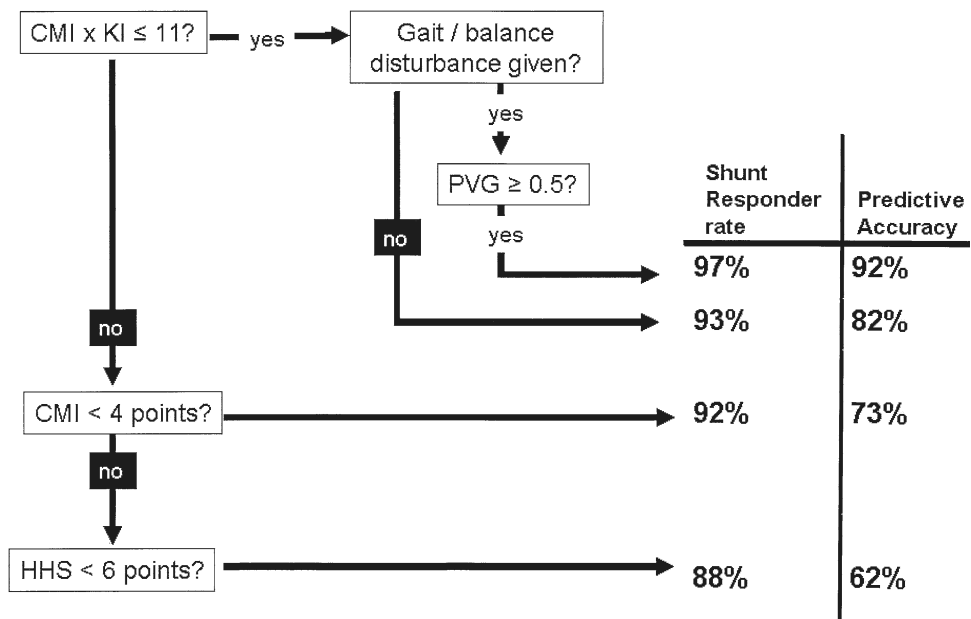
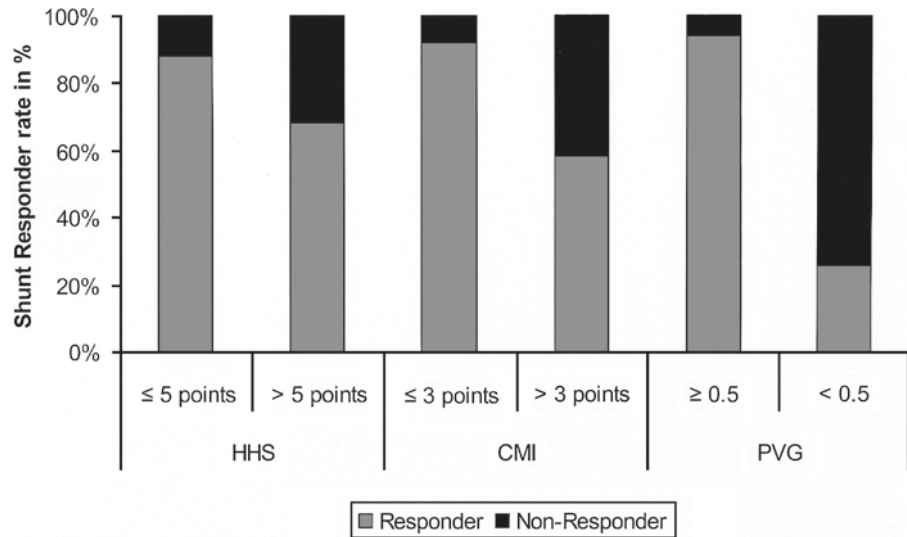


Fig. 3 Algorithm to judge whether patients will benefit from shunting. This algorithm utilizes the clinical gradings of CMI and HHS. The precision of outcome prediction is also indicated. If patients have preconditions that do not fit the criteria in the algorithm, their chance of shunt response is about 60%

and his or her HHS is ≤ 5 points but gait/balance disturbances lack, the shunt responder rate can be still high (88%), but the accuracy of this prediction is only at 62%.

Discussion

These data underline our and others' earlier findings of the outstanding importance of comorbidity for the rehabilitation potential of chronic hydrocephalus (especially for iNPH) (5, 8, 10, 13). Similarly, as in a previous study, we confirmed that older age and a longer anamnesis may worsen clinical outcomes (4, 11, 17, 18). The fact that we did not find significantly different shunt responder rates between iNPH, sNPH and non-communicating hydrocephalus may be due to the fact that the number of patients of each hydrocephalus etiology is quite different and accordingly not valid for outcome comparison.

This study also confirmed earlier findings that stated that patients with predominant gait disturbances had the best prognosis to recover, while patients with symptoms of incontinence and mental disturbances which dominate clinical appearance are less likely to improve after shunting (2, 3, 7, 10, 14, 15, 19, 21).

This knowledge was the basis for our creation of the predictive value of gait (PVG), and we have shown that there is an excellent recovery rate in patients who have mainly gait disturbances in contrast to patients with other symptoms (mental dysfunction, incontinence). PVG provides a useful extension of HHS grading to demonstrate the predominance of gait disturbance.

Against this background, we developed an algorithm that predicts the probability of successful shunting using HHS, CMI and PVG values as inputs. Depending on the patients' individual clinical state, shunt responder rates greater than 90% can be expected with high accuracy (62–92%). With this algorithm, the outcome of patients with good clinical preconditions (HHS ≤ 5 points, CMI ≤ 3 points, and PVG ≥ 0.5) can be assessed with high accuracy. Patients in worse clinical states have significantly lower chances to benefit from shunting (about 60%), but the predictive accuracy is very low too. Studies of more patients who have such worse clinical preconditions will be necessary to establish a useful algorithm extension allowing precise outcome prediction in these patients at worse preconditions too. Yet ancillary tests are necessary in this subgroup.

Conclusion

Using our clinical and comorbidity grading with a specific focus on gait disturbance, it is possible to predict the probability of successful shunting with high accuracy. The drawback

to our established algorithm is its limited applicability to patients with unfavourable preconditions.

Conflict of interest statement Dr.Kiefer has received some honoraria from Codman and Aesculap to speak about hydrocephalus. Issues of this study were not involved.

References

1. Anderson RC, Kan P, Klimo P, Brockmeyer DL, Walker ML, Kestle JR (2004) Complications of intracranial pressure monitoring in children with head trauma. *J Neurosurg* 101(1 Suppl):53–58
2. Black PM (1980) Idiopathic normal-pressure hydrocephalus. Results of shunting in 62 patients. *J Neurosurg* 52:371–377
3. PMcL B, Ojemann RG, Tzouras A (1985) CSF shunts for dementia, incontinence, and gait disturbance. *Clin Neurosurg* 32:632–651
4. Boon AJ, Tans JT, Delwel EJ, Egeler-Peerdeman SM, Hanlo PW, Wurzer HA, Avezaat CJ, de Jong DA, Gooskens RH, Hermans J (1997) Dutch normal-pressure hydrocephalus study: prediction of outcome after shunting by resistance to outflow of cerebrospinal fluid. *J Neurosurg* 87:687–693
5. Boon AJ, Tans JT, Delwel EJ, Egeler-Peerdeman SM, Hanlo PW, Wurzer HAL, Hermans J (1999) Dutch normal-pressure hydrocephalus study: An evaluation 25 years following the initial description. *Fortschr Neurol Psychiatr* 58:178–190
6. Carrion E, Hertzog JH, Medlock MD, Hauser GJ, Dalton HJ (2001) Use of acetazolamide to decrease cerebrospinal fluid production in chronically ventilated patients with ventriculopleural shunts. *Arch Dis Child* 84:68–71
7. Dauch WA, Zimmermann R (1990) Normal pressure hydrocephalus. An evaluation 25 years following the initial description. *Fortschr Neurol Psychiatr* 58:178–190
8. Graff-Radford NR, Godersky JC, Jones MP (1989) Variables predicting surgical outcome in symptomatic hydrocephalus in the elderly. *Neurology* 39:1601–1604
9. Greenberg BM, Williams MA (2008) Infectious complications of temporary spinal catheter insertion for diagnosis of adult hydrocephalus and idiopathic intracranial hypertension. *Neurosurgery* 62:431–436
10. Hebb AO, Cusimano MD (2001) Idiopathic normal pressure hydrocephalus: a systematic review of diagnosis and outcome. *Neurosurgery* 49:1166–1186
11. Kiefer M, Eymann R, Steudel WI (2006) Outcome predictors for normal-pressure hydrocephalus. *Acta Neurochir Suppl* 96:364–367
12. Klinge P, Marmarou A, Bergsneider M, Relkin N, Black PM (2005) Outcome of shunting in idiopathic normal-pressure hydrocephalus and the value of outcome assessment in shunted patients. *Neurosurgery* 57(3 Suppl):40–52
13. Krauss JK, Regel JP (1997) The predictive value of ventricular CSF removal in normal pressure hydrocephalus. *Neurol Res* 19:357–360
14. Krauss JK, Droste DW, Vach W, Regel JP, Orszagh M, Borremans JJ, Tietz A, Seegers W (1996) Cerebrospinal fluid shunting in idiopathic normal-pressure hydrocephalus of the elderly: effect of periventricular and deep white matter lesions. *Neurosurgery* 39:292–299
15. Krauss JK, Regel JP, Droste DW, Orszagh M, Borremans JJ, Vach W (1997) Movement disorders in adult hydrocephalus. *Mov Disord* 12:53–60
16. Marmarou A, Bergsneider M, Klinge P, Relkin N, Black PM (2005) The value of supplemental prognostic tests for the preoperative assessment of idiopathic normal-pressure hydrocephalus. *Neurosurgery* 57(3 Suppl):17–28
17. Meier U (2004) Predictors of the clinical course of patients with normal-pressure hydrocephalus. *Zentralblt Neurochir* 65:41–48 (in German)

18. Rem JA (1986) Dementia – normal-pressure hydrocephalus. *Schweiz Rundschau Med (Praxis)* 75:569–570 (in German)
19. Savolainen S, Hurskainen H, Paljarvi L, Alafuzoff I, Vapalahti M (2002) Five-years outcome of normal pressure hydrocephalus with and without a shunt: predictive value of the clinical signs, neuropsychological evaluation and infusion test. *Acta Neurochir (Wien)* 144:515–523
20. Sternbach G (1985) Lumbar puncture. *J Emerg Med* 2: 199–203
21. Vanneste J, Augustijn P, Dirven C, Tan WF, Goedhart ZD (1992) Shunting normal-pressure hydrocephalus: do the benefits outweigh the risks? Multicenter study and literature review. *Neurology* 42:54–59

What Can Be Found Inside Shunt Catheters

Z. Czernicki, R. Strzałkowski, N. Walasek, and B. Gajkowska

Abstract Obstruction of shunt catheters is one of the main causes of shunt malfunction. The fragments of shunts removed from five patients were examined using scanning electron microscopy with a (SEM) JEOL JSM-6390 LV microscope. Fifteen catheters from the brain ventricle, lumbar space, and peritoneal space were studied. SEM studies showed that the catheters' surfaces were not sufficiently smooth. The inner surface was often covered by a web of collagen fibrils. Aggregates of red and white blood cells, platelets, lymphocytes, mast cells, and macrophages were trapped in the collagen web. Such cellular aggregates formed a coherent, delicate web mainly consisting of ultrastructurally unchanged cellular elements and were well preserved. Other types of aggregates contained completely destroyed cells that appeared to be submerged in thick collagen web fibrils.

We also found a few ultrastructural abnormalities among morphologically unchanged cellular elements. The presence of abnormal red cells showing unusual variability in their shape and size including spherocytosis (thickened, spheroid, and crenate red cells), elliptocytosis (elongated, rod-shaped,

or tear-drop red cells), the thalassaemic phenotype of red cells (with inclusion of precipitated unstable hemoglobin in the form of Heinz bodies distorting the red cells, leading to their lysis) was a striking finding. Under scanning electron microscopy, we also recognized swollen or crumpled red cells that looked like potato crisps. Aggregation of thickened blood platelets and white cells was observed frequently. Our study confirmed the importance of the smoothness of the inner surface of the catheter. Smoothness can prevent the formation of cell and protein deposits.

Keywords Shunt catheters • hydrocephalus • thrombotic aggregates • scanning electron microscopy

Introduction

Shunt systems are implanted so that they may function for many years. The main problems with these systems are infectious complications and obstructions. In many studies, authors have looked for presence of bacterial and fungal colonization of catheters (1,5,6). However, catheter infection is not the only reason for complications. The malfunction is often caused by catheter obstruction. To date, non-microbiological intracatheter deposits have not been sufficiently studied (2).

Materials and Methods

The morphology of unused and explanted plastic shunt catheters, as well as their interior and exterior spaces in longitudinal and transversal sections, was studied by scanning electron microscopy (SEM). The shunt catheters were fixed in 2.5% glutaraldehyde and 2.0% paraformaldehyde in 0.1 M phosphate-buffered saline (PBS). Fixation was initiated at room temperature, followed by storage in the fixative for 4–7 days at 4°C. The fixed material was washed in this same buffer and post-fixed with 1% OsO₄ in PBS for 30 min. After washing, the catheters were dehydrated using increasing

B. Gajkowska (✉)
Department of Cell Ultrastructure, M. Mossakowski
Medical Research Centre,
Polish Academy of Sciences, 5 Pawinskiego Street,
Warsaw 02-106, Poland and
Department of Cell Ultrastructure, M. Mossakowski
Medical Research Centre,
Polish Academy of Sciences, Warsaw, Poland
e-mail: gajk@cmdik.pan.pl

Z. Czernicki
Department of Neurosurgery, M. Mossakowski
Medical Research Centre,
Polish Academy of Sciences, Warsaw, Poland and
Department of Neurosurgery, Medical Research Center,
Polish Academy of Sciences and Department of Neurosurgery
2nd Faculty of Medicine, Medical University of Warsaw,
Poland

R. Strzałkowski
Department of Cell Ultrastructure, M. Mossakowski
Medical Research Centre,
Polish Academy of Sciences, Warsaw, Poland

N. Walasek
Department of Neurosurgery, M. Mossakowski Medical Research
Centre, Polish Academy of Sciences, Warsaw, Poland

acetone concentrations (30–100%), each step lasting 10 min at room temperature. Afterwards, the catheters were placed in a critical-point drier and thinly coated with gold (Polaron SC 7620). The morphology of the shunt catheters was observed in a JEOL JSM 6390LV scanning electron microscope at 20 kV acceleration voltage.

Results

The inner surfaces of catheters were ragged (Fig. 2, high magnification). These surface irregularities enable the attachment of collagen fibrils and the formation of deposits.

In the present study, fragments of 15 explanted catheters from the brain ventricle, lumbar spaces, and peritoneal spaces of five patients were examined using SEM.

In the interior spaces of catheters on longitudinal and transversal sections we recognized ultrastructurally altered protein deposits (Fig. 1, low magnification) and amorphous aggregates.

High magnification of aggregates revealed variability of their morphology. Some of them were focally attached inside of the catheter's surface and showed aggregates of red and white blood cells, platelets, lymphocytes, macrophages, and mast cells (Fig. 3).

Many ultrastructurally unchanged cellular blood elements were caught in delicate networks consisting of thin fibrin fibers (Figs. 4–6). We also observed another type of aggregate

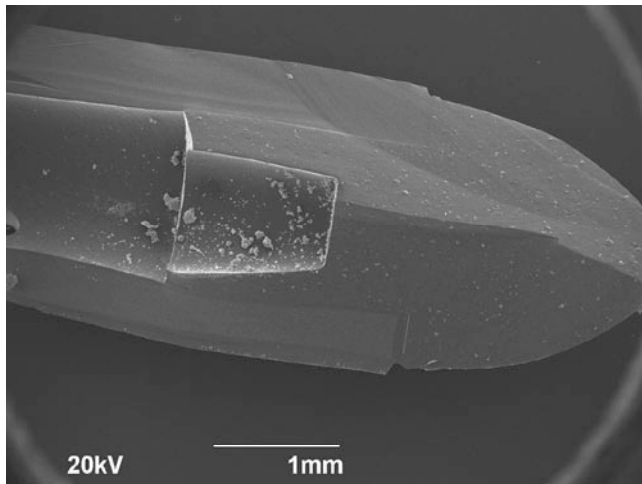


Fig. 1 The inner surface of a used shunt catheter in longitudinal section at a low magnification. Note that the internal surface is covered by aggregates

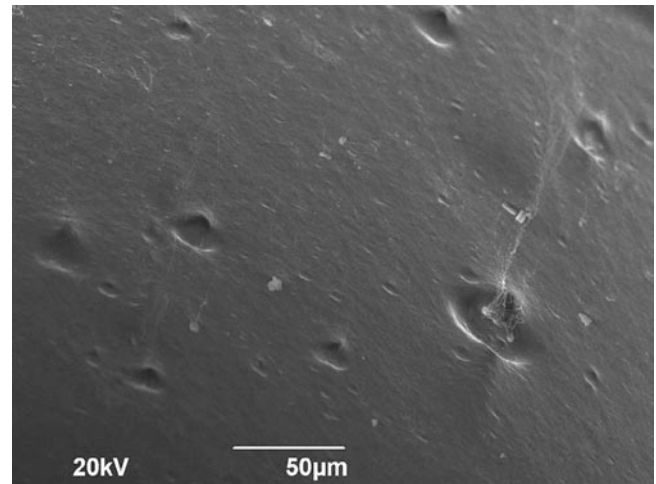


Fig. 2 The inner surface of a shunt catheter

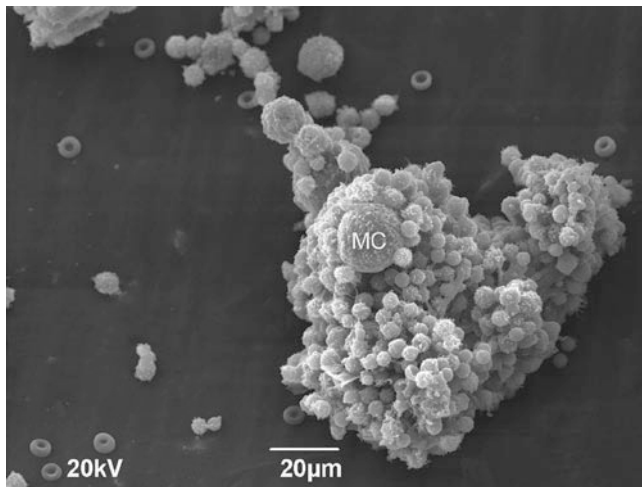


Fig. 3 The aggregate, which is composed of red blood cells, white blood cells, and mast cells (MC)

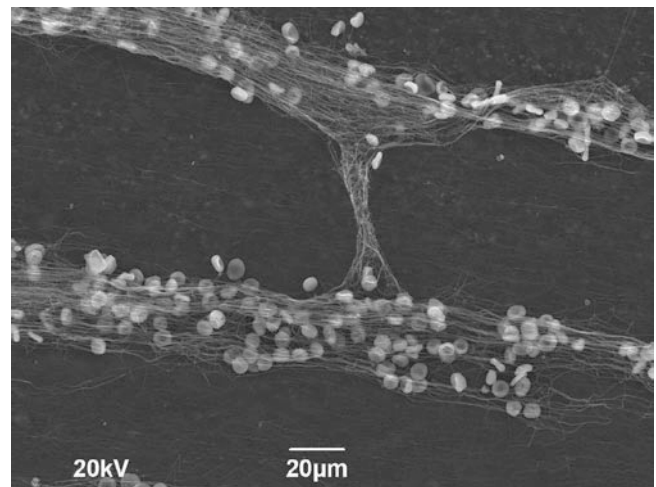


Fig. 4 The ultrastructurally unchanged red blood cell aggregates inside delicate networks of fibrin fibrils

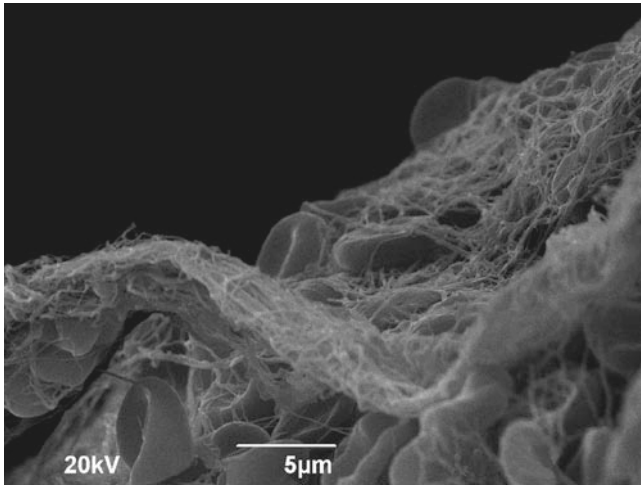


Fig. 5 Red blood cells in mesh fibrin fibrils

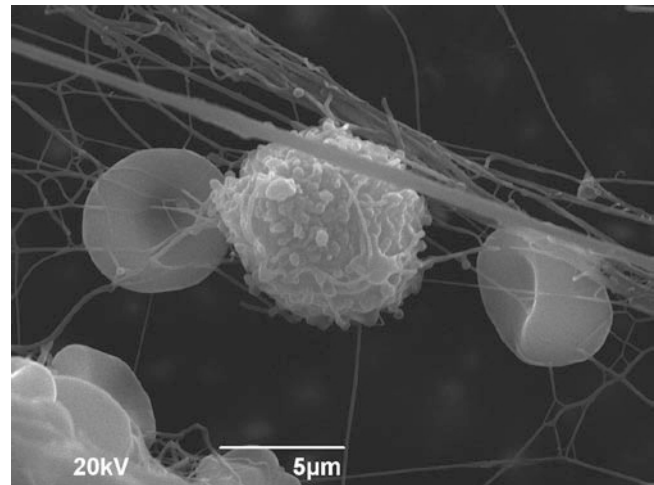


Fig. 6 Higher magnification of two red blood cells and one white blood cell in a network consisting of fibrin and collagen fibrils

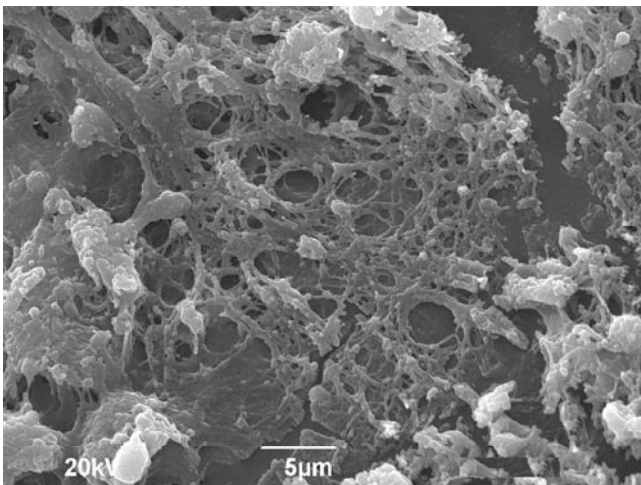


Fig. 7 The aggregate substance, which mainly consists of cell debris, appears to be covered by network bundles of collagen fibrils on the entire surface

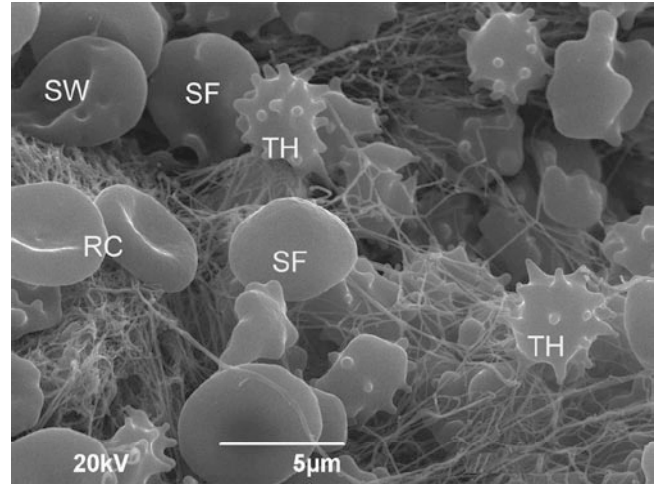


Fig. 8 Among ultrastructurally unchanged red blood cells (RC), which are discs with a concave surface, note the abnormal morphology of red blood cells consistent with thalassaemic (TH) and spherocytosis (SF) phenotypes and swollen red blood cells (SW)

containing completely destroyed cells that appeared to be submerged under thin fibrin fibers and thick collagen fibrils (Fig. 7).

Among the morphologically unchanged red blood cells anchored in webs of fibers, the striking finding was the presence of ultrastructurally changed red cells, which showed unusual variability in their shape and size, including spherocytosis (thickened, spheroid, and crenate red cells) elliptocytosis (elongated, rod-shaped, or tear-drop red cells), the thalassaemic phenotype of red cells (with inclusion of precipitated unstable hemoglobin in the form of Heinz bodies distorting the red cells, leading to their lysis) (Figs. 8 and 9).

Under scanning electron microscopy, we recognized aggregates that also contained mast cells in the process of

degranulation in close contact with white cells (Fig. 10) or large macrophages (Fig. 11). Some of the aggregates were being digested by these macrophages (Fig. 12). Aggregation of thickened blood platelets and white blood cells was frequently observed (Figs. 3 and 8).

Discussion

Further studies of the complex analysis of different catheter types are needed. Of particular interest are the new catheter types, which are covered with an extra smooth layer. Attention should be paid to morphological elements present in the CSF, especially in situations when blood cells can

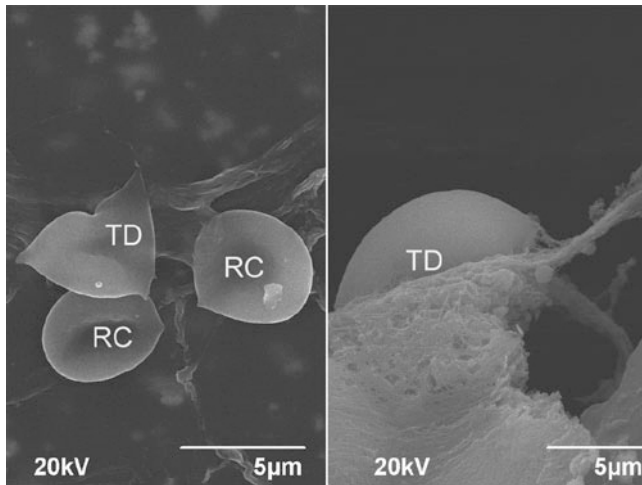


Fig. 9 Normal and elliptocytosis (TD) phenotype of red blood cells (tear-drop red cells)

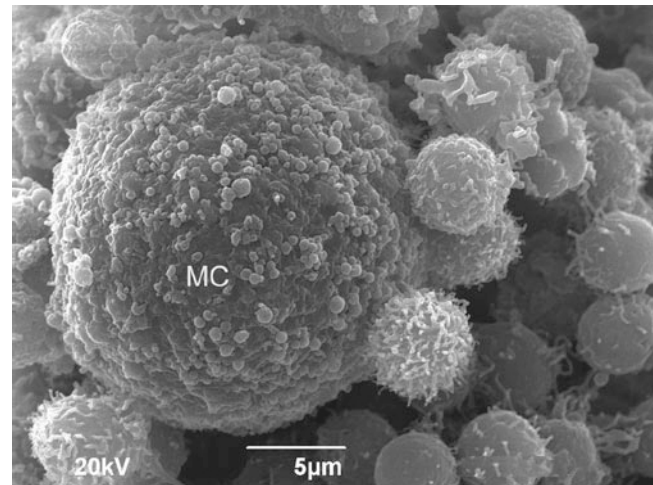


Fig. 10 Aggregate consisting of a mast cell (MC) in the process of degranulation and small white blood cells with other cellular elements attached

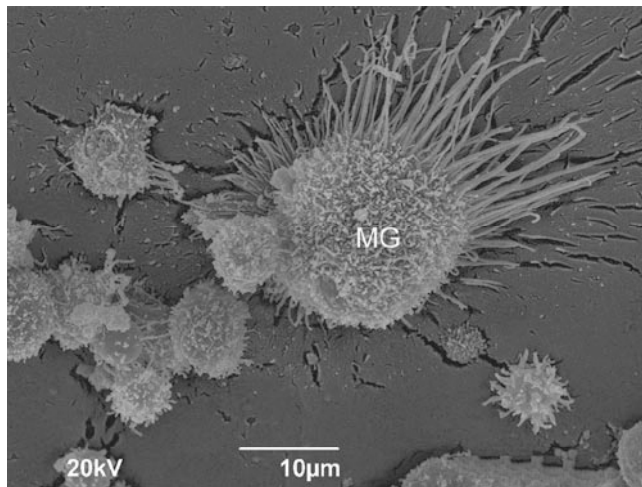


Fig. 11 Large macrophage with long microvilli (MG) corresponding to white blood cell aggregates

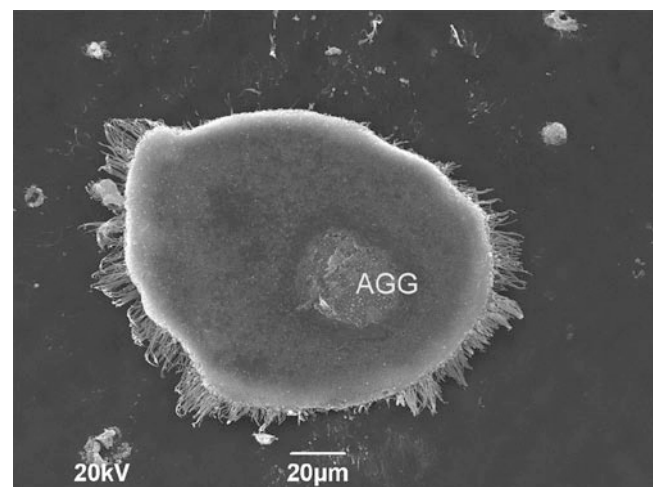


Fig. 12 The picture clearly shows an aggregate/deposit (AGG) being digested by a macrophage

migrate to the CSF. A common problem in shunt-treated patients is shunt malfunction due to system obstruction. The main known causes of obstruction are blood cells and protein deposits. SEM analysis of unused plastic catheters indicated characteristic, fine fissures or notches on their internal and external surfaces. We hypothesize that these fissures were generated mechanically, leading to the attachment of thrombotic aggregates.

The finding of various phenotypes of red blood cells in the catheters' aggregates analyzed by SEM was an important result. Some of these phenotypes, such as the thalassemic phenotype, illustrate a feature of conformational disease (3).

Precipitation of denatured hemoglobin in red cells due to mutations in the globin protein or to unbalanced chain synthesis, as in the common alpha thalassaemias, results in the

aggregation of hemoglobin as discrete inclusion bodies (9). These inclusions distort the cell and lead to a physical loss of membrane and eventually to lysis.

Elliptocytosis is an abnormality of blood characterized by the occurrence of elongated red blood cells, which are mostly represented by elliptic plates and tear-drop red blood cells (7,8).

Red blood cells are also known to be highly sensitive to the osmotic pressure of their medium. In hypertonic situations, they become flattened or crenate, whereas in hypotonic ones they swell into rounded forms (4,8).

In conclusion, SEM analysis of unused and explanted catheters has confirmed the importance of the inner surface of the catheter (dead smoothness) to prevent their malfunction.

Conflict of interest statement We declare that we have no conflict of interest.

References

1. Bayston R, Ashraf W, Bhundia C (2004) Mode of action of an antimicrobial material for use in hydrocephalus shunt. *J Antimicrob Chemother* 53:778–782
2. Brydon HL, Keir G, Thompson EJ, Bayston R, Hayward R, Harkness W (1998) Protein adsorption to hydrocephalus shunt catheters: CSF protein adsorption. *J Neurosurg Neuropsychiatry* 64:643–697
3. Carrell RW (2005) Cell toxicity and conformational disease. *Trends Cell Biol* 15:574–580
4. Clarke JA, Salsbury AJ (1967) Surface ultrastructure of human blood cells. *Nature* 215:402–404
5. Davis LE, Cook G, Costerton W (2002) Biofilm on ventriculoperitoneal shunt tubing as a cause of treatment failure on coccidioidal meningitis. *Research*. 8(4):376–379
6. Kockro RA, Hampl JA, Jansen B, Peters G, Scheiling M, Giaconelli R, Kunze S, Aschoff A (2000) Use of scanning electron microscopy to investigate the prophylactic efficacy of rifampin-impregnated CSF shunt catheters. *J Med Microbiol* 49:441–450
7. Salsbury AJ, Clarke JA (1967) New method for detecting changes in the surface appearance of human red blood cells. *J Clin Pathol* 20:603–610
8. Tokunaga J, Fujita T, Hattori A (1969) Scanning electron microscopy of normal and pathological human erythrocytes. *Arch Histol Jap* 31:21–35
9. Williamson D (1993) The unstable haemoglobins. *Blood Rev* 7:146–163

Glue Instead of Stitches: A Minor Change of the Operative Technique with a Serious Impact on the Shunt Infection Rate

Regina Eymann and Michael Kiefer

Abstract

Introduction Shunt infections are still one of the most important complications of shunt surgery. We observed shunt infections coming from wound breakdown due to minimal CSF leakage from subcutaneous CSF accumulation, which is often unavoidable in babies over the borehole, along the fibers of stitches that close the superficial skin. Whether such secondary shunt infections might be overcome by avoiding stitches has been studied.

Materials and Methods We examined 90 children experiencing their first shunt insertion between September 1998 and April 2008. We divided the children into two groups. Wound closure was performed with absorbable subcutaneous one-on-one sutures with counter-sunk knots in both groups. In one group, octylcyanoacrylate tissue adhesive was used for the final layer closure of the skin (44 children); in the other group, non-absorbable one-on-one single skin sutures were used (46 children).

Results Using the glue, we reduced the wound dehiscence rate from 24% to 2% and the infection rate from 17% to 0%.

Conclusion A minimal change of operative technique substantially affects the shunt infection rate due to the extermination of the “wick-effect” along filaments used to close the skin. Furthermore, Dermabond® itself has a bactericidal effect.

Keywords Hydrocephalus • shunts • children • octylcyanoacrylate tissue adhesive • shunt infection • wound dehiscence • complications

Introduction

Shunt infections are still one of the most important complications of shunt surgery (2). On closer inspection they have to be separated into primary and secondary infections. The latter are caused by wound dehiscence and/or cerebral spinal fluid (CSF) leakage from subcutaneous CSF accumulation along the fibers of sutures. Additionally, sutures may introduce bacteria from the skin into the wound via punctures of the skin that generate a migration path through the skin along which common skin bacteria can migrate (4). Like every foreign material brought into human tissue (e.g., shunt catheters), the surface of the suture material can serve as an opportunistic site for bacterial colonization and potential biofilm cultivation. Shunted patients present optimal conditions for infections, regarding the fact having two foreign materials closely together. Shunt catheter and sutures, which are eventually in direct contact with each other in the subcutaneous tissue, exponentially increase the risks of a shunt infection.

The development of 2-octylcyanoacrylate (Dermabond®, Ethicon, Summerville, NJ, USA) was a new advancement in the wound closure field. This tissue adhesive was introduced in the summer of 1998, and it appears to prevent skin sutures from contacting both CSF accumulations around shunt catheter and the catheter itself. The aim of the prospective study was to find out whether wound closure with octylcyanoacrylate tissue adhesive (ota) is an appropriate method for preventing secondary shunt infections in children.

Materials and Methods

Patient Population, Study Design

We examined 90 children suffering from hydrocephalus who received their first shunt implantation between September 1998 and April 2008, inclusive. The average age of all children at the

R. Eymann (✉)
Department of Neurosurgery, Medical School, Saarland University,
Kirrberger Street, Building 90, Homburg-Saar, Saarland 66421, Germany
e-mail: Regina.Eymann@uks.eu

M. Kiefer
Department of Neurosurgery, Saarland University Medical School,
Kirrberger Street, Building: 90.1, Homburg-Saar 66421, Germany

time of shunt insertion was 9.2 ± 20.2 months (range: 1 day–127 months). We randomly divided the children into a “gluing group” (GG) and a “stitching group” (SG). Each child was arbitrarily assigned to a specific surgeon. One group of surgeons routinely performed gluing of the wound with octylcyanoacrylate tissue adhesive, whereas the other used single skin sutures (sss). Rather than the personal preference of a surgeon, assignment was arbitrarily made to a surgeon with the pre-defined treatment protocol (ota or sss). Quality management examinations revealed no significant shunt infection rate differences between the groups of neurosurgeons over time. Consequently, the final wound closure was performed with gluing in 44 children and suturing in 46 children.

All surgeries were performed by, or under the direction of, one of the pediatric neurosurgeons at a single medical center (Medical school of the Saarland University, Department of Neurosurgery, Homburg-Saar, Germany).

Technique

Surgical procedures were performed in a routine manner with overall three skin incisions in total with any shunt insertion. Skin incisions ranged between 0.5 and 2 cm in size.

In the GG, meticulous closure of the subcutaneous tissue with one-on-one absorbable sutures with a counter-sunk knot was required to achieve appropriate alignment of the final layer of the skin or scalp (Fig. 1). The skin was then dried with a dabber. With the help of fingers or forceps to bring the wound edges close together in a good alignment, the final layer of the skin was closed with octylcyanoacrylate tissue adhesive. After crushing the vial, the adhesive was squeezed to the foam tip. The octylcyanoacrylate tissue adhesive was slightly painted over the apposed wound edges, taking care to prevent the adhesive from running into the depth of the wound. Polymerization of the first layer occurs within 60 s. Second and third layers were made at 30 s intervals. The wound was covered with a soft plaster in order to prevent the child from scraping off the glue. Care was taken not to bring the adhesive of the plaster in contact with the octylcyanoacrylate tissue adhesive.

In the SG, the operation procedure was exactly the same as that in the GG. Subcutaneous absorbable sutures were first inserted in the wound as in the GG. All skin incisions were directly closed with non-absorbable fibers making deep one-on-one skin sutures (Fig. 1). Plaster was stitched onto the wound.

Statistics

For statistical analysis, we used the χ^2 and the Mann–Whitney U tests at a significance level of $\alpha = 0.05$.

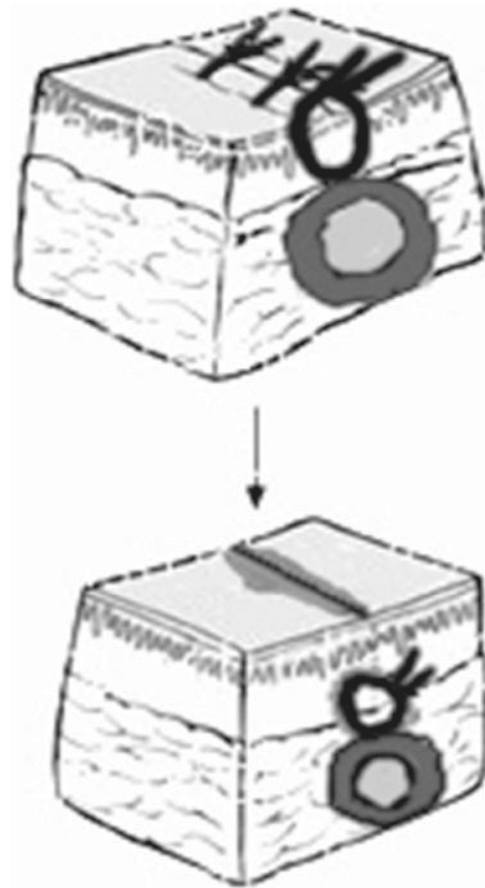


Fig. 1 This figure shows two different methods for wound closing. The *upper drawing* demonstrates the typical suture touching the catheter, whereas the *lower drawing* shows a glued wound without any stitches on the skins surface

Results

The average age of the children in the GG and SG were 7.5 ± 14 months (average values \pm standard deviation) and 10.8 ± 25 months, respectively. Neither the age ($p = 0.641$) nor the body weight ($p = 0.303$; GG 5200 ± 4300 g and SG 6900 ± 7000 g) differed significantly between the two groups at the time of shunt insertion.

We found a significant difference in the rate of wound dehiscence ($p = 0.01$) as well as the consecutive shunt infection rate ($p = 0.05$), which were both worse in the SG. In the GG, there was one dehiscence (2%) of the wound due to the fact that the liquid tissue adhesive had flowed unintentionally between the wound edges into the subcutaneous tissue and impeded normal healing. In this child, no infection occurred (secondary shunt infection rate: 0%). In contrast to the low rate of wound healing complications in the GG, 24% of the children in the SG showed CSF or serous fluid flow through the stitches to the surface of the skin and secondary wound dehiscence (Fig. 2). The wounds involved were located behind the ear in four children, and the frontal scalp wound showed

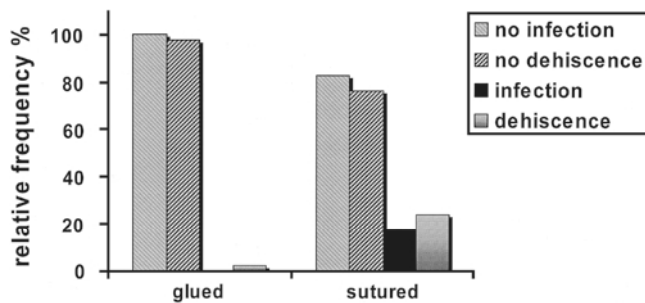


Fig. 2 This figure illustrates the relative frequencies of infection and dehiscence of sutured wounds compared to glued wounds

disturbed healing in four additional children. Eight of the eleven children with a wound healing disorder suffered from a consequent serious shunt infection (17%) with ventriculitis. The causative organisms were coagulase – negative Staphylococci in six cases and Staphylococcus aureus in two cases. The average time until the signs of ventriculitis occurred were 43 ± 34 days (range 10–90 days) after shunt insertion.

Discussion

This analysis is an impressive demonstration of the benefits of using a tissue adhesive instead of single skin sutures for wound healing. The secondary shunt infection rate was reduced from 17% to 0%, and the frequency of wound healing disorders was lowered from 24% to 2%. Wound healing of the skin provides especially challenging circumstances, due to the foreign body beneath the cutis that is eventually surrounded by a small film of fibrinolytic CSF. It is therefore particularly advantageous in such cases to close the upper layer of the skin with a tissue adhesive. This result contrasts with the previous recommendations from another prospective analysis of wound closure with octylcyanoacrylate tissue adhesive (9) in pediatric neurosurgical procedures (10). In sutured wounds, however, the fiber can act as a wick. Serous fluid of the subcutaneous tissue and CSF that gathers around the catheter is transported to the top of the skin. Moving in the opposite direction, bacteria of the normal skin can negotiate through the whole layer of the skin into the subcutaneous tissue. They may migrate on the surface of the shunt catheter through the epithelizing stitches within days (11). The application of octylcyanoacrylate tissue adhesive eliminates the need for deep skin sutures. Interestingly, Wang demonstrated that CSF leakage can be overcome by reapplication of glue even though this author did not recommend its use. Unlike others (gluing scars) (6,10), we avoided different starting conditions to achieve significant rigor and therefore restricted our study only to children undergoing their first shunt insertion. An additional effect

of octylcyanoacrylate tissue adhesive may arise from its actions as a microbial barrier (1). The only child of our series in whom the glue flowed into the wound did not suffer a wound or shunt infection even though the tissue adhesive was in direct contact with the catheter. In our series, secondary shunt infections after a wound dehiscence in sutured wounds occurred with the bacteria of the normal healthy skin (5). The germs causing the shunt infections were coagulase negative Staphylococci and Staphylococci aureus. Our results demonstrate that these infections probably could have been prevented through the use of an octylcyanoacrylate tissue adhesive instead of deep skin sutures. This is very important with regard to the morbidity following ventriculitis in children, which can cause mental and motor function retardation, the development of seizures (7), and nephritis and intraperitoneal cysts (8). In addition to reducing the expenses (3) due to infection treatments, the use of octylcyanoacrylate tissue adhesive could also have prevented the negative personal consequences for these children.

Conflict of interest statement We declare that we have no conflict of interest. We did not achieve any financial support from Ethicon.

References

- Bhende S, Rothenburger S, Spangler DJ, Dito M (2002) In vitro assessment of microbial barrier properties of Dermabond® topical skin adhesive. *Surg Infect* 3(3):251–257
- Enger P, Svendsen F, Wester K (2003) CSF shunt infections in children: experiences from a population-based study. *Acta Neurochirurg (Wien)* 145:243–248
- Eymann R, Chehab S, Strowitzki M, Steudel WI, Kiefer M (2008) Clinical and economical consequences of antibiotic impregnated CSF shunt catheters. *J Neurosurg* 1(6):444–450
- Ghristina AG, Price JL, Hobgood CD, Webb LX, Costerton JW (1985) Bacterial colonisation of percutaneous sutures. *Surgery* 98(1):12–19
- Kulkarni AV, Drake JM, Lamberti-Pasculli M (2001) Cerebrospinal shunt infection: a prospective study of risk factors. *J Neurosurg* 94:195–201
- Lee KW, Sherwin T, Won DJ (1999) An alternate technique to close neurosurgical incisions using octylcyanoacrylate tissue adhesive. *Pediatr Neurosurg* 31:110–114
- Renier D, Sainte-Rose C, Pierre-Kahn A, Hirsch HF (1988) Prenatal hydrocephalus: outcome and prognosis. *Childs Nerv Syst* 4:213–22
- Roitberg BZ, Tomita T, Mc Lone DG (1998) Abdominal cerebrospinal fluid pseudocyst: a complication of ventriculoperitoneal shunt in children. *Pediatr Neurosurg* 29:267–273
- Singer AJ, Thode HC (2004) A review of the literature on octylcyanoacrylate tissue adhesive. *Am J Surgery* 187:238–248
- Wang MY, Levy ML, Mittler MA, Liu CY, Johnston S, Mc Comb G (1999) A prospective analysis of the use of octylcyanoacrylate tissue adhesive for wound closure in paediatric neurosurgery. *Pediatr Neurosurg* 30:186–188
- Yaron M, Halperin M, Huffer W, Cairns C (1995) Efficacy of tissue glue for laceration repair in an animal model. *Acad Emerg Med* 2:259–263

Animal Experiments to Evaluate Complications of Foreign Materials on Silicone with Shunt Catheters: Preliminary Results

Regina Eymann, Ullrich Meier, and Michael Kiefer

Abstract

Objective Use of silicone to manufacture hydrocephalus shunts has been critical for the successful introduction of modern shunt therapy. However reactions to foreign material cause biodegradation, calcification, and massive scarring, and their impact on the still high shunt failure rate might have been undervalued in the past. We established an animal model to simulate the conditions and reactions with the silicone catheter in human patients.

Methods We implanted catheters from different hydrocephalus shunt manufacturers available on the world market in 12 four-week old Wistar rats. To mimic shearing forces and tensile stress, the tubes were firmly fixed proximally and distally in a growing rat. The catheters remained in the subcutaneous tissue for 1 year before being removed and studied using scanning electron microscopy and histological studies.

Results All of the implanted long catheters showed fractures and calcification on their surfaces, whereas the short fragmented catheters did not.

Conclusion The immunological reactions with silicone and the biodegradation of the material can be simulated in this animal model to study details of the pathophysiology of this process.

Keywords Hydrocephalus • shunt catheter • silicone • immune reaction • complication • biodegradation

R. Eymann (✉)
Department of Neurosurgery, Medical School, Saarland University,
Kirrberger Street, Building 90, Homburg-Saar, Saarland 66421,
Germany
e-mail: Regina.Eymann@uks.eu

M. Ullrich
Department of Neurosurgery, Unfallkrankenhaus Berlin,
Warener Straße 7, Berlin D-12683, Germany
e-mail: ullrich.meier@ukb.de

K. Michael
Department of Neurosurgery, Saarland University Medical School,
Kirrberger Street, Building: 90.1, Homburg-Saar 66421, Germany

Introduction

Use of silicone to manufacture hydrocephalus shunts has been one key to the successful introduction of modern shunt therapy. Although this material is one of the main causes of late shunt complications (1), and despite improvements in materials, devices and surgical techniques, no alternatives to silicone have been identified to this day. Based on series reviews and case reports, it is apparent that late shunt complications arise almost entirely due to problems associated with foreign body reactions on the silicone catheter and/or aging of the shunt material. There are two different types of reactions to silicone shunts: the degradation and mineralization of the catheter by itself and as a consequence to immune reactions several biological reactions.

1. Biodegradation and mineralization of the catheter (5)

- Calcification with fixing scarring (1,10)
- Fractures of the silicon catheter (1)
- Corrosion of the material (1)

2. Potential consecutive biological reactions

- Abdominal cerebrospinal fluid pseudo cysts (3,7,12)
- Atrial thrombosis and cardiopulmonary complications (14,15)
- Perforation of the catheter through the skin and organs such as bowel perforation (9,13)
- Occlusion of the distal and ventricular catheter (4)
- Increasing patients malpositioning during the growth

Biodegradation and mineralization of silicone catheters make shunt revisions necessary, particularly in a growing child (1). As it is located in subcutaneous tissue, the catheter calcifies, resulting in a fixation of the catheter with scars. Therefore, surgeons intention by implanting 50 cm of the catheter length into the intraperitoneal cavity in the hope that the catheter would extricate from the abdomen into the subcutaneous tissue step by step during the patient grows, led as absurdum. We performed an animal study to verify whether immunological reactions in the subcutaneous tissue in combination with calcification and

denaturation of the material in patients, especially in children, can be reproduced in an animal model. The animal experiments were approved by the local ethics committee.

Methods

In a first attempt we implanted various shunt catheters from different manufacturers in 12 anaesthetized rats. All the surgeons wore latex-free gloves during the whole procedure. Anesthesia was initiated with CO₂ inhalation until the rat was asleep, followed by full anesthesia administered intraperitoneally (dosage of 0.1 ml per 100g of bodyweight) using a mixture of 1 ml (RS)-(±)-2-(2-Chlorophenyl)-2-(methylamino)cyclohexane-1-on (Ketavet®) (0,1%) with 0.24 ml 2-(2,6-Dimethylphenylamino)-5,6-dihydro-4H-thiazin (Rompun®) (2%). All catheters inserted are available on the world market and most are typical component parts of the shunt kits. In each 4-week old Wistar rat, one long (6 cm) catheter was implanted subcutaneously on the left side using 5 mm skin incisions on the shoulder and hip. The long catheter was drawn with a pusher through the subcutaneous tissue from incision to incision, imitating the catheter insertion of shunt implantation. Slightly stretching the catheter mimicked the tensile stress during operation. Both ends were fixed to the muscle with a non-absorbable suture. One fixation point was

the shoulder and the other end was sutured to the muscle of the hip on the same side of the body. With this maneuver, the catheter was not stretched, as it lay in the subcutaneous tissue. During the first months of growth, the distance between the shoulder and hip of the rat increases. Thus, the catheter was stretched until the resistance increased and imitation scoliosis of the vertebral column occurred. With this experimental set up, we intended to imitate the angular tensile strength and shearing forces in the flexible subcutaneous tissue of a child. On the reverse side of the animal, three different complementary catheters of 1 cm length were inserted subcutaneously without fixation. Wound closure was performed with octylcyanoacrylate tissue adhesive after subcutaneous reabsorbable one-on-one sutures were performed. All implants remained in the subcutaneous tissue of the rats for 1 year. Rats were then euthanized with Pentobarbital, catheters were removed, and histological and scanning electron microscope (SEM) studies were performed.

Results

No infections occurred in the subcutaneous tissue around the catheters and no wound infections occurred.

All long and short pieces of the catheters were found embedded in membranous tissue.

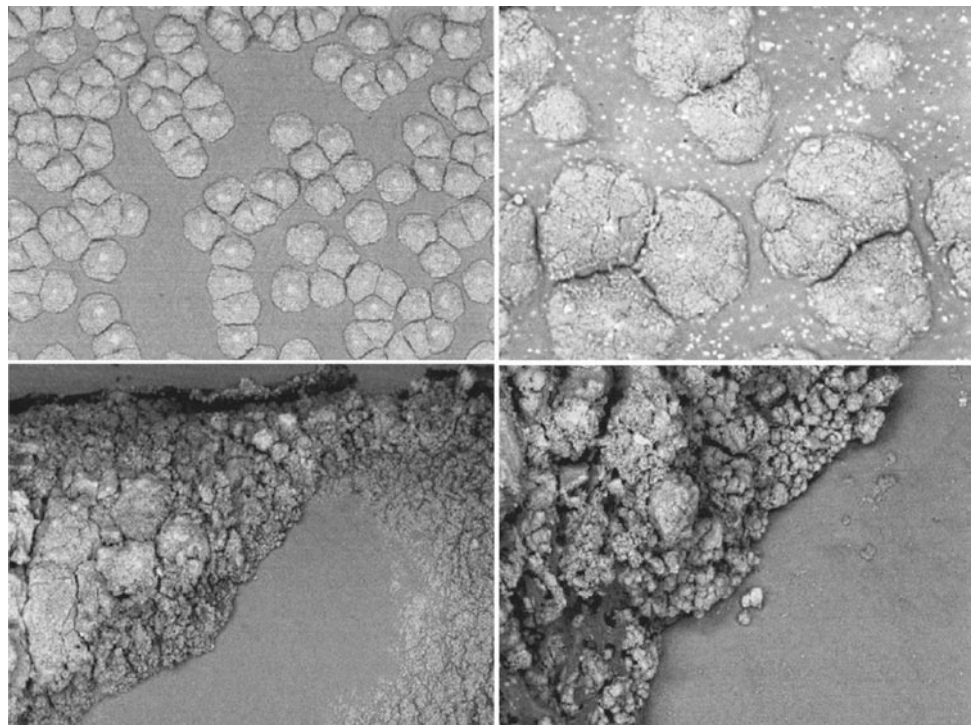
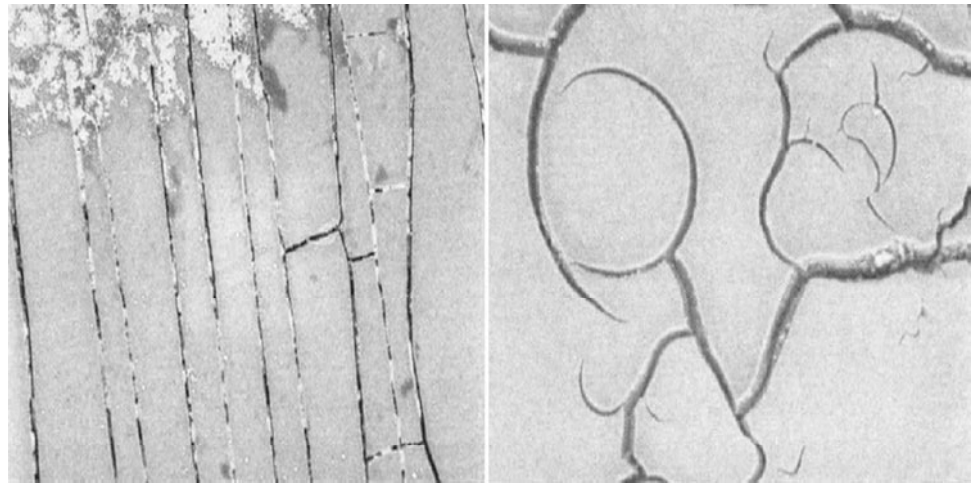


Fig. 1 Calcifications on the surface of long silicone catheters (SEM)

Fig. 2 Fractures and cracks in the surface of the long silicone catheter



- All long catheters showed:
 - Calcifications on the surface area (Fig. 1)
 - Fractures and grooves extending deep into the silicone material (Fig. 2)

One short catheter showed calcification on the surface.

Discussion

This is the first animal model mimicking the in situ situation of the shunt catheter. In particular the tensile strength and shearing forces in the subcutaneous tissue of a growing child, additionally provoked by its movements could be imitated. Fractures of the catheter occurred mainly directly beneath the valve (6,8). In the area of the neck, chest and waist, the catheter is located in flexible subcutaneous tissue. During development and growth of a child, the dimension of movement increases, especially in the region of the neck, so that the catheter is at a higher risk to break. However, increased longevity of the catheter in a biologically active tissue and the consistent biodegradation and calcification additionally increases the risk of fracture (2,8,11). These phenomena interact with each other as calcification and mineralization of the catheter in the subcutaneous tissue stressed with shearing forces due to increasing movement of the child result in scarring and consecutive fixing of the catheter in the tissue, resulting in a vicious circle. About 30% of all shunt revisions are due to catheter problems which arise during growth of a child (1). Indicative therefor is the fact, that all long catheters demonstrated deep cracks and fractures whereas the short, unfixed catheter pieces did not. With this model, further investigations can be performed to study details of the pathophysiology of the immunological processes caused by silicone catheters in soft tissue.

Conflict of interest statement We declare that we received a financial support to realise this study from Raumedic AG.

References

1. Boch AL, Hermelin E, Sainte-Rose C, Sgouros S (1998) Mechanical dysfunction of ventriculoperitoneal shunts caused by calcification of the silicone rubber catheter. *J Neurosurg* 88(6):957–982
2. Couldwell WT, LeMay DR, McComb JG (1996) Experience with use of extended length peritoneal shunt catheters. *J Neurosurg* 85(3):425–427
3. Di Rocco C, Palma P, Pancani S, Velardi F (1993) Postprandial and postural dyspnea a clinical sign of intraperitoneal pseudo cyst in patients with hydrocephalus and ventriculoperitoneal shunt. *Pediatr Med Chir.* 15(2):179–82
4. Del Biogio MR (1998) Biological reactions to cerebrospinal fluid shunt devices: a review of the cellular pathology. *Neurosurgery* 42(2):319–326
5. Echizenya K, Satoh M, Murai H, Ueno H, Abe H, Komai T (1987) Mineralization and biodegradation of CSF shunting systems. *J Neurosurg* 67:584–591
6. Eichler I (1986) Complications following implantation of ventricular-atrial and ventriculoperitoneal shunts. *Zentralbl Neurochir* 47(2): 161–166
7. Hashimoto M, Yokota A, Urasaki E, Tsujigami S, Shimono M (2004) A case of abdominal CSF pseudocyst associated with silicone allergy. *Childs Nerv Syst* 20:761–764
8. Hemmer R (1967) Komplikationen beim atrio-ventrikulären shunt und ihre Vermeidung. *Z Kinderchir* 5:10–24
9. Jimenez DF, Keating R, Goodrich JT (1994) Silicone allergy in ventriculoperitoneal shunts. *Childs Nerv Syst* 10:59–63
10. Kazan S, Acikbas C, Rahat Ö, Tuncer R (2000) Proof of the patent subcutaneous fibrous tract in children with V-P shunt malfunction. *Childs Nerv Syst* 16:351–356
11. Potthoff PC, Wolf J (1985) The transcervical cardiac catheter: the transverse pre-tracheal placement in the treatment of cardiac catheter complications with ventriculo-atrial shunts in infantile hydrocephalus. *Z Kinderchir* 40:323–328
12. Roitberg BZ, Tomita T, Mc Lone DG (1998) Abdominal cerebrospinal fluid pseudocyst: a complication of ventriculoperitoneal shunt in children. *Pediatr Neurosurg* 29:267–273
13. Shanklin DR, Smalley DL (1999) Dynamics of wound healing after silicone device implantation. *Exp Mol Pathol* 67:26–39
14. Sinha RP, Ducker TB (1971) Cardiopulmonary complications of ventriculoatrial shunt in hydrocephalic children. *67(10):421–3*
15. Vernet O, Rilliet B (2001) Late complications of ventriculoatrial ventriculoperitoneal shunts. *The Lancet* 358:1569–1570

Huge Thrombosis as a Consequence of VA-Shunts

Michael Kiefer and Regina Eymann

Abstract

Objective Thrombosis is a rare but serious consequence of VA-shunts. We present two cases of near fatal thrombosis and its successful (but in case 2, atypical) management.

Results Case 1: A 38-year-old woman with VA-shunt suffered from rapidly progressing heart failure and later from progressing underdrainage signs nine years after shunting due to a thrombus on the atrial shunt catheter that occluded >80% of the right atrium. Cardio-surgical removal of thrombus and VA-shunt catheter and VP-shunting normalized neurological and cardiological state. Case 2: A 40-year-old woman received a VA-shunt 5 years before she suddenly suffered dyspnea and venous congestion. Secondly, underdrainage occurred. The underlying huge thrombosis of the superior caval vein could not be excised because the necessary thoracotomy would have interrupted vital venous bypasses along the thoracic wall. Anticoagulants (heparin, cumarin) and ETV relieved all neurological and cardiological symptoms.

Conclusion Sudden or unexpected symptoms of cardiac failure in the presence of a VA-shunt must be recognized as serious. Interestingly, despite distal shunt occlusion, underdrainage symptoms might be initially mild.

Keywords Hydrocephalus • complication • thrombosis • VA-shunt • shunt • side-effects • venous congestion • vena cava syndrome • pulmonary hypertension • foreign material reaction • thromboplastin

Introduction

With the introduction of modern hydrocephalus shunt therapy, the right atrium has been the preferred site for cerebrospinal fluid (CSF) diversion because the initial experiences with ventriculo-peritoneal (VP) shunts were unfavorable (6) (probably due to the materials used (4)). As the incidence of VP-shunt failure dropped with the usage of silicone catheters, VP-shunts became the preferred technique in the 1970s. Some, however, continued to prefer ventriculo-atrial (VA) shunts until the 1990s, when gravitational shunts became available because overdrainage risk was higher with VP-shunts (4, 11, 15–17). However, nowadays, preconditions such as multiple intraperitoneal adhesions after repeated abdominal interventions or intraperitoneal infections or other conditions (1, 12, 27, 28) might force VA-shunting. We report two cases of huge thrombosis due to VA-shunts and its different treatments and discuss as well treatment and prophylaxis options as the still enigmatic incidence and pathophysiology of cardio-pulmonary complications of VA-shunts.

Case Reports

Case 1

A 26-year-old patient with a triventricular hydrocephalus initially had a stereotactically guided third ventriculostomy, followed by VA-shunting some months later due to lack of symptom resolution after ventriculostomy, despite open stoma. After shunting, imaging revealed slit ventricles over several years, but the patient remained asymptomatic. Nine years after shunt insertion, the first signs of shunt dysfunction with fatigue, mental disturbances, and episodes of confusion and symptoms of progressive cardiac failure with dyspnea occurred. Consequently, she lost her job and abandoned all sport activity. However, it was another 3 years before she was admitted to our department with signs of

M. Kiefer (✉)

Department of Neurosurgery, Saarland University Medical School, Kirrberger Street, Building 90.1, Homburg-Saar 66421, Germany
e-mail: Michael.Kiefer@uks.eu

R. Eymann

Department of Neurosurgery, Medical School, Saarland University, Kirrberger Street, Building 90, Homburg-Saar, Saarland 66421, Germany

significant increased intracranial pressure (ICP) (fatigue, headache, mental deficits, and Parinaud's syndrome) and global heart failure (dyspnea while resting in bed). Computer- and magnetresonance-tomography (CCT, MRT) revealed massively enlarged ventricles and periventricular lucencies. Chest X-ray, transthoracic (TTE) and transesophageal (TEE) echocardiography, and thoracic computertomography demonstrated: (1) a partially calcified mass of 4 cm in diameter, which occluded the right atrium by about 80%, in close contact with the distal VA-shunt catheter (Fig. 1), (2) global heart failure with an ejection fraction of 46%, (3) pulmonary hypertension (>50 mm Hg mean pressure), and (4) tricuspid and mitral valve insufficiency. There were no signs of acute or older pulmonary embolism and acute or chronic infections. To overcome ICP crisis, a VP-shunt was inserted, which improved the ICP crisis-related symptoms dramatically. Endoscopic third ventriculostomy (ETV) was abandoned because of the initial failure of third ventriculostomy. In parallel, intravenous antibiotic and heparin treatment was initiated. The calcified mass of the right atrium and the VA-shunt were removed via a transthoracic approach in cardiac arrest using a heart-lung machine. The histological examination of the removed mass confirmed the supposed calcified thrombus with some signs of long-persistent, low-virulent infection. The patient regained complete normalization of her cardiac and mental functions, enabling normal daily activity with sports and full-time employment within 1 year.



Fig. 1 Thoracic computertomography of case 1, demonstrating a mostly calcified mass in the right atrium, which occludes the atrium by minimally 80%. The tip of the VA-shunt ends in this mass. The heart is clearly enlarged

Case 2

A 16-year-old girl was treated in 1982 for aqueduct stenosis with Torkildsen drainage, which resolved hydrocephalus-related symptoms for 17 years, until she presented with Sylvian Aqueduct Syndrome. ETV was refused by the patient and a VP-shunt inserted, which had to be revised multifold within some months due to occluding scars on the distal tip of the peritoneal catheter. A later diagnosed silicone allergy might have been responsible for this. Furthermore, refusing ETV, she was VA-shunted and despite using a gravitational valve, the patient developed asymptomatic slit ventricles. As a medical professional and knowing VA-shunts' thromboembolic complications, she took 100 mg acetylsalicylic acid per day of her own accord. After 6 asymptomatic years, she had a 2 weeks episode of face and neck swelling in 2006. After another asymptomatic interval of 3 months, she suffered again from swelling of the face, neck, and both arms along with tracheal cough. Atypical pneumonia was diagnosed, despite her physician having noted a worse discrimination of the atrial shunt catheter on a chest X-ray. Finally, on admission in our department, she presented with a serious vena cava superior syndrome and moderate dyspnea. The formerly slit-like ventricles were mildly enlarged but shunt failure-related symptoms were lacking. Thoracic CT revealed a vast thrombosis of the complete superior caval vein, which reached into the right atrium, the venae brachiocephalica, azygos (until the confluence with the vena hemiazygos), and the right venae subclavia and jugularis interna, respectively (Fig. 2). The thrombosis was bypassed via the vena hemiazygos (left side) and distended veins on the thoracic wall (right side). The latter prevented thoracotomy for thrombectomy. Accordingly, intravenous heparin and, later, oral cumarin treatment aiming INR-values >3 remained the only therapeutic options. Despite sufficient anticoagulation, the patient suffered within the next 6 months several episodes of pulmonary thromboembolism, which was proved by repeated thoracic CT examinations. TEE demonstrated recurrent free floating thrombi on the distal tip of the VA-shunt as the source of embolism. Signs of shunt failure were lacking until November 2007, when the patient presented with an ICP crisis and significantly enlarged ventricles. Because the thrombosis did not resolve due to the lack of vascular remodeling during the past 1.5 years, the vital venous bypasses on the thoracic wall impeded thrombectomy furthermore and ETV was accepted by her now. After successful ETV, all hydrocephalus-associated symptoms disappeared. It is worth mentioning that there was never an episode indicating shunt or any other generalized infection during the years after VA-shunting.



Fig. 2 Thoracic computed tomography of case 2 after contrast medium application. The most distal intravascular course of the VA-shunt catheter is visible. Contrast medium can be seen in the right Venae jugularis, and subclavia, in the inferior vena cava and all visible parts of the heart. A complete thrombosis of the vena cava superior and aneurysm in the left venae jugularis and subclavia is obvious. Heart has normal dimensions

Discussion

Typical clinical cardiopulmonary, thromboembolic complications of VA-shunts are: (1) thrombosis of the superior and/or inferior vena caval or of the right atrium, (2) acute and/or chronic pulmonary embolism, and (3) pulmonary hypertension (e.g. chronic thromboembolic hypertension (CTEPH)) and its consequence (cor pulmonale).

Frequency

Incidence and prevalence of these complications remain enigmatic. The large discrepancy between the reported clinical prevalence of 0.3% and 50% has become further contrasted by autopsy findings of 60% pulmonary embolism, 34% intracavitary thrombi, and 6% pulmonary hypertension and/or cor pulmonale in VA-shunt carriers (7, 8, 14, 18, 19, 21).

Such contradictory data have been debated as the result of a lack of clinical diagnosis of these complications (3) (due to minor and misleading symptoms) over the years. From our viewpoint, the provided figures of an annual incidence of thromboembolic VA-shunt complications of 0.05% and 0.3% (18, 22, 29) have yet to be substantiated.

Pathophysiology

The roles of preceding shunt infections and foreign material presence in thromboembolic VA-shunt complications have been debated over many years (9, 18, 22). Presently, evidence exists that both are not directly involved in the initiation of complications. *The key to understanding the initiation of complications is that the distal tip of VA-shunts is mobile (in contrast to fixated pacemaker leads, which have a clearly lower potential to provoke similar complications 30) and, accordingly, able to violate the vascular endothelium.* Such violation or any other septic or aseptic inflammation up-regulates *TNF- α* , which initiates *thromboplastin* production in endothelial cells and macrophages. With the next endothelial violation by the catheter, thromboplastin and *F VIIa* induce thrombogenesis by catalyzing the conversion of F X to F Xa. The increased thrombosis risk in growing children when the catheter slips into smaller vessels (23) is not due to a more turbulent blood flow, but due to the higher chance of endothelial violation in smaller vessels. Beside direct involvement in thrombogenesis, thromboplastin and *F VIIa* also play an important role during pulmonary angio-neogenesis, which is a key feature of CTEPH. CSF is, beside endothelial lesions, another important source of thromboplastin in VA-shunts. It is dissolved in CSF in a high concentration (7), especially in slit ventricles, which is consistent with the finding that both presented cases had slit ventricles before they developed thromboembolic complications. Thromboembolic VA-shunt complications can obviously be initiated without any preceding septic event, but the evidence of a specific role of shunt infections for the complications remains impressive as bacterial DNA (restricted to the thrombus solely) was found in 85% of surgically removed thrombi in VA-shunt carriers (3). Bacteria strongly induce *TNF α* production. *TNF α* , however, initiates: (1) endothelial thromboplastin formation, (2) transforming growth factor (*TGF β*) production, and (3) connective tissue growth factor (*CTGF*) production. *TGF β* and *CTGF* hinder thrombolysis and promote thrombus fibrosis. Furthermore, *plasminogen activator inhibitor* and *von Willebrand's factor* are increased in the endothelial layer of septic thrombi, which induce in situ (in the pulmonary artery) thrombogenesis and abnormal local vascular remodeling after

thromboembolism (3), similar to F VIIa and thromboplastin. CTEPH is not, as formerly thought (22), the consequence of recurrent thromboembolic showers and cannot be reproduced in this way in animal models consequently (26). Rather, it is the consequence of abnormal intrinsic dynamics of the pulmonary vessels (13). Staphylococcus aureus infections, as one of the most important sources of primary shunt infection (10), are particularly harmful due to additional serious characteristics: (1) Staphylococcus aureus phagocytosis exterminates macrophages (hindering thrombolysis); (2) the bacteria strongly activate CTGF and TGF β production (protein A on this bacterial surface mimics TNF α) (3).

Some formerly misunderstood phenomena can be understood through the role of infected thrombi in CTEPH pathophysiology. The discrepancy between the prevalence of pulmonary thromboembolism and CTEPH does not result from long-term preceding asymptomatic thromboembolism (21, 22), but from the fact that only a minority of thrombi is infected. Yet, if infected thrombi have reached pulmonary vessels, they promote autonomic CTEPH development, even if the source of thromboembolism and/or infection (VA-shunt) has been removed (21). This might also explain the fact that CTEPH lacks venous thrombosis risk factors (except antiphospholipid antibodies and F VII excesses) and systemic or local defective fibrinolysis.

Clinical Consequences

Contraindications of VA-Shunts

Against this pathophysiological background, VA-shunt carriers are always at an incalculable, - despite low -, risk for thromboembolic complications, justifying recommendations to shunt VA-shunting. However, if a VA-shunt is unavoidable, some relative contraindications must be excluded before VA-shunting: (1) thrombophilia (F V-Leiden, prothrombin mutation G20210A, antiphospholipid syndrome, protein C/S deficiency, antithrombin deficiency, homocysteine increase, F VII increase), (2) thrombophilic treatment (e.g., contraceptive) or unfavourable preconditions (immobility, dehydration, cardiac insufficiency, malignancy), and (3) sleep apnea and Chiari malformation (often associated with sleep apnea). The reason for the relative contraindication of sleep apnea is its pulmonary vasoconstriction, which might worsen an already established CTEPH (2).

Prophylaxis and Therapy

Against this pathophysiology, *platelet aggregation inhibitors* (PAI) are useless for prophylaxis as well as for the treat-

ment of these complications. The normalization of the typically decreased platelets' lifespan (25) in thromboembolic VA-shunt complications by PAI must be regarded as an epiphenomenon. Anticoagulants such as *heparin or cumarin* and concerns about potentially *thrombogenic substances* (e.g., contraceptive) might be justified to prevent aseptic thromboembolic complications (22) in patients at a high risk. In a risk-benefit analysis, the apparently low incidence of such complications, argues against the general lifelong usage of heparin and cumarin in all VA-shunt carriers. For therapy of thromboembolic VA-shunt complications, both substances can be useful in resolving smaller (aseptic) thrombi (which underlines the meaning of the early recognition of such complications) before size and fibrosis (especially in septic forms) prevent resolution. They are also indicated as long as the source of thrombosis and/or infection (atrial catheter) has not been removed and if massive pulmonary embolization superimposes already established CTEPH or if thromboembolism persists despite removal of the potential source of thromboembolism (22). Experience with local thrombolysis using rt-PA is not provided in the literature, but its usage might be reasonable. The most essential elements of the treatment of thromboembolic VA-shunt complications are the *removal of the atrial catheter* (22, 24) as it is a source of chronic endothelial lesion and infection and the treatment of the (potential) infection with calculated antibiotics, even if general infection markers are normal. If thoracotomy is necessary for shunt or thrombus removal, detailed studies of venous bypasses are mandatory to avoid the interruption of vital bypasses, as demonstrated in case 2. From the viewpoint of prevention, any efforts to *reduce bacterial inoculation* during shunting procedures are justified to avoid the life-threatening septic thromboembolic complications in VA-shunts.

Screening and Follow-Up Examination

The difficulty of early detection of such complications has been widely debated (22) and meticulous follow-up is mandatory. Unspecific findings and complaints such as dyspnea, pharyngeal cough (mostly misunderstood as "asthma bronchiale"), cardiac arrhythmia, new or modified cardiac murmur, and chronic fatigue must be understood as serious alarming signals. Regular checks of D-dimers, CRP and platelets' lifespan (5, 24, 25) and detailed pulmonary function tests (20) are reasonable. According to our experience, biannual TEE might also be valuable because small thrombi can be detected early enough to be suitable for conservative resolution with anticoagulation. In patients at a higher risk (after shunt infection or thromboembolic events and other predestining conditions), more frequent examination might be justified while chest X-ray, TTE, detailed cardiac

examination, and ventilation-perfusion scintigraphy are not indicated because of low sensitivity or because of potentially serious side effects (5, 24).

Conclusion

Thromboembolic complications are serious and potentially life-long side-effects of VA-shunting that may be difficult to detect. Prophylaxis and treatment must orientate on the recently more clarified pathophysiology of such complications, but individual strategies are mandatory in each case.

Conflict of interest statement Dr.Kiefer has received some honoraria to speak about hydrocephalus. Issues discussed in this paper were not involved.

References

- Adegbite AB, Khan M (1982) Role of protein content in CSF ascites following ventriculoperitoneal shunting. Case report. *J Neurosurg* 57(3):423–425
- Bayard R (1996) Mechanisms of sudden death and autopsy findings in patients with Arnold–Chiari malformation and ventriculoatrial catheters. *Am J Forensic Med Pathol* 17(3):260–263
- Bonderman D, Jakowitsch J, Redwan B, Bergmeister H, Renner MK, Panzenböck H, Adlbrecht C, Georgopoulos A, Klepetko W, Kneussl M, Lang IM (2008) Role for staphylococci in misguided thrombus resolution of chronic thromboembolic pulmonary hypertension. *Arterioscler Thromb Vasc Biol* 28(4):678–684
- Borgbjerg BM, Gjerris F, Albeck MJ, Hauerberg J, Borgesen SV (1998) A comparison between ventriculo-peritoneal and ventriculo-atrial cerebrospinal fluid shunts in relation to rate of revision and durability. *Acta Neurochir (Wien)* 140:459–465
- Bounameaux H, Cirafici P, de Moerloose P, Schneider PA, Slosman D, Reber G, Unger PF (1991) Measurement of D-dimer in plasma as diagnostic aid in suspected pulmonary embolism. *Lancet* 337:196–200
- Davidson RI (1976) Peritoneal bypass in the treatment of hydrocephalus: historical review and abdominal complications. *J Neurol Neurosurg Psychiatry* 39:640–646
- Emery JL, Hilton HB (1961) Lung and heart complications of the treatment of hydrocephalus by ventriculoauriculostomy. *Surgery* 50:309–314
- Emery JL, Mahgreffe B (1969) Weights of heart ventricles in children with hydrocephalus treated with ventriculo-caval shunts. *Br Heart J* 31:613–615
- Erdohazi M, Eckstein HB, Crome L (1966) Pulmonary embolisation as a complication of ventriculo-atrial shunts inserted for hydrocephalus. *Dev Med Child Neurol Suppl* 11:36–44
- Eymann R, Chehab S, Strowitzki M, Steudel WI, Kiefer M (2008) Clinical and economical consequences of antibiotic impregnated CSF shunt catheters. *J Neurosurg* 1(6):444–450
- Fernell E, Wendt L (1985) Ventriculoatrial or ventriculoperitoneal shunts in the treatment of hydrocephalus in children. *Z Kinderchir* 40(Suppl 1):12–14
- Gottfried ON, Binning MJ, Sherr G, Couldwell WT (2005) Distal ventriculoperitoneal shunt failure secondary to *Clostridium difficile* colitis. *Acta Neurochir (Wien)* 147(3):335–338
- Harris WH, Salzman EW, Athanasoulis CA, Waltman AC, DeSanctis RW (1977) Aspirin prophylaxis of venous thromboembolism after total hip replacement. *N Engl J Med* 297:1246–1249
- Kadar K, Hartyanski I, Kiraly L, Bendig L (1991) Right heart thrombus in infants and children. *Pediatr Cardiol* 12(1):24–27
- Keucher TR, Mealey J (1979) Long-term results after ventriculoatrial and ventriculoperitoneal shunting for infantile hydrocephalus. *J Neurosurg* 50:179–186
- Kiefer M, Eymann R, Strowitzki M, Steudel WI (2005) Gravitational shunts in longstanding overt ventriculomegaly in adults. *Neurosurgery* 57:109–119
- Liptak GS, Masiulis BS, McDonald JV (1985) Ventricular shunt survival in children with neural tube defects. *Acta Neurochir (Wien)* 74:113–117
- Lundar T, Langmoen IA, Hovind KH (1991) Fatal cardiopulmonary complications in children treated with ventriculoatrial shunts. *Childs Nerv Syst* 7:215–217
- McGrail KM, Muzzi DA, Lsoasso TJ, Meyer FB (1992) Ventriculoatrial shunt distal catheter placement using transesophageal echocardiography: technical note. *Neurosurgery* 30(5):747–749
- Nadel JA, Gold WM, Burgess JH (1968) Early diagnosis of chronic pulmonary vascular obstruction. Value of pulmonary function tests. *Am J Med* 44:16–25
- Pascual JMS, Prakash UBS (1993) Development of pulmonary hypertension after placement of a ventriculoatrial shunt. *Mayo Clin Proc* 68:1177–1182
- Piatt JH Jr, Hoffman HJ (1989) Cor pulmonale: a lethal complication of ventriculoatrial CSF diversion. *Childs Nerv Syst* 5:29–31
- Sinha RP, Ducker TB (1971) Cardiopulmonary complications of ventriculo-atrial shunt in hydrocephalic children. *J S C Med Assoc* 67:421–423
- Sleigh G, Dawson A, Penny WJ (1993) Cor pulmonale as a complication of ventriculo-atrial shunts reviewed. *Dev Med Child Neurol* 35:74–78
- Stuart MJ, Murphy S, Oski FA, Evans AE, Donaldson MH, Gardner FH (1972) Platelet function in recipients of platelets from donors ingesting aspirin. *N Engl J Med* 287:1105–1109
- Rich S, Brundage BH (1989) Pulmonary hypertension: a cellular basis for understanding the pathophysiology and treatment. *J Am Coll Cardiol* 14:545–550
- Weinzierl MR, Collmann H, Korinth MC, Gilsbach JM, Rohde V (2007) Management of hydrocephalus in children with plasminogen deficiency. *Eur J Pediatr Surg* 17(2):124–128
- West GA, Berger MS, Geyer JR (1994) Childhood optic pathway tumors associated with ascites following ventriculoperitoneal shunt placement. *Pediatr Neurosurg* 21(4):254–258
- Yavuzgil O, Özerkan F, Ertürk Ü, Islekel S, Atay Y, Buket S (1999) A rare cause of right atrial mass: thrombus formation and infection complicating a ventriculoatrial shunt for hydrocephalus. *Surg Neurol* 52:54–55
- Zager J, Berberich SN, Eslava R, Klieman C (1978) Dynamic tricuspid valve insufficiency produced by a right ventricular thrombus from a pacemaker. *Chest* 74:455–456

Does Idiopathic Normal Pressure Hydrocephalus Always Mean a Poor Prognosis?

Michael Kiefer, Ulrich Meier, and Regina Eymann

Abstract

Objective The objective was to assess whether idiopathic normal-pressure hydrocephalus (iNPH) has a worse prognosis than other forms of hydrocephalus, as has been suggested.

Methods A total of 125 patients with chronic hydrocephalus, 75 of whom suffered from iNPH and the remaining (non-iNPH) from sNPH or non-communicating hydrocephalus, were shunted using gravitational valves. Clinical state was assessed with our clinical grading (KI) and a co-morbidity index (CMI). Average follow-up was 5.1 ± 1.6 years. Statistics: Spearman, Kruskal–Wallis, ANOVA, χ^2 - and the Wilcoxon U tests at a significance level of $p < 0.05$ were used.

Results Shunt responder rates for iNPH and non-iNPH were 72% and 86%, respectively. With shorter anamnesis (≤ 1 year) or preoperative KI < 6 points, iNPH patients had a similar or even better outcome than non-iNPH patients with longer anamnesis or a worse KI. Most impressive was the influence of co-morbidity: 86% of iNPH patients with a low CMI (≤ 3 points) experienced clinical improvement after shunting, which was contrasted by a responder rate of 64% for non-iNPH with worse CMI.

Conclusion The diagnosis of iNPH does not by itself mean a worse prognosis, and iNPH patients with favorable preconditions may have a similar or better prognosis than patients with any other kind of hydrocephalus. The worse overall clinical results of iNPH result from late recognition and in most instances worse preconditions.

Keywords Hydrocephalus • shunt • clinical results • outcome • co-morbidity • normal pressure hydrocephalus • iNPH

M. Kiefer (✉)

Department of Neurosurgery, Saarland University Medical School, Kirrberger Str., Building: 90.1, Homburg-Saar 66421, Germany
e-mail: Michael.Kiefer@uks.eu

R. Eymann

Department of Neurosurgery, Medical School, Saarland University, Kirrberger Street, Building 90, Homburg-Saar, Saarland 66421, Germany

Introduction

Idiopathic normal pressure hydrocephalus (iNPH) is typically thought to have a worse prognosis than other forms of chronic hydrocephalus (3,6,14). Other forms of chronic hydrocephalus (non-iNPH) such as secondary normal pressure hydrocephalus or non-communicating hydrocephalus were found to respond to shunting 74% and 87% percent of the time, respectively (3,6,9,14). In contrast, the provided responder rates in iNPH seldom exceed 50% (3,6,12,14), leading to the question of whether risk-benefit analysis would not argue against iNPH shunting (14). On closer inspection, however, iNPH patients should typically be older, are diagnosed later and should have more severe co-morbidity compared with patients with sNPH or non-communicating hydrocephalus. We have recently found that the clinical state and co-morbidity prior to shunting are important predictors of outcome (10). Worse preconditions may significantly contribute to worse outcomes for iNPH.

The aim of this prospective study was to analyze whether iNPH might have a similar prognosis as non-iNPH if iNPH patients are in the good clinical precondition, which is typically the norm for non-iNPH hydrocephalus.

Material and Methods

Patients, Follow-Up and Documentation

iNPH was diagnosed in 75 patients (45♂, 30♀) and non-iNPH in 50 (18♂, 32♀) patients. The non-iNPH group consisted of 9 patients suffering from sNPH, 26 patients with aqueduct stenosis who preferred shunting instead of endoscopic third ventriculostomy (ETV) ($n = 18$) or with unfavorable preconditions for ETV ($n = 8$), four hydrocephalic patients with Chiari malformations who were shunted before posterior fossa decompression, and another 15 patients with various other (mostly congenital) forms

of non-communicating hydrocephalus, who refused or were unsuitable for endoscopic treatment.

Patients with iNPH had to present at least two symptoms of Hakim's triad. In non-iNPH patients the prerequisites for invasive diagnostics were signs of intracranial pressure (ICP) elevation (e.g., headache, papilla prominence with visual disturbances, etc.) or, as in iNPH, the presence of at least two symptoms of Hakim's triad, which could also be combined with signs of ICP increase. The second prerequisite for invasive diagnostics in both groups was an Evans-Index greater than 0.3.

The clinical state and the state of co-morbidity were meticulously assessed preoperatively and for documentation we used our modified clinical grading (KI) (Table 1), the Recovery-Index (RI) (8) and the co-morbidity index (CMI) (10). A patient was termed a "shunt responder" if RI was ≥ 3 at the time of the last follow-up examination. The Evans-Index was used for ventricular size documentation, which was measured through the obligatory preoperative magnetic resonance imaging (MRI). Follow-up examinations including cerebral computer tomography (CCT) were performed 2–3 months, 12 months, and thereafter annually after shunting. Minimal follow-up time was 1 year and the average follow-up was 5.1 ± 1.6 years (range: 1–8 years). The average follow-up times for iNPH (5.2 ± 1.8 , range: 1–7.5 years) and non-iNPH (4.9 ± 2.2 , range: 1.5–8 years) were quite similar ($p = 0.835$).

Indication Policy and Group Allocation

In potential shunt candidates, ICP was measured for 48 h and cerebrospinal fluid (CSF) dynamics were studied using a Spiegelberg III probe connected to a personal computer with specific software for ICP analysis (7). Only patients with a

mean ICP < 15 mmHg were allocated to the iNPH group. Patients with values above this threshold, who according to anamnesis and/or MRI-flow-studies could not be assigned to either sNPH or non-communicating hydrocephalus, were completely excluded from this analysis because a clear allocation to the iNPH or non-iNPH group was not possible. According to the previous findings of the meaning of the Pressure Volume Index (PVI) for shunt indication (10), both PVI and Resistance to outflow (Rout) were considered for shunt indication. Patients with a PVI < 30 mL or with Rout > 13 mmHg/mL/min were shunted.

Shunt Hardware

All patients were provided with ventriculo-peritoneal (VP) adjustable gravitational shunts. We used the Aesculap-Miethke adjustable PRO-GAV valve (Miethke KG, Potsdam, Germany) in 44 patients (22 iNPH, 22 non-iNPH) and the adjustable Codman-Hakim valve (Codman, Johnson and Johnson, Boston, MA, USA) in 81 patients (41 iNPH, 40 non-iNPH), each set to 120 mm H₂O initially, combined with an Aesculap-Miethke Shunt-Assistant (Miethke KG, Potsdam, Germany) with an opening pressure according to hydrostatic pressure in upright position. During follow-up, adjustments of any range were allowed to compensate for signs and symptoms of over- or under-drainage, respectively.

Statistics

Mann–Whitney U, Spearman, Kruskal–Wallis, ANOVA and χ^2 -tests at a significance level of $p < 0.05$ were used.

Table 1 Modified clinical grading (Kiefer-Index: KI). According to the severity of symptoms/handicap in the given five domains, values from 0 to 6 points for each domain were assigned, and the summed values represent the given clinical state (KI)

Points	Gait/balance	Mental	Incontinence	Headache	Dizziness
0	Able to stand on one leg >30 s	Normal	Normal	Not present	Not present
1	Able to stand on one leg <30 s, minor disturbance with turning or bi-pedal gait	Forgetful, weak concentration, lives independently		Headache affecting ADL	Intermittent and spontaneous or by challenges
2	Wide-legged, atactic gait, standing heels together >30 s		Urge incontinence		Permanent
3	Tendency to fall, foot-corrections necessary, standing heels together <30 s	Forgetful, weak concentration, not completely independent, some intermittent help necessary	Intermittent incontinence, no diaper		
4	Gait with auxiliary equipment (e.g. crutches), wide-legged standing >30 s possible	Apathy, still fundamentally oriented, some daily care necessary	Intermittent incontinence, diaper necessary	Headache affecting ADL	
5	Gait with aid of one or two persons, wide-legged standing <30 s	Apathy, not completely oriented, permanent help needed (for example with personal hygiene)	Permanent incontinence (blister catheter necessary)		
6	Unable to walk, help needed for standing, wheelchair bound	Totally confused, impairment of higher cortical functions, permanent support/care necessary	Urine and bowel incontinence		

Results

Clinical Data

Average age in the iNPH and non-iNPH groups was 68.2 ± 12 years (range: 48–86) and 56.6 ± 18 years (range: 18–72) and accordingly quite different ($p < 0.032$). Increasing age and worse outcome were correlated in both iNPH ($p = 0.003$) and non-iNPH ($p = 0.013$) patients but age alone was not an independent outcome predictor (iNPH: $p = 0.532$; non-iNPH: $p = 0.744$). Interestingly, the time spans between the first overt clinical signs and the treatment of hydrocephalus were quite similar in iNPH (average: 3.0 ± 3.3 years; range: 0.3–5 years) and non-iNPH (average: 3.2 ± 5.2 years; range: 0.5–11 years) patients ($p = 0.782$). In particular, younger patients with non-communicating hydrocephalus symptoms such as headache or dizziness were misconstrued over the years in many instances. While longer anamnesis decreased the shunt responder rate in iNPH ($p = 0.026$), a similar correlation could not be found in non-iNPH patients ($p = 0.145$); at the same time it was found to be an independent outcome predictor in iNPH only ($p = 0.036$), but not in non-iNPH ($p = 0.242$). The preoperative clinical state was worse in iNPH patients (average KI: 9.8 ± 5.8 points; range: 4–22 points) compared with non-iNPH patients (average KI: 7.1 ± 2.8 points; range: 2–15 points) ($p = 0.026$). Similar to the anamnesis duration, a worse preoperative clinical state decreased the shunt responder rate in iNPH patients ($p = 0.029$), but not in non-iNPH patients ($p = 0.183$), and a worsened outcome as measured with the RI was only found to be significant in iNPH ($p = 0.018$), but not in non-iNPH patients ($p = 0.056$). Regarding the whole cohort (not separating iNPH and non-iNPH patients) the preoperative clinical state, age and anamnesis duration were strong, - but not independent -, predictors of shunt success ($p = 0.005$, $p < 0.000$, $p = 0.002$). Co-morbidity as measured with the CMI was significantly different between the iNPH group (average CMI: 5.8 ± 3.6 points, range: 0–9 points) and the non-iNPH group (average CMI: 2.1 ± 2.4 points, range: 0–8 points) ($p < 0.00012$). One reason for this clear difference between both groups was that nearly all (89%) iNPH patients but only 60% of non-iNPH patients suffered from *at least one* co-morbidity ($p = 0.001$). The influence of CMI on outcome was notable. On the one hand, a worse CMI typically worsened the preoperative KI ($p = 0.013$), which indirectly worsens the outcome. On the other hand, a worse CMI directly impaired the clinical benefit of shunting, independently from its influence on the KI ($p = 0.0197$). Typically the CMI increased with age (iNPH: $p = 0.031$; non-iNPH: $p = 0.012$), but both CMI and age were independent outcome predictors in both groups (iNPH: $p = 0.036$; non-iNPH: $p = 0.042$).

Comparison of iNPH and Non-iNPH

In the iNPH group, 54 patients (72%) had at least a “fair” ($RI \geq 3$) outcome and were taken as shunt responders, which is at the first glance contrasted by 43 shunt responders (86%) in the non-iNPH group. The corresponding odds ratio (non-iNPH versus iNPH) of shunt success was 2.3, indicating a twice as great chance for non-iNPH patients to benefit from shunting compared with those with iNPH. This obvious difference initially seems to be consistent with the traditional opinion of a worse iNPH prognosis, but was contrasted somehow by a lack of significance between both shunt responder rates ($p = 0.068$). From a restricted perspective, it becomes evident that some outcome-influencing parameters can be found significantly more often in iNPH patients compared with non-iNPH patients; the odds ratios (iNPH versus non-iNPH) for CMI > 3 points, KI > 5 points and anamnesis duration > 1 year were 2.9 ($p = 0.041$), 5.0 ($p < 0.000$) and 1.1 ($p = 0.848$), respectively. Additionally the frequency of how often these worse prognostic factors occurred in iNPH and non-iNPH patients was strikingly different ($p < 0.000$): no co-morbidity: 6% iNPH/36% non-iNPH, one co-morbidity: 12% iNPH/36% non-iNPH, two co-morbidities: 43% iNPH/18% non-iNPH, and three or more co-morbidities: 39% iNPH/10% non-iNPH. Similar clear discrepancies existed regarding age distribution, while more than 80% of the patients with non-iNPH were younger than 70 years, more than 50% of iNPH patients were older than 70 years. This age difference was the most important one between both groups: iNPH patients were typically older and had accordingly worse co-morbidity. Regarding shunt responder rates, depending on given age ranges (<60 years, 60–69 years, 70–79 years, ≥ 80 years), the difference between iNPH and non-iNPH patients (71%/86%, 77%/84%, 75%/77%, 50%/NA) was insignificant ($p < 0.00012$) yet. The most impressive results, however, can be found, if patients having similar preconditions with regard to co-morbidity, preoperative clinical state and symptoms duration are compared (Fig. 1). I-NPH and non-iNPH patients with a low co-morbidity (CMI ≤ 3 points), milder preoperative deficits (KI ≤ 5 points) and shorter anamnesis (≤ 1 year) had a quite similar shunt responder rate, which exceeded 80%, independent of the type of hydrocephalus. Similarly, with worse preconditions (CMI > 3 points, KI > 5 points), shunt responder rates dropped in both iNPH and non-iNPH patients. CMI worsened the outcome significantly (iNPH: $p = 0.0256$; non-iNPH: $p = 0.0182$) in both groups. The only exceptions were that the worsening effects of worse preoperative conditions and a longer anamnesis on the shunt responder rates were more serious in iNPH patients (KI: $p = 0.041$; anamnesis duration: $p = 0.0251$) than in non-iNPH patients (KI: $p = 0.157$; anamnesis: $p = 0.169$). The latter was the only outcome difference between iNPH and non-iNPH patients at

comparable preconditions. While non-iNPH patients with an anamnesis duration >1 year benefited from shunting 77% of the time, only 57% of iNPH patients with such a prolonged anamnesis responded to shunting ($p = 0.003$).

Most striking was the enormous influence of the CMI, which seemed to “abolish” any effect of aging (Fig. 2). Given a $CMI \leq 3$ points, the shunt success rate exceeded 80% independent of age. Even those patients that at first glance had a low chance to benefit from shunting because of an age older

than 80 years and iNPH hydrocephalus had a favorable outcome in 84% of the cases.

Discussion

I-NPH is typically considered to have a poor prognosis and shunt responder rate; a success rate of shunting below 50% is considered the norm (3,6,14). Some improvement apparently came with the introduction of gravitational shunts because they allowed sufficient drainage while lying down and effectively prevented over-drainage in the upright position (8,9,12,13), in as much that iNPH responder rates of about 70% could be achieved together with a lowered total complication rate. These results, however, need substantiation by a randomized trial, which is already in progress.

However from a pathophysiological point of view, it has always remained enigmatic why iNPH should have a worse prognosis than any other form of hydrocephalus. Actually two pathophysiological models of hydrocephalus exist in parallel. Traditionally increase of resistance to outflow (R_{out}) is claimed as underlying pathology. More recently R_{out} elevation is considered as epiphenomenon, while reduced cranio-spinal compliance is regarded as the fundamentally disturbed parameter. CSF drainage via a shunt however, corrects both impaired CSF absorption with elevated R_{out} and decreased intracranial compliance (4). Accordingly, there

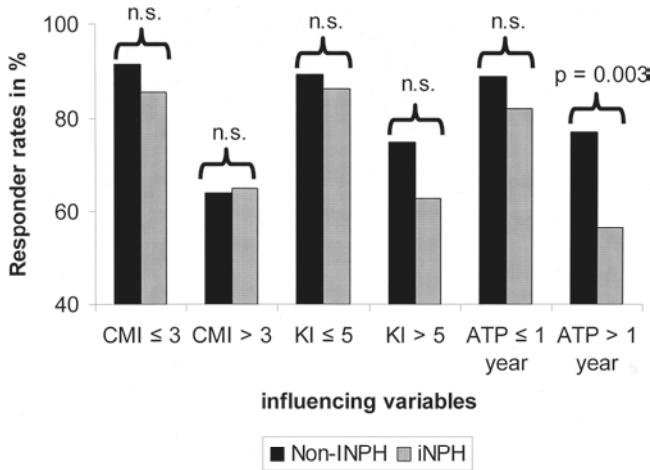


Fig. 1 Shunt responder rate depending on given preconditions (CMI = Co-morbidity index, KI = clinical grading, ATP = anamnesis time period) and indication of statistical significance (n.s. = not significant)

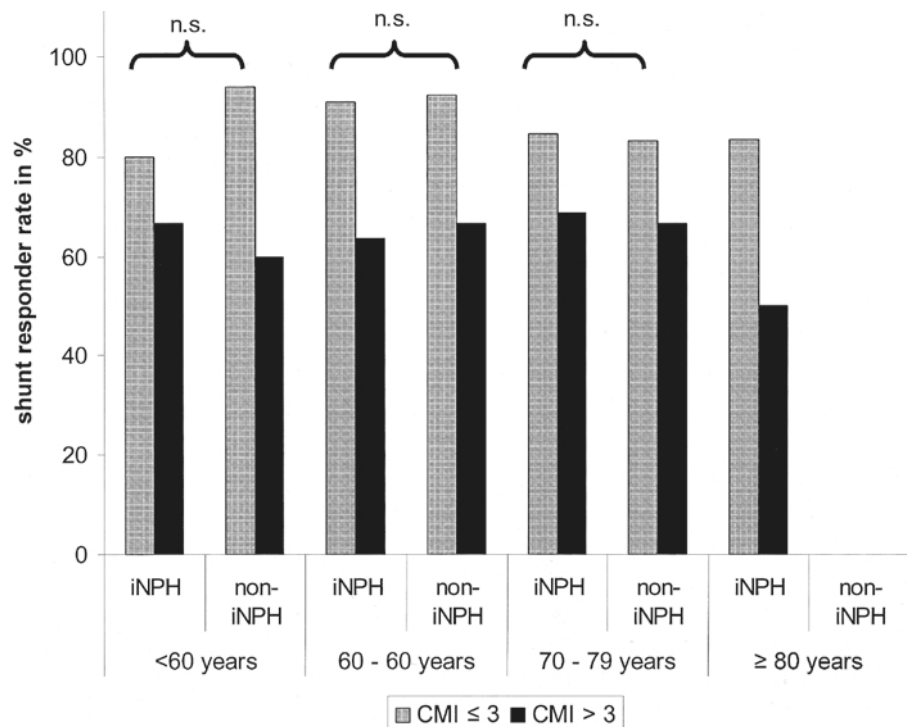


Fig. 2 Shunt responder rate depending on age and CMI in iNPH and non-iNPH patients

is not an obvious reason why iNPH should have lower rehabilitation potency than any other chronic hydrocephalus form. The only overt difference between iNPH and other forms of chronic hydrocephalus is that iNPH typically affects patients during the sixth to eighth decade of life, while other forms of chronic hydrocephalus mostly become clinically apparent about two decades earlier at the latest. It is not astonishing that the elderly typically suffer from more (especially cardio-vascular) co-morbidity, as it holds true in our cohort too. In the literature the evidence, that cardio-vascular and other co-morbidity worsens prognosis of iNPH, is overwhelming (1,2,5,11). Previously, we found that beside co-morbidity, the preoperative clinical state and the period of time that hydrocephalus-related symptoms persisted before treatment might influence the rehabilitation potency as well (10).

In contrast, iNPH and other forms of chronic hydrocephalus should have a comparable good prognosis if preoperative preconditions are similarly favorable as in the most forms of non-communicating hydrocephalus in younger patients. This can be demonstrated with our data: iNPH with favorable preconditions (low co-morbidity, only mild-moderate preoperative handicaps and/or with short anamnesis) had a shunt success rate that was quite similar to other forms of chronic hydrocephalus (non-communicating hydrocephalus of younger patients), which are typically claimed to have a better prognosis compared with iNPH. Probably even more impressive was that with favorable preconditions, iNPH patients clearly had a better chance of benefiting from shunting compared to non-iNPH hydrocephalus patients with worse preoperative preconditions. For us, the most amazing finding was the over 80% chance for iNPH patients with favorable preconditions (especially a low CMI) to benefit from shunting even beyond 80 years of age, indicating that age per se must be not taken as an argument against shunting in otherwise “healthy” iNPH patients. Our findings also argue against an older paradigm whereupon the best shunt candidates would be those presenting the complete triad. Our data indicate that any prolongation of treatment can reduce the chance of rehabilitation.

iNPH has the same prognosis as any other chronic hydrocephalus with comparable preconditions. The problem with iNPH, however, is that the cohort often consists of patients who are older, who have more serious co-morbidity and who are mostly diagnosed late compared to patients with other types of chronic hydrocephalus. The odds ratios of non-iNPH versus iNPH patients to suffer from no or only one co-morbidity are 7.8 and 4.1, respectively, which is contrasted by an odds ratio of 0.17 each for patients suffering from two or three co-morbidities. Similarly, the chance of an iNPH patient to present with only one worse precondition (e.g. only long anamnesis or only worse CMI or only worse KI) instead of having two or three worse preconditions (e.g.

long anamnesis AND worse CMI AND worse KI) is 11-fold lower than in patients with non-iNPH.

The worse prognosis of iNPH – from a clinical perspective – is apparently solely an epiphenomenon due to the fact that the chance for favorable preconditions is more than tenfold lower in the iNPH cohort than in other chronic forms of hydrocephalus.

Conclusion

iNPH per se does not indicate a worse prognosis, but instead has a similar rehabilitation potency as any other chronic hydrocephalus with similar preconditions. However, the frequency of patients with favorable preconditions and iNPH is more than tenfold lower than in other forms of chronic hydrocephalus. The fact that the group of iNPH patients typically includes a preponderance of hydrocephalics with worse preconditions causes the apparent overall worse outcome, but is in reality only an epiphenomenon of the precondition state.

Conflict of interest statement Dr.Kiefer has received some honoraria from Codman and Aesculap to speak about hydrocephalus. Yet issues of this paper were not involved.

References

1. Boon AJ, Tans JTJ, Delwel EJ, Egeler-Peerdeman SM, Hanlo PW, Wurzer HAL, Hermans J (1999) Dutch normal-pressure hydrocephalus study: the role of cerebrovascular disease. *J Neurosurg* 90:221–226
2. Caruso R, Cervoni L, Vitale AM, Salvati M (1989) Idiopathic normal pressure hydrocephalus in adults: results of shunting correlated with clinical findings in 18 patients and review of the literature. *Neurosurg Rev* 20:104–107
3. Dauch WA, Zimmermann R (1990) Normal pressure hydrocephalus. An evaluation 25 years following the initial description. *Fortschr Neurol Psychiatr* 58:178–190
4. Greitz D (2004) Radiological assessment of hydrocephalus: new theories and implications for therapy. *Neurosurg Rev* 27:145–165
5. Haidri NH, Modri SM (1977) Normal pressure hydrocephalus and hypertensive cerebrovascular disease. *Dis Nerv Syst* 38:918–921
6. Hebb AO, Cusimano MD (2001) Idiopathic normal pressure hydrocephalus: a systematic review of diagnosis and outcome. *Neurosurgery* 49:1166–1186
7. Jetzki S, Kiefer M, Eymann R, Walter M, Leonhardt S (2007) Analysis of pulse waves in intracranial pressure. *Conf Proc IEEE Eng Med Biol Soc* 2007:2863–2866
8. Kiefer M, Eymann R, Meier U (2002) Five years experience with gravitational shunts in chronic hydrocephalus of adults. *Acta Neurochir (Wien)* 144:755–767
9. Kiefer M, Eymann R, Strowitzki M, Stuedel WI (2005) Gravitational shunts in longstanding overt ventriculomegaly in adults. *Neurosurgery* 57:109–119
10. Kiefer M, Eymann R, Stuedel WI (2006) Outcome predictors for normal-pressure hydrocephalus. *Acta Neurochir Suppl* 96:364–367

11. Krauss JK, Regel JP, Vach W (1997) White matter lesion in patients with idiopathic normal pressure hydrocephalus and in age-matched control group: a comparative study. *Neurosurgery* 40:491–495
12. Meier U, Kiefer M, Neumann U, Lemcke J (2006) On the optimal opening pressure of hydrostatic valves in cases of idiopathic normal-pressure hydrocephalus: a prospective randomized study with 123 patients. *Acta Neurochir Suppl* 96:358–363
13. Pujari S, Kharkar S, Metellus P, Shuck J, Williams MA, Rigamonti D (2007) Normal pressure hydrocephalus: very long term outcome after shunt surgery. *J Neurol Neurosurg Psychiatry* . doi:[10.1136/jnnp.123620](https://doi.org/10.1136/jnnp.123620)
14. Vanneste J, Augustijn P, Dirven C, Tan WF, Goedhart ZD (1992) Shunting normal pressure hydrocephalus: do the benefits outweigh the risk? Multicenter study and literature review. *Neurology* 42:54–59

Gravitational Shunt Complications After a Five-Year Follow-Up

Michael Kiefer and Regina Eymann

Abstract

Introduction Gravitational shunts (G-valves) for ventriculo-peritoneal (VP) shunting have been available since 1996. We analyzed shunt complications in patients with a complete minimum follow-up of 5 years.

Material and Methods Between 1996 and 2002, we implanted 282 VP G-valves in various forms of adult chronic hydrocephalus, of which 130 provided a complete data set with an annual follow-up. Adjustable and non-adjustable G-valves were used: the Miethke Dual-Switch valve, the Miethke GAV-valve and a combination of adjustable Codman-Hakim valves with the Miethke Shunt-Assistant. In cases of supposed mechanical shunt failure, the explanted shunts were examined in a bench test.

Results The total complication rate was 21%:3% shunt infections, 3% catheter dislocation/fracture, 5% underdrainage and 9% overdrainage occurred. Half of the overdrainage complications could be managed conservatively. Underdrainage complications resulted from the chosen opening pressure being too high ($n = 3$), a secondary increase in intraperitoneal pressure ($n = 2$) or from “real” shunt failure in one case according to bench test results.

Conclusion G-valves demonstrate sufficient long-term performance over multiple years, and real shunt-related complications are rare. The frequency of revision due to overdrainage is low (4.5%).

Keywords Hydrocephalus • iNPH • shunt • gravitational shunts • complication • disconnection • dislocation • shunt infections • overdrainage • underdrainage

M. Kiefer (✉)

Department of Neurosurgery, Saarland University Medical School, Kirrberger Street, Building: 90.1, Homburg-Saar 66421, Germany
e-mail: Michael.Kiefer@uks.eu

R. Eymann

Department of Neurosurgery, Medical School, Saarland University, Kirrberger Street, Building 90, Homburg-Saar, Saarland 66421, Germany

Introduction

The introduction of modern shunts in hydrocephalus therapy in the 1950s revolutionized hydrocephalus therapy. Given that they are usually necessary for the whole life of the patient, the fact that up to 50% of the shunts must be revised within 10 years after implantation (3,6,8,15) seems unacceptably high. The failure rates are obviously independent of the shunt type used (1,4,9,17), as the few existing prospective randomized trials have demonstrated. One reason for shunt revision is shunt infection that may be reduced with the usage of antibiotic-impregnated catheters (5). However, another important source of shunt failure is valve-related failure, with 30–70% of shunt revisions being due to hydraulic mismanagement (1). Classical differential pressure (DP) valves must overdrain in an upright position if their opening pressure (OP) has been chosen for sufficient drainage while lying. In contrast, when choosing a high OP to avoid overdrainage, drainage in a lying position is insufficient as demonstrated by observations of poor clinical results (1). Most measures or technical solutions to overcome this obvious paradox reduce the overdrainage rate at the cost of increased underdrainage, and vice versa. Based on the basic principles that were developed two decades ago by S. Hakim and independently by Yamada (16), gravitational valves (G-valves) for ventriculo-peritoneal and/or atrial insertion have been generally available since the mid-1990s. G-valves vary their OP depending on posture and should overcome hydraulic mismanagement accordingly (10,11,13). Initial experiences with G-valves were favorable (10–12,14), but data with longer follow-ups are lacking.

As one of the first neurosurgical departments worldwide which routinely use G-valves, we have a large body of experience regarding the long-term performance and failures of these valves. In a retrospective study, we analyzed the performance and failures of G-valves with a minimal follow-up of 5 years.

Material and Methods

Between 1996 and 2002, a total of 268 gravitational shunts were implanted in our department to treat various forms of chronic hydrocephalus. Normal follow-up examination was performed three and 12 months postoperatively, and thereafter, annually. The minimal follow-up was 5 years and the average follow-up was 8.1 ± 1.7 years (range: 5–11 years). Only patients with the minimal follow-up of 5 years when their follow-up could be performed as described were considered. If only one follow-up examination was lacking, the patients were excluded. Another precondition for inclusion in this study was that the last follow-up should not date back more than 14 months. Besides clinical examination, cerebral computer tomography (CCT) was performed at every check-up, even if the patient was asymptomatic. In the case of complaints or given signs of complications, the patients were checked in addition to the control routine. During the follow-up, 49 patients were lost as a consequence of non-shunt-related mortality ($n = 12$) and 32 patients moved and the follow-up (if any) that was performed in another department was not compatible with the study protocol. Five patients were “lost without a trace.” Due to incomplete data sets lacking at least one follow-up examination or one CCT check, 89 patients had to be excluded from the analysis. In most instances ($n = 72$), patients were not willing to come for the annual check-up or refused CCT if they were asymptomatic, but we also excluded these patients for reasons of scientific rigor (otherwise asymptomatic subdurals may have been overseen and the patients could have been counted as lacking any complication). The endpoints of the study were a completely documented uneventful clinical course of a minimum of 5 years with a maximum of 14 months backdated to the last follow-up examination, or a shunt explantation independent of the underlying reason for the original shunt insertion.

Shunts All patients were provided with ventriculo-peritoneal (VP) adjustable or non-adjustable gravitational shunts. The Aesculap-Miethke Dual-Switch valve (DSV) (Miethke KG, Potsdam, Germany) was the first available G-valve, and therefore the most often used ($n = 82$) between 1996 and 2002 (10). The Aesculap-Miethke Shunt-Assistant (Miethke KG, Potsdam, Germany) combined with an adjustable Codman-Hakim valve (Codman, Johnson and Johnson, Boston, MA, USA) (CHSA) was used in 25 studied patients throughout the study period, but was used mostly in patients with non-communicating hydrocephalus because at that time, it was the only adjustable G-valve used in our department (10,11). With the launch of the Aesculap-Miethke Gravity-Assisted Valve (GAV) (Miethke KG, Potsdam, Germany) in 2002, this valve was commonly used instead of the DSV (13). The distribution of treated pathologies was quite different between the three valve types ($p < 0.0002$).

The DSV was mainly used for idiopathic normal pressure hydrocephalus (iNPH) ($n = 64$) and secondary normal pressure hydrocephalus (sNPH) ($n = 13$), while only five patients with non-communicating hydrocephalus received this valve. This is contrasted by the usage of the CHSA chiefly in non-communicating hydrocephalus (92%), while only two patients with iNPH were provided with this configuration. SNPH, non-communicating hydrocephalus and iNPH were diagnosed in 11, 6 and 6 patients who received the GAV, respectively. The opening pressure of the DSV was 8/40 cm H₂O in 19 patients, 10/40 cm H₂O in 21 patients, and 13/40 cm H₂O in 36 patients, while the remaining six patients received DSV valves with a lower opening pressure (30 cm H₂O) for the upright position and an opening pressure between 8 cm H₂O and 13 cm H₂O for the lying position. The most often used opening pressures of the GAV were 5/35 cm H₂O ($n = 11$) and 5/40 cm H₂O ($n = 10$), while only one patient each received a 5/30 cm H₂O GAV and a 10/40 cm H₂O GAV. The opening pressure of the 25 Shunt-Assistants ranged between 20 cm H₂O and 35 cm H₂O, depending on the hydrostatic pressure. The opening pressure of the adjustable Codman-Hakim valve was, as part of the protocol of another study, initially set at 20 cm H₂O and thereafter decreased stepwise (11). During the year 2002, we routinely used, in addition to perioperative systemic antibiotics, antibiotic-impregnated catheters (Bactiseal®, Codman, Johnson and Johnson, Boston, MA, USA) (5).

The definitions used for over- and underdrainage, for primary shunt infections have been described in detail elsewhere (5,10), and were also applied in this study because they are the standard in our department. To characterize the severity of complications, we separated mild, moderate and severe complications. Signs or symptoms that did not require shunt revision and could accordingly be treated conservatively were termed “mild”. Moderate and severe complications were characterized by the fact that operative revision was necessary. If the revision required immediate emergency intervention, we termed it as a “severe complication,” while elective revisions were characterized as “moderate complications”.

Shunts that had to be explanted due to supposed hydraulic mismanagement were preserved in 0.9% NaCl solution and sent to the manufacturer for a bench test of the valves’ performance. To avoid misinterpretations, obviously underdraining shunts were not flushed, which may have removed particles (of any origin) in the valve that obstructed the pathway. Cases of supposed hydraulic mismanagement as the reason for shunt explantation were only included in the study when the results of the bench test were available. The data were available for all patients who reached this endpoint of the study.

Statistics Mann–Whitney U, Spearman, Kruskal–Wallis, ANOVA and χ^2 -tests at a significance level of $p < 0.05$ were used.

Results

Overall, 27 complications were registered during the study period, giving a Kaplan-Meier “shunt-survival rate” of 79% after a maximum of 11 years (Fig. 1). Primary shunt infections and disconnections each occurred in 3% of the patients. Overdrainage necessitating shunt revision was found in 5% of patients, while overdrainage requiring no revision was observed in 4% of the patients (Fig. 2). The consequences of overdrainage that could be managed conservatively given asymptomatic small subdural effusions (<1.5 cm thickness) without mass effects. These subdurals were resolved in two patients in the DSV group without any measures taken. Another three patients from the DSV group suffered from

orthostatic headache and were successfully treated with increased fluid uptake. Two patients in the DSV group had, as consequence of overdrainage, slit ventricles after shunting that led to proximal shunt failure necessitating revision. Another two DSV patients had subdural effusions with moderate mass effects, which had to be removed operatively. All four overdrainage cases of DSV resulted from a hydrostatic compensation that was initially too low, and a new DSV with higher opening pressure was inserted at revision. Bench tests of these four valves demonstrated normal function according to their specification. One small subdural effusion in the CHSA group was cured by increasing the valve’s opening pressure. One case of orthostatic headache and one case of bilateral subdural effusion in the CHSA group did not

Fig. 1 “Shunt survival” according to the Kaplan–Meier method for all shunts, and separately for Dual-Switch valves (DSV), Gravity-Assisted valves (GAV), and the combination of adjustable Codman-Hakim and Shunt-Assistant (CHSA)

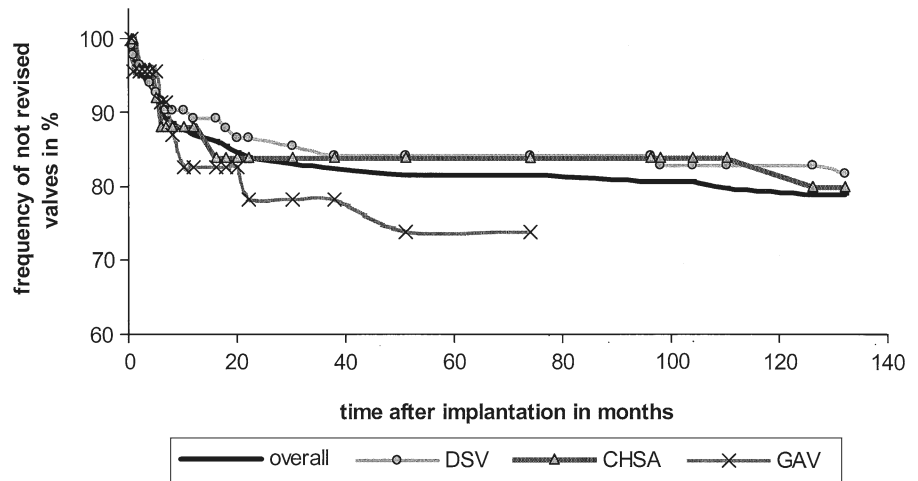
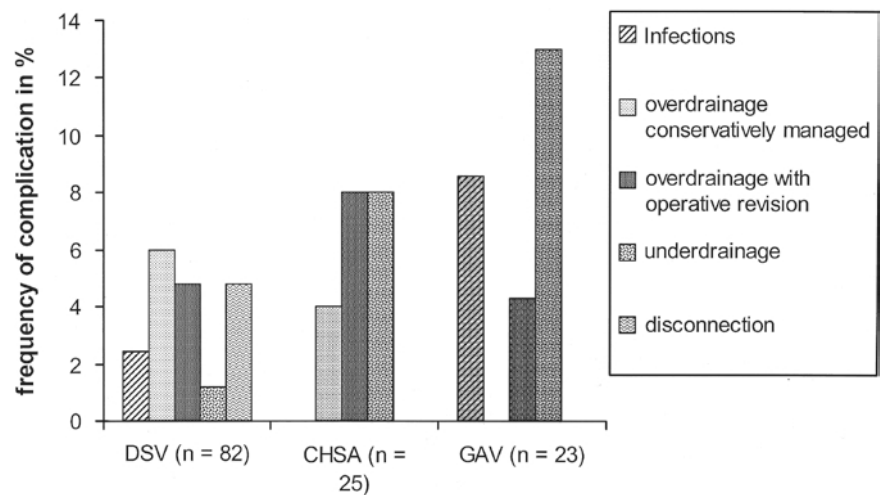


Fig. 2 Observed complications separated for the three studied shunts. It is essential to understand that complication rates refer to the number of studied valves in each group



improve with opening pressures' resetting on the valves' maximal opening pressure (20 cm H₂O), and operative revision was necessary in both cases. Again, the reason for overdrainage in both cases was a hydrostatic compensation that was too low, as the bench test results of both explanted Shunt-Assistants revealed no abnormalities. Overdrainage exclusively occurred within the first weeks after shunting in both CHSA and DSV.

In contrast, six patients were diagnosed to be suffering from underdrainage. Underdrainage was found throughout the study period. In at least one case, underdrainage was attributed to be a direct consequence of shunt failure that was confirmed during in-vitro bench tests. In this specific case, the Tantalum ball of a Shunt-Assistant was stuck and closed the valve permanently. In the remaining five cases of underdrainage, bench tests demonstrated that the valves' performance was within the ranges of tolerance, and these were regarded as functional. A massive weight gain after shunt implantation with a concomitant increase in intraperitoneal pressure was the underlying reason for functional underdrainage in the two patients from the CHSA group. A resetting of the valves' opening pressure to its minimum (3 cm H₂O) could not overcome underdrainage, and operative revision with the implantation of a Shunt-Assistant with a lower opening pressure was necessary. The reason for the functional underdrainage of the remaining three patients in the GAV group was clearly due to an opening pressure that was initially too high in these severely disabled, bedridden sNPH patients. Exchange of the valve and using valves with lower opening pressures for both the upright and lying positions cured the symptoms of underdrainage.

Interesting only from a historical perspective because the underlying systemic weakness has been corrected by the manufacturer, four cases of catheter fracture in the DSV group were discovered. Typically, these fractures occurred near the valve itself, directly beyond the inlet or outlet of the catheter from the valves' housing where the catheters had been fixed. We only observed this phenomenon in DSV valves.

The vast majority of complications (18%) were mild or moderate and were definitely not life-threatening. Only 3% of the observed complications were termed "severe complications" according to our definition (Fig. 3). Comparing the three different valves and the distribution of the severity of complications, it must be stressed that these data are biased by the fact that the apparent worse results of GAV valves resulted from the fact that two of the shunt infections, which by definition are termed "severe," occurred in this, the smallest group. Both shunt infections occurred in sNPH patients who were shunted after a long preceding period of intensive care unit (ICU) treatment, which increases shunt infection risk because normal skin flora typically becomes exchanged and typical nosocomial bacteria dominate the skin flora.

Discussion

The provided data must be interpreted with care for several reasons. Most importantly, the data include the learning curve of both authors with the usage of G-valves, when they were first launched in the 1990s. The correct choice for the

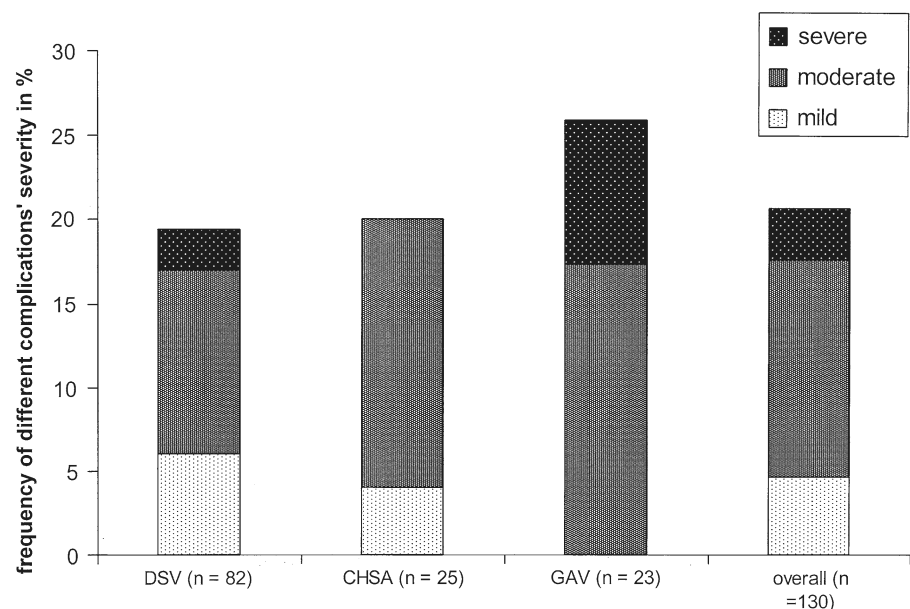


Fig. 3 Severity of shunt complications: apparent differences between the studied shunt types must be regarded against the divergent numbers for a correct validation

optimal opening pressure of G-valves was not so clear initially. Furthermore, the consequences of the choice of the opening pressure of the two different types of G-valves – the counterbalancer type and the switcher type – was also not yet clarified (13). With this in mind, the initial opening pressures that were obviously too high or too low in seven patients (5%) must be understood. Meanwhile, a better understanding of the different G-valves' function allows a more precise selection of the optimal opening pressure. Furthermore, it must be stressed that this retrospective analysis cannot compare the performances of the three tested shunt types. The size and constitution of the groups are too divergent to allow any meaningful conclusions. The fact that we excluded any patient without a complete data set might also be considered a weakness of this analysis, because by doing so, we lost 89 patients. However, because clinically unapparent overdrainage could be recognized in some instances only with early imaging performed after shunting, abandonment of such data could adulterate the results in both directions.

Yet, we found it worthwhile to analyze these data because they provide the first long-term experience (8 years in average, and maximally 11 years) of G-valves' performance. Furthermore, the fact that each explanted valve has been studied in a bench test to determine whether hydraulic mismanagement came from poor valve performance or whether it was due to a functional under- or overdrainage, strengthens the scientific rigor of this analysis.

The "shunt survival rate" as a measured value of a valve's performance is rightly under debate from our perspective, because it depends so much on the investigators' vigilance in recognizing minor shunt complications. It is undefined how precisely and by which means secondary non-responders must be separated from patients suffering functional underdrainage. The general lack of definitions of the severity of shunt complications makes the "shunt survival rate" a relatively weak tool to compare different shunt-types. However, in the absence of alternatives, it is the first figure that has to be compared. In contrast to the literature that describes shunt failure rates of 20–40% (2,3,7,8,17) after a significantly shorter follow-up, our "shunt survival rate" of about 80% after an average follow-up of 8 years appears favorable. Another factor to use in assessing shunt performance is the severity of complications. An overall low complication rate means nothing if the majority of the complications are life-threatening. A valve with a higher failure rate, but a lower risk profile may be superior. Again, lacking generally accepted definitions of the severity of shunt complications impedes comparisons with the literature. Similarly, as in most series of adult shunt surgery over the last decade, our shunt-related mortality was 0% (8). However, severe complications with permanent deficits have recently been shown to occur in 6% of patients (2,7,8,17). In our analysis, there

was not any permanent deficit due to shunt failure. What we termed a severe complication is often regarded as a moderate complication. From this viewpoint, G-valves may have a favorable risk profile compared with other valve designs.

The specific aim of G-valve design is to overcome overdrainage without increasing the underdrainage rate (1). Regarding our observed over- and underdrainage rates necessitating operative revisions of 5% each and comparing these figures with the literature, the performance of G-valves again appears favorable (1,3,8). The fact that hydraulic mismanagement resulted directly from shunt failure in only one case, while all remaining cases resulted from functional over- or underdrainage due to poorly chosen opening pressures or unexpected alterations of intraperitoneal pressure is promising.

One systemic weakness of G-valves has been discovered with the finding of catheter fracture of the DSV beyond the catheters' inlet or outlet of the housing. This may be due to shearing forces in a short region of the catheter where it leaves the housing in the transient zone of the rigid housing. This may also be due to immunological reactions against the subcutaneously-fixed catheter silicone. It typically took several years for this complication to occur. The manufacturer has fixed this problem by reinforcing the material of this critical region, but we lack the experience to determine whether the problem has been overcome by this change.

Conclusion

From a long-term perspective, the frequency and profile of G-valve complications appear comparatively favorable. For definitive conclusions, however, prospectively randomized series are needed.

Conflict of interest statement Dr.Kiefer has received some honoraria from Codman and Aesculap to speak about hydrocephalus. Issues of this paper were not involved.

References

1. Boon AJ, Tans JT, Delwel EJ, Egeler-Peerdeman SM, Hanlo PW, Wurzer HA, Avezaat CJ, de Jong DA, Gooskens RH, Hermans J (1998) Randomized comparison of low- and medium pressure shunts : Dutch Normal-pressure Hydrocephalus Study. *J Neurosurg* 88:490–495
2. Cochrane DD, Kestle JR (2003) The influence of surgical operative experience on the duration of first ventriculoperitoneal shunt function and infection. *Pediatr Neurosurg* 38:295–301
3. Dauch WA, Zimmermann R (1990) Normal pressure hydrocephalus. An evaluation 25 years following the initial description. *Fortschr Neurol Psychiatr* 58:178–190
4. Drake JM, Kestle J, Milner R, Cinalli G, Boop F, Piatt J, Haines S, Schiff SJ, Cochrane DD, Steinbok P, Mac Neil N (1998) Randomized

- trial of cerebrospinal fluid shunt valve design in pediatric hydrocephalus. *Neurosurgery* 43:294–303
5. Eymann R, Chehab S, Strowitzki M, Steudel WI, Kiefer M (2008) Clinical and economical consequences of antibiotic-impregnated cerebrospinal fluid shunt catheters. *J Neurosurg Pediatrics* 1:444–450
 6. Grumme T, Kolodziejczyk D (1995) *Komplikationen in der Neurochirurgie. Volume 2: Kranielle, zerebrale und neuropädiatrische Chirurgie.* Blackwell Berlin-Wien 543–540
 7. Hanlo PW, Cinalli G, Vandertop WP, Faber JA, Bogeskov L, Bogeskov SE, Boschert J, Chumas P, Eder H, Pople IK, Serlo W, Vitzthum E (2003) Treatment of hydrocephalus determined by the European Orbis Sigma Valve II survey: a multicenter prospective 5-years shunt survival study in children and adults in whom a flow-regulating shunt was used. *J Neurosurg* 99:52–57
 8. Hebb AO, Cusimano MD (2001) Idiopathic normal pressure hydrocephalus: a systematic review of diagnosis and outcome. *Neurosurgery* 49:1166–1186
 9. Jain H, Sgouros S, Walsh AR, Hockley AD (2000) The treatment of infantile hydrocephalus: “differential-pressure” or “flow-control” valves. A pilot study. *Child Nerv Syst* 16:242–246
 10. Kiefer M, Eymann R, Meier U (2002) Five years experience with gravitational shunts in chronic hydrocephalus of adults. *Acta Neurochir (Wien)* 144:755–767
 11. Kiefer M, Eymann R, Strowitzki M, Steudel WI (2005) Gravitational shunts in longstanding overt ventriculomegaly in adults. *Neurosurgery* 57:109–119
 12. Kiefer M, Eymann R, Steudel WI (2006) Outcome predictors for normal-pressure hydrocephalus. *Acta Neurochir Suppl* 96:364–367
 13. Kiefer M, Meier U, Eymann R (2006) Gravitational valves: relevant differences with different technical solutions to counteract hydrostatic pressure. *Acta Neurochir Suppl* 96:343–347
 14. Meier U, Kiefer M, Sprung C (2004) Evaluation of the Miethke Dual Switch valve in patients with normal pressure hydrocephalus. *Surg Neurol* 61:119–127
 15. Sainte-Rose C, Hoffman HJ, Hirsch JF (1989) Shunt failure. *Concepts Pediatr Neurosurg* 9:7–20
 16. Yamada H (1982) A flow-regulating device to control differential pressure in CSF shunt systems. Technical note. *J Neurosurg* 57:570–573
 17. Zemack G, Bellner J, Siesjo P, Stromblad LG, Romner B (2003) Clinical experience with the use of a shunt with an adjustable valve in children with hydrocephalus. *J Neurosurg* 98:471–476

Is It Possible to Minimize Overdrainage Complications with Gravitational Units in Patients with Idiopathic Normal Pressure Hydrocephalus? Protocol of the Randomized Controlled SVASONA Trial (ISRCTN51046698)

J. Lemcke, U. Meier, C. Müller, M. Fritsch, R. Eymann, M. Kiefer, U. Kehler, N. Langer, V. Rohde, H-Ch. Ludwig, F. Weber, V. Remenez, M. Schuhmann, and D. Stengel

Abstract Overdrainage is a common complication observed after shunting patients with idiopathic normal-pressure hydrocephalus (iNPH), with an estimated incidence up to 25%. Gravitational units that counterbalance intracranial pressure changes were developed to overcome this problem. We will set out to investigate whether the combination of a programmable valve and a gravitational unit (proGAV, Aesculap/Miethke, Germany) is capable of reducing the incidence of overdrainage and improving patient-centered outcomes compared to a conventional programmable valve (Medos-Codman, Johnson & Johnson, Germany).

SVASONA is a pragmatic randomized controlled trial conducted at seven centers in Germany. Patients with a high probability of iNPH (based on clinical signs and symptoms, lumbar infusion and/or tap test, cranial computed tomography [CCT]) and no contraindications for surgical drainage will randomly be assigned to receive (1) a shunt assistant

valve (proGAV) or (2) a conventional, programmable shunt valve (programmable Medos-Codman).

We will test the primary hypothesis that the experimental device reduces the rate of overdrainage from 25% to 10%. As secondary analyses, we will measure iNPH-specific outcomes (i.e., the Black grading scale and the NPH Recovery Rate), generic quality of life (Short Form 36), and complications and serious adverse events (SAE). One planned interim analysis for safety and efficacy will be performed halfway through the study. To detect the hypothesized difference in the incidence of overdrainage with a type I error of 5% and a type II error of 20%, correcting for multiple testing and an anticipated dropout rate of 10%, 200 patients will be enrolled.

The presented trial is currently recruiting patients, with the first results predicted to be available in late 2008.

Keywords Overdrainage • gravitational • idiopathic • hydrocephalus • SVASONA trial

J. Lemcke(✉)

Department of Neurosurgery, Unfallkrankenhaus Berlin, Warener Straße 7, Berlin D-12683, Germany
e-mail: Johannes.lemcke@ukb.de

M. Fritsch

Department of Neurosurgery, Ernst-Moritz-Arndt-University of Greifswald, Germany

R. Eymann

Department of Neurosurgery, Medical School, Saarland University, Kirrberger Street, Building 90, Homburg-Saar, Saarland 66421, Germany

M. Kiefer

Department of Neurosurgery, Saarland University Medical School, Kirrberger Street, Building: 90.1, Homburg-Saar 66421, Germany

U. Kehler and N. Langer

Department of Neurosurgery, Asklepios Hospital Altona, Hamburg, Germany

F. Weber

Department of Neurosurgery, Hospital Cologne-Merheim, Germany

D. Stengel

Center for Clinical Research, Department of Trauma and Orthopaedics, Unfallkrankenhaus Berlin and Ernst-Moritz-Arndt-University of Greifswald, Germany

Background

In the Dutch Normal-Pressure Hydrocephalus Study, improvement was found in 74% (95% confidence interval [CI] 59–85%) of patients randomized to low-pressure shunts (Medos-Hakim valve, Johnson & Johnson) as compared to 53% (95% CI 38–68%) with medium-pressure shunts (3). This was, however, accompanied by complication rates of 51% (95% CI 37–65%) and 28% (95% CI 15–41%), respectively. In our own clinical series of 128 patients undergoing shunting with a Miethke dual-switch valve (Aesculap/Miethke), good or excellent outcomes were achieved in 63% (95% CI 54–71%) of all subjects (7).

Tuning the opening pressure to the individual patient's optimum level is a challenging task. A mismatch commonly leads to siphoning and overdrainage, which manifests if the patient rises from the supine into an upright position. Overdrainage is the adverse shunting event that is most important and difficult to control. If intractable after pressure adjustment, surgical shunt revision may be necessary.

Recently, a programmable valve with a gravitational unit (proGAV) (1) that is able to compensate intracranial pressure (ICP) changes with different body positions was developed. It was recently FDA-approved and showed promising effects in an early clinical sample of patients for whom conventional approaches for relieving the symptoms of overdrainage had failed (8,10).

It is, however, unclear whether supplementation of established shunt systems with the shunt assistant leads to a clinically relevant decrease in the incidence of symptomatic and/or therapeutically relevant overdrainage (4). In this pragmatic, multicenter RCT, we aim to demonstrate that shunt-assisted drainage of CSF lowers the incidence of overdrainage in adults with iNPH and improves patient-centered outcomes.

Methods and Design

Eligible patients will be randomized according to a computer-generated list with permuted blocks to undergo shunting with:

1. The shunt-assistant valve (proGAV, Aesculap/Miethke, Germany, experimental arm). The proGAV device aims to control overdrainage in addition to another valve. The gravity of a tantalum sphere counterbalances the negative hydrostatic pressure in the shunt system of the patient. It works independent of posture and subcutaneous pressure. Technical details of the implant have previously been described (1).
2. The established Medos-Codman programmable valve system (Johnson & Johnson, Germany, control arm) (9). This is a device that provides constant intraventricular pressure and drainage of CSF. It features 18 pressure ranges. These ranges enable subtle alterations to the opening pressure. Each adjustment can easily be made through a programmer interface.

Random codes will be sealed in opaque envelopes, stored in the operating theatres, and opened immediately before implantation. The opening pressure of both devices will initially be set at 100 mm H₂O. After 3 months, both valves will be programmed to 70 mm H₂O (low pressure setting). A resetting to 100 mmH₂O or more represents an endpoint of the study. No other changes in post-operative aftercare or further treatment will apply for study purposes.

Primary Hypothesis

We will test the primary hypothesis that draining with the proGAV device decreases the rate of overdrainage from 25% to 10% compared to the Medos-Codman shunt 3 months after index surgery.

Overdrainage will be assumed in case of (1) clinical signs and symptoms suggestive of overdrainage (e.g., headache, vomiting, dizziness), (2) imaging results (e.g., subdural hematoma, slit-ventricle syndrome), and/or (3) any therapeutic interventions intended to resolve overdrainage.

Secondary Outcomes

Specific iNPH outcomes (i.e., the Black grading scale (2) and NPH Recovery Rate) and generic quality of life (Short-Form [SF] 36, German Version 2.0) will be measured after 3 and 6 months, and, optionally, after 1 year of follow-up.

Complications and adverse events will synoptically be recorded and reviewed during regular investigators' meetings. Halfway through the study, the clinical investigators together with the statistical consultant will perform an exploratory safety analysis and decide whether to proceed or to stop patient recruitment.

Trial Flow, Documentation, and Follow-Up

The trial flow resembles clinical practice and, apart from screening and baseline documentation, stipulates two scheduled follow-up visits at 3 and 6 months, both of which include a clinical examination (5,6), recording of iNPH outcome scales, and a CCT scan. Investigators are free to invite patients for a 1 year follow-up examination. CCT images will be independently rated by two investigators to (1) verify compliance with trial entry criteria and detect violations of exclusion criteria and (2) validate the radiological diagnosis of overdrainage.

Conclusion

The SVASONA trial is now recruiting and we hope to present first results by the end of 2008. If the hypothesized difference in overdrainage rates can be proven, the shunt-assistant valve may evolve as the new standard of care for patients with iNPH.

Conflict of interest statement We declare that we have no conflict of interest.

References

1. Allin DM, Czosnyka ZH, Czosnyka M, Richards HK, Pickard JD (2006) In vitro hydrodynamic properties of the Miethke ProGAV hydrocephalus shunt. *Cerebrospinal Fluid Res* 3:9

2. Black PM, Ojemann RG, Tzouras A (1998) CSF shunts for dementia, incontinence, and gait disturbance. *Clin Neurosurg* 32:632–651
3. Boon AJ, Tans JT, Delwel EJ, Egeler-Peerdeman SM, Hanlo PW, Wurzer HA, Avezaat CJ, de Jong DA, Gooskens RH, Hermans J (1998) Dutch Normal-Pressure Hydrocephalus Study: randomized comparison of low- and medium-pressure shunts. *J Neurosurg* 88:490–495
4. Esmonde T, Cooke S (2002) Shunting for normal pressure hydrocephalus (NPH). *Cochrane Database Syst Rev* CD003157
5. Klinge P, Marmarou A, Bergsneider M, Relkin N, Black PM (2005) Outcome of shunting in idiopathic normal-pressure hydrocephalus and the value of outcome assessment in shunted patients. *Neurosurgery* 57:S40–S52
6. Kiefer M, Eymann R, Komenda Y, Steudel WI (2003) A grading system for chronic hydrocephalus. *Zentralbl Neurochir* 64:109–115
7. Meier U, Kiefer M, Neumann U, Lemcke J (2006) On the optimal opening pressure of hydrostatic valves in cases of idiopathic normal-pressure hydrocephalus: a prospective randomized study with 122 patients. *Acta Neurochir Suppl* 96:358–363
8. Meier U, Lemcke J (2006) First clinical experiences in patients with idiopathic normal-pressure hydrocephalus with the adjustable gravity valve manufactured by Aesculap (proGAV). *Acta Neurochir Suppl* 96:368–372
9. Sprung C, Miethke C, Trost HA, Lanksch WR, Stolke D (1996) The dual-switch valve. A new hydrostatic valve for the treatment of hydrocephalus. *Childs Nerv Syst* 12:573–581
10. Tokoro K, Suzuki S, Chiba Y, Tsuda M (2002) Shunt assistant valve: bench test investigations and clinical performance. *Childs Nerv Syst* 18:492–499

Early Shunting Using the Parallel Shunt System in Hemorrhagic Hydrocephalus: In Vitro Testing of Handling, Technical Complications and Clogging Rate

F. Al-Zain, U. Meier, and J. Lemcke

Abstract In order to minimize the duration of external cerebrospinal fluid (CSF) drainage after hemorrhagic hydrocephalus we are testing a parallel shunt system that can be implanted very early after bleeding. It should be able to tolerate a high load of protein and blood in the CSF. After clearance of the CSF, the valveless arm of the shunt is closed by a percutaneous manipulation and the valve-arm is opened.

Keywords Hemorrhagic hydrocephalus • parallel shunt system • infection rate

Introduction

The current standard of care in intraventricular haemorrhage (IVH) in adults is an external ventricular drainage (EVD) system to monitor the intracranial pressure and treat hydrocephalus and to drain the bloody cerebrospinal fluid. After IVH, erythrocytes and high protein concentrations are sustained in the CSF for a long time. This requires a long-standing external CSF drainage before shunting. The reported infection risk of this two-step procedure ranges up to 50%. The purpose of this study is to significantly decrease the rate of ventriculitis by early shunting using a parallel dual shunt after a maximum of 5 days of EVD.

Materials and Methods

After insertion of an EVD system into all patients, a further procedure is carried out in a randomized exploratory phase-II study with 15 patients in each patient group. One patient

group will undergo early shunting on days 3–5 after EVD according to the CSF properties and radio-morphological findings (Fig. 1, Table 1), and early shunting is carried out with the parallel dual shunt system (modified by Pizzi) (Fig. 2). The other sample group will undergo late shunting after normalization of the CSF-properties. The optimal time for closing the valveless arm depends on radiological criteria. For conformation, puncture of the burr-hole reservoir for analysing the CSF properties is optional. The patients will be followed up by the Glasgow Outcome Scale. Blood infection parameter and serial cranial CT will be carried out in the follow-up during the in-hospital period, after 4 weeks and after 3 months (Table 2). Two parallel shunt systems are implanted, sharing one burr-hole and ventricular catheter with a larger diameter (1.5 mm), coupled by a Y-connector and one peritoneal catheter. One end of this arrangement carries an Integra Hakim valve system (Integra Neuroscience, Germany). To prevent blood from passing through the valve arm, an up-stream on–off switch has been introduced. The other end is a valveless shunt with low filtration properties and an upstream on–off switch. The position of the upper part of the body and head will regulate the CSF flow rate in the valveless arm. The optimal time of closing this arm has been previously mentioned. We are about to develop a diverting unit to replace the first Y-connector and the two upstream on–off switches that can be adjusted on either one of the arrangement’s arms by an external magnetic device. *In vitro-testing was done in our hospital with bloody CSF-like artificial solution in numerous valve systems.*

Results

We will primarily record the number of infections, handling issues, technical complications, and treatment successes in terms of imaging and outcome scoring results. In this hypothesis-generating, randomized phase-II trial, we set out to describe the feasibility, safety, and tolerability of this technique compared to the current standard of care.

U. Meier (✉), F. Al-Zain, and J. Lemcke
Department of Neurosurgery, Unfallkrankenhaus Berlin, Warener
Straße 7, Berlin D-12683, Germany
e-mail: ullrich.meier@ukb.de

Fig. 1 Example of the GRAEB classification for radiomorphological grading severity of IVH: 1 left lateral ventricle + 1 right lateral ventricle + 1 third ventricle (blood without expansion) + 1 fourth ventricle (blood without expansion) = total score 4

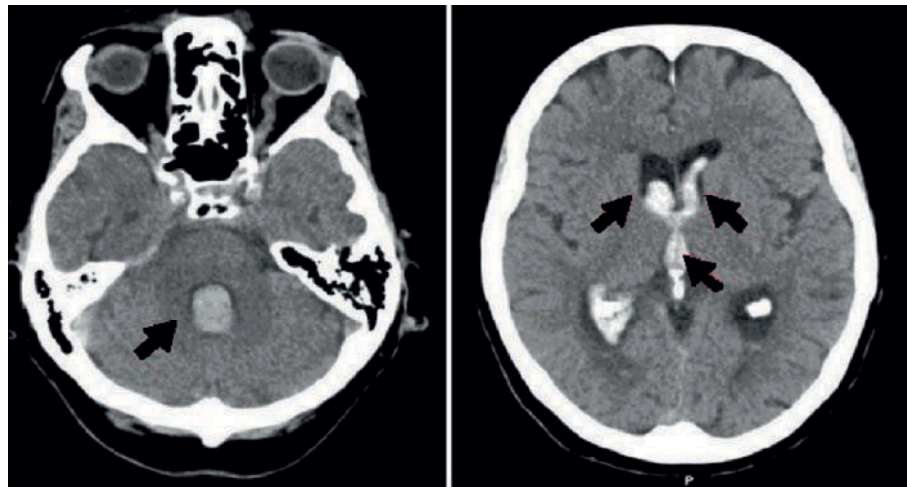


Table 1 A GRAEB score >6 is an exclusion criterion for implanting our shunt system

Points	Lateral (each ventricle is scored separately)	Third and fourth ventricle
1	Trace of blood or mild bleeding	Blood present, ventricle size normal
2	Less than the half ventricle filled with blood	Ventricle filled with blood and expanded
3	More than the half ventricle filled with blood	
4	Ventricle filled with blood and expanded	
	4 × 2	2 × 2

Discussion

Due to the perforation of the physiological barriers by the external ventricular drainage, infections of the cerebrospinal fluid are one of the most common complications of EVD systems (3, 4, 7, 10). Whilst gram-positive cocci of physiological skin flora dominate the microbiological findings in the international literature, the infection rate correlates with the duration of the external ventricular CSF drainage system (5, 6, 8, 9, 11–18). Infection rates of up to

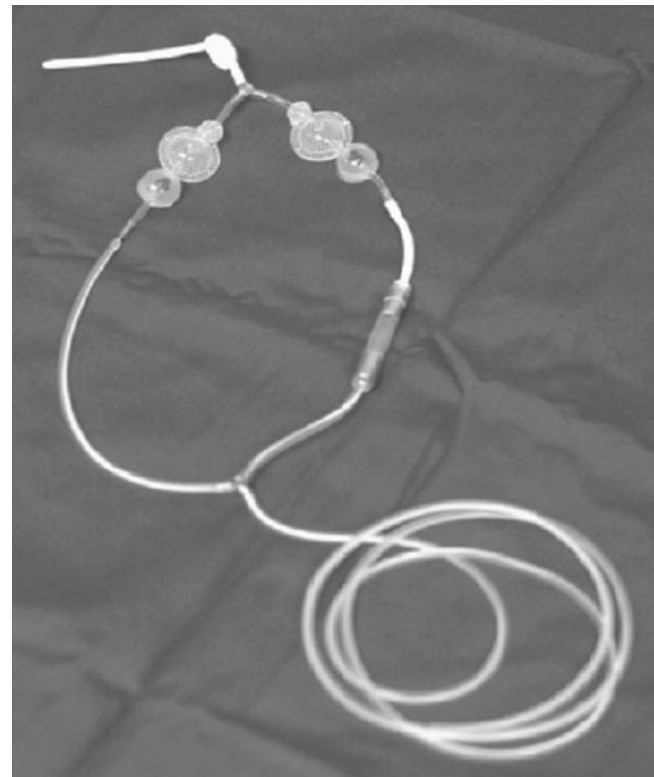


Fig. 2 Prototype of the parallel shunt system

Table 2 Follow-up scheme for the pilot study

	Baseline	Preop.	Postop. (24 h)	1 Week	4 Weeks	3 Months
Clinical examination	☒		☒	☒	☒	☒
CSF study	☒	☒		☒		
CT-scan	☒	☒	☒	☒	☒	☒
Glasgow Outcome Scale				☒	☒	☒
C-reactive protein	☒	☒		☒	☒	☒
AE and SAE			☒	☒	☒	☒

50% (1, 2) have been published. Against this background the duration of external CSF drainage should be minimized by the early implantation of a shunt system.

Conclusion

If the modified shunt system proves safe and effective (that is, if it allows for early shunting with a low infection rate), it is likely to change therapeutic principles in IVH management.

Conflict of interest statement We declare that we have no conflict of interest.

References

1. Chan KH, Mann KS (1988) Prolonged therapeutic external ventricular drainage: a prospective study. *Neurosurgery* 23(4): 436–438
2. Hasan D, Vermeulen M, Wijdicks EFM et al (1989) Management problems in acute hydrocephalus after subarachnoid hemorrhage. *Stroke* 20:747–753
3. Khanna RK, Rosenblum ML, Rock JP et al (1995) Prolonged external ventricular drainage with percutaneous long-tunnel ventriculostomies. *J Neurosurg* 83(5):791–794
4. Lo CH, Spelman D, Bailey M et al (2007) External ventricular drain infections are independent of drain duration: an argument against elective revision. *J Neurosurg* 106(3):378–383
5. Lozier AP, Sciacca RR, Romagnoli MF et al (2002) Ventriculostomy-related infections: a critical review of the literature. *Neurosurgery* 51(1):170–182
6. Lyke KE, Obasanjo OO, Williams MA et al (2001) Ventriculitis complicating use of intraventricular catheters in adult neurosurgical patients. *Clin Infect Dis* 33(12):2028–2033
7. Mayhall CG, Archer NH, Lamb VA et al (1984) Ventriculostomy-related infections: a prospective epidemiologic study. *NEJM* 310(9):553–559
8. Öhrström JK, Skou JK, Ejlertsen T et al (1989) Infected ventriculostomy: bacteriology and treatment. *Acta Neurochir* 100(1–2): 67–69
9. Paramore CG, Turner DA (1994) Relative risks of ventriculostomy infection and morbidity. *Acta Neurochir* 128(1–2):79–84
10. Park P, Garton HJ, Kocan MJ, Thompson BG (2004) Risk of infection with prolonged ventricular catheterization. *Neurosurgery* 55(3):594–601
11. Pfisterer W, Mühlbauer M, Czech T, Reinprecht A (2003) Early diagnosis of external ventricular drainage infection: results of a prospective study. *J Neurol Neurosurg Psych* 74(7):929–932
12. Schade RP, Schinkel J, Visser LG et al (2005) Bacterial meningitis caused by the use of ventricular or lumbar cerebrospinal fluid catheters. *J Neurosurg* 102(2):229–234
13. Smith RW, Alksne JF (1976) Infections complicating the use of external ventriculostomy. *J Neurosurg* 44(5):567–570
14. Steinbok P, Cochrane DD, Kestle JRW (1996) The significance of bacteriologically positive ventriculoperitoneal shunt components in the absence of other signs of shunt infection. *J Neurosurg* 84:617–623
15. Stenager E, Gerner-Smidt P, Kock-Jensen C (1986) Ventriculostomy-related infections – an epidemiological study. *Acta Neurochir* 83(1–2):20–23
16. Sundbärg G, Kjallquest A, Lundberg N, Ponten U (1972) Complications due to prolonged ventricular fluid pressure recording in clinical practice. In: Brock M, Dietz H (eds) *Intracranial pressure I: Experimental and clinical aspects*. Springer, Berlin, Germany, pp 348–351
17. Sundbärg G, Nordström CH, Söderström S (1988) Complications due to prolonged ventricular fluid pressure recording. *Brit J Neurosurg* 2(4):485–495
18. Zingale A, Ippolito S, Pappalardo P et al (1999) Infections and re-infections in long-term external ventricular drainage: a variation upon a theme. *J Neurosurg Sci* 43(2):125–133

Intracranial Irregularities Beside Hydrocephalus in H-Tx Rats

Michael Kiefer, Guenther Schneider, and Regina Eymann

Abstract

Introduction It has been well documented that up to 70% of H-Tx rats' offspring suffer from severe hydrocephalus, which can be fatal if it remains untreated. Some offspring also have non-fatal moderate hydrocephalus allowing a normal life expectancy. The objective of this study was finding other morphological intracranial abnormalities that are not directly related to hydrocephalus.

Method An MRT for small animals (Bruker, Biospec, Erlangen Germany) with a 2.4 T magnet at 100 MHz has been used to study 98 apparently non-hydrocephalic H-Tx rats. T2-weighted 2D-RARE, T2-weighted 3D-Turbo-RARE sequence and T1-weighted 3D-gradient-echo sequences were used.

Results Apart from 36% of animals with moderate or mild hydrocephalus, we found one animal with a cystic cerebellar malformation similar to an arachnoid cyst with minimal space occupying effects. Nine rats had a mild or moderate-sized unilateral enlargement of one lateral ventricle, but a causative occlusion of the Foramen of Monroe could not be verified. Finally, one animal with huge hydrocephalus had a midline cystic malformation between both cerebral hemispheres.

Conclusion Aside from the well-documented hydrocephalus, H-Tx rats may develop other intracranial malformations that have not yet been documented in the literature.

Keywords Hydrocephalus • H-Tx rats • arachnoid cyst • unilateral hydrocephalus • midline cyst • midline malformation

Introduction

H-Tx rats typically have inherited hydrocephalus with ventricular dilatation starting in late gestation due to obstruction of the cerebral aqueduct (7,13). Depending on environment, parity and other factors (5), the frequency of severely affected pups varies between 15% and 70% (11,13), which is compatible with the mode of inheritance of hydrocephalus (5). Untreated severely affected rats die from intracranial pressure excess at 4–6 weeks of age. Severely affected animals suffer from non-communicating hydrocephalus due to aqueduct stenosis normally, but some cases with probably different underlying pathology may occur (1, 25).

While a milder hydrocephalus form characterized by a later onset occasionally occurred in a colony maintained in Florida (USA) (5), others have found higher frequencies of moderate hydrocephalus in their colonies. A colony maintained in Japan was found with 5% and 14% moderate, compensated and mild hydrocephalus, respectively (20,23,27). The incidence of mild and moderate hydrocephalus, allowing long-term survival without treatment, was 36% in our colony.

The outer skull appearance allows the identification of severely affected pups at day 1 or 2 after birth, but the skull dimensions of animals with mild or moderate hydrocephalus are similar to those of H-Tx rats without hydrocephalus normally (11). To identify specifically animals with moderate or mild hydrocephalus, magnetic resonance imaging (MRI) had to be performed on all animals that were not apparently severely affected.

While the varying severity of hydrocephalus (5,11,20, 23,27), microstructural variations (11,18,20,25), genetical alterations (5,6,8,19) and CSF hydrodynamics (9,10) have been studied extensively in H-Tx rats, further intracranial central nervous system (CNS) abnormalities apart from hydrocephalus and alterations around the Foramen of Monroe (1) have not yet been described. We describe several incidentally found alterations, which were found during MRI scanning of our colony for mild and moderate hydrocephalus.

M. Kiefer (✉)

Departments of Neurosurgery, Saarland University Medical School, Kirrberger Street, Building: 90.1, Homburg-Saar 66421, Germany
e-mail: Michael.Kiefer@uks.eu

G. Schneider

Department of Diagnostic and Interventional Radiology, Saarland University Medical School, Kirrberger Street, Building: 90.1, Homburg-Saar 66421, Germany

R. Eymann

Department of Neurosurgery, Medical School, Saarland University, Kirrberger Street, Building 90, Homburg-Saar, Saarland 66421, Germany

Materials and Methods

Animals

H-Tx rats bred at the Saarland University were conventionally housed rats that originated from three several inbred pairs provided in 1996 by N.G. Harris, King's College, London. The strain was formed and maintained by strict brother-sister mating. Male and female rats were not continuously paired to avoid newborns' violations by male rats, as observed in our H-Tx colony maintained during the 1980s. The pairs were typically allowed to breed for three litters. The F5-generation of this strain consisted of 16% severely, overt hydrocephalic animals. This comparatively low incidence of severely affected rats remained stable between F2 and F5 (range: 16–20%).

We studied 98 rats with MRI, which had no overt hydrocephalus at the inspection on day 2 after birth. The animals' age at the time of examination was, on average, 6 ± 2 months (range: 3–8 months).

Anesthesia

Rats were anesthetized using 0.01% (RS)-(±)-2-(2-Chlorophenyl)-2-(methylamino)cyclohexan-1-on (Ketavet®) (2 mL/kg) and 2% 2-(2,6-Dimethylphenylamino)-5,6-dihydro-4H-thiazin (Rompun®) (0.2 mL/kg), intraperitoneally providing sufficient narcosis for about 90 min without the need for artificial ventilation.

MRI-Examination

All MR images were obtained using special scanner and a special coil for small animals (Biospect®, Bruker, Erlangen Germany), operating at 100 MHz in conjunction with a 2.4 T magnet. The imaging spectrometer was checked and calibrated weekly. Variations in the linear and angular distortion from test images of standardized phantoms were calculated and compensated for all three axes. Initially, a low resolution scan was performed for localization. Three different sequences were implemented for the examination, using the following parameters:

- *T2-weighted, 2D-RARE sequence*: TR, 5000 ms; TE, 24 ms; matrix 256×192 ; FOV, 2×2 cm; Pulse Length, 2,000 μ s; 2 averages; RARE-factor, 8; slice thickness, 2 mm; interslice gap, 1 mm; 20 slices
- *T2-weighted 3D-Turbo-RARE sequence*: TR, 500 ms; TE, 17 ms; matrix $256 \times 256 \times 32$; FOV, 2×2 cm; 1 aver-

age; RARE-factor, 16; slap-thickness, 16 mm; effective slice thickness, 0.5 mm

- *T1-weighted 3D-gradient-echo sequence*: TR, 160 ms; TE, 6.5 ms; pulse angle, 30°; matrix $256 \times 128 \times 64$; FOV, 2×2 cm; 1 average; slap-thickness, 16 mm; effective slice thickness, 0.25 mm

Typically the three sequences lasted no longer than 45 min. Images were analyzed on a SUN-4 workstation. For scoring the ventricular size, we used the T2-weighted 2D-RARE sequences.

If atypical findings, as described here, were detected, the T1-sequence was repeated approximately 10 min after contrast material injection. A total of 0.25 mmol/kg Gadolinium diethylenetriaminepentaacetic acid (Gd-DTPA) solution was injected via the tail vein.

According to Jones et al. (5), the brains were scored as severe hydrocephalus when lateral ventricular dilatation was visible on at least six images. If dilated lateral ventricles were seen on 3–4 or 1–2 images, the hydrocephalus was termed “moderate” or “mild,” respectively.

Ventriculo-Peritoneal Shunting and Postoperative Monitoring

A borehole 2 mm in diameter was made 2 mm laterally and 2 mm behind the bregma using a microsurgical drill. Dura mater was carefully coagulated and incised thereafter. The cortical surface was coagulated too, and the lateral ventricle was punctured using a silicone ventricular catheter with an outer diameter of 0.7 mm. CSF flow was verified. Another of our projects was to produce overdrainage in shunted rats. Therefore, we drained about 0.8–1.0 mL CSF via ventricular drainage before the catheter was subcutaneously tunneled and inserted into the peritoneal cavity (12). MRI imaging as described above for screening was performed as well, 2 days after shunting.

Results

Mild or moderate hydrocephalus, which was restricted to the lateral ventricles only, was seen in 35 of 98 (36%) examined rats. None of these rats developed the typical symptoms of raised intracranial pressure as seen in animals with severe forms of hydrocephalus. Compared to normal controls and non affected H-Tx rats, rats with a mild or moderate hydrocephalus were mentally retarded in general, which could be seen in learning and balancing tests (X-maze test, balance test) (unpublished data).

Unilateral Enlarged Ventricle

Unilaterally mild ($n = 4$) or moderate ($n = 5$) enlarged lateral ventricles together with a normal configuration for the remaining ventricles could be demonstrated in nine H-Tx rats (9%) (Fig. 1). No significant differences in learning and balancing test results were found in comparison to unaffected H-Tx rat. Obvious occluding lesions in or around the Foramen of Monro could not be seen. If CSF circulation disturbances caused ventricular enlargement, the causative lesions in the Foramen of Monro must have been very small, because lesions of minimally 0.25 mm diameter could have been visualized with the MRI sequences used. The outer CSF spaces on the affected hemisphere were not significantly larger than on the unaffected side, which should have been the case if local cerebral developmental deficits had caused ex vacuo enlargement of the ventricle. The histological examination of these nine H-Tx rats with unilateral mild or moderate ventricular enlargement might help to clarify the etiology. T1-weighted Gd-DTPA images provided no further information.

Midline Cyst

One of 98 screened animals without overt hydrocephalus at the inspection on day 2 after birth and with normal skull dimensions compared to H-Tx rats with overt hydrocephalus suffered unexpectedly from severe hydrocephalus, as revealed by MRI (Fig. 2). Yet ventricular dilatation

was restricted to the lateral ventricles exclusively supposing bilateral Foramen of Monro occlusion. This animal performed particularly worse in the balancing test. By MRI, we saw a midline cyst extending from the region of the bregma dorsally between both hemispheres. In an effort to establish a model of overdrainage in severely affected H-Tx rats by shunting in parallel, we decided to shunt and overdrain this animal. The next MRI was performed 2 days after shunting, showing clearly the effects of overdrainage with subdural effusions over both cerebral hemispheres. The shunted ventricle was subtotally collapsed, while the contralateral ventricle was clearly decreased in size. The remainder of intraventricular hemorrhage was also visible in the shunted ventricle. Remarkably, the midline cyst increased in size in the overdrained rat. This finding indicates that the cyst did not communicate with the outer CSF space.

Cerebellar Cyst

One of the 98 screened H-Tx rats presented with a right-sided cerebellar cystic lesion (Fig. 3). It can be speculated that this cystic lesion might be segmented, but this was not clearly visible on MRI. The unfinished histological examination of this lesion will clarify this issue. However, MRI demonstrates clearly that there is no or minimal mass effect of the cystic lesion. T1-weighted images with Gd-DTPA did not demonstrate any contrast medium affinity between the cyst's wall and its surrounding structures.

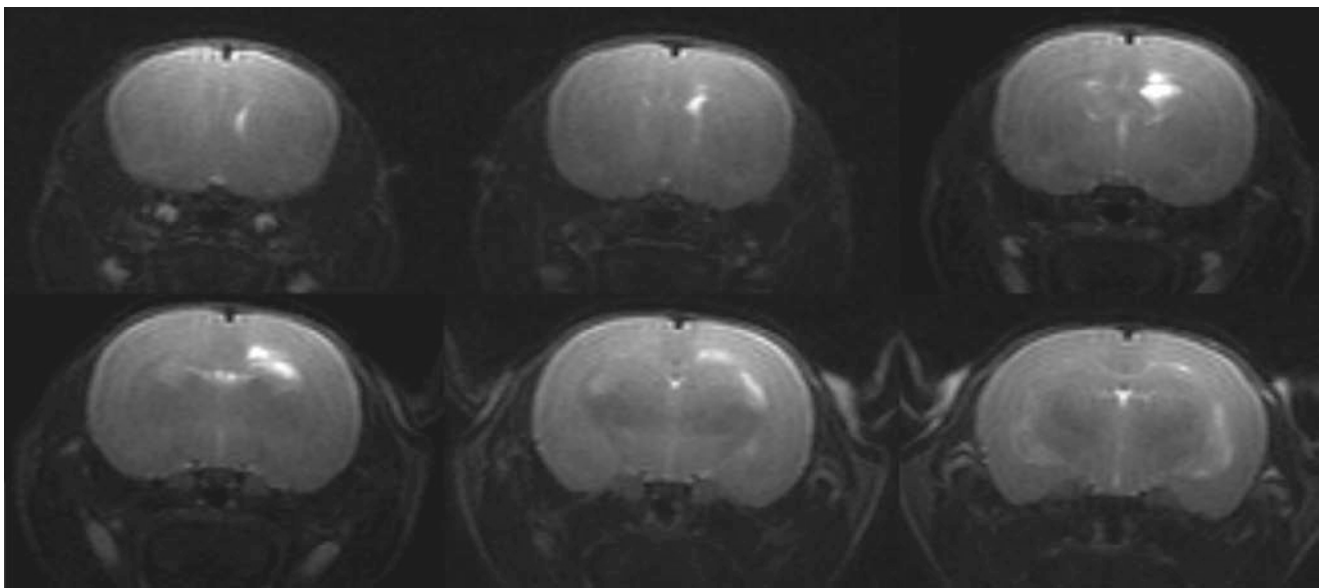


Fig. 1 Unilateral moderate enlarged lateral ventricle in coronal orientation. T2-weighted 3D-Turbo-RARE sequence

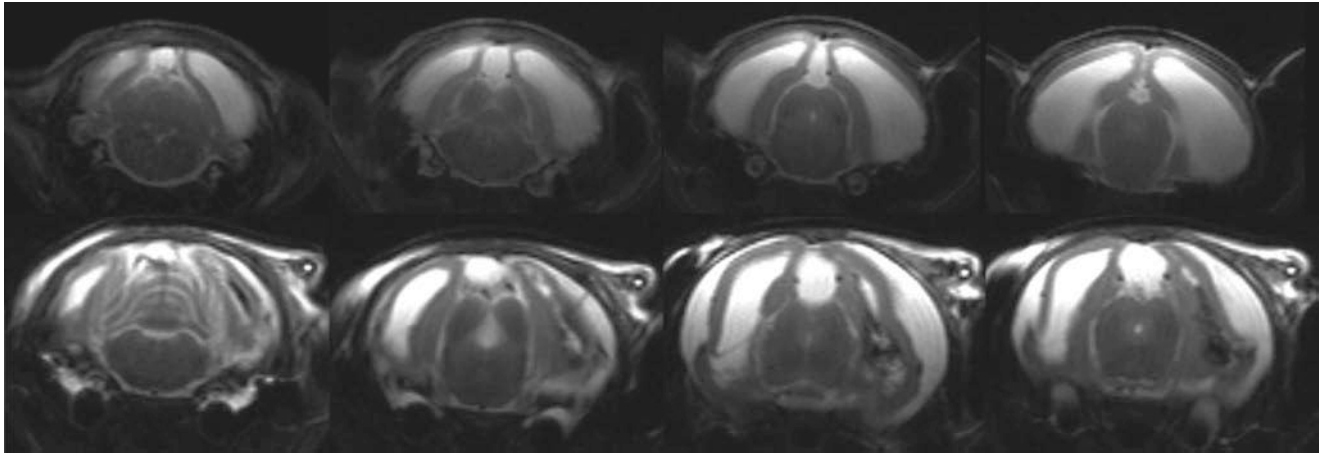


Fig. 2 Interhemispheric midline cyst; upper row: clearly enlarged dorsal part of lateral ventricles and an interhemispheric cystic lesion before shunting; lower row: same animal after shunting and intended overdrainage with left side collapsed and right side clearly shrunken

lateral ventricle, bilateral subdural effusions and intraventricular hemorrhage in the shunted ventricle are visible. The midline cyst appears larger than before shunting. T2-weighted 3D-Turbo-RARE sequence

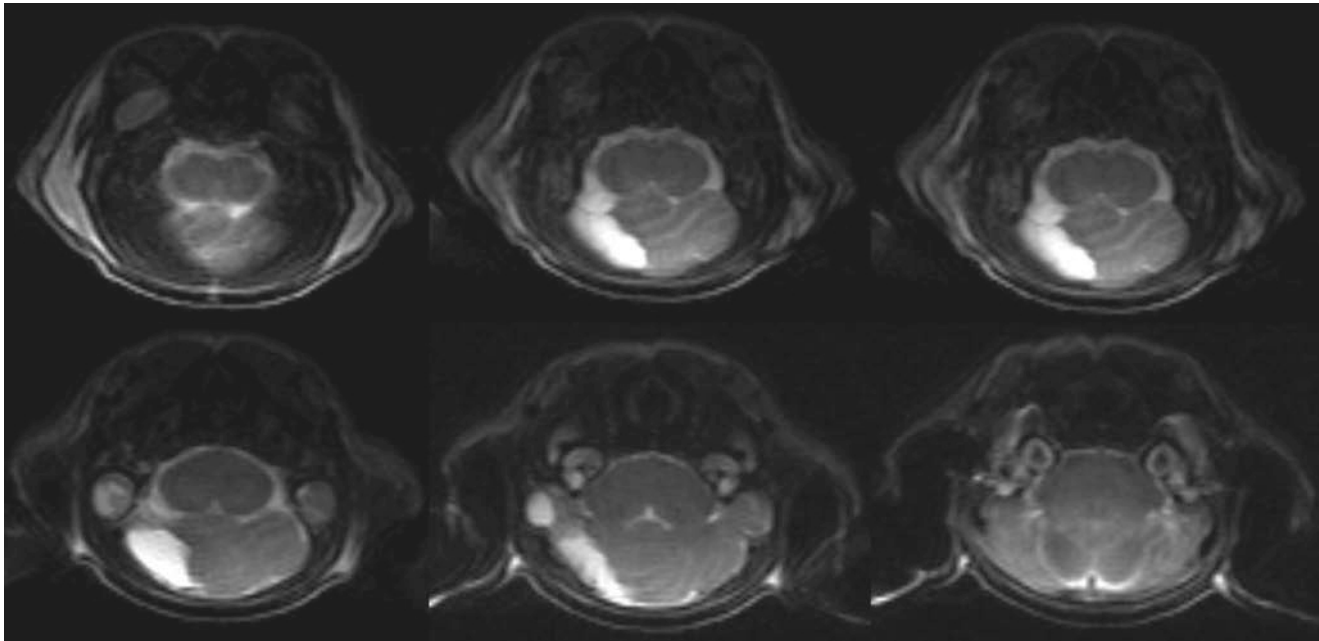


Fig. 3 Cerebellar cyst with minimal or lacking mass effect. Whether gross anatomy of cerebellar hemispheres is distorted and the hemispheres probably fused or whether most of the right cerebellar

hemisphere is lacking cannot be distinguished clearly. Similarly, it cannot be determined whether the cyst is segmented. T2-weighted 3D-Turbo-RARE sequence

Discussion

H-Tx rats are an inbred strain with inherited hydrocephalus of a variable proportion in the offspring. At least three different loci on different chromosomes have been identified to have linkage to hydrocephalus (6). However, epigenetic phenomena may have a significant influence on the frequency of severely affected animals (6). In Kohn's original colony,

severe hydrocephalic offspring occurred in about 70% of the pups, but other colonies produced severe hydrocephalic rats with a lower frequency (30–50%) (2,5,13,25,27). Interestingly the incidence of severe hydrocephalus in our colonies was comparatively low (15–20%) over two decades, despite our receipt of inbred pairs from different colonies. The first colony bred at the Saarland University was based upon inbred pairs provided in the 1980s by the Max Planck Institute Cologne (Germany). Our second and third bred colonies in

the early and the late 1990s of the last century were derived from colonies in Switzerland (G.Kaiser, Inselspital, Bern) and the United Kingdom (NG. Harris, King's Collage, London). Nevertheless the frequency of severe hydrocephalic offspring remained comparatively low. Yet in contrast to other colonies, the incidence of mild or moderate hydrocephalic H-Tx rats was comparatively high (30–40%). Mild or moderate hydrocephalic rats had normal life expectancy but performed slightly worse compared to unaffected H-Tx controls in balancing and learning tests (unpublished data). H-Tx rats with mild or moderate forms of hydrocephalus, which do not affect life expectancy, have also been reported by colonies in Florida (USA) and Japan (20,23,25,27) with an incidence between 4% and 15%, respectively. This variation in phenotypes between colonies is compatible with the complex mode of inheritance, which can be proven by many genetical analyses in H-Tx rats (5–8,19), given different husbandry and breeding conditions (5). While severe hydrocephalus occurs in our colonies as well, mostly in the presence of aqueduct stenosis, evidence exists that aqueduct stenosis is not a necessary prerequisite for severe hydrocephalus in H-Tx rats (25), as observed in various H-Tx colonies (11,13,21,27).

An underdevelopment of the subcommissural organ (SCO), which can be found typically in hydrocephalic H-Tx rats during late gestation, seems to play an important role in the development of hydrocephalus (25). The linkage between hydrocephalus and an underdeveloped SCO, however, is not fully understood. Before the SCO produces the Reissner's fiber during late gestation, it secretes soluble glycoproteins that are important for normal cerebral ontogeny. Nestin is an intermediate filament protein expressed in dividing cells during the early stages of CNS development. Upon differentiation, nestin is typically downregulated. During neuro- and gliogenesis, nestin is replaced by cell type-specific intermediate filaments, e.g., neurofilaments and glial fibrillary acidic protein (GFAP). Interestingly, nestin expression is reinduced in the adults during pathological situations, such as the formation of the glial scars after CNS injury and in active hydrocephalus (4,24,26,28). Normal SCO cells have nestin immunoreactivity regularly (3), but, consistently with the underdevelopment of SCO in (hydrocephalic) H-Tx rats, the nestin immunoreactivity level is low in newborn H-Tx rats (25).

Against the background of an outstanding importance of SCO function for normal cerebral ontogenesis, it is reasonable to assume that hydrocephalus CNS abnormalities may occur with defective SCO function during gestation. Apparently, our colony is subject to specific epigenetic phenomena that significantly affect the proportion of severe and moderate hydrocephalic offspring. Given such obviously

specific developmental aberrations (e.g., cerebellar cyst, midline cyst) as reported here, these might also be the consequence of abnormal SCO function.

While this is the first description of an obvious Foramen of Monro obstruction in mature H-Tx rats leading to mild, moderate or severe uni- or bilateral ventricular widening, observations exist of alterations of the Foramen of Monro and displaced choroid plexus in the anterior part of the lateral ventricle of H-Tx rats during gestation (1). It has been demonstrated that the Foramen of Monro may have a smaller extent in H-Tx fetuses, and its orifice was decreased further by a displaced choroid plexus (1). It seems reasonable to assume that these fetal morphological changes might also result in uni- or bilateral ventricular dilation in adult H-Tx rats. Notably, the alterations of and around the Foramen of Monro precede the formation of fetal aqueduct stenosis, which might explain the quite high frequency of moderate or mild hydrocephalus in our H-Tx colony. Supposing specific local preconditions provoking alteration of or around the Foramen of Monro, a hydrocephalus evolution of the lateral ventricles might be triggered before aqueduct stenosis can become relevant for hydrocephalus development. If it develops later in parallel its effect should be restricted because the preceding Foramen of Monro occlusion represents the earlier and accordingly most relevant CSF pathway obstruction. Typically such hydrocephalus was restricted to dilated lateral ventricles in the presence of a normal sized third ventricle, suggesting the existence of bilateral Foramen of Monro obstruction.

Overall, evidence exists suggesting a more generalized developmental alteration of the neuroepithelium during fetal development in H-Tx rats that may affect different cerebral regions at different stages (1, 28). Such an alteration may also be responsible for defective development of the subarachnoidal space, culminating in alterations affecting the midline and provoking an interhemispheric cyst, as described here.

However, we do not think that the alterations seen in H-Tx rats are closely related to the hereditary cerebellar vermis defect (CVD), which has been reported in another rat mutant (14,17). CVD rats suffer from agenesis of the cerebellar vermis, cerebellar cyst formation, fused cerebellar hemispheres and a mildly disorganized microstructure of the cerebellar hemispheres (14–17), which “clinically” results in hind-leg paralysis. This manifestation is similar to the “clinical” appearance of severely affected H-Tx rats some days before they die due to excessive hydrocephalus and not typical for the abnormality described here. Yet, the genetic background of CVD and H-Tx rats is completely different (5,17).

Conclusion

Apart from hydrocephalus, H-Tx rats may present with a multitude of other CNS abnormalities, suggesting generalized developmental alteration of the neuroepithelium during fetal CNS development. This aberrant development may affect different cerebral regions at different stages, possibly influenced by as yet undiscovered epigenetic effects. This explanation could potentially reconcile current disagreement regarding whether or not aqueduct stenosis represents the sole cause of hydrocephalus in H-Tx rats. Further research will be necessary to completely understand the basic pathology of H-Tx rats.

Conflict of interest statement Dr.Kiefer has received some honoraria from Codman and Aesculap to speak about hydrocephalus. Issues of this paper were not involved.

References

- Boillat CA, Jones HC, Kaiser GL (2001) Inherited hydrocephalus in the H-Tx rat: the ventricular system in late-gestation and neonatal aqueduct stenosis. *Eur J Pediatr Surg* 11(1):43–44
- Cai X, McGraw G, Pattisapu JV, von Kalm L, Willingham S, Socci DJ, Gibson JS (2000) Hydrocephalus in the H-Tx rat: a monogenic disease? *Exp Neurol* 163:131–135
- Chouaf-Lakhdar L, Fèvre-Montange M, Brisson C, Strazielle N, Gamrani H, Didier-Bazès M (2003) Proliferative activity and nestin expression in periventricular cells of the adult rat brain. *Neuroreport* 14:633–636
- Guérette D, Khan PA, Savard PE, Vincent M (2007) Molecular evolution of type VI intermediate filament proteins. *BMC Evol Biol* 7:164
- Jones HC, Loppman BA, Jones TW, Carter BJ, Depelteau JS, Morel L (2000) The expression of inherited hydrocephalus in H-Tx rats. *Childs Nerv Syst* 16:578–584
- Jones HC, Carter BJ, Depelteau JS, Roman M, Morel L (2001) Chromosomal linkage associated with disease severity in the hydrocephalic H-Tx rat. *Behav Genet* 31:101–111
- Jones HC, Yehia B, Chen GF, Carter BJ (2004) Genetic analysis of inherited hydrocephalus in a rat model. *Exp Neurol* 190:79–90
- Jones HC, Chen GF, Yehia BR, Carter BJ, Akins EJ, Wolpin LC (2005) Single and multiple congenic strains for hydrocephalus in the H-Tx rat. *Mammalian Genome* 16:251–261
- Kaiser G, Jones HC (1991) Cerebrospinal fluid pressure in 10-day-old rats with congenital hydrocephalus. *Eur J Pediatr Surg* 1(Suppl. 1):20–22
- Kiefer M, Eymann R, Hollanda M, Schneider J, Reiche W (1997) Development of a long term VP-shunt model in hydrocephalic rats. In: 11th International congress of Neurological Surgery, Volume 2, Monduzzi Editore, International Proceedings Division Bologna, 2233–2236; ISBN: 88-323-0706-5
- Kiefer M, Eymann R, von Tiling S, Muller A, Steudel WI (1998) The ependyma in chronic hydrocephalus. *Childs Nerv Syst* 14:263–270
- Kiefer M, Eymann R, Steudel WI (2000) The dynamic infusion test in rats. *Childs Nerv Syst* 16:451–456
- Kohn DF, Chinookoswong N, Chou SM (1981) A new model of congenital hydrocephalus in the rat. *Acta Neuropathol (Berl)* 54:211–218
- Kuwamura M, Yoshida T, Yamate J, Kotani T, Sakuma S (1994) Hereditary cerebellar vermis defect in the Lewis rat. *Brain Res Dev Brain Res* 83:294–298
- Kuwamura M, Ishida A, Yamate J, Kato K, Kotani T, Sakuma S (1997) Chronological and immunohistochemical observations of cerebellar dysplasia and vermis defect in the hereditary cerebellar vermis defect (CVD) rat. *Acta Neuropathol* 94:549–556
- Kuwamura M, Morikawa T, Yamate J, Kato K, Kotani T, Sakuma S (2000) Glial pathology in development of cerebellar dysplasia in the hereditary cerebellar vermis defect (CVD) rat. *Acta Neuropathol* 99:305–309
- Kuwamura M, Yoshida T, Ishida A, Tsudzuki M, Yamate J, Kotani T, Sakuma S (1996) Cerebellar vermis defect: a new neurological mutation in the rat. *J Hered* 87:161–162
- Miller JM, McAllister JP II (2007) Reduction of astrogliosis and microgliosis by cerebrospinal fluid shunting in experimental hydrocephalus. *Cerebrospinal Fluid Res* 4:5
- Miller JM, Kumar R, McAllister JP II, Krause GS (2006) Gene expression analysis of the development of congenital hydrocephalus in the H-Tx rat. *Brain Res* 1075:36–47
- Miyazawa T, Sato K, Ikeda Y, Nakamura N, Matsumoto K (1997) A rat model of spontaneously arrested hydrocephalus. *Childs Nerv Syst* 13:189–193
- Nojima Y, Enzan H, Hayashi Y, Nakayama H, Kiyoku M, Mori K (1998) Neuroepithelial and ependymal changes in HTX rats with congenital hydrocephalus: an ultrastructural and immunohistochemical study. *Pathol Int* 48:115–125
- Owen-Lynch PJ, Draper CE, Mashayeki F, Bannister CM, Miyan JA (2003) Defective cell cycle control underlies abnormal cortical development in the hydrocephalic Texas rat. *Brain* 126:623–631
- Shen XQ, Miyajima M, Ogino I, Arai H (2006) Expression of the water-channel protein aquaporin 4 in the H-Tx rat: possible compensatory role in spontaneously arrested hydrocephalus. *J Neurosurg* 105(6 Suppl Pediatrics):459–464
- Shi M, Wei LC, Cao R, Chen LW (2002) Enhancement of nestin protein-immunoreactivity induced by ionizing radiation in the forebrain ependymal regions of rats. *Neurosci Res* 44:475–481
- Somera KC, Jones HC (2004) Reduced subcommissural organ glycoprotein immunoreactivity precedes aqueduct closure and ventricular dilatation in H-Tx rat hydrocephalus. *Cell Tissue Res* 315:361–373
- Takano T, Rutka JT, Becker LE (1996) Overexpression of nestin and vimentin in ependymal cells in hydrocephalus. *Acta Neuropathol* 92:90–97
- Wada M (1988) Congenital hydrocephalus in HTX-rats: incidence, pathogenesis and developmental impairment. *Neurol Med Chir* 28:955–964
- Wei LC, Shi M, Chen LW, Cao R, Zhang P, Chan YS (2002) Nestin-containing cells express glial fibrillary acidic protein in the proliferative regions of the central nervous system of postnatal developing and adult mice. *Brain Res Dev Brain Res* 139:9–17

Co-morbidity as a Predictor of Outcome in Patients with Idiopathic Normal-Pressure Hydrocephalus

Ullrich Meier and Johannes Lemcke

Abstract

Introduction A critical question in the diagnosis and treatment of idiopathic normal-pressure hydrocephalus (iNPH) is which preoperative factors can most reliably predict outcomes following shunt insertion. The number and type of co-morbidities are increasingly being viewed as important predictive indicators.

Materials and Methods Between 1997 and 2005, 100 patients were implanted with a gravitational ventriculo-peritoneal shunt as a treatment for iNPH. All coincident disease processes were recorded. Eighty-two of these patients underwent follow-up of 2 years post-operation. The results of this prospective follow-up examination (Kiefer Score, NPH Recovery Rate) were compared with the preoperative Co-morbidity Index (CMI).

Results Of the patients with a CMI score of 0–1 ($n = 18$), 67% experienced an excellent outcome, 28% a good outcome, and 5% and 0% fair and poor outcomes, respectively. A CMI score of 2–3 was associated with markedly poorer outcomes ($n = 33$); 42% excellent, 30% good, 18% fair and 10% poor. A score of 4–5 was related to 14% excellent, 27% good, 23% fair and 36% poor outcomes ($n = 22$). Remarkably, a few patients scoring between 6 and 8 on the CMI scale experienced a favorable outcome. The outcomes for this latter group were 0% excellent, 10% good, 45% fair and 45% poor ($n = 9$).

Conclusion Co-morbidity is a statistically significant predictor of the quality of clinical outcome for patients with iNPH undergoing shunt therapy.

Keywords Co-morbidity • outcome • idiopathic normal-pressure hydrocephalus (iNPH)

Introduction

Patients with idiopathic normal-pressure hydrocephalus (iNPH) are usually elderly and, as such, often present multiple co-morbidities. In this prospective audit, we aim to evaluate whether a Co-morbidity Index (CMI) (7) can be used to provide a prognostic indicator for the quality of clinical outcomes following shunt surgery for iNPH.

Materials and Methods

In the Department of Neurosurgery at the Unfallkrankenhaus Berlin, Germany between September 1997 and July 2005, 100 patients were diagnosed with iNPH and treated surgically. The 65 men and 35 women had an average age of 67 at diagnosis (range 27–83). All patients underwent implantation of gravitational valves (54 x Miethke-Aesculap® Dual switch valve, 20 x programmable Codman® Medos valve with Miethke-Aesculap® gravitational assistant valve, 26 x Miethke-Aesculap® proGAV). It was possible to follow-up 82 of these patients over a 2 year postoperative period. Twelve patients died from causes unrelated to either the shunt operation or their iNPH between 10 and 19 months postoperatively (six from heart disease, three from neoplastic disease, two from pneumonia and one from renal failure). One patient died perioperatively from a pulmonary embolism despite thromboprophylaxis (1% perioperative mortality). Five patients were lost to follow-up.

Diagnosis

Patients who displayed gait ataxia in addition to other cardinal symptoms of iNPH and who showed neuroradiological evidence of ventricular enlargement were further assessed with an intrathecal infusion test. To determine the individual CSF flow parameters, a dynamic infusion test was performed via lumbar

U. Meier (✉) and J. Lemcke
Department of Neurosurgery, Unfallkrankenhaus Berlin, Warener
Straße 7, Berlin D-12683, Germany
e-mail: ullrich.meier@ukb.de

puncture using a computer-assisted constant flow technique with an infusion rate of 2 mL/min. A resistance of 13 mmHg or higher was defined as pathological. Immediately following the dynamic infusion test a diagnostic drainage of at least 60 mL CSF was carried out using the same puncture site. An improvement in the clinical picture over the ensuing 2 or 3 days served as an indication for the implantation of a ventriculo-peritoneal shunt. If the patient's symptoms, particularly the gait ataxia, did not initially improve, then 2–3 days of further external lumbar drainage was performed. Once more, if symptoms improved over this period, shunting was initiated.

Clinical Grading

The Black Grading System for Shunt Assessment and the NPH Recovery Rate (based on the clinical grading for NPH by Kiefer) were used to express the results of the clinical examinations. All graded examination results were split into four clinical outcome groups; excellent (restoration of pre-morbid activity levels), good (limited reduction in activity levels), fair (partial improvement) and poor (transient or no improvement). The first group was defined by an NPH Recovery Rate of ≥ 7.5 (75–100% improvement), the second by a rate of ≥ 5 (50–74% improvement), the third by a rate of ≥ 2 (20–49% improvement) and the fourth by a rate of < 2 (partial improvement up to 19% or deterioration).

$$\text{NPH Recovery Rate} = \frac{\text{NPH Grading}_{\text{preoperative}} - \text{NPH Grading}_{\text{postoperative}}}{\text{NPH Grading (Kiefer)}_{\text{postoperative}}} \times 10$$

Co-morbidity Index (CMI)

Kiefer et al. (7) introduced an assessment tool for various pathologies and their clinical effect when present in NPH.

By collecting the scores for each co-morbid disease process found in Table 1, a CMI score of between 0 and 23 can be calculated.

Results

Of the 82 patients studied, 29 (35%) experienced an excellent outcome, 22 (27%) a good outcome and 16 (20%) a fair outcome. Fifteen patients (18%) experienced a poor outcome. Thus, 67 patients responded to treatment, for a responder rate of 82%. Figure 1 graphically relates the preoperative CMI score to the clinical outcomes of all iNPH patients who underwent follow-up examinations postoperatively. Ninety-five percent of patients with a CMI score of 0–1 achieved an excellent or good outcome. A CMI score of 2–3 was associated with a noticeable decrease in the quality of outcomes (n = 33: excellent 42%, good 30%, fair 18%, poor 10%). Patients scoring 4–5 (n = 22: 14%, 27%, 23%, 36%) or

Table 1 Co-morbidity Index (CMI)

Risk factors	1 Point	2 Points	3 Points
Vascular	Hypertension	Diabetes mellitus	
	Aortofemoral bypass	Peripheral vascular disease	
	Stent	Vascular occlusion	
Cerebro-vascular	Posterior circulatory insufficiency	Vascular encephalopathy	Cerebral infarction
	ICA stenosis	TIA/PRIND	
Cardiac	Arrhythmia		
	Valve disease		
	Heart failure/stent		
	Aortocoronary bypass		
	Myocardial infarction		
Others		Parkinson's disease	

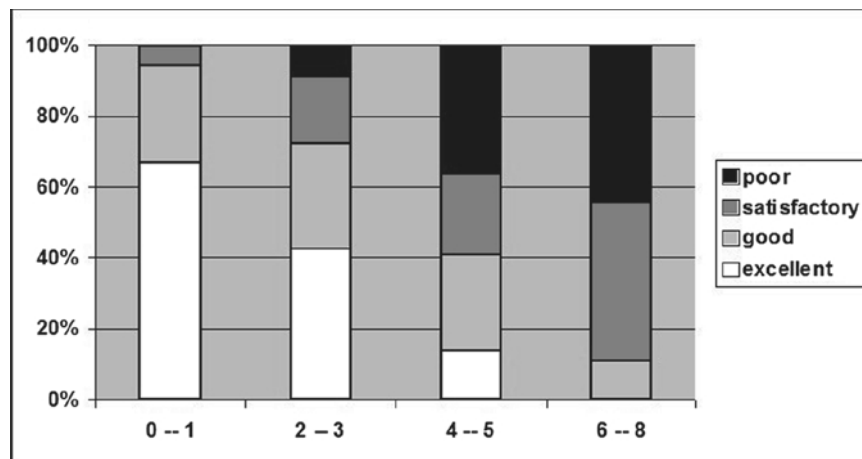


Fig. 1 Responder rate

Outcome \ CMI	0 - 3	4 - 8
excellent / good	41	10
satisfactory / poor	10	21

Fig. 2 Kiefer's CMI on postoperative outcomes in patients with iNPH is associated with a sensitivity of 80% and a specificity of 68%

6–8 (n=9: 0%, 10%, 45%, 45%) on the preoperative CMI scale experienced markedly poorer postoperative outcomes.

As a predictive tool, Kiefer's CMI on postoperative outcomes in patients with iNPH is associated with a sensitivity of 80% and a specificity of 68%. Outcomes in patients with a CMI score between 0 and 3 were significantly better than those of patients with a CMI greater than 3 (Fig. 2).

Discussion

In all branches of medicine, a multidisciplinary approach involving various specialties is necessary for two important reasons. Firstly, for an intervention to be effective, it must be ascertained that the observed symptoms are indeed caused by the disease process targeted by the treatment method and not by some other pathology. Secondly, it is important to recognize situations in which the detrimental effect of co-morbidity on the probable outcome of a given intervention is such that little or no improvement can be expected. Both of these possibilities represent a potential contraindication to operative therapy (8,9).

Co-morbidity

A review of the international literature yields a mean reported rate of co-morbidity in iNPH of 43% (5). Cerebrovascular insufficiency is described in 45% of these patients. The most common co-morbidity (78–100%) is vascular encephalopathy. Parkinson's disease or Parkinsonianism were present in 10% of cases, and 10% had histologically unconfirmed but clinically suspected Alzheimer's dementia (11). In order to distinguish the clinical picture of iNPH from other dementing syndromes, Golomb et al. (4) and Savolainen et al. (10) describe the coincidence of Alzheimer's disease and iNPH. Centrally limited motor disturbances can likewise result in an overlapping entity. In the patient population reported in this study, 8% were found to have Parkinson's disease in addition to iNPH. The exclusion of progressive cerebrovascular

dementia as a differential diagnosis in iNPH is an important motivation for the use of invasive diagnostic procedures. Co-morbidities can be clinically quantified in terms of risk factors. Such a system – the Co-morbidity Index – was introduced in 2006 by Kiefer (6,7). In it, the most common co-morbid pathologies are assigned between one and three points, which, when totaled as a CMI score, can be referred to an empirical threshold value above which the likelihood of a good to excellent outcome significantly decreases. This indirect correlation (Fig. 3) between outcome and CMI is unequivocally demonstrated in this study – those patients with a CMI score of 0 or 1, 67%, had an excellent outcome, while 45% of patients with a CMI of between 6 and 8 experienced an unsatisfactory outcome. Kiefer et al. (7) suggest a CMI of three as a threshold value dividing patient groups with a statistically favorable prognosis from those with a tendency towards a poor outcome. The data from this study serve to confirm the value of this cut-off point; of the patients who experienced a good or excellent outcome 80% (41/51) had a CMI \leq 3. Only 10/31 patients (32%) with a CMI > 3 experienced a comparable improvement in symptoms.

Outcome

The general improvement rates reported in the literature for patients with NPH undergoing a shunt operation vary around a mean of 53% (range 31–96%). In one meta-analysis, Vanneste (12) gives a figure of between 30% and 50%. Hebb and Cusimano (5) report an immediate improvement rate following iNPH shunt operations of 59%, falling to 29% in the long term. The results of our study show an overall improvement rate at 2 years post-shunt of 82%, in keeping with the international literature (1–3).

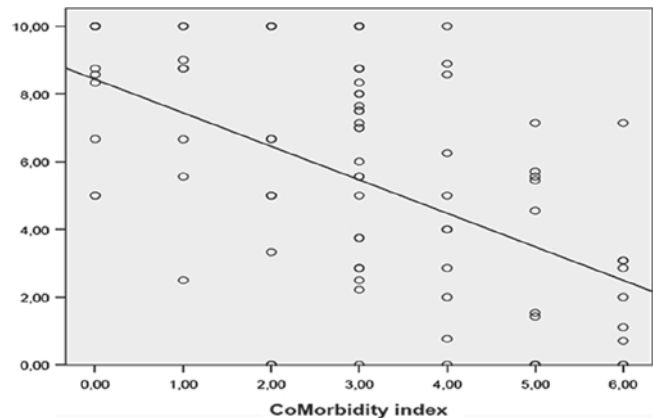


Fig. 3 Correlation of Kiefer's CMI and outcome after shunting

Conclusion

Co-morbidity is a statistically significant predictor of the quality of the clinical outcome for patients with iNPH undergoing shunt therapy (sensitivity = 80%; specificity = 68%). A CMI score of less than three points allows for a good post-operative prognosis. A CMI of more than three significantly decreases the chance of a good outcome and this should form part of the assessment when the risks and benefits of surgery are considered. Due to factors arising from co-morbidity, a successful outcome in patients with a CMI of six or more is unlikely.

Conflict of interest statement We declare that we have no conflict of interest.

References

1. Bech RA, Waldemar G, Gjerris F (1999) Shunting effects in patients with idiopathic normal pressure hydrocephalus: correlations with cerebral and leptomeningeal biopsy findings. *Acta Neurochir (Wien)* 141:633–639
2. Boon AJ, Tans JT, Delwei EJ, Egeler-Peerdeman SM, Hanlo PW, Wurzer HA, Hermans J (1999) Dutch Normal Pressure Hydrocephalus Study: the role of cerebrovascular disease. *J Neurosurg* 90(2): 221–226
3. Borgesen SE (1984) Conductance to outflow of CSF in normal pressure hydrocephalus. *Acta Neurochir (Wien)* 71:1–15
4. Golomb J, Wisoff J, Miller DC, Boksay I, Kluger A, Weiner H, Salton J, Graves W (2000) Alzheimer's disease comorbidity in normal pressure hydrocephalus: prevalence and shunt response. *J Neurol Neurosurg Psychiatr* 68(6):778–781
5. Hebb AO, Cusimano MD (2001) Idiopathic normal pressure hydrocephalus: a systematic review of diagnosis and outcome. *Neurosurgery* 49:1166–1186
6. Kiefer M, Eymann R, Meier U (2002) Five years experience with gravitational shunts in chronic hydrocephalus of adults. *Acta Neurochir (Wien)* 144:755–767
7. Kiefer M, Eymann R, Steudel WI (2006) Outcome predictors for normal pressure hydrocephalus. *Acta Neurochir (suppl.)* 96: 364–367
8. Meier U, Kiefer M, Sprung C (2003) Normal-pressure hydrocephalus: pathology, pathophysiology, diagnostics, therapeutics and clinical course. PVV Science, Ratingen
9. Meier U, Zeilinger FS, Kintzel D (1999) Signs, symptoms and course of normal pressure hydrocephalus in comparison with cerebral atrophy. *Acta Neurochir (Wien)* 141(10):1039–1048
10. Savolainen S, Paljarvi L, Vapalahti M (1999) Prevalence of Alzheimer's disease in patients investigated for presumed normal pressure hydrocephalus: a clinical and neuropathological study. *Acta Neurochir (Wien)* 141(8):849–853
11. Tulberg M (2000) CSF sulfatide distinguishes between NPH and subcortical atherosclerotic encephalopathy. *J Neurol Neurosurg Psychiatr* 69:74–81
12. Vanneste JA (2000) Diagnosis and management of normal-pressure hydrocephalus. *J Neurol* 247(1):5–14

Subarachnoid Hemorrhage and Intracerebral Hemorrhage

Effects of Magnesium Sulfate Infusion on Cerebral Perfusion in Patients After Aneurysmal SAH

George Kwok-Chu Wong, Rachael Kwok, Karen Tang, David Yeung, Anil Ahuja, Ann Dorothy King, and Wai-Sang Poon

Abstract

Background A meta-analysis of current data suggests that magnesium sulfate infusion improves the outcome after aneurysmal subarachnoid hemorrhage through a reduction in delayed ischemic neurological deficit. Two multi-center randomized controlled trials are currently underway to investigate this hypothesis. The possible pharmacological basis of this hypothesis includes neuroprotection and vasodilatation. We aim to investigate the cerebral hemodynamic effects of magnesium sulfate infusion in aneurysmal subarachnoid hemorrhage patients.

Method A total of 12 patients who had experienced aneurysmal subarachnoid hemorrhage were randomized to magnesium sulfate infusion ($n = 6$) or placebo infusion ($n = 6$) for 14 days. Each patient had two perfusion MRIs performed, one in the first week after subarachnoid hemorrhage and one in the second week after subarachnoid hemorrhage.

Findings Age, sex, and Fisher CT grade were not different between the two groups. All but one patient were of WFNS Grade I to II on presentation. There was no increase in rCBV, rCBF and MTT between the two perfusion scans within the same group or between the two groups.

Conclusion Magnesium sulfate infusion, in the dosage of current clinical trials, did not increase cerebral blood volume and cerebral blood flow, as postulated by dilation of small vessels and/or collateral pathways.

Keywords Cerebral blood flow • cerebral blood volume • magnesium sulfate • subarachnoid hemorrhage

Introduction

Delayed ischemic neurological deficits or clinical vasospasm remain a major cause for delayed neurological morbidity and mortality for patients with aneurysmal subarachnoid hemorrhage. With the goal of improving the outcome of patients with aneurysmal subarachnoid hemorrhage by alleviating the harmful effects of delayed ischemic neurological deficits, magnesium sulfate infusion has been tested in six randomized controlled pilot studies (3,4,6,9–11). Four of these studies were eligible for the following meta-analysis. One study was excluded due to lack of 3 to 6 month follow up data; another was excluded due to the unconventional omission of nimodipine in the treatment group (4,6). Using the random effects model, the pooled odds ratio for symptomatic vasospasm or delayed cerebral ischemia was, 0.620, 95% CI 0.389 to 0.987, statistically significant. Similarly, the pooled odds ratio for unfavorable outcome is 1.598, 95% CI 1.074 to 2.377, statistically significant. Two multi-center randomized controlled trials are currently underway to investigate the above hypothesis.

In an experimental model of drug or SAH-induced vasospasm, magnesium blocked voltage-dependent calcium channels and antagonized the action on N-methyl-D-aspartate receptors in the brain, preventing glutamate release and decreasing calcium influx during ischemic injury. The angiographic antispasmodic effect was not certain at the dosage of the current clinical trials (2). It remains a possibility that the vasodilatory effect predominantly acted on microcirculation level. We aim to investigate the cerebral hemodynamic effects, at the microcirculation level, of magnesium sulfate infusion in aneurysmal subarachnoid hemorrhage patients, using perfusion magnetic resonance imaging.

Methods and Materials

A total of 12 patients after aneurysmal subarachnoid hemorrhage were randomized to magnesium sulfate infusion ($n = 6$)

G.K.-C. Wong (✉), K. Karen, R. Kwok, and W.-S. Poon
Division of Neurosurgery, The Chinese University of Hong Kong,
Prince of Wales Hospital, Shatin, NT, Hong Kong SAR
e-mail: georgewong@surgery.cuhk.edu.hk

D. Yeung, A. Ahuja, and A.D. King
Department of Diagnostic Radiology and Organ Imaging,
Prince of Wales Hospital, The Chinese University of Hong Kong,
Shatin, NT, Hong Kong SAR

or placebo infusion ($n = 6$) for 14 days. Each patient had two perfusion MRIs performed, one in the first week after subarachnoid hemorrhage, one in the second week after subarachnoid hemorrhage. Using a 1.5T MR system (Philips Intera NT), dynamic perfusion imaging was acquired on the whole brain after a bolus injection of gadoteric acid (Dotarem; Guerbet) at a concentration of 0.4 mmol/kg body weight, injected at a rate of 5 mL/s. Dynamic images were analyzed using brain perfusion analysis software (ViewForum, Philips) to obtain mean transit time (MTT), negative integral (rCBV), and index map (rCBF) values from the (ACA, PCA, MCA) in both the right and left sides of the brain. Data analysis was carried out with SPSS for Windows Version 14.0. Statistical significance was taken as $P < 0.05$ (two-tailed). Categorical data was compared using Fisher's exact tests and numerical data was compared with unpaired t tests.

Results

The mean age of the cohort was 56 years and the female to male ratio was 1:1. All patients except one (WFNS grade IV) were WFNS Grade I to II upon admission. For all patients, the Fisher CT Grade on admission was 3. Eight patients had ruptured anterior communicating artery aneurysm; three patients had ruptured posterior communicating artery aneurysm; one patient had ruptured internal carotid artery aneurysm. All were treated by endovascular coiling. There was one patient in each group who developed clinical vasospasm at the time of second MR scan. Both had complete recovery from the neurological deficits. Mean transit times were not significantly different in all vascular territories between both groups in both MR scans (Fig. 1). Paradoxically, the cerebral

blood volume and thus the cerebral blood flow in anterior circulation of the magnesium sulfate treated group were significantly lower than the control group.

Discussion

Our results showed that magnesium sulfate infusion did not have a vasodilatory effect in microcirculation. Paradoxically, the magnesium sulfate group had decreased cerebral blood volume, and thus cerebral blood flow, over the anterior circulation, as compared to the control group. The mean transit times were the same across both groups, signifying the parameter change in cerebral blood volume and cerebral blood flow were clinically insignificant. Whether it is related to changes in cerebral autoregulation remains to be determined.

A remaining possible mechanism to explain magnesium sulfate's effect may be that it improves clinical outcome through its neuroprotective effects. Assessment of this hypothesis requires studies of cerebrospinal fluid and intracellular magnesium levels during intravenous magnesium infusion. Studies into the pharmacological actions of magnesium sulfate are important and would guide us in describing its role in aneurysmal subarachnoid hemorrhage with nimodipine, statins, and agents like endothelin antagonists (1,5,7,8). In conclusion, magnesium sulfate infusion, in the dosage used in current clinical trials, did not increase cerebral blood volume and cerebral blood flow, as we postulated based on its dilation of small vessels and/or collateral pathways.

Conflicts of interest statement We declare that we have no conflict of interest.

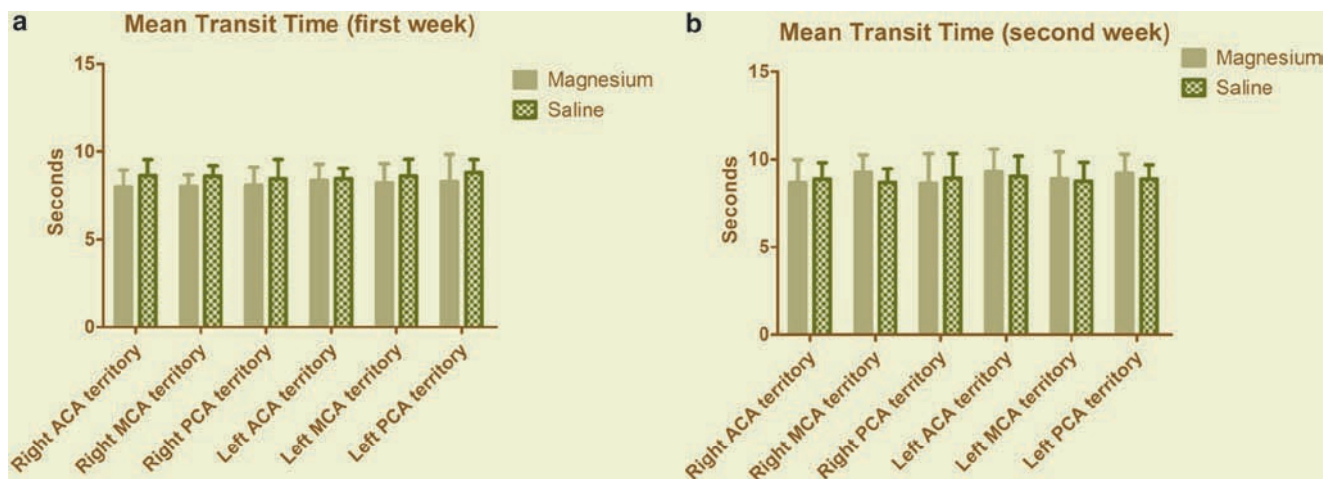


Fig. 1 Mean transit time of the magnesium sulfate treated group and control group: (a) during the first week and (b) during the second week

References

- Lynch JR, Wang H, McGirt MJ, Floyd J, Friedman AH, Coon AL, Blessing R, Alexander MJ, Graffagnino C, Warner DS, Laskowitz DT (2005) Simvastatin reduced vasospasm after aneurysmal subarachnoid hemorrhage. Results of a pilot randomized clinical trial. *Stroke* 36:2024–2026
- Macdonald RL, Curry DJ, Aihara Y, Zhang ZD, Jahromi BS, Yassari R (2004) Magnesium and experimental vasospasm. *J Neurosurg* 100(1):106–110
- Muroi C, Terzic A, Fortunati M, Yonekawa Y, Keller E (2008) Magnesium sulfate in the management of patients with aneurysmal subarachnoid hemorrhage: a randomized, placebo-controlled, dose-adapted trial. *Surg Neurol* 69:33–39
- Prevedello DM, Cordeiro JG, Leito de Morais A, Saucedo NS, Chen IB, Araujo JC (2006) Magnesium sulfate: role as possible attenuating factor in vasospasm morbidity. *Surg Neurol* 65(S1):14–21
- Rinkel GJ, Feign VL, Algra A, van den Bergh WM, Vermeulen M, van Gijn J (2005) Calcium antagonists for aneurysmal subarachnoid haemorrhage. *Cochrane Database Syst Rev*, Issue 1. Art. No.:CD000277 doi: 10.1002/14651858.CD000277.pub2.
- Schmid-Elsaesser R, Kunz M, Zausinger S, Prueckner S, Briegel J, Steiger HJ (2006) Intravenous magnesium versus nimodipine in the treatment of patients with aneurysmal subarachnoid hemorrhage: a randomized study. *Neurosurgery* 58:1054–1065
- Tseng MY, Czosnyka M, Richards H, Pickard JD, Kirkpatrick XX (2005) Effects of acute treatment with Pravastatin on cerebral vasospasm, autoregulation, and delayed ischemic deficits after aneurysmal subarachnoid hemorrhage: a phase II randomized placebo-controlled trial. *Stroke* 36:1627–1632
- Vajkoczy P, Meyer B, Weidauer S, Raabe A, Thome C, Ringel F, Breu V, Schniedek P, and the other study participants (2005) Clazosentan (AXV-034343), a selective endothelin A receptor antagonist, in the prevention of cerebral vasospasm following severe aneurysmal subarachnoid hemorrhage: results of a randomized, double-blind, placebo-controlled, multicenter Phase IIa study. *J Neurosurg* 103:9–17
- van den Bergh WM, on behalf of the MASH study group (2005) Magnesium sulfate in aneurysmal subarachnoid hemorrhage. *Stroke* 36:1011–1015
- Veyna RS, Seyfried D, Burke DG, Zimmerman C, Mlynarek M, Nichols V, Marrocco A, Thomas AJ, Mitsias PD (2002) Magnesium sulfate therapy after aneurysmal subarachnoid hemorrhage. *J Neurosurg* 96:510–514
- Wong GK, Chan MT, Boet R, Poon WS, Gin T (2006) Intravenous magnesium sulfate after aneurysmal subarachnoid hemorrhage: a prospective randomized pilot study. *J Neurosurg Anesthesiol* 18:142–148

Timing of Serum Active MMP-9 and MMP-2 Levels in Acute and Subacute Phases After Spontaneous Intracerebral Hemorrhage

Massimiliano Castellazzi, Carmine Tamborino, Giuseppe De Santis, Francesco Garofano, Angelica Lupato, Vania Ramponi, Alessandro Trentini, Ilaria Casetta, Tiziana Bellini, and Enrico Fainardi

Abstract Serum active matrix metalloproteinase (MMP)-9 and -2 levels and their tissue inhibitors TIMP-1 and -2 were measured in 28 patients with spontaneous intracerebral hemorrhage (SICH) at 24 h, 48 h and 7 days after bleeding. Perihematomal edema volume was calculated on non-enhanced computed tomography scans by using the formula $A \times B \times C / 2$ at the same time points. Mean levels of serum active MMP-9 and MMP-2, as well as perihematomal edema volume, were significantly different over time ($p < 0.0001$). In comparison to values observed at 24 h, serum active MMP-9 mean concentrations increased at 48 h and reached their peak at 7 days, serum active MMP-2 mean levels progressively declined at 48 h and at 7 days, whereas perihematomal edema volume increased at 48 h and at 7 days. Perihematomal edema volume was positively correlated with active MMP-9 and MMP-2 at 24 h ($p < 0.02$ and $p < 0.05$, respectively) and with active MMP-9 at 48 h ($p < 0.05$), but was inversely correlated with active MMP-2 at 7 days ($p < 0.02$). These findings suggest a different involvement of active MMP-9 and MMP-2 in perihematomal-associated inflammatory response occurring in the transition from acute to subacute phases after SICH.

Keywords Matrix metalloproteinases • activity assay • spontaneous intracerebral hemorrhage • perihematomal brain edema

E. Fainardi (✉) and V. Ramponi
Neuroradiology Unit, Department of Neurosciences and Rehabilitation, Azienda Ospedaliera-Universitaria, Arcispedale S. Anna Corso della Giovecca 203, 44100 Ferrara, Italy

M. Castellazzi, C. Tamborino, G. De Santis, A. Lupato, and I. Casetta
Section of Neurology, Department of Medical and Surgical Sciences of the Communication and Behaviour, University of Ferrara, Arcispedale S. Anna Corso della Giovecca 203, 44100 Ferrara, Italy

Francesco Garofano
Neurosurgery Unit, Department of Neurosciences and Rehabilitation, Azienda Ospedaliera-Universitaria, Arcispedale S. Anna Corso della Giovecca 203, 44100 Ferrara, Italy

A. Trentini and T. Bellini
Section of Biochemistry and Clinical Biochemistry, Department of Biochemistry and Molecular Biology, University of Ferrara, 44100 Ferrara, Italy

Introduction

Spontaneous intracerebral hemorrhage (SICH) accounts for about 10–20% of all strokes, is associated with poor prognosis and high mortality rates, and is commonly caused by hypertension or amyloid angiopathy (12). However, because the pathogenesis of SICH is currently poorly understood, no appropriate therapeutic strategy has been identified. In fact, while it is well known that hematoma formation produces irreversible damage due to tissue destruction by the extravasated blood, the fate of the perihematomal edematous region remains to be established (12). In this context, the presence of an intense inflammatory reaction has recently been proven in the edematous tissue surrounding the hemorrhagic core (11). In particular, it has been proposed that matrix metalloproteinases (MMPs) can contribute to perihemorrhagic inflammatory response through the opening of the blood–brain barrier (BBB) leading to leukocyte migration into the brain and edema development (11,12). These enzymes are a family of zinc-containing and calcium-requiring endopeptidases that are synthesized under the influence of pro-inflammatory cytokines and are secreted into extracellular space as latent inactive proform that becomes activated after proteolytic cleavage. Tissue inhibitors of metalloproteinases (TIMPs) are able to bind to either activated MMPs or their proforms, and thereby ultimately regulate MMP activity (13). As MMPs are responsible for remodelling and degrading extracellular matrix (ECM) constituents contained in the subendothelial basement membranes associated to brain capillaries and glia limitans, their overexpression, not sufficiently counterbalanced by TIMPs, could trigger the breakdown of ECM components of the BBB. Among the various MMPs, MMP-9 (Gelatinase B) is currently thought to play a central role in this process since elevated blood levels of this enzyme have been correlated to perihematomal edema formation (1,2) and hematoma enlargement (9). In addition, high blood concentrations of MMP-9 have been found in the edematous brain tissue located adjacent to hematoma (8,10), whereas increased blood levels of MMP-9 have been observed in ischemic stroke patients with hemorrhagic transformation (5). Conversely, the significance

of MMP-2 (Gelatinase A) in neuroinflammation occurring in SICH is at present unclear. In any case, no data are available on active MMP-9 and MMP-2, which are the only enzyme forms exerting catalytic activity. Considering these observations, the aim of this study was to investigate the temporal profile of serum active MMP-9 and MMP-2 concentrations and their relationships with perihematomal edema in a group of patients with SICH evolving from acute to subacute phases. To address these questions, we employed a sensitive activity assay system to quantify serum levels of active MMP-9 and MMP-2 and used an ELISA method to measure TIMP-1 and TIMP-2.

Materials and Methods

Patient Characteristics

Twenty-eight patients (18 males and 10 females; mean age \pm SD = 71.4 \pm 10.8 years) with diagnosis of acute supratentorial SICH proven by an admission non-enhanced computed tomography (CT) scan carried out within 24 h of onset were prospectively included in the study. Time of onset was considered as the last time the patient was known to be neurologically normal. Exclusion criteria at the time of enrollment were: (1) occurrence of infratentorial hemorrhage; (2) hematoma related to tumor, trauma, coagulopathy, aneurysms, vascular malformations; (3) hemorrhagic transformation of brain infarction; (4) intraventricular extension of hemorrhage; (5) surgical hematoma evacuation performed after the first non-contrast CT scans; (6) age <20 years; or (7) evidence of pregnancy. Disease severity was scored in all patients using the National Institutes of Health Stroke Scale (NIHSS) (3) at 24 h (admission), 48 and 7 days (follow-up) from onset.

CT Examination

All CT scans were performed using a single-section CT scanner (CT HiSpeed ZX/i; GE Medical System, Milwaukee, Wis) at the same time points as NIHSS calculation: 24 h (baseline), 48 h and 7 days (follow-up) after bleeding. Based on their location, hematomas were classified as either basal ganglia or lobar. Accordingly, SICH was located within basal ganglia regions in 18 patients and within lobar regions in the remaining 10 patients. Hematoma volume was calculated on the non-enhanced CT scan using the formula $A \times B \times C / 2$ where A, B and C represent the dimensions of CT hyperdensity in three axes perpendicular to each other (7). The volume of hematoma plus that of perihematomal low density area was determined with the same method. Perihematomal edema volume

was measured by subtracting the hematoma volume from the combined hematoma and perihematomal low density area volumes. Hematoma expansion was defined as a volume increase >33% between the baseline CT scan obtained at 24 h and the follow-up CT scan performed at 48 h (4). Informed consent was obtained from each patient or from his or her close relatives before the CT was performed.

Laboratory Procedures

Serum samples were obtained by centrifugation at room temperature for blood specimens previously withdrawn by puncture of an antero-cubital vein. Specimens were collected under sterile conditions at the same time points as NIHSS calculation and CT scan performance: 24 h (baseline), 48 h and 7 days (follow-up) after SICH. Serum specimens were then stored in aliquots at -70°C until assay. As reported elsewhere (6), serum concentrations of active MMP-9 and MMP-2 were measured by using a commercially available Activity Assay System kit (Activity Assay System, Biotrak, Amersham Biosciences, UK), according to the manufacturer's instructions. Serum samples were diluted at 1:20 for MMP-9 and at 1:100 for MMP-2 determinations. The lower limit of quantification was 0.125 ng/mL for MMP-9 and 0.19 ng/mL for MMP-2. Serum levels of TIMP-2 were measured by using a commercially available "sandwich" enzyme-linked immunosorbent assay (ELISA) kit (Biotrak, Amersham Biosciences, UK) according to the manufacturer's instructions. Serum samples were diluted at 1:40 for TIMP-1 and at 1:4 for TIMP-2 determinations. The limit of sensitivity of the assay was 3 ng/mL for both TIMP-1 and TIMP-2.

Statistical Analysis

After checking data for normality by using the Kolmogorov-Smirnov test, repeated measures ANOVA followed by post-hoc Scheffè test, Friedman ANOVA followed by post-hoc Mann-Whitney test, Spearman rank correlation coefficient test and linear regression analysis were used when appropriate. A value of $p < 0.05$ was considered as statistically significant.

Results

MMPs and TIMPs Time Course

As illustrated in Fig. 1, mean levels of serum active MMP-9 and MMP-2 were statistically different over time ($p < 0.0001$). Specifically, in comparison to baseline mean values

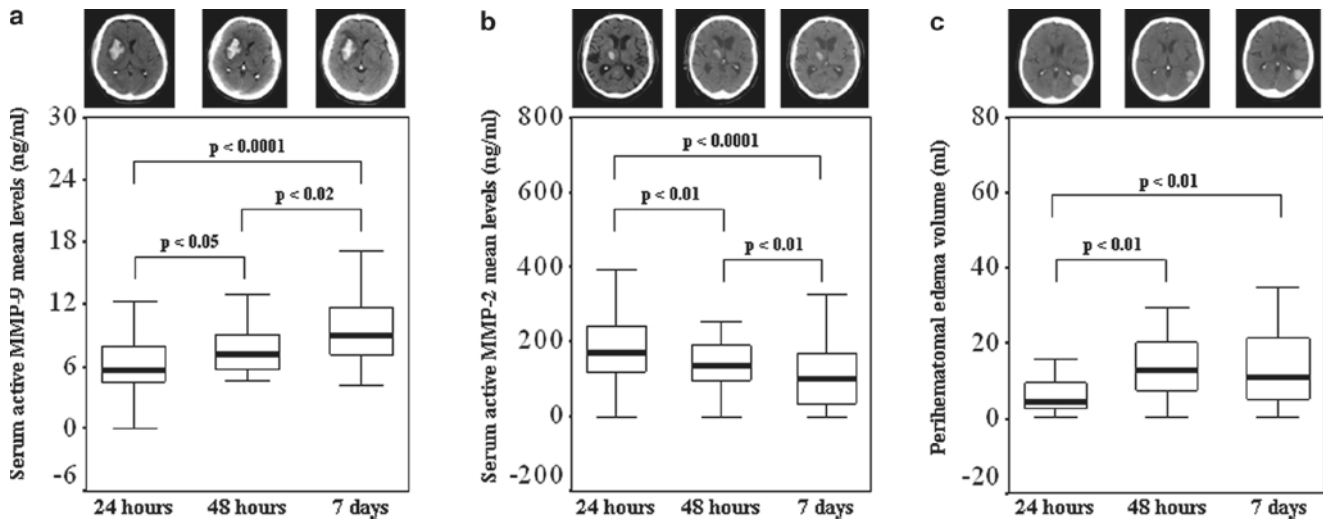


Fig. 1 Temporal profile of serum active MMP-9 and MMP-2 levels and perihematomal edema volume in 28 patients with spontaneous intracerebral hemorrhage (SICH) expressed as median and interquartile range (IQR). Serum mean concentrations of active MMP-9 were significantly higher at 48 h ($p < 0.05$) and at 7 days ($p < 0.0001$) than at 24 h and at 7 days than at 48 h ($p < 0.02$). (Panel A) Serum mean levels of active MMP-2 were significantly lower at 48 h ($p < 0.01$) and at 7 days ($p < 0.0001$) than at 24 h and at 7 days than at 48 h ($p < 0.01$) (Panel B).

Perihematomal edema volume was significantly greater at 48 h ($p < 0.01$) and at 7 days ($p < 0.01$) than at 24 h (Panel C). The boundaries of the box represent the 25th–75th quartiles. The line within the box indicates the median. The whiskers above and below the box correspond to the highest and lowest values, excluding outliers. At the top, sequential CT scans from three illustrative cases showing the time course of hematoma and surrounding perihematomal edema in basal ganglia (above Panels A and B) and lobar SICH (above Panel C)

observed at 24 h (6.1 ± 3.7 ng/mL), serum active MMP-9 mean concentrations were significantly higher at 48 h (7.5 ± 4.0 ng/mL; $p < 0.05$) and at 7 days (9.5 ± 4.1 ng/mL; $p < 0.0001$). In addition, serum active MMP-9 mean levels were significantly more elevated at 7 days than at 48 h ($p < 0.02$). On the other hand, serum mean titers of active MMP-2 were significantly lower at 48 h (154.5 ± 110.9 ng/mL; $p < 0.01$) and at 7 days (117.8 ± 93.7 ng/mL; $p < 0.0001$) than at baseline (194.1 ± 122.7 ng/mL). Moreover, serum active MMP-2 mean levels were significantly decreased at 7 days as compared to 48 h ($p < 0.01$). No statistical differences were found among the time points examined for serum mean levels of TIMP-1 and TIMP-2 (data not shown).

Hematoma and Edema Volumes Time Course

Hematoma volume did not statistically differ among the time points selected since similar mean values were detected at baseline (15.8 ± 21.4 mL), at 48 h (18.4 ± 26.2 mL) and at 7 days (6.4 ± 21.6 mL). In this setting, a hematoma enlargement was present in 5/28 (17.9%) SICH patients. In contrast, as shown in Fig. 1, perihematomal edema volume was statistically different over time ($p < 0.0001$). Specifically, its mean values were significantly increased at 48 h (18.4 ± 26.2 mL;

$p < 0.01$) and at 7 days (18.77 ± 27.1 mL; $p < 0.01$) compared to those found at 24 h (8.9 ± 13.3 mL).

Relationships Between Serum MMPs and TIMPs Levels and Findings from CT and Clinical Examinations

As reported in Table 1, hematoma volume was positively associated with mean serum concentrations of active MMP-9 and MMP-2 at 24 h ($p < 0.05$) and to mean levels of serum active MMP-9 at 48 h ($p < 0.02$), whereas it was negatively correlated to serum active MMP-2 mean levels at 7 days ($p < 0.05$). Similarly, perihematomal edema volume was positively correlated with serum active MMP-9 and MMP-2 mean titers at 24 h ($p < 0.02$ and $p < 0.05$, respectively) and with serum mean levels of active MMP-9 at 48 h ($p < 0.05$), but it was inversely correlated with serum active MMP-2 mean concentrations at 7 days ($p < 0.02$). No further definite associations were identified between the temporal profiles of serum MMP-9, MMP-2, TIMP-1 and TIMP-2 mean levels and hematoma and perihematomal edema volumes (data not shown). Serum MMP and TIMP measurements were not significantly correlated to NIHSS in the different time points analyzed.

Table 1 Significant correlations between mean serum levels of MMP-9 and MMP-2 and hematoma and perihematomal edema volumes in 28 patients with spontaneous intracerebral hemorrhage (SICH)

Spearman's correlation	Correlation coefficient	Significance
MMP-9 vs. hematoma volume at 24 h from onset	$r = 0.394$	$p < 0.05$
MMP-9 vs. hematoma volume at 48 h from onset	$r = 0.447$	$p < 0.02$
MMP-2 vs. hematoma volume at 7 days from onset	$r = -0.405$	$p < 0.05$
MMP-9 vs. edema volume at 24 h from onset	$r = 0.460$	$p < 0.02$
MMP-9 vs. edema volume at 48 h from onset	$r = 0.422$	$p < 0.05$
MMP-2 vs. edema volume at 24 h from onset	$r = 0.385$	$p < 0.05$
MMP-2 vs. edema volume at 7 days from onset	$r = -0.471$	$p < 0.02$

Discussion

Recent studies have demonstrated that increased blood levels of MMP-9 can be associated to perihematomal edema development (1,2) and hematoma expansion (9), suggesting the potential role of this enzyme in SICH-related inflammation. However, little is known about the relevance of MMP-2 in perihematomal inflammatory response and the temporal profile of gelatinases in SICH (2). More importantly, MMP-9 and MMP-2 levels have been determined by various methods, such as ELISA, zymography, immunoblotting, immunohistochemistry and in situ hybridization, which are not able to detect the active form of gelatinases. For these reasons, in this study serum levels of active MMP-9 and MMP-2 in patients with SICH were measured by using a sensitive activity assay system that allowed us to have a clear representation of gelatinase proteolytic net activity. Here we found that serum active MMP-9 mean concentrations rose at 48 h and reached their peak at 7 days. Moreover, serum active MMP-2 mean levels progressively declined at 48 h and at 7 days when compared to corresponding baseline values observed at 24 h after bleeding. In contrast, no significant changes in serum TIMP-1 and TIMP-2 mean titers were found over time. These data are only partially in agreement with those reported previously (2) likely due to the methodological differences in determination techniques. Interestingly, according to prior findings (12), a gradual increase in perihematomal edema volume was seen at 48 h and at 7 days compared to baseline values obtained at 24 h from onset. Of note, serum MMP-9 and MMP-2 mean levels and perihematomal edema volume, were positively associated at 24 and 48 h and became inversely correlated at 7 days after SICH, respectively. Therefore, our results indicate that the combined temporal profile of MMP-9 and MMP-2, and their relationships with perihematomal edema volume over time, appear to be reciprocal in the transition from acute to subacute phases after SICH. This potentially

indicates different roles for these two gelatinases in ongoing inflammatory response taking place in the edematous tissue surrounding hematoma. In fact, as hypothesized for ischemic stroke (14), MMP-9 may be detrimental in promoting a disruption of the BBB that exacerbates perihematomal edema formation. Conversely, MMP-2 might exert a protective function favouring the resolution of perihematomal neuroinflammation and tissue repair. Nevertheless, further studies are required to clarify the actual involvement of gelatinases in the inflammatory mechanisms orchestrating perihematomal edema development.

Conflict of interest statement We declare that we have no conflict of interest.

References

- Abilleira S, Montaner J, Molina CA, Monasterio J, Castillo J, Alvarez-Sabín J (2003) Matrix metalloproteinase-9 concentration after spontaneous intracerebral hemorrhage. *J Neurosurg* 99:65–70
- Alvarez-Sabín J, Delgado P, Abilleira S, Molina CA, Arenillas J, Ribó M, Santamarina E, Quintana M, Monasterio J, Montaner J (2004) Temporal profile of matrix metalloproteinases and their inhibitors after spontaneous intracerebral hemorrhage. Relationship to clinical and radiological outcome. *Stroke* 35:1316–1322
- Brott T, Adams HP, Olinger CP, Marler JR, Barsan WG, Biller J, Spilker J, Holleran R, Eberle R, Hertzberg V, Rorick M, Moomaw CJ, Walker M (1989) Measurements of acute cerebral infarction: a clinical examination scale. *Stroke* 20:864–870
- Brott T, Broderick J, Kothari R, Barsan W, Tomsick T, Sauerbeck L, Spilker J, Duldner J, Khoury J (1997) Early hemorrhage growth in patients with intracerebral hemorrhage. *Stroke* 28:1–5
- Castellanos M, Leira R, Serena J, Pumar JM, Lizasoain I, Castillo J, Dávalos A (2003) Plasma metalloproteinase-9 concentration predicts hemorrhagic transformation in acute ischemic stroke. *Stroke* 34:40–46
- Castellazzi M, Tamborino C, Fainardi E, Manfrinato MC, Granieri E, Dallochio F, Bellini T (2007) Effects of anticoagulants on the activity of gelatinases. *Clin Biochem* 40:1272–1276
- Kothari RU, Brott T, Broderick JP, Barsan WG, Sauerbeck LR, Zuccarello M, Khoury J (1996) The ABCs of measuring intracerebral hemorrhage volume. *Stroke* 27:1034–1035
- Rosell A, Ortega-Aznar A, Alvarez-Sabín J, Fernández-Cadenas I, Ribó M, Molina CA, Lo EH, Montaner J (2006) Increased brain expression of matrix metalloproteinase-9 after ischemic and hemorrhagic human stroke. *Stroke* 37:1399–1406
- Silva Y, Leira R, Tejada J, Lainez JM, Castillo J, Dávalos A (2005) Molecular signatures of vascular injury are associated with early growth of intracerebral hemorrhage. *Stroke* 36:86–91
- Tejima E, Zhao B-Q, Tsuji K, Rosell A, van Leyen K, Gonzalez RG, Montaner J, Wang X, Lo EH (2007) Astrocytic induction of matrix metalloproteinase-9 and edema in brain hemorrhage. *J Cereb Blood Flow Metab* 27:460–468
- Wang J, Doré S (2007) Inflammation after intracerebral hemorrhage. *J Cereb Blood Flow Metab* 27:894–908
- Xi G, Keep RF, Hoff JT (2006) Mechanisms of brain injury after intracerebral haemorrhage. *Lancet Neurol* 5:53–63
- Yong VW (2005) Metalloproteinases: mediators of pathology and regeneration in the CNS. *Nat Rev Neurosci* 6:931–944
- Zhao B-Q, Tejima E, Lo EH (2007) Neurovascular proteases in brain injury, hemorrhage and remodelling after stroke. *Stroke* 38 (part 2):748–752

Timing of Serum Soluble HLA-G Levels in Acute and Subacute Phases After Spontaneous Intracerebral Hemorrhage

Enrico Fainardi, Roberta Rizzo, Angelica Lupato, Vania Ramponi, Giuseppe De Santis, Francesco Garofano, Marina Stignani, Carmine Tamborino, Massimiliano Castellazzi, Ilaria Casetta, and Olavio Roberto Baricordi

Abstract Serum levels of sHLA-G (sHLA-G1/HLA-G5) antigens and their soluble isoforms, sHLA-G1 and HLA-G5, were measured by ELISA in 22 patients with spontaneous intracerebral hemorrhage (SICH) at 24 h, 48 h and 7 days after bleeding. The perihematomal edema volume was calculated on non-enhanced computed tomography scans using the formula $A \times B \times C / 2$ at the same time points. The mean serum concentrations of sHLA-G1/HLA-G5 and sHLA-G1 as well as the perihematomal edema volume changed significantly over time ($p < 0.0001$, $p < 0.001$ and $p < 0.0001$, respectively), whereas no statistical differences were found in serum HLA-G5 concentrations over the course of the experiment. In comparison to the values found at 24 h, sHLA-G1/HLA-G5 and sHLA-G1 increased at 48 h and then decreased at 7 days, whereas the perihematomal edema volume was more elevated at 48 h and, to a lesser extent, at 7 days. A positive correlation was detected between mean serum sHLA-G1/HLA-G5 and sHLA-G1 levels and perihematomal edema volume at 24 h ($p < 0.02$) and at 48 h ($p < 0.01$). Our results may indicate a role for sHLA-G in inflammatory mechanisms related to SICH, where these proteins probably act as anti-inflammatory molecules and are predominantly produced as the sHLA-G1 isoform.

Keywords sHLA-G1 • HLA-G5 • spontaneous intracerebral hemorrhage • perihematomal brain edema

E. Fainardi and V. Ramponi
Neuroradiology Unit, Department of Neurosciences and Rehabilitation,
Azienda Ospedaliera-Universitaria, Arcispedale S. Anna
Corso della Giovecca 203, 44100 Ferrara, Italy

R. Rizzo, M. Stignani, and O.R. Baricordi
Section of Medical Genetics, Department of Experimental and
Diagnostic Medicine, University of Ferrara, 44100 Ferrara, Italy

A. Lupato, G. De Santis, C. Tamborino, M. Castellazzi, and I. Casetta,
Section of Neurology, Department of Medical and Surgical Sciences
of the Communication and Behaviour, University of Ferrara,
Arcispedale S. Anna Corso della Giovecca 203, 44100 Ferrara, Italy

Francesco Garofano
Neurosurgery Unit, Department of Neurosciences and Rehabilitation,
Azienda Ospedaliera-Universitaria, Arcispedale S. Anna
Corso della Giovecca 203, 44100 Ferrara, Italy

Introduction

Spontaneous intracerebral hemorrhage (SICH) is a devastating cerebrovascular disease that represents about 10–20% of all strokes and is characterized by high disability and mortality rates (13). Currently, there is no proven effective treatment for SICH due to the limited understanding of its pathogenesis. In particular, although it is widely accepted that bleeding occurring in the central part of the hematoma results in tissue destruction and irreversible damage, the mechanisms implicated in hematoma enlargement and perihematomal edema formation still remain a matter of debate. In fact, these two critical events are considered the major factors affecting outcome because together their effects could lead to clinical deterioration and death as a consequence of an increase in intracranial pressure (13). In this regard, a growing body of evidence suggests that a strong inflammatory response could contribute to secondary injury promoted by edema developing in the region peripheral to the hematoma (11). Recently, the potential role of Human Leukocyte Antigen-G molecules in soluble form (sHLA-G) as regulatory factors of the inflammatory process operating in various neoplastic, viral and autoimmune diseases of the central nervous system (CNS) has received increasing attention (4,12). HLA-G are non-classical class Ib HLA antigens structurally related to classical class Ia HLA products (HLA-I), which display a limited polymorphism, a restricted tissue distribution and alternative splicing of their primary transcript encoding seven distinct isoforms, which include four membrane bound (G1,G2,G3 and G4) and three soluble (G5,G6,G7) proteins (3). Among these different isoforms, membrane-bound HLA-G1 and soluble HLA-G5 (HLA-G5) are considered the most important functionally active soluble HLA-G (sHLA-G) isoforms (9,10). HLA-G5 proteins are directly secreted in this form and represent the soluble counterparts of membrane-bound HLA-G1, whereas HLA-G1 can be released as soluble molecules (sHLA-G1) after being shed from the cell surface. Although the biological functions of these two different sHLA-G isoforms remain unclear, sHLA-G are believed to exhibit tolerogenic and anti-inflammatory properties (3). Nevertheless, no data are

presently available on the presence of sHLA-G molecules in the blood of patients with SICH. Therefore, the purpose of this study was to assess the chronological changes in the serum levels of sHLA-G antigens and their isoforms, HLA-G5 and sHLA-G1, and the relationships between these molecules and perihematomal edema in a group of patients with SICH during the conversion from the acute to the subacute phases.

Materials and Methods

Patient Selection

Twenty-two patients (14 males and 8 females; mean age \pm SD = 71.6 \pm 11.9 years) with a diagnosis of acute supratentorial SICH, demonstrated by an admission non-enhanced computed tomography (CT) scan carried out within 24 h of onset, prospectively entered the study. The time of onset was considered as the last time the patient was known to be neurologically normal. Exclusion criteria at the time of enrollment were: (1) occurrence of infratentorial hemorrhage; (2) hematoma related to tumor, trauma, coagulopathy, aneurysms, vascular malformations; (3) hemorrhagic transformation of brain infarction; (4) intraventricular extension of hemorrhage; (5) surgical hematoma evacuation performed after the first non-contrast CT scans; (6) age <20 years; (7) evidence of pregnancy. Disease severity was scored in all patients using the National Institutes of Health Stroke Scale (NIHSS) (1) at 24 h (admission), 48 h and 7 days (follow-up) from onset.

CT Evaluation

All CT scans were performed using a single-section CT scanner (CT HiSpeed ZX/i; GE Medical System, Milwaukee, Wis) at the same time points as NIHSS calculation: 24 h (baseline), 48 h and 7 days (follow-up) after bleeding. The hematoma location was categorized as basal ganglia and lobar. Accordingly, SICH was located within basal ganglia regions in 15 patients and within lobar regions in the remaining 7 patients. The hematoma volume was calculated on the non-enhanced CT scan using the formula $A \times B \times C / 2$ where A, B and C represent the dimensions of CT hyperdensity in three axes perpendicular to each other (8). The volume of the hematoma plus that of the perihematomal low density area was determined by the same method. The perihematomal edema volume was measured by subtracting the hematoma volume from the combined hematoma and perihematomal low density area volumes. Hematoma expansion was defined as

a volume increase >33% between the baseline CT scan obtained at 24 h and the follow-up CT scan performed at 48 h (2). Informed consent was obtained from each patient or from close relatives before the CT was performed.

Immunoassay Methods

Serum samples were obtained by centrifugation at room temperature of blood specimens previously withdrawn by puncture of an antecubital vein, collected under sterile conditions at the same time points as NIHSS calculation and CT scan performance: 24 h (baseline), 48 h and 7 days (follow-up) after SICH. Serum specimens were then stored in aliquots at -70°C until assay. Measurements of serum sHLA-G (sHLA-G1/HLA-G5) and HLA-G5 levels were obtained by enzyme-linked immunosorbent assay (ELISA) using undiluted serum samples, as previously described (4–6). The limit of sensitivity was 1 ng/mL for both sHLA-G (sHLA-G1/HLA-G5) and HLA-G5. After ELISA measurements of the serum levels of sHLA-G1/HLA-G5 and HLA-G5, the amount of sHLA-G1 was expressed as the difference between the sHLA-G1/HLA-G5 and HLA-G5 concentrations.

Statistics

After checking data for normality using the Kolmogorov–Smirnov test, repeated measures ANOVA followed by post-hoc Scheffè test, a Friedman ANOVA followed by post-hoc Mann–Whitney test, the Spearman rank correlation coefficient test and linear regression analysis were used when appropriate. A value of $p < 0.05$ was accepted as statistically significant.

Results

sHLA-G1/HLA-G5, sHLA-G1 and HLA-G5 Time Course

As shown in Fig. 1, the mean serum levels of sHLA-G1/HLA-G5 and sHLA-G1 were statistically different over time ($p < 0.0001$ and $p < 0.01$, respectively). More precisely, in comparison to baseline mean values observed at 24 h (17.8 \pm 4.8 ng/mL), the mean serum concentrations of sHLA-G1/HLA-G5 were significantly greater at 48 h (21.8 \pm 6.5 ng/mL; $p < 0.01$) and significantly reduced at 7 days (14.0 \pm 5.1 ng/mL; $p < 0.02$). In addition, the mean serum titers of

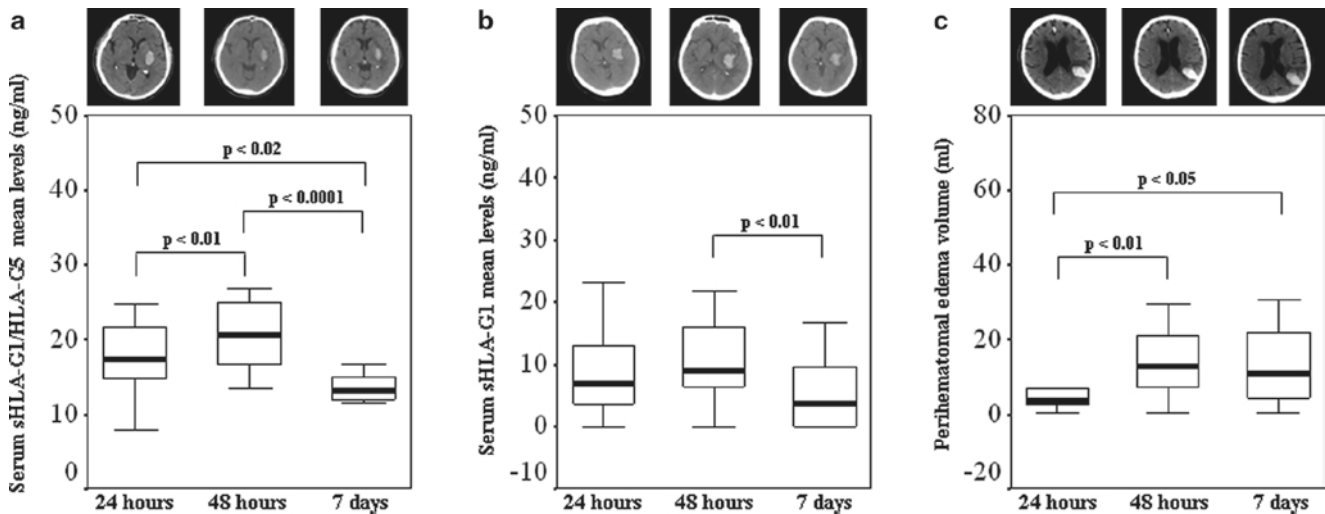


Fig. 1 Temporal profile of serum sHLA-G1/HLA-G5 and sHLA-G1 levels and perihematomal edema volume in 22 patients with spontaneous intracerebral hemorrhage (SICH), expressed as median and interquartile range (IQR). The mean serum concentrations of sHLA-G1/HLA-G5 were significantly higher at 48 h ($p < 0.01$) and significantly reduced at 7 days ($p < 0.02$) than at 24 h. In addition, the mean serum titers of sHLA-G1/HLA-G5 were significantly decreased at 7 days than at 48 h ($p < 0.0001$) (Panel A). The mean serum levels of sHLA-G1 were significantly lower at 7 days than at 48 h

($p < 0.01$) (Panel B). The perihematomal edema volume was significantly greater at 48 h ($p < 0.01$) and at 7 days ($p < 0.05$) than at 24 h (Panel C). The box boundaries represent the 25th–75th quartile. The line within the box indicates the median. The whiskers above and below the box correspond to the highest and lowest values, excluding outliers. On the top, sequential CT scans from three illustrative cases show the time course of hematoma and surrounding perihematomal edema in basal ganglia (above Panels A and B) and lobar SICH (above Panel C)

sHLA-G1/HLA-G5 showed a significantly greater decrease at 7 days than at 48 h ($p < 0.0001$). A similar trend was also observed for mean serum sHLA-G1 levels, which were higher at 48 h (11.0 ± 8.5 ng/mL) and lower at 7 days (5.1 ± 6.3) than at baseline (8.1 ± 5.9 ng/mL). However, these differences did not reach statistical significance. Conversely, the mean serum concentrations of sHLA-G1 were significantly lower at 7 days than at 48 h ($p < 0.01$). On the other hand, the mean serum HLA-G5 levels were equivalent at 24 h (9.9 ± 4.6 ng/mL), 48 h (11.0 ± 5.3 ng/mL) and 7 days (10.0 ± 6.1).

Relationships Between sHLA-G1/HLA-G5, sHLA-G1 and HLA-G5 and CT and Clinical Findings

As shown in Table 1, hematoma volume was positively associated with mean serum concentrations of sHLA-G1/HLA-G5 and sHLA-G1 at 24 ($p < 0.05$) and 48 h ($p < 0.05$).

Table 1 Significant correlations between the mean serum levels of sHLA-G1/HLA-G5 and sHLA-G1 and hematoma and perihematomal edema volumes in 22 patients with spontaneous intracerebral hemorrhage (SICH)

Spearman’s correlation	Correlation coefficient	Significance
sHLA-G1/HLA-G5 vs. hematoma volume at 24 h from onset	$r = 0.433$	$p < 0.05$
sHLA-G1/HLA-G5 vs. hematoma volume at 48 h from onset	$r = 0.460$	$p < 0.05$
sHLA-G1 vs. hematoma volume at 24 h from onset	$r = 0.422$	$p < 0.05$
sHLA-G1 vs. hematoma volume at 48 h from onset	$r = 0.467$	$p < 0.05$
sHLA-G1/HLA-G5 vs. edema volume at 24 h from onset	$r = 0.512$	$p < 0.02$
sHLA-G1/HLA-G5 vs. edema volume at 48 h from onset	$r = 0.544$	$p < 0.01$
sHLA-G1 vs. edema volume at 24 h from onset	$r = 0.518$	$p < 0.02$
sHLA-G1 vs. edema volume at 48 h from onset	$r = 0.559$	$p < 0.01$

Time Course of Changes in Hematoma and Edema Volumes

Hematoma volume did not differ statistically among the time points selected since similar mean values were detected at baseline (17.1 ± 23.6 mL), at 48 h (20.1 ± 28.7 mL) and at 7 days (17.9 ± 23.5 mL). A hematoma enlargement was present in 4/22 (18.2%) SICH patients. In contrast, as shown in Fig. 1, perihematomal edema volume changed statistically over time ($p < 0.0001$). Specifically, the mean values were significantly increased at 48 h (34.5 ± 100.2 mL; $p < 0.01$) and at 7 days (19.8 ± 30.2 mL; $p < 0.05$) with respect to those found at 24 h (9.3 ± 14.9 mL).

Similarly, perihematomal edema volume was positively correlated with sHLA-G1/HLA-G5 and sHLA-G1 mean levels at 24 h ($p < 0.02$) and at 48 h ($p < 0.01$). No further definite associations were identified between the temporal profile of serum sHLA-G1/HLA-G5, sHLA-G1 and HLA-G5 mean levels and hematoma and perihematomal edema volumes (data not shown). Serum sHLA-G1/HLA-G5, sHLA-G1 and HLA-G5 measurements were not significantly correlated to NIHSS at the different time points evaluated.

Discussion

An intense inflammatory reaction is currently believed to have an important influence on the secondary injury occurring in the edematous tissue surrounding the hemorrhagic core after SICH (11). As sHLA-G molecules and their two principal isoforms, HLA-G5 and sHLA-G1, could exert anti-inflammatory functions in some CNS inflammatory diseases of infectious, tumoral, and autoimmune origin (4,12), in the present report we investigated the time course of their serum concentrations in a series of SICH patients by employing specific ELISA techniques. Our final objective was to establish whether a link between these antigenic structures and perihematomal edema evolution could exist. Data emerging from this study seems to indicate that serum sHLA-G mean levels show a characteristic temporal profile after hematoma appearance since they increased at 48 h and then decreased at 7 days when compared to corresponding baseline values observed at 24 h after the start of the bleeding. In addition, comparison of the 24 and 48 h time points revealed that the mean serum levels of sHLA-G reached their highest values at 48 h from onset. Of note, the mean serum sHLA-G1 concentrations exhibited an analogous time course after hematoma formation and peaked at 48 h from onset as well. In contrast, no significant changes in serum mean concentrations of HLA-G5 were found over time after SICH. On the other hand, as expected (13), a progressive enlargement in perihematomal edema volume was observed at 48 h and at 7 days compared to baseline values obtained at 24 h of onset. Of interest was the positive correlation between the mean serum sHLA-G and sHLA-G1 levels and the perihematomal edema volume observed at 24 and at 48 h after SICH. Taken together, our findings suggest the potential involvement of sHLA-G in the ongoing inflammatory response associated with the perihematomal edema development that occurs during the transition from the acute to the subacute phase after SICH. In this context, sHLA-G proteins may play a protective role since they may act as anti-inflammatory molecules leading to the downregulation of SICH-related neuroinflammation by the suppression of natural killer (NK) and CD8+ cytotoxic T effector cells infiltrating the CNS via

Fas/FasL-dependent apoptotic mechanisms, by the inhibition of CD4+ T cell activation, but also by the secretion of T helper 2-type anti-inflammatory cytokines (3). Intriguingly, the evidence that leukocyte migration into the hematoma peaks at 2 to 3 days after onset (11), and that apoptosis reaches its maximum at 3 days after bleeding (7), seems to support this speculation. Furthermore, measurable serum sHLA-G levels in SICH were predominantly composed of the sHLA-G1 isoform, which probably accounts for the time course of the changes in serum sHLA-G concentrations and their relationship to perihematomal edema formation observed in SICH evolution from the acute to the subacute phase. Although evidence of a difference in functional activity between HLA-G5 and sHLA-G1 isoforms is currently lacking (9), these results lead to the hypothesis that the supposed anti-inflammatory properties of sHLA-G molecules in SICH may be due to the HLA-G1 isoform. Interestingly, the sHLA-G isoform profile appears to be different in patients with chronic CNS inflammatory disorders such as multiple sclerosis, in whom we have recently reported a prevalence of HLA-G5 (6). Therefore, future studies are warranted to clarify the actual significance of sHLA-G molecules in the inflammatory mechanisms operating during perihematomal edema development.

Conflict of interest statement We declare that we have no conflict of interest.

References

1. Brott T, Adams HP, Olinger CP, Marler JR, Barsan WG, Biller J, Spilker J, Holleran R, Eberle R, Hertzberg V, Rorick M, Moomaw CJ, Walker M (1989) Measurements of acute cerebral infarction: a clinical examination scale. *Stroke* 20:864–870
2. Brott T, Broderick J, Kothari R, Barsan W, Tomsick T, Sauerbeck L, Spilker J, Duldner J, Khoury J (1997) Early hemorrhage growth in patients with intracerebral hemorrhage. *Stroke* 28:1–5
3. Carosella ED, Moreau P, LeMaout J, Rouas-Freiss N (2008) HLA-G: from biology to clinical benefits. *Trends Immunol* 29: 125–132
4. Fainardi E, Rizzo R, Melchiorri L, Vaghi L, Castellazzi M, Marzola A, Govoni V, Paolino E, Tola MR, Granieri E, Baricordi OR (2003) Presence of detectable levels of soluble HLA-G molecules in CSF of relapsing-remitting multiple sclerosis: relationship with CSF soluble HLA-I and IL-10 concentrations and MRI findings. *J Neuroimmunol* 142:149–158
5. Fainardi E, Rizzo R, Melchiorri L, Castellazzi M, Paolino E, Tola MR, Granieri E, Baricordi OR (2006) Intrathecal synthesis of soluble HLA-G and HLA-I molecules are reciprocally associated to clinical and MRI activity in patients with multiple sclerosis. *Mult Scler* 12:2–12
6. Fainardi E, Rizzo R, Melchiorri L, Stignani M, Castellazzi M, Caniatti ML, Baldi E, Tola MR, Granieri E, Baricordi OR (2007) Soluble HLA-G molecules are released as HLA-G5 and not as soluble HLA-G1 isoforms in CSF of patients with relapsing-remitting multiple sclerosis. *J Neuroimmunol* 192:219–225

7. Gong C, Boulis N, Quian J, Turner DE, Hoff JT, Keep RF (2001) Intracerebral hemorrhage-induced neuronal death. *Neurosurgery* 48:875–883
8. Kothari RU, Brott T, Broderick JP, Barsan WG, Sauerbeck LR, Zuccarello M, Khoury J (1996) The ABCs of measuring intracerebral hemorrhage volume. *Stroke* 27:1034–1035
9. LeMaoult J, Le Discorde M, Rouas-Freiss N, Moreau P, Menier C, McCluskey J, Carosella ED (2003) Biology and functions of human leukocyte antigen-G in health and sickness. *Tissue Antigens* 62:273–284
10. Rebmann V, LeMaoult J, Rouas-Freiss N, Carosella ED, Grosse-Wilde H (2007) Quantification and identification of soluble HLA-G isoforms. *Tissue Antigens* 69:143–149
11. Wang J, Doré S (2007) Inflammation after intracerebral hemorrhage. *J Cereb Blood Flow Metab* 27:894–908
12. Wiendl H (2007) HLA-G in the nervous system. *Hum Immunol* 68:286–293
13. Xi G, Keep RF, Hoff JT (2006) Mechanisms of brain injury after intracerebral haemorrhage. *Lancet Neurol* 5:53–63

Minocycline Attenuates Brain Edema, Brain Atrophy and Neurological Deficits After Intracerebral Hemorrhage

J. Wu, S. Yang, Y. Hua, W. Liu, R. F. Keep, and G. Xi

Abstract Evidence suggests that microglia activation contributes to brain injury after intracerebral hemorrhage (ICH). The present study aimed to determine if minocycline, an inhibitor of microglia activation, can reduce brain edema, brain atrophy and neurological deficits after ICH.

Male Sprague-Dawley rats received an infusion of 100- μ L autologous whole blood into the right basal ganglia. Rats received minocycline or vehicle treatment. There were two sets of experiments in this study. In the first set of experiments, the effects of minocycline on ICH-induced brain edema were examined at day 3. In the second set, behavioral tests were performed at days 1, 3, 7, 14 and 28. Rats were killed at day 28 for brain atrophy measurement (caudate and lateral ventricle size).

Minocycline reduced perihematomal brain edema in the ipsilateral basal ganglia (78.8 ± 0.4 vs. $80.9 \pm 1.1\%$ in the vehicle-treated group, $p < 0.01$). Minocycline also improved functional outcome. In addition, minocycline reduced brain tissue loss in the ipsilateral caudate ($p < 0.01$) and ventricular enlargement ($p < 0.05$).

In conclusion, minocycline attenuates ICH-induced brain edema formation, neurological deficits and brain atrophy in rats suggesting an important role of microglia in ICH-related brain injury.

Keywords Brain atrophy • brain edema • cerebral hemorrhage • minocycline

Introduction

Inflammation aggravates hemorrhagic brain injury. An inflammatory response in the surrounding brain occurs shortly after ICH and peaks several days later (2). Neutrophil

infiltration develops within 2 days in rats and activated microglial cells persist for a month (3,5). Microglia are cells within the brain that are activated in response to injury. Depending upon specific conditions they can have neurotrophic or neurotoxic actions (10). Activated microglia are associated with ischemic and hemorrhagic brain injury including intracerebral hemorrhage (ICH), and there is evidence that microglia contribute to ICH-induced brain damage (3,17). Inhibition of microglia activation with tuftsin fragment 1-3 reduces brain damage after ICH (15).

Minocycline, a second generation tetracycline-based molecule, is a potent inhibitor of microglia activation (13). It is a highly lipophilic compound and penetrates the brain-blood barrier easily (7). Minocycline has been reported to provide neuroprotection by inhibiting microglia. An in vitro study showed that minocycline reduced excitotoxicity in primary neuronal culture by preventing excitotoxin-induced microglial proliferation (12). It also inhibits macrophage/microglia activation after ICH in the rat (8,16).

In this study, we examined the effects of minocycline on brain edema formation, neurological deficits and brain atrophy in rat ICH model.

Materials and Methods

Animal Preparation and Intracerebral Injection

The University of Michigan Committee on the Use and Care of Animals approved the protocols for these animal studies. Male Sprague-Dawley rats aged 3 to 4 months (Charles River Laboratories, Wilmington, MA) were used. Rats were anesthetized with pentobarbital (50 mg/kg, i.p.) and the right femoral artery was catheterized for continuous blood pressure monitoring and blood sampling. Blood from the catheter was used to determine pH, PaO₂, PaCO₂, hematocrit, and glucose. It was also the source for the intracerebral blood

G. Xi (✉), J. Wu, S. Yang, Y. Hua, W. Liu, and R.F. Keep
R5018 Biomedical Science Research Building, Department
of Neurosurgery, University of Michigan, 109 Zina Pitcher Place,
Ann Arbor, MI 48109-2200, USA
e-mail: guohuaxi@umich.edu

infusion. The animals were positioned in a stereotactic frame (David Kopf Instruments, Tujunga, CA). Blood was injected into the right caudate nucleus through a 26-gauge needle at a rate of 10 μL per minute using a microinfusion pump (Harvard Apparatus, Inc., Holliston, MA). The coordinates were 0.2 mm anterior to bregma, 5.5 mm ventral, and 4.0 mm lateral to midline.

Experimental Groups

Male Sprague-Dawley rats received an infusion of 100- μL autologous whole blood into the right basal ganglia. Rats received minocycline injection intraperitoneally at dose of 45 mg/kg immediately and 12 h after ICH, followed by 22.5 mg/kg twice a day for 2 days. In the control group, rats received vehicle only. There were two sets of experiments in this study. In the first set of experiments, the effects of minocycline on ICH-induced brain edema were examined at day 3. In the second set, behavioral tests were performed at days 1, 3, 7, 14 and 28. Rats were killed at day 28 for brain atrophy measurement (caudate and lateral ventricle size).

Brain Water and Ion Content Measurements

Rats were killed under deep pentobarbital anesthesia at day 3. The brains were removed immediately and a 4-mm thick coronal section was taken 3 mm from the frontal pole. The brain sample was then divided into cortex or basal ganglia (ipsilateral or contralateral). Tissue samples were weighed to obtain the wet weight (WW). The tissue was then dried in a gravity oven at 100°C for more than 24 h to determine the dry weight (DW). Tissue water content (%) was calculated as $([WW - DW]/WW) \times 100$. Dehydrated brain samples were digested in 1 mL of 1 N nitric acid for 1 week. Sodium and potassium ion contents in this solution were measured by flame photometry and expressed in micro-equivalents per gram of dehydrated brain tissue ($\mu\text{Eq/g}$ dry wt).

Brain Atrophy Examination

Rats were anesthetized with pentobarbital (60 mg/kg, i.p.) and perfused with 4% paraformaldehyde in 0.1 M pH 7.4 phosphate-buffered saline. Removed brains were kept in 4% paraformaldehyde for 4 to 6 h, then immersed in 25% sucrose for 3 to 4 days at 4°C. The brains were embedded in O.C.T compound (Sakura Finetek USA Inc.) and sectioned

on a cryostat (18 μm thick). Coronal sections from 1 mm anterior and 1 mm posterior to the blood injection site were used for hematoxylin and eosin staining (1). Caudate and lateral ventricular areas were measured using NIH image.

Behavioral Tests

All animals underwent behavioral testing before and after surgery and were scored by experimenters who were blinded to both neurological and treatment conditions. To assess behavioral deficits both forelimb placing and forelimb use asymmetry tests were used (4).

Statistical Analysis

All data in this study were presented as mean \pm standard deviation. Data were analyzed using Student t test or ANOVA with a Scheffe's post-hoc multiple comparison test. Behavioral data were analyzed by Kruskal-Wallis test. Significance levels were set at $p < 0.05$.

Results

All physiologic variables were measured immediately before intracerebral injections. Mean arterial blood pressure (MABP), pH, arterial oxygen and carbon dioxide tensions (PO_2 and PCO_2), hematocrit, and blood glucose were controlled within normal range (MABP, 80–120 mmHg; PO_2 , 80–120 mmHg; PCO_2 , 35–45 mmHg; hematocrit, 38–43%; blood glucose, 80–120 mg/dL).

Normal rat brain water content in the basal ganglia is about 78% and ICH causes brain edema in the perihematomal zone. Minocycline reduced perihematomal brain edema in the ipsilateral basal ganglia (78.8 ± 0.4 vs. $80.9 \pm 1.1\%$ in the vehicle-treated group, $p < 0.01$). Minocycline also reduced sodium ion accumulation (219 ± 22 vs. 324 ± 89 $\mu\text{Eq/g}$ dry wt in the vehicle-treated group, $p < 0.01$) and potassium ion loss (394 ± 16 vs. 327 ± 48 $\mu\text{Eq/g}$ dry wt in the vehicle-treated group, $p < 0.01$) in the perihematomal zone.

Minocycline also improved functional outcome (Fig. 1). For example, the forelimb placing score was increased by minocycline treatment (day 1: 12 ± 10 vs. $0 \pm 0\%$ in the vehicle-treated group, $p < 0.05$; day 14: 98 ± 4 vs. $60 \pm 36\%$, $p < 0.05$, Fig. 1). In addition, minocycline reduced brain tissue loss in the ipsilateral caudate ($5 \pm 7\%$ vs. $17 \pm 5\%$ loss in the vehicle-treated group, $p < 0.01$) and ventricular enlargement ($p < 0.05$, Fig. 2).

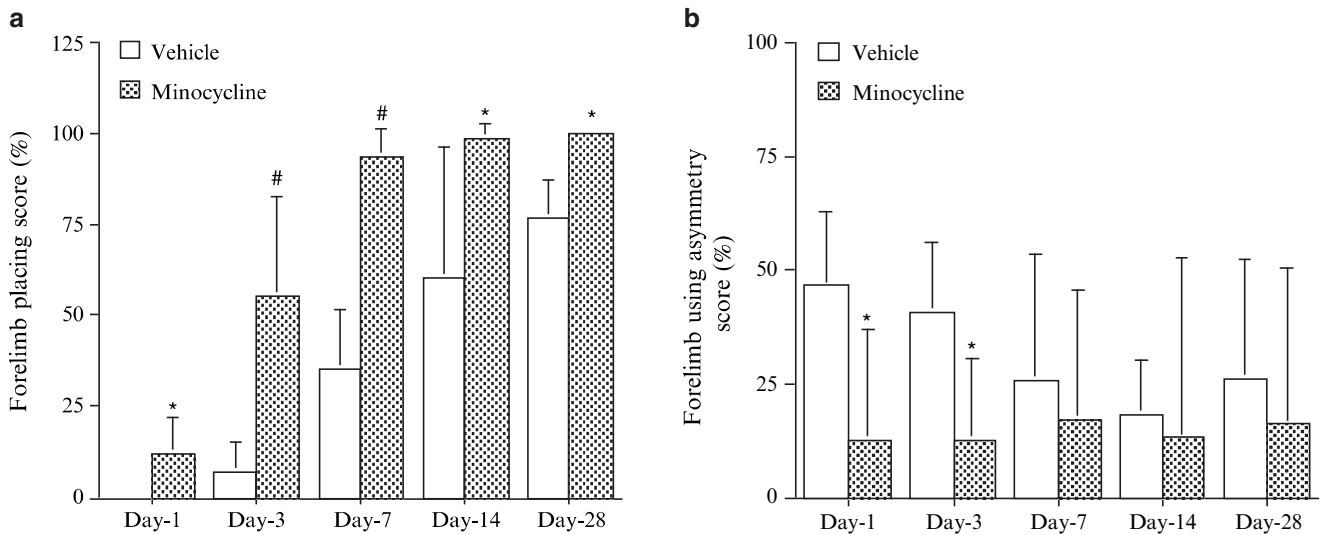


Fig. 1 Forelimb placing (a) and forelimb using asymmetry (b) score in the rats after ICH. The rats were treated with vehicle or minocycline. For forelimb placing, normal rats have a score of 100% and lower

scores indicate a deficit. For forelimb use asymmetry, normal rats have a score of 0% and high scores indicate a deficit. Values are mean \pm SD, $n = 5-7$, * $p < 0.05$, # $p < 0.01$ vs. vehicle; Kruskal–Wallis test

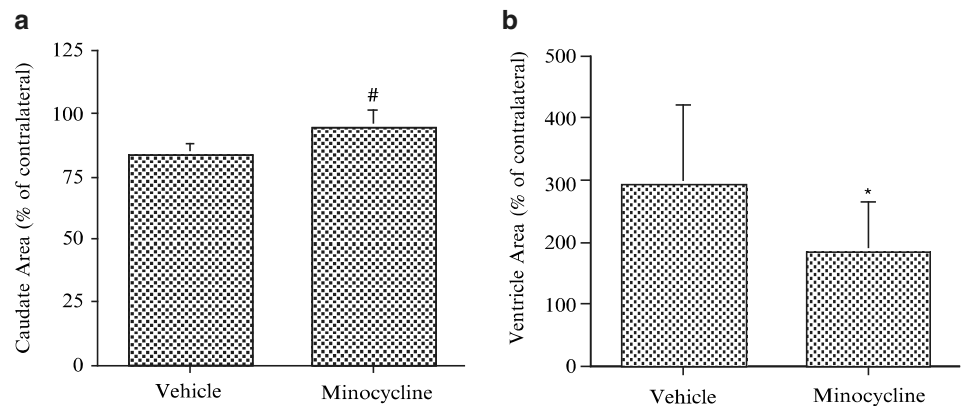


Fig. 2 Caudate (a) and ventricle (b) sizes 28 days after ICH in rats treated with vehicle or minocycline. For both caudate and ventricle measurements, the ipsilateral size was expressed a percent of contralateral. Values are mean \pm SD, $n = 5-7$, * $p < 0.05$, # $p < 0.1$ vs. vehicle; Student t test

Discussion

In this study, we demonstrated that minocycline can reduce perihematomal edema, brain tissue loss and neurological deficits in a rat model of ICH.

Activation of microglia around the hematoma occurs after ICH (2,3). Microglia are cells within the brain that are activated in response to injury. In normal brain, microglia are in a quiescent state, but in the event of injury they become highly phagocytic and they are involved in clearing debris from the damaged site (10). The activation of microglia that occurs after acute CNS injury is marked by changes in cellular morphology, size and number. In human brain, microglia become progressively more activated with age (9). Our previous study found many more activated microglia in aged compared to young rats 3 days after ICH (3).

Microglia activation is associated with brain edema formation following ICH since minocycline, an inhibitor of microglia activation, results in less perihematomal edema. We have previously found that microglial activation is associated with severe brain swelling in aged rats after ICH (3). Many factors, including thrombin and complement factors, contribute to brain edema formation after ICH (17), and both thrombin and complement can activate microglia (11,18). It is unclear, however, whether or not thrombin-or complement-mediated brain edema is through microglia activation.

Minocycline reduces ICH-induced brain tissue loss and improves functional outcomes suggesting that acute microglia activation after ICH may be harmful. Microglia secrete many toxic materials such as free radicals and can cause brain damage (6). Our results are supported by a study by Wang et al. who found that microglial inhibition decreases

injury volume and improves neurobehavioral deficits in a collagenase-induced ICH mouse model (14). However, it should be noted that although microglial activation is a brain injury marker for many central nervous system diseases, microglia can also have neurotrophic actions (10).

Conflict of interest statement We declare that we have no conflict of interest.

Acknowledgments This study was supported by grants NS-017760, NS-039866, and NS-047245 from the National Institutes of Health (NIH), 0755717Z from American Heart Association (AHA), and NSFC30600195 from National Natural Science Foundation of China (NSFC). The content is solely the responsibility of the authors and does not necessarily represent the official views of the NIH, AHA, or NSFC.

References

1. Felberg RA, Grotta JC, Shirzadi AL, Strong R, Narayana P, Hill-Felberg SJ, Aronowski J (2002) Cell death in experimental intracerebral hemorrhage: the “black hole” model of hemorrhagic damage. *Ann Neurol* 51:517–524
2. Gong C, Hoff JT, Keep RF (2000) Acute inflammatory reaction following experimental intracerebral hemorrhage. *Brain Res* 871(1):57–65
3. Gong Y, Hua Y, Keep RF, Hoff JT, Xi G (2004) Intracerebral hemorrhage: effects of aging on brain edema and neurological deficits. *Stroke* 35:2571–2575
4. Hua Y, Schallert T, Keep RF, Wu J, Hoff JT, Xi G (2002) Behavioral tests after intracerebral hemorrhage in the rat. *Stroke* 33:2478–2484
5. Jenkins A, Maxwell W, Graham D (1989) Experimental intracerebral hematoma in the rat: sequential light microscopic changes. *Neuropathol Appl Neurobiol* 15:477–486
6. Klegeris A, McGeer PL (2000) Interaction of various intracellular signaling mechanisms involved in mononuclear phagocyte toxicity toward neuronal cells. *J Leukocyte Biol* 67:127–133
7. Klein NC, Cunha BA (1995) Tetracyclines. *Med Clin North America* 79:789–801
8. Power C, Henry S, Del Bigio MR, Larsen PH, Corbett D, Imai Y, Yong VW, Peeling J (2003) Intracerebral hemorrhage induces macrophage activation and matrix metalloproteinases. *Ann Neurol* 53:731–742
9. Streit WJ, Sparks DL (1997) Activation of microglia in the brains of humans with heart disease and hypercholesterolemic rabbits. *J Mol Med* 75:130–138
10. Streit WJ, Walter SA, Pennell NA (1999) Reactive microgliosis. *Prog Neurobiol* 57:563–581
11. Suo Z, Wu M, Ameenuddin S, Anderson HE, Zoloty JE, Citron BA, Andrade-Gordon P, Festoff BW (2002) Participation of protease-activated receptor-1 in thrombin-induced microglial activation. *J Neurochem* 80:655–666
12. Tikka T, Fiebich BL, Goldsteins G, Keinänen R, Koistinaho J (2001) Minocycline, a tetracycline derivative, is neuroprotective against excitotoxicity by inhibiting activation and proliferation of microglia. *J Neurosci* 21:2580–2588
13. Tikka TM, Koistinaho JE (2001) Minocycline provides neuroprotection against N-methyl-D-aspartate neurotoxicity by inhibiting microglia. *J Immunol* 166:7527–7533
14. Wang J, Rogove AD, Tsirka AE, Tsirka SE (2003) Protective role of tuftsin fragment 1–3 in an animal model of intracerebral hemorrhage. *Ann Neurol* 54:655–664
15. Wang J, Tsirka SE (2005) Tuftsin fragment 1–3 is beneficial when delivered after the induction of intracerebral hemorrhage. *Stroke* 36:613–618
16. Wasserman JK, Schlichter LC (2007) Neuron death and inflammation in a rat model of intracerebral hemorrhage: effects of delayed minocycline treatment. *Brain Res* 1136:208–218
17. Xi G, Keep RF, Hoff JT (2006) Mechanisms of brain injury after intracerebral haemorrhage. *Lancet Neurol* 5:53–63
18. Yang S, Nakamura T, Hua Y, Keep RF, Younger JG, He Y, Hoff JT, Xi G (2006) The role of complement C3 in intracerebral hemorrhage-induced brain injury. *J Cereb Blood Flow Metab* 26:1490–1495

Myocardial Dysfunction in Subarachnoid Hemorrhage: Prognostication by Echo Cardiography and Cardiac Enzymes. A Prospective Study

Prasad Vannemreddy, Prasanna Venkatesh, Kumar Dinesh, Pratap Reddy, and Anil Nanda

Abstract

Background The myocardial dysfunction in nontraumatic sub-arachnoid hemorrhage (SAH) is not well understood. Borderline elevations of cardiac biomarkers, electrocardiographic repolarization abnormalities and systolic dysfunction have been reported but the clinical significance of these abnormalities is uncertain.

Methods Patients without history of cardiac disease were prospectively evaluated for cardiac dysfunction. Myocardial regional wall motion and left ventricular ejection fraction (LVEF) were serially studied by transthoracic echocardiogram along with cardiac enzymes.

Results The mean age of the study population was 53 years. Majority of the patients had aneurysms (N = 38). The mean LVEF was $55 \pm 15\%$. Eight patients had evidence of WMA, mostly global hypokinesia (63%). The mean LVEF of patients with WMA was significantly lower compared to those without WMA ($p < 0.001$) at day 0. Systolic function recovered in 25% of these patients. The mean value of troponin was significantly higher in those with WMA ($p < 0.001$) and mean GCS upon admission was significantly lower ($p < 0.001$). On multivariate analysis, WMA were associated with poor GCS ($p < 0.01$) and increased hospitalization ($P < 0.01$).

Conclusions WMA with systolic dysfunction occurred in 20% of patients and recovered within 3 days in 25%. Patients with evidence of WMA had a significant myocardial dysfunction, higher troponin levels and poor GCS.

Keywords Subarachnoid hemorrhage • echo cardiography • myocardial dysfunction • ejection fraction • cardiac enzymes

P. Vannemreddy (✉)

Department of Neurosurgery, LSUHSC-Shreveport, LA, 71103, USA
e-mail: pvanne@lsuhsc.edu; prasad4458@hotmail.com

P. Venkatesh, K. Dinesh, P. Reddy and A. Nanda
Departments of Cardiology, LSUHSC-Shreveport, LA 71103, USA

Introduction

The association between SAH and myocardial dysfunction cannot be overemphasized. There is paucity of information on the natural history of left ventricular systolic dysfunction in patients who survive a SAH. Cheng published his report of a patient who presented with SAH mimicking acute myocardial infarction (5). Similar but more dramatic was the presentation by Galasko et al about a patient with SAH presenting as acute myocardial infarction with electromechanical arrest (9). This patient had a normal coronary angiography but extensive SAH on CT scan of brain and died after 16 h of admission. Previous studies suggested that significant cardiac dysfunction can occur in patients with acute intracranial hemorrhage, particularly in those with subarachnoid hemorrhage (6,11).

Materials and Methods

Patients admitted with nontraumatic SAH but without known preexisting cardiac disease were evaluated by serial cardiac enzyme, ECG and echocardiographic studies. Exclusion criteria included a delayed admission of 7 or more days after hemorrhage, death before angiography and a history of preexisting cardiac disease (coronary artery disease (CAD), valvular heart disease, or arrhythmia). From the eligible patients, details of both clinical and investigative modalities like age, gender, premorbid conditions, risk factors, SAH-CT grading, Hunt and Hess grading of SAH, ECG findings, cardiac enzymes (troponin1, CK-MB) were recorded. Diagnosis of aneurysmal SAH was documented by CT angiogram and/or conventional four vessel cerebral angiography. Initial echo was done on the day of admission. Standard parasternal long axis, short axis, and apical 2- and 4-chamber views were obtained for analysis of left ventricular function. Serial EKG, Echo cardiography and enzyme studies were obtained on day 0, day 1 and day 3.

Results

The mean age (\pm SD) of the study population was 53 (\pm 13) years. Females comprised 58% of the population. The majority of these patients had evidence of intracranial aneurysms (38/42). All aneurysms were treated and 15 of them had postoperative complications. The mean GCS upon admission was 13.1. The mean LVEF for total population was $55 \pm 15\%$. Ten patients (20%) had evidence of WMA. The WMA seen were mostly global hypokinesia (5/8 = 63%) and the rest were regional WMA involving the anterior wall, septum or basal inferior walls. The mean LVEF of patients who demonstrated WMA was significantly lower compared to those without WMA (30% vs 62%, $p < 0.001$) at day 0. Systolic function recovered in 25% of these patients by day 3. The mean level of troponin for the study population was 0.262. The mean value of troponin was significantly higher in those with WMA compared to those without WMA (0.938 vs 0.077, $p < 0.001$).

Moreover, the mean GCS upon admission was significantly lower in patients with WMA compared to those without WMA (8.2 vs 14.1, $p < 0.001$).

On multivariate regression analysis, WMA were associated with poor GCS ($P < 0.01$) and increased hospital stay ($P < 0.01$). The details of relationships among the cardiac dysfunction and other variables show that poor neurological status had significant correlation with myocardial dysfunction. These associations, in turn had shown statistically significant association with patient outcomes.

Discussion

Intracranial hemorrhage is associated with high mortality and morbidity. Following initial hemorrhage 10% die before reaching the hospital and about 8% die from progressive deterioration from the initial hemorrhage; of those reaching the neurosurgical intensive care 7% die because of vasospasm and another 7% get severely disabled. Overall, half of the patients succumb to SAH in the first month itself (9).

In SAH, many abnormalities are noted in ECG and echocardiography depending upon the severity of the intracranial hemorrhage. ECG abnormalities occur frequently but there is no consistent relation between these abnormalities and actual cardiac injury or ischemia in SAH. Abnormalities in echocardiogram or left ventriculogram in cases with SAH include transient global or segmental left ventricular hypokinesia or akinesia. Histologically apparent cardiac lesions and ECG abnormalities seen in these patients are similar to those observed in hyperadrenergic animals as well as patients with pheochromocytoma or who received norepinephrine infusion

before death (13,14). Braunwald and Kloner attributed stunned myocardium to a delayed recovery of ATP concentration because the process of recovery of post ischemic intracellular ATP depletion following the re-establishment of perfusion was found to occur in parallel with the recovery of myocardial contractility (3). It is pertinent to note that coronary angiography in many of these cases with stunned myocardium did not reveal coronary vasospasm and occlusion (10). In rare cases there may be enzymatic evidence of myocardial necrosis. So dramatic may be the presentation of myocardial stunning that often death ensues even before evaluation of intracranial pathology (8).

It is suggested that hypothalamic ischemia in these patients with vasospasm can precipitate an intense sympathetic discharge that causes myocardial injury. Interestingly, hypothalamic hemorrhage and infarction are frequently found in conjunction with myocardial damage in SAH at autopsy of these patients (12). The cardiac enzymes may not be significantly elevated in these patients reflecting the minimal extent of myocardial necrosis (15). Yuki et al also reported cases where coronary angiography was normal even though the EKG changes were consistent with myocardial ischemia (16). This kind of myocardial stunning phenomenon was thought to be due to reversible cellular disturbances due to free radicals. The degree of cardiac dysfunction evident on echocardiogram is more closely associated with the severity of SAH and with poor neurological status than it is with ECG changes (4). This probably would explain the high risk of mortality and morbidity in patients with poor neurological status.

Deibert et al reported that in seven of the 12 patients with elevated troponin-1 levels, there was echocardiographic evidence of left ventricular dysfunction, which later returned to normal (5). These patients underwent further evaluation and no evidence of CAD was found. In another study abnormal left ventricular wall motion occurred exclusively in patients with peak CK-MB levels $>2\%$, poor neurological grade, and female sex (11).

Elrifai et al studied cardiac effects of acute SAH in nine adult mongrel dogs; microscopic examination of the heart showed evidence of myocardial changes in one animal with the use of light microscopy and in all nine with the use of electron microscopy (7).

Activation of the sympathetic nervous system after SAH typically results in a hyperdynamic cardiovascular state and even small elevations in myocardial enzymes reflect relative cardiac decompensation and failure of the left ventricle to meet these inotropic demands. Benedict and Loach found that plasma epinephrine and norepinephrine levels were significantly raised in patients recovering from SAH, and higher levels on admission were associated with a poor outcome (1,2).

Conclusions: Echocardiography was abnormal in aneurysmal SAH compared to non aneurysmal SAH. Regional wall motion abnormalities (RWMA) seen in SAH were

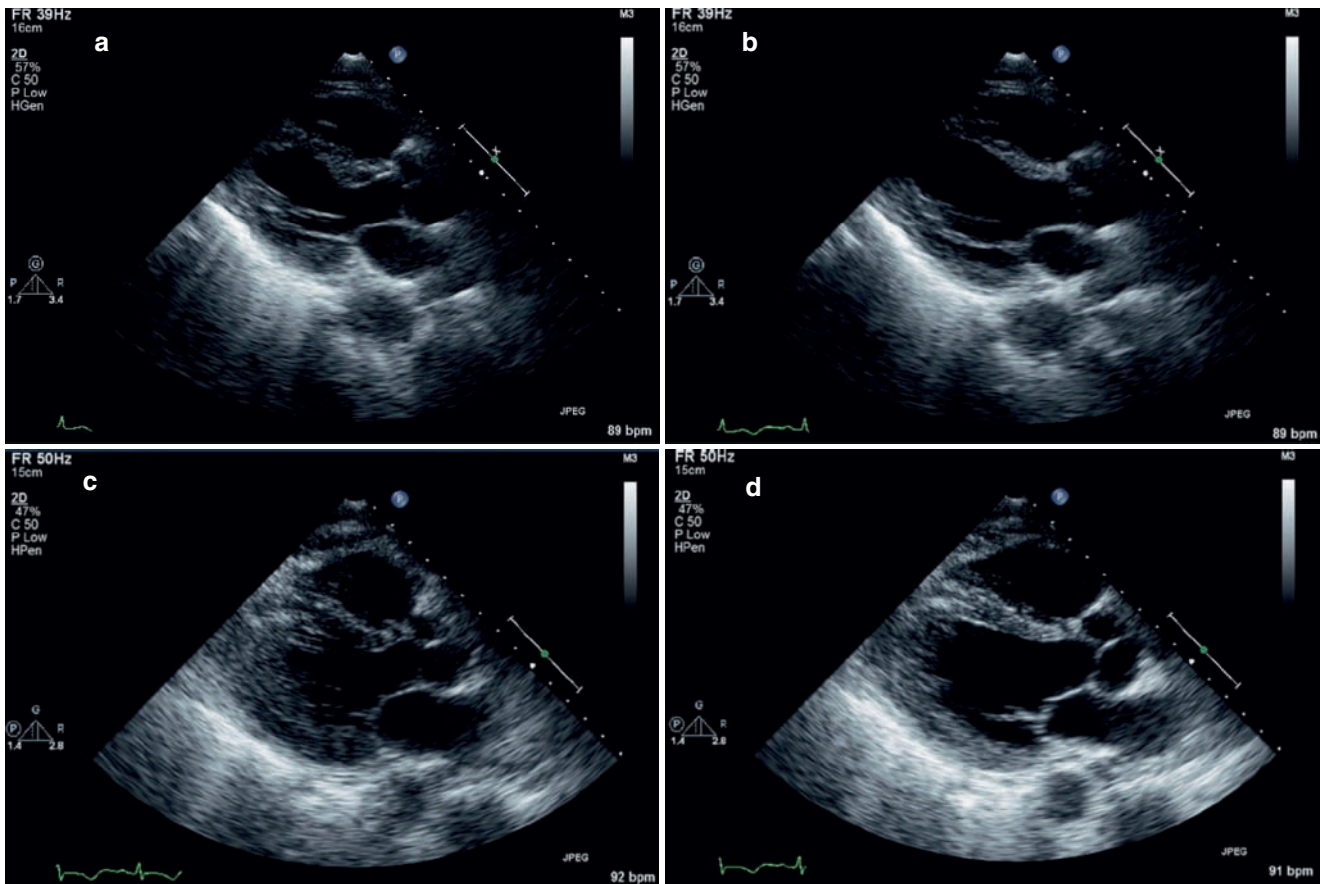


Fig.1 Panels (a) and (b) show the parasternal long axis views at end-systole and end-diastole respectively from a patient with SAH at the time of admission. There is severe global hypokinesis, mid septal akinesis, with reduced LVEF. The reduced systolic thickening of the ventricular walls and the akinesis of the mid septum can be appreciated in

this view. Panels (c) and (d) show parasternal long axis views at end-systole and end-diastole respectively from the same patient 12 days later. Compared to the previous echo, there is improvement in the wall thickening, wall motion and systolic function. The mid septal akinesis is no longer evident

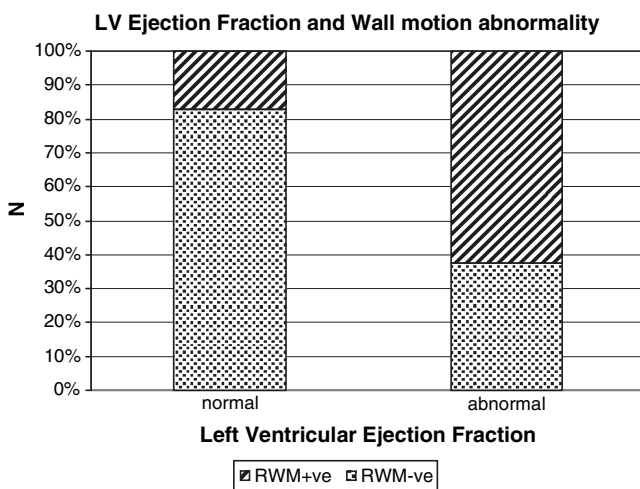


Fig. 2 Left ventricular regional wall motion abnormalities had significant relationship with abnormal ejection fraction ($P < 0.01$)

distinct from patterns seen in coronary heart disease. Clinical grade had significant correlation with RWMA. Reversal of the RWMA was seen in follow up echocardiography, suggesting that these changes are transient. LV dysfunction and RWMA had association with mortality (Figs. 1 and 2).

Conflict of interest statement We declare that we have no conflict of interest.

References

1. Benedict CR, Loach AB (1978) Clinical significance of plasma adrenaline and noradrenaline concentrations in patients with subarachnoid haemorrhage. *J Neurol Neurosurg Psychiatry* 41(2):113–117
2. Benedict CR, Loach AB (1978) Sympathetic nervous system activity in patients with subarachnoid hemorrhage. *Stroke* 9(3): 237–244

3. Braunwald E, Kloner RA (1982) The stunned myocardium: prolonged, postischemic ventricular dysfunction. *Circulation* 66(6): 1146-1149
4. Bulsara KR, McGirt MJ, Liao L, Villavicencio AT, Borel C, Alexander MJ, et al. (2003) Use of the peak troponin value to differentiate myocardial infarction from reversible neurogenic left ventricular dysfunction associated with aneurysmal sub arachnoid hemorrhage. *J Neurosurg* 98(Mar):524-528
5. Cheng T (2004) Subarachnoid hemorrhage mimicking acute myocardial infarction. *Int J Card* 95:361-362
6. Davies KR, Gelb AW, Manninen PH, Boughner DR, Bisnaire D (1991) Cardiac function in aneurysmal subarachnoid haemorrhage: a study of electrocardiographic and echocardiographic abnormalities. *Br J Anaesth* 67(Jul):58-63
7. Deibert E, Barzillai B, Braverman AC, Edwards DF, Aiyagari V, Dacey R, et al. (2003) Clinical significance of elevated troponin I levels in patients with nontraumatic subarachnoid hemorrhage. *J Neurosurg* 98(Apr):741-746
8. Elrifai AM, Bailes JE, Shih SR, Dianzumba S, Brillman J (1996) Characterization of the cardiac effects of acute subarachnoid hemorrhage in dogs. *Stroke* 4:737-741
9. Galasko GIW, Dubowitz M, Senior R (2001) Subarachnoid hemorrhage presenting as acute myocardial infarction with electromechanical dissociation arrest. *Heart* 86:340-341
10. Jain R, Deveikis J, Thompson BG (2004) Management of patients with stunned myocardium associated with subarachnoid hemorrhage. *Am J Neuroradiol* 25:126-129
11. Mayer SA, Fink ME, Homma S, Sherman D, LiMandri G, Lennihan L et al (1994) Cardiac Injury associated with neurogenic pulmonary edema following subarachnoid hemorrhage. *Neurology* 44(5):815-820
12. Pine DS, Tierney L (1996) A stressful interaction. *NEJM* 334: 1530-1534
13. Szakacs JE, Cannon A (1958) L-Norepinephrine myocarditis. *Am J Clin Pathol* 30(5):425-434
14. Todd GL, Baroldi G, Pieper GM, Clayton FC, Eliot RS (1985) Experimental catecholamine-induced myocardial necrosis. II. Temporal development of isoproterenol-induced contraction band lesions correlated with ECG, hemodynamic and biochemical changes. *J Mol Cell Cardiol* 17(7):647-656
15. Wells C, Cujec B, Johnson D, Goplen G (1995) Reversibility of severe left ventricular dysfunction in patients with subarachnoid hemorrhage. *Am Heart J* 139:409-412
16. Yuki K, Kodama Y, Onda J, Emoto K, Morimoto T, Uozumi T (1991) Coronary Vasospasm following subarachnoid hemorrhage as a cause of stunned myocardium. *J Neurosurg* 75: 308-311

The Effects of Tetrahydrobiopterin on Intracerebral Hemorrhage-Induced Brain Injury in Mice

Reiko Tsuchiyama, Takumi Sozen, Elena Titova, John H. Zhang, and Jiping Tang

Abstract Tetrahydrobiopterin (BH4) is an essential cofactor for nitric oxide synthase (NOS) and is presently used clinically to treat forms of phenylketonuria. BH4 has been reported to restrain superoxide generation of NOS and chemically reduce superoxide. However, there has been no report concerning the effects of BH4 in intracerebral hemorrhage (ICH). In the present study, we investigated the neuroprotective effect of BH4 against ICH-induced brain injury in a mouse model.

A total of 26 male CD1 mice (31–39 g) were divided into sham, ICH-vehicle, and ICH-treated with BH4 groups (n = 8 in each group). ICH was induced by collagenase injection into the right basal ganglia. BH4 (20 mg/kg) was administered intraperitoneally at 1 h after ICH. The effect of BH4 was measured by neurological score and brain water content at 24 h after ICH.

Our data demonstrates that ICH caused significant neurological deficit that is associated with brain edema. Treatment with BH4 did not reduce brain edema and neurological deficits at 24 h after ICH in mice. Further study is required to investigate the long-term effect of BH4 in ICH-induced brain injury.

Keywords Tetrahydrobiopterin(BH4) • ICH • mice • brain edema

Introduction

Intracerebral hemorrhage (ICH) is a common and often fatal subtype of stroke and carries high mortality and morbidity. Except the initial hemorrhagic impact, secondary brain

injury contributes to the poor clinical outcomes. Oxidative stress is considered a major contributor to ICH-induced secondary brain injury (1).

Hemoglobin (Hb) autoxidation and the iron release due to hemoglobin degradation start a chain of Hb-driven oxidative reactions (1). Reactive oxygen species (ROS) including superoxide anion, hydrogen peroxide and peroxynitrite (ONOO-) are produced. In addition, it has been reported that the inducible NO synthase (NOS)-derived peroxynitrite (ONOO-) contributes to ischemic brain injury (6). Blockade of endogenous brain tetrahydrobiopterin (BH4) (an essential cofactor for NOS activity) synthesis attenuates cerebral infarction via inhibiting iNOS and ONOO- (6). It was described that formation of superoxide (14) and hydrogen peroxide (7) in part is controlled by BH4 and BH4 efficiently inhibits superoxide generation from the heme group at the oxygenase domain of eNOS (13). However, a possible role of BH4 in secondary brain injury after ICH has not been examined. The goal of the presented study was to test whether BH4 administration may reduce brain edema formation and thus reduce neurological deficit after ICH.

Materials and Methods

Animal Preparation

A total of 26 male CD1 mice (31–39 g) were divided into sham (n = 8), ICH-vehicle (n = 9), and ICH-treated with BH4 (n = 9). ICH was induced by collagenase injection into the right basal ganglia as described by Rosenberg et al. (8). (6R)-5,6,7,8-Tetrahydrobiopterin dihydrochloride (BH4, Sigma-Aldrich, St. Louis, MO) was administered intraperitoneally at 1 h after ICH. All surgical procedures were approved by the Loma Linda University Institutional Committee for Animal Care and Handling. Animals were housed under 12:12 h light/dark cycle with access to water and food ad libitum.

J. Tang (✉), R. Tsuchiyama, T. Sozen, J.H. Zhang
Department of Physiology and Pharmacology, Loma Linda University
Medical Center, 11041 Campus Street, Risley Hall Room 133, Loma
Linda, California, 92354, USA
e-mail: jtang@llu.edu

E. Titova
Department of Radiation Medicine, Loma Linda University,
Loma Linda, CA 92350, USA

Neurological Deficits and Mortality

Neurological scores were assessed 24 h after ICH by an independent researcher blinded to the procedure using a modification of scoring (21 points) reported by Garcia et al. (2) (minimum score = 0, maximum score (healthy mouse) = 21). In addition, Beam Balance and Wire Hang scoring were also performed. Beam L (90 cm, \varnothing 1 cm) and Wire L (50 cm, \varnothing 1 mm) were bridges built between platforms. Mice were put on the center of Beam or Wire and time and behavior were evaluated until they reached one platform, when they scored five grades. This was repeated three times and an average (minimum score = 0, maximum score (healthy mouse) = 5) score was calculated.

Brain Water Content

Brains were divided into ipsilateral basal ganglia and cortex, contralateral basal ganglia and cortex, and cerebellum for the measurement of water content as described previously (12). Tissue samples were weighed on an electronic analytical balance (APX-60; Denver Instrument, Denver, CO, USA) to obtain the wet weight (WW), then dried at 100°C for 24 h to determine the dry weight (DW). Brain water content (%) was calculated as $[(WW-DW)/ww] \times 100$.

Results

The mortality rate at 24 h after collagenase injection did not differ between vehicle and treated group (11%, 1 of 9). The collagenase-induced hemorrhage detected in both vehicle and BH4 group (Fig. 1) resulted in significant neurological deficit versus sham animals (* $p < 0.05$, ** $p < 0.01$ vs sham, ANOVA). However, performed neurological tests did not show significant difference between vehicle and BH4-treated groups at 24 h after ICH induction. (Fig. 2a, b).

ICH induction resulted in markedly increased brain edema as compared with sham-operated animals (* $p < 0.05$, ANOVA). Again, no statistically significant difference was found between vehicle and treated groups (Fig. 3).

Discussion

Tetrahydrobiopterin (BH4) is a cofactor of aromatic amino acid hydroxylases, which are regarded as key enzymes in the biosynthesis of several neurotransmitters, including catecholamines and serotonin (5). In addition, BH4 is

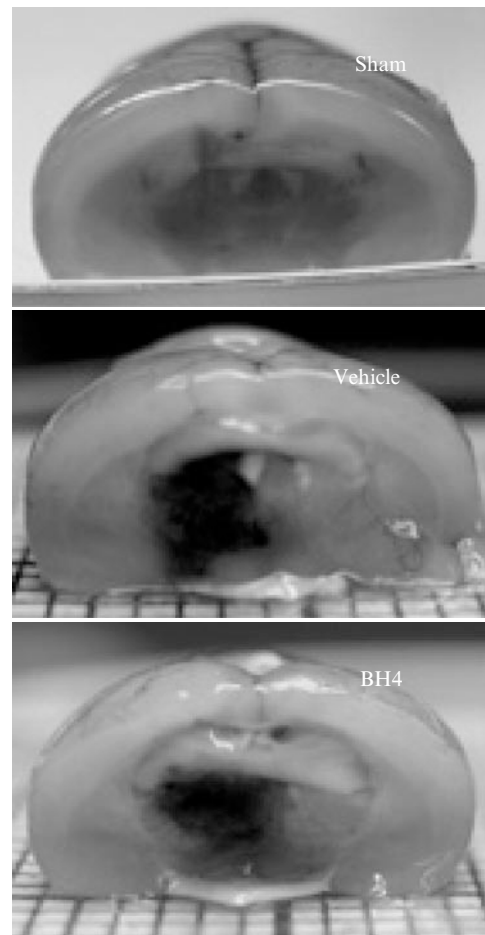


Fig. 1 Representative photographs of sham, vehicle-treated and BH4-treated mice brains. The hemorrhage volumes did not differ between both ICH-induced groups at 24 h after surgery

required for the activity of all NO synthase (NOS) isoforms: neuronal NOS (nNOS), endothelial NOS (eNOS), and inducible NOS (iNOS). It was shown that deficiency of BH4 leads to NOS-driven generation of superoxide anion instead of NO. Exogenous BH4 administration has been reported to restore impaired eNOS in endothelial dysfunction (10). In animal models it leads to reduced ischemia/reperfusion injury in the heart, stomach, kidney, and lung (3,4,9,11).

However, the effect of BH4 in cerebral hemorrhage model has not been tested. Our study presents the first experience of BH4 usage in ICH animal model. In this study, at its present stage, no neuroprotective effect of tetrahydrobiopterin in neurological functional tests and in brain edema formation was shown due to the short-term examination. The long-term effect of BH4 in secondary brain injury after ICH and a possible role of BH4 antagonist which was reported to reduce ischemic brain injury (6) will be studied.

Conflict of interest statement We declare that we have no conflict of interest.

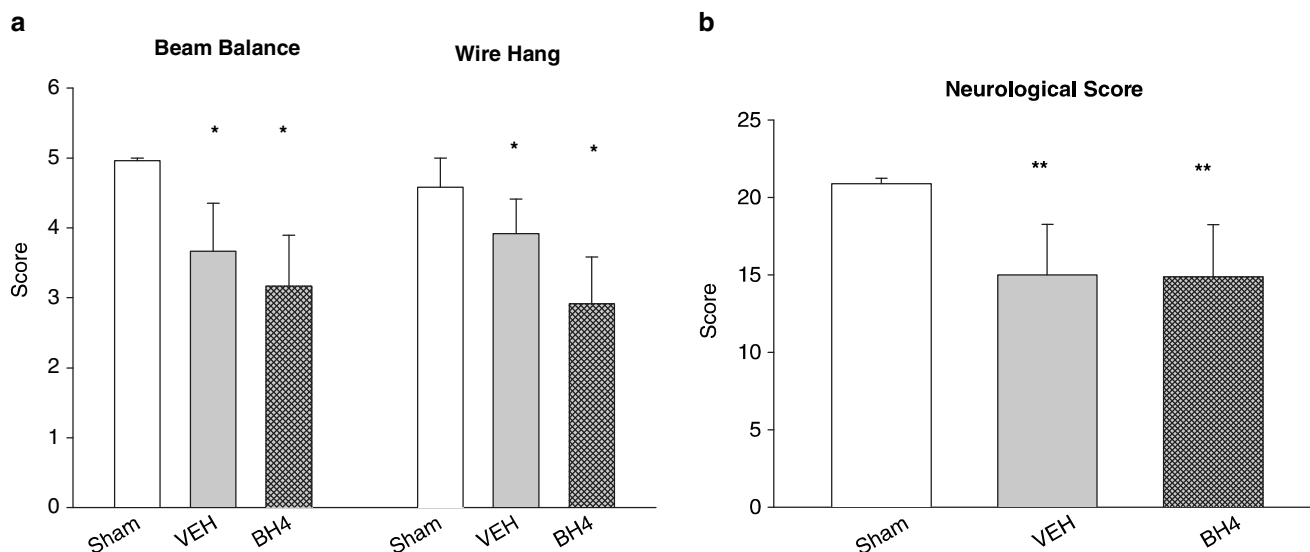


Fig. 2 (a and b) Neurological function was markedly impaired after ICH induction (* $p < 0.05$, ** $p < 0.01$ vs. sham, ANOVA). However, there was no difference between vehicle and BH4-treated groups at 24 h after ICH

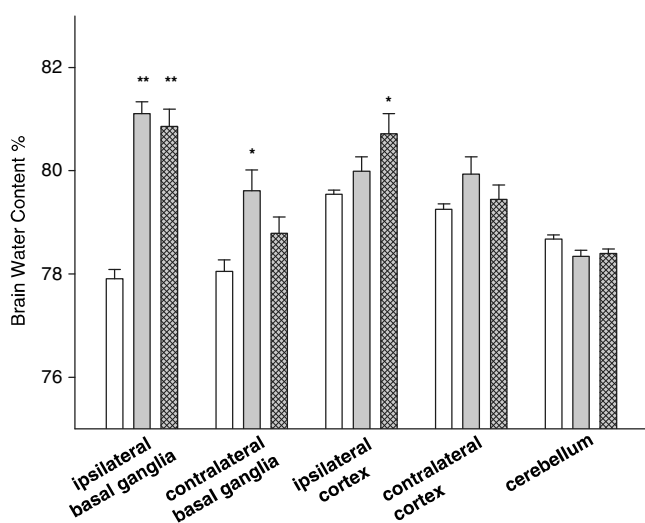


Fig. 3 Brain edema detected in ipsilateral basal ganglia was significantly higher in both ICH groups when compared with sham-operated animals (** $p < 0.001$ vs. sham, ANOVA). Brain edema was found in contralateral basal ganglia and ipsilateral cortex in vehicle and treated groups, respectively (* $p < 0.05$ vs. sham, ANOVA). However, BH4 treatment did not result in reduction of brain edema ($p > 0.05$ vehicle vs. BH4, ANOVA)

References

- Chen M, Regan RF (2007) Time course of increased heme oxygenase activity and expression after experimental intracerebral hemorrhage: correlation with oxidative injury. *J Neurochem* 103:2015–2021
- Garcia JH, Wagner S, Liu KF, Hu XJ (1995) Neurological deficit and extent of neuronal necrosis attributable to middle cerebral artery occlusion in rats. Statistical validation. *Stroke* 26:627–634
- Ishii M, Shimizu S, Nawata S, Kiuchi Y, Yamamoto T (2000) Involvement of reactive oxygen species and nitric oxide in gastric

ischemia-reperfusion injury in rats: protective effect of tetrahydrobiopterin. *Dig Dis Sci* 45:93–98

- Kakoki M, Hirata Y, Hayakawa H, Suzuki E, Nagata D, Tojo A, Nishimatsu H, Nakanishi N, Hattori Y, Kiuchi K, Nagano T, Omata M (2000) Effects of tetrahydrobiopterin on endothelial dysfunction in rats with ischemic acute renal failure. *J Am Soc Nephrol* 11:301–309
- Kaufman S (1993) New tetrahydrobiopterin-dependent systems. *Annu Rev Nutr* 13:261–286
- Kidd GA, Hong H, Majid A, Kaufman DI, Chen AF (2005) Inhibition of brain GTP cyclohydrolase I and tetrahydrobiopterin attenuates cerebral infarction via reducing inducible NO synthase and peroxynitrite in ischemic stroke. *Stroke* 36: 2705–2711
- Ortiz de Montellano PR, Nishida C, Rodriguez-Crespo I, Gerber N (1998) Nitric oxide synthase structure and electron transfer. *Drug Metab Dispos* 26:1185–1189
- Rosenberg GA, Mun-Bryce S, Wesley M, Kornfeld M (1990) Collagenase-induced intracerebral hemorrhage in rats. *Stroke* 21:801–807
- Schmid RA, Hillinger S, Walter R, Zollinger A, Stammberger U, Speich R, Schaffner A, Weder W, Schoedon G (1999) The nitric oxide synthase cofactor tetrahydrobiopterin reduces allograft ischemia-reperfusion injury after lung transplantation. *J Thorac Cardiovasc Surg* 118:726–732
- Shinozaki K, Nishio Y, Okamura T, Yoshida Y, Maegawa H, Kojima H, Masada M, Toda N, Kikkawa R, Kashiwagi A (2000) Oral administration of tetrahydrobiopterin prevents endothelial dysfunction and vascular oxidative stress in the aortas of insulin-resistant rats. *Circ Res* 87:566–573
- Teruaki Wajima, Shunichi Shimizu, Toshihito Hiroi, Masakazu Ishii, Yuji Kiuchi (2006) Reduction of myocardial infarct size by tetrahydrobiopterin: possible involvement of mitochondrial KATP channels activation through nitric oxide production. *J Cardiovasc Pharmacol* 47:243–249
- Titova E, Ostrowski RP, Sowers LC, Zhang JH, Tang J (2007) Effects of apocynin and ethanol on intracerebral haemorrhage-induced brain injury in rats. *Clin Exp Pharmacol Physiol* 34:845–850
- Vásquez-Vivar J, Kalyanaraman B, Martásek P (2003) The role of tetrahydrobiopterin in superoxide generation from eNOS: enzymology and physiological implications. *Free Radic Res* 37: 121–127
- Vásquez-Vivar J, Kalyanaraman B, Martásek P, Hogg N, Masters BSS, Karoui H, Tordo P, Pritchard KA Jr (1998) Superoxide generation by endothelial nitric oxide synthase: the influence of cofactors. *Proc Natl Acad Sci USA* 35:9220–9225

Estrogen Reduces Iron-Mediated Brain Edema and Neuronal Death

Y. Gu, G. Xi, W. Liu, R. F. Keep, and Y. Hua

Abstract Our previous studies found that 17- β estradiol attenuates edema formation after intracerebral hemorrhage (ICH). As brain iron overload occurs after ICH and contributes to ICH-induced brain injury, the present study examined the effects of estrogen on iron-induced brain injury in vivo and in vitro.

There were two sets of experiments in this study. In the first set, male Sprague-Dawley rats were pretreated with 17- β estradiol or vehicle prior to an intracerebral injection of ferrous iron. Ferrous iron was injected into the right caudate and the rats were killed 24 h later for brain edema measurement. In the second set, primary cultured neurons were pretreated with different doses of 17- β estradiol or vehicle for 24 h. The cells were then exposed to ferrous iron for 48 h when culture medium was collected for lactate dehydrogenase measurement. Neuronal death was also assessed by live/dead cell assay.

Estrogen pretreatment reduced brain water content ($p < 0.01$) 24 h after iron injection. Estrogen also protected against iron-induced cell death in cultured neurons. Estrogen reduces iron-induced brain edema in vivo and neuronal death in vitro suggesting estrogen could be a potential therapeutic agent for ICH.

Keywords Brain edema • cerebral hemorrhage • estrogen • iron

Introduction

Iron, a hemoglobin degradation product, accumulates in the brain after intracerebral hemorrhage (ICH) (18). ICH-induced brain iron overload contributes to both early and delayed brain injury (5,10,11).

Y. Hua (✉), Y. Gu, G. Xi, W. Liu, and R.F. Keep
R5018 Biomedical Science Research Building
Department of Neurosurgery
University of Michigan
109 Zina Pitcher Place
Ann Arbor, MI 48109-2200, USA
e-mail: yahua@umich.edu

Estrogen has been shown to confer strong brain protection in experimental cerebral ischemia (7,17) and we have found that brain edema is reduced when estrogen is given before or after ICH (9,12). The mechanisms involved in estrogen-induced protection are unknown. The present study investigated whether or not estrogen reduces iron-induced brain edema in vivo and neuronal death in vitro.

Materials and Methods

Experimental Groups

There were two groups of experiments in this study. In the first group, male Sprague-Dawley rats were pretreated with 17- β estradiol (5 mg/kg) or vehicle at 24 and 2 h prior to an intracerebral injection of ferrous iron. Ferrous iron (0.2 mM, 50 μ L) was injected into the right caudate and the rats were killed 24 h later for brain water content measurement. In the second group, primary cultured neurons were pretreated with different doses of 17- β estradiol (10 nM to 10 μ M) or vehicle for 24 h. The cultured neurons were then exposed to ferrous iron (500 μ M) for 48 h when culture medium was collected for lactate dehydrogenase (LDH) measurement. Neuronal death was also assessed by live/dead cell assay.

Animal Preparation and Intracerebral Injection

The University of Michigan Committee on the Use and Care of Animals approved the protocols for these animal studies, which used male Sprague-Dawley rats aged 3 to 4 months (Charles River Laboratories, Wilmington, MA). Septic precautions were used for all surgical procedures, and body temperature was maintained at 37.5°C using a feedback-controlled heating pad. Rats were anesthetized with pentobarbital (50 mg/kg, i.p.) and the right femoral artery was catheterized

for continuous blood pressure monitoring and blood sampling. Blood from the catheter was used to determine pH, PaO₂, PaCO₂, hematocrit, and glucose. The animals were positioned in a stereotactic frame (David Kopf Instruments, Tujunga, CA). Ferrous iron was injected into the right caudate nucleus through a 26-gauge needle at a rate of 10 μ L/min using a microinfusion pump (Harvard Apparatus, Inc., Holliston, MA). The coordinates were 0.2 mm anterior to bregma, 5.5 mm ventral, and 4.0 mm lateral to midline. After intracerebral injection, the needle was removed and the skin incision closed with suture.

Brain Water and Ion Content Measurements

Rats were killed under deep pentobarbital anesthesia at 24 h after iron injection. The brains were removed immediately and a 4-mm thick coronal section was taken 3 mm from the frontal pole. The brain sample was then divided into cortex or basal ganglia (ipsilateral or contralateral). Tissue samples were weighed to obtain the wet weight (WW). The tissue was then dried in a gravity oven at 100°C for more than 24 h to determine the dry weight (DW). Tissue water content (%) was calculated as $([WW-DW]/WW) \times 100$. Dehydrated brain samples were digested in 1 mL of 1 N nitric acid for 1 week. Sodium and potassium ion contents in this solution were measured by flame photometry and expressed in micro-equivalents per gram of dehydrated brain tissue (μ Eq/gm dry wt).

Primary Cortical Neuronal Culture

Neuronal cultures were established from embryonic day-17 Sprague-Dawley rat cerebral cortex. Cultures were prepared according to a previously described procedure with some modifications (8).

Measurement of Lactate Dehydrogenase

LDH activity in cell culture media was measured using a commercially available kit (Roche, Pleasanton, CA) according to the manufacture's instructions. The activity of LDH in the medium was expressed as mU/mL.

Live/Dead Cell Assay

Cell viability was assessed using a commercial kit (Live/Dead Viability/Cytotoxicity assay kit, Molecular Probes, Eugene, OR) according to the manufacture's instructions.

Samples were viewed under a microscope. For each sample, four randomly spots were selected. Quantification of dead cells (percent of red cells/red + green cells) was performed by 1.62 NIH image system.

Statistical Analysis

All data in this study are presented as mean \pm standard deviation. Data were analyzed with Student's t test or ANOVA test. Significance levels were set at $p < 0.05$.

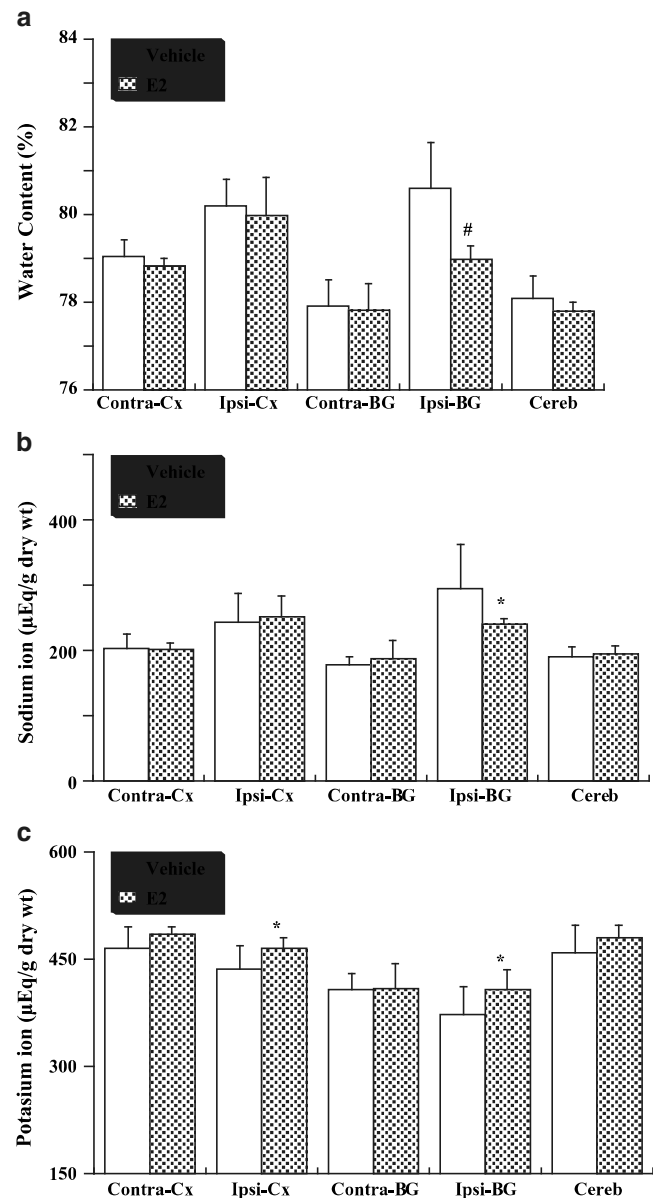


Fig. 1 Brain water (a), sodium (b) and potassium (c) contents in the ipsilateral (ipsi) and contralateral (contra) basal ganglia (BG) and cortex (Cx) 24 h after intracerebral injection of ferrous iron. Rats were pretreated with 17- β estradiol (E2; 5 mg/kg) or vehicle 24 and 2 h prior to ferrous iron injection. Values are mean \pm SD, $n = 5-7$, * $p < 0.05$, # $p < 0.01$ vs. vehicle

Results

Physiological variables including mean arterial blood pressure, blood pH, PaO₂, PaCO₂, hematocrit, and blood glucose level were controlled within normal ranges.

Intracerebral injection of ferrous iron caused brain edema in the ipsilateral basal ganglia (80.6 ± 0.9 vs. $78.2 \pm 0.6\%$ in the contralateral side, $p < 0.05$) at 24 h. Estrogen pretreatment reduced the water content (79.0 ± 0.3 vs. $80.6 \pm 0.5\%$ in the vehicle-treated group, $p < 0.01$, Fig. 1a) in the ipsilateral basal ganglia 24 h after iron injection. This was accompanied by a reduction in brain sodium content (239.9 ± 9.2 vs. 294.7 ± 67.7 $\mu\text{Eq/g}$ dry wt in the vehicle-treated group, $p < 0.05$, Fig. 1b) and reduced brain potassium loss (407.1 ± 27.7 vs. 458.7 ± 39.2 $\mu\text{Eq/g}$ dry wt in vehicle-treated group, $p < 0.05$, Fig. 1c).

Estrogen also protected against iron-induced cell death in cultured neurons. The LDH release induced by ferrous chloride was significantly reduced by 17- β estradiol pretreatment at all doses (e.g. at dose of 1 μM : 41 ± 7 vs. 58 ± 13 mU/mL in the vehicle-treated group, $p < 0.05$, Fig. 2a). In addition, iron-induced cell death (percentage to total cells) was less after 17- β estradiol treatment ($p < 0.05$, Fig. 2b).

Discussion

Our previous study showed that 17 β -estradiol attenuates ICH-induced brain edema (9). Perihematomal brain edema is commonly observed during the acute and subacute stage following ICH, contributing to poor outcomes (14,15,20).

Although the mechanisms of edema formation following ICH are not fully resolved, several mechanisms are responsible for edema development. These include hydrostatic pressure during hematoma formation and clot retraction; coagulation cascade activation and thrombin production; erythrocyte lysis and iron toxicity (19). Iron has an important role in brain edema formation following ICH. We have demonstrated that deferoxamine, an iron chelator, can reduce perihematomal brain edema (11). In the present study we found that estrogen reduces iron-induced brain edema. The result suggests that estrogen-induced attenuation of brain edema following ICH may result from less iron toxicity.

Estrogen can also reduce iron-induced neuronal death. Recent studies have demonstrated that brain atrophy occurs after ICH in rats and in humans (5). Felberg et al. reported a 20% reduction in ipsilateral striatum volume and an increase in the ipsilateral ventricular size at 100 days after experimental ICH (2). Our data also found that brain atrophy develops gradually and peaks between 1 and 2 months after ICH in the rat and that deferoxamine can reduce ICH-induced brain atrophy implicating iron in such atrophy (5). Future studies should examine whether or not estrogen can reduce brain atrophy after ICH.

The precise mechanisms of estrogen-induced neuroprotection are not well understood, but estrogen reduces inflammation, diminishes programmed cell death and attenuates oxidative brain damage (3,4,6,16). There is also evidence that it can upregulate potentially protective heat shock proteins within the brain (1). Several estrogen receptors have been discovered including estrogen receptor (ER)- α , - β , -X and a membrane estrogen receptor (13). Evidence indicates that estrogen-induced neuroprotection can be estrogen receptor-mediated or non-estrogen receptor-mediated (13).

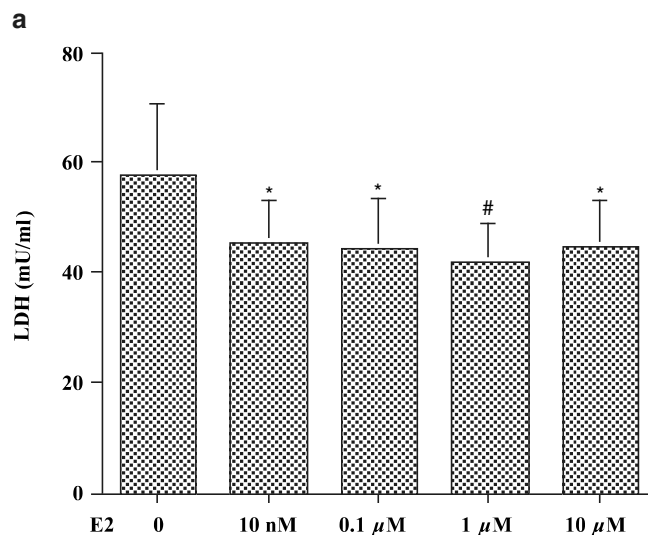
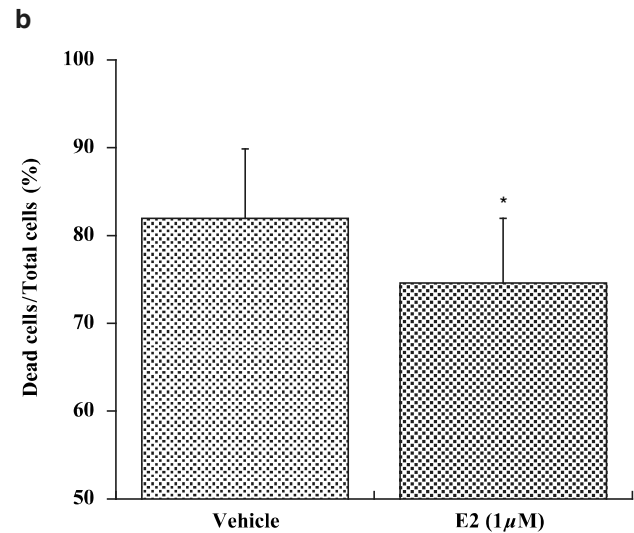


Fig. 2 (a) LDH levels in the neuronal culture medium 48 h after FeCl₂ (500 μM) treatment. Neurons were pretreated with 17- β estradiol (E2) at different concentrations (0, 10 nM, 0.1 μM , 1 μM and 10 μM) for 24



h. Values are mean \pm SD, * $p < 0.05$ and # $p < 0.01$ vs. E2 = 0. **(b)** 17- β Estradiol reduced neuronal death induced by FeCl₂ (500 μM). Values are mean \pm SD, * $p < 0.05$ vs. vehicle

In summary, estrogen reduces brain edema and neuronal death induced by iron suggesting that acute use of estrogen could be a new therapy for ICH.

Conflict of interest statement We declare that we have no conflict of interest.

Acknowledgments This study was supported by grants NS-017760, NS-039866, and NS-057539 from the National Institutes of Health (NIH), and 0755717Z and 0840016N from American Heart Association (AHA). The content is solely the responsibility of the authors and does not necessarily represent the official views of the NIH or AHA.

Reference

- Behan M, Zabka AG, Mitchell GS (2002) Age and gender effects on serotonin-dependent plasticity in respiratory motor control. *Resp Physiol Neurobiol* 131:65–77
- Felberg RA, Grotta JC, Shirzadi AL, Strong R, Narayana P, Hill-Felberg SJ, Aronowski J (2002) Cell death in experimental intracerebral hemorrhage: the “black hole” model of hemorrhagic damage. *Ann Neurol* 51:517–524
- Garcia-Segura LM, Azcoitia I, DonCarlos LL (2001) Neuroprotection by estradiol. *Prog Neurobiol* 63:29–60
- Gerlach M, Ben-Shachar D, Riederer P, Youdim MB (1994) Altered brain metabolism of iron as a cause of neurodegenerative diseases? *J Neurochem* 63:793–807
- Hua Y, Nakamura T, Keep RF, Wu J, Schallert T, Hoff JT, Xi G (2006) Long-term effects of experimental intracerebral hemorrhage: the role of iron. *J Neurosurg* 104:305–312
- Hurn PD, Brass LM (2003) Estrogen and stroke: a balanced analysis. *Stroke* 34:338–341
- Hurn PD, Macrae IM (2000) Estrogen as a neuroprotectant in stroke. *J Cereb Blood Flow Metab* 20:631–652
- Jiang Y, Wu J, Hua Y, Keep RF, Xiang J, Hoff JT, Xi G (2002) Thrombin-receptor activation and thrombin-induced brain tolerance. *J Cereb Blood Flow Metab* 22:404–410
- Nakamura T, Hua Y, Keep RF, Park JW, Xi G, Hoff JT (2005) Estrogen therapy for experimental intracerebral hemorrhage in rats. *J Neurosurg* 103:97–103
- Nakamura T, Keep RF, Hua Y, Hoff JT, Xi G (2005) Oxidative DNA injury after experimental intracerebral hemorrhage. *Brain Res* 1039:30–36
- Nakamura T, Keep RF, Hua Y, Schallert T, Hoff JT, Xi G (2004) Deferoxamine-induced attenuation of brain edema and neurological deficits in a rat model of intracerebral hemorrhage. *J Neurosurg* 100:672–678
- Nakamura T, Xi G, Hua Y, Schallert T, Hoff JT, Keep RF (2004) Intracerebral hemorrhage in mice: model characterization and application for genetically modified mice. *J Cereb Blood Flow Metab* 24:487–494
- Rau SW, Dubal DB, Bottner M, Gerhold LM, Wise PM (2003) Estradiol attenuates programmed cell death after stroke-like injury. *J Neurosci* 23:11420–11426
- Ropper AH (1986) Lateral displacement of the brain and level of consciousness in patients with an acute hemispherical mass. *N Eng J Med* 314:953–958
- Ropper AH, King RB (1984) Intracranial pressure monitoring in comatose patients with cerebral hemorrhage. *Arch Neurol* 41:725–728
- Santizo RA, Anderson S, Ye S, Koenig HM, Pelligrino DA (2000) Effects of estrogen on leukocyte adhesion after transient forebrain ischemia. *Stroke* 31:2231–2235
- Wise PM, Dubal DB, Wilson ME, Rau SW, Bottner M, Rosewell KL (2001) Estradiol is a protective factor in the adult and aging brain: understanding of mechanisms derived from in vivo and in vitro studies. *Brain Res – Brain Res Rev* 37:313–319
- Wu J, Hua Y, Keep RF, Nakamura T, Hoff JT, Xi G (2003) Iron and iron-handling proteins in the brain after intracerebral hemorrhage. *Stroke* 34:2964–2969
- Xi G, Keep RF, Hoff JT (2006) Mechanisms of brain injury after intracerebral haemorrhage. *Lancet Neurol* 5:53–63
- Zazulia AR, Diringner MN, Derdeyn CP, Powers WJ (1999) Progression of mass effect after intracerebral hemorrhage. *Stroke* 30:1167–1173

Part V
Imaging and Diagnosis

Improving Diagnostic Value of CT Examinations in Hyperacute Ischemic Stroke

A. Przelaskowski, J. Walecki, K. Sklinda, and G. Ostrek

Abstract This paper presents a computer assisted support of ischemic stroke diagnosis based on nonenhanced CT examinations acquired in the hyperacute phase of stroke. Computational analysis, recognition, and image understanding methods were used for extraction of the subtlest signs of hypodensity in diagnostically important areas. Starting from perception improvement, suggestive and coarse image data visualization was designed as a complement of the standard diagnosis procedure based on CT scan soft-copy review. The proposed method includes an evidence-based description of ischemic conditions and changes, de-skulling and segmenting of unusual areas, the analysis of hypodensity signs across scales and subbands with noise reduction, and hypodensity extraction. Following visualization, forms of empowered hypodensity symptoms localize suggested ischemic areas in source brain image space. Increased visibility of cerebral ischemia for difficult-to-diagnose cases was experimentally noticed and improved diagnostic value of CT was concluded.

Keywords Computer aided diagnosis • hyperacute stroke detection • multiscale image analysis • image content extraction

Introduction

The recent advent of thrombolytic therapy for hyperacute stroke treatment makes the earliest detection of areas of hypoattenuating ischemic parenchyma exceedingly important (1–4). However, although CT plays a crucial role in the evaluation of stroke patients, it is not sufficient for

visualizing infarcted cerebral tissues in the hyperacute stage. On the initial CT-scan, performed during the hyperacute phase of stroke (0–6 h), a hypodense area (direct infarct sign defined as any area in the brain with density lower than normal) surrounding brain tissues does not need to be seen. Early indirect findings, such as obscuration of gray/white matter differentiation and effacement of sulci or “insular ribbon sign”, may be sometimes noticed instead. Afterwards, it becomes possible to detect a slight hypodense area of infarction either in the cortices or the basal ganglia. Initially, the low density region is poorly defined, becoming more sharply delineated in the following hours (1–7). However, many infarcts do not emerge on CT until hours after the onset of stroke; 50–60% of stroke cases have normal CT before 12 h after stroke onset (8). Hence, effective and reliable computer assistance, which has become one of the major research subjects in medical imaging and diagnostic radiology (9), is considered to improve diagnostic value of CT examinations for those cases.

Computer aided diagnosis (CAD) is a sophisticated program that supports the doctor’s interpretations and findings. Automatic detection and characterization of lesions, perception enhancement, and other suggested indications in radiological images are based on image processing, computer vision, artificial intelligence, or computational intelligence completed by semantic technologies with formalized domain knowledge. For some clinical cases in which radiologists are confident about their judgments, radiologists may disagree and then disregard the computer. Otherwise, for cases in which radiologists are less confident, it is expected that the final decision can be improved by use of reliable computer output. The potential gain is due to the synergistic effect obtained by combining the radiologist’s competence and the computer’s capability (9). Computer suggestions can be utilized by radiologists, but not replace the judgment of the radiologists. Distinct computer aid is extremely useful for reliable support of as early as possible diagnosis for hyperacute cases. Ischemic stroke diagnosis based on nonenhanced CT examinations acquired in the hyperacute phase of stroke is an important and difficult computer assistance challenge (10–12). All available domain knowledge (i.e.,

A. Przelaskowski (✉) and G. Ostrek
Institute of Radioelectronics, Warsaw University of Technology,
Warsaw, Poland
e-mail: arturp@ire.pw.edu.pl

J. Walecki
Department of Radiology and Department of Experimental
Pharmacology, Centre of Experimental and Clinical Medicine,
Polish Academy of Science, Warsaw, Poland

K. Sklinda
Department of Radiology CMKP, CSK MSWiA, Warsaw, Poland

disease and imaging modality conditioning) is useful for optimizing CAD tool efficiency.

Focal hypodense changes were found to be the most frequent and reliable signs of early cerebral ischemia. A decline in cerebral blood flow causes the brain tissue to take up water immediately. Thus, in the early stage of cerebral ischemia, the tissue changes mainly consist of alterations in water and electrolyte content. Parallel intracellular increase of sodium and a decrease of potassium concentration occur. A 2–4% increase in brain tissue water within 4 h of MCA occlusion was noticed in several experiments (1). Increase of water content causes the lowering of brain attenuation coefficients in hyperacute ischemia, which leads to a discrepant decrease of about 1.3–2.6 HU for 1% change in water content (2). The discrepancy of water uptake and density changes might suggest an incompleteness of ischemic physiology model and unclear impact of other factors (e.g., decreased lipids, increased protein, and electrolyte changes).

Furthermore, the attenuation coefficients of brain parenchyma vary, mainly due to the differing thickness of the cranial vault. Dense bone lowers the energy of the beam and, thus, increases attenuation. M. Bendszus et al. (10) found inter-individual differences (i.e., bone artifacts) of up to 14 HU in brain parenchyma at comparable scan levels. The sufficient accuracy, stability, and linearity of CT number (HU) and degradation of contrast resolution caused by noise are the next problem. The CT number for water should ideally be zero, but the actual value changes because of variations in the stability of the detector system or x-ray source. Normally, these variations (i.e., standard deviation of the water value) are very small and most scanners should be able to stay within 2 HU of zero for water. The mean CT number measured over the central test ROI (region of interests) should be in the range of 4 HU, which is close to the early changes within ischemic region.

Diffusely interspersed changes in grey shade can hardly be distinguished in noisy areas because of a low brightness contrast, bone artifacts, and non-optimum scanning. That is why ischemic area is not well outlined, contrasted, or even noticeable. Nevertheless, it is evident that the early changes with ischemia occur, but may vary within the limited range of HU scale depending on cerebral infarct case, discrepant patient characteristics, and acquisition and technological conditioning. Because of the human eye limitations, these first ischemic signs can often be out of visibility range. The typical preview window of width 80 HU gives maximum noticeable change of 1–2 grey shade within the first 4 h of ischemia. Computer capability of signal extraction may be useful to make hidden hypodensity signs visible.

Methods and Materials

A stroke CAD method called Stroke Monitor was designed to improve diagnostic value of emergency CT scans through increased perception of hypodensity changes in hyperacute ischemic stroke cases. The suggested processing method was based on multiscale image data processing, de-noising, and identified lesion pattern extraction optimized by visualization procedure (13). Although experimental verification of Stroke Monitor confirmed improved diagnostic efficiency, some limitations caused further optimization research. Retrospective evaluation of 52 sets of examinations conducted in patients admitted with symptoms suggestive of stroke was undertaken by four radiologists unaware of the final clinical findings. All of the selected cases were considered as having no direct signs of hyperacute ischemia in the localization corresponding with clinical manifestation and follow-up studies (reported more exhaustively in (13)). At the first stage, only the CTs performed at admission were evaluated; after a month, the same scans were evaluated again with additional use of wavelet-based Stroke Monitor for stroke perception improvement. Subtle tissue attenuation changes were investigated, de-noised, extracted, and visualized. Follow-up CT exam and/or clinical picture confirmed or excluded the diagnosis. Sensitivity of 0.641 and specificity of 0.688 was gained for the wavelet-based stroke monitor aided diagnosis. Statistical significance of $p = 0.031$ for diagnosis improvement in comparison to conventional image review was noticed. However, for certain cases, prior Stroke Monitor was completely ineffective, causing reduction of sensitivity and specificity in comparison to conventional diagnosis. Considering these results with concluded efficiency limitations, an additional post-processing method based on complementary distinct hypodensity extraction has been designed.

An image data visualization method that extracts and distinctly communicates hypodensity as a signature of ischemia to the observers was proposed. Distinct Hypodensity Extraction (DHE) complements conventional CT scan view with highly specific to infarct cases display. Multiscale image transformations were used to analyze image content basing on spatially distributed soft tissue properties over different scales and subbands. Hypodensity may be effectively identified through hierarchical local data representation with signal energy compaction and information ordering; next, data analysis and processing in transform domain; finally, data reconstruction and adjusted visualization. Post-processing in space-scale domain is less susceptible to local perturbations, artifacts, and beneficial noise suppression. Adaptive local contrast enhancement and clear tissue density distinction is possible.

Initial two-stage segmentation of the regions susceptible to subtle ischemic density changes was applied to eliminate false indications in diagnostically unusual areas. False positives must be avoided since treating ineligible patients with intravenous thrombolysis is associated with an unacceptable risk of hemorrhage and death. De-skulling was the first stage. Moreover, clearly noticeable low density areas (e.g., sulci, prior ischemic scars) are not the subject of interest and should be omitted for processing. Thus, brain tissue areas with low density were segmented and fulfilled with higher density tissue (certainly not ischemic), providing continuous representation of white and gray matter region. Modified images were processed for final visualization. The essential procedure of hypodensity extraction was based on multiscale data processing. Multiscale image decomposition based on successive transformations with non-perfect reconstruction wavelet basis of separated horizontal-vertical kernels and curvelet basis of 2D kernels were used for de-noising and semantically defined stroke features extraction. Curvelets ensure better description of margin curvature to recognize that the boundary is smooth (14). Adaptive thresholding of the coefficients distributed across scales and subbands were used to model disease signatures more effectively. Algorithm arrangement is as follows:

Distinct Hypodensity Extraction Algorithm

1. Image conditioning with segmentation of ROIs

- (a) The brain extraction through de-skulling in CT volume; region growing arranged in 3D space of successive slices was used, where the initial set of seeds were grown-up across successive slices to regular region of the brain tissue identified in CT acquisition expanse.
- (b) Selection of the only tissue regions that are susceptible to ischemia; clear brain sulci, prior ischemic scars, and other structures useless in acute stroke detection were discarded; designed method of mixed growing-thresholding was applied with weighted average filtering for noise reduction, detection of low density seeds based on adaptive thresholding, growing low density regions with adaptive membership function, adjusting of indicated areas to make them regular, smooth, and large enough in size.
- (c) smooth complement of diagnostic ROIs with mean values of neighbor areas providing the continuity of density function and absence of any lower density fields.

2. Hypodensity extraction

- (a) Non-perfect orthogonal wavelet transform with *t spline2* kernel defined by low pass analysis filter

($\tilde{h} = [1/4, 2/4, 1/4]$) for coarse de-noising, gray-level scale quantization and contrast enhancement across subbands on scales.

- (b) Curvelet transform according to FDCT implementation (15) with adaptive soft thresholding (λ – threshold value) of complex curvelet coefficients c :

$$\tilde{c}_\lambda = \frac{c}{|c|} \cdot (|c| - \lambda) \text{ for } |c| > \lambda \text{ with zeroing other coefficients; de-noising and extraction of smooth edges of hypodense areas was the result.}$$

- (c) Reconstructed brain tissue mapping to source CT scans and merging with background view of the scans; the brain areas processed in multiscale domain are reconstructed, adaptively converted to suitable presentation scales, and respectively fitted to the source image with skull, scalp, and surrounding tissue in the best view window.

3. Hypodensity visualization

- (a) Display arrangement with contrast enhancement by adaptive histogram equalization of processed data in brain tissue area
- (b) Alternative 3D view of extracted hypodensity areas, stroke segmented regions, or structures to assess brain and stroke morphology more clearly

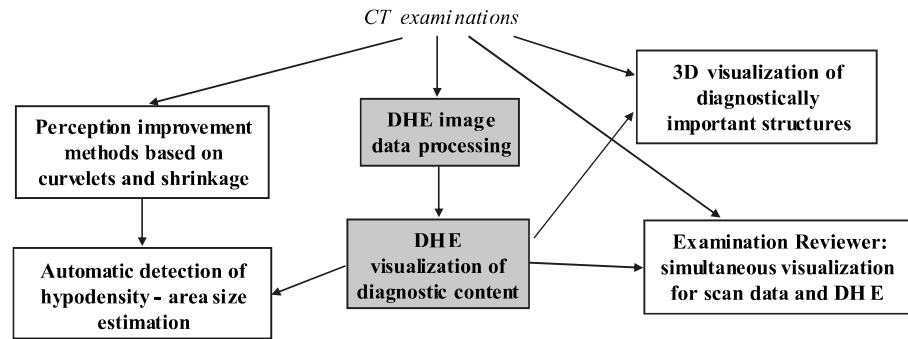
Proposed DHE was suggested to be applied in extended Stroke Monitor application (Fig. 1).

DHE was designed to improve and complete prior Stroke Monitor implementation based on perception improvement. Preliminary subjective tests were performed to verify the efficiency of DHE implementation as a supplement to prior Stroke Monitor verification. A test set consisted of six CT exams of brains selected as extremely difficult to diagnose based on false decision of specialists and unusual role of Stroke Monitor in the experiments. For three clinically confirmed cases of acute stroke appearance, the time between the onset of symptoms and the early CT examination ranged from 1 to 5 h. The other three were clinically confirmed normal cases. The valid presence and indicated position of asymmetric hypodense signs compared to the reference diagnosis (the location and size of the infarct) based on follow-up CT and MR scans were the performance criteria.

Results

First, clear and unambiguous DHE indications for extremely difficult cases were tested. According to simple test rules, monitor usefulness was verified even by non-specialists, biomedical engineers, or medicine students with the aim of

Fig. 1 Diagram of Stroke Monitor method as an extension of DHE – general view



preliminary assessment of DHE with simplified form of visualization. Nine observers participated in the experiments: one radiologist, four instructed medical students, and four instructed students of engineering.

The observer conviction of hypodensity extraction and any false suggestions dominantly affected responses in ischemic stroke detection procedure. Distinct extraction of hypodensity for diagnostically difficult cases significantly improved prior Stroke Monitor assistance (see Table 1). We found it useful in comparison to conventional diagnosis. The examples of DHE output are presented in Fig. 2.

Discussion

According to observers' opinions and collected results, DHE method improved the diagnosis for difficult cases because of clear, distinct visibility of hypodense signs or generally ischemic susceptibility for test examinations. Extraction of subtle tissue density changes and hard indications of lower density areas made image content assessment and interpretation more accurate and simple. Even engineers achieved satisfactory results based on elementary knowledge and assessment of asymmetric distribution of dark areas in visualized image form. Generally, significantly increased stroke detection efficiency was noticed. Combining the effects of standard CT scans review with DHE assistance provided a better diagnosis of stroke. Hypodensity-oriented distinct extraction with clearly indicated ischemic areas may facilitate the interpretation of CT scans in hyperacute infarction.

Optimized multiscale extraction of ischemic changes with complementary forms of semantic content visualization extends capabilities of computer assistance tools in a way that is useful for inexperienced observers, especially for difficult cases of ischemia. Consequently, the proposed

Table 1 A comparison of diagnosis efficiency for conventional-windowed image review, prior Stroke Monitor with perception improvement and DHE; mean results for nine observers were presented;

used measures are defined as follows: precision = $\frac{TP + TN}{TP + TN + FP + FN}$, sensitivity = $\frac{TP}{N_{stroke}}$, specificity = $\frac{TN}{N_{normal}}$, PVP = $\frac{TP}{TP + FP}$.

Method	Precision	Sensitivity	Specificity	PVP
Conventional	0.63	0.58	0.67	0.47
Prior Stroke Monitor (13)	0.42	0.5	0.33	0.38
DHE (nine observers)	0.80	0.89	0.70	0.74
DHE (radiologist)	0.833	0.666	1	1
DHE (four medical students)	0.708	0.833	0.583	0.625
DHE (four engineering students)	0.85	1	0.75	0.8

computer aided diagnosis tool with expressive display of distinct hypodensity symptoms can considerably improve stroke diagnosis by increased objectivity, unambiguous content extraction, and clear observer conviction, resulting in higher decision sensitivity and specificity. Increased usefulness of hyperacute CT examinations because of improved diagnostic value of visualized image content was noticed for test cases.

Further optimization of computer-based understanding of stroke presence in CT scans includes integrated assistance of DHE with tissue density perception enhancement, automatic detection and characteristic of ischemia, 3D visualization of underlined brain structures, and reliable estimation of segmented structures parameters. Moreover, multimodal analysis is required for time series of CT examinations and MR or perfusion complement.

Conflict of interest statement We declare that we have no conflict of interest.

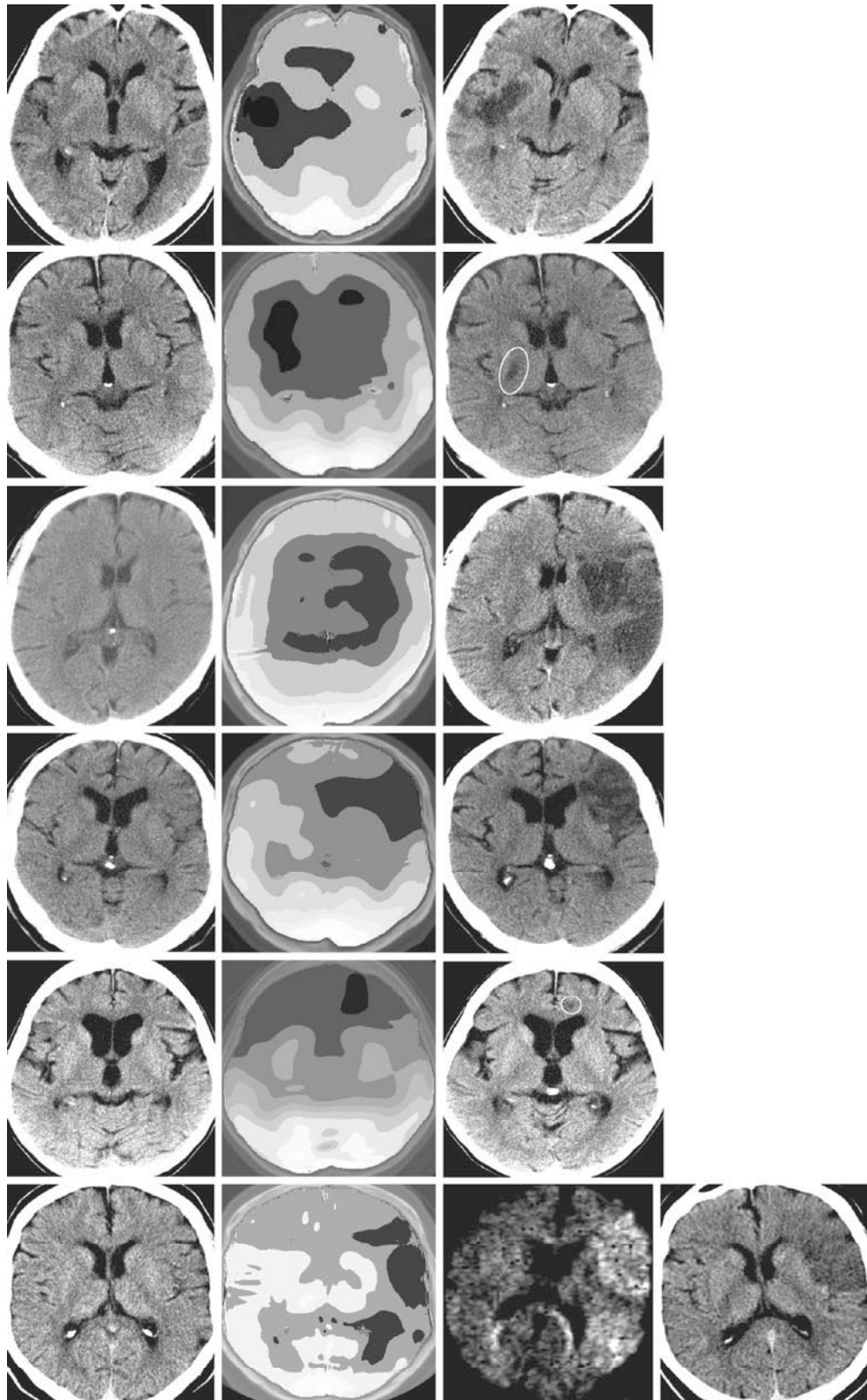


Fig. 2 The Stroke Monitor outputs (middle column) compared to early CT examinations (*left*) and follow-up confirmation (*right*) – small hypodensities were indicated; for the last case, early MR image was

presented with bright expression of two ischemic regions confirmed by Stroke Monitor, but only one of them was visible in follow-up CT (what suggests that this region was changed irreversibly)

References

1. von Kummer R (2005) The impact of CT on acute stroke treatment. In: Lyden P (ed) *Thrombolytic therapy for stroke*. Humana, Totowa, NJ, USA
2. Tomura N, Uemura K et al (1988) Early CT finding in cerebral infarction. *Radiology* 168:463–467
3. Bozzao L, Bastianello S et al (1989) Correlation of angiographic and sequential CT findings in patients with evolving cerebral infarction. *AJNR Am J Neuroradiol* 10:1215–1222
4. von Kummer R, Allen KL et al (1997) Acute stroke: usefulness of early CT findings before thrombolytic therapy. *Radiology* 205:327–333
5. Hacke W, Kaste M, Fieschi C et al (1995) Intravenous thrombolysis with recombinant tissue plasminogen activator for acute hemispheric stroke (ECASS). *JAMA* 274:1017–1025
6. Hacke W, Kaste M, Fieschi C et al (1998) Randomised double-blind placebo-controlled trial of thrombolytic therapy with intravenous alteplase in acute ischaemic stroke (ECASS II). *Lancet* 352:1245–1251
7. Wardlaw JM, Mielke O (2005) Early signs of brain infarction at CT: observer reliability and outcome after thrombolytic treatment systematic review. *Radiology* 235:444–453
8. Osborn AG (1994) *Diagnostic Neuroradiology*. Mosby Inc
9. Doi K (2007) Computer-aided diagnosis in medical imaging: historical review, current status and future potential. *Comp Med Im Graph* 31:198–211
10. Bendszus M, Urbach H, Meyer B, Schultheiss R, Solymosi L (1997) Improved CT diagnosis of acute middle cerebral artery territory infarcts with density-difference analysis. *Neuroradiology* 39(2):127–131
11. Maldjian JA, Chalela J et al (2001) Automated CT segmentation and analysis for acute middle cerebral artery stroke. *AJNR Am J Neuroradiol* 22:1050–1055
12. Grimm C, Hochmuth A, Huppertz HJ (2005) Voxel-based CT analysis for improved detection of early CT signs in cerebral infarction. *Eur Radiol* B315–B315 (ECR—European Congress of Radiology)
13. Sklina K, Bargiel P, Przelaskowski A, Bulski T, Walecki J, Grieb P (2007) Multiscale extraction of hypodensity in hyperacute stroke. *Med Sci Monit* 13(Suppl 1):5–10
14. Candes EJ, Donoho D (1999) Curvelets – a surprisingly effective nonadaptive representation for objects with edges. In: Schumaker LL et al (eds) *Curves and surfaces*. Vanderbilt University Press, Nashville, TN
15. Candes EJ, Demanet L, Donoho D, Ying L (2005) Fast discrete curvelet transforms. *Multiscale Model Simul* 5:861–899

Pattern Recognition Methods in ^1H MRS Monitoring In Vivo of Normal Appearing Cerebellar Tissue After Treatment of Posterior Fossa Tumors

Łukasz Boguszewicz, Sławomir Blamek, and Maria Sokół

Abstract The objective of this study was to investigate the metabolic responses of normal appearing cerebellar tissue after posterior fossa tumor treatment, and to identify characteristics of the particular treatment method. Moreover, this work examined the metabolic alterations of normal appearing tissue induced by a particular tumor state including resection, stagnation, progression, and recurrence. The studied group consisted of 29 patients treated for posterior fossa tumors. All of them were irradiated with a total dose of 54 Gy at 1.8 Gy/fraction (median values). In addition, 13 underwent chemotherapy, 25 underwent total tumor resection, 18 were tumor-free in control examinations, 5 had a stable disease, and tumor progression or recurrence was observed in 2 and 4 cases, respectively. The 69 spectra, acquired using a MRI/MRS 2T system, were analyzed using Partial Least Squares Discriminant Analysis (PLS-DA) with orthogonal signal correction (OSC) spectral filtering. A significantly elevated spectral region (0.97–1.55 ppm) was observed in patients after total resection in comparison to non-operated subjects. Patients treated with chemotherapy showed an elevated band between 1.15–1.75 and 2.7–3.0 ppm and had decreases in the remaining parts of the spectra. Increases in lactate and decreases in the remaining metabolites were characteristic for the tumor progression/recurrence group. Pattern recognition methods coupled with MRS revealed significant treatment-dependent alterations in normal appearing cerebellar tissue, as well as metabolic changes induced by tumor progression/recurrence.

Keywords Magnetic resonance spectroscopy • pattern recognition • brain tumor • treatment monitoring

Introduction

Central nervous system (CNS) tumors are some of the most frequent childhood malignancies and are characterized by a relatively high occurrence in the posterior fossa (19). Although treatment methods are consistently improving and have increased the long-term survival of those suffering from this condition, the treatment induced side effects are major limitations of many therapies. Besides the associated neurological and cognitive impairments (5), there is a higher risk of impairment in children who have undergone exclusive surgical treatment (1). Furthermore, there is often radiotherapy induced brain tissue necrosis (2) with additional necrosis developing after subsequent or adjuvant chemotherapy (12), as well as direct chemotherapy induced brain injury (3).

In vivo proton magnetic resonance spectroscopy (MRS) is a powerful and noninvasive tool for investigating metabolic changes in the intact brain (6). The MRS studies have revealed severe metabolic disturbances in low-dose irradiated adult brain tissue in comparison to the pre-treatment state (16). Similar observations have been made in the frontal lobe of children treated for posterior fossa tumors, where these disturbances were significantly altered after receiving chemotherapy (15). Previous work has demonstrated the usefulness of the pattern recognition (PR) analysis of in vivo ^1H spectra for the detection and characterization of brain tumors (4,11). In this study, we combined MRS and PR methods in order to investigate the response of normal appearing cerebellar tissue after posterior fossa tumor treatment, and to provide information on metabolic alterations characteristic for a particular treatment method. Furthermore, we examined the metabolic alterations of normal appearing tissue induced by the following tumor states: total resection, stagnation, progression, and recurrence.

Ł. Boguszewicz (✉)

Department of Medical Physics, Maria Skłodowska-Curie Memorial Cancer Center and Institute of Oncology, Gliwice Branch, Wybrzeże Armii Krajowej 15, Gliwice 44-101, Poland
e-mail: lboguszewicz@io.gliwice.pl

S. Blamek

Department of Radiotherapy, Maria Skłodowska-Curie Memorial Cancer Center and Institute of Oncology, Gliwice Branch, Wybrzeże Armii Krajowej, Gliwice 15, 44-101, Poland

M. Sokół

Department of Medical Physics, Center of Oncology, Maria Skłodowska-Curie Memorial Cancer Center and Institute of Oncology, Gliwice Branch, Wybrzeże Armii Krajowej 15, Gliwice 44-101, Poland

Materials and Methods

Patients

The studied group consisted of 27 patients (with a median age of 16 years) treated for posterior fossa tumors. All patients were irradiated with a total dose of 54 or 55.5 Gy with a day fraction 1.8 or 1.5 Gy. In addition, 13 (48.2%) patients were treated with chemotherapy and 23 (85.2%) of them underwent total tumor resection. According to control examinations, the patients were divided into one of the four following groups: tumor free (16 cases – 59.3%), stagnation (5 cases – 18.5%), recurrence (4 cases – 14.8%), and progression (2 cases – 7.4%). Control examinations were performed from one to several times.

¹H NMR In Vivo

The 69 MRI localized in vivo ¹H MRS spectra were obtained using a 2T whole-body MRI/MRS system (Elscent Prestige, Haifa, Israel). The PRESS sequence was applied with the following parameters: TR = 1500 ms, TE = 35 ms, and 50 Acq. The volumes of interest of 1.5 × 1.5 × 1.5 cm³ were located contralaterally to the tumor or tumor site. The recording of the spectra was preceded by the automated global and local shimming procedures. Water suppression was achieved using CHESS techniques and no zero filling was applied. After a Fourier transformation and manual zero (and first, if necessary) order phase correction, the spectra were normalized in PeakFit 4.0 (by SPSS Inc., Chicago, USA). The spectra were normalized to the Cr peak to remove any relative shifts and analyzed in the range from 0.2 to 4.0 ppm.

Multivariate Analyses

The analyzed data gathered in the **X** matrix were composed of *k* spectra as rows and with columns of *n* = 929 spectral points representing chemical shifts. PLS-DA modelled the relations between the **X** and **Y** matrices, where **Y** was the (*k* × *j*) matrix containing information pertaining to group membership, and the number of columns (*j*) was equal to the number of groups. The relationship was expressed by means of score (latent) vectors. Geometrically, the **X** and **Y** matrices were understood as *k* points in two spaces with *n* and *j* axes. The PLS-DA modeling corresponded with hyper planes fit to both the **X** and **Y** data points and projected the matrices down on the hyper planes in such way so as to maximize the

covariance between the observation (spectra) positions on these hyper planes. The coordinates of this projection were the X- and Y-scores (18). Before the analyses, the NMR spectra were pre-processed using a spectral filter orthogonal signal correction (OSC) to improve the separation among groups. The OSC removed from the X variables the extraneous variance that was unrelated to Y, and the correction was made without removing information from X (17). The multivariate analyses were performed in SIMCA-P 11 Demo (Umetrics AB, Umeå, Sweden).

Results

In order to examine the data according to the influence of tumor resection on cerebellar tissue, the **X** data matrix was subjected to PLS-DA with OSC preprocessing. Figure 1a demonstrates a distinct separation between the spectra of non-operated patients and patients who underwent tumor resection. An interpretation of the scores plot was possible by comparing it with the X-weights plot (Fig. 1b), which displays each original variable (i.e. the chemical shift) as a single point. The further away a variable was from the plot origin, the greater was its influence on the distribution of the spectra along a given component of the scores plot. Figure 1a, b demonstrates a greatly elevated signal for mobile lipids and lactate (0.95–1.55 ppm) in post-operated patients.

Examining the influence of chemotherapy treatment resulted in a slightly worse clustering (Fig. 2a) than in the previous case, although both groups were distinguishable. X-weights plot (Fig. 2b) revealed a strongly elevated spectral range between 1.15 and 1.75 ppm, with maximum differences in the methylene lipids and a lactate peak at 1.3–1.33 ppm, as well as decreases in the remaining metabolites of the chemotherapy treated group. In patients without chemotherapy, strong increase of mobile lipids (0.9 ppm) and myoinositol (3.65 ppm) were visible.

Metabolic alterations induced by the tumor state were clearly visible in Fig. 3a, b. Distinct clustering among the tumor-free state, stagnation, and progression/recurrence were observed (Fig. 3a). Interestingly, the two latter groups remained non-separated, which suggests that differences between them are much less important against the background of the other groups. Figure 3b shows markedly increased lactate signals in the progression/recurrence group with slightly decreased choline (3.2 ppm), NAA (2.02 ppm), and mI (3.65 ppm) signals, which were in direct opposition to the stagnation group. In addition, the tumor-free group was characterized by relatively higher mobile lipids levels at 0.9 ppm.

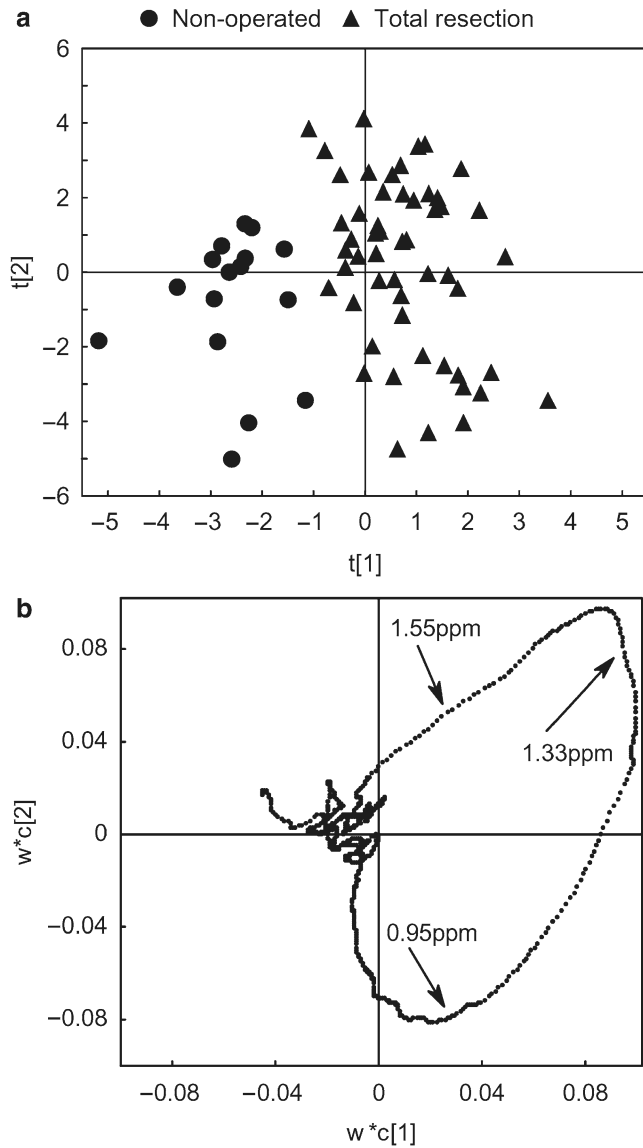


Fig. 1 PLS-DA scores plot (a) and corresponding X-weights plot (b) derived from the investigation of surgical influences on normal appearing tissue

Discussion

The combination of the in vivo ¹H MRS and pattern recognition methods have been effectively applied to differentiate between metabolic alterations induced by the specific treatment method, as well as tumor recurrence/progression or stagnation. The main advantage of this study was that the extracted discrimination features were clearly presented in graphical form and in terms of the original variables (the chemical shifts). Moreover, analyses were performed on the full spectra instead of metabolite proportions, thereby giving insight into the alterations of metabolites that are often omitted,

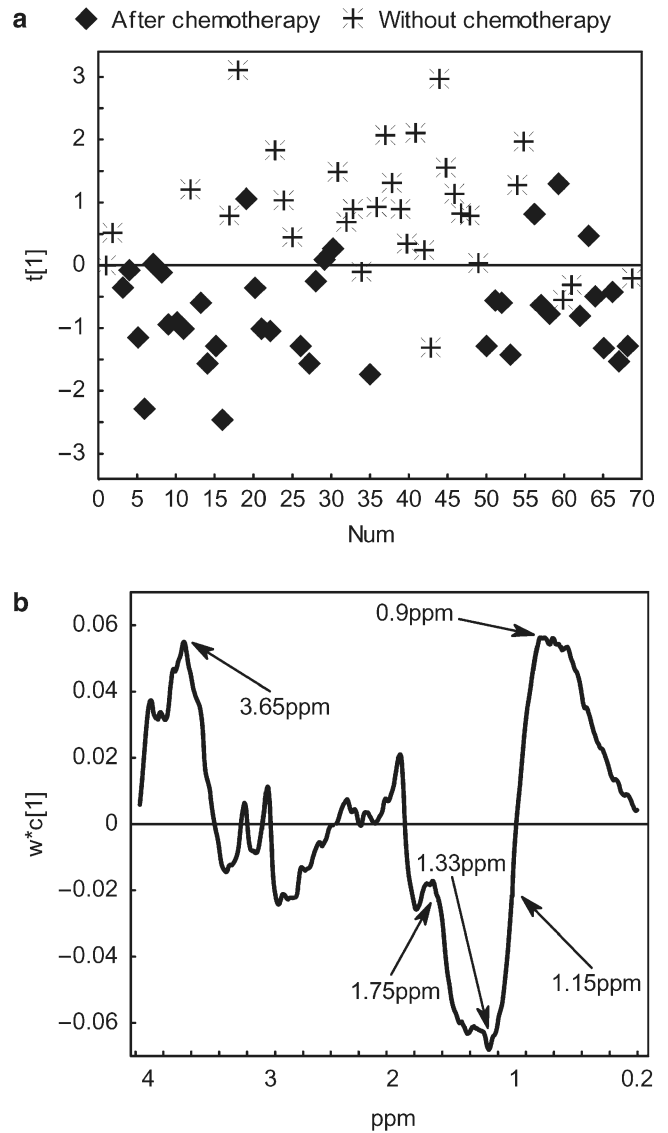


Fig. 2 PLS-DA scores plot (a) and corresponding X-weights plot (b) derived from the investigation of chemotherapy influences on normal appearing tissue

e.g. mobile lipids or lactate. The results obtained for the operated/non-operated group were comparable with other studies where increased Lip and Lac signals (in the ratio to NAA) were detected in the “normal brain” in non-irradiated patients who underwent tumor resection (7,13). The same ratios were markedly higher after receiving radiotherapy and were not dose-dependent (13). The authors suggested that the appearance of Lip signals in a normal appearing brain was caused by severe damage to the cell membranes. While the Lac signal could accumulate as a result of anaerobic glycolysis, hypoxia (13), or due to infiltration of tumor cells into the adjacent regions (7). However, the metabolic profile of patients treated with chemotherapy was less specific.

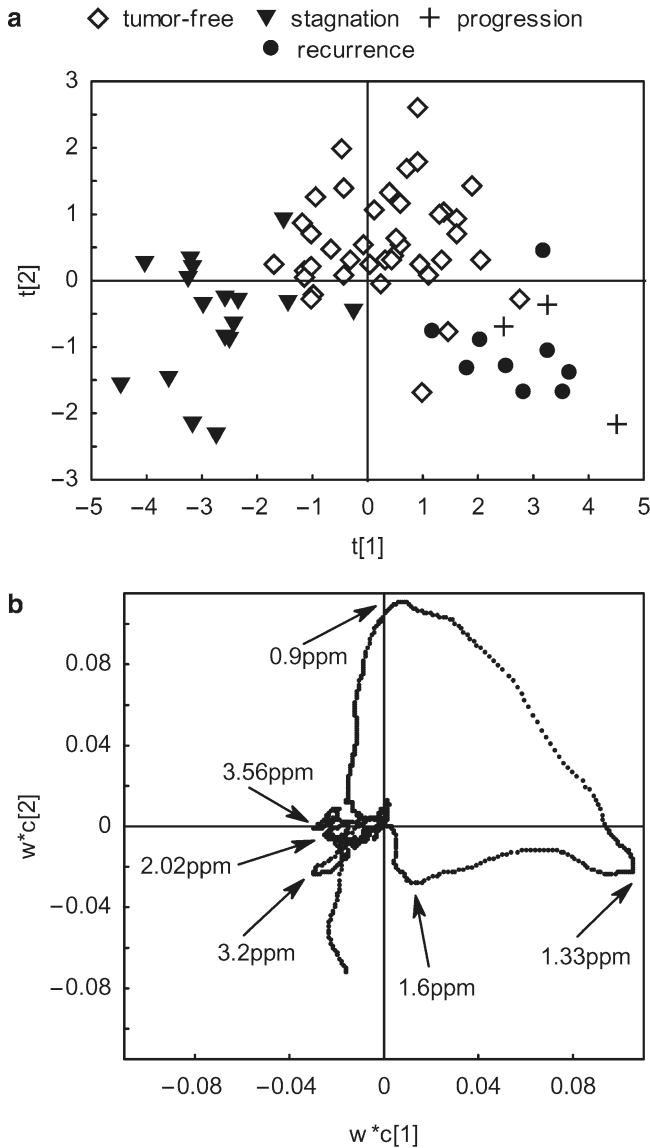


Fig. 3 PLS-DA scores plot (a) and corresponding X-weights plot (b) derived from the investigation of tumor state on normal appearing tissue

Moreover, publications examining the metabolic changes in a normal appearing brain due to chemotherapy are sparse and usually mobile lipids and lactate signals are excluded from the analyses (3,15). Nevertheless, some studies have focused on predicting resistance or responsiveness of non-irradiated tumor cells to chemotherapy. These findings indicate that the lipid (methylene) intensities were increased (1.3 ppm) and that the Cho resonance decreased as a treatment specific reaction resulting from apoptotic cell death (8,9). The strong difference in mI levels between the two groups was unclear, yet the increase of mI (in ratio to Cr) was observed in post-surgical irradiated patients who were not treated with chemotherapy and this was hypothesized to be

closely associated with local irradiation injury (16). Thus, there was an assumption that chemotherapy may act inversely to radiotherapy on mI levels. The second important aspect of tumor treatment is the prediction of treatment side effects. MRS has proved its usefulness as a reliable and reproducible prognostic marker that is capable of revealing a strong negative correlation between Lac/NAA ratio in patients treated for malignant gliomas and their survival rates (14). Another study proposed an increased ratio of lipid methylene (CH_2) to methyl (CH_3) signals as a possible recurrence marker (10). In addition, elevated Cho levels reflecting an increased membrane turnover as a result of inflammation and/or myelin breakdown are usually observed in tumor tissue. In this study, a slightly increased Cho signal was associated with the influence of a stable tumor in “normal tissue”. Even though analyses were performed on one group of spectra, where several metabolic effects may overlap (e.g. influence of resection was studied after irradiation and chemotherapy), the usefulness of pattern recognition methods as an automatic tool for analyzing ^1H MRS spectra cannot be underestimated. In combination with OSC spectral filtering PLS-DA, these techniques were able to reveal subtle metabolic differences in normal appearing cerebellar tissue and assign them to a specific factor responsible for the observed alterations. Research supported by grant No. KBN 2P05E06829.

Conflict of interest statement We declare that we have no conflict of interest.

References

1. Beebe DW, Ris MD, Armstrong FD, Fontanesi J, Mulhern R, Holmes E, Wisoff JH (2005) Cognitive and adaptive outcome in low-grade pediatric cerebellar astrocytomas: evidence of diminished cognitive and adaptive functioning in national collaborative research studies (CCG 9891/POG 9130). *J Clin Oncol* 23:5198–5204
2. Chong VFH, Khoo JBK, Chan LL, Rumpel H (2002) Neurological changes following radiation therapy for head and neck tumours. *Eur J Radiol* 44:120–129
3. Chu WC, Chik KW, Chan YL, Yeung DK, Roebuck DJ, Howard RG, Li CK, Metreweli C (2003) White matter and cerebral metabolite changes in children undergoing treatment for acute lymphoblastic leukemia: longitudinal study with MR imaging and ^1H MR spectroscopy. *Radiology* 229:659–669
4. Devos A, Lukas L, Suykens JAK, Vanhamme L, Tate AR, Howe FA, Majos C, Moreno-Torres A, van der Graaf M, Arus C, van Huffel S (2004) Classification of brain tumours using short echo time ^1H MR spectra. *J Magn Reson* 170(1):164–175
5. George AP, Kuehn SM, Vassilyadi M, Richards PMP, Parlow SE, Keene DL, Ventureyra ECG (2003) Cognitive sequelae in children with posterior fossa tumors. *Pediatr Neurol* 28:42–47
6. Gujar SK, Maheshwari S, Bjorkman-Burtscher I, Sundgren PC (2005) Magnetic Resonance Spectroscopy. *J Neuro-Ophthalmol* 25:217–226
7. Li X, Vigneron DB, Cha S, Graves EE, Crawford F, Chang SM, Nelson SJ (2005) Relationship of MR-derived lactate, mobile lipids, and relative blood volume for gliomas in vivo. *Am J Neuroradiol* 26:760–769

8. Lindskog M, Spenger C, Jarvet J, Graslund A, Kogner P (2004) Predicting resistance or response to chemotherapy by proton magnetic resonance spectroscopy in neuroblastoma. *J Natl Cancer Inst* 96:1457–1466
9. Lindskog M, Spenger C, Klason T, Jarvet J, Gräslund A, Johnsen JI, Ponthan F, Douglas L, Nordell B, Kogner P (2005) Proton magnetic resonance spectroscopy in neuroblastoma: Current status, prospects and limitations. *Cancer Lett* 228:247–255
10. Matulewicz Ł, Sokół M, Wydmański J, Hawrylewicz L (2006) Could lipid CH₂/CH₃ analysis by in vivo ¹H MRS help in differentiation of tumor recurrence and post-radiation effects? *Folia Neuropathol* 44(2):116–124
11. Menze BH, Lichy MP, Bachert P, Kelm BM, Schlemmer HP, Hamprecht FA (2006) Optimal classification of long echo time in vivo magnetic resonance spectra in the detection of recurrent brain tumors. *NMR Biomed* 19:599–609
12. Ruben JD, Dally M, Bailey M, Smith R, McLean CA, Fedele P (2006) Cerebral radiation necrosis: incidence, outcomes, and risk factors with emphasis on radiation parameters and chemotherapy. *Int J Radiat Oncol Biol Phys* 65:499–508
13. Rutkowski T, Tarnawski R, Sokół M, Maciejewski B (2003) ¹H-MR spectroscopy of normal brain tissue before and after postoperative radiotherapy because of primary brain tumors. *Int J Radiat Oncol Biol Phys* 56(5):1381–1389
14. Tarnawski R, Sokół M, Pieniążek P, Maciejewski B, Walecki J, Miszczuk L, Krupska T (2002) ¹H-MRS in vivo predicts the early treatment outcome of postoperative radiotherapy for malignant gliomas. *Int J Radiat Oncol Biol Phys* 52(5):1271–1276
15. Waldrop SM, Davis PC, Padgett CA, Shapiro MB, Morris R (1998) Treatment of brain tumors in children is associated with abnormal MR spectroscopic ratios in brain tissue remote from the tumor site. *Am J Neuroradiol* 19:963–970
16. Walecki J, Sokół M, Pieniążek P, Maciejewski B, Tarnawski R, Krupska T, Wydmański J, Brzeziński J, Grieb P (1999) Role of short TE ¹H-MR spectroscopy in monitoring of post-operation irradiated patients. *Eur J Radiol* 30:154–161
17. Wold S, Anttja H, Lindgren F, Öhman J (1998) Orthogonal signal correction of near-infrared spectra. *Chemom Intell Lab Sys* 44:175–185
18. Wold S, Sjostrom M, Eriksson L (2001) PLS-regression: a basic tool for chemometrics. *Chemom Intell Lab Sys* 58:109–130
19. Young G, Toretsky JA, Campbell AB, Eskenazi AE (2000) Recognition of common childhood malignancies. *Am Fam Physician* 61:2144–2154

Metabolic Changes in Rat Brain Following Intracerebroventricular Injections of Streptozotocin: A Model of Sporadic Alzheimer's Disease

M. Labak, T. Foniok, D. Kirk, D. Rushforth, B. Tomanek, A. Jasiński, and P. Grieb

Abstract A decrease in cerebral glucose metabolic uptake is an early and characteristic sign of Alzheimer's disease (AD). Streptozotocin (STZ) is a bacterial toxin which damages insulin-producing cells and insulin receptors. Intracerebroventricular (icv) application of STZ in rats has been found to chronically decrease cerebral glucose uptake and produce other effects that bear a resemblance to several other molecular and pathological features of AD. In the present experiments in vivo ^1H MR Spectroscopy with short echo time (3 ms) was used to non-invasively obtain a neurochemical profile of rat brains, 3 weeks and 2 months after double icv injections of STZ or vehicle. Seventeen metabolites were quantified from 27 μL tissue volume which included hippocampus and a part of cerebral cortex, using the LCModel and unsuppressed water signal as an internal reference. Three weeks after icv STZ several metabolites were significantly decreased, the most prominent changes noted in glycerophosphocholine and phosphocholine ($-38 \pm 5\%$), glutathione ($-37 \pm 4\%$), taurine ($-30 \pm 19\%$), glutamate ($-26 \pm 14\%$), phosphocreatine ($-23 \pm 15\%$) and N-acetylaspartate ($-16 \pm 6\%$). On the contrary, the concentration of N-acetylaspartylglutamate was found significantly increased ($+38 \pm 18\%$). After 2

months some of these changes were even more pronounced. We conclude that in vivo ^1H MRS of rat brain following icv STZ injections provides a new input into a better understanding of the critical dependency of neural function and structure on brain glucose consumption, and may be of relevance in further studies of AD pathomechanism.

Keywords Sporadic Alzheimer's disease • streptozotocin • H-MR spectroscopy • LCModel • neurochemical profile • brain metabolites • MR spectra quantification

Introduction

Despite intense research the pathogenesis of Alzheimer disease (AD) remains a matter of debate (1). Currently the most popular "amyloid cascade" hypothesis assumes that the primary pathogenetic event in AD comprises formation of neurotoxic $\text{A}\beta$ deposits. Another leading hypothesis assumes that the central pathogenetic event in AD is hyperphosphorylation of tau protein which leads to neurofibrillary triangles formation. Both aforementioned hypotheses have in common the implicit assumption that decreases in brain glucose and oxygen consumption are secondary to neurotoxicities caused by primary pathogenetic events.

Several observations indicate that decrease in brain regional glucose consumption occurs very early in AD (5), and is not an artifact due to increase in extracellular fluid space induced by brain atrophy but a true metabolic reduction per gram of tissue (7). Moreover, the decrease in glucose consumption is more pronounced than the concomitant decrease in oxygen consumption, reflecting an apparent metabolic shift from glycolytic to oxidative metabolism (2). In the face of such observations an alternative hypothesis according to which early in the pathogenesis of dementia of the Alzheimer's type the control of brain glucose metabolism is perturbed due to insulin signal transduction failure (4,18) is likely to gain wider acceptance. According to this hypothesis senile plaques and neurofibrillary tangles

M. Labak

and A. Jasiński

Department of Magnetic Resonance Imaging, H. Niewodniczanski Institute of Nuclear Physics, Polish Academy of Sciences, Radzikowskiego 152, Krakow 31-342, Poland

T. Foniok, D. Kirk, and D. Rushforth

National Research Council of Canada Institute for Biodiagnostics and Experimental Imaging Centre, Calgary, Canada

B. Tomanek

Department of Magnetic Resonance Imaging, H. Niewodniczanski Institute of Nuclear Physics, Polish Academy of Sciences, Radzikowskiego 152, Krakow 31-342, Poland and National Research Council of Canada Institute for Biodiagnostics and Experimental Imaging Centre, Calgary, Canada

P. Grieb (✉)

Department of Experimental Pharmacology, Mossakowski Medical Research Centre, Polish Academy of Sciences, Pawinskiego 5, 02-106 Warsaw, Poland
e-mail: pgrieb@cmdik.pan.pl

may be the effect rather than the cause of failure in brain glucose metabolism.

A rat model of chronic brain glucose metabolism failure has been developed where streptozotocin (STZ), a bacterial toxin able to selectively damage insulin-producing cells as well as insulin receptors, is injected intracerebroventricularly (icv), i.e., to the lateral brain ventricles. In a rat icv STZ dose of 1–3 mg/kg body weight is devoid of peripheral effects but produces a range of central effects including, inter alia, a decrease in brain glucose utilization, increased release of lactate from the brain, decrease of the level of ATP and phosphocreatine in brain tissues, and disturbances in learning and memory abilities (3,8,9). These effects resemble abnormalities seen in humans suffering from AD.

Recent developments in high-field in vivo MR Spectroscopy have resulted in the ability to simultaneously quantification of several brain metabolites noninvasively, which is termed neurochemical profiling (14). The purpose of our present study was to quantify the neurochemical profile in the brain area of icv STZ-treated rats as compared to the control (solvent-injected) animals.

Materials and Methods

Animals

Experiments were performed according to procedures approved by the joint NRC IBD (West) and University of Calgary Animal Care Committee. Twelve adult male *Wistar* rats, 290–330 g were used throughout the studies. The animals were housed in individual cages in an air-conditioned room with free access to standard pellet diet and water ad libitum. Two groups of rats were utilized: experimental (STZ-injected) group (n = 6) and control group injected with vehicle (n = 6). MR measurements were performed at 3 weeks and 2 months after the first injection of either STZ or sodium citrate buffer. During measurements body temperature was maintained at 37°C by warm water circulation and verified by rectal temperature sensor.

For intracerebroventricular injections and in vivo MRI/MRS measurements, the animals were anesthetized with a gas mixture of O₂:N₂ = 3:7 with 1.5% isoflurane. The head was placed in the stereotactic apparatus and a midline sagittal incision was made in the scalp. The following coordinates were used for icv injection: 0.8 mm posterior to bregma, 1.5 mm lateral to sagittal suture, 3.6 mm beneath the surface of brain. To minimize decomposition of STZ (Sigma, Canada), it was dissolved in the vehicle consisting of 50 mM sodium citrate buffer (pH 4.4) just prior to injection. The experimental group was injected bilaterally with icv STZ (3 mg/kg

body weight) on day 1 and 3. Each rat was given 5 µL into each lateral ventricle (0.5 mg/side) with the use of a Hamilton micro-syringe. Rats in the control group were given icv injection of the same volume of citrate buffer on the first and third day.

¹H MR Spectroscopy

¹H MR spectra were measured with a Bruker Avance II spectrometer with a 9.4T/21 cm magnet (Magnex, UK). The actively shielded, 116 mm inside diameter gradient coil with a minimum rise time of 100 µs and the maximum field gradient strength of 400 mT/m, and a transmit/receive elliptical (25 × 20 mm) RF surface coil resonating at 400 MHz were used. A stimulated echo acquisition mode (STEAM) sequence with a very short echo time (T_E = 3 ms, mixing time T_M = 5 ms) combined with outer volume saturation (OVS) was applied for localization. The repetition time (T_R) was 5 s, which minimized effects due to potential T₁ variation. The water signal was suppressed with variable power RF pulses and optimized relaxation delays (VAPOR). First- and second-order shimming was performed using a fully adiabatic version of FASTMAP (fast, automatic shimming technique by mapping along projections). ¹H MR spectra were acquired from the 3 × 3 × 3 mm³ (27 µL) VOIs centered in a brain region including the hippocampus and a part of the cerebral cortex. The position of VOI was based on pilot Rapid Acquisition with Relaxation Enhancement (RARE) images (T_E = 60 ms, matrix 128 × 128, number of slices = 10, slice thickness = 1 mm, number of transients = 7, T_R = 5 s).

MRS Quantification and Statistics

Metabolite concentrations were quantified by the LCModel (Linear Combination of Model spectra of metabolite solutions) (15) using the unsuppressed water signal as internal reference and taking water content of 0.83 mL/g. Nineteen metabolites were quantified from 27 µ volume, including alanine (Ala), ascorbate (Asc), aspartate (Asp), creatine (Cr), γ-aminobutyric acid (GABA), glucose (Glc), glutamate (Glu), glutamine (Gln), glutathione (GSH), glycerophosphorylcholine (GPC), glycine (Gly), phosphorylcholine (PCho), *myo*-inositol (Ins), lactate (Lac), *N*-acetylaspartate (NAA), *N*-acetylaspartylglutamate (NAAG), phosphocreatine (PCr), phosphorylehtanolamine (PE) and taurine (Tau). In addition, the simulated spectrum of fast relaxing macromolecules (MM) was included in the basis set. Metabolite concentrations were expressed in micromoles per gram wet weight. Due to the short T_E of 3 ms and long T_R of 5 s, T₂ and T₁ relaxation effects on MR signal intensity did not appreciably influence resonance intensity and were neglected. Metabolite

concentrations in control animals were compared to concentrations in icv STZ rats at two time points, 3 weeks and 2 months after icv injections.

The results are expressed in mM as mean \pm standard deviation (SD). The data for each metabolite were tested for the normality of the distributions (Shapiro–Wilk test, $p > 0.05$) and homogeneity of variances (Levene test, $p > 0.05$). For each metabolite the differences between groups were analyzed by two-tailed t tests for independent samples, and $p < 0.05$ were considered significant.

Gross Brain Weights

At the conclusion of the second MRI/MRS measurement performed 2 months after the first icv STZ injection the anesthetised rats were transcardially perfused with 5% paraformaldehyde solution. Brains were removed from the skull, weighted and stored for further histopathological examinations (not included in the present report).

Results

The mean values of metabolite concentrations measured 3 weeks and 2 months after intracerebroventricular injections are presented in Figs. 1 and 2. At 3 weeks after injection of STZ, statistically significant differences ($p < 0.05$, two-tailed t -test) between icv STZ and control rats were reductions in the methylene groups of proteins and lipids ($-9 \pm 4\%$), PCr ($-23 \pm 15\%$), Glu ($-26 \pm 14\%$), GSH ($-37 \pm 4\%$), NAA ($-16 \pm 6\%$), Tau ($-30 \pm 19\%$), and the sum of [Cr + PCr] ($-20 \pm 11\%$), [NAA + NAAG] ($-13 \pm 7\%$), [Glu + Gln] ($-22 \pm 10\%$), [GPC + PC] ($-38 \pm 5\%$). Increase in NAAG ($p < 0.05$) by ($+38 \pm 18\%$) and lactate ($+20 \pm 16\%$) (statistically not significant, $p > 0.05$) in the icv STZ group were also found. Other metabolites, including PE, Glc, Gln, Asp and Asc were in the range of the values measured from the control rat brain.

After 2 months some of these changes were more pronounced in spectra from icv STZ rats compared with controls. Concentrations of methylene groups in macromolecules, PCr, NAA and total [NAA + NAAG] continued to decrease ($-17\% \pm 1\%$, $-29\% \pm 18\%$, $-22\% \pm 14\%$, $-18\% \pm 8\%$ respectively). Glu ($-27 \pm 15\%$), total [Glu + Gln] ($-22 \pm 9\%$) and total [Cr + PCr] ($-15 \pm 7\%$) decreased slightly, but significantly ($p < 0.05$). However, decrease found in total choline compounds [GPC] + [PC] ($-19 \pm 9\%$) and Tau ($-16 \pm 8\%$) were not significant ($p > 0.05$). Further increase was observed in NAAG ($+115 \pm 12\%$), whereas that of lactate ($+29 \pm 12\%$) was not statistically significant ($p > 0.05$). A decrease in *myo*-inositol in icv STZ group was also not

significant. However, when calculated relative to total creatine, increases in *myo*-inositol concentrations [Ins]/[Cr + PCr] by $+10 \pm 3\%$ after 3 weeks and by $11 \pm 5\%$ after 2 months, were significant. Ala and Gly, although included in the LCModel database, were eliminated from further analysis, because were quantified with Cramer-Rao lower bounds (CRLB) of 50%.

Discussion

To the best of our knowledge this is the first report on in vivo ^1H MRS in this experimental paradigm. Our proton resonance data collected with a very short echo time provided the non-invasive measurement of absolute metabolite concentrations from a defined brain region.

Two months after intracerebroventricular STZ injections a reduction of gross brain wet weight by 20% has been observed, probably reflecting brain atrophy and substituting cells with extracellular fluid. Concomitantly the decrease of total creatine, on average by 20% and 15%, 3 weeks and 2 months later icv STZ, respectively, was found. Several other metabolites showed statistically significant reductions after icv injections of STZ, although the degree of reduction cannot be accounted for by the aforementioned atrophy of brain tissues since it was not uniform and in some cases apparently larger than the reduction in Cr + PCr.

Three weeks after icv STZ the most prominent decrease was observed in choline compounds. Of note is that, according to a recent publication (19), the Cho signal intensity observed by ^1H MRS in rat brain regions may be an indicator of regional acetylcholine levels. In the context of the well known fact that cholinergic insufficiency is a neurochemical hallmark of AD, our present observation lends further support to considering the icv STZ rat paradigm as a simple animal model recapitulating multiple characteristic features of AD. However, it is also worth noting that 2 months after icv STZ the decrease of cholines was less pronounced and statistically not significant.

The decrease similar in magnitude to that of choline compounds was noted in the reduced glutathione, an important intracellular antioxidant that protects against a variety of different oxidant species. This concurs with observations of other authors concerning the presence of brain tissue oxidative stress following icv STZ (17). However, although brain oxidative stress is suspected to be an important factor in human AD (16), brain GSH levels in AD patients appeared to be unaffected (13). A bit smaller in magnitude, but also statistically significant decreases of taurine and glutamate were also observed in the present study; they may also resemble the situation seen in brain cortex areas of AD patients by some authors (6,10), although the others (13) did not confirm such findings.

Fig. 1 Concentration of brain metabolites 3 weeks after the injection of Streptozotocin: icv STZ group (n = 6) and control group (n = 6). Error bars show standard deviations. Significance level (two tailed *t* test for independent samples): **p* < 0.05

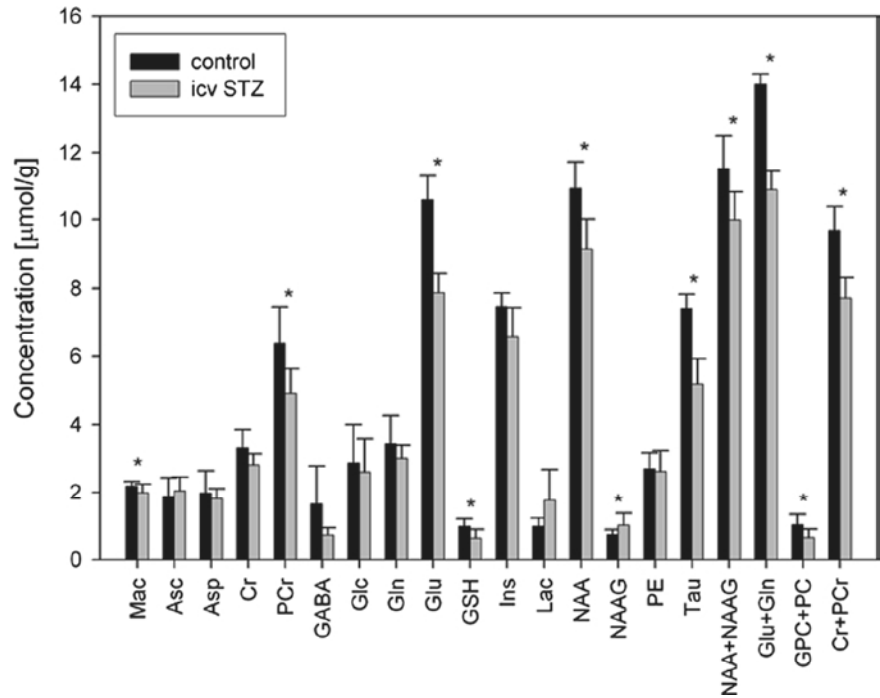
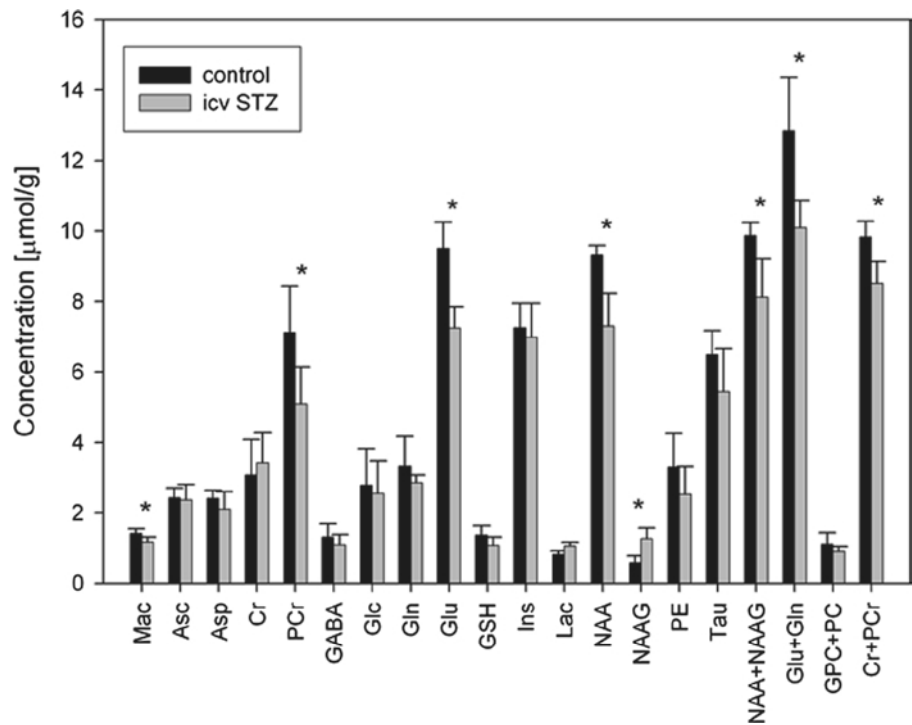


Fig. 2 Concentration of brain metabolites 2 months after the injection of Streptozotocin: icv STZ group (n = 6) and control group (n = 6). Error bars show standard deviations. Significance level (two tailed *t* test for independent samples): **p* < 0.05



In contrast to the significant decreases of the aforementioned metabolites we have observed a marked and significant increase in the N-acetylaspartylglutamate (NAAG), contrasting with the slight decrease in NAA. In this respect the effects of icv STZ differ from the situation in brains of patients with AD, where a decrease in both NAA and NAAG has been reported by invasive or post mortem methods (11).

In the normal brain glucose is the basic energy fuel, regional metabolism of glucose seems to be coupled to regional intensity of glutamatergic neurotransmission (12), and the coupling mechanism may involve release of NAAG from neurons to the brain extracellular space and its subsequent hydrolysis. When brain cannot utilize glucose efficiently, the aforementioned mechanism may become obsolete. Further research is needed to describe an alternative mechanism (if it does exist) of coupling blood flow and oxygen delivery to the level of glutamatergic neurotransmission in glucose-deprived brain; the icv STZ model may be an interesting approach to study this issue.

Our studies emphasize the potential and utility of high field in vivo ¹H MR Spectroscopy to detect neurochemical changes in the brain region in a small animal model. The non-invasive nature of MRS makes such studies particularly attractive. This technique may allow monitoring long-term consequences of brain glucose deprivation, and provide assistance to the development of an alternative fuel able to maintain basic metabolism in the glucose-deprived brain.

Conflict of interest statement We declare that we have no conflict of interest.

Acknowledgements The study was supported in part by the Polish State Committee for Scientific Research (KBN) project no. N518 040 32/3101 and by the MSHE Scientific Network 28/E-32/SN-0053/2007, and by Foundation for the Development of Diagnostics and Therapy, Warsaw, Poland.

References

1. Armstrong RA (2006) Plaques and tangles and the pathogenesis of Alzheimer's disease. *Folia Neuropathol* 44:1–11
2. Fukuyama H, Ogawa M, Yamauchi H, Yamaguchi S, Kimura J, Yonekura Y, Konishi J (1994) Altered cerebral energy metabolism in Alzheimer's disease: a PET study. *J Nucl Med* 35:1–6
3. Grünblatt E, Salkovic-Petrisic M, Osmanovic J, Riederer P, Hoyer S (2007) Brain insulin system dysfunction in streptozotocin intracerebroventricularly treated rats generates hyperphosphorylated tau protein. *J Neurochem* 101:757–770
4. Hoyer S (1998) Is sporadic Alzheimer disease the brain type of non-insulin dependent diabetes mellitus? A challenging hypothesis. *J Neural Transm* 105:415–422
5. Hunt A, Schönknecht P, Henze M, Seidl U, Haberkorn U, Schröder J (2007) Reduced cerebral glucose metabolism in patients at risk for Alzheimer's disease. *Psychiatry Res* 155:147–154
6. Hyman BT, Van Hoesen GW, Damasio AR (1987) Alzheimer's disease: glutamate depletion in the hippocampal perforant pathway zone. *Ann Neurol* 22:37–40
7. Ibáñez V, Pietrini P, Alexander GE, Furey ML, Teichberg D, Rajapakse JC, Rapoport SI, Schapiro MB, Horwitz B (1998) Regional glucose metabolic abnormalities are not the result of atrophy in Alzheimer's disease. *Neurology* 50:1585–1593
8. Lannert H, Hoyer S (1998) Intracerebroventricular administration of streptozotocin causes long-term diminutions in learning and memory abilities and in cerebral energy metabolism in adult rats. *Behav Neurosci* 112:1199–1208
9. Lester-Coll N, Rivera EJ, Soscia SJ, Doiron K, Wands JR, de la Monte SM (2006) Intracerebral streptozotocin model of type 3 diabetes: relevance to sporadic Alzheimer's disease. *J Alzheimers Dis* 9:13–33
10. Lowe SL, Bowen DM, Francis PT, Neary D (1990) Ante mortem cerebral amino acid concentrations indicate selective degeneration of glutamate-enriched neurons in Alzheimer's disease. *Neuroscience* 38:571–577
11. Passani LA, Vonsattel JP, Coyle JT (1997) Distribution of N-acetylaspartylglutamate immunoreactivity in human brain and its alteration in neurodegenerative disease. *Brain Res* 772:9–22
12. Patel AB, de Graaf RA, Mason GF, Kanamatsu T, Rothman DL, Shulman RG, Behar KL (2004) Glutamatergic neurotransmission and neuronal glucose oxidation are coupled during intense neuronal activation. *J Cereb Blood Flow Metab* 24:972–985
13. Perry TL, Yong VW, Bergeron C, Hansen S, Jones K (1987) Amino acids, glutathione, and glutathione transferase activity in the brains of patients with Alzheimer's disease. *Ann Neurol* 21:331–336
14. Pfeuffer J, Tkáč I, Provencher SW, Gruetter R (1999) Toward an in vivo neurochemical profile: quantification of 18 metabolites in short-echo time ¹H NMR spectra of the rat brain. *J Magn Res* 141:104–120
15. Provencher SW (1993) Estimation of metabolite concentrations from localized in vivo proton NMR spectra. *Magn Reson Med* 30:672–679
16. Reddy PH, Beal MF (2008) Amyloid beta, mitochondrial dysfunction and synaptic damage: implications for cognitive decline in aging and Alzheimer's disease. *Trends Mol Med* 14:45–53
17. Sharma M, Gupta YK (2003) Effect of alpha lipoic acid on intracerebroventricular streptozotocin model of cognitive impairment in rats. *Eur Neuropsychopharmacol* 13:241–247
18. Steen E, Terry BM, Rivera EJ, Cannon JL, Neely TR, Tavares R, Xu XJ, Wands JR, de la Monte SM (2005) Impaired insulin and insulin-like growth factor expression and signaling mechanisms in Alzheimer's disease – is this type 3 diabetes? *J Alzheimers Dis* 7:63–80
19. Wang XC, Du XX, Tian Q, Wang JZ (2008) Correlation between choline signal intensity and acetylcholine level in different brain regions of rat. *Neurochem Res* 33:814–819

MR Spectroscopic Evaluation of Brain Tissue Damage After Treatment for Pediatric Brain Tumors

Stawomir Blamek, Dawid Larysz, Kornelia Ficek, Maria Sokół, Leszek Miszczyk, and Rafał Tarnawski

Abstract

Purpose The aim of this study was to evaluate the metabolic profile of uninvolved brain tissue after treatment for pediatric brain tumors.

Material A group of 24 patients aged 4–18 years was analyzed after combined treatment for brain tumors. In this group, there were nine medulloblastomas, seven low-grade gliomas, three high-grade gliomas, two ependymomas and three children with conservatively treated diffuse brainstem gliomas.

Methods Short echo-time (TE=30 ms) point-resolved spectra were acquired using a 2 T clinical scanner (Elscent Prestige). The ratios of signal intensities for N-acetylaspartate (NAA), choline (Cho), myo-inositol (mI), lactate (Lac), and lipids (Lip) were calculated using the creatine (Cr) signal as an internal reference. The spectra were acquired both from the tumor bed and from contralateral uninvolved brain tissue; only control spectra were analyzed. The first examination was made between the third and sixth month after therapy (24 spectra), the second examination occurred 8–12 months after treatment (15 spectra available), and the third was performed approximately 18 months after completion of therapy (eight spectra available). The results were compared using the *t*-test for dependent samples.

Results At all time points, the metabolite ratios showed alterations indicating brain tissue damage. The most impor-

tant were the decrease of NAA/Cr and increase of Lac/Cr and Lip/Cr ratios. The mean NAA/Cr values were 0.91, 0.91, and 0.86, respectively, for the three examinations, while the Lac/Cr and Lip/Cr values were 1.66, 2.11, 1.19 and 12.24, 12.05, 5.69, respectively. Interestingly, in children with supratentorial tumors, a significant increase in NAA/Cr value was observed (from 0.82 to 1.11 in the first and second examinations, respectively; $p = 0.0487$), which may be indicative of neuronal function recovery.

Conclusions MRS examinations of uninvolved brain tissue indicate long-lasting metabolic disturbances. However, the NAA/Cr ratio increase may be a sign of at least partial recovery of metabolic function of the brain.

Keywords Magnetic resonance spectroscopy • children • brain tumors • radiotherapy • radiation damage

Background and Purpose

Radiation-induced alterations of brain function and metabolism are important sequelae of radiotherapy for brain tumors, especially in patients with good prognoses. The importance of these phenomena is even more pronounced in children, as a significant number of patients treated for brain tumors will be long-term survivors and thus, any treatment-induced impairment can significantly influence their quality of life (1, 3).

Most publications concerning proton magnetic resonance spectroscopy (MRS) in pediatric brain tumors concentrate on examination of tumor tissue and the value of MRS examination as a prognostic factor (7, 17). The usefulness of MRS in distinguishing tumor recurrence from radiation necrosis is also the subject of numerous reports and reviews (6, 11, 13). However, evaluation of treatment-induced early metabolic alterations and the duration of changes by repeated spectroscopic examinations has been less intensively investigated. This is especially significant when it comes to normal-appearing brain areas, which are not involved primarily by

S. Blamek (✉), K. Ficek, L. Miszczyk, and R. Tarnawski
Department of Radiotherapy, Maria Skłodowska-Curie Memorial
Cancer Center and Institute of Oncology, Gliwice Branchul,
Wybrzeże Armii Krajowej 15, Gliwice 44-100, Poland
e-mail: blamek@gmail.com

M. Sokół
Department of Medical Physics, Maria Skłodowska-Curie Memorial
Cancer Center and Institute of Oncology, Gliwice Branchul,
Wybrzeże Armii Krajowej 15, Gliwice 44-101, Poland

D. Larysz
Department of Neurosurgery, Medical University
of Silesia, Katowice, U1 Medyków 16, Katowice 40-752, Poland

neoplastic tissue but are exposed to ionizing radiation and/or chemotherapeutic agents (12, 16).

The aim of our study was to evaluate the metabolic profile of uninvolved brain tissue in children after treatment for brain tumors and further, to assess the stability of metabolic alterations and their duration.

Material and Methods

A group of 24 patients was investigated. The patients ranged in age from 4 to 18 years at the time of treatment, and included 11 boys and 14 girls. Histopathologic findings are summarized in Table 1.

Sixteen tumors were located in the posterior fossa, with the remainder diagnosed as supratentorial tumors. Total or subtotal excision of the tumor was performed in 21 children. In three cases, a diagnosis of diffuse brainstem glioma was based solely on imaging results and no surgery was performed. All but three patients received chemotherapy, and all of them were irradiated. The radiation doses ranged between 45 and 59.4 Gy delivered with a dose of 1.8 Gy per daily fraction.

During control examinations, both magnetic resonance imaging (MRI) and MRS were performed. Short echo-time (TE = 30 ms) point-resolved spectra were acquired using a 2 T magnet (Elscent Prestige). The ratios of signal intensities for N-acetylaspartate (NAA), choline (Cho), myo-inositol (mI), lactate (Lac), and lipids (Lip) were calculated using the creatine (Cr) signal as an internal reference. The spectra were acquired both from the tumor bed and contralateral uninvolved brain tissue. In the case where the tumor was located centrally (for example, in a brainstem tumor), the control voxel was placed laterally, e.g., in the cerebellar hemisphere, always away from any visible abnormalities that could be attributed to the presence of neoplastic tissue. Only the control spectra were taken for analysis. The first examination was made between the third and sixth month after therapy (24 spectra), the second at 8–12 months after treatment (15 spectra available), and the third was performed approximately 18 months after completion of therapy (eight spectra available). The results were compared using the *t*-test for dependent samples, and the significance level α was set to 0.05. Interpretation of the results was based on comparisons with

normal values of metabolite ratios defined as mean \pm 2SD of values obtained from healthy young adult volunteers.

Results

The metabolite ratios in subsequent examinations are summarized in Table 2. At all time points the metabolite ratios showed alterations indicating brain tissue damage. The most important were the decrease of NAA/Cr and increase of Lac/Cr and Lip/Cr ratios. The mean NAA/Cr values were 0.91, 0.91, and 0.86 in the first, second, and third examinations, respectively, while the Lac/Cr and Lip/Cr values were 1.66, 2.11, 1.19 and 12.24, 12.05, 5.69, respectively. No significant aberrations in Cho/Cr and mI/Cr ratios were observed, and these were within the normal range in all examinations, based on MRS examination of healthy volunteers.

Interestingly, in children with supratentorial tumors, a significant increase in the NAA/Cr ratio was observed (from 0.82 to 1.11 in the first and second examinations, respectively; $p = 0.0487$). The results of MRS examinations in children with supratentorial tumors are summarized in Table 3. There was also a statistically significant difference in the Cho/Cr ratios between the second and third examinations; however, due to a limited number of data (three spectra for supratentorial tumors available in the third examination), these data are difficult to interpret.

Analysis of metabolite ratios in children with posterior fossa tumors did not show any statistically significant difference between subsequent examinations, in spite of an evident decrease of Lip/Cr ratio in the third examination. The detailed results are shown in Table 4.

Discussion

In all examinations the reduction of NAA/Cr is clearly visible, as compared to the mean values obtained for healthy volunteers (1.53, SD = 0.23). This observation is true both for children with supratentorial and infratentorial tumors. In the group with supratentorial tumors, however, a slight increase in the NAA/Cr ratio is visible in consecutive examinations. This difference reached statistical significance between the first and second examinations. NAA is synthesized in neuronal mitochondria and is believed to be a marker of neuronal function or viability (8). A decrease in NAA signal intensity or NAA/Cr signal proportion after radiotherapy was also observed in other studies, and is commonly associated with neuronal loss or dysfunction (10, 15, 18). A significant increase of NAA/Cr could be therefore interpreted as a sign of neuronal recovery after temporary damage caused by the applied

Table 1 Histopathology of brain tumors in the examined group

Histopathologic type	Number
Medulloblastoma	9
Low-grade glioma	7
High-grade glioma	3
Ependymoma	2
Diffuse brainstem glioma ^a	3

^aDiagnosis based on imaging only; no attempt at biopsy or excision was made.

Table 2 Results of MRS examinations of the entire group. The values shown in the table are means of metabolite ratios \pm standard deviation (SD)

Metabolite ratio	First examination	Second examination	Third examination	p-Value (first/second)	p-Value (second/third)
NAA/Cr	0.91 \pm 0.27	0.91 \pm 0.26	0.86 \pm 0.35	0.8819	0.5531
Cho/Cr	1.01 \pm 0.19	1.08 \pm 0.20	1.01 \pm 0.40	0.4471	0.4932
mI/Cr	0.61 \pm 0.37	0.55 \pm 0.35	0.75 \pm 0.35	0.3170	0.4040
Lac/Cr	1.66 \pm 1.84	2.11 \pm 1.97	1.19 \pm 1.11	0.7667	0.9068
Lip/Cr	12.24 \pm 13.70	12.05 \pm 9.87	5.69 \pm 4.29	0.7265	0.6256

Table 3 Results of MRS examinations in the group of patients with supratentorial tumors. The values shown in the table are means of metabolite ratios \pm standard deviation (SD)

Metabolite ratio	First examination	Second examination	Third examination	p-Value (first/second)	p-Value (second/third)
NAA/Cr	0.90 \pm 0.16	1.11 \pm 0.30	1.15 \pm 0.32	0.0487	0.6538
Cho/Cr	1.15 \pm 0.16	1.05 \pm 0.20	1.26 \pm 0.23	0.3989	0.0048
mI/Cr	0.70 \pm 0.49	0.72 \pm 0.46	0.91 \pm 0.23	0.3705	0.2862
Lac/Cr	0.79 \pm 0.88	1.16 \pm 1.33	0.14 \pm 0.79	0.3576	0.7266
Lip/Cr	4.44 \pm 4.03	6.55 \pm 4.67	6.74 \pm 5.40	0.1807	0.9523

Table 4 Results of MRS examinations in the group of patients with posterior fossa tumors. The values shown in the table are means of metabolite proportion values \pm standard deviation (SD)

Metabolite ratio	First examination	Second examination	Third examination	p-Value (first/second)	p-Value (second/third)
NAA/Cr	0.91 \pm 0.32	0.81 \pm 0.19	0.69 \pm 0.26	0.3129	0.8163
Cho/Cr	0.94 \pm 0.17	1.10 \pm 0.21	0.85 \pm 0.43	0.0942	0.2931
mI/Cr	0.57 \pm 0.30	0.47 \pm 0.28	0.66 \pm 0.39	0.5342	0.3298
Lac/Cr	2.10 \pm 2.05	2.58 \pm 2.12	1.45 \pm 1.28	0.9349	0.3565
Lip/Cr	16.15 \pm 15.21	14.79 \pm 10.81	5.06 \pm 4.04	0.9986	0.4764

treatment. This observation is in concordance with the natural course of radiation-induced brain toxicity; after a temporary decrease of cognitive abilities, patients usually recover to, or slightly below the baseline. In contrast, the NAA/Cr ratio measured in the healthy tissue of children with posterior fossa tumors seems to decrease over time, although the observed differences did not reach statistical significance.

Cho/Cr values seem to be stable over time and are close to normal values (0.98, SD = 0.20) except for an increase in the third examination values in the group with supratentorial tumors. This value is close to that obtained in the first examination ($p = 0.1298$). Moreover, due to a limited number of observations in the third examination (three spectra,) these data are ambiguous and difficult to interpret.

In all cases the mI/Cr values oscillate near normal values (0.70, SD = 0.18), with no significant changes detected over time. Because myo-inositol is believed to be a marker of glial cell density (2), no significant glial tissue proliferation or depletion could be anticipated, which is in good agreement with MRI not showing any abnormalities in the examined areas.

A lactate signal should not be observed in healthy brain tissue. It is, however, apparent in all analyzed examinations, with the tendency to be higher in the posterior fossa. Elevation of the Lac/Cr ratio could be attributed to impaired glucose metabolism or lactate washout (14). The latter seems to be

even more probable because of vascular damage caused by ionizing radiation, which can influence the ability of effective lactate washout. It is worth noting that control areas in the posterior fossa received the full dose of radiotherapy, whereas supratentorial control areas were not exposed to the full prescribed dose of ionizing radiation. This fact may be explanatory for the difference between mean Lac/Cr values in supra- and infratentorial areas.

The most pronounced aberrations were observed in the Lip/Cr values. The presence of lipid signals is usually connected with disintegration of cell membranes and increased levels of free mobile lipids (9), and lipid signals should not be present in healthy brain areas. The high Lip/Cr proportion values in the posterior fossa could be explained in part by signal contamination from adjacent fatty tissue, but voxels located in supratentorial areas were usually distant from bone marrow or epicranium. In spite of this, the Lip/Cr ratio is also elevated in these areas, although to a somewhat lesser degree. As no foci of recurrence or necrosis were observed in the examined area, it could be hypothesized that the increased Lip/Cr ratio could be a sign of radiation-induced subclinical cell damage and result from increased concentration of mobile lipids in this area. Similar observations confirming the presence of lipid signal after brain tissue irradiation have been made by other authors, giving further support to this hypothesis (4, 5, 10).

Conclusions

MRS examinations of uninvolved brain tissue indicate long-lasting and mostly stable metabolic disturbances that may be attributed to the applied treatment. The increase of NAA/Cr ratio in the supratentorial area, however, may be a sign of at least partial recovery of metabolic function of the brain. Because this study involved a small group of patients and thus, an insufficient number of evaluable spectra, interpretation of these data and the conclusions drawn require utmost prudence. Nevertheless, the obtained results do allow for the assumption that uninvolved brain tissue in children with brain tumors is strongly affected by treatment and further investigation is required to elucidate the meaning and importance of the observed metabolic alterations.

Conflict of interest statement We declare that we have no conflict of interest

References

1. Aarsen FK, Paquier PF, Reddingius RE, Streng IC, Arts WF, Evera-Preesman M, Catsman-Berreoets CE (2006) Functional outcome after low-grade astrocytoma treatment in childhood. *Cancer* 106(2):396–402
2. Brand A, Richter-Landsberg C, Leibfritz D (1993) Multinuclear NMR studies on the energy metabolism of glial and neuronal cells. *Dev Neurosci* 15(3–5):289–298
3. Brière ME, Scott JG, McNall-Knapp RY, Adams RL (2008) Cognitive outcome in pediatric brain tumor survivors: delayed attention deficit at long-term follow-up. *Pediatr Blood Cancer* 50(2):337–340
4. Graves EE, Nelson SJ, Vigneron DB, Verhey L, McDermott M, Larson D, Chang S, Prados MD, Dillon WP (2001) Serial proton MR spectroscopic imaging of recurrent malignant gliomas after gamma knife radiosurgery. *AJNR Am J Neuroradiol* 22(4):613–624
5. Kizu O, Naruse S, Furuya S, Morishita H, Ide M, Maeda T, Ueda S (1988) Application of proton chemical shift imaging in monitoring of gamma knife radiosurgery on brain tumors. *Magn Reson Imaging* 16(2):197–204
6. Matulewicz Ł, Sokół M, Wydmański J, Hawrylewicz L (2006) Could lipid CH₂/CH₃ analysis by in vivo ¹H MRS help in differentiation of tumor recurrence and post-radiation effects? *Folia Neuropathol* 44(2):116–124
7. Marcus KJ, Astrakas LG, Zurakowski D, Zarifi MK, Mintzopoulos D, Poussaint TY, Anthony DC, De Girolami U, Black PM, Tarbell NJ, Tzika AA (2007) Predicting survival of children with CNS tumors using proton magnetic resonance spectroscopic imaging biomarkers. *Int J Oncol* 30(3):651–657
8. Miller BL (1991) A review of chemical issues in ¹H NMR spectroscopy: N-acetyl-L-aspartate, creatine and choline. *NMR Biomed* 4(2):47–52
9. Rand SD, Prost P, Haughton V, Mark L, Stainer J, Johansen J, Kim TA, Chetty VK, Mueller W, Meyer G, Krouwer H (1997) Accuracy of single-voxel proton mr spectroscopy in distinguishing neoplastic from nonneoplastic brain lesions. *AJNR Am J Neuroradiol* 18:1695–1704
10. Rutkowski T, Tarnawski R, Sokół M, Maciejewski B (2003) ¹H-MR spectroscopy of normal brain tissue before and after postoperative radiotherapy because of primary brain tumors. *Int J Radiat Oncol Biol Phys* 56(5):1381–1389
11. Schlemmer HP, Bachert P, Henze M, Buslei R, Herfarth KK, Debus J, van Kaick G (2002) Differentiation of radiation necrosis from tumor progression using proton magnetic resonance spectroscopy. *Neuroradiology* 44(3):216–222
12. Steffen-Smith EA, Wolters PL, Albert PS, Baker EH, Shimoda KC, Barnett AS, Warren KE (2008) Detection and characterization of neurotoxicity in cancer patients using proton MR spectroscopy. *Childs Nerv Syst* 24(7):807–813
13. Tarnawski R, Sokół M, Blamek S (2005) Differentiation of radiation effect from glioma progression by MRS. In: Tosi R, Tugnoli V (eds) *Nuclear magnetic resonance spectroscopy in the study of neoplastic tissue*. Nova Science, New York, pp 95–122
14. Tomoi M, Kimura H, Yoshida M, Itoh S, Kawamura Y, Hayashi N, Yamamoto K, Kubota T, Ishii Y (1997) Alterations of lactate (+lipid) concentration in brain tumors with in vivo hydrogen magnetic resonance spectroscopy during radiotherapy. *Invest Radiol* 32(5):288–296
15. Usenius T, Usenius JP, Tenhunen M, Vainio P, Johansson R, Soimakallio S, Kauppinen R (1995) Radiation-induced changes in human brain metabolites as studied by ¹H nuclear magnetic resonance spectroscopy in vivo. *Int J Radiat Oncol Biol Phys* 33(3):719–724
16. Waldrop SM, Davis PC, Padgett CA, Shapiro MB, Morris R (1998) Treatment of brain tumors in children is associated with abnormal MR spectroscopic ratios in brain tissue remote from the tumor site. *AJNR Am J Neuroradiol* 19:963–970
17. Warren KE, Frank JA, Black JL, Hill RS, Duyn JH, Aikin AA, Lewis BK, Adamson PC, Balis FM (2000) Proton magnetic resonance spectroscopic imaging in children with recurrent primary brain tumors. *J Clin Oncol* 18(5):1020–1026
18. Walecki J, Sokół M, Pieniążek P, Maciejewski B, Tarnawski R, Krupska T, Wydmański J, Brzeziński J, Grieb P (1999) Role of short TE ¹H-MR spectroscopy in monitoring of post-operation irradiated patients. *Eur J Radiol* 30:154–161

The Incidence of Imaging Abnormalities after Stereotactic Radiosurgery for Cerebral Arteriovenous and Cavernous Malformations

Sławomir Blamek, Marek Boba, Dawid Larysz, Adam Rudnik, Kornelia Ficek, Bartosz Eksner, Leszek Miszczyk, and Rafał Tarnawski

Abstract

Objective The aim of the study was to evaluate the incidence of postirradiation imaging changes after stereotactic radiosurgery for arteriovenous malformations (AVM) and cerebral cavernous malformations (CCM).

Material and Methods A group of 85 patients treated for arteriovenous malformations (62 patients, 73%) and cavernomas (23 patients, 27%) between October 2001 and December 2005 was analyzed.

All patients were treated with stereotactic radiosurgery with doses ranging from 8-28 Gy. After the irradiation, magnetic resonance imaging (MRI) or computed tomography (CT) was performed at 6 to 12-month intervals to assess the effects of the treatment. The mean follow-up time for the whole group was 27.3 months; AVM group – 26 months; CCM group – 30.9 months.

All the imaging data were carefully reviewed to identify the radiological symptoms of postradiosurgical damage. T2 or FLAIR hyperintensity, T1-hypointensity and contrast enhancement on MRI and the presence of hypodense areas and contrast enhancement on CT examinations were assessed.

Results Imaging abnormalities were found in 28 (33%) patients. The symptoms of postradiosurgical damage were observed in 21 (33.9%) patients in the AVM group and 7 (30.4%) patients in the CCM group. Radiological symptoms of radiation necrosis associated with neurological deterioration were identified in two patients with cavernomas, while no

radiation necrosis was found in the AVM group. Patients in whom radiological signs of focal brain edema or gliosis existed were asymptomatic.

Conclusions Radiological symptoms of postradiosurgical damage affected about one third of the irradiated patients, typically without any clinical manifestations. Patients irradiated for CCMs seem to be more prone to develop symptomatic postradiosurgical necrosis; this observation, however, requires further investigation.

Keywords Stereotactic radiosurgery • arteriovenous malformations • cavernomas • radiation injury

Background and Purpose

Although stereotactic radiosurgery (SRS) is a widely recognized method of treatment for cerebral arteriovenous malformations (AVMs), its usefulness in the treatment of cerebral cavernous malformations (CCMs) is still a subject of debate. Most reports concerning the effects of AVM or CCM treatment concentrate on the rate of AVM obliteration and the incidence of cerebral hemorrhages from AVMs or CCMs after radiosurgical treatment. Although incidence and factors influencing the probability of developing radiation-induced imaging abnormalities after stereotactic radiosurgery for AVMs are also systematically investigated, relatively few data concerning radiation-induced toxicity of CCMs irradiation is available (1–6,9,11,13). The aim of our study was to evaluate the incidence of postirradiation imaging changes suggestive of gliosis, edema or necrosis after stereotactic radiosurgery for cerebral arteriovenous malformations (AVM) and cavernous malformations (CCM).

Material and Methods

The studied group consisted of 85 patients treated for arteriovenous malformations (62 patients, 73%) and cavernomas (23 patients, 27%) between October 2001 and December

S. Blamek (✉), K. Ficek, L. Miszczyk, and R. Tarnawski
Department of Radiotherapy, Maria Skłodowska-Curie Memorial Cancer Center and Institute of Oncology, Gliwice Branch, Wybrzeże Armii Krajowej 15, Gliwice 44-100, Poland
e-mail: blamek@gmail.com

M. Boba and B. Eksner
Department of Radiology, Maria Skłodowska-Curie Memorial Cancer Center and Institute of Oncology, ul. Wybrzeże Armii Krajowej 15, Gliwice Branch, 44-100, Gliwice, Poland

D. Larysz and A. Rudnik
Department of Neurosurgery, Medical University of Silesia, Katowice, U1 Medyków 16, Katowice 40-752, Poland

2005. All patients were treated with linac-based stereotactic radiosurgery, with doses ranging from 8–28 Gy.

The AVM volumes ranged from 0.14 to 63 mL, with a mean volume of 11.7 mL. All AVMs were scored according to the Spetzler–Martin grading system (12). There were 2 grade I, 22 grade II, 26 grade III, 9 grade IV and 2 grade V lesions. According to the radiosurgery-based scoring system, there were nine lesions with an AVM score <1, 31 with an AVM score between 1 and 2 and 22 with an AVM score >2 (10). The mean dose delivered to the AVMs was 15.9 Gy (range 8–28 Gy).

The mean CCM volume was 1.72 mL and ranged from 0.25 to 8.34 mL. The doses delivered to CCMs ranged between 7 and 20 Gy (mean 16.1 Gy).

After the irradiation, patients underwent magnetic resonance imaging (MRI) or computed tomography (CT) at 6 to 12-month intervals to assess the effects of the treatment. The mean follow up time for the whole group was 27.3 months; AVM group – 26 months, CCM group – 30.9 months. The imaging data were carefully reviewed to identify the radiological symptoms of postradiosurgical damage. T2 or FLAIR hyperintensity, T1-hypointensity and contrast enhancement on MRI and the presence of hypodense areas and contrast enhancement on CT examinations were assessed. The diameters of visible lesions were measured whenever possible and maximal diameters were used for comparisons.

Student's *t*-test for independent samples was used for statistical analysis of the maximal diameters of the lesions between the AVM and CCM groups and to compare the doses and volumes between groups of patients with and without imaging alterations. A chi-square test was used to compare the incidence of necrotic and non-necrotic lesions between groups.

Results

Imaging abnormalities were found in 28 (33%) patients. Radiological symptoms of postradiosurgical damage were observed in 21 (33.9%) patients in the AVM group and seven (30.4%) patients in the CCM group. 25/28 (89%) imaging changes appeared within the first 2 years of follow-up. Five lesions partially resolved after 8–19 months of further observation, in two patients imaging abnormalities resolved completely. Sample images of MR-visible radiation-induced lesions are presented in Figs. 1 and 2.

The incidence of imaging abnormalities did not differ statistically between the AVM and the CCM group ($p=0.8306$). Mean maximal diameter of the postradiation lesions in the whole group was 1.73 cm and ranged between 0.2 and 4.3 cm. Mean maximal diameter of the lesion was 1.61 and 2.07 cm

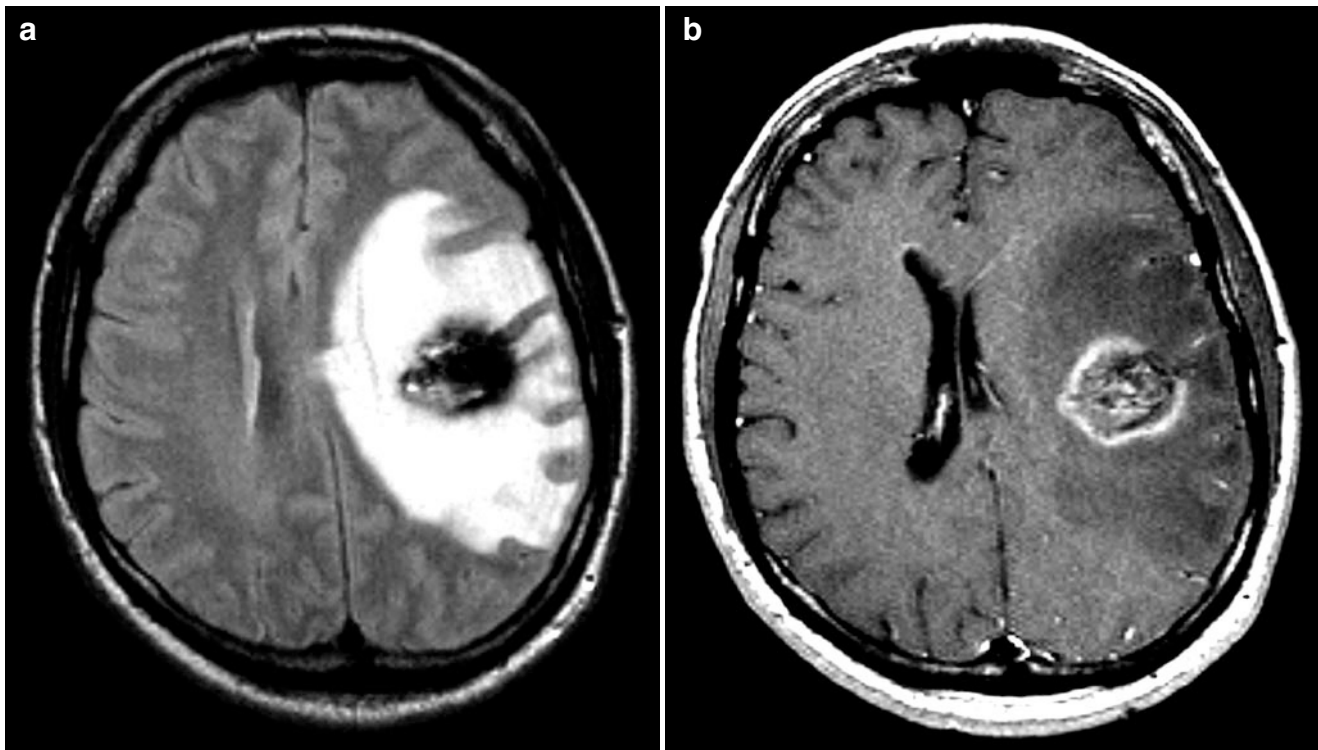


Fig. 1 Imaging abnormalities after stereotactic irradiation for cavernous malformation with single dose of 18 Gy. On FLAIR images a wide region of hyperintensity with an approximate diameter of 3 cm is visible around the cavernoma (a). On T1-weighted images a ring of contrast enhancement and wide area of hypointensity is present (b)

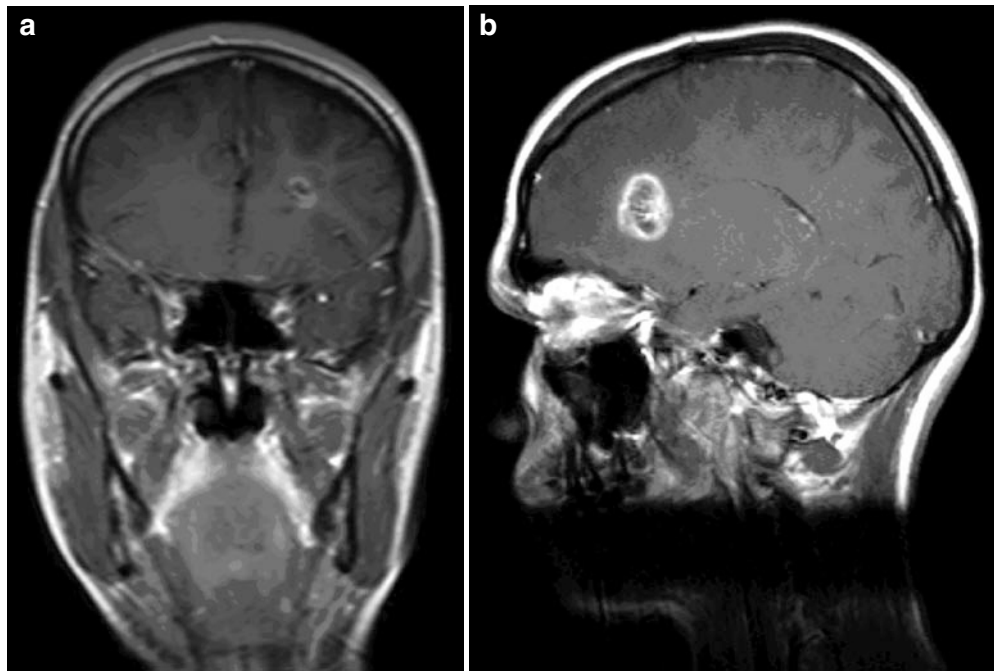


Fig. 2 T1-weighted frontal (a) and sagittal (b) sections through a cavernoma irradiated also with a dose of 18 Gy with radiation-induced alterations of relatively smaller intensity. A ring of contrast enhancement around the lesion with some signs of edema is visible

in the AVM and CCM groups, respectively ($p = 0.4968$). Imaging abnormalities in the CCM group were significantly more frequent in patients irradiated with higher doses ($p = 0.0008$, mean dose 18.1 vs 15.3 Gy in the group with and without imaging abnormalities, respectively). No association between dose, volume or any clinical parameters like bleeding prior to embolization, presenting symptoms, sex or age and the incidence of imaging abnormalities after treatment could be found in the AVM group. The mean doses delivered to the AVMs and CCMs did not differ significantly ($p = 0.8097$). In two patients with cavernomas radiological symptoms of radiation necrosis associated with neurological deterioration were identified; no radiation necrosis was found in the AVM group ($p = 0.0188$, chi-square test; $p = 0.1225$ with Yates correction). Patients with radiological signs of focal brain edema or gliosis were asymptomatic in all cases. To date, no cyst formation has been observed in our patients.

Discussion

Imaging abnormalities in brain tissue after stereotactic irradiation are a relatively common finding. They can be caused by focal brain edema, easily recognized on MR images as hyperintense areas on FLAIR and T2-weighted images or

regions of hypointensity on T1-weighted images, whereas areas of contrast enhancement are the evidence of blood-brain barrier breakdown, which also can be attributed to damaging effect of ionizing radiation delivery.

The incidence of radiation-induced imaging abnormalities after stereotactic radiosurgery for brain AVMs is usually reported at the level of 26–30%. Here it reached 33.9%, which is in good agreement with the literature (1–3,8,13). It is noteworthy that the presence of imaging alterations was not associated with clinical neurological symptoms, whereas some reports indicate that imaging changes are associated with neurological deficits in 5–10% of cases (8,15). This finding can be explained by the fact that the mean radiation dose in our material was lower than reported in other papers and thus it can be assumed that the risk of symptomatic radiological alterations was also reduced. Nevertheless, two symptomatic radiation necroses were diagnosed in the CCM group despite the fact that the mean radiation dose was similar to the mean dose in the AVM group. A strong influence of radiation dose on the incidence of imaging alterations was also revealed. These observations suggest that patients with CCMs are more prone to radiation-induced brain toxicity after stereotactic radiosurgery than patients with AVMs. Similar results were obtained by Pollock et al. They found that patients irradiated stereotactically for CCMs experience radiation-induced complications more often than patients

harboring AVMs of similar size and location (11). In addition, Karlsson et al. reported a relatively high number of symptomatic radiation-induced complications (26%) in patients treated for CCMs, much higher than expected for AVMs of similar parameters (6). It has been suggested that the increased susceptibility of neural tissue surrounding cavernomas to radiation-induced toxic effects is caused by the sensitizing action of hemoglobin metabolites deposited around the lesion as a result of repeated subclinical microhemorrhages or overt hemorrhage (4). As deposits of hemoglobin metabolites around CCMs were a common finding in our diagnostic studies, the results of our study could be another argument in favor of that hypothesis. On the other hand, Huang et al. reported a relatively low incidence of radiation-induced complications after SRS for cavernomas (6.7% of 30 patients had imaging alterations in MR studies) and suggested that this treatment modality can be a safe technique of treatment for deep seated or residual CCMs, unfit for microsurgery, although its effectiveness requires further study (5).

The time from irradiation to diagnosis of imaging abnormalities did not exceed 2 years in most cases, which is concordant with other reports (9,14). A longer follow-up period would allow for assessment of the evolution and the kinetics of imaging alterations. Our observations suggest that these changes are not permanent and at least in some cases can finally resolve. The need for more intensive investigation of the imaging alterations after SRS for cavernomas has also been proposed by other authors otherwise suggesting potential usefulness of this technique in the treatment of inoperable CCMs (7).

Conclusions

Radiological symptoms of postradiosurgical damage affect about one third of irradiated patients, usually without clinical manifestations. The probability of the occurrence of radiation-induced brain damage is strongly associated with the dose of ionizing radiation administered to patients with cavernomas. Moreover, patients irradiated for CCMs seem to be more prone to develop symptomatic postradiosurgery necrosis, this observation however demands further investigation.

Conflict of interest statement We declare that we have no conflict of interest.

References

1. Flickinger JC, Kondziolka D, Kalend AM, Maitz AH, Lunsford LD (1996) Radiosurgery-related imaging changes in surrounding brain: multivariate analysis and model evaluation. *Radiosurgery* 1:229–236
2. Flickinger JC, Kondziolka D, Maitz AH, Lunsford LD (1998) Analysis of neurological sequelae from radiosurgery of arteriovenous malformations: how location affects outcome. *Int J Radiat Oncol Biol Phys* 40(2):273–278
3. Flickinger JC, Kondziolka D, Pollock BE, Maitz AH, Lunsford LD (1997) Complications from arteriovenous malformation radiosurgery: multivariate analysis and risk modeling. *Int J Radiat Oncol Biol Phys* 38(3):485–490
4. Hasegawa T, McInerney J, Kondziolka D, Lee JYK, Flickinger JC, Lunsford D (2002) Long-term results after stereotactic radiosurgery for patients with cavernous malformations. *Neurosurgery* 50(6):1190–1197
5. Huang YC, Tseng CK, Chang CN, Wei KC, Liao CC, Hsu PW (2006) LINAC radiosurgery for intracranial cavernous malformation: 10-year experience. *Clin Neurol Neurosurg* 108(8):750–756
6. Karlsson B, Kihlström L, Lindquist C, Ericson K, Steiner L (1998) Radiosurgery for cavernous malformations. *J Neurosurg* 88(2):293–297
7. Kim DG, Choe WJ, Paek SH, Chung HT, Kim IH, Han DH (2002) Radiosurgery of intracranial cavernous malformations. *Acta Neurochir (Wien)* 144(9):869–878
8. Kondziolka D, Lunsford LD, Flickinger JC (2003) Gamma knife radiosurgery for brain arteriovenous malformations. *Oper Tech Neurosurg* 2(6):75–82
9. Levegrün S, Hof H, Essig M, Schlegel W, Debus J (2004) Radiation-induced changes of brain tissue after radiosurgery in patients with arteriovenous malformations: Correlation with dose distribution parameters. *Int J Radiat Oncol Biol Phys* 59(3):796–808
10. Pollock BE, Flickinger JC (2002) A proposed radiosurgery-based grading system for arteriovenous malformations. *J Neurosurg* 96:79–85
11. Pollock BE, Garces YI, Stafford SL, Foote RL, Schomberg PJ, Link MJ (2000) Stereotactic radiosurgery for cavernous malformations. *J Neurosurg* 93(6):987–991
12. Spetzler RF, Martin NA (1986) A proposed grading system for arteriovenous malformations. *J Neurosurg* 65:476–483
13. Tomura N, Izumi J, Sakuma I, Takahashi S, Omachi K, Otani T, Anbai A, Watarai J, Suzuki A, Mizoi K (2004) Radiation-induced changes in the brain following stereotactic irradiation evaluated by sequential MRI. *Comp Med Imag Graph* (28):73–79
14. Voges J, Treuer H, Sturm V, Büchner C, Lehrke R, Kocher M, Staar S, Kuchta J, Müller RP (1996) Risk analysis of linear accelerator radiosurgery. *Int J Radiat Oncol Biol Phys* 36(5):1055–1063
15. Yamamoto M, Hara M, Ide M, Ono Y, Jimbo M, Saito I (1998) Radiation-related adverse effects observed on neuro-imaging several years after radiosurgery for cerebral arteriovenous malformations. *Surg Neurol* 49(4):385–397

Magnetic Resonance Spectroscopic Evaluation of Brain Tissue Metabolism After Irradiation for Pediatric Brain Tumors in Long-Term Survivors: A Report of Two Cases

Sławomir Blamek, Jerzy Wydmański, Maria Sokół, Łukasz Matulewicz, and Łukasz Boguszewicz

Abstract

Objective The aim of our study was to evaluate the metabolic profile of brain tissue of two long-term survivors of childhood brain tumors.

Materials Two males who were 25 and 33 years old at the time of examination and had been irradiated for brain tumors at the age of 17 and 13 years respectively. The first subject had been operated on radically for medulloblastoma and received craniospinal axis irradiation composed of a whole brain radiotherapy with boost to the posterior fossa (total dose (TD) = 59.4 Gy in 33 fractions) and spinal canal irradiation (TD = 30 Gy in 20 fractions) according to the protocol at the time of treatment. The second subject had previously received whole brain irradiation (TD = 45 Gy in 19 fractions) because of inoperable central region tumor of unknown histology.

Methods Short echo-time (TE = 30ms) point-resolved spectra were obtained using a 2 T magnet. Ratios of N-acetylaspartate (NAA), choline (Cho), myo-inositol (mI), lactate (Lac) and lipids (Lip) signal intensities were calculated using the creatine (Cr) signal as an internal reference. The spectra were acquired both from the tumor bed area and uninvolved brain tissue in the first subject, and from uninvolved brain areas of frontal and occipital lobes in the second subject.

Results In both cases, MRS examination revealed ratios of NAA/Cr, Cho/Cr and mI/Cr within normal range in most spectra. Nevertheless, a slight elevation of Lac/Cr (2.47 and 1.05) and a more pronounced elevation of Lip/Cr proportions (45.77 and 3.97 respectively, in uninvolved sites) were detected in both patients.

Conclusions Metabolic parameters correlated with neuronal function (NAA/Cr) and cell membrane metabolites turnover (Cho/Cr) seem to recover to normal values in long-term survivors of brain tumors. Lac/Cr and Lip/Cr proportions could be considered parameters indicating permanent radiation-induced brain damage; however, this proposal requires further investigation.

Keywords Magnetic resonance spectroscopy • pediatric brain tumors • long-term survivors • radiotherapy • adverse effects

Introduction

Management of brain tumors in children requires an aggressive therapy usually composed of surgery, chemotherapy, and irradiation. Late sequelae of this regimen are attracting growing attention because of the increasing number of long-term survivors of childhood brain cancer. Most reports concentrate on white matter damage, cognitive impairment, and results of neuropsychological testing (2,10,11). The assessment of the metabolic profile of the brain has not been so intensively investigated, and available reports deal with patients just a few months or years after completion of the treatment. Our aim is to present two cases of long-term survivors of pediatric brain tumors and to evaluate the results of magnetic resonance spectroscopic examination (MRS) of areas both proximal and distal from the original site of the neoplasm in conjunction with the results of clinical examination and imaging.

Case Reports

Case 1

A 17-year-old male referred to our institution after the implantation of ventriculo-peritoneal valve and subtotal removal of cerebellar tumor in 1996. The tumor was located in the left cerebellar hemisphere and had invaded the

S. Blamek (✉), and J. Wydmański
Department of Radiotherapy, Maria Skłodowska-Curie Memorial
Cancer Center and Institute of Oncology, Gliwice Branchul,
Wybrzeże Armii Krajowej 15, Gliwice 44-100, Poland
e-mail: blamek@gmail.com

M. Sokół, Ł. Matulewicz, and Ł. Boguszewicz
Department of Medical Physics, Maria Skłodowska-Curie Memorial
Cancer Center and Institute of Oncology, Gliwice Branchul,
Wybrzeże Armii Krajowej 15, Gliwice 44-101, Poland

Table 1 Results of MRS examinations

	Voxel location	NAA/Cr	Cho/Cr	Cho/NAA	mI/Cr	Lac/Cr	Lip/Cr
Case 1	Cerebellum L	1.07	1.13	1.05	0.73	6.32	15.71
	Cerebellum R	1.79	1.09	0.61	0.62	2.47	45.77
Case 2	Frontal L	1.05	1.16	1.11	0.72	1.05	3.97
	Occipital L	1.13	1.15	1.02	0.50	0.94	3.24
	Occipital R	1.49	1.08	0.72	0.78	0.00	3.05
Norm		1.53	0.98	0.64	0.70	0 ^a	0 ^a

NAA – N-acetylaspartate, Cr – creatine, Cho – choline, mI – myo-inositol, Lac – lactate, Lip – lipids, L – left, R – right.^a It was assumed that lactate and lipid signals are not visible in the healthy brain.

left cerebello-pontine angle and pons. The histopathologic diagnosis was medulloblastoma. In 1996, the patient received craniospinal radiotherapy. According to the protocol at that time, the whole brain was irradiated with a daily fraction of 1.8 Gy and total dose of 45 Gy with boost to posterior fossa to total dose of 59.4 Gy. The medulla oblongata and upper part of cervical spinal cord received 36 Gy. The spinal field was irradiated with a total dose of 30 Gy with 1.5 Gy/fraction. Control examinations after radiotherapy did not reveal either tumor mass in the posterior fossa or dissemination in the spinal canal. MRS examination was performed in 2004. Voxels were placed in the left cerebellar hemisphere, in the vicinity of tumor bed and in the contralateral cerebellar hemisphere for comparison. Results of the examination are summarized in Table 1.

Case 2

The second subject is a 13-year-old male who was admitted with diagnosis of central region tumor. The diagnosis was established after a CT scan was performed because the patient complained of headaches, decreased vision acuity, and vomiting. The CT examination showed a solid mass in the posterior part of third ventricle associated with a widening of third and lateral ventricles. The tumor was deemed inoperable at the time of diagnosis. Because of symptoms of increasing intracranial pressure, a Pudenz valve was implanted and the patient was referred to radiotherapy. The patient was in good performance status (WHO/ECOG 1). Neurological examination revealed discrete horizontal nystagmus and positive Parinaud, Kerning and Babinski signs. Ophthalmologic examination revealed slight signs of papilledema. The patient had been irradiated in 1983, initially with orthovoltage machine and, because of machine defect during treatment, the remainder of planned dose was delivered with a cobalt unit. Radiotherapy fields encompassed the whole brain, and the total dose delivered was 45 Gy. The dose of 10 Gy was delivered with X-rays with daily fraction of 2 Gy and next 35 Gy with gamma-rays with 2.5 Gy per fraction.

Nineteen years after the initial treatment, another brain tumor was diagnosed. MRI examination performed in 2002 revealed a contrast-enhancing mass in the left occipital lobe. The third ventricle was slightly widened posteriorly, but with no evidence of tumor. Total excision was performed in May 2002 and was confirmed with postoperative MRI. Histopathologic examination of tumor specimens revealed a grade II meningioma. After surgery, the patient was in good performance status (WHO/ECOG 1) without obvious neurological deficits. However, the patient displayed decreased intellectual function on neuropsychological testing, especially in the area of short-term memory. This finding was attributed to prior whole-brain radiotherapy.

A control MRI/MRS examination was performed in September 2002. No evidence of tumor was found on MRI. Magnetic resonance spectroscopy was performed using voxels placed in the left and right occipital and left frontal lobes. Results of the examination are presented in Table 1.

Discussion

In both cases, MRS was performed after a relatively long period of time since high dose whole brain radiotherapy. Most reports concerning post-irradiation metabolic alterations in brain tissue concentrate on early effect of radiation on nervous tissue. Decreases of the NAA signal intensity or the NAA/Cr ratio are the most prevalent early consequences of irradiation (13,16). However, literature dealing with the duration of metabolic changes and long-term metabolic effects of radiation on brain tissue is scant and inconclusive.

In the two cases presented above, the metabolic activities of neurons both proximal and distal to primary tumor site seem to be nearly normal as assessed by the NAA/Cr ratio. The reference value for NAA/Cr proportion based on measurements in healthy adult volunteers in our center is 1.53 (SD = 0.23). In both clinical cases we presented, the NAA/Cr ratio is within the normal range in most voxels, with a slight tendency to be lower in tumor bed proximity. This phenomenon is particularly visible in the medulloblastoma

case. According to numerous reports, decrease of the NAA/Cr ratio is a commonly occurring consequence of brain irradiation (13,16,17). Results of our investigation suggest that, in the long-term, post-irradiation NAA/Cr proportion can achieve values within the normal range for a healthy population.

Normalization of the NAA/Cr ratio could not only reflect the normalization of the NAA signal intensity, but also a decreased Cr signal intensity. In our two cases, analysis of Cho/Cr and Cho/NAA signal intensities showed that they were also mostly within the normal range. This suggests that the obtained NAA/Cr values for our cases are primarily due to normalization of NAA signal intensity rather than a diminished Cr signal. This observation could reflect at least partial recovery of neuronal function after damage caused by ionizing radiation; however, further investigation is needed to provide stronger evidence of neuronal function restoration.

The NAA/Cr ratio in left frontal lobe in the second case is somewhat below values expected in healthy brain. This could be a sign of neuronal loss or dysfunction. This explanation correlates well with the clinical findings of impaired intellectual ability in this patient including impaired short-term memory and decreased performance on cognitive tasks and learning problems. There are numerous publications dealing with the correlation of MRS-visible brain metabolites and intellectual functions. Ross et al. described a significant correlation between NAA/Cr signal intensity in the frontal lobe region and the speed of information processing (12). These findings are consistent with our observations in this patient. Moreover, it was reported that radiation-induced intellectual impairment depends on dose and volume of irradiated brain, and is more prominent in patients after whole brain radiotherapy than after localized irradiation (3,4,6). Thus, we believe the observed intellectual dysfunction and slightly reduced NAA/Cr ratio in the frontal lobe are consequences of the precedent treatment.

An elevation of Cho/Cr ratio can indicate increased cell membrane turnover and cellular density usually associated with tumor recurrence (7). In both presented cases, the Cho/Cr ratio had similar values to the value observed in healthy volunteers: 0.98 (SD = 0.2). Therefore, it can be assumed that the observed signal intensities of certain metabolites are connected to radiation therapy consequences rather than to possible residual or recurrent tumor in subclinical stage.

The presence of lactate signal is usually associated with altered glucose metabolism, local hypoxia, or impaired lactate washout (15). Additionally, the lactate signal was recorded in brain tissue of patients with glial cell tumors with poor prognosis (14). In the presented cases, the lactate signal can be justified by vascular damage caused by ionizing radiation, which can result in impaired tissue perfusion and impaired glucose/lactate turnover (1).

A striking observation in both cases is the presence of a high Lip/Cr ratio, especially in the cerebellar region. The lipid signal is usually associated with cell membrane disintegration resulting in an increased concentration of mobile lipids. Strong lipid signals are commonly seen in regions of severe brain damage or necrosis or in highly malignant brain tumors (5,8,9). MR imaging did not reveal brain necrosis in any region of the brain of the two subjects or any signs of tumor recurrence. Increased lipid signals in the cerebellum could be in part explained by signal contamination caused by fatty tissue adjacent to skull base. However, the lipid signal is also visible in voxels distant from fatty tissue of epicranium and bone marrow. Its presence could therefore be attributed to radiation damage being below the detection threshold of MR imaging.

Resumé

Analysis of the presented cases suggests that the long-term metabolic activity of the brain after whole brain radiotherapy may resemble brain metabolic activity in healthy subjects who have never undergone brain radiotherapy. The similarities are particularly visible in the Cho/Cr, mI/Cr, and NAA/Cr ratios, which suggests that metabolism of neural and glial tissues can recover to normal level after a period of aberrations caused by ionizing radiation.

Elevation of the Lac/Cr and Lip/Cr ratios could be used as a marker of persistent brain damage. However, this observation requires further investigation because other factors potentially influencing the Lac and Lip signal intensities such as partial volume effect and signal contamination could not be excluded.

Conflict of interest statement We declare that we have no conflict of interest.

References

1. Belka C, Budach W, Kortmann RD, Bamberg M (2001) Radiation induced CNS toxicity – molecular and cellular mechanisms. *Br J Cancer* 85(9):1233–1299
2. Fouladi M, Chintagumpala M, Laningham FH, Ashley D, Kellie SJ, Langston JW, McCluggage CW, Woo S, Kocak M, Krull K, Kun LE, Mulhern RK, Gajjar A (2004) White matter lesions detected by magnetic resonance imaging after radiotherapy and high-dose chemotherapy in children with medulloblastoma or primitive neuroectodermal tumor. *J Clin Oncol* 22(22):4551–4560
3. Fuss M, Poljanc K, Hug EB (2000) Full Scale IQ (FSIQ) changes in children treated with whole brain and partial brain irradiation. A review and analysis. *Strahlenther Onkol* 176(12):573–581
4. Hoppe-Hirsch E, Brunet L, Laroussinie F, Cinalli G, Pierre-Kahn A, Rénier D, Sainte-Rose C, Hirsch JF (1995) Intellectual outcome in children with malignant tumors of the posterior fossa: influence

- of the field of irradiation and quality of surgery. *Childs Nerv Syst* 11(6):340–345
5. Kizu O, Naruse S, Furuya S, Morishita H, Ide M, Maeda T, Ueda S (1988) Application of proton chemical shift imaging in monitoring of gamma knife radiosurgery on brain tumors. *Magn Reson Imaging* 16(2):197–204
 6. Merchant TE, Kiehna EN, Li C, Shukla H, Sengupta S, Xiong X, Gajjar A, Mulhern RK (2006) Modeling radiation dosimetry to predict cognitive outcomes in pediatric patients with CNS embryonal tumors including medulloblastoma. *Int J Radiat Oncol Biol Phys* 65(1):210–221
 7. Miller BL, Chang L, Booth R, Ernst T, Cornford M, Nikas D, McBride D, Jenden DJ (1996) In vivo 1H MRS choline: correlation with in vitro chemistry/histology. *Life Sci* 58(22):1929–1935
 8. Negendank WG, Sauter R, Brown TR, Evelhoch JL, Falini A, Gotsis ED, Heerschap A, Kamada K, Lee BC, Mengeot MM, Moser E, Padavic-Shaller KA, Sanders JA, Spraggins TA, Stillman AE, Terwey B, Vogl TJ, Wicklow K, Zimmerman RA (1996) Proton magnetic resonance spectroscopy in patients with glial tumors: a multicenter study. *J Neurosurg* 84(3):449–458
 9. Rand SD, Prost P, Haughton V, Mark L, Stainer J, Johansen J, Kim TA, Chetty VK, Mueller W, Meyer G, Krouwer H (1997) Accuracy of single-voxel proton MR spectroscopy in distinguishing neoplastic from nonneoplastic brain lesions. *AJNR Am J Neuroradiol* 18:1695–1704
 10. Reddick WE, Glass JO, Palmer SL, Wu S, Gajjar A, Langston JW, Kun LE, Xiong X, Mulhern RK (2005) Atypical white matter volume development in children following craniospinal irradiation. *Neuro Oncol* 7(1):12–19
 11. Reeves CB, Palmer SL, Reddick WE, Merchant TE, Buchanan GM, Gajjar A, Mulhern RK (2006) Attention and memory functioning among pediatric patients with medulloblastoma. *J Pediatr Psychol* 31(3):272–280
 12. Ross AJ, Sachdev PS, Wen W, Valenzuela MJ, Brodaty H (2005) Cognitive correlates of 1H MRS measures in the healthy elderly brain. *Brain Res Bull* 66(1):9–16
 13. Rutkowski T, Tarnawski R, Sokol M, Maciejewski B (2003) 1H-MR spectroscopy of normal brain tissue before and after postoperative radiotherapy because of primary brain tumors. *Int J Radiat Oncol Biol Phys* 56(5):1381–1389
 14. Tarnawski R, Sokol M, Pieniazek P, Maciejewski B, Walecki J, Miszczyk L, Krupska T (2002) 1H-MRS in vivo predicts the early treatment outcome of postoperative radiotherapy for malignant gliomas. *Int J Radiat Oncol Biol Phys* 52(5):1271–1276
 15. Tomoi M, Kimura H, Yoshida M, Itoh S, Kawamura Y, Hayashi N, Yamamoto K, Kubota T, Ishii Y (1997) Alterations of lactate (+lipid) concentration in brain tumors with in vivo hydrogen magnetic resonance spectroscopy during radiotherapy. *Invest Radiol* 32(5):288–296
 16. Usenius T, Usenius JP, Tenhunen M, Vainio P, Johansson R, Soimakallio S, Kauppinen R (1995) Radiation-induced changes in human brain metabolites as studied by 1H nuclear magnetic resonance spectroscopy in vivo. *Int J Radiat Oncol Biol Phys* 33(3):719–724
 17. Yousem DM, Lenkinski RE, Evans S, Allen D, O'Brien R, Curran W, Schnell M, Bennett M, Wehrli SL, Grossman RI (1992) Proton MR spectroscopy of experimental radiation-induced white matter injury. *J Comput Assist Tomogr* 16(4):543–548

Evaluation of the Late Effects of CNS Prophylactic Treatment in Childhood Acute Lymphoblastic Leukemia (ALL) Using Magnetic Resonance Spectroscopy

Kornelia Ficek, Sławomir Blamek, Dorota Syguła, Leszek Miszczyk, Danuta Sońta-Jakimczyk, and Rafał Tarnawski

Abstract

Purpose The aim of the study was to evaluate the late changes seen in Magnetic Resonance Spectroscopy (MRS) of the brain in Acute Lymphoblastic Leukemia (ALL) survivors to assess neurotoxicity following prophylactic treatment with cranial irradiation (CRT) and/or intrathecal (ITMTX) and systemic MTX.

Materials and Methods The study was performed on two groups of patients. The first group consisted of 30 children who received CRT and ITMTX, and the second group was comprised of 15 children treated only with ITMTX. All patients were ALL survivors treated between 1994 and 2002. Radiotherapy was performed using two opposite fields for a total dose of 18 Gy. The children were examined from 6 to 12 years after treatment. All children underwent a physical and neurological examination and MRI/MRS studies. ¹H-MR spectra were acquired from frontal and occipital regions of the brain. Mean values and standard deviations were calculated for following metabolite ratios: NAA/Cr, Cho/Cr, Cho/NAA, and mI/Cr.

Results Three of the 45 children (11%) presented with white matter changes upon MRI examination. All children with MRI abnormalities received CRT. In 13 (31%) children, changes in ¹H-MRS metabolite ratios were seen. We observed decreased NAA/Cr and Cho/Cr ratios. MR spectroscopy showed a significant reduction ($P < .05$) of the mean NAA/Cr ratio in children given CRT.

Conclusion MRS is a sensitive detector of late metabolic changes after prophylactic treatment for ALL in childhood. It is able to detect metabolic effects of treatment in patients even when no morphologic changes are visible upon MRI.

K. Ficek (✉)

Department of Radiotherapy, Center of Oncology Maria Skłodowska Curie Memorial Institute-Branch, Wybrzeże Armii Krajowej 14, 44-101, Gliwice, Poland
e-mail: bertaf@poczta.onet.pl

D.S. Jakimczyk

Department of Paediatric Oncology Organization Medical University, Center of Oncology Maria Skłodowska Curie Memorial Institute-Branch, 3 Maja 15, 41-800 zabrze

Keywords Brain injury • late effects after cancer therapy • MRS • childhood leukemia

Introduction

Prophylactic central nervous system therapy is an essential component of the treatment for childhood acute lymphoblastic leukemia (1). Cranial irradiation (CRT) and intrathecal methotrexate (ITMTX) have been introduced as prophylactic treatments that reduce the CNS relapse rate. It is well documented that radiotherapy and chemotherapy, either alone or in combination, may lead to structural and functional changes in the central nervous system.

The children who were irradiated develop long-term neurocognitive sequelae affecting intellectual functions and psychological status (2,3). Imaging changes revealed upon CT or MRI after prophylactic treatment are useful in the detection of CNS complications, but neurointellectual disturbances have been observed without any imaging changes in some cases (4,5).

Proton Magnetic Resonance Spectroscopy (MRS) is a safe, non-invasive diagnostic method that may provide more information concerning neurotoxicity after prophylactic treatment than conventional imaging. Because many neurological complications of leukemia are treatable, early diagnosis is essential. The aim of our study was to evaluate the late changes detected in MRS of the brain in pediatric ALL survivors to assess neurotoxicity following prophylactic CNS treatment with cranial irradiation and/or intrathecal and systemic administration of methotrexate (MTX).

Materials and Methods

The study was performed on two groups of patients. The first group consisted of 30 children receiving cranial irradiation and intrathecal MTX, whereas the second group consisted of 15 children treated with intrathecal MTX only.

All patients are ALL survivors treated from 1994 to 2002.

Radiotherapy was performed using two lateral opposed fields with total dose of 18 Gy and 1.8–2.0 Gy per fraction. MTX chemotherapy doses depended on the risk group to which the patient was assigned (Table 1).

The children were examined 6 to 12 years after treatment.

MRI and MRS studies were performed on a 2 T Elscint Prestige device using a standard head coil. Localized ¹H-MR spectra were acquired from frontal and occipital regions of the brain. The mean values and standard deviations were calculated for each of following metabolite ratios: NAA/Cr, Cho/Cr, Cho/NAA, and mI/Cr. For comparison between groups with and without RT, t-tests for independent samples were used. $P < 0.05$ was considered statistically significant.

Results

There were no unusual neurological findings in either group. The groups were comparable in gender and age distribution. Three of the 45 children (7%) showed white matter changes upon MRI that can be described as demyelination. The children with MRI-visible changes received cranial radiotherapy. All children treated with intrathecal chemotherapy had normal imaging examinations. In 14 cases (31%), changes in ¹H-MRS metabolite ratios were seen. In that subgroup, ten children underwent radiotherapy and four underwent ITMTX alone. We observed decreased NAA/Cr ($p = 0.00003$) and Cho/Cr ($p = 0.0002$) ratios in the group with metabolic changes in comparison to patients who had normal metabolite ratios. MRI changes were strongly correlated with the reduction of the NAA/Cr ratio (χ^2 test $p = 0.00001$).

MR spectroscopy revealed no statistically significant differences of mean NAA/Cr, Cho/Cr, or Cho/NAA ratios between the group with cranial irradiation and the group without radiotherapy (Table 2).

Table 1 Characteristics of the patients

Group characteristics	With RT and MTX	Only MTX
Sex	M-15 F-15	M-7 F-8
Age	4–16 Median 11	4–17 Median 8

Table 2 Summary of metabolite ratios. The presented values are calculated means and standard deviations

Metabolite ratios	Group with RT		Group without RT	
	Mean	SD	Mean	SD
NAA/Cr	1.04	0.45	1.27	0.4
Cho/Cr	0.94	0.36	1.01	0.32
Cho/NAA	0.75	0.25	0.73	0.18
mI/Cr	0.64	0.21	0.32	0.15

Discussion

In our study, we evaluated late neurotoxicity after prophylactic CNS treatment due to childhood leukemia. The children underwent examinations from 6 to 12 years after the conclusion of their treatment.

Morphologic changes after treatment are well described in several studies, and those most frequently recognized are demyelination, mineralizing microangiopathy, and atrophy (10). The majority of changes were observed either during the treatment or a short time after the conclusion of chemotherapy, which suggests that some changes could be reversible (5–7). A relatively low incidence of abnormal imaging more than 5 years after treatment was also observed. In a study by Yu-Leung Chan et al., only 10% of patients had imaging changes from 5.6 to 19 years after diagnosis (8). Kramer et al. found abnormalities in 10% of leukemia survivors who received cranial radiotherapy with doses ranging from 18 to 24 Gy (9). In our study, the imaging changes were relatively rare; only 7% of the children who received cranial irradiation exhibited late changes in MRI that were described as demyelination.

A significant number of publications provide evidence that children's cognitive functions are compromised by prophylactic therapy (11–14). Conventional MR imaging is not very useful for detecting long-term CNS damage, because neurological disturbances were also observed in patients who exhibited normal imaging (5).

Magnetic Resonance Spectroscopy has the potential to recognize metabolic disturbances that may be associated with neurological and intellectual side-effects of the treatment. The high sensitivity of ¹H MRS in detecting neuronal abnormalities has been documented in a study involving patients with dementia as well as children with developmental delays and different neurological disorders (14–16).

In our study, 14 children presented metabolic changes characterized by a reduction of the NAA/Cr and Cho/Cr ratios. The children with abnormal imaging findings also exhibited metabolic changes. Our results are concordant with those from the study by Yu-Leung Chan, in which reduction of the NAA/Cr ratio correlated with white matter changes upon MRI (7). The most characteristic metabolic abnormalities after prophylactic brain irradiation in our material were the reduction of the NAA/Cr and Cho/Cr ratios.

Conclusion

Magnetic Resonance Spectroscopy is a sensitive detector of late metabolic changes in patients after prophylactic treatment due to childhood ALL. MRS has the potential to detect

adverse metabolic effects of prophylactic treatment in patients who do not exhibit morphological changes on MRI images.

Conflict of interest statement We declare that we have no conflict of interest.

References

1. Clarke M, Gaynon P, Hann I (2003) CNS-directed therapy for childhood acute lymphoblastic leukemia. *J Clin Oncol* 21:1798–1809
2. Mulhern RK, Palmer SL (2003) Neurocognitive late effects in pediatric cancer. *Curr Probl Cancer* 27:177–197
3. Spiegler B, Kennedy K, Mazze M (2006) Comparison of long-term cognitive outcomes in young children with ALL treated with cranial radiation or high-dose or very high-dose intravenous methotrexate. *J Clin Oncol* 24:3858–3864
4. Brecher ML, Berger P, Freeman AI (1985) Computerized tomography scan findings in children with acute lymphocytic leukemia treated with three different methods of central nervous system prophylaxis. *Cancer* 56:2430–2433
5. Paakko E, Talvessari K, Pyhitnen J (1994) Late cranial MRI after cranial irradiation in survivors of childhood. *Cancer* 36:652–655
6. Ch Cheng-Yu, Zimmerman R, Farro S et al (1996) Childhood leukemia: Central Nervous System abnormalities during and after treatment. *Am J Neuroradiol* 17:295–310
7. Chu W, Ch C, Chan Y (2003) White matter and cerebral metabolite changes in children undergoing treatment for Acute Lymphoblastic Leukemia: longitudinal study with MR imaging and 1H MR spectroscopy. *Radiology* 229:659–669
8. Chan L, Roebuck T, Yuen M (2001) Long term cerebral metabolite changes on proton magnetic resonance spectroscopy in patients cured of acute lymphoblastic leukemia with previous intrathecal metotrexate and cranial irradiation prophylaxis. *Int J Radiat Oncol Biol Phys* 50:759–763
9. Kramer JH, Norman D, Brandt-Zawadzki M (1988) Absence of white matter changes on magnetic resonance imaging in children treated with CNS prophylaxis therapy for leukemia. *Cancer* 61:928–930
10. Contantinae LS, Ekholm S, McDonald S (1988) Adverse effects of brain irradiation correlated with MR and CT imaging. *Int J Radiat Oncol Biol Phys* 15:319–330
11. Balsom Wr, Bleyer Wa, Robinson L (1991) Intellectual function in long-term survivors of childhood acute lymphoblastic leukemia. *Med Pediatr Oncol* 19:486–492
12. Copeland D, Moore B, Francis D (1996) Neuropsychological effects of chemotherapy on children with cancer. *J Clin Oncol* 14:2826–2835
13. Mabbot D, Spiegler B, Greenberg M et al (2005) Serial evaluation of academic and behavioral outcome after treatment with cranial irradiation. *J Clin Oncol* 23:2256–2263
14. Raymond-Spenden E, Tripp G, Lawrence B (2000) Intellectual, neuropsychological and academic functioning I long-term survivors of leukenmia. *J Ped Psychol* 25:59–68
15. Fayed N, Morales H, Mordego P (2006) White matter proton MR spectroscopy in children with isolated developmental delay: does it mean delayed myelination. *Acad Radiol* 13:229–235
16. Voorn P, Pouvles P, Augustinus A (2006) Childhood white matter disorders quantitative MR imaging and spectroscopy. *Radiology* 241:510–517
17. Friedman S, Show D, Artru A et al (2006) Grey and white matter brain chemistry in young children with autism. *Arch Gen Psychiatry* 63:786–794

A Non-invasive Assessment of Intracranial Volume Reserve by Measuring Cerebrospinal Fluid Volume with the Aid of CT Imaging

Mariusz Glowacki, Karol Budohoski, Piotr Marszalek, Jerzy Walecki, and Zbigniew Czernicki

Abstract

Introduction Monitoring changes in the intracranial volume (ICV) reserve and intracranial pressure (ICP) is one of the key issues in the treatment of intracranial pathologies. The aim of this study is to develop a method of monitoring the ICV reserve by analyzing CSF volume measured using CT in specific regions.

Materials and Methods A total of 20 patients with cerebral injury were evaluated. Analysis was performed using imaging software. On selected scans (three at the basal cistern level and three at the pineal level), the following regions were analyzed: total cerebral surface (TC1, TC2) and bilateral ambient cistern (AC) only at the basal cistern level for cerebrospinal fluid (CSF) volume. Results were correlated with patients' Glasgow Coma Scale (GCS) scores.

Results An increase of CSF volume was observed with an improvement in the GCS. From the examined regions, only AC volume showed a statistically significant linear correlation ($p < 0.0005$) with GCS. Mean AC: 0.021, 0.454, and 0.678 mL CSF/scan in severe (3–8 pts GCS), moderate (9–12 pts GCS), and mild (13–15 pts GCS) TBI groups, respectively.

Discussion Assessment of CSF volume changes in mL CSF/scan can be conducted using CT. Counting voxels corresponding to the CSF eliminates mistakes due to inaccurate

region demarcation. The obtained results (AC volume) show a high correlation with patient state.

Keywords Intracranial pressure • intracranial volume reserve • traumatic brain injury • non-invasive ICP monitoring • voxel

Introduction

Intracranial volume (ICV) reserve and intracranial pressure (ICP) are two key factors taken into consideration when monitoring a patient with traumatic brain injury (TBI) (1, 7, 17, 19, 20). The decision of whether supportive or surgical intervention is indicated is made predominantly based on these factors in combination with the patient's state assessed using the Glasgow Coma Scale (GCS) (10–13). When the patient is comatose, intubated, or under anesthesia with supportive treatment implemented, ICP monitoring with cerebral perfusion pressure (CPP) calculation and diagnostic imaging become the sole indicators for surgery since it is impossible to clinically assess the state of the patient (7, 16, 17). However, controversy still remains whether invasive monitoring of ICP has any influence on morbidity and mortality after TBI; a number of authors suggest an even worse outcome in patients who have undergone invasive ICP monitoring (2, 20). Invasive ICP monitoring nonetheless remains the “gold standard” on neurocritical care units, although it is reserved for patients with severe neurological conditions (7, 8, 17, 19). The invasiveness of this method and potential risks arising from infections, improper handling, and decalibration in long term observations, however, may outweigh the benefits of constant bedside monitoring (2, 17, 20). This problem highlights the need for other less invasive methods of monitoring the ICV reserve. Emphasis has thus far been placed on transcranial Doppler (TCD) ultrasonography (8, 9), but different methods (e.g., pulsed phase lock loop technology (PPLL) (23) and CT analysis (4, 5, 18)) are also being developed. Therefore, there is still a need to develop and evaluate methods for the non-invasive assessment of ICV reserve.

M. Glowacki (✉) and P. Marszalek
Department of Neurosurgery,
M. Mossakowski Medical Research Center,
Polish Academy of Sciences, 5 Pawinskiego street, 20–016,
Warsaw, Poland

J. Walecki
Department of Radiology and Department of Experimental
Pharmacology, Polish Academy of Sciences
Medical Research Center, Warsaw, Poland

K. Budohoski and Z. Czernicki
Department of Neurosurgery, M. Mossakowski
Medical Research Center, Polish Academy of Sciences, Warsaw,
Poland and Department of Neurosurgery, Medical Research Center,
Polish Academy of Sciences and Department of Neurosurgery,
2nd Faculty of Medicine, Medical University of Warsaw, Poland

The aim of this study is to develop a method of non-invasive, objective assessment of intracranial volume reserve.

Materials and Methods

A total of 20 patients (age 38–60) diagnosed with traumatic brain injury (concussion, diffuse brain injury, epidural, and traumatic subdural intracerebral hemorrhage with the exclusion of traumatic subarachnoid hemorrhage (SAH)) were evaluated in the study. The control group consisted of 10 patients aged 41–63 who were being diagnosed for the cause of persistent headaches with normal CT imaging. Patients were divided into three groups based on their initial GCS scores: severe: 3–8 pts, n = 7; moderate: 9–12 pts, n = 6; mild: 13–15 pts, n = 7 (21). Cerebral CT scans at admission were analyzed at two levels: the basal cistern level and the pineal level. At the basal cistern level, demarcated and quantified regions included the ambient cistern (AC) and total cerebral surface (TC1). At the pineal level, only the total cerebral surface (TC2) was demarcated and quantified (Fig. 1). For the analysis, software dedicated for teleradiology and digital medical imaging was used (PaxStation, CompArt Medical Systems). The software quantified the number of voxels corresponding to the cerebrospinal fluid

(CSF) (0–18 Hounsfield units, Hu) in demarcated regions as the mean from three consecutive scans. The obtained number of voxels was then transformed to mL CSF/scan. Statistical analysis was performed using Statistica 7 (StatSoft).

Results

A difference in CSF volume in all demarcated regions was observed between the three groups with TBI and the control group. However, the difference was statistically significant only in the AC region ($p < 0.05$): severe: 0.021 mL CSF/scan, moderate: 0.143 mL CSF/scan, mild: 0.454 mL CSF/scan, control: 0.678 mL CSF/scan. Other regions (TC1 and TC2) showed a statistically significant difference only between the mild group and control group: TC1: 2.79 mL CSF/scan and 5.227 mL CSF/scan in the mild and control groups, respectively ($p < 0.05$); TC2: 4.315 mL CSF/scan and 7.358 mL CSF/scan in the mild and control groups, respectively ($p < 0.05$) (Fig. 2). A linear relationship between AC, TC1, and TC2 volume and GCS score was shown. However, only the correlation index (r) of AC volume to GCS was statistically significant ($p < 0.0005$) (Fig. 3). While the volume of the AC decreases steadily with the deterioration of the patient's

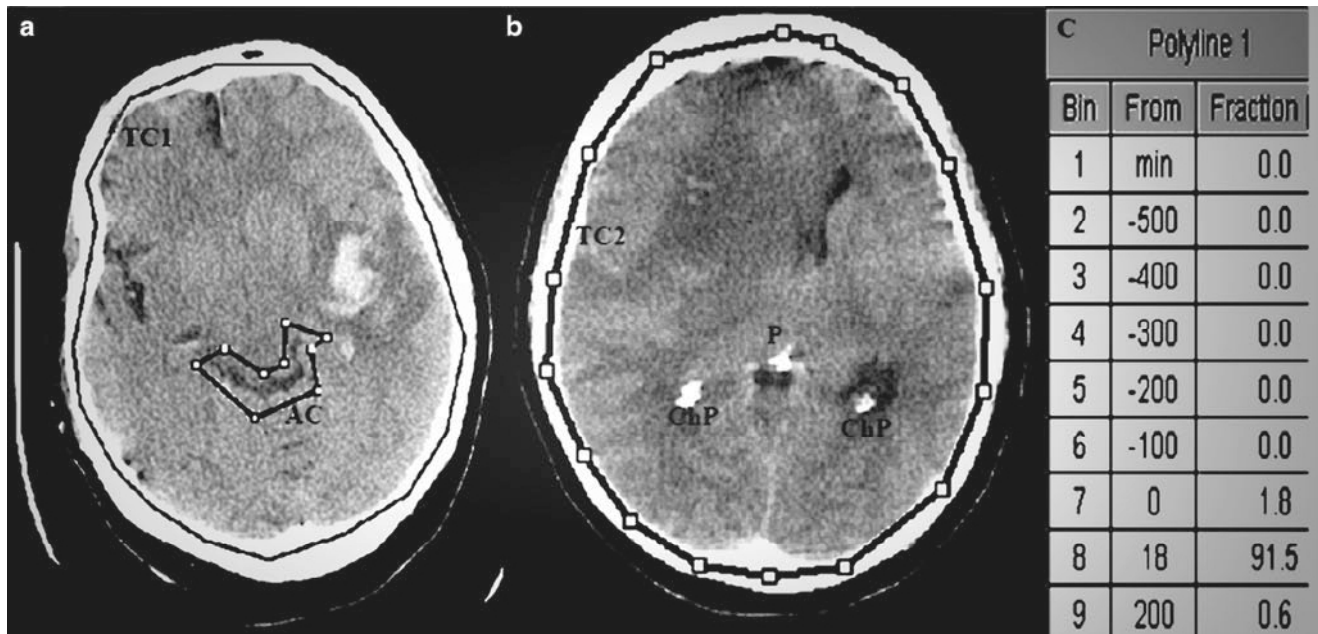


Fig. 1 (a) Scan at the level of the basal cisterns with demarcated regions for quantification: AC-ambient cistern, TC1-total cerebral surface at basal cisterns level. (b) Scan at the pineal level. Choroid plexus (ChP) calcifications and pineal gland (P) calcifications were used as

markers for proper patient positioning. TC2-total cerebral surface at the pineal level. (c) Example quantification of the voxel percentage within specified Hu ranges for the AC region. Values of 0–18 Hu correspond to the CSF: 1.8%

state, analysis has also shown that there is a minimal increase of volume in TC1 and TC2 from the mild to moderate group (Fig. 2). The reason for this inconsistency remains to be determined.

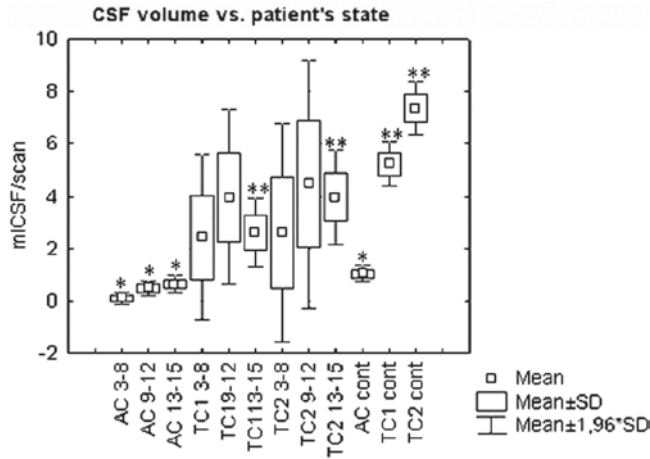


Fig. 2 CSF volume in analyzed regions divided into TBI groups: 3–8: severe, 9–12: moderate, 13–15: mild, cont.: control group. * Statistically significant ($p < 0.05$) differences in AC volume between TBI groups and control group, ** statistically significant ($p < 0.05$) differences in TC1 and TC2 only between mild TBI group and control group

Discussion

The results obtained show that assessment of ICV reserve is possible from routine CT scans using software designed for digital radiology even though different regions of the brain show differential sensitivities. The results show that ambient cistern volume, which was measured as the mean from three consecutive scans, correlates best with the patient's state ($p < 0.0005$). After division of TBI patients based on the GCS score into mild, moderate, and severe TBI groups, a significant difference in AC volume was observed between all TBI groups and the control group. Evaluating TC1 and TC2 revealed an increase of CSF volume among moderate compared to mild TBI patients. The reason for this difference remains to be determined. However the authors believe that it may be caused by unexpected CSF shifts due to pathological intracranial mass in the acute stage (1, 3, 4, 14, 22). Additionally, quantifying the total cerebral surface may lead to potential methodological mistakes resulting from parenchymal edema and/or dissolving hematoma that mimics CSF in CT imaging by falling into the same Hounsfield unit range. There is, however, a need to address this problem and determine whether other factors like patient age (the impact of age was minimized in the present study by choosing a cohort

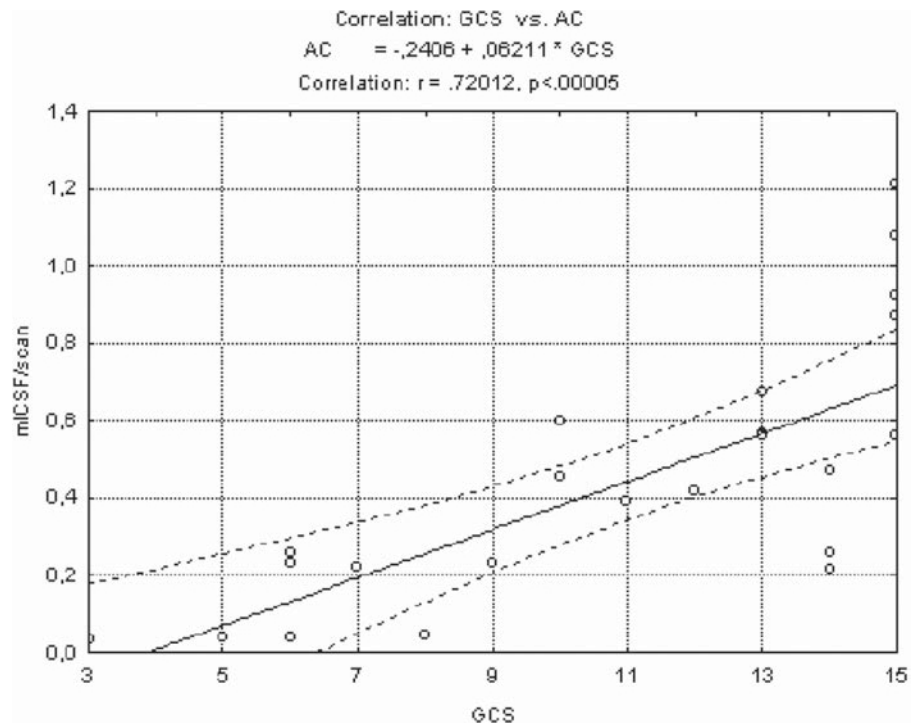


Fig. 3 Positive correlation between patient state (GCS-Glasgow Coma Scale) and AC volume in mL CSF/scan. Curved lines show the 95% CI. $p < 0.0005$

of patients with an age range of 38–63) and lesion localization play a role in this inconsistency (3, 4, 9, 15, 22, 24).

A drawback of the method is the inability to calculate accurately the ICV reserve in patients with traumatic SAH. This is due to a difference in H_u between the CSF and clotted blood, which in the computerized quantification process mimics severe ICV reserve depletion. For this reason, any evidence of traumatic SAH upon initial CT examination was considered an exclusion criterion.

This method has potential clinical applications for monitoring edema development in TBI patients with the advantage that it is non-invasive and avoids a subjective diagnostic image evaluation. Because of the high correlation between the AC volume and patient state, it may also be used as an additional tool in initial patient evaluation in long-distance consultations as well as one of the indicators for implementing surgical treatment (6, 10–13).

Conflict of interest statement We declare that we have no conflict of interest.

References

- Børgeesen SE, Albeck MJ, Gjerris F, Czosnyka M, Laniewski P (1992) Computerized infusion test compared to steady pressure constant infusion test in measurement of resistance to CSF outflow. *Acta Neurochir (Wien)* 119(1–4):12–16
- Cremer OL, van Dijk GW, van Wensen E, Brekelmans GJ, Moons KG, Leenen LP, Kalkman CJ (2005) Effect of intracranial pressure monitoring and targeted intensive care on functional outcome after severe head injury. *Crit Care Med* 33(10):2207–2213
- Czernicki Z, Berdyga J, Stepińska G, Jurkiewicz J (1995) Evaluation of craniospinal system condition using standardized volume-pressure loadings. *Acta Neurochir (Wien)* 133(3–4):191–194
- Czernicki Z, Walecki J (1990) Evaluation of oedema spreading and intracranial volume reserve using CT image numerical analysis. *Acta Neurochir Suppl (Wien)* 51:407–408
- Czernicki Z, Walecki J, Jurkiewicz J, Grochowski W, Tychmanowicz K (1992) Intracranial volume reserve determination using CT images, numerical analysis and lumbar infusion tests. An experimental study. *Acta Neurochir (Wien)* 115(1–2):43–46
- Czernicki Z, Glowacki M, Walecki J, Jurkiewicz J, Walasek N (2007) Optimization of the neurosurgical care – a multicentre telemedical project. In: International Proceedings, reprinted from 13th European Congress of Neurosurgery, Glasgow, September, 2–7, 719–722
- Czosnyka M, Pickard JD (2004) Monitoring and interpretation of intracranial pressure. *J Neurol Neurosurg Psychiatry* Jun; 75(6):813–821
- Fountas KN, Sitkauskas A, Feltes CH, Kapsalaki EZ, Dimopoulos VG, Kassam M, Grigorian AA, Robinson JS, Ragauskas A (2005) Is non-invasive monitoring of intracranial pressure waveform analysis possible? Preliminary results of a comparative study of non-invasive vs. invasive intracranial slow-wave waveform analysis monitoring in patients with brain injury. *Med Sci Monit* Feb; 11(2):CR58–CR63
- Geeraerts T, Merceron S, Benhamou D, Vigué B, Duranteau J (2008) Non-invasive assessment of intracranial pressure using ocular sonography in neurocritical care patients. *Intensive Care Med* Nov 34(11). [Epub 2008 May 29; 2062–7]
- Głowacki M, Czernicki Z, Jurkiewicz J (2004) Teleconsulting in multidisciplinary approach to the trauma patient. In: Abstracts of the Proceedings of 9th Congress of the Euroacademia Multidisciplinaria Neurotraumatologica, Bucharest, Romania, 19–22 May; *Acta Neurochir (2006)* 148:II
- Głowacki M, Czernicki Z, Jurkiewicz J, Walasek N (2005) Teleradiology in neurosurgery, based on the experience of the Department of Neurosurgery, Polish Academy of Sciences. *Pol J Radiol* 70(4): 27–34
- Głowacki M, Czernicki Z, Mierzejewski M, Jurkiewicz J (2003) Teleconsulting in the Management of Acute Neurotrauma. *Euroacademia Multidisciplinaria Neurotraumatologica* 155:61–67
- Głowacki M (2006) Teleradiology in clinical practice. *Pol J Radiol* 71(4):99–117
- Kosteljanetz M (1987) Intracranial pressure: cerebrospinal fluid dynamics and pressure–volume relations. *Acta Neurol Scand Suppl* 111:1–23
- Kroin JS, Nagalla SK, Buvanendran A, McCarthy RJ, Tuman KJ, Ivankovich AD (2002) The mechanisms of intracranial pressure modulation by epidural blood and other injectates in a postdural puncture rat model. *Anesth Analg* Aug; 95(2): 423–429
- Louis PT, Goddard-Finegold J, Fishman MA, Griggs JR, Stein F, Laurent JP (1993) Barbiturates and hyperventilation during intracranial hypertension. *Crit Care Med* Aug; 21(8):1200–1206
- Mauritz W, Steltzer H, Bauer P, Dolanski-Aghamanoukjan L, Metnitz P (2008) Monitoring of intracranial pressure in patients with severe traumatic brain injury: an Austrian prospective multicenter study. *Intensive Care Med* Jul; 34(7):1208–1215. Epub 2008 Mar 26
- Narayan RR (1994) Intracranial pressure and CT. *J Neurosurg* Nov; 81(5):810–811
- Ng SC, Poon WS, Chan MT (2005) Cerebral haemodynamic assessment in patients with thalamic haemorrhage: a pilot study with continuous compliance monitoring. *Acta Neurochir Suppl* 95:299–301
- Shafi S, Diaz-Arrastia R, Madden C, Gentilello L (2008) Intracranial pressure monitoring in brain-injured patients is associated with worsening of survival. *J Trauma* Feb; 64(2):335–340
- Styrke J, Stålnacke BM, Sojka P, Björnstig U (2007) Traumatic brain injuries in a well-defined population: epidemiological aspects and severity. *J Neurotrauma* Sep; 24(9):1425–1436
- Sullivan HG, Miller JD, Becker DP, Flora RE, Allen GA (1977) The physiological basis of intracranial pressure change with progressive epidural brain compression. An experimental evaluation in cats. *J Neurosurg* Oct; 47(4):532–550
- Ueno T, Macias BR, Yost WT, Hargens AR (2005) Noninvasive assessment of intracranial pressure waveforms by using pulsed phase lock loop technology. Technical note. *J Neurosurg* Aug; 103(2):361–367
- Zwetnow NN, Schrader H, Löfgren J (1986) Effects of continuously expanding intracranial lesions on vital physiological parameters. An experimental animal study. *Acta Neurochir (Wien)* 80(1–2):47–56

Is Neuroradiological Imaging Sufficient for Exclusion of Intracranial Hypertension in Children? Intracranial Hypertension Syndrome Without Evident Radiological Symptoms

Dawid Larysz, Patrycja Larysz, Andrzej Klimczak, and Marek Mandera

Abstract There are still many important questions about algorithms and clinical scenarios in the context of children with clinical intracranial hypertension symptoms (IHS) without radiological findings. Such conditions could appear in different clinical situations, including slit ventricle syndrome, overdrainage syndrome, normal volume hydrocephalus, or idiopathic intracranial hypertension. Many articles have defined specific treatment strategies for various forms of IHS, including ventriculoperitoneal shunting, medication for shunt-related migraine, steroids, and valve upgrades with antisiphoning devices or programmable systems. This study is an attempt to define the proper diagnostic procedures and treatment options for patients with various forms of IHS without evident neuroradiological findings. The authors discuss possible pathological mechanisms leading to IHS in the pediatric population. The authors present six children treated in their center. All of the children presented clinical manifestation of intracranial hypertension without evident neuroradiological findings in CT and/or MRI examinations. In three cases, the final diagnosis was slit ventricle syndrome; in two cases, normal volume hydrocephalus; in another case, idiopathic intracranial hypertension. The treatment options included short-term steroid (dexamethasone) administration and ventriculoperitoneal shunting using programmable systems. In one case of idiopathic intracranial hypertension, ICP monitoring was also performed. The authors discuss possible diagnostic and treatment strategies for the aforementioned cases. There are still many controversies about management of children with clinical symptoms of intracranial hypertension that are not confirmed in neuroimaging. It seems that our understanding of intracranial hypertension in the pediatric population is not nearly as sophisticated or complete as we might have imagined. Ventriculoperitoneal shunting with antisiphoning devices and/or short-term dexamethasone administration seem to be the best treatment options in these cases.

D. Larysz (✉) and P. Larysz,
Division of Pediatric Neurosurgery, Medical University of Silesia,
Katowice, Ul. Medykow 16, Katowice 40-752, Poland
e-mail: dawilar@poczta.onet.pl

A. Klimczak and M. Mandera
Division of Pediatric Neurosurgery, Medical University of Silesia,
Katowice, Ul. Medykow 16, Katowice 40-752, Poland

Keywords Hydrocephalus • slit ventricle syndrome • children • neuroimaging

Background and Purpose

There are still controversies about diagnostic procedures and therapeutic management of children admitted to hospitals with clinical symptoms of intracranial hypertension syndrome (IHS) but without any, or with very slight, evidence of IHS in neuroimaging. Such conditions could appear in different clinical situations, including slit ventricle syndrome (SVS), overdrainage syndrome, normal volume hydrocephalus, or idiopathic intracranial hypertension. Many articles have defined specific forms of treatment for a variety of specific forms of IHS, including ventriculoperitoneal shunting, medication for shunt-related migraine, and valve upgrades with devices that retard siphoning for overdrainage syndrome (7, 10).

Aim of the Study

This study is an attempt to define the proper diagnostic procedures and treatment options for patients with various forms of IHS without evident neuroradiological findings. The authors discuss possible pathological mechanisms leading to IHS in the pediatric population.

Material

In the last 2 years, seven children were admitted to the Division of Pediatric Neurosurgery, Medical University of Silesia in Katowice with evident clinical symptoms of intracranial hypertension but without, or with only minimal, pathological neuroradiological findings in CT or MRI. The studied group consisted of three girls and four boys. The studied group's characteristics are presented in Table 1.

Case 1

One case was a 14-year-old boy with congenital hydrocephalus. In his first month of life, he was treated by implantation of a VP shunt (medium pressure valve). The postoperative period was without any complications. The boy developed normally, without any psychomotor delays or neurological deficits. He was admitted to our hospital due to a history of 2 weeks of morning headaches with vomiting. The pediatric examination did not reveal any symptoms of infection or any other

pathological symptoms except mild bradycardia. In the examination, we did not find any neurological deficits. Episodes of intense headaches with vomiting had been repeated a few times a day. CT examination revealed normal-sized, thin, symmetrical ventricles. A ventricular catheter was located within the frontal horn of the left lateral ventricle. The examination did not reveal any pathological findings (Fig. 1a, b).

The boy was admitted to the hospital for clinical observation. Because of increasing headaches, he had another CT examination 3 days later (Fig. 1c, d). In this CT scan, we saw, once again, normal-sized, thin, symmetrical ventricles but, compared to the previous CT, the ventricles had become slightly wider.

The diagnosis was slit ventricle syndrome with proximal catheter dysfunction, and the boy was operated on. Reimplantation of the intraventricular catheter and reimplantation of the valve mechanism (flow-regulated valve) were performed. After surgery, we noted a quick regression of headaches and vomiting. In the neurological examination, the boy was without any symptoms of intracranial hypertension. A control CT examination revealed a normal postoperative image of the brain (Fig. 2).

Table 1 Studied group characteristics

Child	Age (years)	Diagnosis
1	3.5	Slit ventricle syndrome
2	3	Slit ventricle syndrome
3	4	Slit ventricle syndrome
4	14	Normal volume hydrocephalus
5	6	Normal volume hydrocephalus
6	16	Idiopathic intracranial hypertension
7	7	Overdrainage syndrome

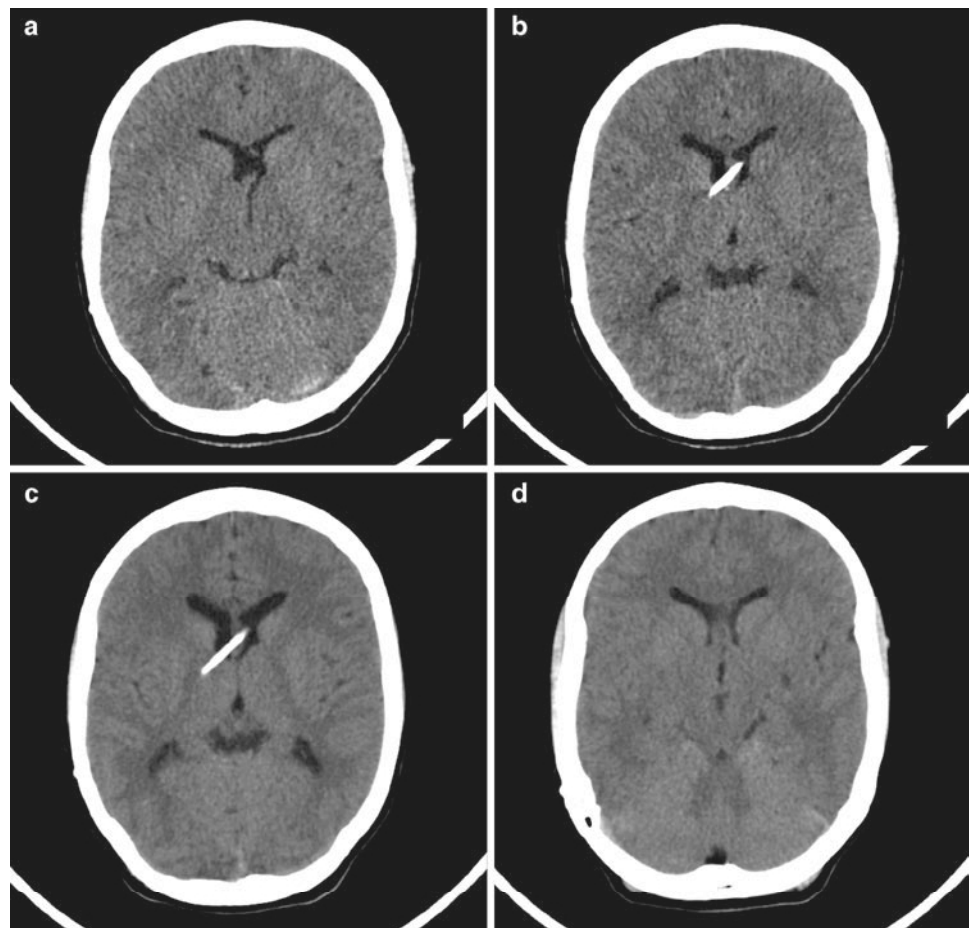


Fig. 1 Case 1. (a) and (b) CT examination on admission. (c) and (d) CT examination 3 days later (note widening of frontal horns)

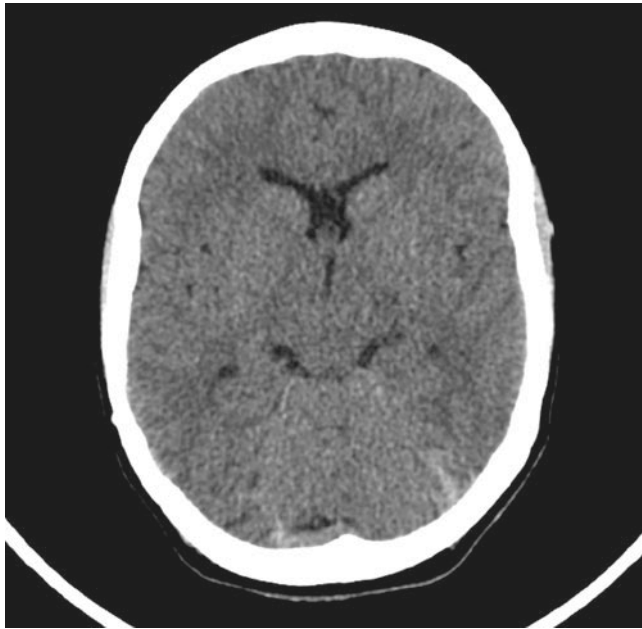


Fig. 2 Case 1. Control CT examination

Case 2

Another case was a 4-year-old girl with congenital hydrocephalus. In her first month of life, she was treated by ETV and then, because of progression of hydrocephalus despite ETV, by implantation of a VP shunt (medium pressure valve) in the second month of life (Fig. 3a, b).

The postoperative period was without any complications. After the surgery, the girl was without symptoms of intracranial hypertension for 3 years. The girl developed with only mild psychomotor delays and without neurological deficits. At the age of three, the child developed recurrent episodes of headaches, vomiting, and drowsiness. She was admitted to our hospital without any neurological deficits. The pediatric examination did not reveal symptoms of infection. CT and MRI scanning revealed a very narrow ventricular system with proper positioning of the ventricular catheter within the frontal horn of the left lateral ventricle (Figs. 3c, d and 4a, b).

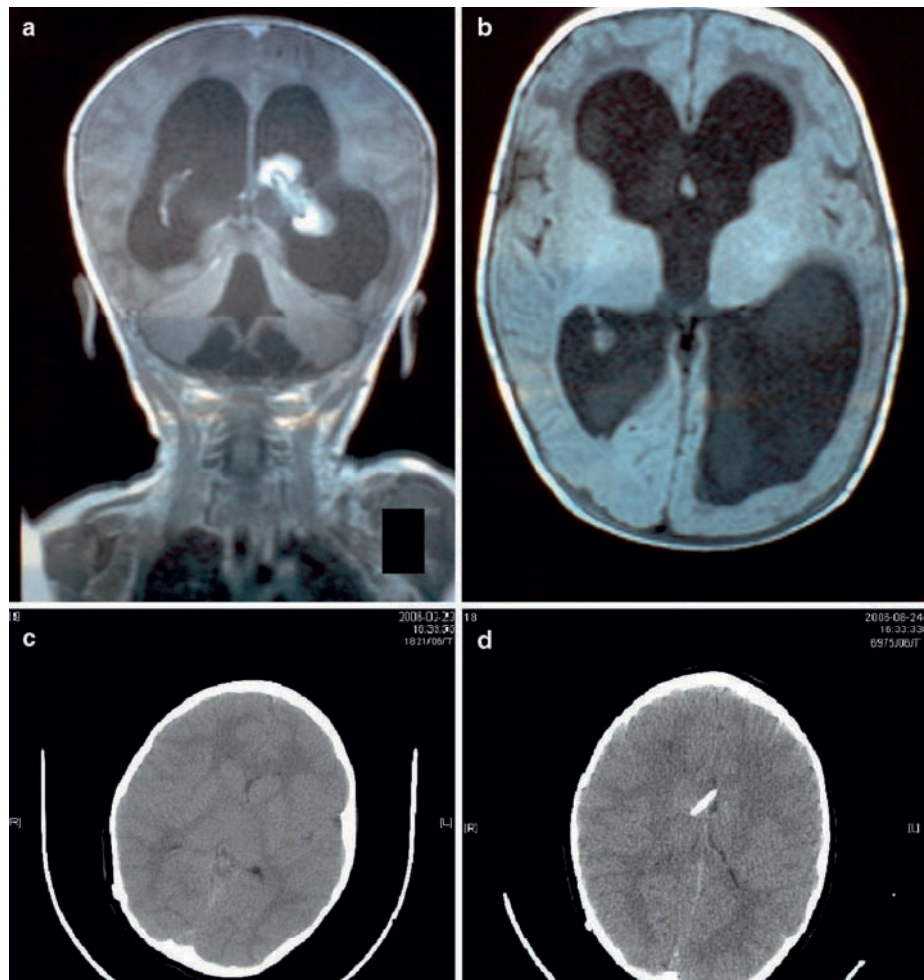
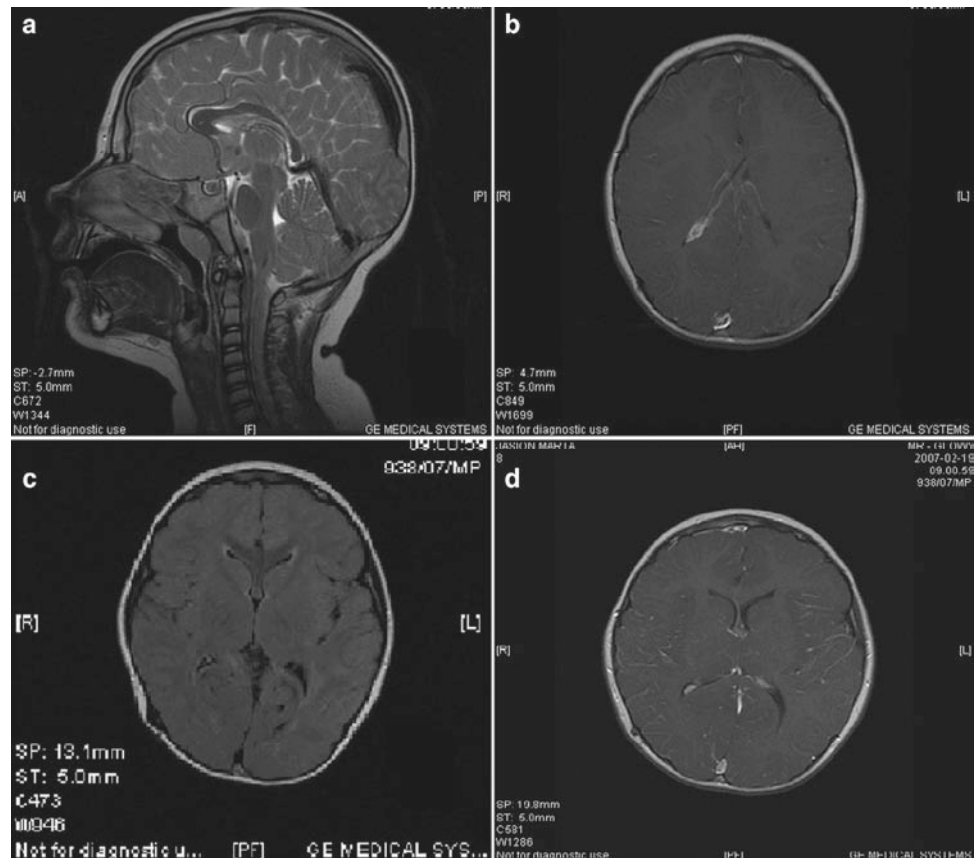


Fig. 3 Case 2. (a) and (b) Congenital hydrocephalus. MRI examination before treatment. (c) and (d) CT examination during headaches

Fig. 4 Case 2. (a) and (b) MRI examination during headaches. (c) and (d) MRI examination after the surgery



The diagnosis was slit ventricle syndrome, and the girl was operated on. Reimplantation of the valve mechanism (flow-regulated valve) was performed. After surgery, MRI revealed slight enlargement of ventricular width (Fig. 4c, d). Clinically, we noted a quick regression of headaches and vomiting. In the neurological examination, the girl was without any symptoms of intracranial hypertension. The girl is now 12 months after surgery and remains without any complaints.

Case 3

Yet another case was a 16-year-old girl with a 1-month history of headaches and progressive blurred vision with narrowing of the visual field. In the ophthalmological examination, significant bilateral papilledema was found with narrowing of the visual field and improper visual acuity. In the clinical examination, the girl was obese, with arterial hypertension and hypercholesterolemia. The cardiologic examination did not reveal any heart disease. After 1 week, we noted further progression of visual deficits. Lumbar puncture was performed. We found significant CSF hypertension

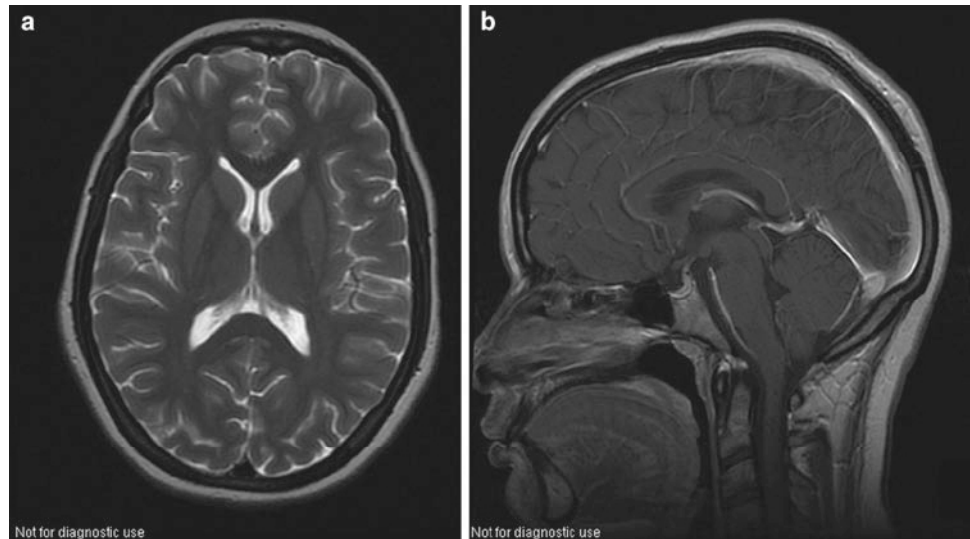
(over 200 mm H₂O). MRI did not divulge any pathological findings (Fig. 5).

The diagnosis was idiopathic intracranial hypertension. The girl was treated with acetazolamide and dexamethasone. Unfortunately, we did not obtain any positive effects. After 1 week of treatment, the girl could only see contours of moving objects. An MRI was performed once more and, again, showed no pathological findings. We decided to implant an intraparenchymal intracranial pressure (ICP) sensor. We noted ICP values of approximately 50–80 mm Hg, because of which, implantation of a VP shunt (programmable valve 130–150 mm Hg) was performed. After surgery, gradual clinical improvement occurred. At present, the girl is able to read and has proper visual acuity; however, improper vision of the color green is still present.

Discussion

Shunt malfunctions are manifested clinically by symptoms of increased intracranial pressure. On imaging studies, they are typically manifested by increasing ventricular size. However, shunted hydrocephalic patients may become symptomatic from

Fig. 5 Case 3. MRI examination on admission



shunt failure without evidence of ventricular enlargement on CT or MRI (10, 11). One of the possibilities of intracranial hypertension syndrome without any neuroradiological findings is the so-called slit ventricle syndrome. SVS is a condition in which the clinical picture is one of acute or semi-acute headache, nausea, vomiting, and/or lethargy. The headaches could be episodic, typically presenting as pressure waves, often terminating in vomiting or hyperventilation, and are sometimes associated with bradycardia and systemic hypertension (7, 10, 11). ReKate divided SVS into five groups of patients: those with (1) extreme low pressure headaches, probably from siphoning of CSF from the brain by the shunt, (2) intermittent obstruction of the proximal shunt catheter, (3) normal volume hydrocephalus with diminished buffering capacity of the CSF, (4) intracranial hypertension associated with working shunts, and (5) headaches (in shunted children) unrelated to intracranial pressure or shunt function (10, 11). It has been postulated that shunt-induced suture ossification may cause slit ventricle syndrome. The mechanism described is that chronic overdrainage of cerebrospinal fluid via the shunt dampens the normal cerebral pressure waves and growth of the calvarium is thus understimulated, leading to ossification of the sutures (1). These observations have led a number of investigators to propose physically increasing the size available to the brain, and improvements after subtemporal decompression and cranial expansion operations have been reported (1, 6). It is very important to realize that the presence of small ventricles after placement of a VP shunt with proper positioning of ventricular catheter is not diagnostic for exclusion of IHS. Proper treatment options in most cases of SVS include implantation of antisiphoning devices and/or reimplantation of a shunt system with application of programmable valve (7, 9, 10). In some cases, short-term dexamethasone administration is a

non-surgical option as a first line of treatment. Treatment with dexamethasone can serve as a prompt way of lowering the intracranial pressure as a temporary measure until a decision regarding the surgical procedure with optimal timing can be made (7). Subtemporal decompression and other alternatives designed to increase the volume of the skull are often considered by parents as being “aggressive,” and these approaches are not always effective (2, 4). Another possibility of intracranial hypertension syndrome without any neuroradiological findings is idiopathic intracranial hypertension, also known as pseudotumour cerebri. This rare condition is presented by all of the signs and symptoms of raised intracranial pressure with headache, papilledema, and a decline in visual acuity being among the most common symptoms in children with idiopathic intracranial hypertension. The ventricles are of normal size but the CSF pressure is raised. Diagnosis is made from a description of the patient’s medical history, an ophthalmology assessment, normal CT and MRI scans, and a lumbar puncture that demonstrates a raised CSF pressure. Treatment options include medical therapies such as acetazolamide and/or dexamethasone. Drainage of CSF, either intermittently with serial lumbar punctures or continuously by placement of a ventriculoperitoneal shunt (if ventricular size permits), may be required when medical therapy fails (3, 5, 8).

Conclusions

There are still many important questions concerning algorithms and clinical scenarios in the context of children with clinical intracranial hypertension symptoms without radiological findings. It seems that our understanding of intracranial

hypertension in the pediatric population is not sufficient. Ventriculoperitoneal shunting with antisiphoning devices and/or short-term dexamethasone administration seem to be the best treatment options in these cases.

Conflict of interest statement WAcKe declare that we have no conflict of interest.

References

1. Albright AL, Tyler-Kabara E (2001) Slit-ventricle syndrome secondary to shunt-induced suture ossification. *Neurosurgery* 48:764–769
2. Buxton N, Punt J (1999) Subtemporal decompression: the treatment of noncompliant ventricle syndrome. *Neurosurgery* 44: 513–519
3. Choux M, Di Rocco C, Hockley A, Walker M (eds) (1999) *Pediatric neurosurgery*. Churchill Livingstone, London, pp 229–230
4. Cohen SR, Dauser RC, Newman MH, Muraszko K (1993) Surgical techniques of cranial vault expansion for increases in intracranial pressure in older children. *J Craniofac Surg* 4:167–176
5. Drake J, Sainte-Rose C (1995) *The shunt book*. Blackwell, Cambridge, MA
6. Epstein F, Lapras C, Wisoff JH (1988) ‘Slit-ventricle syndrome’: etiology and treatment. *Pediatr Neurosci* 14:5–10
7. Fattal-Valevski A, Beni-Adani L, Constantini S (2005) Short-term dexamethasone treatment for symptomatic slit ventricle syndrome. *Childs Nerv Syst* 21:981–984
8. Fishman RA (1984) The pathophysiology of pseudotumor cerebri. *Arch Neurol* 41:257–258
9. Jain H, Sgouros S, Walsh AR, Hockley AD (2000) The treatment of infantile hydrocephalus: “differential-pressure” or “flow-control valves”. A pilot study. *Childs Nerv Syst* 16:242–246
10. ReKate HL (2004) The slit ventricle syndrome: advances based on technology and understanding. *Pediatr Neurosurg* 40:259–263
11. ReKate HL (1993) Classification of slit-ventricle syndrome using intracranial pressure monitoring. *Pediatr Neurosurg* 19:15–20

Part VI
Trauma and Brain Tissue Injury

Substance P Immunoreactivity Increases Following Human Traumatic Brain Injury

Andrew C. Zacest, Robert Vink, Jim Manavis, Ghafar T. Sarvestani, and Peter C. Blumbergs

Abstract Recent experimental evidence suggests that neuropeptides, and in particular substance P (SP), are released following traumatic brain injury (TBI) and may play a significant role in the aetiology of cerebral edema and increased intracranial pressure. Whether SP may play a similar role in clinical TBI remains unknown and was investigated in the current study. Archival post-mortem material was selected from patients who had sustained TBI, had died and had undergone post-mortem and detailed neuropathological examination (n=13). A second cohort of patients who had died, but who showed no neuropathological abnormality (n=10), served as case controls. Changes in SP immunoreactivity were examined in the cerebral cortex directly beneath the subdural haematoma in 7 TBI cases and in proximity to contusions in the other 6 cases. Increased SP perivascular immunoreactivity was observed after TBI in 10/13 cases, cortical neurones in 12/13 and astrocytes in 10/13 cases. Perivascular axonal injury was observed by amyloid precursor protein (APP) immunoreactivity in 6/13 TBI cases. Co-localization of SP and APP in a small subset of perivascular fibres suggests perivascular axonal injury could be a mechanism of release of this neuropeptide. The abundance of SP fibres around the human cerebral microvasculature, particularly post capillary venules, together

with the changes observed following TBI in perivascular axons, cortical neurones and astrocytes suggest a potentially important role for substance P in neurogenic inflammation following human TBI.

Keywords Neurotrauma • edema • brain swelling • neurogenic inflammation • tachykinin • substance P

Introduction

A number of studies have now demonstrated that much of the mortality and morbidity in survivors following traumatic brain injury (TBI) is associated with the development of a secondary injury cascade that occurs between hours and days after the insult (23). While a number of factors have been identified as participating in this secondary injury, it has been recognised that edema formation is a critical determinant of outcome after TBI. Our recent experimental studies have shown that neurogenic inflammation may play an important role in edema formation following CNS insults (9,21,26).

Neurogenic inflammation is a neurally elicited reaction that has typical characteristics of an inflammatory reaction including vasodilation, protein extravasation and tissue swelling. Studies of peripheral nerves have demonstrated that neurogenic inflammation is the result of the stimulation of C-fibres, which causes the release of neuropeptides (1). These neuropeptides cause plasma protein extravasation from blood vessels and associated edema formation. Although a number of neuropeptides have been implicated in this process, it is generally accepted that substance P (SP) increases microvascular permeability leading to edema formation whilst calcitonin gene related peptide (CGRP) is an extremely potent vasodilator (17). Substance P has been shown to be primarily associated with the formation of vasogenic edema by numerous potential interactions with target cells that produce vasoactive mediators (20,22), and with the endothelium (19,28) which leads to changes in vascular ultrastructure (8,11).

R. Vink (✉), P.C. Blumbergs
Discipline of Pathology, School of Medical Sciences, University of Adelaide, Adelaide, SA 5005, Australia and Hanson Institute Center for Neurological Diseases, Institute of Medical and Veterinary Sciences, Adelaide, SA 5000, Australia
e-mail: Robert.Vink@adelaide.edu.au

A.C. Zacest
Disciplines of Pathology, University of Adelaide, South Australia 5005, Australia

J. Manavis
Hanson Institute Centre for Neurological Diseases, Institute of Medical and Veterinary Sciences, Adelaide, SA 5000, Australia

G.T. Sarvestani
Division of Haematology, Institute of Medical and Veterinary Sciences, Adelaide, SA 5000, Australia

Although traditionally known to be involved in nociception and neurogenic inflammation, recent work has suggested additional potentially important roles for SP and neurokinin antagonists in ischaemic neurological injury (5,25), apoptosis (6), epilepsy (16,27), the glial response to injury (15,18) and cerebral edema (9,21). Given that all of these pathologies may occur to a varying extent following human TBI, the potential for neuroprotection against several types of secondary injury with neurokinin antagonists would seem to be promising. In light of the above findings, we sought to determine whether SP might have a role in human TBI by characterising the SP immunoreactivity of the nerve fibres in the cerebral cortex, around cerebral vessels of the microvasculature, in white matter and in the spinal trigeminal tract of the caudal medulla, in victims of TBI versus age-matched controls.

Materials and Methods

Case Selection

Archival post mortem material was selected from patients who had sustained head injuries, had died and had undergone post mortem and detailed neuropathological examination (n=13). A second cohort of patients with a known past medical history of epilepsy, who had died but showed no neuropathological abnormality in subsequent post mortem examination (n=10), served as case controls for the purpose of this study. Cases were age-matched (2–86 years of age) but could not always be sex-matched. The 13 cases of fatal TBI had survival times ranging from instant death to 1 week survival, and showed a heterogeneous mixture of different cellular lesions at different stages of evolution including contusions (9/13), acute sudural haematomas (7/13), subarachnoid haemorrhage (7/13), hypoxic–ischemic encephalopathy (4/13), and increases of intracranial pressure (9/13). For all cases the cerebral cortex was sampled, and in the TBI cases this was directly beneath existing ASDHs in 7 cases and in proximity to contusions in the remaining 6 cases. The spinal trigeminal tract of the caudal medulla was also examined because of its intense SP immunoreactivity in mammals and humans (4,7). A level between the inferior olivary nucleus and commencement of the cervical cord was selected.

Immunohistochemistry

Wax blocks containing sections of medulla and cortex were selected from the human archival material for sectioning.

Sections of 5 μm thickness were cut by tissue microtome, picked up onto APT coated slides and routinely stained for haematoxylin and eosin (H&E), and immunolabelled with amyloid precursor protein (APP) (Chemicon, clone 22C11; 1:10,000) or a goat polyclonal antibody directed against substance P (Santa Cruz; 1:2,000). For double immunolabelling, sections were also labelled with a rabbit polyclonal antibody directed against glial fibrillary acidic protein (GFAP) (Dako Cytomation; 1:20,000), a well established marker for astrocytes (10), or a mouse monoclonal antibody directed against protein gene product (PGP) 9.5 (Ultraclone; 1:20,000), primarily as a marker for nerve fibres (24). APP was used as a marker for injured axons (2). Sections were immersed in 0.3% H_2O_2 /methanol for 30 min then washed in PBS. Those with prominent formalin pigment staining were treated with picric acid solution for 15 min prior to immersion in methanol. Heat induced antigen retrieval was then performed using either citrate buffer (pH 6.0) for APP, GFAP and PGP 9.5, or EDTA (pH 8.0) for substance P. Sections were washed in PBS and blocked in normal horse serum (NHS/PBS pH 7.40) for 30 min, then incubated with the primary antibody overnight. After washing in PBS, sections were incubated with biotin-conjugated secondary antibodies for 30 min (Vector Laboratories) washed in PBS followed by 1-h incubation with a streptavidin–peroxidase conjugate (Pierce Laboratories). Immunoreactivity was visualised using diaminobenzidine–hydrogen peroxide reaction. Sections were then counterstained with haematoxylin, dehydrated, cleared, and mounted.

For confocal microscopy, 10 μm thick paraffin sections from selected cases were examined using double immunofluorescent staining with the substance P antibody (1:200) plus PGP 9.5 (1:2000), APP (1:200) and GFAP (1:2000), respectively. Sections were incubated overnight in the primary antibodies, then secondary antibodies for 1 h. Secondary antibodies used were an Alexa Fluor 546 donkey anti goat (Molecular Probes) for the substance P, Alexa Fluor 488 donkey anti rabbit for GFAP (Molecular Probes), and Cy5 donkey anti mouse (Jackson ImmunoResearch) for the PGP 9.5 and APP. After washing in PBS, slides were mounted using an aqueous mounting solution with antifade and sealed using varnish. Positive and negative controls were routinely used for all antibodies. Sections were examined using a confocal fluorescence microscope (BioRad Radiance 2100).

Tissue Analysis

H&E analysis was important in the identification of haemorrhage and neuronal red cell change. APP immunostaining was used to characterise axonal injury by the presence of

axonal swellings and retraction balls, particularly in perivascular nerve fibres. SP immunostaining was used to observe patterns of SP staining and also in conjunction with double immunolabelling for PGP 9.5, APP and GFAP to positively identify the anatomical distribution of SP in perivascular nerve fibres, injured axons and astrocytes in normal and post traumatic tissue. To control for variability of immunostaining including background staining that might confound comparative tissue analysis, immunostaining of all final data sets was performed in one sitting.

Confocal Microscopy

Confocal images were produced using the BioRad Radiance 2100 confocal microscope (BioRad Microscience Ltd, UK) equipped with three lasers: Argon ion 488 nm (14 mw); Green HeNe 543 nm (1.5 mw); Red Diode 637 nm (5 mw) outputs, and an Olympus IX70 inverted microscope. The objective used was a 10–60× UPLAPO with NA=1.4 oil. The dual labelled cells were imaged with two separate channels in a sequential setting. The FITC was excited with an Ar

488 nm laser and the emission was viewed through an HQ515/30 nm narrow band filter in PMT1. The Cy5 was excited with Green HeNe 543 nm laser light and the emission was viewed through a long pass barrier (E600LP) to allow only far red light wavelengths longer than 600 nm to pass through PMT2. Automatically all signals from PMTs 1 and 2 were merged. The imaged data were stored on a CD for further analysis using a confocal assistant software program for Microsoft Windows (Todd Clark Brelje, USA).

Results

SP Immunoreactivity in Control Cases

Prominent SP staining of human cerebral cortical pyramidal cells and to a lesser extent other cortical neurones was observed in control cases of all ages (Fig. 1a). An extensive perivascular distribution of SP nerve endings could also be demonstrated in the cerebral cortical microvasculature, and this was confirmed with confocal analysis (PGP 9.5 and SP).

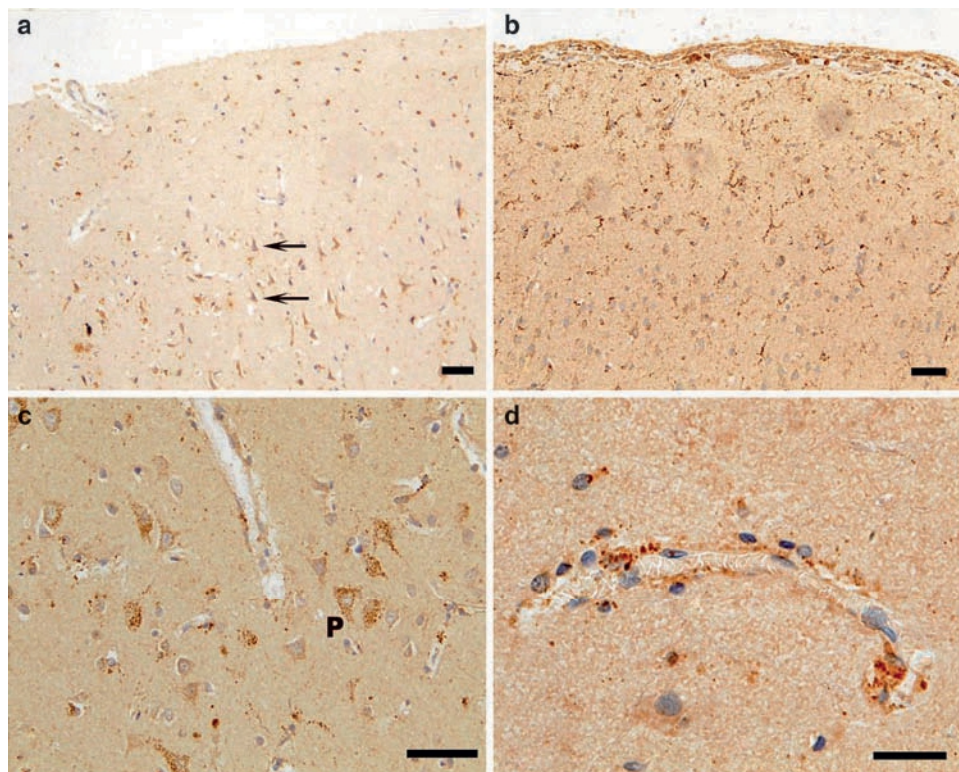


Fig. 1 Alterations in SP immunoreactivity after TBI; SP immunostain, haematoxylin counterstain. (a) Frontal cortex from a control case showing SP immunoreactivity (arrows) of some of the cortical neurones. (b) Prominent SP immunostaining in the frontal cortex of a 23 year-old with cerebral contusion who survived 6 days. (c) Frontal cortex underlying

acute subdural haematoma in a 41 year-old man who survived 1 day showing prominent SP immunostaining of cortical neurones (labelled as P). (d) Cortical venule showing perivascular SP immunoreactivity in a 21 year-old man with an acute subdural haematoma who died at the roadside (Bar=50 μm)

Human perivascular astrocytes in control cases exhibited no colocalisation of GFAP with SP on confocal analysis. SP could not be identified in human endothelial cells of the microvasculature. The spinal trigeminal tract and nucleus was examined between the closure of the fourth ventricle and the commencement of the dorsal horns of the cervical spinal cord. At this level the tract assumed a characteristic bilateral crescent morphology as the intensely immunostained end fibres of the tract with varicose terminals encircled the spinal nucleus. Neurones of the spinal nucleus caudalis were unstained as were surrounding blood vessels.

Changes in SP Immunoreactivity Following TBI

Cortical SP immunoreactivity increased after trauma (Fig. 1b), although there was clear heterogeneity within the trauma population. SP immunoreactivity was increased in cortical pyramidal neurones early after injury in 12/13 trauma cases compared to controls (Fig. 1c). Increased SP perivascular immunoreactivity was also observed after TBI in 10/13 cases (Fig. 1d). Such SP immunoreactivity was often co-localised with neuronal PGP 9.5 (Fig. 2a–c), with only small foci of colocalisation of SP and GFAP on reactive astrocytes (Fig. 2d–f). Nonetheless, there was overall increased SP staining of glial cells in 10/13 cases following injury, particularly after several days. We also noted the regular presence of SP positive polymorphonuclear leukocytes, which were located within the lumen, on the endothelium and in the perivascular spaces in the human trauma material. No specific changes in SP immunoreactivity could be identified in the trigeminal tract or nucleus following injury. APP positive cortical perivascular nerve fibres were identified in 6/13 traumatic cases, although only a small subset of vessels showed this abnormality. Confocal analysis confirmed that a subset of APP immunopositive perivascular fibres also contained SP (Fig. 2g–i).

Discussion

Recent experimental work has suggested an important role for tachykinins in blood brain barrier permeability following ischaemic (25,26) and post-traumatic cerebral injury (9,21). In the present study extensive cortical neuronal staining of SP was observed and increased immediately following clinical TBI. Similar changes in neuronal SP immunoreactivity have been previously observed in experimental TBI (9) as well as experimental ischemia (25), where increased SP immunoreactivity in lamina II,III and V pyramidal neurones of rodent cortex in the ischaemic penumbra was noted following MCA

occlusion. SP has also been implicated in the gliotic response following nerve injury and inflammatory processes in the CNS (13,14). In the present study, although SP immunostaining of astrocytes was present in 10/13 cases, confocal colocalisation of SP with GFAP was only demonstrated in 1/3 cases suggesting that SP might be bound to a surface receptor, possibly the neurokinin 1 receptor to which SP preferentially binds.

Perivascular nerve fibres may be the source of SP released and measurable in peripheral blood following clinical cerebral ischaemia. Consistent with this, Bruno et al. (5) showed serum SP levels were elevated at 12 h following the clinical onset of cerebral ischaemia. Ischaemic brain injury, as defined by neuronal red cell change, was present in the current study in 8/13 cases. The subsequent observation of a subset of APP positive SP containing perivascular fibres and increased SP perivascular profiles following TBI in this study demonstrates that perivascular SP fibres are injured in human TBI and could be a source of released and potentially vasoactive neuropeptide. We hypothesise that APP positive nerve fibres may be an indication of post traumatic vascular “deafferentation”, which might be important in the disturbance of autoregulation of the cerebral microvasculature following trauma. It may also potentially result in nociceptor sensitisation following TBI, which may be important in post traumatic headache. The dramatic changes in SP immunoreactivity around cortical blood vessels contrasted markedly with those observed at the central end of the SP containing nerve fibres in the caudal medulla of our cases. These observations strongly suggest that in human traumatic brain injury, SP is more likely to be released from the peripheral terminal ends of the trigeminovascular system, which is congruous with previous data demonstrating that four times as much neuropeptide is transported peripherally than centrally (3).

Hokfelt (12) originally described “substance P containing nerve endings” in human cerebral cortex but did not identify them as perivascular fibres. One important observation from the present study was of the extensive perivascular SP positive nerve fibres involving the cerebral cortical microvasculature and absence of SP immunoreactivity from the human microvasculature endothelium. This is of particular relevance to the study of human TBI because of the involvement of the microvasculature in TBI. While our results do not allow us to make definite conclusions regarding a role for neuropeptides in the development of cerebral edema secondary to neurogenic inflammation, they demonstrate an abundant innervation of the cerebral microvasculature, particularly post capillary venules with SP fibres, and support the potential for a critical role in post-traumatic edema as previously shown in experimental TBI studies (21).

In conclusion, this study has characterised cortical perivascular changes in SP immunoreactivity that occur following human TBI. Our findings suggest that SP is present in perivascular axons of the cerebral microvasculature, is

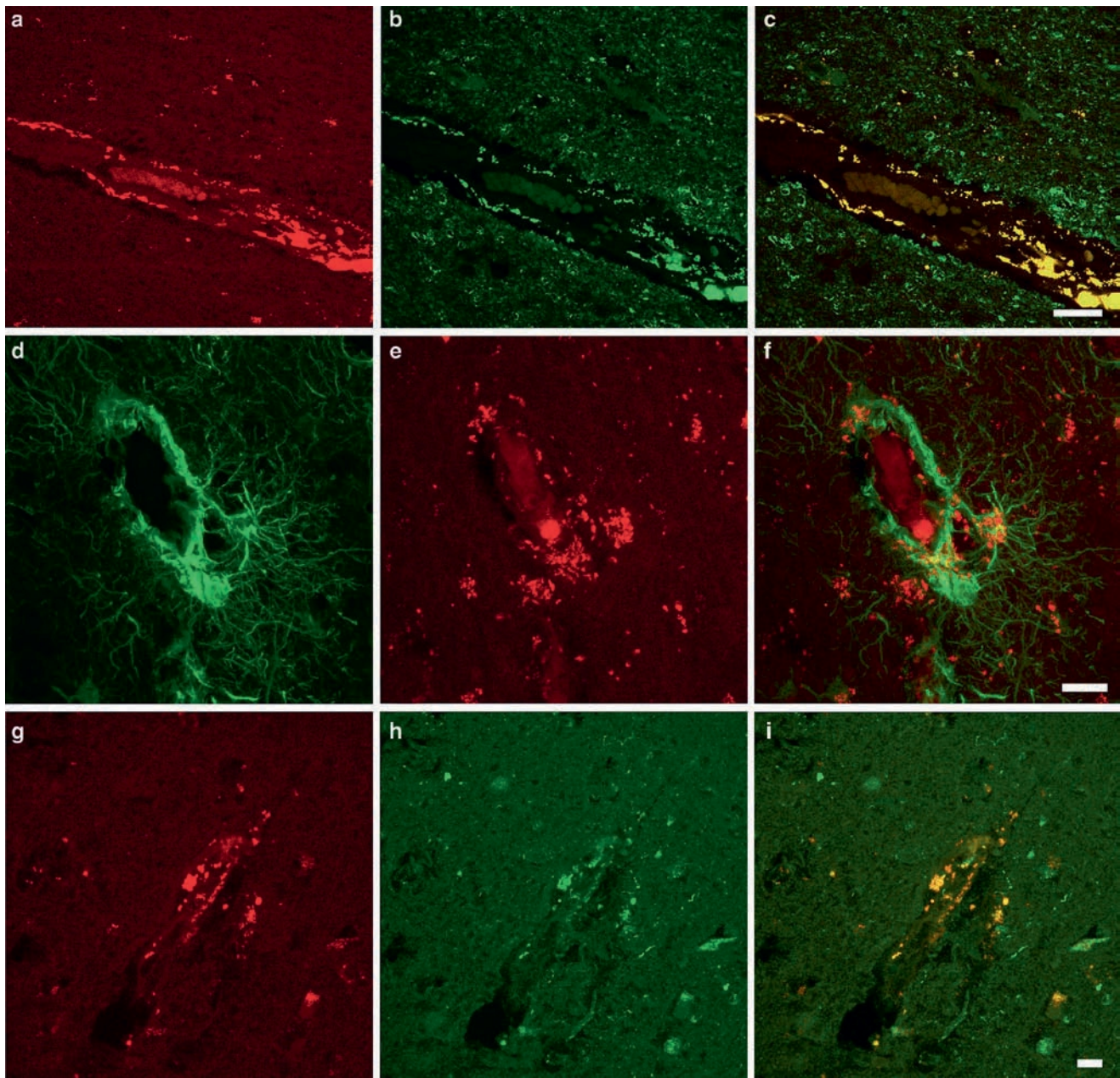


Fig. 2 Colocalisation of SP with neuronal PGP 9.5, astrocytic GFAP and APP. (a–c) *Confocal images* of a human cortical venule showing (a) red neuronal PGP 9.5, (b) green SP and (c) their colocalisation in yellow. (d–f) *Confocal images* of a human cortical venule showing

(d) glial GFAP, (e) SP, and (f) their lack of colocalisation in most areas. Small foci of yellow colocalisation are present in a few areas. (g–i) *Confocal images* of a human cortical venule showing (g) red APP, (h) green SP and (i) their colocalisation in yellow (Bar=20 μ m)

released early following injury and is markedly upregulated in pyramidal cortical neurones. Mechanical injury and ischaemia may be important variables associated with these changes in immunoreactivity. These observations complement growing evidence in the literature of cerebral neurogenic inflammation in response to noxious stimuli.

Conflict of interest statement We declare that we have no conflict of interest.

Acknowledgment Supported, in part, by the Motor Accident Commission of SA.

References

1. Black PH (2002) Stress and the inflammatory response: a review of neurogenic inflammation. *Brain Behav Immun* 16:622–653
2. Blumbergs PC, Scott G, Manavis J, Wainwright H, Simpson DA, McLean AJ (1995) Topography of axonal injury as defined by amyloid

- precursor protein and the sector scoring method in mild and severe closed head injury. *J Neurotrauma* 12:565–572
3. Brimijoin S, Lundberg JM, Brodin E, Hokfelt T, Nilsson G (1980) Axonal transport of substance P in the vagus and sciatic nerves of the guinea pig. *Brain Res* 191:443–457
 4. Brown JL, Liu H, Maggio JE, Vigna SR, Mantyh PW, Basbaum AI (1995) Morphological characterization of substance P receptor-immunoreactive neurons in the rat spinal cord and trigeminal nucleus caudalis. *J Comp Neurol* 356:327–344
 5. Bruno G, Tega F, Bruno A, Graf U, Corelli F, Molfetta R, Barucco M (2003) The role of substance P in cerebral ischemia. *Int J Immunopathol Pharmacol* 16:67–72
 6. Castro-Obregon S, Del Rio G, Chen SF, Swanson RA, Frankowski H, Rao RV, Stoka V, Vesce S, Nicholls DG, Bredesen DE (2002) A ligand–receptor pair that triggers a non-apoptotic form of programmed cell death. *Cell Death Differ* 9:807–817
 7. Del Fiacco M, Dessi ML, Atzori MG, Levanti MC (1983) Substance P in the human brainstem. Preliminary results of its immunohistochemical localization. *Brain Res* 264:142–147
 8. Dimitriadou V, Buzzi MG, Theoharides TC, Moskowitz MA (1992) Ultrastructural evidence for neurogenically mediated changes in blood vessels of the rat dura mater and tongue following antidromic trigeminal stimulation. *Neuroscience* 48:187–203
 9. Donkin JJ, Turner RJ, Hassan I, Vink R (2007) Substance P in traumatic brain injury. *Prog Brain Res* 161:97–109
 10. Eng LF, Ghirnikar RS, Lee YL (2000) Glial fibrillary acidic protein: GFAP-thirty-one years (1969–2000). *Neurochem Res* 25:1439–1451
 11. Ghabriel MN, Lu MX, Leigh C, Cheung WC, Allt G (1999) Substance P-induced enhanced permeability of dura mater microvessels is accompanied by pronounced ultrastructural changes, but is not dependent on the density of endothelial cell anionic sites. *Acta Neuropathol (Berl)* 97:297–305
 12. Hokfelt T, Meyerson B, Nilsson G, Pernow B, Sachs C (1976) Immunohistochemical evidence for substance P-containing nerve endings in the human cortex. *Brain Res* 104:181–186
 13. Kennedy PG, Rodgers J, Jennings FW, Murray M, Leeman SE, Burke JM (1997) A substance P antagonist, RP-67, 580, ameliorates a mouse meningoencephalitic response to *Trypanosoma brucei*. *Proc Natl Acad Sci USA* 94:4167–4170
 14. Kostyk SK, Kowall NW, Hauser SL (1989) Substance P immunoreactive astrocytes are present in multiple sclerosis plaques. *Brain Res* 504:284–288
 15. Lin RC (1995) Reactive astrocytes express substance-P immunoreactivity in the adult forebrain after injury. *Neuroreport* 7:310–312
 16. Liu H, Mazarati AM, Katsumori H, Sankar R, Wasterlain CG (1999) Substance P is expressed in hippocampal principal neurons during status epilepticus and plays a critical role in the maintenance of status epilepticus. *Proc Natl Acad Sci USA* 96:5286–5291
 17. Maggi CA (1995) Tachykinins and calcitonin gene-related peptide (CGRP) as co-transmitters released from peripheral endings of sensory nerves. *Prog Neurobiol* 45:1–98
 18. Mantyh PW, Johnson DJ, Boehmer CG, Catton MD, Vinters HV, Maggio JE, Too HP, Vigna SR (1989) Substance P receptor binding sites are expressed by glia in vivo after neuronal injury. *Proc Natl Acad Sci USA* 86:5193–5197
 19. Nakagawa N, Sano H, Iwamoto I (1995) Substance P induces the expression of intercellular adhesion molecule-1 on vascular endothelial cells and enhances neutrophil transendothelial migration. *Peptides* 16:721–725
 20. Newbold P, Brain SD (1995) An investigation into the mechanism of capsaicin-induced oedema in rabbit skin. *Br J Pharmacol* 114:570–577
 21. Nimmo AJ, Cernak I, Heath DL, Hu X, Bennett CJ, Vink R (2004) Neurogenic inflammation is associated with development of edema and functional deficits following traumatic brain injury in rats. *Neuropeptides* 38:40–47
 22. Ohlen A, Thureson-Klein A, Lindbom L, Persson MG, Hedqvist P (1989) Substance P activates leukocytes and platelets in rabbit microvessels. *Blood Vessels* 26:84–94
 23. Reilly PL (2001) Brain injury: the pathophysiology of the first hours. ‘Talk and Die revisited’. *J Clin Neurosci* 8:398–403
 24. Stjernholm Y, Sennstrom M, Granstrom L, Ekman G, Johansson O (1999) Protein gene product 9.5 – immunoreactive nerve fibers and cells in human cervix of late pregnant, postpartal and non-pregnant women. *Acta Obstet Gynecol Scand* 78:299–304
 25. Stumm R, Culmsee C, Schafer MK, Kriegelstein J, Weihe E (2001) Adaptive plasticity in tachykinin and tachykinin receptor expression after focal cerebral ischemia is differentially linked to gabaergic and glutamatergic cerebrocortical circuits and cerebrovascular endothelium. *J Neurosci* 21:798–811
 26. Turner RJ, Blumbergs PC, Sims NR, Helps SC, Rodgers KM, Vink R (2006) Increased substance P immunoreactivity after reversible ischemic stroke. *Acta Neurochir Suppl* 96:263–266
 27. Zachrisson O, Lindfors N, Brene S (1998) A tachykinin NK1 receptor antagonist, CP-122, 721–1, attenuates kainic acid-induced seizure activity. *Brain Res Mol Brain Res* 60:291–295
 28. Ziche M, Morbidelli L, Geppetti P, Maggi CA, Dolara P (1991) Substance P induces migration of capillary endothelial cells: a novel NK-1 selective receptor mediated activity. *Life Sci* 48:PL7–11

Hyperbaric Oxygen Preconditioning Reduces Postoperative Brain Edema and Improves Neurological Outcomes After Surgical Brain Injury

Vikram Jadhav, Robert P. Ostrowski, Wenni Tong, Brenden Matus, Connie Chang, and John H. Zhang

Abstract The present study was designed to examine if hyperbaric oxygen preconditioning (HBO-PC) is neuroprotective in a mouse model of surgical brain injury (SBI). C57BL mice were administered 100% oxygen for 1 h at 2.5 ATA for 5 consecutive days and subjected to SBI on the following day. The HBO-PC+SBI animals were compared to sham and normoxia+SBI groups for brain water content in different brain regions at 24 and 72 h after surgery. Blood–brain barrier (BBB) permeability was evaluated using Evan’s blue dye extravasation at 24 h. Neurological assessment of the animals was done by a blinded observer at 24 and 72 h. The results showed that brain water content was significantly increased in the right (ipsilateral) frontal lobe surrounding the site of resection. This was attenuated by HBO-PC at 24 and 72 h. However, HBO-PC did not have any effect on the increased BBB permeability observed after SBI. Significant neurological deficits were observed after SBI. HBO-PC improved neurological deficits at 72 h on the 21-point sensorimotor scale and at 24 and 72 h on the wire hang and beam balance scoring. In conclusion, HBO-PC attenuates post-operative brain edema and improves neurological outcomes following SBI.

Keywords Hyperbaric oxygen • surgical brain injury • brain edema • neuroprotection

Introduction

Hyperbaric oxygen (HBO) has been shown to protect against different forms of brain injury in various experimental models (8, 9, 11, 12). Recent evidence has shown that HBO is

J.H. Zhang (✉)

Department of Physiology and Pharmacology, Department of Neurosurgery, Department of Anesthesiology, Linda University School of Medicine, Risley Hall, Room 219, Loma Linda, CA 92350, USA
e-mail: johnzhang3910@yahoo.com

V. Jadhav, R. Ostrowski, W. Tong, B. Matus, and C. Chang
Department of Physiology and Pharmacology, Linda University School of Medicine, Risley Hall, Room 219, Loma Linda, CA 92350, USA

also beneficial when used in a preconditioning paradigm (1, 5, 7–10, 12). HBO preconditioning (HBO-PC) has shown to provide neuroprotection against ischemic injuries in the brain and spinal cord as well as brain injuries due to hemorrhagic etiologies. Surgical brain injury (SBI) is the inevitable brain injury to the normal yet susceptible brain that occurs during neurosurgical procedures due to intraoperative hemorrhage, unavoidable incisions to access deeper structures, retraction, and electrocauterization (2–4). SBI is critical in clinical settings as it can contribute to the morbidity and mortality in the form of post-operative complications such as brain edema and blood–brain barrier (BBB) disruption (2–4). Furthermore, it has immense medicolegal implications as the practice of defensive medicine results in excessive expenditure of 120 billion dollars in United States alone (2).

In the present study, we investigated if HBO-PC provided neuroprotection against SBI using a standard mouse model to evaluate post-operative outcomes such as brain edema, blood–brain barrier (BBB) permeability and assessment of neurological status.

Materials and Methods

Surgical Brain Injury Modeling

This protocol was evaluated and approved by the Institutional Animal Care and Use Committee at Loma Linda University, Loma Linda, CA. The mouse model of SBI was used as described before with modifications (6). In brief, following anesthesia with ketamine (100 mg/kg) plus xylazine (10 mg/kg) i.p., a square cranial window (5 mm edge) was drilled such that the left lower corner of the square was at the bregma. The dura was incised and reflected to expose the underlying right frontal lobe. A monopolar electrocautery was used to incise and sever a part of the frontal brain 1 mm lateral of sagittal and 1 mm proximal of coronal sutures in a piecemeal manner progressively from the top (cortex) to the base of the

skull alternating with hemostasis measures using packing and saline irrigation. After confirmation of hemostasis the wound was closed and skin sutured with 3–0 silk (Ethicon) on a reverse cutting needle. Sham surgery includes only craniotomy without any dural incisions. Vital signs and core body temperature were monitored throughout the procedure.

Treatment Groups

C57BL mice were randomly assigned to three groups: sham-operated, Normoxia+SBI, and HBO-PC+SBI. HBO-PC paradigm was as follows: 100% oxygen administered for 1 h at 2.5 ATA for 5 consecutive days based on previously used successful protocols (8). Mice were subjected to SBI the following day.

Brain Water Content

The animals were sacrificed under deep anesthesia at different time points (24 and 72 h) and the brains were divided into frontal ipsilateral, frontal contralateral, parietal ipsilateral, parietal contralateral, brain stem and cerebellum on ice. These parts were weighed immediately (wet weight) and again after drying in an oven at 105°C for 48 h (dry weight) as previously reported (3, 4, 6). The percent of water content was calculated as [(wet weight–dry weight)/wet weight] × 100%.

Blood–Brain Barrier Permeability

The BBB permeability was evaluated by measuring the extravasation of Evan's blue dye in different brain regions at 24 h by spectrophotometric analysis as reported previously (3).

Neurological Evaluation

The neurological assessment of animals was performed by a blinded observer at different time points (24 and 72 h) using a 21 point sensorimotor scale as reported previously (6). Wire hang test examined the animal's ability to hang using fore-limbs and then additionally use hind-limbs and tail to move across stretched wire (80 cm) to a platform at either end within 45 s. Similarly, beam balance test examined the animal's ability to walk on beam (100 × 0.62 cm diameter) and reach platform at either end when placed in the middle

within 40 s. Scores ranging from 0 to 5 were awarded depending on time taken and distance traversed and average of three tests was used for data analysis.

Statistical Analysis

Data are expressed as mean ± S.E.M. Statistical significance was verified by one-way analysis of variance (ANOVA) for multiple comparisons. Probability value of $p < 0.05$ was considered statistically significant.

Results

The results (Table 1) indicated that brain water content was significantly increased in the right frontal (ipsilateral) lobe at 24 and 72 h and in the right parietal lobe at 72 h in the normoxia+SBI group as compared to sham group. This was significantly attenuated in the HBO-PC+SBI group at both 24 and 72 h. There was no significant difference in brain water content amongst all other groups.

Increased Evan's blue dye extravasation was observed in the right frontal lobe at 24 h in both SBI groups compared to sham group. There was no significant difference between the two groups subjected to SBI.

Twenty-one point sensorimotor scoring indicated significant neurological deficits in both SBI groups at 24 and 72 h compared to respective sham groups. HBO-PC+SBI group, however, showed significant improvement in neurological score at 72 h compared to normoxia+SBI group. Wire hang and beam balance tests showed significantly decreased scores in both SBI groups at 24 and 72 h compared to the respective sham groups. The HBO-PC+SBI group showed significant improvement in scores at 24 and 72 h compared to normoxia+SBI group.

Discussion

The present study shows that preconditioning with hyperbaric oxygen reduces postoperative brain edema after SBI in mice. The study also shows that HBO-PC improved neurological outcomes after SBI. Previous studies have shown that protecting the BBB translates into decreased brain edema after SBI (3). However, in the present study, HBO-PC did not attenuate the BBB disruption observed after SBI. Recent studies have shown that HBO-PC can upregulate anti-oxidant enzymes and also provide neuroprotection via anti-apoptotic mechanisms

Table 1 Brain edema, blood–brain barrier permeability and neurological outcomes after SBI

Groups	Sham	Normoxia + SBI	HBO-PC + SBI
Brain water content			
% (brain edema)			
24 h after SBI			
	(8)	(10)	(12)
Right frontal	81.16 ± 0.69	86.86 ± 0.63 ^a	84.61 ± 0.65 ^{a,b}
Left frontal	81.32 ± 0.57	82.73 ± 0.68	82.19 ± 0.60
Right parietal	79.43 ± 0.35	80.23 ± 0.43	80.16 ± 0.40
Left parietal	79.45 ± 0.38	79.57 ± 0.38	79.66 ± 0.37
Cerebellum	80.12 ± 0.67	80.11 ± 0.58	79.86 ± 0.49
Brain stem	76.32 ± 0.57	76.46 ± 0.37	76.33 ± 0.49
72 h after SBI			
	(5)	(5)	(5)
Right frontal	80.89 ± 0.54	86.54 ± 0.77 ^a	83.38 ± 0.26 ^{a,b}
Left frontal	80.10 ± 0.40	81.52 ± 0.54	80.65 ± 0.32
Right parietal	78.69 ± 0.03	79.83 ± 0.19 ^a	78.71 ± 0.15 ^b
Left parietal	78.72 ± 0.21	78.50 ± 0.13	78.47 ± 0.13
Cerebellum	78.85 ± 0.30	78.20 ± 0.35	78.99 ± 0.35
Brain stem	75.48 ± 0.31	75.00 ± 0.34	76.14 ± 0.20
Evan's blue dye µg/g brain			
(BBB permeability – 24 h)			
	(4)	(6)	(8)
	6.58 ± 1.1	14.54 ± 1.1 ^a	15.51 ± 1.2 ^a
Neurological evaluation			
21 Point sensorimotor scale			
24 h (n ≥ 11 in each group)			
	20.81 ± 0.1	12.88 ± 0.5 ^a	13.59 ± 0.6 ^a
72 h (n = 5 in each group)			
	21.00 ± 0.0	11.00 ± 1.9 ^a	16.00 ± 0.3 ^{a,b}
Wire hang (0–5 points)			
24 h (n ≥ 11 in each group)			
	4.97 ± 0.0	0.58 ± 0.1 ^a	1.37 ± 0.2 ^{a,b}
72 h (n = 5 in each group)			
	5.00 ± 0.0	0.93 ± 0.6 ^a	2.99 ± 0.5 ^{a,b}
Beam balance (0–5 points)			
24 h (n ≥ 11 in each group)			
	4.90 ± 0.0	0.67 ± 0.1 ^a	1.25 ± 0.2 ^{a,b}
72 h (n = 5 in each group)			
	5.00 ± 0.0	0.99 ± 0.3 ^a	3.66 ± 0.4 ^{a,b}

Note: The table shows brain water content in different regions of the brain as indicated, extravasated Evan's blue dye levels in right frontal lobe, and neurological evaluation by 21 point sensorimotor scale, wire hang and beam balance tests in different groups. Increased brain water content was seen in the right frontal (ipsilateral) lobe at 24 and 72 h and right parietal (ipsilateral) at 72 h in the normoxia + SBI group compared to sham. This was attenuated in the HBO-PC + SBI group. Compared to sham group, there was significantly more extravasated Evan's blue dye in the right frontal lobe in both normoxia + SBI and HBO-PC + SBI groups, but there was no significant difference between these SBI groups themselves. 21-point sensorimotor scoring indicated neurological deficits in both SBI groups at 24 and 72 h compared to respective sham groups, however, there was significant improvement in score in HBO-PC + SBI group compared to normoxia + SBI group at 72 h. Wire hang and beam balance tests both show significantly lower scores in both SBI groups at 24 and 72 h compared to respective sham groups. There was significant improvement in scores in HBO-PC + SBI group compared to normoxia group at 24 h as well as 72 h. $P < 0.05$ was considered as significant, "a" indicates significance v/s respective sham group and "b" indicates significance vs. respective normoxia group. Animal numbers are indicated in parentheses.

in ischemic brain injuries (5, 8). Our recent study showed that decreasing the oxidative stress in susceptible brain tissue after SBI resulted in improved neurological outcomes (6). HBO-PC has also been shown to upregulate hypoxia inducible factor 1 α and erythropoietin in vivo (1). Whether these mechanisms are involved in HBO-PC mediated decrease in brain edema needs to be further elucidated.

Presently HBO is used for few clinical indications such as carbon monoxide poisoning, gas embolism and decompression sickness, however not in any neuroprotective therapeutic regimens (13). SBI is an important clinical and medicolegal issue (2). The present study suggests that HBO is a promising therapeutic modality to provide blanket neuroprotection against SBI.

Conflict of interest statement We declare that we have no conflict of interest.

Acknowledgements This study was partially supported by grants from NIH NS45694, NS53407, and NS43338 to JHZ.

References

1. Gu GJ, Li YP, Peng ZY, Xu JJ, Kang ZM, Xu WG, Tao HY, Ostrowski RP, Zhang JH, Sun XJ (2008) Mechanism of ischemic tolerance induced by hyperbaric oxygen preconditioning involves upregulation of hypoxia-inducible factor-1 α and erythropoietin in rats. *J Appl Physiol* 104(4):1185–1191
2. Jadhav V, Zhang JH (2008) Surgical brain injury: prevention is better than cure. *Front Biosci* 13:3793–3797
3. Jadhav V, Matchett G, Hsu FP, Zhang JH (2007) Inhibition of Src tyrosine kinase and effect on outcomes in a new in vivo model of surgically induced brain injury. *J Neurosurg* 106(4):680–686
4. Jadhav V, Solaroglu I, Obenaus A, Zhang JH (2007) Neuroprotection against surgically induced brain injury. *Surg Neurol* 67(1):15–20
5. Li J, Liu W, Ding S, Xu W, Guan Y, Zhang JH, Sun X (2008) Hyperbaric oxygen preconditioning induces tolerance against brain ischemia-reperfusion injury by upregulation of antioxidant enzymes in rats. *Brain Res* 1210:223–229
6. Lo W, Bravo T, Jadhav V, Titova E, Zhang JH, Tang J (2007) NADPH oxidase inhibition improves neurological outcomes in surgically-induced brain injury. *Neurosci Lett* 414(3):228–232
7. Nie H, Xiong L, Lao N, Chen S, Xu N, Zhu Z (2006) Hyperbaric oxygen preconditioning induces tolerance against spinal cord ischemia by upregulation of antioxidant enzymes in rabbits. *J Cereb Blood Flow Metab* 26(5):666–674
8. Ostrowski RP, Graupner G, Titova E, Zhang J, Chiu J, Dach N, Corleone D, Tang J, Zhang JH (2008) The hyperbaric oxygen preconditioning-induced brain protection is mediated by a reduction of early apoptosis after transient global cerebral ischemia. *Neurobiol Dis* 29(1):1–13
9. Prass K, Wiegand F, Schumann P, Ahrens M, Kapinya K, Harms C, Liao W, Trendelenburg G, Gertz K, Moskowitz MA, Knapp F, Victorov IV, Megow D, Dirnagl U (2000) Hyperbaric oxygenation induced tolerance against focal cerebral ischemia in mice is strain dependent. *Brain Res* 871(1):146–150
10. Qin Z, Song S, Xi G, Silbergleit R, Keep RF, Hoff JT, Hua Y (2007) Preconditioning with hyperbaric oxygen attenuates brain edema after experimental intracerebral hemorrhage. *Neurosurg Focus* 22(5):E13
11. Veltkamp R, Siebing DA, Sun L, Heiland S, Bieber K, Marti HH, Nagel S, Schwab S, Schwaninger M (2005) Hyperbaric oxygen reduces blood-brain barrier damage and edema after transient focal cerebral ischemia. *Stroke* 36(8):1679–1683
12. Wada K, Miyazawa T, Nomura N, Tsuzuki N, Nawashiro H, Shima K (2001) Preferential conditions for and possible mechanisms of induction of ischemic tolerance by repeated hyperbaric oxygenation in gerbil hippocampus. *Neurosurgery* 49(1):160–166
13. Zhang JH (2007) Hyperbaric oxygen in neurological diseases. *Neurol Res* 29(2):113–115

Following Brain Trauma, Copeptin, a Stable Peptide Derived from the AVP Precursor, Does Not Reflect Osmoregulation but Correlates with Injury Severity

A. Kleindienst, G. Brabant, N.G. Morgenthaler, K.C. Dixit, H. Parsch, and M. Buchfelder

Abstract The incidence of water and electrolyte disturbances following traumatic brain injury (TBI) is considerable and has been attributed to a dysregulation of the hypothalamic peptide arginine-vasopressin (AVP). Copeptin, the C-terminal part of the AVP prohormone, reflects AVP activity.

In 71 TBI patients we measured copeptin in serum by a sandwich immunoassay. Injury severity was assessed by Glasgow Coma Score (GCS) and computed tomography, and recovery by Glasgow Outcome Score (GOS). Neuroendocrine and osmoregulation regulation were examined on day 0, 3 and 7, and 24 months post-injury.

Copeptin was highest on admission (40.0 ± 72.3 pmol/l), stabilized on day 3 and 7 (21.2 ± 18.3 resp. 20.3 ± 17.1 pmol/l), and normalized at follow-up (4.2 ± 1.7 pmol/l). On admission, there was a correlation between serum sodium and urine excretion ($p=0.003$), but the correlation got lost on day 3 and 7. Copeptin did not reflect the individual 24 h urine excretion or serum sodium levels indicating an uncoupling of copeptin/AVP release and renal water excretion. High copeptin level on day 3 were correlated with a low GCS ($p<0.001$), midline shift ($p=0.019$), intracerebral hemorrhage ($p=0.026$), SAPS score ($p=0.001$), as well as with a low GOS ($p=0.031$). Copeptin was significantly decreased following skullbase fracture ($p=0.016$).

Our data reveal a loss of hypothalamic osmoregulation following TBI. The measurement of Copeptin/AVP release reveals a significant predictive function for the severity of TBI.

Keywords Neuroendocrine function • osmoregulation • outcome • traumatic brain injury

Introduction

The existence of neuroendocrine dysfunction following traumatic brain injury (TBI) has increasingly attracted attention, and different studies reveal a broad spectrum of post-traumatic neuroendocrine dysfunction (14). Especially in the immediate post-trauma period, the incidence of water and electrolyte disturbances is considerable and contributes to the early morbidity (6). The impaired osmoregulation has been attributed to a dysregulation of the hypothalamic peptide arginine-vasopressin (AVP) subsequently affecting the prognosis of the individual patient. Agha et al. reported 26% of TBI patients to suffer from diabetes insipidus in the acute period (plasma sodium >145 mmol/l, plasma osmolality >300 mosmol/kg, ratio osmolality urine/plasma <2 , polyuria >3.5 l/24 h), and 14% demonstrated symptoms suggestive for an inappropriate antidiuretic hormone (syn. AVP) secretion (SIADH, plasma sodium <130 mmol/l, plasma osmolality <270 mosmol/kg, urine osmolality >100 mosmol/kg, urinesodium >40 mM) (1). The diabetes insipidus persisted in 6% of patients while all patients recovered from SIADH.

Because of methodological problems, the hypothalamic-posterior pituitary function has been poorly investigated, yet. In the study mentioned above, both diabetes insipidus and SIADH have been diagnosed on the basis of water and electrolyte dysbalances alone but were not confirmed by AVP measurements (1). Copeptin, the C-terminal part of the AVP prohormone, is concomitantly secreted together with mature AVP (5). Due to an ex vivo stability lasting several days, copeptin can be readily assayed in serum or plasma. In the present study, we investigated the copeptin release in the acute period following TBI, and after more than 24 months combined with a repetitive neurological examination. In parallel, we performed a comprehensive assessment of different osmoregulatory parameter.

A. Kleindienst (✉), and M. Buchfelder
Department of Neurosurgery, Friedrich-Alexander-University
Erlangen-Nuremberg, Schwabachanlage 6, Erlangen D-91054, Germany
e-mail: andrea.kleindienst@uk-erlangen.de

G. Brabant and K.C. Dixit
Department of Endocrinology, Christie Hospital, Manchester,
United Kingdom

H. Parsch
University Erlangen-Nuremberg, Central Laboratory, Erlangen, Germany

N.G. Morgenthaler
Research Department, B.R.A.H.M.S. AG, Biotechnology Centre,
Hennigsdorf, Berlin, Germany

Methods

Seventy-one consecutive patients (57 male, 14 female, mean age 53 years, range 18–87 years), who were admitted to our neurosurgical unit, were studied. According to the Glasgow Coma Score (GCS, 15), 24 patients suffered from mild (GCS 13–15), 32 from moderate (GCS 9–12), and 15 from severe (GCS 3–8) TBI. All patients underwent routinely an initial computerized tomography (CT) scan. The CT demonstrated an open TBI in 19, a skull fracture in 36, a cranio-facial fracture in 6, a skull base fracture in 17, a subdural hematoma in 14, an epidural hematoma in 8, an intracerebral hemorrhagic contusion in 20, a subarachnoid hemorrhage in 17, a midline shift in 2, and findings suggestive of a diffuse axonal injury in 2 patients. The study protocol was approved by the local Ethical Committee. Informed written consent was given by the patient or the next-of-kin, in each case. Exclusion criteria were an age below 18 years, pregnancy, an extremely poor prognosis, a pre-existing endocrine dysfunction, and whenever the patient's or their relatives' consent could not be obtained.

The patients were neurologically assessed daily, and the GCS was documented. On admission to the intensive care unit (ICU), the GCS was 12.09 ± 3.94 , and improved to 14.27 ± 2.04 on day 7. The daily fluid balance was recorded, an output above 3.5 l was considered suspicious of diabetes insipidus. The simplified acute physiology (SAPS) II score (estimation of hospital mortality ~21% at 32 [9]) was 40.43 ± 20.64 . Blood samples for serum sodium, osmolality and copeptin were obtained on day 0 (n=66), on day 3 (n=69) and on day 7 (n=52). Venous blood samples were drawn in the morning between 7:00 and 9:00 a.m. into pre-cooled tubes. Clotted samples were promptly centrifuged at 3,000Xg for 15 min at 4°C, and then the plasma was frozen at -80°C until analysis. Sodium (mmol/l) was measured by indirect potentiometry (predilution 1:20) with an ion-sensitive electrode on an AU2700 analyzer (sodium, potassium and chloride-unit with a reference-electrode) manufactured by Olympus Diagnostics Coop., Japan. Precision is less than 1.3%. Osmolality (mosmol/kg) measurements (reproducibility $\pm 1.0\%$) were done by freezing-point depression with an autosampler (Osmomat Auto, Gonotec Inc.). Copeptin (CT-proAVP) measurements were performed in a blinded fashion in a single batch with a commercial sandwich immunoluminometric assay (B.R.A.H.M.S LUMitest CT-proAVP, B.R.A.H.M.S AG, Hennigsdorf/Berlin, Germany), as described in detail elsewhere (11). The Glasgow Outcome Score (GOS) assessed outcome at 6 months (1=death, 2=vegetative, 3=severely disabled, 4=moderately disabled, 5=good recovery, [4]). Twenty-three patients consented to undergo a follow-up examination 24 to 36 months after the injury. The results are expressed as the mean \pm SD. The correlation between variables was sought calculating the Pearson coefficient with the commercially available SPSS software.

Results

The incidence of polyuria (>3.5 l/day) was initially 21% and increased to 65% on day 7. Serum sodium was 135 ± 7.9 mmol/l on admission, 135 ± 9.1 mmol/l on day 3, and 133 ± 7.9 mmol/l on day 7. Copeptin was highest on admission (40.0 ± 72.3 pmol/l), stabilized on days 3 and 7 (21.2 ± 18.3 and 20.3 ± 17.1 pmol/l, respectively) and was normalized at follow-up in all but one patient (4.2 ± 1.7 pmol/l, Fig. 1). On the day of admission, a high urine output was correlated with high serum sodium levels ($r=0.536$, $p=0.003$, Fig. 2a). However, while polyuria resulted in a lowered urine osmolality ($r=-0.556$, $p=0.009$), the positive correlation between

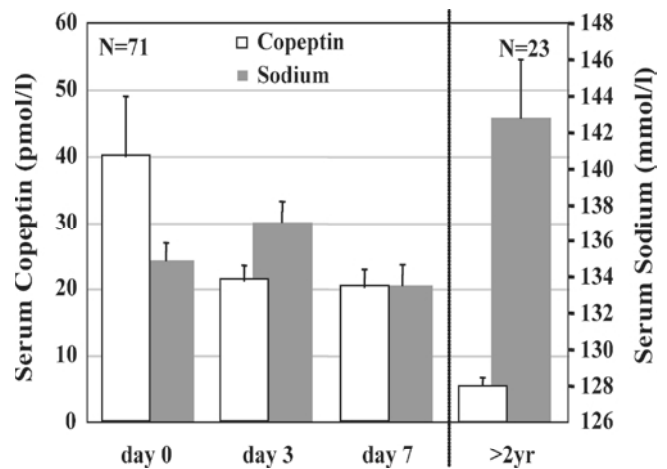


Fig. 1 Serum copeptin and sodium concentrations are displayed at different time points following TBI

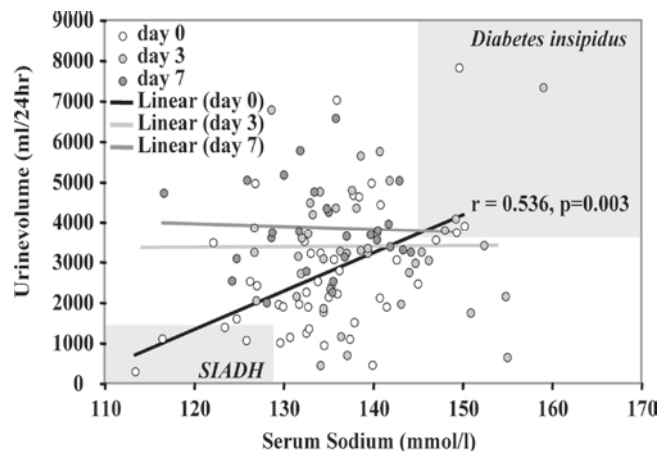


Fig. 2 Pearson correlation between the daily urine volume and the serum sodium concentration in the acute phase after TBI. The physiological positive correlation still exists on the day of injury, and gets lost thereafter

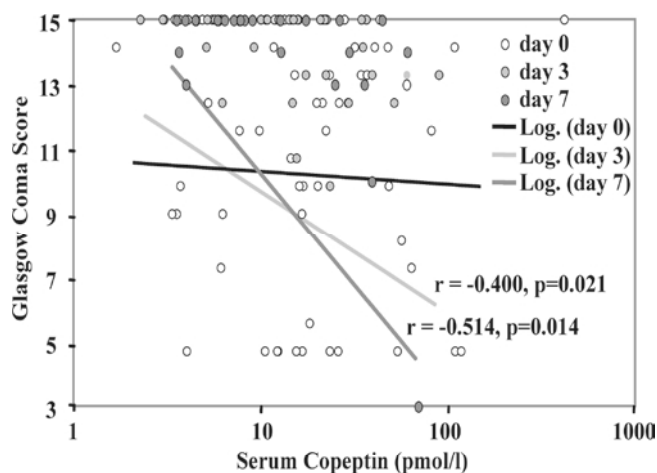


Fig. 3 Pearson correlation between the neurological function as assessed with the Glasgow Coma Score and serum copeptin levels reflecting the AVP activity. On day 3 and 7, the correlation between GCS and copeptin becomes significantly negative

urine volume, serum sodium and serum osmolality was lost on day 7 ($r = -0.041$, $r = 0.571$ and $r = -0.132$, $p = 0.512$). The correlation of serum sodium and serum osmolality was re-established at the follow-up examination ($r = 0.894$, $p < 0.001$).

Interestingly, copeptin level did not correlate with urine volume, serum and urine sodium or osmolality within the acute period after TBI, and on follow-up. However, copeptin level correlated with a poorer neurological performance when they were persistently high on day 3 and 7 post-injury, i.e. with a low GCS ($r = -0.396$, $r = 0.020$ and $r = -0.520$, $p = 0.011$, Fig. 3). Copeptin level reflected the morphological severity of injury as assessed by the CT, i.e. intracerebral hemorrhage ($r = 0.334$, $p = 0.043$) and midline shift ($r = -0.350$, $p = 0.034$), as well as an unfavorable intensive care score SAPS II ($r = 0.530$, $p = 0.002$) and a low GOS score ($r = -0.302$, $p = 0.031$), when not declined by day 7. Notably, skull base fractures were associated with an increased serum osmolality on day 0 and 3 ($r = 0.517$, $r < 0.001$ and $r = 0.320$, $p = 0.012$) and with decreased copeptin levels on day 7 ($r = -0.343$, $p = 0.038$).

Discussion

With respect to the mechanism of brain injury, the primary trauma or direct damage to the pituitary or its stalk has to be differentiated from a secondary insult due to the TBI induced hypoxia, hypotension, brain edema or other intracranial pathology with subsequent effects on the hypothalamic-pituitary complex. The bony encasement of the pituitary within

the sella turcica and its blood supply from different sources are anatomic features protecting the delicate organ from injury. Fractures of the sella turcica and the petrous bone are a possible cause of direct damage to the pituitary and have been reported to occur with variable frequency (2,7,13). In those patients presenting with sellar fractures, the frequency of endocrine deficiencies increases dramatically (3,17). A case series from our group (12) described the endocrinological findings of 11 head injured patients with skull base fractures involving the sella turcica. Diabetes insipidus was present in 8 patients in the acute phase, but was transient in 6 of them. In the present study, we found a skull base fracture to result significantly more often in a high serum osmolality and low copeptin levels on day 7 post-injury, thereby suggesting a damage of the hypothalamo-posterior pituitary complex with a subsequent AVP deficiency.

Beside the direct trauma to the pituitary-hypothalamic system, both TBI in general and consecutive critical illness may induce an adaptive endocrine response (16). We demonstrated that the hypothalamic osmoregulation is still present immediately after injury, but gets lost during the further course of illness. Instead, our data reveal that the enhanced AVP activity in the early phase following TBI as assessed by the copeptin release reflects the seriousness of the condition. The homeostatic correction to cope with the catastrophic event of serious brain injury may engage a shift of AVP's osmoregulatory responsibilities towards its vasopressor effects (10). This has been shown in life threatening conditions such as cardiopulmonary resuscitation (8). Thus, copeptin may be used as a surrogate parameter for the severity of brain injury, and even more importantly for the outcome of the patients.

Conflict of interest statement NGM is employed by BRAHMS AG, a company developing, marketing and selling in vitro diagnostic products, including a Copeptin assay.

References

1. Agha A, Thornton E, O'Kelly P, Tormey W, Phillips J, Thompson CJ (2004) Posterior pituitary dysfunction after traumatic brain injury. *J Clin Endocrinol Metab* 89:5987–5992
2. Dublin AB, Poirier VC (1976) Fracture of the sella turcica. *AJR Am J Roentgenol* 127:969–972
3. Edwards OM, Clark JD (1986) Post-traumatic hypopituitarism. Six cases and a review of the literature. *Medicine (Baltimore)* 65: 281–290
4. Jennett B (1975) Outcome of severe damage to the central nervous system. Scale, scope and philosophy of the clinical problem. *Ciba Found Symp* 34:3–21
5. Katan M, Muller B, Christ-Crain M (2008) Copeptin: a new and promising diagnostic and prognostic marker. *Crit Care* 12:117
6. Kaufman HH, Timberlake G, Voelker J, Pait TG (1993) Medical complications of head injury. *Med Clin North Am* 77:43–60

7. Kojima T, Waga S, Furuno M (1985) Fracture of the sella turcica. *Neurosurgery* 16:225–229
8. Krismer AC, Wenzel V, Stadlbauer KH, Mayr VD, Lienhart HG, Arntz HR, Lindner KH (2004) Vasopressin during cardiopulmonary resuscitation: a progress report. *Crit Care Med* 32: S432–S435
9. Le Gall JR, Lemeshow S, Saulnier F (1993) A new simplified acute physiology score (SAPS II) based on a European/North American multicenter study. *JAMA* 270:2957–2963
10. Lindner KH, Prengel AW, Pfenninger EG, Lindner IM, Strohmenger HU, Georgieff M, Lurie KG (1995) Vasopressin improves vital organ blood flow during closed-chest cardiopulmonary resuscitation in pigs. *Circulation* 91:215–221
11. Morgenthaler NG, Struck J, Alonso C, Bergmann A (2006) Assay for the measurement of copeptin, a stable peptide derived from the precursor of vasopressin. *Clin Chem* 52:112–119
12. Nomikos P, Buchfelder M, Honegger J, Fahlbusch R (1997) Head injuries with fractures of the sella turcica. *Ann Endocrinol* 58(Suppl):1S130
13. Ortega FJ, Longridge NS (1975) Fracture of the sella turcica. *Injury* 6:335–337
14. Schneider M, Schneider HJ, Yassouridis A, Saller B, von Rosen F, Stalla GK (2008) Predictors of anterior pituitary insufficiency after traumatic brain injury. *Clin Endocrinol (Oxf)* 68: 206–212
15. Teasdale G, Jennett B (1974) Assessment of coma and impaired consciousness. A practical scale. *Lancet* 2:81–84
16. Vanhorebeek I, Van den Berghe G (2006) The neuroendocrine response to critical illness is a dynamic process. *Crit Care Clin* 22:1–15
17. Young HA, Olin MS, Schmidek HH (1980) Fractures of the sella turcica. *Neurosurgery* 7:23–29

The Effects of Selective Brain Hypothermia and Decompressive Craniectomy on Brain Edema After Closed Head Injury in Mice

Jacek Szczygielski, Angelika E. Mautes, Karsten Schwerdtfeger, and Wolf-Ingo Steudel

Abstract Intractable brain edema remains one of the main causes of death after traumatic brain injury (TBI). Brain hypothermia and decompressive craniectomy have been considered as potential therapies. The goal of our experimental study was to determine if selective hypothermia in combination with craniectomy could modify the development of posttraumatic brain edema. Male CD-1 mice were anesthetized with halothane and randomly assigned into the following groups: sham-operated (n=5), closed head injury (CHI) alone (n=5), CHI followed by craniectomy at 1 h post-TBI (n=5) and CHI+craniectomy and selective hypothermia (focal brain cooling using cryosurgery device) maintained for 5 h (n=5). Animals were sacrificed at 7 h posttrauma and brains were removed, sagittally dissected and dried. The brain water content of separate hemispheres was calculated from the weight difference before and after drying. In the CHI alone group there was no significant increase in brain water content in both the ipsi- and contralateral hemispheres ($80.59 \pm 1\%$ and $78.74 \pm 0.9\%$ in the CHI group vs. $79.31 \pm 0.7\%$ and $79.01 \pm 0.3\%$ in the sham group, respectively). Brain edema was significantly increased ipsilaterally in the trauma+craniectomy group ($82.11 \pm 0.6\%$, $p < 0.05$), but not in the trauma+craniectomy+hypothermia group ($81.52 \pm 1.1\%$, $p > 0.05$) as compared to the sham group ($79.31 \pm 0.7\%$). These data suggest that decompressive craniectomy leads to an increase in brain water content after CHI. Additional focal hypothermia may be an effective approach in the treatment of posttraumatic brain edema.

Keywords Traumatic brain injury • closed head injury • brain edema • selective brain cooling • hypothermia • decompressive craniectomy • mice

Introduction

Traumatic Brain Injury (TBI) is considered a major cause of death and disability among individuals at productive ages in developed countries (4). One of the fatal consequences of brain trauma is an intractable increase in intracranial pressure (ICP) due to refractory brain edema (3). To date, the multiple methods of treatment of uncontrolled posttraumatic increases in ICP have been tested both experimentally and clinically. These methods include controlled hyperventilation, infusion of hypertonic solutions, pharmacological suppression of cerebral metabolism, hypothermia and decompressive craniectomy (DC) (1,15,32). The last two methods bear the most interesting and controversial potential for therapeutic use. Although both treatment modes – DC and brain hypothermia – have already been used separately in clinical practice, little information is available about a potential synergistic effect of these two methods. The purpose of this study was to analyze the effect of combined treatment of DC and hypothermia on the development of posttraumatic brain edema in a mouse model of closed head injury.

Methods

Male CD-1 mice were used in this study, and the following experimental groups were created: (1) sham-operated (sham); (2) closed head injury (CHI) alone (CHI); (3) CHI followed by DC at 1 h post-TBI (CHI+DC); and (4) CHI+DC and selective hypothermia (H) maintained for 5 h (CHI+DC+H). To induce brain trauma, a well-established mouse model of CHI was used (adapted from Chen et al. [5]). The principles of this model are based on transmission of weight drop energy to an intact, non-trephined mouse skull. Briefly, mice were anesthetized with halothane (initial dose 3%, maintenance 0.8–1.3% in O₂). The animals were placed on a heating pad, and an additional heat lamp was used if necessary (target core temperature $37 \pm 0.5^\circ\text{C}$ as measured by rectal

J. Szczygielski (✉), A.E. Mautes, K. Schwerdtfeger, and W.I. Steudel
Department of Neurosurgery, Saarland University Hospital,
Kirrberger Straße, Homburg, Saar, Germany
e-mail: ncjszc@uniklinikum-saarland.de

probe was maintained during the whole experiment). The skull was exposed by a scalp incision. The animals were placed on the base of the weight drop device (Laboratory Tools Workshop, Department of Pharmacology, School of Pharmacy, The Hebrew University of Jerusalem, Israel), and head trauma was applied. For the purpose of this study, the following settings were used: brass rod weight: 75 g, height of the fall: 16 cm. In the CHI+DC and CHI+DC+H groups, unilateral DC was performed 1 h after trauma according to the description of Doerfler et al. (8). A bone flap was created in the parietal and temporal bone using a dental drill. Then, the temporal bone was removed down to the skull base using microscissors and microforceps. A dura opening over the occipital lobe was created using surgical microforceps. Thereafter, the skin was closed using 5–0 polypropylene sutures (Premilene®, Aesculap AG). In the hypothermia group (CHI+DC+H), additional selective brain cooling was applied using a carbon dioxide-driven cryosurgery device (Erbokryo AE, ERBE Elektromedizin GmbH). The suitable 3 mm cooling probe with thermocouple (ERBE Elektromedizin GmbH) was placed on the skin covering the craniectomized area and then chilled to 4°C. After reaching this target temperature, the cooling was maintained during the next 5 h of the experiment. In order to demonstrate a cooling effect in the hypothermia groups, two needle temperature probes (ERBE Elektromedizin GmbH) connected with an electronic thermometer (Erbe ET1, ERBE Elektromedizin GmbH) were placed in the scalp tissue at a distance of 2 and 5 mm from the cooling probe. Cerebral edema was evaluated by determining brain water content for each hemisphere separately. After 7 h of anesthesia, the animals were sacrificed by cervical dislocation, and their brains were removed. The brain stem and cerebellum were discarded and the remaining tissue was sagittally dissected into two separate hemispheres and weighed. Thereafter, each hemisphere was dried in a desiccator oven for 24 h at 96°C and reweighed. The water content in the tissue was calculated as a percent ratio of the wet weight according to the formula: water content = $[\text{wet weight} - \text{dry weight}] / \text{wet weight} \times 100\%$. Data for initial body weight, halothane concentration, core temperature and brain water content were expressed as mean \pm SEM. Statistical analyses were performed using a one-way analysis of variance (ANOVA) followed by a post-hoc *t*-test with Bonferroni correction for individual comparisons. Significance was set at $p < 0.05$.

Results

Measurement of body weight in subgroups of animals prior to surgery revealed no significant differences. Also, the analysis of the mean core temperature and mean halothane

concentration used during anesthesia showed no differences between the subgroups.

Cooling Effect

The assessment of the temperature in the scalp tissue surrounding the cooling probe showed that the temperature gradient between both probes was achieved promptly after initiation of cooling and could be maintained during the five consecutive hours of hypothermia treatment. The mean temperatures measured during the cooling phase were: $23.17 \pm 0.95^\circ\text{C}$ for the 2 mm probe and $25.19 \pm 0.76^\circ\text{C}$ for the 5 mm probe, with a core temperature of $36.98 \pm 0.38^\circ\text{C}$ (Fig. 1.) In order to validate the method, we also measured the scalp temperature in one animal from the CHI group and one animal from the CHI+DC group in the same manner. The scalp temperature was lower than the core temperature, but there was no difference between temperatures measured by both thermoprobes ($30.53 \pm 0.8^\circ\text{C}$ and $30.37 \pm 0.67^\circ\text{C}$ with a core temperature of $36.52 \pm 0.63^\circ\text{C}$ for the CHI animal; $27.33 \pm 1.13^\circ\text{C}$ and $27.43 \pm 1.18^\circ\text{C}$ with a core temperature of $36.8 \pm 0.8^\circ\text{C}$ for the CHI+DC animal).

Evaluation of Edema

Cerebral water content for the four experimental groups (ipsi- and contralateral hemispheres separately) are shown in Fig. 2 ($n=5$ for each experimental group, ANOVA). There was no significant difference in the brain water content of the contralateral hemispheres between experimental groups.

Regarding the ipsilateral hemispheres, there was no significant increase in brain water content between the trauma alone group compared to the sham group. The CHI group showed no significant differences between the CHI+DC or the CHI+DC+H groups. In addition, the difference between the CHI+DC and the CHI+DC+H groups did not reach statistical significance. However, ipsilateral brain edema was significantly increased in the CHI+DC group but not in the CHI+DC+H when compared with the sham group.

Discussion

We examined the impact of combined therapy of DC and local hypothermia on posttraumatic brain edema formation in a CHI model. The design of our model was based on the events seen in clinical practice: injury to the closed skull,

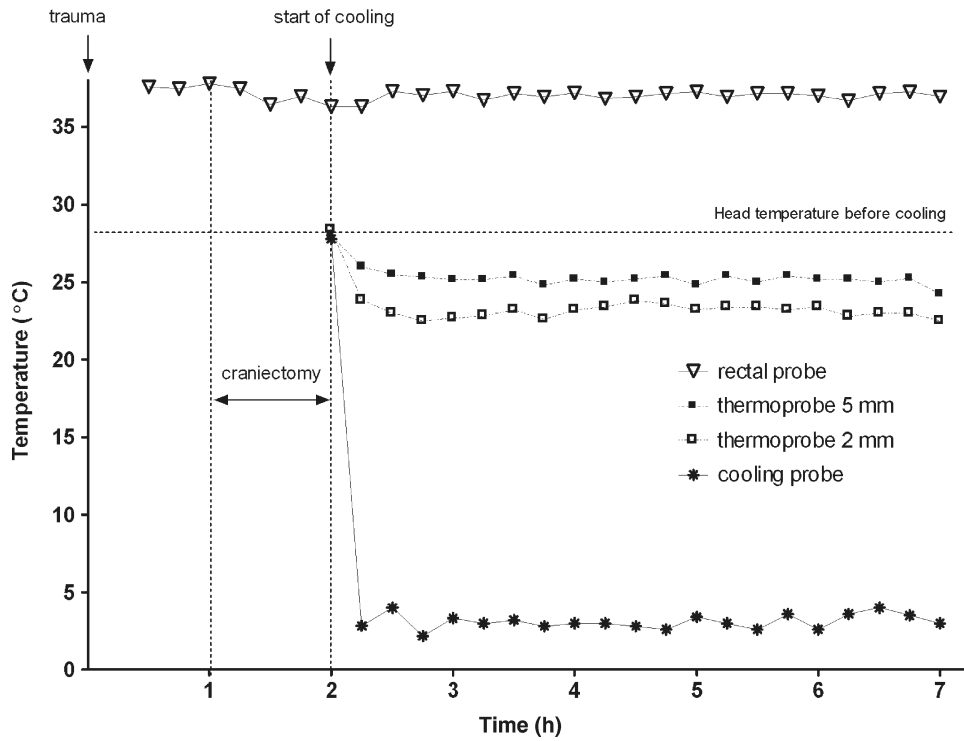


Fig. 1 Graph demonstrating the time course of head cooling initiated 2 h after closed head injury in the trauma+craniectomy+hypothermia group. Data points represent the mean temperature of five animals in this group. The effect of selective head cooling was seen as an immediate

drop in scalp tissue temperature and as the temperature gradient between thermoprobes placed at a distance of 2 and 5 mm from the cooling probe. This effect could be maintained for five consecutive hours of hypothermia treatment

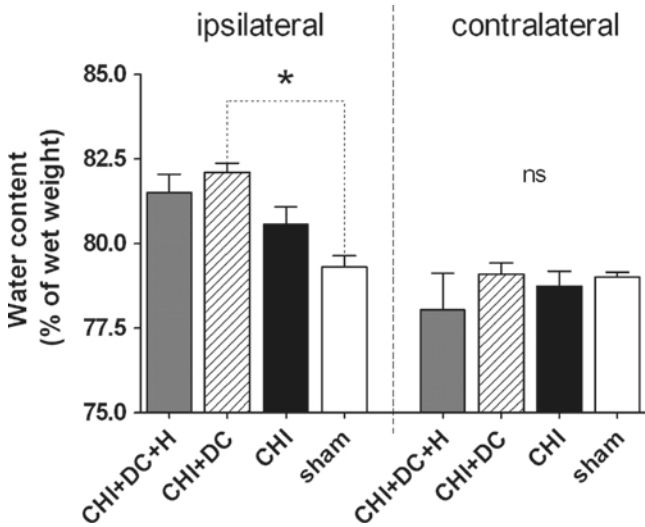


Fig. 2 Histogram showing brain water content 7 h after sham injury or closed head injury and single (craniectomy) or combined (craniectomy and hypothermia) treatment in mice. The brain hemispheres ipsilateral (left) and contralateral (right) to the injury site were dissected and analyzed separately. Brain water content was not elevated by closed head injury alone. Brain edema formation was significantly increased by posttraumatic craniectomy: * $p < 0.05$ compared with the sham injury group. This effect was not present if additional selective brain cooling was applied; $p > 0.05$ compared with the sham injury group. CHI=closed head injury, DC=decompressive craniectomy, H=hypothermia

early surgical decompression and the application of hypothermia during intensive care therapy.

Experimental DC was first introduced in brain ischemia studies. Doerfler et al. showed in a rat middle cerebral artery (MCA) occlusion model that surgical decompression improves mortality, neurological performance and infarction size (8). An ameliorated cerebral perfusion was proposed as the mechanism of action (11). Recently, craniectomy was also thoroughly analyzed in neurotrauma experiments. Zweckberger et al. studied DC in a murine controlled cortical impact (CCI) model of TBI. They described that in animals in which pre-CCI craniotomy was left open, there was no significant increase in posttraumatic ICP and the expansion of the contusion volume was reduced by 40% at 24 h posttrauma, i.e., at the time point of maximal lesion expansion. Moreover, the neurological outcome in craniotomized mice (assessed using beam walking tests) was significantly better compared to animals in which the craniotomy was closed after application of trauma (30,40).

In our craniectomy model, we showed that at 7 h posttrauma, there was a significant increase in brain water content in animals subjected to both CHI and craniectomy, as compared to sham animals. Such significant differences could not be observed in animals subjected to trauma alone. This suggests that at least at the analyzed time point, the DC

promotes formation of brain edema. A similar effect of decompression has been reported in dogs subjected to cortical cold lesion (7). Notably, a rise in water content itself does not directly imply an increased secondary injury after craniectomy. Postoperative swelling and the bulging of the brain through the area of decompression is occasionally observed in craniectomized patients with preoperatively increased ICP (2). The results from clinical studies suggest that despite this morphological phenomenon, surgical decompression improves cerebral perfusion and cerebral oxygen supply as well as induces changes in vascular reactivity (14,34,37,38). Thus, such brain swelling after craniectomy should be considered evidence of sufficient decompression of elevated ICP and may be attributed to an alteration in cerebrovascular reactivity rather than to increased neurological damage (37,38). This view is also supported by the time point of the analysis of brain water content in our study (7 h posttrauma). This result is consistent with a rise in ICP that was previously described in another experimental model of murine TBI (40).

One important aspect is the optimal time point of craniectomy. According to current view in the field, the craniectomy remains a last resort therapy rather than a standard first line neurosurgical procedure in TBI (1,15,33). Nevertheless, growing clinical data demonstrates that earlier decompression may be beneficial for the posttraumatic outcome, especially in the pediatric population (19,36). Moreover, a recent experimental evaluation showed that in mice subjected to CCI, a craniectomy prevents the expansion of the contusion and the formation of brain edema only if animals were craniectomized early (up to 3 h posttrauma) (30,39). Therefore, we chose immediate decompression, which, due to the technique of the surgical procedure, could be completed at 2 h posttrauma.

We have shown that applying local hypothermia prevents the formation of brain edema following CHI and DC. These results are consistent with previous reports in which hypothermia applied after CCI decreased the magnitude of edema in rats (13,28). In addition, the hypothermia was able to reduce, at least transiently, posttraumatic brain water content in an immature rat TBI model (27). The reduction of brain edema by hypothermia was also presented in rat models of subdural hematoma (20), intracerebral hemorrhage (12,26) and MCA infarction (22,29). In addition to other authors, we presume that the antiedematous effect of cooling in our experimental setting results from the prevention of blood-brain barrier breakdown (17,28). In clinical settings, hypothermia reduces cerebral hyperemia without impairing metabolism or the oxygen supply (35). Hypothermia can also alleviate vasogenic brain edema in a rat model of cold-induced cortical lesion (6,24). This fact is important, especially in the postcraniectomy situation, where disturbed vascular reactivity may promote this type of brain swelling (37). Although the efficacy of hypothermia as a solo therapy

remains disputable, the combination of craniectomy and hypothermia may be clinically useful; according to our results, hypothermia could reduce herniation of the brain over the craniectomy site, thereby preventing the deleterious effect of venous kinking and allowing cranioplasty to be performed early. On the other hand, if hypothermia is planned, an initial craniectomy could prevent a secondary rise in ICP during the rewarming stage (16,21,25). This treatment combination has already been investigated in experimental stroke (9,18,23). In the study of Doerfler et al., rats treated by hypothermia and subsequent craniectomy after MCA occlusion presented a better neurological outcome and reduced infarction size compared to controls and the craniectomy alone group (9). Our data indicates a therapeutic potential for hypothermia administered after TBI and following craniectomy. In addition, recent studies in stroke and TBI patients showed the clinical safety and efficacy of combined craniectomy-hypothermia therapy (10,31).

Taken together, our experimental model closely resembles the clinical situation of combined surgical/conservative therapy of acute TBI. Thus, our experimental approach may be of high value for testing several hypotheses concerning how and why DC and brain hypothermia impact posttraumatic outcome.

Conflict of interest statement We declare that we have no conflict of interest.

References

1. Guidelines for the management of severe traumatic brain injury (2007). *J Neurotrauma* 24(Suppl 1):S1–S106
2. Aarabi B, Hesdorffer DC, Ahn ES, Aresco C, Scalea TM, Eisenberg HM (2006) Outcome following decompressive craniectomy for malignant swelling due to severe head injury. *J Neurosurg* 104:469–479
3. Balestreri M, Czosnyka M, Hutchinson P, Steiner LA, Hiler M, Smielewski P, Pickard JD (2006) Impact of intracranial pressure and cerebral perfusion pressure on severe disability and mortality after head injury. *Neurocrit Care* 4:8–13
4. Bruns J Jr, Hauser WA (2003) The epidemiology of traumatic brain injury: a review. *Epilepsia* 44:2–10
5. Chen Y, Constantini S, Trembovler V, Weinstock M, Shohami E (1996) An experimental model of closed head injury in mice: pathophysiology, histopathology, and cognitive deficits. *J Neurotrauma* 13:557–568
6. Clasen RA, Pandolfi S, Russell J, Stuart D, Hass GM (1968) Hypothermia and hypotension in experimental cerebral edema. *Arch Neurol* 19:472–486
7. Cooper PR, Hagler H, Clark WK, Barnett P (1979) Enhancement of experimental cerebral edema after decompressive craniectomy: implications for the management of severe head injuries. *Neurosurgery* 4:296–300
8. Doerfler A, Forsting M, Reith W, Staff C, Heiland S, Schabitz WR, von Kummer R, Hacke W, Sartor K (1996) Decompressive craniectomy in a rat model of “malignant” cerebral hemispheric stroke: experimental support for an aggressive therapeutic approach. *J Neurosurg* 85:853–859

9. Doerfler A, Schwab S, Hoffmann TT, Engelhorn T, Forsting M (2001) Combination of decompressive craniectomy and mild hypothermia ameliorates infarction volume after permanent focal ischemia in rats. *Stroke* 32:2675–2681
10. Els T, Oehm E, Voigt S, Klisch J, Hetzel A, Kassubek J (2006) Safety and therapeutical benefit of hemicraniectomy combined with mild hypothermia in comparison with hemicraniectomy alone in patients with malignant ischemic stroke. *Cerebrovasc Dis* 21:79–85. Epub 2005 Nov 2028
11. Engelhorn T, Doerfler A, Kastrop A, Beaulieu C, de Crespigny A, Forsting M, Moseley ME, Faraci FM (1999) Decompressive craniectomy, reperfusion, or a combination for early treatment of acute “malignant” cerebral hemispheric stroke in rats? Potential mechanisms studied by MRI. *Stroke* 30:1456–1463
12. Fingas M, Clark DL, Colbourne F (2007) The effects of selective brain hypothermia on intracerebral hemorrhage in rats. *Exp Neurol* 208:277–284
13. Heegaard W, Biros M, Zink J (1997) Effect of hypothermia, dichloroacetate, and deferoxamine in the treatment for cortical edema and functional recovery after experimental cortical impact in the rat. *Acad Emerg Med* 4:33–39
14. Ho CL, Wang CM, Lee KK, Ng I, Ang BT (2008) Cerebral oxygenation, vascular reactivity, and neurochemistry following decompressive craniectomy for severe traumatic brain injury. *J Neurosurg* 108:943–949
15. Hutchinson P, Timofeev I, Kirkpatrick P (2007) Surgery for brain edema. *Neurosurg Focus* 22:E14
16. Iida K, Kurisu K, Arita K, Ohtani M (2003) Hyperemia prior to acute brain swelling during rewarming of patients who have been treated with moderate hypothermia for severe head injuries. *J Neurosurg* 98:793–799
17. Jiang JY, Lyeth BG, Kapasi MZ, Jenkins LW, Povlishock JT (1992) Moderate hypothermia reduces blood-brain barrier disruption following traumatic brain injury in the rat. *Acta Neuropathol (Berl)* 84:495–500
18. Jieyong B, Zhong W, Shiming Z, Dai Z, Kato Y, Kanno T, Sano H (2006) Decompressive craniectomy and mild hypothermia reduces infarction size and counterregulates Bax and Bcl-2 expression after permanent focal ischemia in rats. *Neurosurg Rev* 29:1–5
19. Kan P, Amini A, Hansen K, White GL Jr, Brockmeyer DL, Walker ML, Kestle JR (2006) Outcomes after decompressive craniectomy for severe traumatic brain injury in children. *J Neurosurg* 105:337–342
20. Kawai N, Nakamura T, Okauchi M, Nagao S (2000) Effects of hypothermia on intracranial pressure and brain edema formation: studies in a rat acute subdural hematoma model. *J Neurotrauma* 17:193–202
21. Kinoshita K, Hayashi N, Sakurai A, Utagawa A, Moriya T (2003) Changes in cerebrovascular response during brain hypothermia after traumatic brain injury. *Acta Neurochir Suppl* 86:377–380
22. Kollmar R, Schabitz WR, Heiland S, Georgiadis D, Schellinger PD, Bardutzky J, Schwab S (2002) Neuroprotective effect of delayed moderate hypothermia after focal cerebral ischemia: an MRI study. *Stroke* 33:1899–1904
23. Koo JS, Kim YJ, Yoon BW (2004) Effects of decompressive craniectomy, hypothermia and their combination in a permanent focal cerebral ischemia model. *Neurosci Res Commun* 35:73–82
24. Laskowski EJ, Klatzo I, Baldwin M (1960) Experimental study of the effects of hypothermia on local brain injury. *Neurology* 10:499–505
25. Lavinio A, Timofeev I, Nortje J, Outtrim J, Smielewski P, Gupta A, Hutchinson PJ, Matta BF, Pickard JD, Menon D, Czosnyka M (2007) Cerebrovascular reactivity during hypothermia and rewarming. *Br J Anaesth* 99:237–244
26. MacLellan CL, Davies LM, Fingas MS, Colbourne F (2006) The influence of hypothermia on outcome after intracerebral hemorrhage in rats. *Stroke* 37:1266–1270
27. Mansfield RT, Schiding JK, Hamilton RL, Kochanek PM (1996) Effects of hypothermia on traumatic brain injury in immature rats. *J Cereb Blood Flow Metab* 16:244–252
28. Markgraf CG, Clifton GL, Moody MR (2001) Treatment window for hypothermia in brain injury. *J Neurosurg* 95:979–983
29. Park CK, Jun SS, Kim MC, Kang JK (1998) Effects of systemic hypothermia and selective brain cooling on ischemic brain damage and swelling. *Acta Neurochir Suppl* 71:225–228
30. Plesnila N (2007) Decompression craniectomy after traumatic brain injury: recent experimental results. *Prog Brain Res* 161:393–400
31. Qiu W, Zhang Y, Sheng H, Zhang J, Wang W, Liu W, Chen K, Zhou J, Xu Z (2007) Effects of therapeutic mild hypothermia on patients with severe traumatic brain injury after craniotomy. *J Crit Care* 22:229–235
32. Raslan A, Bhardwaj A (2007) Medical management of cerebral edema. *Neurosurg Focus* 22:E12
33. Schirmer CM, Ackil AA Jr, Malek AM (2008) Decompressive craniectomy. *Neurocrit Care* 8:456–470
34. Schneider GH, Bardt T, Lanksch WR, Unterberg A (2002) Decompressive craniectomy following traumatic brain injury: ICP, CPP and neurological outcome. *Acta Neurochir Suppl* 81:77–79
35. Shiozaki T, Sugimoto H, Taneda M, Yoshida H, Iwai A, Yoshioka T, Sugimoto T (1993) Effect of mild hypothermia on uncontrollable intracranial hypertension after severe head injury. *J Neurosurg* 79:363–368
36. Taylor A, Butt W, Rosenfeld J, Shann F, Ditchfield M, Lewis E, Klug G, Wallace D, Henning R, Tibballs J (2001) A randomized trial of very early decompressive craniectomy in children with traumatic brain injury and sustained intracranial hypertension. *Childs Nerv Syst* 17:154–162
37. Timofeev I, Czosnyka M, Nortje J, Smielewski P, Kirkpatrick P, Gupta A, Hutchinson P (2008) Effect of decompressive craniectomy on intracranial pressure and cerebrospinal compensation following traumatic brain injury. *J Neurosurg* 108:66–73
38. Yamakami I, Yamaura A (1993) Effects of decompressive craniectomy on regional cerebral blood flow in severe head trauma patients. *Neurol Med Chir (Tokyo)* 33:616–620
39. Zweckberger K, Eros C, Zimmermann R, Kim SW, Engel D, Plesnila N (2006) Effect of early and delayed decompressive craniectomy on secondary brain damage after controlled cortical impact in mice. *J Neurotrauma* 23:1083–1093
40. Zweckberger K, Stoffel M, Baethmann A, Plesnila N (2003) Effect of decompression craniotomy on increase of contusion volume and functional outcome after controlled cortical impact in mice. *J Neurotrauma* 20:1307–1314

Outcome of Patients with Severe Head Injury After Decompressive Craniectomy

J. Lemcke, S. Ahmadi, and U. Meier

Abstract Decompressive craniectomy is an operative option for the neurosurgeon in cases of generalized traumatic brain edema. While the outcome of patients after decompressive craniectomy is often poor, we tried to identify predictors of a favorable course of the injury. Therefore, 131 patients who received a decompressive craniectomy at the Unfallkrankenhaus Berlin (ukb) between September 1997 and September 2005 due to severe traumatic brain injury were followed up. Overall outcome was measured using the Glasgow Outcome Scale (GOS). Sixty-three patients (48%) died during their initial hospital stay and another 27 (21%) were discharged in a vegetative state (GOS 2). Thirty-two patients (24%) were discharged with severe disability, while another nine (7%) had moderate disability at discharge. At an average of 49 months after surgery, 75 patients (68%) were either dead or in a vegetative state (GOS 1 and 2). The results stress again that the prognosis after traumatic brain injury (TBI) with decompressive craniectomy (DC) is unfavorable. Age, midline shift, and status of the basal cisterns on cranial computed tomography (cCT) were associated with the long-term outcome. When weighing whether to initiate the last resort intervention of decompressive craniectomy, the predictive factors detailed here should be taken into consideration.

Keywords Severe head injury • decompressive craniectomy • outcomes • predictive factors

Introduction

Primary brain injury in severe head trauma occurs at the moment of the mechanical insult. With this in mind, the neurosurgeon must decide how to intervene therapeutically in order to at least minimize secondary brain injury. Decompressive craniectomy represents the neurosurgeon's *ultima ratio* – last

resort – in terms of operative therapy. The decision for or against this measure depends largely on the prognostic indications of the individual patient. The goal of our study was to determine if factors exist that can reliably predict the quality of outcome in these patients.

Patients and Methods

All 131 patients who underwent decompressive craniectomy for severe head injury in our department between September 1997 and September 2005 were included in this partially prospective study. Their clinical records were prospectively evaluated and a number of preoperative factors were recorded. These included basic epidemiological information as well as the Glasgow Coma Scale (GCS) score on admission, the initial cCT scan results, pupil reactivity on admission, and the position of the midline on cCT on admission. A retrospective follow-up examination was conducted at least 12 months after discharge from the Unfallkrankenhaus Berlin, in which the condition of the patient was determined using the Glasgow Outcome Scale (GOS).

Results

The mean age of the 99 men (76%) and 32 (24%) women was 36 ± 20 years at the time of the operation. The commonest causes of head injury were as follows: road traffic accidents (53%; $n = 69$), falls (26%; $n = 34$), and physical violence (including suicide attempts) (14%; $n = 18$). Other causes accounted for the remaining ten (7%) patients' injuries. It was possible to follow-up 95% of the patients ($n = 124$). The mean period between the initial trauma and follow-up was 49 ± 25 months. At the time of follow-up, 75 patients (61%) had died (GOS 1) and nine patients (7%) remained in a persistent vegetative state (GOS 2). Fourteen patients (12%) were severely disabled (GOS 3), while 13 patients (10%)

U. Meier (✉), J. Lemcke, S. Ahmadi
Department of Neurosurgery, Unfallkrankenhaus Berlin,
Warener Straße 7, Berlin D-12683, Germany
e-mail: johannes.lemcke@ukb.de

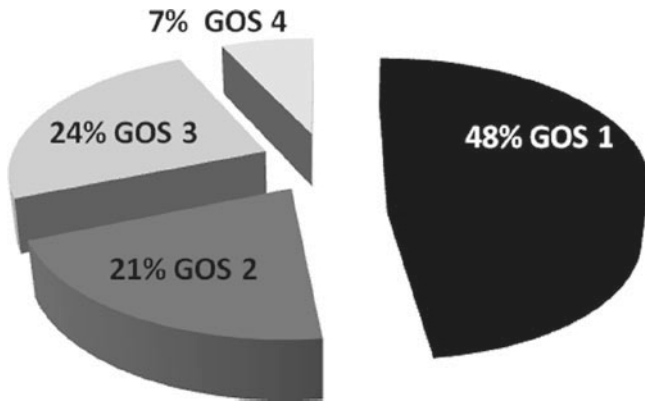


Fig. 1 Outcome at discharge (n = 131, GOS 5 = 0%)

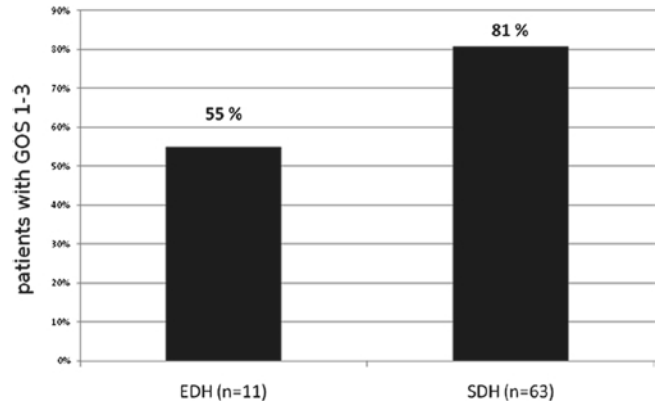


Fig. 5 Patients with epidural and subdural hematomas have different outcomes

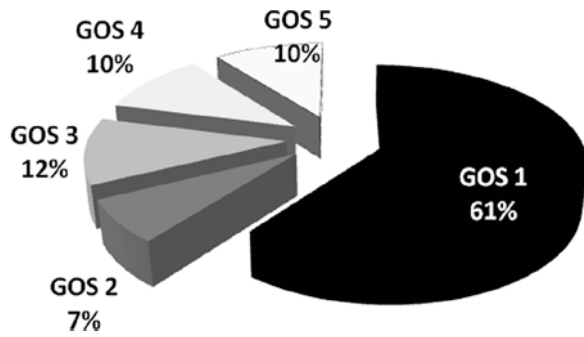


Fig. 2 Long-term outcome (49 ± 25 months after surgery, n = 124, follow-up rate 95%)

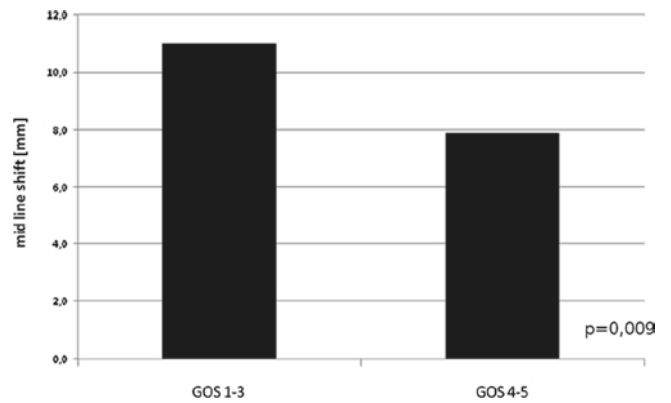


Fig. 6 The degree of midline shift predicts the outcome (significant)

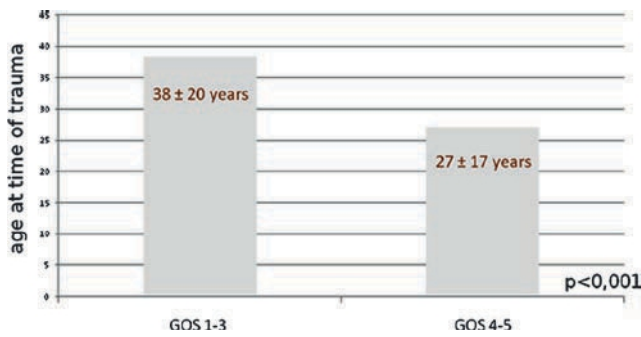


Fig. 3 Age vs. outcome (significant)

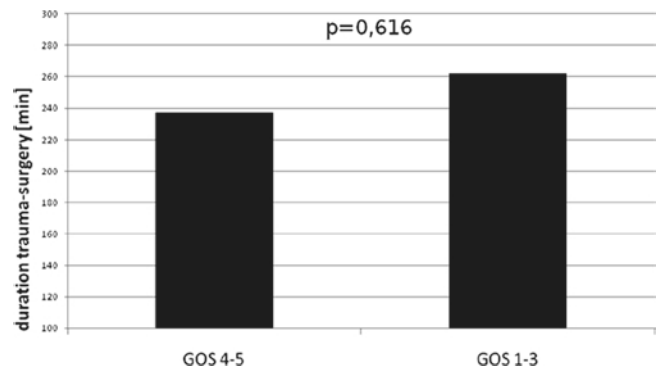


Fig. 7 We did not find a significant correlation between the duration of time from trauma to surgery and the outcome

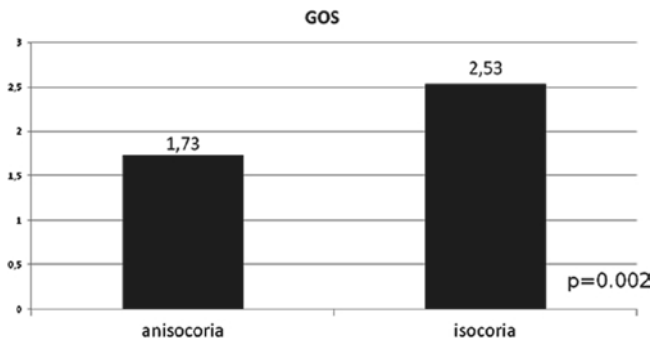


Fig. 4 Isocoria vs. outcome (significant)

were moderately disabled and 13 patients (10%) had made a good recovery (GOS 5).

When the specific indicators and the GOS score at follow-up were compared, a number of significant relationships were demonstrated (Fig. 1–7). Patients with an initial GCS of less than eight were significantly more likely to go on to

have a GOS of 1–3 at follow-up. Pathological pupil reactivity on admission similarly led to a significantly higher chance of a poor outcome. A marked midline shift at the time of admission was also highly predictive of an unsatisfactory GOS (1–3) at follow-up. Pre-existing and perioperatively apparent clotting disorders as well as post-traumatic hydrocephalus internus were also revealed as predictors of a poor outcome (high percentage of GOS 1–3). Hyperglycemia and/or initial acidosis were likewise associated with poor outcomes at follow-up.

Discussion

At the present time, no large prospective studies of decompressive craniectomy for severe head injury have been performed. Therefore, the neurosurgeon faced with deciding for or against decompressive craniectomy has only a combination of generally accepted opinion and his/her own personal experience to draw upon. The demographics of the population in the current study are comparable to those reported in the international literature (3–6). The results of the Rescue ICP Study, which began in 2006 with a target population of 500 patients, are not expected until 2008 or 2009.

The findings of this study add to the consensus in the international literature regarding predictors of outcome in craniectomy. In this study, the demonstration of a relationship between a low GCS score at the scene of the injury or on admission and a poor prognosis (high percentage of GOS 1–3) – the principal finding of various other studies (1,3) – is replicated. Pathological pupil reactivity in terms of initial anisocoria or an absent reaction to light has also been proposed as a negative predictor of outcome by other authors (2). In this study, shift of the midline on cCT was significantly correlated with the quality of outcome. Patients with a poor outcome (GOS 1–3) had a mean midline shift of 9.8 ± 6.7 mm, whereas patients with a good outcome (GOS 4–5) showed a mean midline shift of 6.7 ± 5.0 mm. The important predictive value of this factor has been confirmed

by Marshall et al. (7), among others. The visibility of the basal cisterns was also shown in this study to be very significantly connected to the quality of outcome at follow-up.

Conclusion

The initial Glasgow Coma Scale (GCS) score, pupil reactivity, visibility of the basal cisterns, and degree of midline shift on cCT are highly significant predictors of outcome in patients undergoing decompressive craniectomy for severe head injury. These predictive factors should be taken into account when physicians decide for or against craniectomy.

Conflict of interest statement We declare that we have no conflict of interest.

References

1. Arabi B, Hesdorffer DC, Ahn ES, Aresco C, Scalea TM, Eisenberg HM (2006) Outcome following decompressive craniectomy for malignant swelling due to severe head injury. *J Neurosurg* 104(4): 469–479
2. Bullock MR, Chesnut RM, Clifton GL, Ghajar J, Marion DW, Narayan RK, Newell DW (2000) Part I: guidelines for the management of severe head injury, management and prognosis of severe traumatic brain injury. Brain Trauma Foundation, New York, pp 7–159
3. Gaab MR, Rittierodt M, Lorenz M, Heissler HE (1990) Traumatic brain swelling and operative decompression: a prospective investigation. *Acta Neurochir Suppl (Wien)* 51:326–328
4. Guerra WK, Gaab MR, Dietz H, Mueller JU, Pieck J, Fritsch MJ (1999) Surgical decompression for traumatic brain swelling: indications and results. *J Neurosurg* 90(2):187–196
5. Meier U, Lemcke J, Reyer T, Gräwe A (2006) Decompressive craniectomy for severe head injury in patients with major extracranial injuries. *Acta Neurochir Suppl* 96:373–376
6. Ransohoff J, Benjamin V (1971) Hemicraniectomy in the treatment of acute subdural haematoma. *J Neurol Neurosurg Psychiatry* 34(1):106
7. Marshall LF, Gattille T, Klauber MR, Eisenberg HM, Jane JA, Luerssen TG, Marmarou A, Foulkes MA (1991) The outcome of severe closed head injury. *J Neurosurg* 75:28–36

Assessing the Neurological Outcome of Traumatic Acute Subdural Hematoma Patients with and without Primary Decompressive Craniectomies

George Kwok-Chu Wong, Yuk-Wah Hung, Charing Chong, Janice Yeung, Stephanie Chi-Ping Ng, Tim Rainer, and Wai-Sang Poon

Abstract

Background We have investigated the impact of primary decompressive craniectomies on neurological outcomes after adjusting for other predictive variables.

Method We have collected data from trauma patients with acute subdural hematomas in a regional trauma center in Hong Kong over a 4-year period. Patient risk factors were investigated using logistic regression.

Results Out of 464 patients with significant head injuries, 100 patients had acute subdural hematomas and were recruited for analysis. Forty-four percent of the patients achieved favorable neurological outcomes after 6 months. Favorable neurological outcomes at 1 year were related to age, pupil dilatation, and motor GCS scores at the time of admission. In the 34 patients who underwent evacuation of acute subdural hematomas, primary decompressive craniectomy was not associated with favorable neurological outcomes.

Conclusion Primary decompressive craniectomy failed to show benefit in terms of neurological outcomes and should be reserved for cases with uncontrolled intra-operative brain swelling.

Keywords Acute subdural hematoma • craniotomy • decompressive craniectomy • neurological outcome

Introduction

Despite studies of the impact of early craniectomy on patients with traumatic acute subdural hematoma (5,7,8) the value of primary decompressive craniectomies remains uncertain. There is only one literature reference that compares mortality rates between normal craniotomies and decompressive craniectomies (10). Woertgen et al. found that there was no difference between the two groups. However, their analysis was not adjusted for age, the Glasgow coma scale or signs of herniation. We sought to judge the value of decompressive craniectomy with reference to functional outcome after taking into account other patient disabilities. We designed the current study to investigate the impact of primary decompressive craniectomy on neurological outcomes as well as other prognostic factors.

Methods and Materials

We collected data from trauma patients with traumatic acute subdural hematomas in a regional trauma center in Hong Kong over a 4-year period. Out of 464 patients who had significant head injuries, 100 patients had acute subdural hematomas and were recruited for analysis. Of the 34 patients who underwent surgical evacuation of their hematomas, 15 were subjected to normal craniotomies, while 19 had decompressive craniectomies (one patient who had a craniotomy also had a secondary craniectomy afterwards). Data regarding the age, sex, Glasgow coma scale (9) (GCS), GCS motor component, signs of herniation (unilateral or bilateral pupil dilatation), extradural hematoma, cerebral contusions, traumatic subarachnoid hemorrhages, extracranial trauma and surgical procedures were recorded. We assessed the patient outcome using the Glasgow outcome scale (GOS) 6 months after injury (3). Favourable outcomes were defined as GOS 4–5 (good recovery and moderate disability including independent daily living activity), while unfavourable outcomes were defined as GOS 1–3 (severe disability, vegetative state or death).

G.K.-C. Wong (✉), Y.-W. Hung, C. Chong, S. Chi-Ping Ng, and W.-S. Poon
Division of Neurosurgery, The Chinese University of Hong Kong, Prince of Wales Hospital, Shatin, NT, Hong Kong SAR
e-mail: georgewong@surgery.cuhk.edu.hk

T. Rainer, and J. Yeung
Accident and Emergency Medicine Academic Unit, The Chinese University of Hong Kong, Prince of Wales Hospital, Shatin, NT, Hong Kong SAR

Statistical analysis was carried out with SPSS for Windows 14.0. Univariate analysis was performed with the Chi-Square test and the Mann–Whitney U test as appropriate. Multivariate analysis was performed using logistic regression. Statistical significance was defined as $p < 0.05$ (two-tailed).

Results

All patients were successfully evaluated after injury in our cohort. The cohort age (mean \pm SD) was 60.0 \pm 24.6 years, and the male to female ratio was 2:1. Thirty-three percent of the hematoma causes were related to road traffic accidents, 14% to falls from heights, 43% from falls at ground level (or below the height of one meter). Twenty-three percent of patients had significant extracranial injury (defined as an abbreviated injury score >2). Nine percent of patients had extradural hematoma, 44% had cerebral contusions and 36% had traumatic subarachnoid hemorrhages. A full 41% of the patients exhibited signs of herniation. The mean intensive care unit stay (mean \pm SD) was 2.8 \pm 5.7 days, and the total hospital stay was on average 12.3 \pm 18.9 days. With regard to the mode of evacuation of subdural hematoma, 15% had craniotomies performed, and 19% had craniectomies performed (18 primary and 1 secondary). Mortality rates were 38%, and 38% of patients required inpatient rehabilitation after hospital discharge. A favourable outcome was seen after 6 months in 44% of the patients.

The characteristics of patients as reported in this study and their relation to the patients' neurological outcomes are displayed in Tables 1 and 2. Univariate analysis showed that

unfavourable outcomes were associated with the conditions of being male, being older, having signs of herniation, having low GCS upon admission, and having a low GCS motor component upon admission.

Using a multivariate analysis, favourable outcomes were related to age (adjusted OR 0.94, 95% CI 0.92–0.97), pupil dilation (adjusted OR 2.15, 95% CI 1.2–114.5) and GCS motor score at admission (adjusted OR 2.15, 95% CI 1.44–3.21). In 34 patients with surgical evacuation of their hematomas, decompressive craniectomy (adjusted OR 0.42, 95% CI 0.08–2.20) was not associated with favourable outcomes after adjustments were made for the age, pupil dilatation and GCS motor scores.

Discussion

The preconditions necessary for surgical evacuation of traumatic acute subdural hematomas have previously been well defined. An acute subdural hematoma with a thickness greater than 10 mm or a midline shift greater than 5 mm as determined from a computed tomography scan should be surgically evacuated (1,4,11). However, there is no consensus regarding which surgical technique should be employed for evacuation of traumatic acute subdural hematomas. Some doctors perform craniotomies, while others perform decompressive craniectomies. In our unit, we used the question mark trauma flap with a bone flap of approximately 10 cm in all patients. Whether to perform a duroplasty and leave the bone flap out was left up to specialist neurosurgeons. Some doctors would leave the bone flap after decompressive craniectomies, while

Table 1 Univariate analysis of the categorical variables and their neurological outcomes

	Unfavourable outcome (56 patients)	Favourable outcome (44 patients)	Odds ratio, 95%CI, p-value
Sex (male)	79.5% (35)	55.4% (31)	0.32, 0.13 to 0.79, $p = 0.011$
Extradural hematoma	8.9% (5)	9.1% (4)	1.02, 0.26 to 4.05, $p = 0.978$
Cerebral contusion	41.1% (23)	47.7% (21)	1.31, 0.59 to 2.90, $p = 0.506$
Traumatic subarachnoid hemorrhage	39.3% (21)	31.8% (14)	0.72, 0.31 to 1.66, $p = 0.440$
Extracranial trauma	19.6% (11)	27.3% (12)	1.53, 0.60 to 3.91, $p = 0.368$
Signs of herniation	62.5% (35)	13.7% (6)	0.10, 0.03 to 0.26, $p < 0.001$
Craniotomy	33.9% (19)	34.1% (15)	1.01, 0.44 to 2.32, $p = 0.986$
Craniectomy	21.4% (12)	15.9% (7)	0.69, 0.25 to 1.94, $p = 0.485$

Table 2 Univariate analysis of continuous variables and their neurological outcomes

Mean \pm SD	Unfavourable outcome (56 patients)	Favourable outcome (44 patients)	p-Value
Age (mean \pm SD)	70.5 \pm 20.3	46.7 \pm 23.1	<0.001
GCS (median, interquartile range)	7.5, 4 to 14.75	14.5, 11 to 15	<0.001
GCS motor (median interquartile range)	4, 1.25 to 6	6, 5.25 to 6	<0.001
ICU stay (mean \pm SD)	2.4 \pm 5.9	3.3 \pm 5.5	<0.001
Hospital stay (mean \pm SD)	11.4 \pm 19.7	15.8 \pm 17.6	0.666

some would try to put the bone flap back if feasible. This provided an opportunity to carry out the current study.

In the literature, there is only one retrospective observational study that compares the mortality rates of patients undergoing craniotomies and those patients undergoing decompressive craniectomies to treat acute subdural hematomas (9). Woertgen et al. reported that decompressive craniectomies do not seem to have therapeutic advantages over craniotomies in traumatic acute subdural hematoma treatment and that they had a higher mortality rate (53% versus 32%). However, the results were not adjusted for other variables, and no data on the neurological outcome were available.

We found that patients undergoing decompressive craniectomies (after adjustment for age, GCS motor component and signs of herniation) did not have improved neurological outcomes at 6 months. However, decompressive craniectomies were not significantly associated with unfavourable outcomes. This may be explained by the fact that some bone flaps were not replaced because of severe intra-operative brain swelling. In the current study, the distribution of concomitant extradural hematomas, cerebral contusions and traumatic subarachnoid hemorrhages did not differ between the two groups.

The limitations of our current study are that it is observational in nature and has a limited sample size. Nevertheless, we were able to demonstrate that there was no benefit in terms of neurological outcome from primary decompressive craniectomies when compared to craniotomies. Given the potential complications arising from craniectomies, primary decompressive craniectomies should be reserved for patients with intractable intra-operative swelling that precludes placement of the bone flap.

It remains possible that some patients would benefit from decompressive craniectomy for treatment of subsequent severe cerebral edemas. Furthermore, there is no class I evidence to support the routine use of secondary decompressive craniectomies to reduce unfavourable neurological outcomes in adults with refractory high intracranial pressure (6). Two randomized controlled trials of decompressive craniectomies (RescueICP and DECRAN) are ongoing and are expected to assess the value of secondary decompressive craniectomies (2,6).

In conclusion, application of primary decompressive craniectomies failed to show patient benefits on neurological

outcomes and should be reserved for cases of uncontrolled intra-operative brain swelling. Whether secondary decompressive craniectomies are beneficial for cases of severe cerebral edema remains to be investigated.

Conflict of interest statement: We declare that we have no conflict of interest.

References

1. Bullock MR, Chesnut R, Ghajar J, Gordon D, Hartl R, Newell DW, Servadei F, Walters BC, Wilberger JE (2006) Surgical management of acute subdural hematomas. *Neurosurgery* 58:S2-16–S2-24
2. Hutchison PJ, Corteen E, Czosnyka M, Mendelow AD, Menon DK, Mitchell P, Murray G, Pickard JD, Rickels E, Sahuquillo J, Servadei F, Teasdale GM, Timofeev I, Unterberg A, Kirkpatrick PJ (2006) Decompressive craniectomy in traumatic brain injury: the randomized multicenter RESCUEicp study (www.RESCUEicp.com). *Acta Neurochir Suppl* 96:17–20
3. Jennett B, Bond M (1975) Assessment of outcome after severe brain damage. *Lancet* 1:480–484
4. Mathew P, Oluoch-Olunya D, Condon B, Bullock R (1993) Acute subdural haematoma in the conscious patient: outcome with initial nonoperative management. *Acta Neurochir (Wien)* 121:100–108
5. Ransohoff J, Benjamin MV, Gage EL, Epstein F (1971) Hemicraniectomy in the management of acute subdural haematoma. *J Neurosurg* 34:70–76
6. Sahuquillo J, Arikian F (2006) Decompressive craniectomy for the treatment of refractory high intracranial pressure in traumatic brain injury. *Cochrane Database Syst Rev*, Issue 1. Art. No.:CD003983. DOI: 10.1002/14651858.CD003983.pub2.
7. Seelig J, Becker D, Miller J, Greenberg R, Ward J, Choi S (1982) Traumatic acute subdural hematoma: major mortality reduction in comatose patients treated within four hours. *N Engl J Med* 304:1511–1518
8. Shigemori M, Syojima K, Nakayama K, Kojima T, Ogata T, Watanabe M, Kuramoto S (1980) The outcome from acute subdural haematoma following decompressive craniectomy. *Acta Neurochir (Wien)* 54:61–69
9. Teasdale G, Jennett B (1974) Assessment of coma and impaired consciousness: a practical scale. *Lancet* 2:81–84
10. Woertgen C, Rothoerl RD, Schebesch KM, Albert R (2006) Comparison of craniotomy and craniectomy in patients with acute subdural haematoma. *J Clin Neurosci* 13:718–721
11. Wong CW (1995) Criteria for conservative treatment of supratentorial acute subdural haematomas. *Acta Neurochir (Wien)* 135:38–43

Changes in the Blood–CSF Barrier in Experimental Traumatic Brain Injury

Mounir N. Ghabriel, Irena M. Zdziarski, Chris Leigh, and Robert Vink

Abstract

Purpose Elevation of intracranial pressure (ICP) is a major complication of traumatic brain injury (TBI), and cerebrospinal fluid (CSF) volume is a key factor in ICP regulation. Choroidal epithelial cells (CEC) form the blood–CSF barrier and their integrity is essential for controlling CSF production. In the current study, the morphology of the CEC was studied from 5 h to 28 day after TBI in the rat.

Methods Male Sprague-Dawley rats were subjected to severe TBI using the impact-acceleration model, and the ultrastructure of the CEC was studied using transmission (TEM) and scanning (SEM) electron microscopy.

Results Radical ultrastructural changes were seen by TEM in CEC in injured animals. At 5 h post-injury cell swelling and incipient cytoplasmic vacuoles were seen. At 24 h most severe changes were noted with extensive widening of intercellular clefts. At 7 day and 14 day post-injury, increased cytoplasmic electron density was evident. At 21 day, most microvilli had bulbous ends, and at 28 day cytoplasmic vacuoles were numerous with widened intercellular clefts. SEM revealed a continuum of changes in all injured animals and most conspicuous was the heterogeneity of surface features, with most cells showing bulbous and cup-shaped microvilli, burr-like processes and pits. Epiplexus cells were hypertrophic and more numerous.

Conclusion At 4 weeks after trauma, choroidal epithelial cells continued to show morphological alterations suggesting that brain homeostasis was still not restored.

Keywords Traumatic brain injury • choroidal epithelium • blood–CSF barrier • transmission electron microscopy • scanning electron microscopy

Introduction

Elevation of intracranial pressure (ICP) is a major complication of traumatic brain injury (TBI). The cerebrospinal fluid (CSF) volume is a major player in ICP regulation (2). It has been suggested that in the initial stages after trauma normal ICP is maintained due to compensatory mechanisms, one of which is the CSF volume, where its production is slowed and drainage increased (2). Once these mechanisms are exhausted, an exponential rise in ICP occurs (17). Choroidal epithelial cells (CEC) are the major producers of CSF via mechanisms that involve Na^+ , K^+ and HCO_3^- ion channels (14–16). These cells form a continuous covering for the choroid plexus, are joined by tight junctions and form the blood–CSF barrier (3,14,15). The structural integrity of CEC is essential for controlling the CSF composition and production.

It has been shown that under conditions of altered intracranial pressure, such as the effect of gravity in head-down tilt and microgravity in spaceflight, the apical morphology of CEC is altered (6,11). Furthermore, CEC ultrastructure is restored after adaptation to the earth's gravity (5). The choroid plexus and epiplexus cells were also shown to be sensitive to blast injury, displaying ultrastructural changes (9). The aim of the current study was to investigate the morphology of CEC in the acute phases post TBI and determine if any changes would be rectified by 4 weeks after trauma.

Materials and Methods

Animals and Induction of Traumatic Brain Injury

All experiments were approved by the Animal Ethics Committee of the University of Adelaide and complied with the Australian code of practice for the care and use of animals

M.N. Ghabriel (✉), I.M. Zdziarski, and C. Leigh
Discipline of Anatomical Sciences, School of Medical Sciences,
University of Adelaide, Adelaide, SA 5005, Australia
e-mail: mounir.ghabriel@adelaide.edu.au

R. Vink
Disciplines of Pathology and Neurosurgery, School of Medical
Sciences, University of Adelaide, Adelaide, SA 5005, Australia and
Hanson Institute Centre for Neurological Diseases, Institute of
Medical and Veterinary Sciences, Adelaide, SA 5000, Australia
e-mail: mounir.ghabriel@adelaide.edu.au

for scientific purposes. Sprague-Dawley male rats, average weight 410 g, were intubated and general anaesthesia achieved by inhalation of 2% isoflurane in oxygen. Severe TBI was induced using the impact acceleration model (10), where a weight of 450 g was dropped onto a protective disc adhered to the exposed skull from a height of 2 m (7,18). Three animals were killed at 5 h, 1 day, 7 day, 14 day, 21 day and 28 day post-injury and three additional animals were not injured and used as controls.

Animal Perfusion and Tissue Preparation

Animals were anaesthetised by intraperitoneal injection of pentobarbitone sodium (60 mg/kg). The circulation was flushed via the left ventricle with phosphate-buffered saline (PBS, pH 7.4, gassed with 95% O₂: 5% CO₂) for 30 s, followed by the fixative, 4% paraformaldehyde–2% glutaraldehyde in 0.1 mol phosphate buffer, pH 7.4, under constant pressure of 100 mmHg. The brain was divided in the midline then post-fixed for 3 h. The choroid plexus was removed from the right and left lateral ventricles and conventionally processed for transmission (TEM) and scanning electron microscopy (SEM) respectively. Philips CM100 and Philips XL30 FEG were used for TEM and SEM respectively.

Results

TEM

In controls (Fig. 1) most CEC had moderately electron dense cytoplasm with basal nuclei and slender long densely-packed microvilli. The lateral membranes of neighbouring cells were closely apposed and joined by tight junctions. A basal lamina ran a straight continuous course against the basal membranes. Complex interdigitations of processes from the basal corners existed in all cells. However, some cells showed relatively electron-lucent cytoplasm with spaced organelles, bulbous-ending microvilli, and occasional small focal widening of the intercellular spaces.

Ultrastructural changes were seen in all injured animals from 5 h to 28 day. At 5 h (Fig. 1C) CEC showed relatively lighter cytoplasm with vacuoles, focal widening of the intercellular clefts and separation of the basal interdigitations. The 24 h time period showed the most severe ultrastructural changes (Fig. 1D), with extreme cellular spacing. Although stretched, epithelial cells maintained some focal points of contact near the ventricular surface, where tight junctions are normally located. The wide intercellular clefts and cytoplasmic vacuoles occupied more surface area than the cell cyto-

plasm. At 7 day, 14 day and 21 day (Fig. 1E–G) cytoplasmic vacuoles were less than at 1 day but intercellular clefts remained wide. Many cells had electron dense cytoplasm and were pulling away from adjacent cells. There was an obvious disruption of microvilli and many had large bulbous ends, complex lamellae and lattice formation. Some bulbous ends appeared ruptured, discharging their contents. Mono-nuclear cells were seen in the intercellular clefts at 7 day. At 28 day (Fig. 1H) microvilli in many cells were thicker and retained bulbous terminations. Many cells had lighter cytoplasm with vacuoles and wide intercellular clefts still seen, although tight junctions were visible at the ventricular end of the cleft.

SEM

The choroid plexus in control animals (Fig. 2A–C) showed uniform morphology of major and minor fronds, each formed of several cells across. Demarcations between cells were apparent as shallow grooves between domed cells. Most cells in controls had thin microvilli, but many of these showed flattened ends forming racket-shaped or spoon-shaped microvilli. A minority of cells showed microvilli with bulbous ends that were taller than surrounding cells. Burr-like projections, tufted processes and a few pits were also seen. Epiplexus cells seen on the ventricular surface had long primary processes with flattened end feet from which projected thin secondary processes.

In injured animals a continuum of changes were seen at all time intervals with heterogeneous cell populations, but each time period had some salient features. At 5 h (Fig. 2D) and 1 day (Fig. 2E) CEC showed a pronounced domed appearance and heterogeneous population as many cells started to show swollen microvilli. At 7 day (Fig. 2F) surface pits were numerous and most cells had microvilli with bulbous ends. At 14 day (Fig. 3A, B) there was an apparent increase in the burr-like protrusions and thick broad lamellar microvilli. Most striking at 21 day (Fig. 3C, D) was the bulbous and cup-shaped long microvilli, with many carrying sessile and pedunculated vesicles. At 28 day (Fig. 3E, F) cup-shaped and bulbous microvilli were still apparent in many cells. At all time periods surface pits were evident. Red blood cells were encountered at earlier time periods at the ventricular surface indicating intra-ventricular haemorrhage. Epiplexus cells were seen in increasing frequency in injured animals and showed hypertrophy.

Discussion

The current study demonstrated severe morphological alterations in CEC in TBI throughout the 4 week study period. It is of interest to consider whether these changes

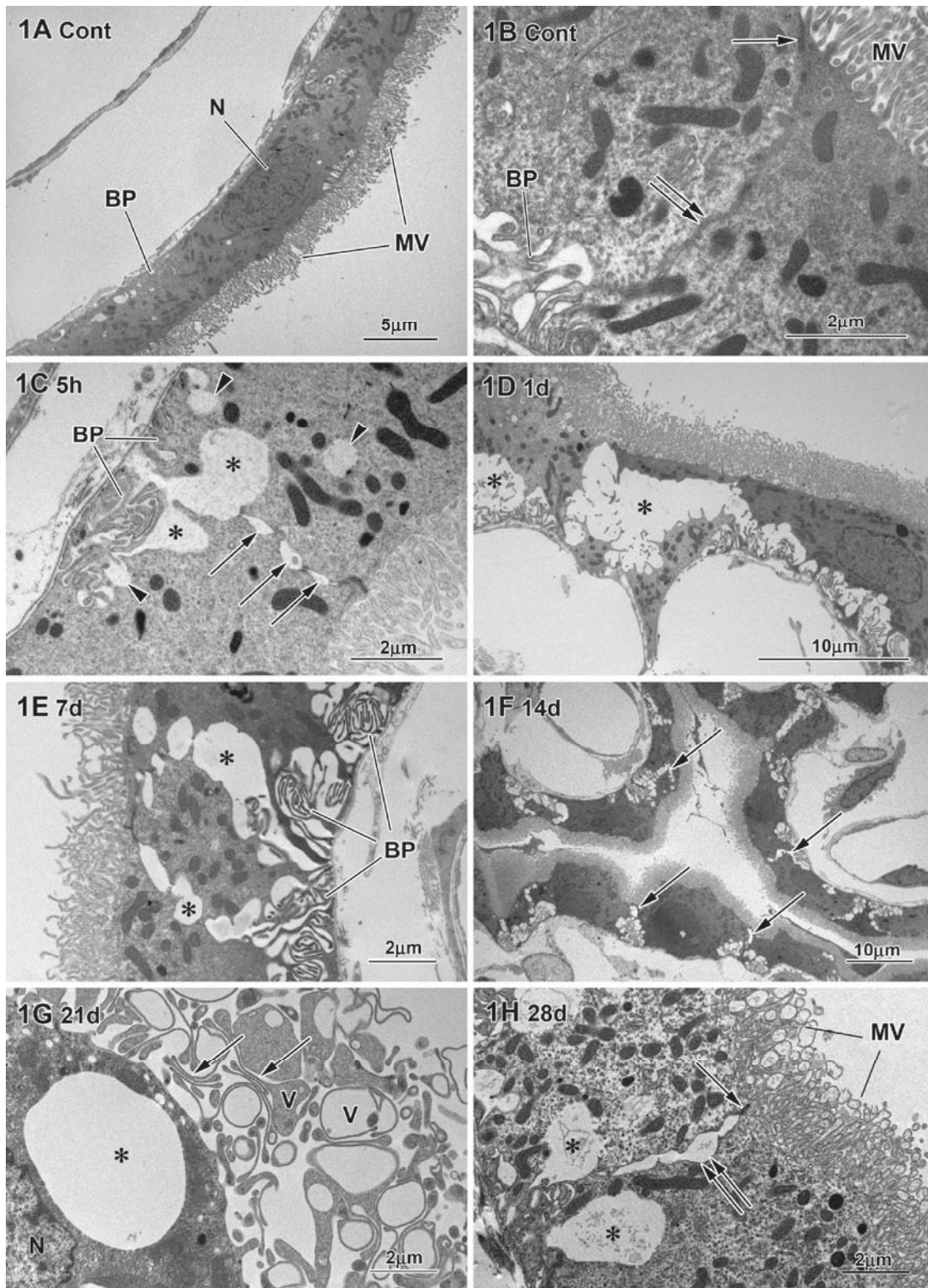


Fig. 1 (A–H) TEM micrographs of choroidal epithelial cells from control animals (A) and (B) showing slender densely packed microvilli (MV), moderately electron dense cytoplasm rich in mitochondria, closely apposed lateral membranes (*double arrows*), a tight junction (*arrow*), basal processes (BP) and a basal nucleus (N). (C) Injured animal at 5 h showing incipient dilations of an intercellular cleft (*arrows*), cytoplasmic vacuoles (*arrowheads*) and large cavities (*asterisks*) communicating with the intercellular cleft. Basal processes (BP) of neighbouring cells are separated. (D) Injured animal at 1 day showing extensive widening of intercellular clefts (*asterisks*). (E) Injured animal

at 7 day showing extensive basal processes (BP) with widened intercellular clefts (*asterisks*). (F) Injured animal at 14 day, the epithelium shows widespread separation of intercellular contacts (*arrows*). (G) Injured animal at 21 day showing lamellar arrangement of microvilli (*arrows*), extensive dilatation of microvilli appear as vesicles (V) some contained cytoplasm and others are empty, and a large cytoplasmic vacuole (*asterisk*) located apical to the nucleus (N). (H) Injured animal at 28 day showing electron-light cytoplasm, a tight junction (*arrow*), bulbous-ending microvilli (MV), dilated intercellular cleft (*double arrow*) and large cytoplasmic vacuoles (*asterisks*)

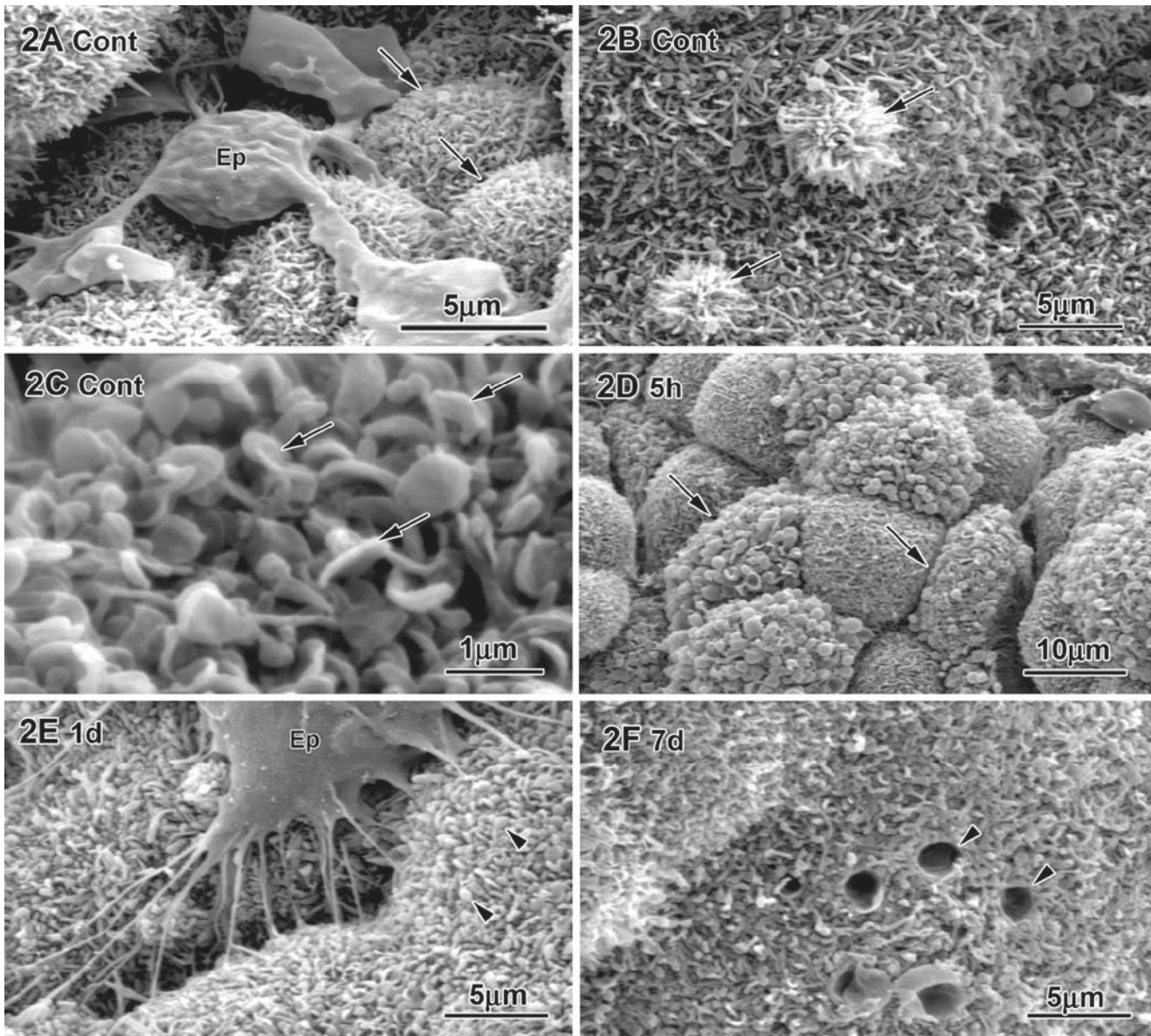


Fig. 2 (A–F) SEM micrographs of choroidal epithelial cells (CEC) from control (A–C) and injured (D–F) animals. (A) CEC have domed surfaces separated by shallow grooves (*arrows*). An epiplexus cell (Ep) has processes with flattened end feet that project secondary thin processes. (B) Shows CEC with finger-like microvilli and burr-like processes (*arrows*). (C) High magnification shows microvilli with flat ends, particularly seen in side view (*arrows*) and some of these have a

curved spoon-shaped appearance. (D) Injured animal at 5 h, CEC show increased dome appearance with more demarcated grooves (*arrows*). Several cells show taller bulbous microvilli. (E) Injured animal at 1 day. Microvilli have moderately distended ends (*arrowheads*). An epiplexus cell shows a distended end foot process (Ep) from which thin long secondary processes are projected. (F) Injured animals at 7 day showing increased number of surface pits (*arrowheads*)

are adaptive to assist brain recovery or are pathological changes (a) produced primarily due to trauma to the choroid plexus, or (b) have occurred secondary to biochemical changes in the brain internal environment. TBI is often associated with subarachnoid and intra-ventricular haemorrhage which may have initiated such morphological changes. Indeed, red blood cells were seen in the current study lying on the microvilli of CEC. Secondly it is important to consider whether the altered morphology of CEC

was causative or consequential to increased intracranial pressure known to occur in TBI.

Severe widening of intercellular clefts was seen particularly at the 1 day to 14 day periods. It is not known from this study if the fluid accumulating in these spaces is derived from the CSF, passing retrogradely between CEC, or if it is derived from the leaky choroidal capillaries in the core of the plexus. Retrograde transport of fluids implies reversal of the polarised function of CEC. Bulbous ending

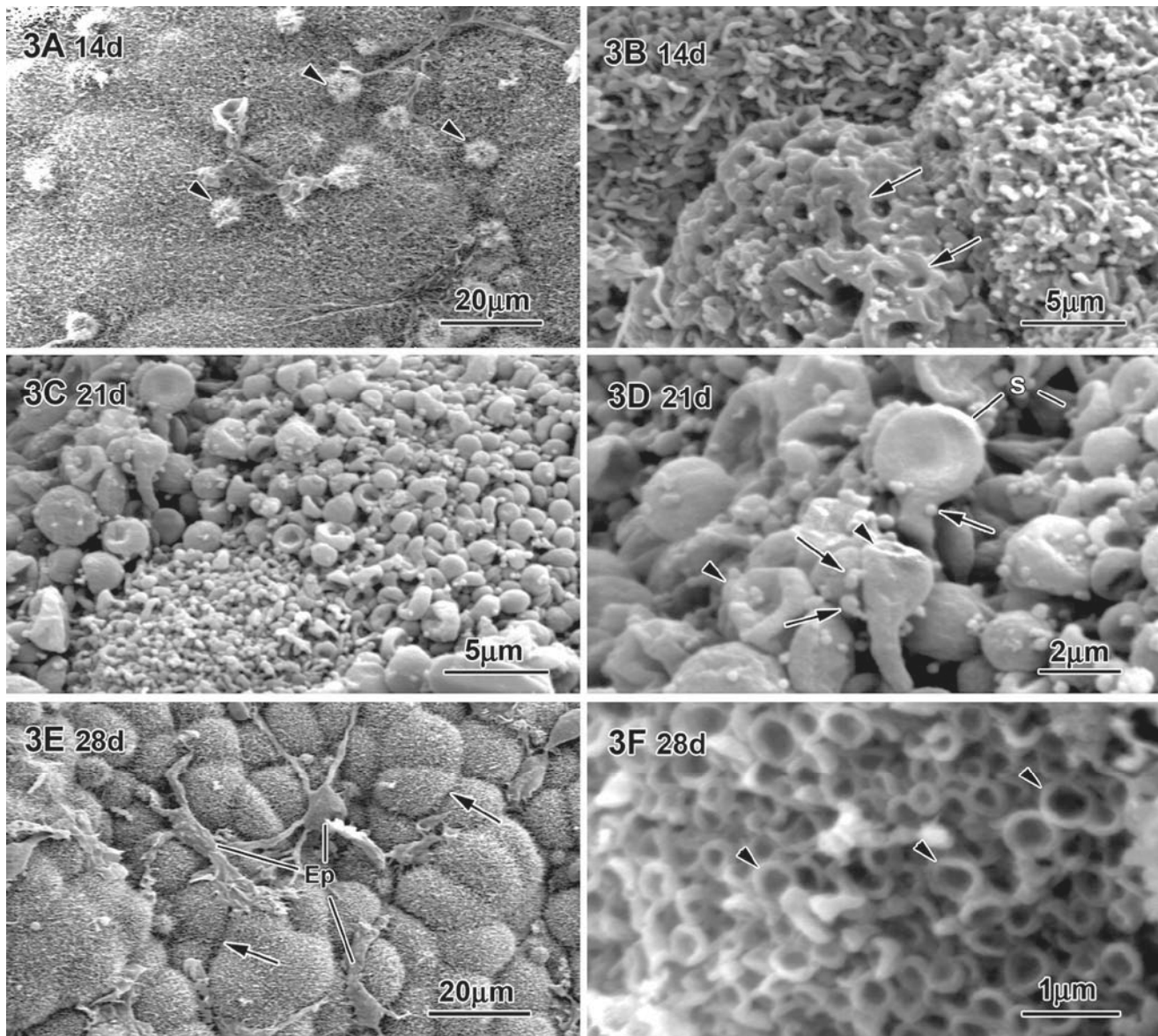


Fig. 3 (A–F) Injured animals. (A) and (B) CEC 14 day post-injury showing increased burr-like processes (*arrowheads*) and broad lamellar processes (*arrows*) likely to have formed by side fusion of microvilli. (C) and (D) Injured animals at 21 day, (C) shows cells with much taller and bulbous-ending microvilli, surrounding a cell with relatively short though

distended microvilli. (D) Is a higher magnification showing spoon-shaped (S) and cup-shaped (*arrowheads*) microvilli with many sessile and pedunculated surface microvesicles (*arrows*). (E) and (F) Injured animals at 28 day showing domed cells demarcated with grooves (*arrows*), many epi-plexus cells (EP), and cup-shaped microvilli (*arrowheads*) seen end-on

microvilli and surface blebs have been suggested as a physiological mechanism for discharging CSF components from the epithelial cells (12). This morphological feature was extensively seen in injured animals, which therefore does not support a retrograde function. Previous studies employing systemic administration of the protein tracer horseradish peroxidase demonstrated its passage between epithelial cells towards the ventricle, but not past the tight junctions, and it was also seen in cytoplasmic vesicles that accumulated beneath the apical membranes but did not dis-

charge into the ventricle (3). Furthermore, intraventricular administration of the tracer did not show any transport towards the core of the plexus (3). Thus a retrograde route for fluid accumulation in the intercellular clefts seen in this study is unlikely.

Although morphological changes were seen throughout the study period, specific features were seen in epithelial cells at certain time periods. The electron-lucent cytoplasm particularly seen at 5 h, 21 day and 28 day in association with organelles dispersion may reflect cell oedema. This

may represent a specific phase in the acute events and prior to recovery. On the other hand, the dark severely distorted cells seen at 7 day and 14 day may reflect a different phase and perhaps a different function. The significance of these morphologically distinct populations and their role is currently unknown.

The use of both TEM and SEM in the current study allowed correlation between 2D sections and 3D images for further interpretation of the morphological changes. In TEM of controls microvilli appeared as thin finger-like processes. However, in SEM many of these microvilli had flattened tips giving a racket-like appearance, and often their flat ends were curved giving a spoon-like shape. Although the surface views in SEM show continuity of cells at all time periods, TEM showed severe distension of the intercellular clefts just under the surface, particularly at 1 day–14 day where the cells had lost much of their normal contact along the lateral membranes.

In the current study of lateral ventricle choroid plexus, SEM demonstrated heterogeneity of CEC in control animals, where cells with slender microvilli, racket-shaped microvilli or spoon-shaped microvilli, surrounded a minority of cells with bulbous-ending microvilli. Bulbous-ending microvilli have been reported previously (9,12) and was considered to be a normal appearance of actively secreting cells and an evidence of diversity in the surface morphology of CEC in normal rats. It is of interest to note here that a previous study has found that bleb-forming cells are much less common in the lateral ventricle but more abundant in the fourth ventricle (4). It was also reported that administration of acetazolamide, which interferes with active transport of chloride ions and reduces the rate of CSF secretion through its carbonic anhydrase inhibition, was accompanied by reduced number of bleb-carrying cells, and that these bleb-forming cells are the specific sites for the extra chloride secretion that is added to the CSF in the fourth ventricle (4). In the current study of injured animals there was extensive increase in the cells carrying bulbous microvilli which may indicate excessive chloride secretion and increased CSF in the injured animals. Under physiological conditions a transient elevation of ICP that may occur during daily activities may be tolerated by some adaptive mechanisms. It has been shown experimentally that the rate of CSF production is decreased when the CSF pressure is increased (8), and that elevation of ICP leads to increased drainage of CSF via arachnoid villi and extracranial lymphatics (2).

Epiplexus cells are considered as resident phagocytes of the brain (1) and their number is augmented from haematogenous monocytes in head trauma in non-human primates (13). In the current study monocytes were encountered during passage through intercellular clefts, and epiplexus cells were more frequently seen in injured animals and showed hypertrophy with extended processes and much irregular

surface. This suggested an increased phagocytic activity perhaps for removal of particulate matter in the CSF, material extruded from CEC, remnants of cell membranes or red blood cells that leaked into the ventricle.

In conclusion, this study demonstrated that 4 weeks after trauma, the choroidal epithelium still displayed altered morphology suggesting that brain homeostasis is not restored. It is suggested that the altered morphology seen here is maladaptive, represents severe pathological changes and is likely to contribute to increased intracranial fluids and pressure. We tentatively suggest that the CSF would contain increased chloride content. Understanding water homeostasis in the brain is crucial for successful management of patients with traumatic brain injury. The morphology, physiology and molecular biology of CEC in TBI merit further investigation.

Conflict of interest statement We declare that we have no conflict of interest.

Acknowledgement We would like to acknowledge the expert assistance of Mr Peter Self of Adelaide Microscopy, and Mr Tavik Morgenstern and Mrs Gail Hermanis of the Discipline of Anatomical Sciences. This Study was supported by a grant from The Faculty of Health Sciences, University of Adelaide.

References

1. Bleier R, Albrecht R, Cruce JAF (1975) Supraependymal cells of the hypothalamic third ventricle: identification as resident phagocytes of the brain. *Science* 189:299–301
2. Boulton M, Armstrong D, Flessner M, Hay J, Szalai JP, Johnston M (1998) Raised intracranial pressure increases CSF drainage through arachnoid villi and extracranial lymphatics. *Am J Physiol* 275 (Regulatory Integrative Comp Physiol 44):R889–R896
3. Brightman MW (1968) The intracerebral movement of proteins injected into blood and cerebrospinal fluid of mice. *Prog Brain Res* 29:19–40
4. Collins P, Morriss GM (1975) Changes in the surface features of choroid plexus of the rat following the administration of acetazolamide and other drugs which affect CSF secretion. *J Anat* 120:571–579
5. Davet J, Clavel B, Datas L, Mani-Ponset L, Maurel D, Herbuté S, Viso M, Hinds W, Jarvi J, Gabrion J (1998) Choroidal readaptation to gravity in rats after spaceflight and head-down tilt. *J Appl Physiol* 84:19–29
6. Gabrion J, Maurel D, Clavel B, Davet J, Farih J, Herbuté S, O'Mara K, Gharib C, Hinds W, Krasnov I, Guell A (1996) Changes in apical organization of choroidal cells in rats adapted to spaceflight or head-down tilt. *Brain Res* 734:301–315
7. Ghabriel MN, Thomas A, Vink R (2006) Magnesium restores altered aquaporin-4 immunoreactivity following traumatic brain injury to a re-injury state. *Acta Neurochir (Wien) [Suppl]* 96:402–406
8. Hochwald GM, Sahar A (1971) Effect of spinal fluid pressure on cerebrospinal fluid formation. *Exp Neurol* 32:30–40
9. Kaur C, Singh J, Lim MK, Ng BL, Yap EP, Ling EA (1996) Studies of the choroid plexus and its associated epiplexus cells in the lateral

- ventricles of rats following an exposure to a single non-penetrative blast. *Arch Histol Cytol* 59:239–248
10. Marmarou A, Foda MA, Van Den Brink W, Campbell J, Kita H, Demetriadou K (1994) A new model of diffuse brain injury in rats. Part I: Pathophysiology and biomechanics. *J Neurosurg* 80:291–300
 11. Maseguin C, Mani-Ponset L, Carcenac C, Herbuté S, Tixier-Vidal A, Gabrion J (2001) Persistence of tight junctions and changes in apical structures and protein expression in choroid plexus epithelium of rats after short-term head-down tilt. *J Neurocytol* 30:365–377
 12. Mathew TC (2007) Diversity in the surface morphology of adjacent epithelial cells of the choroid plexus: an ultrastructural analysis. *Mol Cell Biochem* 301:235–239
 13. Maxwell WL, Hardy IG, Watt C, McGadey J, Graham DI, Adams JH, Gennarelli TA (1992) Changes in the choroid plexus, responses by intrinsic ependymal cells and recruitment from monocytes after experimental head acceleration injury in the non-human primate. *Acta Neuropathol* 84:78–94
 14. Redzic ZB, Segal MB (2004) The structure of the choroid plexus and the physiology of the choroid plexus epithelium. *Adv Drug Deliv Rev* 56:1695–1716
 15. Segal MB (2000) The choroid plexus and the barriers between the blood and the cerebrospinal fluid. *Cell Mol Neurobiol* 20:183–196
 16. Speake T, Whitwell C, Kajita H, Majid A, Brown PD (2001) Mechanisms of CSF secretion by the choroid plexus. *Microsc Res Tech* 52:49–59
 17. Steiner LA, Andrews PJD (2006) Monitoring the injured brain: ICP and CBF. *Br J Anaesth* 97:26–38
 18. Vink R, O'Connor CA, Nimmo AJ, Heath DL (2003) Magnesium attenuates functional deficits following diffuse traumatic brain injury in rats. *Neurosci Lett* 336:41–44

Dynamics of S100B Release into Serum and Cerebrospinal Fluid Following Acute Brain Injury

A. Kleindienst, S. Meissner, I.Y. Eyupoglu, H. Parsch, C. Schmidt, and M. Buchfelder

Abstract High S100B serum levels are considered to reflect brain injury severity. However, the dynamics of S100B passage from the cerebral compartment into the blood remain unclear. We examined the temporal profile of S100B release into the cerebrospinal fluid (CSF) and blood in acute brain injury.

In patients treated with ventricular drainage (subarachnoid hemorrhage, SAH, $n = 23$; traumatic brain injury, TBI, $n = 19$), we measured S100B levels in the serum and CSF. The Glasgow Coma Score (GCS) was assessed daily. Statistical analysis was performed by the Mann–Whitney rank sum test for group differences and by the Pearson correlation.

In normal controls ($n = 6$), S100B levels in the serum ($0.05 \pm 0.01 \mu\text{g/L}$) comprised around 10% of the CSF concentration ($0.66 \pm 0.08 \mu\text{g/L}$). Following brain injury, S100B levels were significantly increased in the serum ($p < 0.05$ in SAH day 2–5, TBI day 1–8) and excessively increased in the CSF ($p < 0.05$ in SAH and TBI day 1–10). For the individual patient, there was no consistent correlation between S100B levels in serum or CSF and GCS. We therefore calculated the ratio of S100B serum/CSF. Following brain injury, the S100B passage from the CSF to the blood was significantly impaired. Further, higher ratios were correlated with better neurological function ($p = 0.002$).

Because stimulated active S100B release may serve as a repair mechanism, a higher S100B serum/CSF ratio may contribute to neurological recovery.

Keywords Biomarker • outcome • neurotrophic factor • traumatic brain injury

Introduction

The early assessment of injury severity and consequent prognosis are major concerns for physicians treating patients suffering from brain injury, and there is a desire for a reliable indicator to accurately determine the extent of the brain damage. The measurement of putative biochemical markers, such as the S100B protein, has been proposed in this role. Over the past decade, numerous studies have reported a positive correlation between S100B serum levels and poor outcome following brain injury (10). However, some evidence raises doubts regarding whether the serum measurement of S100B is a valid biomarker of brain damage (7).

The neurotrophic protein S100B belongs to a multigenic family of low molecular weight (9–13 kD) calcium-binding S100 proteins (5). S100B is most abundant in glial cells of the central nervous system, predominately in astrocytes (3). Experimental findings demonstrate that S100B is secreted from astroglia within a few minutes after receptor activation, and release may last up to 10 h (2, 12). Although injury-induced S100B release continues to increase up to 48 h in cell cultures (11, 13), S100B serum levels in patients are highest directly after the injury and become normalized within 24 h in a high percentage of cases (even in those patients with a bad outcome) (6). The underlying mechanism describing the passage of S100B through the blood–brain-barrier (BBB) has not yet been clarified, nor do data exist regarding cerebral S100B levels and their correlation to serum S100B levels.

The purposes of the present study were to (1) examine the temporal profile of S100B release into the cerebrospinal fluid (CSF) and blood in patients with acute brain injury and (2) correlate the respective S100B levels with the neurological function. By calculating the ratio of S100B in the CSF/serum, we aimed to estimate the blood–CSF–barrier integrity and correlate the ratio to neurological recovery.

Methods

Thirty-nine consecutive patients admitted to our neurosurgical intensive care unit due to severe traumatic brain injury (TBI,

A. Kleindienst (✉), S. Meissner, I.Y. Eyupoglu, C. Schmidt, and M. Buchfelder

Department of Neurosurgery, Friedrich-Alexander-University Erlangen-Nuremberg, Schwabachanlage 6, Erlangen D-91054, Germany
e-mail: andrea.kleindienst@uk-erlangen.de

H. Parsch
University Erlangen-Nuremberg, Central Laboratory, Erlangen, Germany

n = 19) or subarachnoid hemorrhage (SAH, Hunt&Hess grade 1 n = 4, H&H 2 n = 5, H&H 3 n = 6, H&H 4 n = 4, H&H 5 n = 4) and treated with a ventricular drainage are included in the study. The mean age of the patients was 39.9 ± 22.8 years in the TBI group and 59.6 ± 14.7 in the SAH group. We measured S100B levels daily in the serum and CSF (Elecsys® S100 Immunoassay, Roche Diagnostics, measuring range 0.005–39 µg/L) for 10 days. Neurological function was assessed by the Glasgow Coma Score (GCS). The control group consisted of six patients (mean age 51.9 ± 18.0) who were treated with a lumbar drainage to control CSF leakage following transsphenoidal pituitary surgery. In the control patients, S100B levels in the serum and CSF were measured daily for 6 days, the lumbar drainage was then removed.

The study protocol was approved by the local ethical committee. Exclusion criteria were an age below 18 years, an infaust prognosis, and failure to obtain consent from either

patients or their relatives. Statistical analysis was performed by the Mann–Whitney rank sum test for group differences and by the Pearson correlation. Statistical significance was accepted at p < 0.05.

Results

The normal values were established in control patients undergoing pituitary surgery. The time course of the S100B concentration in the CSF and serum is displayed in Fig. 1. S100B levels in the serum were increased on day 1 in control patients, whereas S100B levels in the CSF were increased on days 1 and 2. Stable basal levels (normal S100B levels in the serum and CSF were 0.05 ± 0.01 and 0.66 ± 0.08 µg/L, respectively) were then achieved. Statistical comparison by

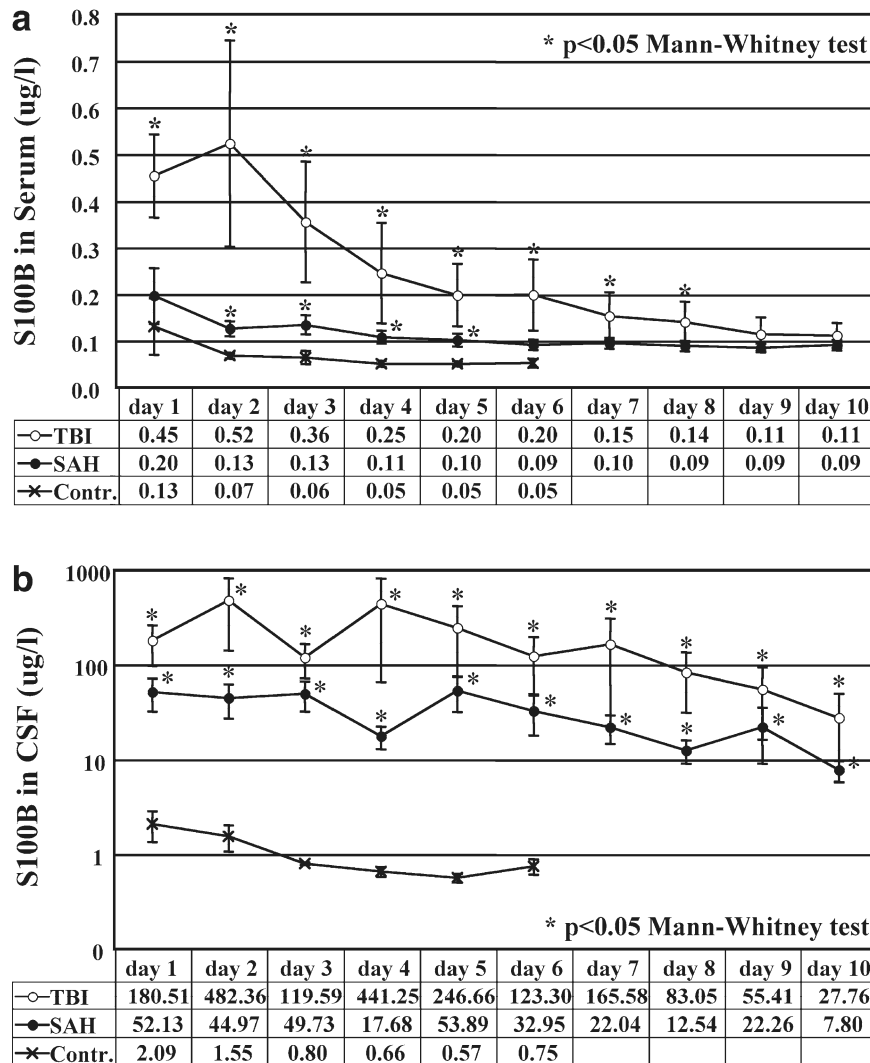


Fig. 1 (a) and (b) Mean S100B levels in the serum and cerebrospinal fluid of patients on day 1 to 10 following subarachnoid hemorrhage or traumatic brain injury and in the control group. The values are given as mean ± SD. An asterisk represents a significant difference compared to the control group

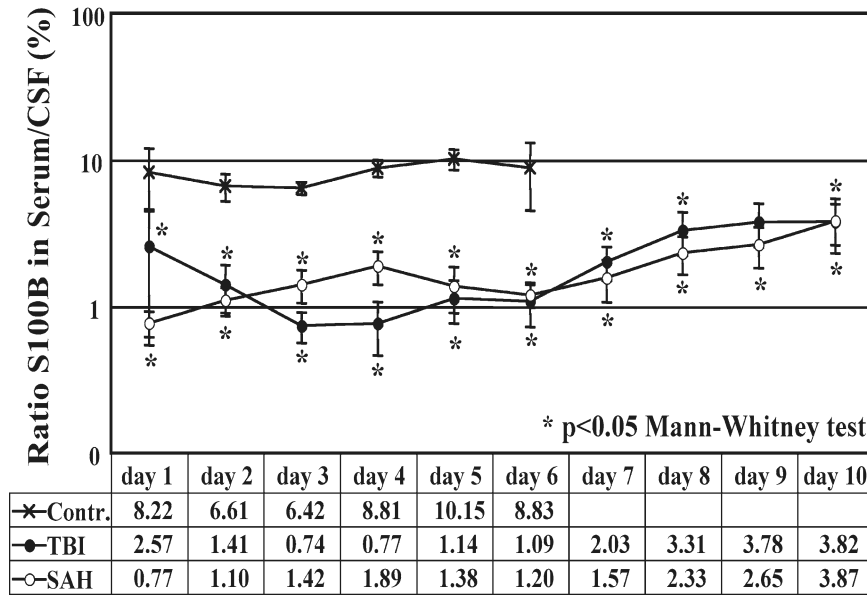


Fig. 2 The ratio of S100B serum/CSF is calculated in order to provide an estimate of the CSF–blood–barrier integrity. The values are given as mean ± SD. In the control group, a constant S100B turnover results in serum levels

of S100B being roughly 10% of the respective CSF levels. Interestingly, this ratio is decreased in patients with acute brain damage, reflecting impaired passage through the endothelial cells of the ventricle plexus

the Whitney–Mann rank sum test demonstrated that following TBI, S100B levels were significantly increased in the serum on day 1 to 8 ($p < 0.05$, day 1: $0.47 \pm 0.39 \mu\text{g/L}$, day 10: $0.12 \pm 0.12 \mu\text{g/L}$) and in the CSF on day 1 to 10 ($p < 0.05$, day 1: $198.52 \pm 340.17 \mu\text{g/L}$, day 10: $29.85 \pm 85.21 \mu\text{g/L}$). Following SAH, S100B levels were significantly increased in the serum on day 2 to 5 ($p < 0.05$, day 1: $0.20 \pm 0.27 \mu\text{g/L}$, day 10: $0.09 \pm 0.04 \mu\text{g/L}$) and in the CSF on day 1 to 10 ($p < 0.05$, day 1: $54.13 \pm 9.27 \mu\text{g/L}$, day 10: $7.80 \pm 7.78 \mu\text{g/L}$). In the control patients, S100B in the serum comprised around 10% of the CSF concentration (Fig. 2). Following both TBI and SAH, this ratio was significantly reduced to 1% to 4% for the investigation period ($p < 0.05$).

Within the groups, there was no consistent correlation between S100B concentrations in either the serum or CSF and GCS (Fig. 3). For example, high serum S100B levels on day 1 following TBI were correlated with a better neurological function on day 4 and 5 ($r = 0.553$, $p = 0.040$ and $r = 0.534$, $p = 0.049$). Patients with a less severe TBI (i.e. high GCS values) upon admission had significantly higher S100B CSF levels on day 3 ($r = 0.722$, $p = 0.018$). On the other hand, patients with impaired neurological function upon admission had significantly higher S100B serum levels on day 1 ($r = -0.739$, $p = 0.036$) and CSF levels on day 2 ($r = -0.689$, $p = 0.040$). When we calculated a ratio of S100B serum/CSF, however, there was a consistent correlation between a higher ratio (i.e. restored passage from the CSF into the blood) and better neurological functioning (e.g. TBI on day 6: $r = 0.622$, $p = 0.023$ and SAH on day 4: $r = 0.724$, $p = 0.002$).

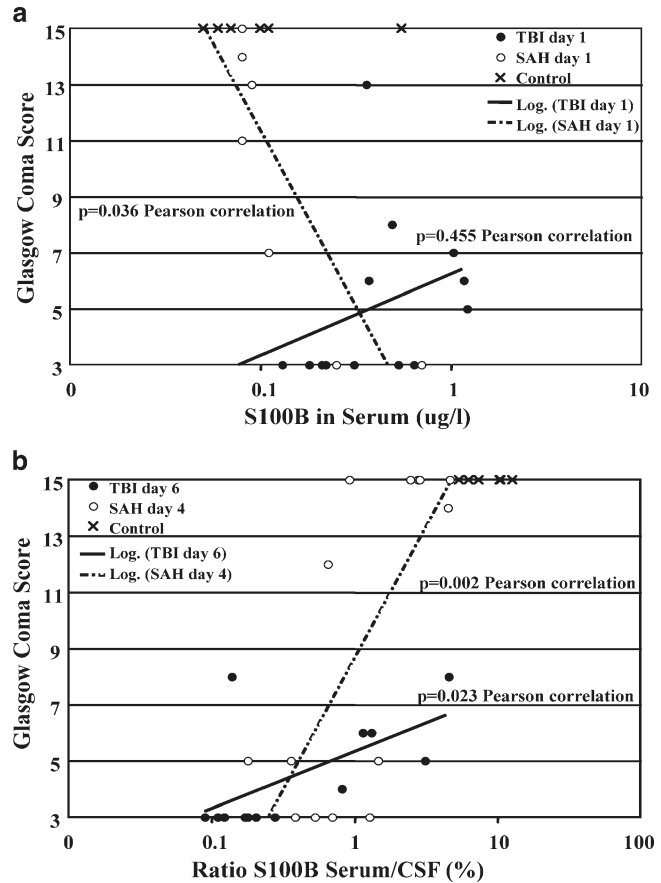


Fig. 3 (a) Pearson correlation between S100B serum levels and neurological function, as assessed by the Glasgow Coma Score on day 1 after admission. (b) Pearson correlation between the ratio of S100B serum/CSF and the Glasgow Coma Score

Discussion

Neither the role of S100B in the acutely injured brain nor the release pattern of S100B into the CSF and blood is well known as of yet. In light of a substantial body of evidence demonstrating an association between S100B and bad outcome after acute brain injury, it is important to be aware that proof of an association is not proof of causation in science; this is especially true for S100B. Increased S100B concentrations in the blood have been attributed to an increased passage of S100B from the brain through an impaired BBB following injury. Furthermore, experimental data provide evidence that S100B does not cross the intact BBB (8). Thus, the initially high S100B serum levels following injury may reflect its increased passage from the brain through a compromised BBB. However, it is important to be aware of the notion that neither high S100B serum levels nor high S100B CSF concentrations reliably reflect impaired neurological function. This finding is in line with evidence for the participation of S100B in neuroregeneration, i.e. learning and memory processes and developmental plasticity (1, 4, 9). Thus, the high S100B CSF concentrations found in our patients may reflect either passive release from damaged astrocytes or active release serving as a repair mechanism.

Little is known about the CSF-blood-barrier in acute brain damage. Ultrastructural examinations of the choroidal epithelial cells forming the CSF-blood-barrier following experimental injury demonstrate pronounced changes lasting up to 4 weeks post-injury (Ghabriel et al., this volume). Accordingly, the decreased passage of S100B from the CSF into the blood found in our patients may result from damaged choroidal epithelial cells. Restoration of the normal passage of S100B through the CSF-blood-barrier is significantly correlated with better neurological functioning.

Conflict of interest statement We declare that we have no conflict of interest.

Acknowledgement This study was supported by a grant of the Hannelore Kohl Stiftung-Kuratorium ZNS to A.K.

References

1. Agelink MW, Andrich J, Postert T, Wurzing U, Zeit T, Klotz P, Przuntek H (2001) Relation between electroconvulsive therapy, cognitive side effects, neuron specific enolase, and protein S-100. *J Neurol Neurosurg Psychiatry* 71:394–396
2. Ciccarelli R, Di Iorio P, Bruno V, Battaglia G, D'Alimonte I, D'Onofrio M, Nicoletti F, Caciagli F (1999) Activation of A(1) adenosine or mGlu3 metabotropic glutamate receptors enhances the release of nerve growth factor and S-100beta protein from cultured astrocytes. *Glia* 27:275–281
3. Donato R (1986) S-100 proteins. *Cell Calcium* 7:123–145
4. Fazeli MS, Errington ML, Dolphin AC, Bliss TV (1990) Extracellular proteases and S100 protein in long-term potentiation in the dentate gyrus of the anaesthetized rat. *Adv Exp Med Biol* 268:369–375
5. Heizmann CW, Fritz G, Schafer BW (2002) S100 proteins: structure, functions and pathology. *Front Biosci* 7:d1356–d1368
6. Jackson RG, Samra GS, Radcliffe J, Clark GH, Price CP (2000) The early fall in levels of S-100 beta in traumatic brain injury. *Clin Chem Lab Med* 38:1165–1167
7. Kleindienst A, Ross Bullock M (2006) A critical analysis of the role of the neurotrophic protein S100B in acute brain injury. *J Neurotrauma* 23:1185–1200
8. Kleindienst A, Toliaas CM, Corwin FD, Muller C, Marmarou A, Fatouros P, Bullock MR (2005) Assessment of cerebral S100B levels by proton magnetic resonance spectroscopy after late-ral fluid-percussion injury in the rat. *J Neurosurg* 102:1115–1121
9. McAdory BS, Van Eldik LJ, Norden JJ (1998) S100B, a neurotrophic protein that modulates neuronal protein phosphorylation, is upregulated during lesion-induced collateral sprouting and reactive synaptogenesis. *Brain Res* 813:211–217
10. Rothermundt M, Peters M, Prehn JH, Arolt V (2003) S100B in brain damage and neurodegeneration. *Microsc Res Tech* 60: 614–632
11. Slemmer JE, Matser EJ, De Zeeuw CI, Weber JT (2002) Repeated mild injury causes cumulative damage to hippocampal cells. *Brain* 125:2699–2709
12. Whitaker-Azmitia PM, Murphy R, Azmitia EC (1990) Stimulation of astroglial 5-HT1A receptors releases the serotonergic growth factor, protein S-100, and alters astroglial morphology. *Brain Res* 528:155–158
13. Willoughby KA, Kleindienst A, Muller C, Chen T, Muir JK, Ellis EF (2004) S100B protein is released by in vitro trauma and reduces delayed neuronal injury. *J Neurochem* 91:1284–1291

Ultrastructural and Immunochemical Studies of Glial Scar Formation in Diabetic Rats

Malgorzata Frontczak-Baniewicz, Lidia Struzynska, Jaroslaw Andrychowski, Jolanta Opertowska, Dorota Sulejczak, and Michal Walski

Abstract We explored the rebuilding of the brain parenchyma after surgical injury due to reactive astrogliosis. In the present study, we investigated the initial stages of rebuilding in the perilesional cortex of streptozotocin-induced diabetic rats. Our methods utilized ultrastructural and immunohistochemical studies as well as Western blot analysis of glial fibrillary acidic protein (GFAP) and vimentin. Data was collected at 2 days, 7 days and 2 months following a unilateral sensorimotor cortex lesion. Electron-microscopic studies revealed not only formation of glial scar tissue but also ultrastructural features of death in the elements of neurovascular unit. Immunohistochemical studies, confirmed by Western blot analysis, demonstrated the enhancement of vimentin and GFAP immunoreactivity (IR) in astrocytes located in the perilesion cortical area of the diabetic rats that were operated upon. We suggest that the process of rebuilding brain parenchyma following surgical injury may be disturbed by the induction of astrocytes and the degeneration of astrocytes, as well as by morphological changes within capillaries that are accompanied by the presence of macrophages.

Keywords Brain injury • glial scar • GFAP • vimentin

Introduction

Neurosurgical procedures associated with disrupted continuity of the meninges, followed by interventions within the cerebral parenchyma, often result in damage to the morphological components of neurovascular units as well as damage to various cells that form the cerebral parenchyma (1–4). One of the results of damage to the nervous system is the formation of glial scars. Glial scar tissue is composed of astrocytes and microglia, as well as a rich mesh of extracellular matrix proteins, including proteoglycans. In our model of surgical brain injury, a part of the cerebral cortex in the fronto-temporal region is removed. Investigating a number of time points following the operation allows us to analyze the process of rebuilding of brain parenchyma.

Diabetes mellitus is the most common serious metabolic disorder, and it is characterized by functional and structural changes in the peripheral as well as in the central nervous system. Earlier studies were not able to fully characterize the effects of diabetes on glial scar formation and the rebuilding of brain parenchyma after brain injury. This difficulty is due in part to the fact that there can be multiple underlying causes of diabetes in the central nervous system. Among these, the blood–brain barrier is one important contributor to the alterations seen in CNS. Diabetes is associated with changes in the barrier as well as in the transport functions of the cerebral microvessels (10). In the current study, we systematically evaluated the effects of diabetes on these processes at the early and the late stages of the glial scar formation using streptozotocin-induced diabetic rats as a model system. We present investigations that provide insight into common ultrastructural, immunohistochemical and immunochemical pathways of glial scar formation in diabetic rats following surgical brain injury. A 60 mg/kg streptozotocin (STZ) dose can begin an autoimmune process that results in the destruction of the Langerhans islets beta cells (13) and of insulin receptors (5,9). It has been shown earlier (13) that a stable diabetic state is established two weeks after the treatment with

M. Frontczak-Baniewicz (✉) and M. Walski
Department of Cell Ultrastructure, M. Mossakowski Medical
Research Centre Polish Academy of Sciences, 5 Pawinskiego Street,
Warsaw 02-106, Poland
e-mail: gosia@cmdik.pan.pl

L. Struzynska
Department of Neurochemistry, M. Mossakowski Medical Research
Centre Polish Academy of Sciences, 5 Pawinskiego Street,
Warsaw 02-106, Poland

J. Andrychowski
Department of Neurosurgery, M. Mossakowski Medical Research
Centre Polish Academy of Sciences, 5 Pawinskiego Street, Warsaw
02-106, Poland

J. Opertowska
Department of Neuropathology, M. Mossakowski Medical Research
Centre Polish Academy of Sciences, 5 Pawinskiego Street,
Warsaw 02-106, Poland

D. Sulejczak
Department of Experimental Pharmacology, M. Mossakowski
Medical Research Centre Polish Academy of Sciences,
5 Pawinskiego Street, Warsaw 02-106, Poland

the STZ. In light of this, the animals in this study were operated on after that time.

Materials and Methods

A local Ethics Committee approved the study. Three groups of animals were used: (1) intact diabetic, (2) operated diabetic and (3) operated non-diabetic (four rats in each group). Male adult Wistar rats weighing 200–250 g were injected intraperitoneally with STZ (Sigma Chemical Company, USA) at a dose of 60 mg/kg body weight. Blood sugar levels were monitored (once a week) as described earlier (6,11).

Two weeks after the injection of STZ, a traumatic brain injury was induced in the frontotemporal region of the cerebral cortex after skull exposure (as described in (4) in two experimental groups – (2) and (3)).

After recovery from anesthesia, rats remained under standard laboratory conditions for 2 days, 7 days or 2 months. At this time, the animals were anesthetized with Nembutal (80 mg/kg b.w.) and perfused through the ascending aorta with 0.01 M phosphate buffered saline (PBS) containing heparin, followed by perfusion with an ice-cold fixative (4% paraformaldehyde in 0.1 M phosphate buffer for light microscopy or 2% paraformaldehyde + 2.5% glutaraldehyde for transmission electron microscopy – TEM). The brains were removed from the skull and postfixed with the same fixative for 2 h. Later, the material for ultrastructural studies was processed for TEM as described earlier (4). Material for immunohistochemistry was infiltrated in 10% sucrose in phosphate buffer, followed by 20% and 30% sucrose solution infiltration for the following 7 days and cut on a cryostat (Leica). Immunohistochemical reactions were carried out on 25- μ m-thick free-floating brain sections. The primary antibodies (Abs) against GFAP (Chemicon) and vimentin (Santa-Cruz) and secondary antibodies conjugated to HRP (Bio-Rad) were used. HRP reaction product was visualized with SG kit (Vector, Vector Labs).

Animals for the western blot studies were anesthetized with Nembutal (80 mg/kg b.w.) and decapitated. The brains were quickly removed from the skull and placed in ice-cold sucrose medium. To obtain homogenates for immunoblots, perilesional cortical areas were dissected. The appropriate regions from the cerebral cortex of diabetic non-operated animals served as control. Material was homogenized, centrifuged and the obtained supernatants were used for immunoblotting analysis. Proteins were separated by SDS-PAGE as described by Laemmli et al. (7), and then electrotransferred to nitrocellulose membranes. Membranes were incubated in PBS + 0.05% Tween 20 (PBS-T) and 5% milk powder for 1.5 h at room temperature, washed in PBS-T and

incubated overnight at 4°C in PBS-T containing 0.1% milk powder and primary antibodies against GFAP (1:1000) and vimentin (1:200). After washing in PBS-T, membranes were incubated for 1 h at room temperature in PBS-T containing 0.1% milk powder and secondary antibody – peroxidase-conjugated anti-mouse IgG (1:1000). Membranes were washed in PBS-T and reactions were detected using a chemiluminescence system (ECL Western Blotting System, Amersham Biosciences).

Results

The intact brain parenchyma of diabetic rats was primarily characterized by ultrastructurally altered capillaries with thickened basement membrane. A characteristic feature of the zone surrounding the traumatic lesion in group of non-diabetic operated animals was the presence of basal membrane-like material defining lesion borders, with adjacent astrocyte plasmatic processes containing numerous glial filaments. Subsequently, the number of glial filaments in astrocytes increased, and the filaments filled morphologically differentiated processes of varying morphology. Studies show those plasma proteins present in the perivascular zone form a scaffold that supports newly formed blood vessels. Our observations show also that populations of perivascular macrophages are present.

In operated diabetic animals during the first week, there is a transient inflammatory reaction in the area immediately adjacent to the operated region, especially around blood vessels. As the core of the injured parenchyma disintegrated, endothelial cells from the periphery proliferate and capillaries grow into the dead tissue. Monocytes from the blood stream enter the lesion through damaged vessels. They ingest the products of degradation of damaged parenchyma and are transformed into macrophages. Macrophage reaction appears early and peaks at one week. Astrocytes from the surrounding undamaged brain proliferate and form a glial scar around the injured area. This process is completed after approximately 2 months. After that time, we observed the ultrastructural features of astrocyte degeneration. However, neurons do not regenerate within this time period. The most common feature of astrocytes is their reaction to CNS damage, including reactive gliosis combined with morphological changes inside the cell and increased synthesis of many proteins, mainly glial fibrillary acidic protein (GFAP). The very interesting feature of the operated diabetic group of animals is degeneration and death of elements forming the neurovascular unit (Fig. 1). We observed not only death of neurons but also degeneration of perivascular astrocytes and endothelial cells in newly formed capillaries.

Immunohistochemical (IHC) studies confirm these findings (data not shown). Immunostaining techniques showed an

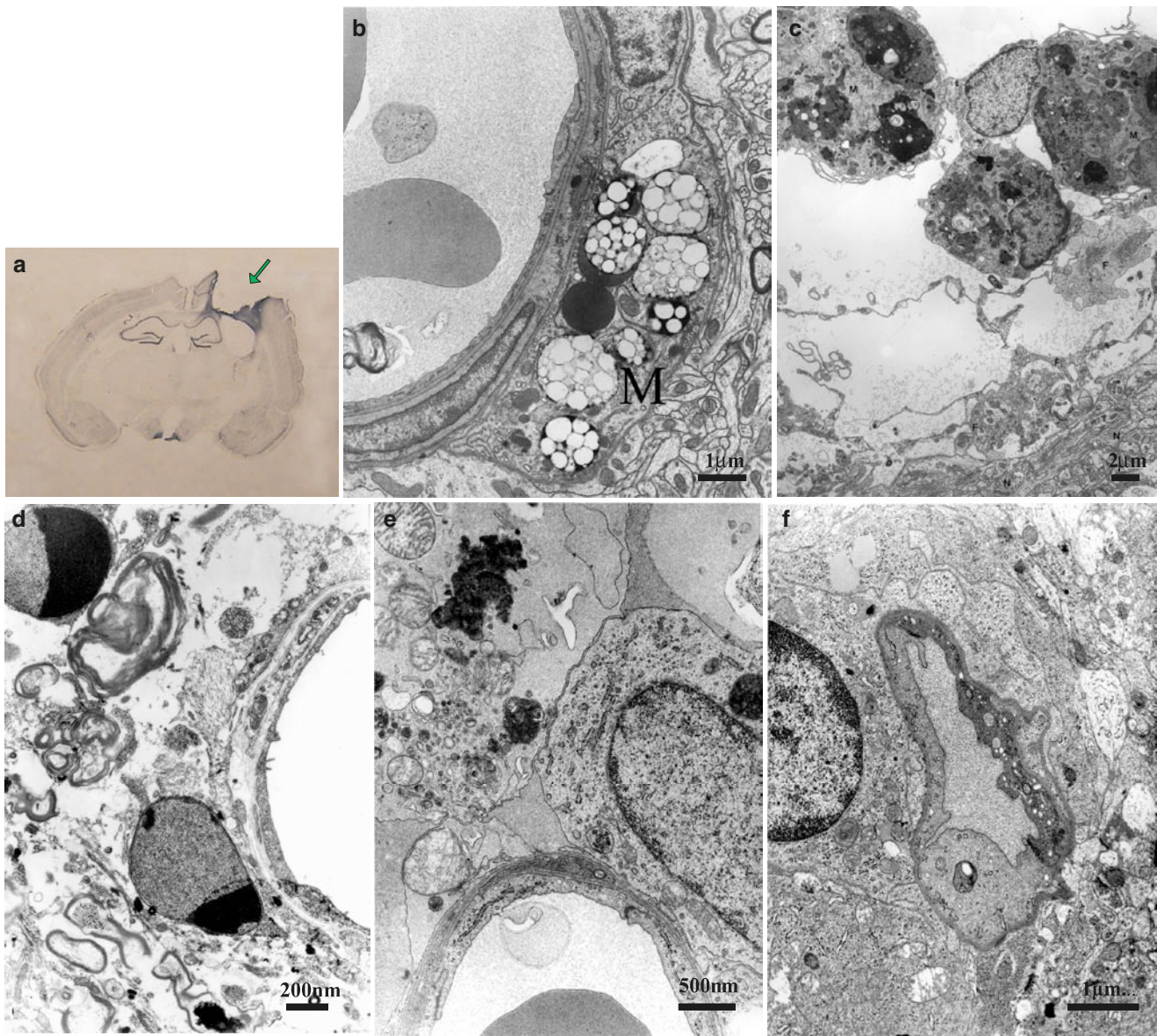


Fig. 1 (a) The area of cortical degeneration at the 4th day following the operation. (b) Perivascular macrophage (M) located between the basement membrane and endothelium. (c) Macrophages located in the vicinity of the scar border. (d) Apoptotic neurons with characteristic nuclear changes. Note the aggregation and marginalization of chromatin.

(e) Blood capillary vessel in the area immediately adjacent to the lesion in diabetic rat. The perivascular space with morphological features indicating neurodegeneration. (f) Young capillary vessel in the perilesion area of diabetic cerebral cortex. Endothelial cells reveal morphological features of apoptosis

increase in the number of GFAP and vimentin positive astrocytes within the perilesion cortical area (Fig. 2). The level of staining was higher than that observed in the tissue derived from controls, including both intact diabetic and operated non-diabetic animals. Western blot analysis of GFAP and vimentin levels (Fig. 3) from operated diabetic rats showed a significant elevation of both investigated proteins in the perilesion cortex after 7 days post-lesion. This result confirms our immunohistochemical data. However, within brains of diabetic rats who survived longer following brain damage (i.e. 2 months) the level of this protein significantly decreased.

Discussion

Brain injury induced breakdown of the blood brain barrier (BBB), which is composed of endothelial cells and astrocytes, occurs concurrently with microglial activation. This breakdown appears in response to the release of various cytokines, reactive oxygen species, glutamate, adenosine triphosphate (ATP), bradykinins, histamine, and nitric oxide from neurons, activated microglia, and the endothelial cells themselves. Breakdown of this barrier facilitates the translocation of plasma-derived molecules into the brain

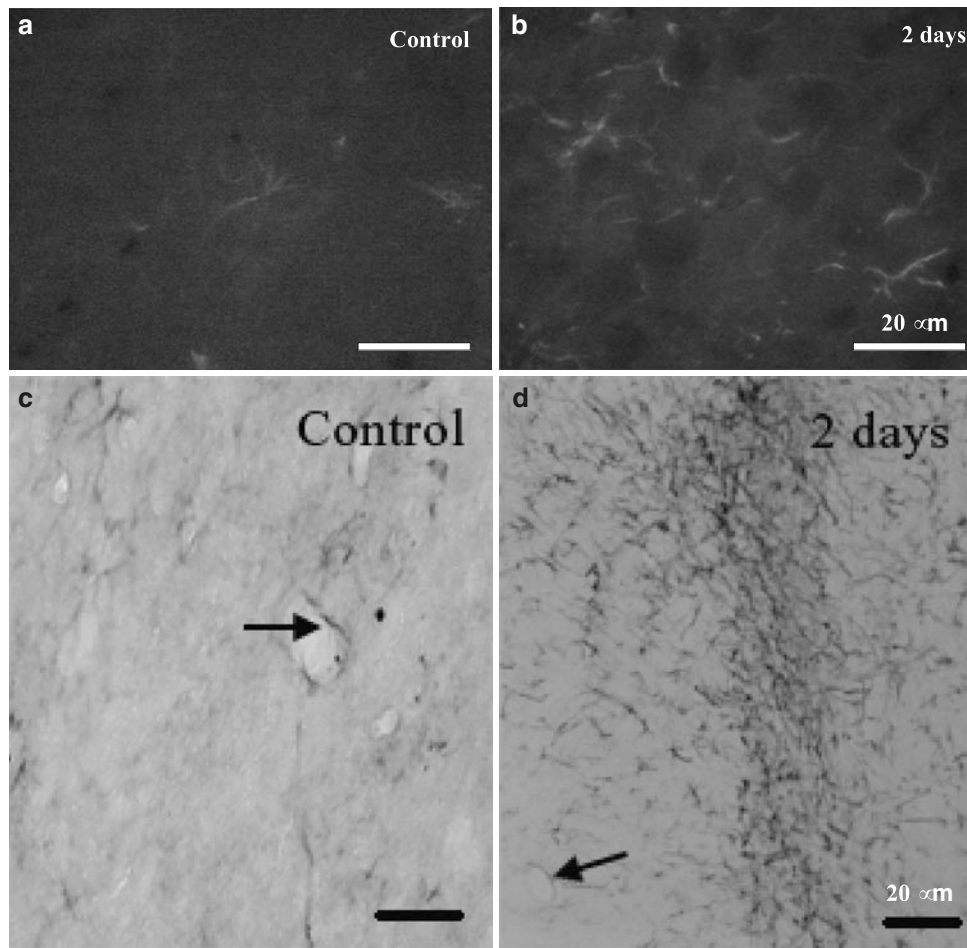


Fig. 2 Immunoreactivity (IR) for GFAP (panels **a** and **b**, immunofluorescence) and vimentin (panels **c** and **d**, light microscopy) in the intact diabetic and injured diabetic rat cortex. In the cortex of intact diabetic rats, GFAP and vimentin-positive astrocytes were detected. The perivas-

cular area (*arrow*) showed only weak immunostaining for vimentin (panel **c**). Two days following the operation many astrocytes immunoreactive for vimentin (panel **d**) and for GFAP (panel **b**) were detected in the perilesion cortical region

(10). Several studies suggest that this influx of blood-derived molecules is a critical step in the formation of a glial scar. Consistent with this notion, areas of greatest glial scarring are often found near regions of the largest BBB breakdown (10). Moreover, breakdown of the BBB contributes to the posttraumatic inflammatory response by increasing extravasation of blood-borne neurotrophins, macrophages, and T- and B-lymphocytes, which may trigger further brain damage (10). Physical and metabolic insults cause rapid changes in the neurovascular unit.

Diabetes mellitus is the most common serious metabolic disorder, and is characterized by functional and structural changes in the peripheral as well as in the central nervous system. In the present study, we aimed to investigate rebuilding in cerebral cortex of streptozotocin-induced diabetic rats following surgical brain injury by determining the ultrastructural and immunohistochemical features of the perilesion area as well as the expression of GFAP and vimentin. One of the important events during astrocyte differentiation

is the increase in expression of glial markers, glial fibrillary acidic protein (GFAP) and vimentin. Our IHC data showed an important enhancement of the number of GFAP immunoreactive (IR) and vimentin IR astrocytes within the perilesional cortical region of operated rats. The level of staining was significantly higher than that observed in the control rat brains. High levels of both investigated proteins were detected up to 2 months following the lesion; but at the same time points, a degeneration of individual astrocytes was observed. Western blot analyses indicated an increase of GFAP and vimentin level in the brains of diabetic rats compared with those of controls. Lin and Cai (8) suggest that vimentin and GFAP play a key role in the formation of glial scar following brain injury. Our findings indicate that streptozotocin-induced diabetes alters degradation and production of GFAP and vimentin. We suppose that induction and degeneration of astrocytes, accumulation of macrophages as well as the morphological changes within capillaries may disturb the process of rebuilding of brain parenchyma fol-

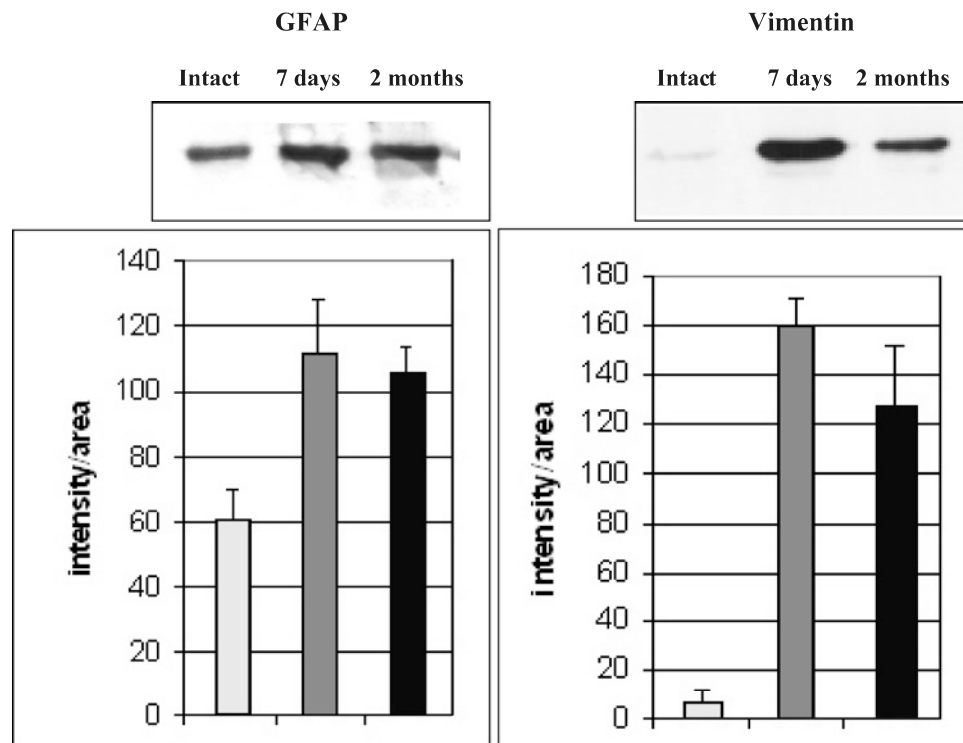


Fig. 3 GFAP and vimentin IR in the intact and operated cerebral cortex. At 7 days as well as at 2 months following the operation, a significant increase of both investigated protein levels was observed

lowing surgical injury. New data reveal a novel regulatory mechanism of vimentin transport during neurite extension that may have implications in diseases featuring transport/trafficking defects and impaired regeneration (12). Thus, determination of GFAP and vimentin may provide a relevant marker in the central nervous system for studying neurodegenerative changes in experimental diabetes mellitus.

Conflict of interest statement We declare that we have no conflict of interest.

References

- Berry M, Maxwell WL, Logan A, Mathewson A, McConnell P, Ashurst DE, Thomas GH (1983) Deposition of scar tissue in the central nervous system. *Acta Neurochir* 32(Suppl):31–53
- Cervos NJ, Lafuente JV (1991) Traumatic brain injuries: structural changes. *J Neurol Sci* 103(Suppl):S3–S14
- Fawcett JW, Asher RA (1999) The glia scar and central nervous system repair. *Brain Res Bull* 49:377–391
- Frontczak-Baniewicz M, Walski M (2006) Glial scar instability after brain injury. *J Physiol Pharmacol* 57(Suppl) 4:97–102
- Kadowaki T, Kasaga M, Akamuma Y, Ezaki O, Takaku F (1984) Decreased autophosphorylation of the insulin receptor-kinase in streptozotocin diabetic rats. *J Biol Chem* 259:14208–14216
- Kumthekar MM, Katyare SS (1992) Altered kinetic attributes of Na⁺ K⁺ ATPase activity in kidney, brain and erythrocyte membranes in alloxan-diabetic rats. *Indian J Expt Biol* 30:26–32
- Laemmli VK (1970) Cleavage of structural proteins during the assembly of the heat of bacteriophage T4. *Nature* 227:680–685
- Lin J, Cai W (2004) Effect of vimentin on reactive gliosis: in vitro and in vivo analysis. *J Neurotrauma* 21(11):1671–1682
- Meyerovitch J, Backer JM, Kahn CR (1989) Hepatic phosphotyrosine phosphatase activity and its alterations in diabetic rats. *J Clin Invest* 84:976–983
- Mooradian AD (1997) Central nervous system complications of diabetes mellitus – a perspective from the blood–brain barrier. *Brain Res Brain Res Rev* 23(3):210–218
- Nerurkar MA, Satav JG, Katyare SS (1988) Insulin-dependent changes in lysosomal cathepsin D activity in rat liver, kidney, brain and heart. *Diabetologia* 31:119–122
- Shim SY, Samuels BA, Wang J, Neumayer G, Belzil C, Ayala R, Shi Y, Shi Y, Tsai LH, Nguyen MD (2008) Ndel1 controls the dynein-mediated transport of vimentin during neurite outgrowth. *J Biol Chem* 283:12232–12240
- Wilson GL, Leiter EH (1990) Streptozotocin interactions with pancreatic cells and the induction of insulin-dependent diabetes. *Curr Top Microb Immunol* 156:27–33

Significance of Monitoring the Initial Intracranial Pressure on Hematoma Irrigation with Trephination Therapy for Acute Subdural Hematomas in Critical Conditions

Naoki Otani, Yoshio Takasato, Hiroyuki Masaoka, Takanori Hayakawa, Yoshikazu Yoshino, Hiroshi Yatsushige, Hiroki Miyawaki, Kyoko Sumiyoshi, Takashi Sugawara, Aoyagi Chikashi, Satoru Takeuchi, and Go Suzuki

Abstract Acute subdural hematoma (ASDH) patients presenting in a severe condition tend to have poor outcomes due to the significant brain edema required to maintain the ICP at less than 20–25 mmHg. This study compared the surgical outcomes of 16 critically ill patients with ASDH who underwent hematoma irrigation with trephination therapy (HITT) based on their initial ICP values. The initial mean GCS score upon admission was four. A unilateral dilated pupil was seen in one and bilateral dilated pupils were seen in seven patients. The co-existence of a brain contusion was seen in seven patients, brain swelling was noted in six patients, and both basal cistern effacement and a midline shift greater than 5 mm were observed in all patients. The mean initial ICP value was 45mmHg (range: 3 to 85 mmHg). Ten patients (62.5%) underwent a rapid external decompression to evacuate the hematoma. By using the Glasgow Outcome Scale upon discharge a score of good recovery (GR) was assigned to two (12.5 %), moderate disability (MD) to four (25.0 %), vegetative state (VS) to two (12.5 %), and death (D) to eight (50.0 %) patients. All six patients who showed an initial ICP greater than 60 mmHg died despite intensive care. Eight patients who showed an initial ICP less than 40 mmHg had a favorable outcome, but two patients deteriorated due to a traumatic cerebrovascular disorder. It seems that the initial ICP monitoring with HITT for ASDH patients in critical condition may be an important factor for predicting both surgical outcome and clinical course.

Keywords Acute subdural hematoma • brain edema • external decompression • intracranial pressure

Introduction

Acute subdural hematoma (ASDH) in patients in severe condition is associated with a poor outcome due to significant brain edema (5). The surgical indications are determined based on careful consideration of the neurological deficit and the radiological findings with the intent to maintain an ICP of less than 25 mmHg (2). If the pathophysiology of the ASDH is complicated with brain edema or cerebral contusion, however, it can overwhelm the surgical strategy. It is sometimes necessary to immediately perform hematoma irrigation with trephination therapy (HITT) to control the ICP (4). This study compared the surgical outcome in critically ill patients with ASDH who underwent HITT based on their initial ICP value.

Patients and Methods

There were 56 patients with ASDH surgically treated between April 2005 and September 2007. Among these 56 patients, 16 patients (mean age 56.8, male 10, female 6) who underwent HITT were analyzed to measure the initial ICP. The patients' hospital records, including medical charts, intensive care unit flow sheets, operative records, and radiological findings (e.g., head CT scans and MRI (A)) were retrospectively reviewed. The patient outcome was assessed upon discharge using the Glasgow Outcome Scale (GOS), which is composed of five levels: good recovery (GR), moderate disability (MD), severe disability (SD), vegetative state (VS), and death (D). All of the patients were managed with the same protocol. After an immediate neurological examination, aggressive resuscitation (e.g., tracheal intubation and adequate ventilation using sedation) was performed in the emergency room. The diagnosis of an ASDH was confirmed by computed tomography (CT) scans. To prevent intracranial hypertension and maintain the cerebral perfusion pressure during the acute stage, the mean blood pressure was increased to more than 90 mmHg. The initial ICP was monitored in all patients using a subdural fiber optic ICP catheter (Camino Laboratories, San Diego, CA, USA) during the HITT. Ten of the patients were

N. Otani (✉), Y. Takasato, H. Masaoka, T. Hayakawa, Y. Yoshino, H. Yatsushige, H. Miyawaki, K. Sumiyoshi, T. Sugawara, A. Chikashi, S. Takeuchi, G. Suzuki
Department of Neurosurgery, National Hospital Organization Disaster Medical Center, 3256 Midoricho, Tachikawa, Tokyo, Japan
e-mail: naotani@tdmc.hosp.go.jp

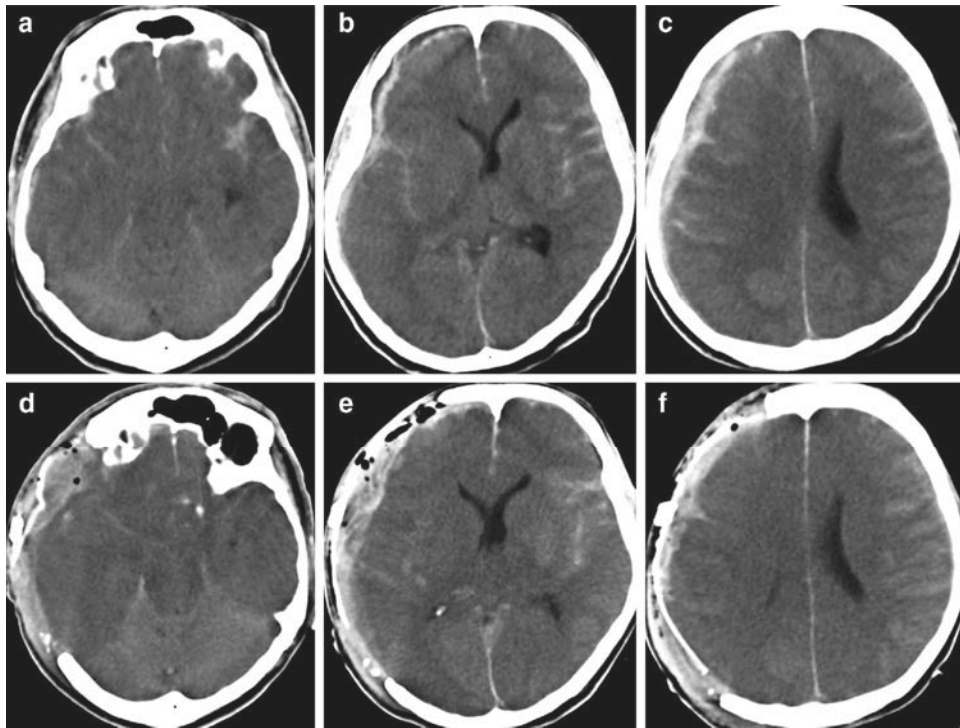


Fig. 1 Case presentation (Case 12). A 56-year-old-male was injured in a traffic accident. His GCS upon admission was E1V1M2 (4). His pupils were dilated bilaterally to 7.0 mm in size, and there was no light reflex. (a–c) An initial CT scan showing a traumatic SAH, ASDH on

the right side with a thickness 12 mm and midline shift of 8 mm. The initial ICP upon HITT was 63 mmHg. A decompressive craniectomy with hematoma evacuation was performed immediately (d–f). The patient died 2 weeks after the injury

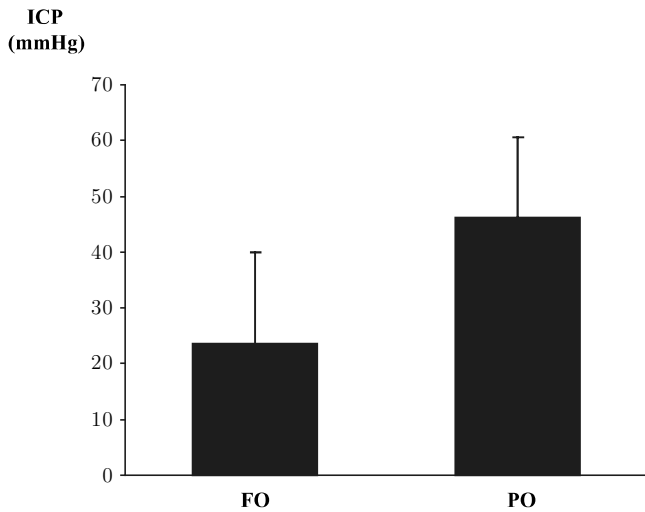


Fig. 2 Correlation between the initial ICP upon HITT and clinical outcome in 10 patients who underwent a DC with hematoma evacuation. Two patients who showed an initial ICP greater than 40 mmHg showed a poor outcome despite receiving intensive care. Conversely, eight patients who showed an initial ICP less than 40 mmHg had a favorable outcome, with the exception of two patients who deteriorated due to a traumatic cerebrovascular disorder. There was no significant difference between favorable and poor outcomes ($P = 0.054$). FO, favorable outcome; GR, MD. PO, poor outcome; SD, VS, D

surgically treated as soon as possible in the operating room. A relatively large craniotomy flap was removed via a large reversed question mark scalp incision with the following margins: anteriorly: frontal to the floor of the anterior cranial fossa; superiorly: within 2 cm of the superior sagittal sinus; posteriorly: within 1 cm of the asterion; inferiorly: to the floor of the middle fossa. The dura was opened in a semicircular fashion with additional dural incisions for the decompression. No internal decompression was performed in any of the patients. The patients were aggressively treated post-operatively in the neurological intensive care unit to avoid intracranial hypertension. The ICP was continuously monitored in all patients for at least one week. When the ICP remained over 20 mmHg after medical treatment, mild hypothermia therapy was induced. In addition, CSF drainage was performed to decrease the ICP caused by hydrocephalus. The cranial bone flap was replaced 1–2 months after the surgery. Statistical analysis was performed using a one-factor ANOVA. Significance was confirmed at values less than 0.05.

Results

All patient characteristics, radiological findings, and surgical outcomes are summarized in Table 1. The cause of the injury was a traffic accident in eight patients, falling in seven, and

Table 1 Patients characteristics and clinical outcome in 16 ASDH patients measured initial ICP on HITT

Patient no.	Age/sex	Cause of injury	Duration for operation (h)		Pupil abnormality	Pupil size (mm)	Light reflex	Brainstem		ASDH	Contusion	Cisternal effacement	Hematoma thickness (mm)	Midline shift (mm)	Hitt initial ICP (mm Hg)	Surgical procedure	ED	GOS
			GCS	for operation (h)				abnormality	Brainstem									
1	35/M	Falling	10	20	-	2.5	+	-	+	+	+	8	8	3	HE	+	MD	
2	77/F	Falling	15	24	-	2.5	+	-	+	+	+	12	13	6	HE	+	GR	
3	51/M	Hitting	4	1	Dilated	5.0	-	+	+	-	+	8	12	23	HE	+	MD	
4	58/M	Traffic accident	3	1	Dilated	6.0	-	+	+	+	+	13	5	30	HE	+	D	
5	20/M	Falling	4	3	-	2.5	+	+	+	-	+	5	8	30	HE	+	MD	
6	20/F	Traffic accident	11	1	-	2.5	+	-	+	+	+	12	5	40	HE	+	GR	
7	22/F	Traffic accident	8	1	-	3.0	-	-	+	+	+	5	10	40	HE	+	MD	
8	68/F	Traffic accident	13	3	+	2.5	-	-	+	+	+	10	9	40	HE	+	VS	
9	61/M	Falling	3	1	+	5.3	-	+	+	+	+	13	16	45	HITT	-	D	
10	32/F	Falling	3	3	Dilated	6.0	-	+	+	-	+	11	13	52	HE	+	VS	
11	58/M	Falling	3	1	-	4.0	-	+	+	+	+	8	7	60	HITT	-	D	
12	56/M	Traffic accident	4	1	Dilated	7.0	-	+	+	+	+	12	8	63	HE	+	D	
13	79/M	Traffic accident	4	2	Dilated	5.0	-	+	+	+	+	15	11	64	HITT	-	D	
14	21/M	Traffic accident	5	1	Dilated	7.0	-	+	+	-	+	2	2	72	HITT	-	D	
15	78/F	Falling	3	3	Dilated	6.0	-	+	+	-	+	17	16	75	HITT	-	D	
16	70/M	Traffic accident	4	1	Dilated	6.0	-	+	+	+	+	16	24	85	HITT	-	D	

GCS, Glasgow Coma Scale; ASDH, acute subdural hematoma; HITT, hematoma irrigation with trephination therapy; HE, hematoma evacuation; GOS, Glasgow outcome scale; GR, good recovery; MD, moderate disability; SD, severe disability; VS, vegetative state; D, death; ED, external decompression; ICP, intracranial pressure.

wbeing hit by a falling body in one. The initial mean GCS score upon admission was 4 and ranged from 3 to 15. Three patients deteriorated after admission. A unilateral dilated pupil was seen in one and bilateral dilated pupils in seven patients. The co-existence of a brain contusion was seen in seven patients, brain swelling was noted in six patients, and both basal cisterns effacement and a midline shift greater than 5 mm was observed in all patients. All patients underwent HITT to measure the initial ICP from 1 to 24 h (mean 1.5 h) after the injury. The mean initial ICP value was 45 mmHg and ranged from 3 to 85 mmHg. Ten patients (62.5%) underwent a rapid external decompression to evacuate the hematoma. The Glasgow Outcome Scale upon discharge assigned a score of GR to two patients (12.5 %), MD to four (25.0 %), VS to two (12.5 %) and D to eight (50.0 %) patients. All six patients who showed an initial ICP greater than 60 mmHg died despite intensive care. Conversely, eight patients who showed an initial ICP less than 40 mmHg had a favorable outcome, with the exception of two patients who deteriorated due to a traumatic cerebrovascular disorder.

Discussion

The factors affecting the clinical outcome in patients with an ASDH in critical condition include the cause of the injury, being in a traffic accident, advanced age greater than 65 years old, GCS score upon admission less than 4, and postoperative ICP greater than 45 mmHg (5). As a consequence, surgical indications are determined with consideration of both neurological deficits and radiological findings to maintain an ICP of less than 25 mmHg and to prevent secondary brain damage. Immediate surgical intervention should therefore be performed in patients with ASDH when there is a hematoma volume greater than 10 mm in thickness or a progressing neurological deficit caused by a mass effect. On the other hand, conservative

treatment is recommended for patients with ASDH who present in critical condition while also showing a complete disruption of brainstem function (2).

It is difficult to select the optimal surgical intervention and timing. For patients with ASDH who present in critical condition, a DC with hematoma evacuation is recommended to reduce the ICP immediately (3). For patients with a rapid progressive neurological decline, however, HITT is useful to regulate the ICP in the emergency room (1). In the present study, all six patients who showed an initial ICP greater than 60 mmHg died despite intensive care. Conversely, eight patients who showed an initial ICP less than 40 mmHg had a favorable outcome, with the exception of two patients who deteriorated due to a traumatic cerebrovascular disorder. It seems that initial ICP monitoring with HITT for an ASDH patient in critical condition may be an important factor for predicting both the surgical outcome and clinical course. Further investigations will thus be needed to clarify the optimal surgical indications and functional outcomes.

Conflict of interest statement We declare that we have no conflict of interest.

References

1. Aruga T, Mii K, Sakamoto T (1984) Significance of hematoma irrigation with trephination therapy (HITT) in the management of acute subdural hematoma. *No To Shinkei* 36:709–716
2. Bullock RM, Chesnut RM, Clifton GL (2000) Guidelines for the management of severe traumatic brain injury. *J Neurotrauma* 17:451–513
3. Shigemori M, Yamamoto F, Tokutomi T (1983) Re-evaluation of decompressive hemicraniectomy for acute subdural hematoma. *Neurol Med Chir (Tokyo)* 23:867–872
4. Springer MF, Baker FJ (1988) Cranial burr hole decompression in the emergency department. *Am J Emerg Med* 6:640–646
5. Wilberger JE, Harris M, Diamond DL (1991) Acute subdural hematoma: morbidity, mortality and operative timing. *J Neurosurg* 74:212–218

Surgical Outcome Following a Decompressive Craniectomy for Acute Epidural Hematoma Patients Presenting with Associated Massive Brain Swelling

Naoki Otani, Yoshio Takasato, Hiroyuki Masaoka, Takanori Hayakawa, Yoshikazu Yoshino, Hiroshi Yatsushige, Hiroki Miyawaki, Kyoko Sumiyoshi, Takashi Sugawara, Aoyagi Chikashi, Satoru Takeuchi, and Go Suzuki

Abstract Acute epidural hematomas (AEDH) are generally managed with rapid surgical hematoma evacuation and bleeding control. However, the surgical outcome of patients with serious brain edema is poor. This study reviewed the clinical outcome for AEDH patients and evaluated the efficacy of the DC, especially in patients with associated massive brain swelling. Eighty consecutive patients surgically treated with AEDH were retrospectively assessed. The patients were divided into two groups: (a) hematoma evacuation (HE: 46 cases) and (b) HE+ an external decompression (ED: 34 cases). The medical charts, operative findings, radiological findings, and operative notes were reviewed. In the poor outcome group, there were 18 patients (72%), with a GCS score of less than 8 (severe injury), and 22 patients (88%) who showed pupil abnormalities. Many more patients showed a midline shift, basal cistern effacement, and brain contusion in comparison to the favorable outcome group. In the favorable outcome group, almost all of the patients (98%) showed less than 12 mm of a midline shift. The influential factors may be age, GCS, pupil abnormalities, size, midline shift, basal cistern effacement, coincidence of contusion and swelling. We conclude that an A DC may be effective to manage the AEDH patients with cerebral contusion or massive brain swelling.

Keywords External decompression • cerebral swelling • surgical outcome • head injury

Introduction

Acute epidural hematomas (AEDHs) are generally managed with rapid surgical hematoma evacuation and bleeding control. In particular, an AEDH greater than 10 mm in thickness, 30

cm³ in hematoma volume, or a 5 mm midline shift in patients with a GCS score of less than 8 and with focal deficits should immediately undergo surgical correction (4). However, the surgical outcome of patients in critical condition with serious brain edema is poor due to the significant mass effect and brain stem compression. (5,9). On the other hand, a decompressive craniectomy (DC) can reduce the morbidity and mortality in critically ill patients with a severe head injury (1,2,7,12). This study reviewed the clinical outcome in a total of 80 surgically treated AEDH patients and evaluated the efficacy of DC, especially in patients with associated massive cerebral contusion or brain swelling.

Patients and Methods

Eighty consecutive patients surgically treated for AEDH between January 1997 and December 2004 were retrospectively assessed. The patients' hospital records, including their medical charts, intensive care unit flow sheets, operative records, anesthesia records and radiological findings such as head CT scans, were reviewed. The patients were divided into two groups: (a) hematoma evacuation (HE: 46 cases) and (b) HE+ an external decompression (ED: 34 cases). The patient outcome was assessed upon discharge using the Glasgow Outcome Scale (GOS) that includes five levels: recovery (GR), moderate disability (MD), severe disability (SD), vegetative state (VS) and death (D). The GOS describes good recovery and moderate disability as favorable outcomes, whereas severe disability, vegetative state and death constitute poor outcomes (Fig. 1).

All patients were managed in the same fashion. After an immediate neurological examination, aggressive resuscitation, such as tracheal intubation and adequate ventilation using sedations, was performed in the emergency room. The diagnosis of an AEDH was confirmed by computed tomography (CT) scans. A generous craniotomy flap was removed via a large reversed question mark scalp incision with the following margins for the DC: anteriorly, frontal to the floor of the

N. Otani (✉)
Department of Neurosurgery, National Hospital Organization
Disaster Medical Center, 3256 Midoricho, Tachikawa, Tokyo, Japan
e-mail: naotani@tdmc.hosp.go.jp

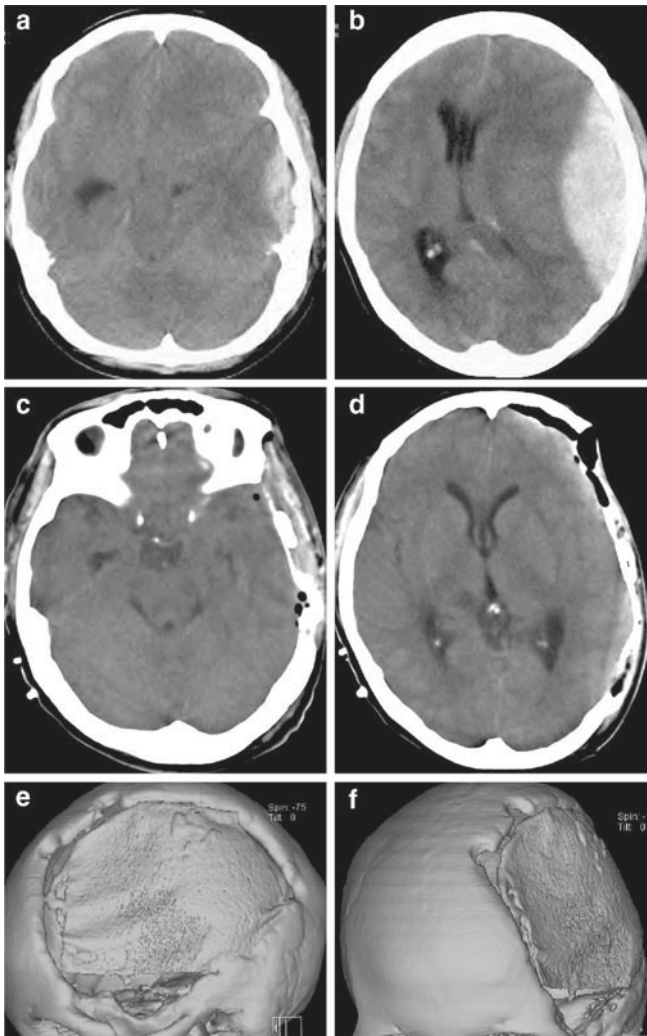


Fig. 1 Case presentation (Case 2). A 35-year-old female was injured due to a fall and was admitted in a state of unconsciousness, with a GCS of 4 (E1V1M2). One pupil (Lt side) was dilated. Computed tomography scans upon admission revealed an AEDH 33 mm in thickness and an 11 mm midline shift. Effacement of the perimesencephalic cistern was confirmed (a, b). A hematoma evacuation was thus immediately performed with a DC (c, d, e, f). The postoperative course was uneventful. Three months after the ictus, the GOS on discharge showed severe disability (SD)

anterior cranial fossa, superiorly, within 2 cm of the superior sagittal sinus, posteriorly, within 1 cm of the asterion and inferiorly, to the floor of the middle fossa. The dura was opened in a semicircular fashion with additional dural incisions for the decompression. An internal decompression was not performed in all patients. Only evacuation of the hematoma was performed, and a free bone flap was replaced with a titan plate. Patients were aggressively treated post-operatively in the neurological intensive care unit to avoid intracranial hypertension. The ICP was continuously monitored in all patients for at least one week. When the ICP remained over 20 mmHg after medical treatment, mild hypothermia therapy was induced. In addition, CSF drainage was performed to

decrease the ICP. The cranial bone flap was replaced 1–2 months after the surgery. The statistical analysis was performed using the Mann–Whitney U test. The significant difference was confirmed at a value of less than 0.05.

Results

The patient's characteristics, radiological findings and surgical outcomes are summarized in Table 1. Among the 80 patients (mean age 37.3 years ranging from 1 to 79, 60 males, 20 females), 46 patients underwent a hematoma evacuation (group A) and 34 patients underwent an additional external decompression (group B). The mean GCS score was lower in group B (GCS 9.1) than in group A (GCS 12.9). There were 27 patients (79.4%) in group B and 13 (28.3%) in group A, who showed a GCS score of less than 8 (severe head injury) upon admission. There were also 27 patients (79.4%) who showed pupil abnormalities. Patients in group B showed thick hematomas or basal cistern effacement at a higher rate than those in group A. In addition, more patients showed co-incident cerebral contusion and brain swelling in group B (Fig. 2). The GOS on discharge indicated a favorable outcome in 36 patients (78.2%) in group A, compared to only 19 patients (55.8%) in group B. In group B, there were significant differences in age, GCS score on admission, and midline shift in CT findings between those with a favorable outcome and a poor outcome. There was no significant correlation between the hematoma thickness and clinical outcome. In addition, there were 5 patients (14.7%) who died in group B. All of them showed a GCS score of less than 6, pupil abnormalities, a hematoma more than 20 mm in thickness, a midline shift of more than 8 mm, and co-incident brain contusion.

Discussion

Immediately aggressive surgery and intensive care for AEDH patients in poor clinical condition can improve the outcome and decrease mortality rates (4). Despite recent advances in the treatment of an AEDH, the surgical outcome remains unfavorable due to uncontrollable intracranial hypertension (5,9). An elevated ICP has been associated with several detrimental effects such as cerebral ischemia and reduced cerebral blood flow. The authors of these studies recommend the rapid control of ICP, which is associated with an improved outcome, and propose that early control of ICP and cerebral blood flow is important for improving patient outcome.

Several clinical studies have suggested that a DC can reduce morbidity and mortality in critically ill patients with a severe head injury (1,2,7,12). Experimental studies have

Table 1 Comparison of patient characteristics between HE and HE + ED group

		HE	n = 46	HE + ED	n = 34
Age		5–79	Mean 37.0	1–78	Mean 38.0
Sex	Male	37	(80.4%)	23	(67.6%)
	Female	9	(19.6%)	11	(32.4%)
Site	R	28	(60.9%)	16	(47.1%)
	L	18	(39.1%)	18	(52.9%)
GCS on admission	<8	13	(28.3%)	27	(79.4%)
	9–12	12	(26.1%)	4	(11.8%)
	13–15	21	(45.6%)	3	(8.8%)
	Mean GCS	12.9		9.1	
Pupil abnormalities		17	(37.0%)	27	(79.4%)
Size	(mm)	8–45	Mean 22.1	12–42	Mean 25.3
Cleavage	Clear	41	(89.1%)	26	(76.5%)
	Obscure	5	(10.9%)	8	(23.5%)
Density	High	25	(54.3%)	13	(38.2%)
	Mixed	21	(45.7%)	21	(61.8%)
Midline shift	(mm)	0–15	Mean 4.9	27	(79.4%)
Basal cistern effacement		17	(37.0%)	44	(55.0%)
	Bone fracture	46	(100.0%)	34	(100.0%)
	Basal fracture	15	(32.6%)	13	(38.2%)
	Contusion	25	(54.3%)	24	(70.6%)
	ASDH	13	(28.3%)	11	(32.4%)
	SAH	16	(34.8%)	14	(41.2%)
	DAI	2	(4.3%)	3	(8.8%)
	Brain swelling	1	(2.2%)	11	(32.4%)
Co-incident trauma	GR	30	(65.2%)	13	(38.2%)
	MD	6	(13.0%)	6	(17.6%)
	SD	8	(17.4%)	9	(26.6%)
	VS	0	0	1	(2.9%)
	D	2	(4.4%)	5	(14.7%)

GCS, Glasgow Coma Scale; GOS, Glasgow Outcome Scale; HE, hematoma evacuation; ED, external decompression; ASDH, acute subdural hematoma; DAI, diffuse axonal injury; GR, good recovery; MD, moderate disability; SD, severe disability; VS, vegetative state; D, death.

suggested that DC results in a significant elevation of the mean cerebral blood flow velocity in most patients with traumatic brain swelling and a significant decrease in the MCA pulsatility index values, thus indicating a reduction in cerebrovascular resistance (10). In addition, a significant decrease of the ICP and an increase in cerebral tissue oxygenation was confirmed after craniectomy or dural enlargement (3). In addition, recent clinical findings suggest that an external decompression might reduce the ICP (6,8,10). A craniectomy and enlarged dural plasty induced a significant decrease of ICP and an increase in cerebral tissue oxygenation (8). Others suggest that external decompression significantly increases cerebral tissue oxygenation (6,11).

In the present study, there were significant differences in age, GCS score upon admission, and midline shift in CT findings between patients with a favorable outcome and poor outcome in the patients who underwent DC. However, there was no significant correlation between the hematoma thickness and the clinical outcome. In summary,

these data indicate that the affecting factors for the clinical outcome in patients with an AEDH may be their age, GCS, pupil abnormalities, size, midline shift, basal cistern effacement, co-occurrence of contusion and swelling. These conclusions are consistent with previous studies. Additionally, an ED may be effective to manage the AEDH patients with intraaxial lesions such as a contusion and brain swelling.

To conclude, we propose that DC improves the outcome due to increased perfusion pressure or reduced intracranial pressure, which would suggest that DC helps to reduce the morbidity and mortality by controlling the ICP for AEDH patients in critical condition due to a massive cerebral contusion or brain edema. However, from the viewpoint of the long-term higher cortical function, further investigations will be required to clarify the usefulness of DC for treating a severe AEDH.

Conflict of interest statement We declare that we have no conflict of interest.

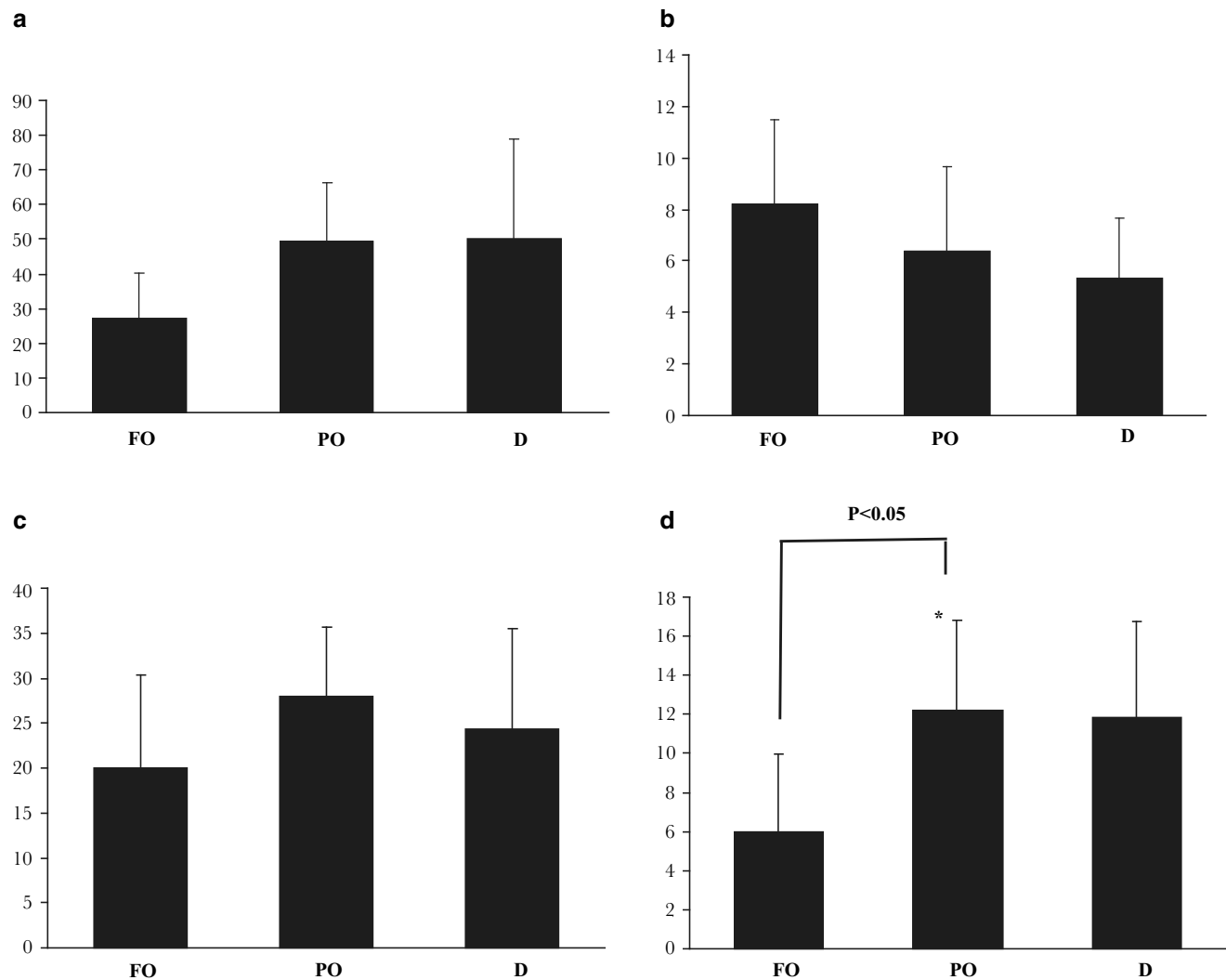


Fig. 2 The correlation between the surgical outcome and the clinical features and the CT findings upon admission in the patients who underwent DC. There were no significant differences in the age (a), GCS score on admission (b) and hematoma thickness (c) in the CT findings

between those with a favorable outcome and a poor outcome. There was no significant correlation between the midline shift and the clinical outcome (d; $P < 0.05$). FO, Favorable outcome; GR, MD. PO, Poor outcome; SD, VS, D

References

1. Aarabi B, Hesdorffer DC, Ahn ES (2006) Outcome following decompressive craniectomy for malignant swelling due to severe head injury. *J Neurosurg* 104:469–479
2. Albanese J, Leone M, Alliez JR (2003) Decompressive craniectomy for severe traumatic brain injury: evaluation of the effects at one year. *Crit Care Med* 31:2535–2538
3. Bor-Seng-Shu E, Hirsch R, Teixeira MJ (2006) Cerebral hemodynamic changes gauged by transcranial Doppler ultrasonography in patients with posttraumatic brain swelling treated by surgical decompression. *J Neurosurg* 104:93–100
4. Bullock MR, Chesnut R, Ghajar D (2006) Surgical management of acute epidural hematomas. *Neurosurgery* 58 (Suppl) S7–S15
5. Caroli M, Locatelli M, Campanella R (2001) Multiple intracranial lesions in head injury: clinical considerations, prognostic factors, management, and results in 95 patients. *Surg Neurol* 56:82–88
6. Jaeger M, Soehle M, Meixensberger J (2003) Effects of decompressive craniotomy on brain tissue oxygen in patients with intracranial hypertension. *J Neurol Neurosurg Psychiatr* 74:513–515
7. Jiang JY, Xu W, Li WP (2005) Efficacy of standard trauma craniectomy for refractory intracranial hypertension with severe traumatic brain injury: a multicenter, prospective, randomized controlled study. *J Neurotrauma* 22:623–628
8. Jourdan C, Convert J, Mottolese C (1993) Evaluation of the clinical benefit of decompression hemicraniectomy in intracranial hypertension not controlled by medical treatment. *Neurochirurgie* 39:304–310
9. Lobato RD, Rivas JJ, Cordobes F (1988) Acute epidural hematoma: an analysis of factors influencing the outcome of patients undergoing surgery in coma. *J Neurosurg* 68:48–57
10. Reithmeier T, Lohr M, Pakos P (2005) Relevance of ICP and $ptiO_2$ for indication and timing of decompressive craniectomy in patients with malignant brain edema. *Acta Neurochir (Wien)* 147: 947–951
11. Stiefel MF, Heuer GG, Smith MJ (2004) Cerebral oxygenation following decompressive hemicraniectomy for the treatment of refractory intracranial hypertension. *J Neurosurg* 101:241–247
12. Ziai WC, Port JD, Cowan JA (2003) Decompressive craniectomy for intractable cerebral edema: experience of a single center. *J Neurosurg Anesthesiol* 15:25–32

Prognosis for Severe Traumatic Brain Injury Patients Treated with Bilateral Decompressive Craniectomy

Hiroshi Yatsushige, Yoshio Takasato, Hiroyuki Masaoka, Takanori Hayakawa, Naoki Otani, Yoshikazu Yoshino, Kyoko Sumiyoshi, Takashi Sugawara, Hiroki Miyawaki, Chikashi Aoyagi, Satoru Takeuchi, and Go Suzuki

Abstract

Purpose Decompressive craniectomy for traumatic brain injury patients has been shown to reduce intracranial hypertension, while it often results in increased brain edema and/or contralateral space-occupied hematoma. The purpose of this study was to determine the prognosis of bilateral decompressive craniectomy in severe head injury patients with the development of either bilateral or contralateral lesions after ipsilateral decompressive craniectomy.

Methods Twelve patients underwent bilateral decompressive craniectomy among 217 individuals who had been treated with decompressive craniectomy with dural expansion from September 1995 to August 2006. The following patient data were retrospectively collected: age, neurological status at admission, time between injury and surgical decompression, time between first and second decompression, laboratory and physiological data collected in the intensive care unit, and outcome according to the Glasgow Outcome Scale.

Results Patient outcomes fell into the following categories: good recovery (three patients); mild disability (one patient); severe disability (two patients); persistent vegetative state (one patient); and death (five patients). Patients with good outcomes were younger and had better pupil reactions and neurological statuses on admission. Other factors existing prior to the operation did not directly correlate with outcome. At 24 h post-surgery, the average intracranial pressure (ICP), cerebral perfusion pressure (CPP), glucose level, and lactate level in patients with poor outcomes differed significantly from those of patients with a good prognosis.

Conclusion Head injury patients with either bilateral or contralateral lesions have poor prognosis. However, bilateral decompressive craniectomy may be a favorable treatment in certain younger patients with reactive pupils, whose ICP and CPP values are stabilized 24 h post-surgery.

Keywords Decompressive craniectomy • bilateral lesion • head injury • intracranial pressure • cerebral perfusion pressure

Introduction

Significant efforts have been made to control brain swelling caused by serious head injury. Decompressive craniectomy, one modality for head trauma, has been practiced since the early nineteenth century (5). Previous studies (10,14) have demonstrated that decompressive craniectomy provides a reduction in intracranial hypertension, and that surgical decompression is superior to medical management in patients with massive brain swelling. However, others (16) have reported increases in either brain edema or contralateral space-occupied hematoma after decompressive craniectomy (7,8), leading to the skepticism with respect to the usefulness of this procedure.

At the National Hospital Organization Disaster Medical Center, intraoperative brain swelling and increased ICP in the intensive care unit after ipsilateral decompressive craniectomy have led us to conduct immediate CT scans, and the development of contralateral lesions with midline shifts on the CT scan led us to perform immediate contralateral decompressive craniectomy. The aim of the study presented herein was to assess the effects of bilateral decompressive craniectomy on severe head injury patients with the development of either bilateral or contralateral lesions after ipsilateral decompressive craniectomy.

H. Yatsushige (✉), Y. Takasato, H. Masaoka, T. Hayakawa, N. Otani, Y. Yoshino, K. Sumiyoshi, T. Sugawara, H. Miyawaki, C. Aoyagi, S. Takeuchi, and G. Suzuki
Department of Neurosurgery, National Hospital Organization Disaster Medical Center, 3256 Midoricho, Tachikawa, Tokyo, Japan
e-mail: hyatsushige@hotmail.com

Materials and Methods

Patient Population

Between September 1995 and August 2006, 217 patients were treated with decompressive craniectomy and dural expansion at our hospital. Twelve patients (5.5%) underwent

bilateral decompressive craniectomy with dural expansion. The indications for bilateral decompressive craniectomy include bilateral space-occupied lesions with severe brain swelling and the development of contralateral lesions with midline shifts on CT scan after ipsilateral decompressive craniectomy. A representative bilateral fronto-temporal decompressive craniectomy is shown in Fig. 1.

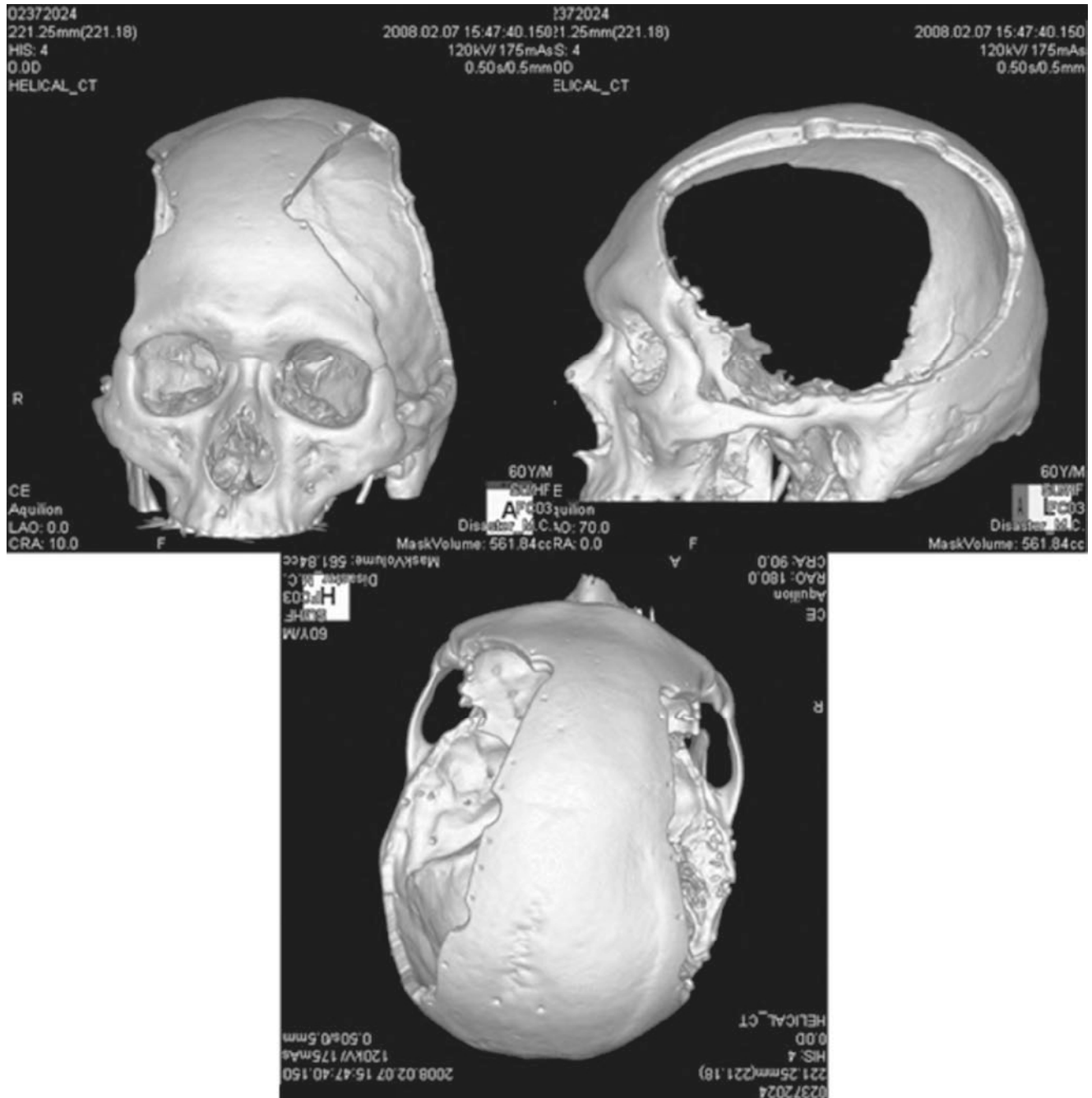


Fig. 1 Representative three-dimensional CT scan showing bilateral fronto-temporal decompressive craniectomy

Data Collection

The following patient data were retrospectively collected from medical records: age, sex, neurological status at admission, initial ICP after bilateral decompression, time between the injury and surgical decompression, time between first and second decompression, laboratory and physiological data collected in the intensive care unit, and outcome according to the Glasgow Outcome Scale (GOS). Twelve patients were divided into two groups consisting of group A (good prognosis) as either good recovery (GR) or mild disability (MD) patients according to the GOS, and group B (poor prognosis) as either severe disability (SD), persistent vegetative state (VS), or dead (D) patients according to the GOS.

Statistical Analysis

To assess the effects of bilateral decompressive craniectomy on severe head injury patients, the collected data were evaluated by statistical analysis. The differences in patient proportions were evaluated using the Fisher's Exact Test. Other data were analyzed by the Mann–Whitney U test. Significance was accepted at a probability value less than 0.05.

Results

Twelve patients were included in this study. Patient outcomes were as follows: GR (three patients), MD (one patient), SD (two patients), VS (one patient), and D (five patients). As such, four patients were assigned to group A, and eight were assigned to group B.

Pre-operative Factors

Table 1 presents information on gender, anisocoria, and light reflex. There were no measured differences between the two groups with regard to gender and anisocoria, although the proportion of observations in light reflex that define the contingency table was significantly different than expected from random occurrence ($p = 0.010$). Additionally, age of the good prognosis group was significantly lower than that of the poor prognosis group (Fig. 2a). Moreover, there was a significant difference in the Glasgow Coma Scale (GCS) on admission between the two groups (Fig. 2b). Other factors, such as duration before surgeries, did not correlate with observed outcomes (Fig. 2c, d).

Table 1 Contingency data on gender, papillary light reflex, and pupil laterality

	Sex		Light reflex		Anisocoria	
	Male	Female	Prompt	Absent	(-)	(+)
Group A	3	1	4	0	3	1
Group B	5	3	1	7	2	5

Post-operative Factors

The time course of ICP, CPP, glucose levels, and lactate levels in the intensive care unit are shown in Fig. 3. The mean ICP at 24 h post-surgery in the poor prognosis group was significantly higher than that of the good prognosis group (Fig. 3a). Moreover, there was a significant difference in CPP between the two groups at both 6 and 24 h post-surgery (Fig. 3b). Glucose levels in the good prognosis group post-surgery were significantly lower relative to the poor prognosis group (Fig. 3c), and there were significant differences in the lactate levels at 24 h post-surgery between the two groups (Fig. 3d).

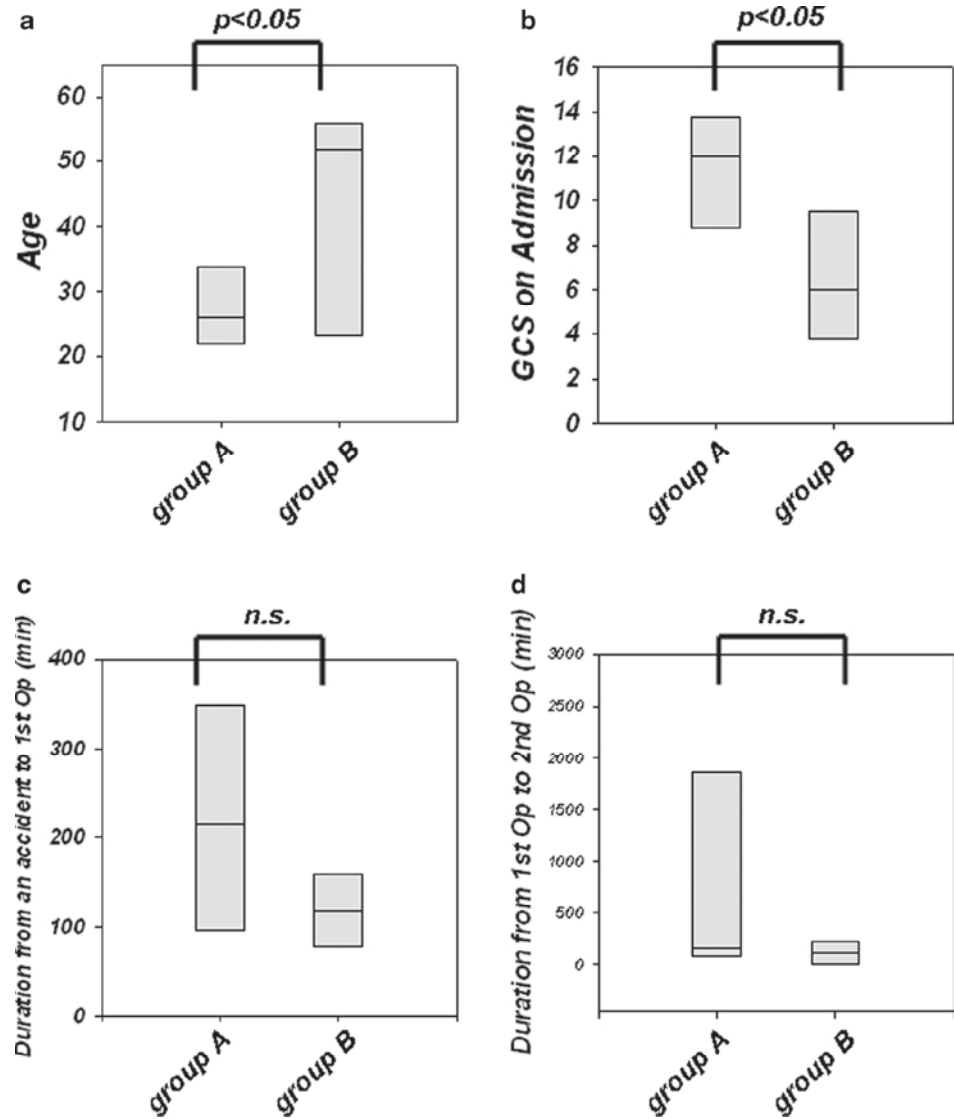
Discussion

The present study strongly suggests that bilateral decompressive craniectomy for the development of either bilateral or contralateral lesions may be a useful treatment in younger patients with light-reactive pupils. Moreover, ICP, CPP, glucose, and lactate levels at 24 h post-surgery should be maintained within normal limits for a good prognosis.

A previous report (9) determined that decompressive craniectomy did not lead to an improvement in outcome despite an improvement in midline shift. However, other studies (11,14) suggest that decompressive craniectomy is an effective treatment for severe head injury. The guidelines of the European Brain Injury Consortium, the Joint Brain Trauma Foundation, and the American Association of Neurological Surgeons for severe head injuries describe decompressive craniectomy as a therapeutic option for brain edema in patients that do not respond to conventional therapeutic measures (1,2,6). Therefore, decompressive craniectomy is a standard therapy at our hospital for head injury patients at risk for severe brain edema with or without space-occupied hematoma.

A negative aspect of decompressive craniectomy and hematoma evacuation is that these procedures can lead to the development of contralateral hematoma. A previous report (7) demonstrated that 5.7% of patients with decompressive craniectomy in whom a bilateral decompressive craniotomy

Fig. 2 Box plot comparing (a) age, (b) GCS on admission, (c) duration from accident to first surgery, and (d) duration from first surgery to second surgery between the two groups. There were significant differences in age and GCS on admission ($p < 0.05$), however, there were no significant differences in the duration between surgeries



was performed developed hematoma opposite to the site of the principal lesion. This figure is approximately the same as was observed in the present study, in which we evaluated the effects of bilateral decompressive craniectomy on the outcomes of severe head injury patients with the development of either bilateral or contralateral lesions after ipsilateral decompressive craniectomy.

This study demonstrated that patients with a good prognosis were younger and displayed a better overall neurological status upon admission. Other recent studies (12,15) have shown that both initial GCS and age were statistically significant in patient outcomes after treatment with decompressive craniectomy. Taken together, an indication for this aggressive therapy should be considered together with these pre-operative prognostic factors.

Although ICP and CPP are interrelated, both should be considered in setting treatment goals. A previous report (4) showed a threefold increase in the risk of later deterioration if the ICP was greater than 20 mmHg, while CPP should be maintained above the expected lower limit of autoregulation. Other recent reports (10,14) have confirmed that the measured ICP immediately after decompressive craniectomy was significantly reduced while the CPP was improved; however, ICP rose again during the first 12 h post-surgery. In this study, there was a significant increase in ICP and a significant decrease in CPP at 24 h post-surgery in patients with unfavorable outcomes. Therefore, ICP and CPP should be maintained at normal levels for at least 24 h after bilateral decompressive craniectomy to maximize chances for a good prognosis.

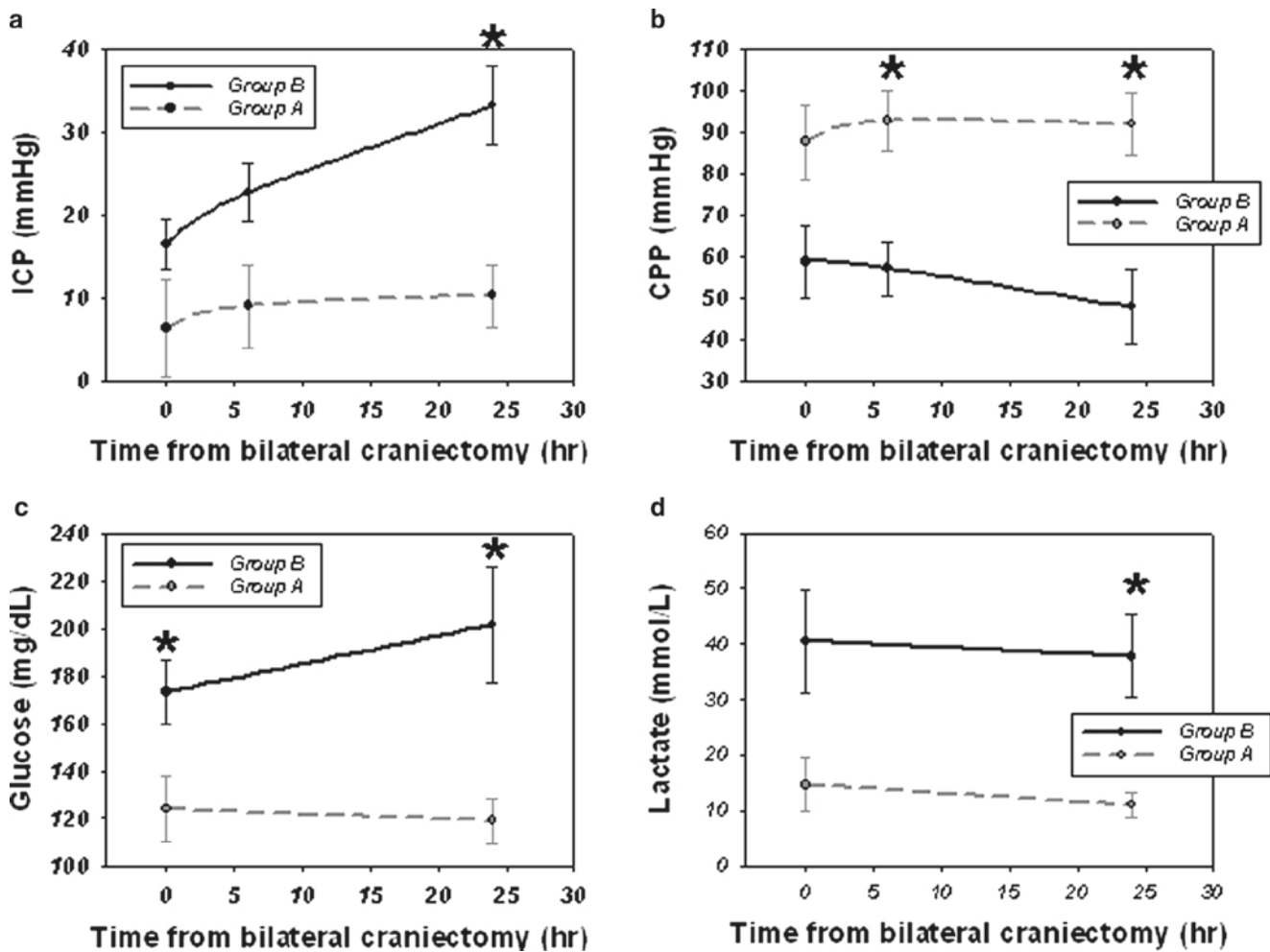


Fig. 3 Time course of (a) ICP, (b) CPP, (c) glucose concentration, and (d) lactate concentration between the two groups. * indicate that values are significantly different between the two groups ($p < 0.05$)

Previous studies (3,13) demonstrated that, during intensive care treatment for head injury, arterial glucose levels were the strongest predictors of neurologic outcomes. Attainment of strict normoglycemia in head injury patients is associated with improved survival. Our results further suggest that glucose levels are directly related to prognosis, and that, in the intensive care unit, the management of glucose metabolism should be closely monitored.

In conclusion, head injury patients who develop either bilateral or contralateral lesions have poor prognoses. However, bilateral decompressive craniectomy may be a treatment with a favorable outcome in certain younger patients with reactive pupils, whose ICP and CPP levels were stabilized 24 h post-surgery.

Conflict of interest statement We declare that we have no conflict of interest.

References

1. BTF Guidelines (2000) The Brain Trauma Foundation. The American Association of Neurological Surgeons. The Joint Section on Neurotrauma and Critical Care. Critical pathway for the treatment of established intracranial hypertension. *J Neurotrauma* 17: 537–538
2. Bullock R, Chesnut RM, Clifton G, Ghajar J, Marion DW, Narayan RK, Newell DW, Pitts LH, Rosner MJ, Wilberger JW (1996) Guidelines for the management of severe head injury. *Brain Trauma Foundation. Eur J Emerg Med* 3:109–127
3. Glenn TC, Kelly DF, Boscardin WJ, McArthur DL, Vespa P, Oertel M, Hovda DA, Bergsneider M, Hillered L, Martin NA (2003) Energy dysfunction as a predictor of outcome after moderate or severe head injury: indices of oxygen, glucose, and lactate metabolism. *J Cereb Blood Flow Metab* 23:1239–1250
4. Juul N, Morris GF, Marshall SB, Marshall LF (2000) Intracranial hypertension and cerebral perfusion pressure: influence on neurological deterioration and outcome in severe head injury. The Executive Committee of the International Selfotel Trial. *J Neurosurg* 92:1–6

5. Kocher ET (1901) Die Therapie des Hirndruckes. In: Nothnagel H (ed) *Specielle Pathologie und Therapie*. Alfred Holder, Wien, pp 255–266
6. Maas AI, Dearden M, Teasdale GM, Braakman R, Cohadon F, Iannotti F, Karimi A, Lapierre F, Murray G, Ohman J, Persson L, Servadei F, Stocchetti N, Unterberg A (1997) EBIC-guidelines for management of severe head injury in adults. *European Brain Injury Consortium. Acta Neurochir (Wien)* 139:286–294
7. Matsuno A, Katayama H, Wada H, Morikawa K, Tanaka K, Tanaka H, Murakami M, Fuke N, Nagashima T (2003) Significance of consecutive bilateral surgeries for patients with acute subdural hematoma who develop contralateral acute epi- or subdural hematoma. *Surg Neurol* 60:23–30; discussion 30
8. Mohindra S, Mukherjee KK, Gupta R, Chhabra R, Gupta SK, Khosla VK (2005) Decompressive surgery for acute subdural haematoma leading to contralateral extradural haematoma: a report of two cases and review of literature. *Br J Neurosurg* 19:490–494
9. Munch E, Horn P, Schurer L, Piepgras A, Paul T, Schmiedek P (2000) Management of severe traumatic brain injury by decompressive craniectomy. *Neurosurgery* 47:315–322; discussion 322–323
10. Olivecrona M, Rodling-Wahlstrom M, Naredi S, Koskinen LO (2007) Effective ICP reduction by decompressive craniectomy in patients with severe traumatic brain injury treated by an ICP-targeted therapy. *J Neurotrauma* 24:927–935
11. Polin RS, Shaffrey ME, Bogaev CA, Tisdale N, Germanson T, Bocchicchio B, Jane JA (1997) Decompressive bifrontal craniectomy in the treatment of severe refractory posttraumatic cerebral edema. *Neurosurgery* 41:84–92; discussion 92–84
12. Pompucci A, De Bonis P, Pettorini B, Petrella G, Di Chirico A, Anile C (2007) Decompressive craniectomy for traumatic brain injury: patient age and outcome. *J Neurotrauma* 24:1182–1188
13. Schirmer-Mikalsen K, Vik A, Gisvold SE, Skandsen T, Hynne H, Klepstad P (2007) Severe head injury: control of physiological variables, organ failure and complications in the intensive care unit. *Acta Anaesthesiol Scand* 51:1194–1201
14. Schneider GH, Bardt T, Lanksch WR, Unterberg A (2002) Decompressive craniectomy following traumatic brain injury: ICP, CPP and neurological outcome. *Acta Neurochir Suppl* 81:77–79
15. Ucar T, Akyuz M, Kazan S, Tuncer R (2005) Role of decompressive surgery in the management of severe head injuries: prognostic factors and patient selection. *J Neurotrauma* 22:1311–1318
16. Woertgen C, Rothoerl RD, Schebesch KM, Albert R (2006) Comparison of craniotomy and craniectomy in patients with acute subdural haematoma. *J Clin Neurosci* 13:718–721

Posterior Fossa Brain Tissue Injury: Developmental, Neuropsychological, and Neurological Consequences of Brain Tumors in Children

Dawid Larysz, Slawomir Blamek, Patrycja Larysz, Katarzyna Pietras, and Marek Mandra

Abstract The aim of the study was the functional neurodevelopmental assessment of children with posterior fossa tumors, specifically examining whether tumor location in particular cerebellar structures determines particular neuropsychological deficits. The examined group consisted of 34 children treated between 1999 and 2007 at the Division of Pediatric Neurosurgery Silesian University Medical School in Katowice, Poland. Twelve girls and 22 boys between 5 and 21 years of age were examined. The mean age was 12.3 years. There were 21 total and 8 subtotal resections of tumor, and marsupialization was performed in cases of arachnoid cysts. Hydrocephalus in 19 patients was fixed surgically. Histopathological diagnoses of tumors were as follows: 4 medulloblastomas, 8 pilocytic astrocytomas, 6 fibrillary astrocytomas, 1 anaplastic astrocytoma, 2 oligodendrogliomas, 4 anaplastic ependymomas, 1 choroid plexus papilloma, and 5 arachnoid cysts. The children were assessed by age-appropriate tests that examine higher mental functions such as cognitive processes, visual–spatial functions, verbal fluency, planning, sequential memory, and emotions. Additionally, speech examination and tests were performed. The clinical state of all patients was also evaluated, including a full neurological examination. Posterior fossa tumors can disturb normal development of higher mental functions, especially in the development of linguistic and emotional traits. Our study aimed to better understand the functional anatomy of the cerebellum in the context of behavioral changes. Exploration of the consequences of damage to posterior fossa structures may lead to a better understanding of their function in the emotional and cognitive development of children. Moreover, this work may enable the prediction of neurobehavioral disorders and offer appropriate strategies for rehabilitation, qualification, and surgical procedures.

P. Larysz, K. Pietras, and M. Mandra
Division of Pediatric Neurosurgery, Medical University of Silesia in Katowice, Ul. Medykow, 16, Katowice 40-752, Poland
e-mail: dawilar@poczta.onet.pl

S. Blamek
Department of Radiotherapy Maria Sklodowska-Curie
Memorial Cancer Center and Institute of Oncology, Gliwice
Branchul Wybrzeże Armii Krajowej, Gliwice 1544-100, Poland

Keywords Higher CNS functions • posterior fossa tumors • cerebellum • children

Background and Purpose

CNS tumors appear significantly more frequently in children than in adults and account for 20% of all neoplasms in childhood, making them the second most frequent neoplasm in the pediatric population (18). Furthermore, the tumor location differs between age groups; specifically, supratentorial tumors are more frequent in adults, whereas in children the infratentorial location is more frequent (i.e., posterior fossa tumors). Cerebellar tumors and brainstem tumors account for half of all brain tumors in children (3). However, initial studies on neuropsychological disorders associated with posterior fossa anomalies were performed mainly in adults. These studies characterized the adult subjects as having cerebellar cognitive affective syndrome, which is characterized by disorders of higher CNS function such as affect regulation, linguistic processing, and spatial cognition (14). To date, there are few studies on long-term neuropsychological changes in children treated for posterior fossa tumors. Riva and Giorgi in 2000 observed in children treated for posterior fossa tumors disturbances of visual and auditory sequential memory, behavioral, linguistic, and visual–spatial changes, and emotional lability (11). Similar symptoms were found in children with tumors located in brainstem. Initially, changes after posterior fossa surgery were interpreted as symptoms of reactive depression. Recent studies reported that the behavioral disorders observed after posterior fossa surgery are the results of organic damage to the cerebellar structure (4,5,15). Behavioral disorders were also described in patients with cerebellar stroke or degeneration and congenital hypoplasia of the cerebellum (2,5). Vermal lesions are often accompanied by disorders in affect regulation, such as mood lability, irritability, excessive weepiness, and autism. Therefore, the vermis is sometimes called the cerebellar limbic system (13). Vermal anomalies also lead to language and speech disturbances, for example, agrammatism or dysarthria, and are also likely responsible for postoperative

mutism. After resection of the vermis or part of the cerebellum, posterior fossa syndrome appears in 15% of children (2,17). The syndrome is characterized by transient postoperative mutism, emotional lability, social difficulties, and apathy.

Treatment scheme depends on histopathology, tumor location, and age of the child. In most cases total resection of the tumor is essential. In some cases of posterior fossa tumors, adjuvant therapy like chemotherapy and/or radiotherapy is needed. In these children neurodevelopmental disturbances can be attributed not only to the tumor resection but also to the effect of the adjuvant therapy (1,12). Another determinant of neurodevelopmental disorders is the age of the patient. It has been observed that in younger children cognitive disturbances are less expressed, which may be the effect of greater brain plasticity in younger children and different histopathology of the tumor in different age ranges (4).

Aim of the Study

The aim of the study was the functional neurodevelopmental assessment of children with posterior fossa tumors, specifically examining whether tumor location, in particular cerebellar structures determines particular neuropsychological deficits.

Material and Methods

The examined group consisted of 34 children treated between 1999 and 2007 in the Division of Pediatric Neurosurgery, Medical University of Silesia in Katowice, Poland. Twelve girls and 22 boys between 5 and 21 years of age were examined. The mean age was 12.3 years. Histopathological diagnoses of tumors were as follows: 4 medulloblastomas, 8 pilocytic astrocytomas, 6 fibrillary astrocytomas, 1 anaplastic astrocytoma, 2 oligodendrogliomas, 4 anaplastic ependymomas, 1 choroid plexus papilloma, and 5 arachnoid cysts. There were 21 total and 8 subtotal resections of tumors. In cases of arachnoid cysts, marsupializations were performed. Hydrocephalus coexisting in 19 patients was fixed surgically by ETV (endoscopic third ventriculocysternostomy) or implantation of ventriculoperitoneal shunt. The studied group was divided into two subgroups. The first subgroup consisted of 14 children with cerebellar tumors and the second consisted of 20 children with extracerebellar tumors localized in posterior

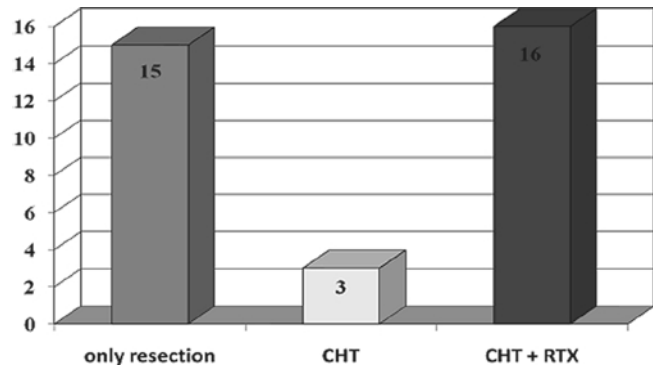


Fig. 1 Applied treatment schemes

fossa. Exact localization of the tumors is presented in Table 1. In the first subgroup of children with localization of the tumor within the cerebellum, in 4 children the tumors were localized in the right hemisphere, in 3 children the tumors were in the left hemisphere, and in 4 children the tumors were localized in the vermis. Four children had the tumor localized in both hemispheres and also in the vermis of the cerebellum. Exact treatment schemes are shown in Fig. 1.

The most interesting subgroup of children in the context of the aims of our study was the subgroup treated by surgical tumor resection only. The children were assessed by means of age-appropriate tests that examine higher mental functions. We used WAIS-R and WISC-R (III Edition) tests. As suggested by David Wechsler, we used Wechsler scales as a clinical tool, rather than as an intelligence test, to assess the development of higher CNS function. We considered three indices: Verbal Comprehension (VCI), Perceptual Reasoning (PRI), and Working Memory (WMI). We used WAIS-R and WISC-R appropriate to the patient age. We also assessed neuropsychological development with the use of some subtests of the Verbal Scale, specifically similarities (asking how two concepts are alike), arithmetics (timed, orally-administered arithmetic questions), and digit span (children are orally given sequences of numbers and asked to repeat them, either as heard or in reverse order), and some subtests of Performance Scale, like picture completion (children are shown artwork of common objects with a missing part and asked to identify the missing part by pointing and/or naming), Picture concepts (children are shown rows of pictures and asked to find a common bond with one picture in each row), and block design (children put together red-and-white blocks in a pattern according to a displayed model). Additionally, we used the Luria Neuropsychological Test to assess visual sequential memory and auditory sequential memory. Moreover, all children during the examination were observed with respect to levels of attention, emotions, memory, and verbal function and fluency. Additionally, a speech examination and neurologopedical test were performed. The clinical state of all patients was also evaluated, including a

Table 1 Localization of the tumor in posterior fossa

Cerebellar tumors	43.75%
Fourth ventricle tumors	25.00%
Brain stem tumors	15.60%
Tumors/cysts of lamina	12.50%
Retrocerebellar cyst	3.10%

Table 2 Neurological deficits

No deficits	4
Mild cerebellar ataxia	22
Considerable cerebellar ataxia and other neurological deficits	6

full neurological examination. Neurological deficits are shown in Table 2. Statistical analysis was performed with the application of SPSS® and Statistica® v 6.0 software. Significance level α was set to 0.05.

Results

We found that patient age at the time of surgery correlated positively with PRI (Perceptual Reasoning Index) outcome ($p < 0.05$). Application of RTX and CHT correlated negatively with PRI (Perceptual Reasoning) outcome ($p < 0.05$). There was no similar significant correlation in other indices of Wechsler subscales and in cases of CHT alone. Such results may also be influenced by more aggressive tumor types, not only by the application of adjuvant therapies. Considering VCI (Verbal Comprehension Index – linguistic processing), we noted better outcome in children with tumor localization in brainstem and vermis, and the lowest values were achieved by children with tumor localized in cerebellar hemispheres and IV ventricle ($p < 0.05$). To verify if the age of the children affects neurodevelopment, we divided our patients by age at time of surgery. Results showed that older children perform working memory tasks considerably better. Moreover, post-operative children younger than 8 years of age were found to have significantly more lability/behavioral deficits when compared to the older children. Seventy-five percent of patients, mainly with vermis damage, demonstrated changes in affect regulation characterized by emotional lability, mood swings, irritability, shyness, lack of self-confidence, and weepiness (Fig. 2).

In the second part of our study we focused on cerebellar functional topography to see if vermal or hemispheric tumor localization determines different neurobehavioral outcome. Recently, evidence has been presented to suggest that right hemisphere disorders affect linguistic processing and sequential auditory memory, whereas left hemisphere disorders affect visual–spatial sequential memory (Fig. 3).

We did not find statistically significant differences by localization, and we noted only a tendency to obtain lower values in verbal comprehension in patients with tumors localized in left cerebellar hemisphere. The lack of statistical significance may have been the effect of a small sample size. Right hemispheric tumor localization seems to predispose patients particularly to working memory disorders and together with vermal tumor localization to perceptual reasoning disorders.

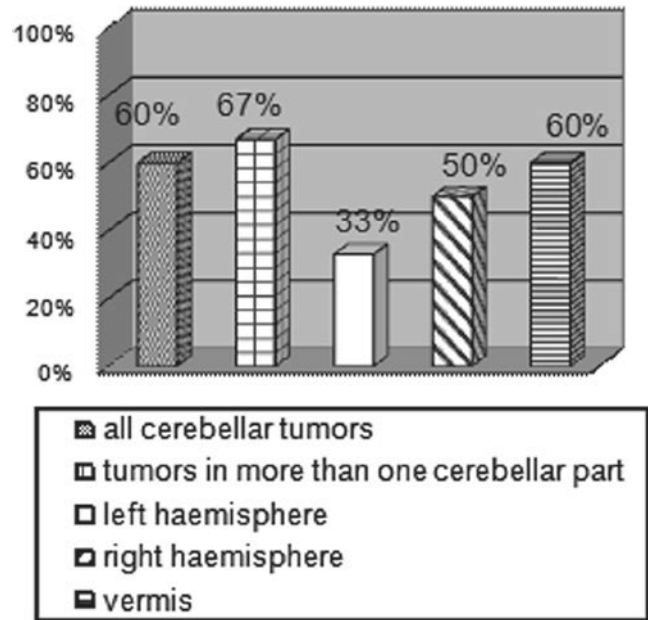


Fig. 2 Neurobehavioral changes in accordance with cerebellar tumor localization

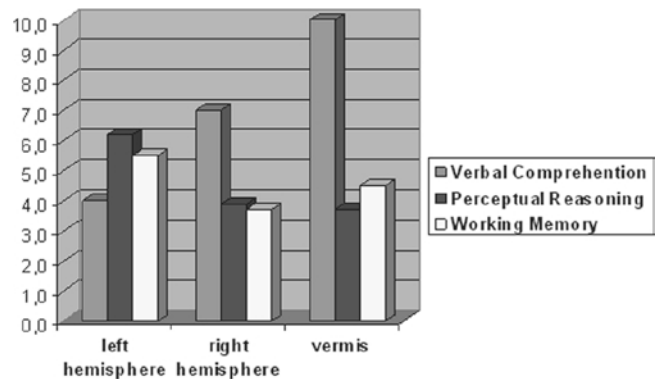


Fig. 3 Results for particular subscales in accordance with cerebellar localization of the tumor

Discussion

Neurobehavioral changes such as emotional lability, irritability, weepiness, impulsiveness, shyness, and uncertainty were found in most (75%) of our patients. It is noteworthy that the disorders were significantly more frequent in patients with vermal lesions, which was confirmed by other authors. Steinlin and colleagues described neurobehavioral changes in 33% of 24 children operated on for cerebellar tumors and yielded significant positive correlations between the location of the pathology in the vermis and the described disorders (16). Similar results were achieved by Levisohn et al. in their study with 48 children (4). In our group, children younger

than 8 years of age demonstrated neurobehavioral changes more frequently than older children. On the other hand, older patients obtained better results in subtests assessing memory functions.

The adjuvant therapy seemed to deteriorate results independently of age, which was confirmed by our study and other papers (6–9). We demonstrated statistically significant differences between results obtained by children, who underwent adjuvant therapy, and children treated only surgically. Recognition of a cerebellar role in the control and development of higher CNS functions supports a possible correlation between tumor location (vermal or hemispheric) and different neurobehavioral anomalies. Previous work has suggested an association between the functional topography of the cerebellum and cognitive alterations, specifically that right cerebellar lesions are probably responsible for deficits in language processing and auditory sequential memory, whereas the left cerebellum may be involved in visual–spatial sequential memory (10,13). We did not find any statistically significant results supporting such differences, although we did observe lower ability in linguistic processing in children with left cerebellar tumors. Right cerebellar tumor location seemed to predispose towards lower ability in working memory tasks, and together with vermal location, a lower perceptual reasoning index was found. Our observations did not correspond to the results of previous studies, which may be the consequence of small group size.

Our results confirm the appearance of behavioral and cognitive disorders in children treated for posterior fossa tumors. Posterior fossa structures are associated not only with motor control but also with higher CNS functions. Posterior fossa tumors are thought to be responsible for deficits in executive, visual–spatial, linguistic, and behavioral functions. In the literature there are few findings describing cognitive and behavioral deficits following cerebellar pathologies in children. Our study supports the aforementioned phenomena and develops a theory of functional organization of the cerebellum. Exploration of the consequences of damage in posterior fossa structures contributes to a better understanding of the cerebellar function in the emotional and cognitive development of children. Moreover, this work may enable the prediction of possible neurobehavioral disorders and offer appropriate strategies for rehabilitation, qualification, and surgical procedures.

Conclusions

Posterior fossa tumors can disturb normal development of higher mental functions, especially in terms of linguistic processes and emotional traits. Exploration of the consequences of damage in posterior fossa structures contributes to better

understanding of cerebellar function in the emotional and cognitive development of children.

Conflict of interest statement We declare that we have no conflict of interest.

References

1. Duffner PK, Cohen ME (1991) The long-term effects of central nervous system therapy on children with brain tumors. *Neurol Clin* 9:479–495
2. Gilberg C, Coleman M (1992) *The biology of autistic syndromes*. MacKeith, London
3. Heideman RL, Packer RJ, Albright LA, Freeman CR, Rorke LB (1993) *Tumors of the central nervous system principles and practice of pediatric oncology*, 2nd edn. JB Lippincott, Philadelphia
4. Levisohn L, Cronin-Golomb A, Schmähmann JD (2000) Neuropsychological consequences of cerebellar tumour resection in children. *Brain* 123:1041–1050
5. Malm J, Kristensen B, Karlsson T, Carlberg B, Fagerlund M, Olsson T (1998) Cognitive impairment in young adults with infratentorial infarcts. *Neurology* 51:433–440
6. Mulhern RK (2001) Risks of young age for selected neurocognitive deficits in medulloblastoma are associated with white matter loss. *J Clin Oncol* 19:472–479
7. Pollack IF, Polinko P, Albright AL, Towbin R, Fitz C (1995) Mutism and pseudobulbar symptoms after resection of posterior fossa tumors in children. *Neurosurgery* 37:885–893
8. Reimers TS, Ehrenfels S, Mortensen EL, Schmiegelow M, Shnderkaer S, Carstensen H, Shmiegelow K, Muller J (2003) Cognitive deficits in long-term survivors of childhood brain tumors: identification of predictive factors. *Med Pediatr Oncol* 40:26–34
9. Ris MD, Packer R, Goldwein J, Jones-Wallace D, Boyett JM (2001) Intellectual outcome after reduced-dose radiation therapy plus adjuvant chemotherapy for medulloblastoma: a Children's Cancer Group study. *J Clin Oncol* 19:3470–3476
10. Riva D, Pantaleoni C, Milani N, Fossati Belani F (1991) Combined treatment modality for medulloblastoma in childhood: effects on neuropsychological functioning. *Neuropediatrics* 22:36–42
11. Riva D, Giorgi C (2000) The cerebellum contributes to higher functions during development. *Brain* 123:1051–1061
12. Riva D, Milani N, Pantaleoni C, Ballerini E, Giorgi C (1989) Impairment of neuropsychological functions in children with medulloblastomas and astrocytomas in the posterior fossa. *Childs Nerv Syst* 5:107–110
13. Schmähmann JD (1991) An emerging concept: the cerebellar contribution to higher function. *Arch Neurol* 48:1178–1187
14. Schmähmann JD, Sherman JC (1998) The cerebellar cognitive affective syndrome. *Brain* 121:567–579
15. Silveri MC, Di Betta AM, Filippini V, Leggio MG, Molinari M (1998) Verbal short-term store-rehearsal system and the cerebellum. Evidence from a patient with a right cerebellar lesion. *Brain* 121:2175–2187
16. Steinlin M, Imfeld S, Zulauf P, Boldshauser E, Lovblad KO, Ridolfi Luthy A, Perring W, Kaufmann F (2003) Neuropsychological long-term sequelae after posterior fossa tumour resection during childhood. *Brain* 126:1–11
17. Van Calenbergh F, Van de Laar A, Plets C, Goffin J, Cesaer P (1995) Transient cerebellar mutism after posterior fossa surgery in children. *Neurosurgery* 37:894–898
18. Young J, Ries LG, Silverberg E, Horn JW, Miller RW (1986) Cancer incidence, survival and mortality for children young than age 15 years. *Cancer* 58:598–602

Part VII
Tumor

The Role of eNOS in Vascular Permeability in ENU-Induced Gliomas

S. Bulnes, E.G. Argandoña, H. Bengoetxea, O. Leis, N. Ortuzar, and J.V. Lafuente

Abstract Brain edema in gliomas is an epiphenomenon related to blood–brain-barrier (BBB) breakdown in which endothelial nitric oxide synthase (eNOS) plays a key role. When induced by vascular endothelial growth factor (VEGF), eNOS synthesizes nitric oxide that increases vascular permeability. We investigated the relationship between eNOS, VEGF and BBB dysfunction in experimental gliomas.

Tumors were produced in Sprague-Dawley rats by transplacental administration of Ethylnitrosourea (ENU). Immunoreexpression of eNOS and VEGF₁₆₅ was studied to identify locations of vascular permeability. BBB permeability was evaluated using gadolinium and intravital dyes and BBB integrity by endothelial barrier antigen (EBA), glucose transporter-1 (GluT-1) and occludin immunostaining.

Low grade gliomas displayed constitutive eNOS expression in endothelial cells and in VEGF-positive astrocytes surrounding vessels. Malignant gliomas overexpressed eNOS in aberrant vessels and displayed numerous adjacent reactive astrocytes positive for VEGF. Huge dilated vessels inside tumors and glomeruloid vessels on the periphery of the tumor showed strong immunopositivity for eNOS and a lack of occludin and EBA staining in several vascular sections. BBB dysfunction on these aberrant vessels caused increased permeability as shown by Gadolinium contrast enhancement and intravital dye extravasation.

These findings support the central role of eNOS in intra- and peritumoral edema in ENU-induced gliomas.

Keywords Brain edema • glioma • tight junction • blood–brain-barrier (BBB) • vascular endothelial growth factor (VEGF) • endothelial nitric oxide synthase (eNOS)

Introduction

Brain edema that occurs in association with gliomas is thought to be related to vasodilation and blood–brain-barrier (BBB) dysfunction mediated by vascular endothelial growth factor (VEGF) and nitric oxide (NO) (11, 12).

When blood flow inside and around the tumor becomes irregular and chaotic, partly due to aberrant microvessels, tissue hypoxia triggers the production of hypoxia inducible factor-1 α (9, 19), which upregulates the expression of VEGF (3). This angiogenic factor induces the synthesis of NO by phosphorylating endothelial NO synthase via PI-3K/Akt kinase (16, 21), thus promoting BBB breakdown and increasing permeability.

Overexpression of NO is proposed to be involved in blood flow alterations and hypoxia-induced BBB permeability changes (14, 15). Once synthesized, NO has a very short half-life (less than 5 s), so the majority of our knowledge of NO is based on the NOS expression.

Endothelial nitric oxide synthase (eNOS) is the tissue-specific isoform that plays a crucial role in the regulation of vascular tone, vascular remodelling, angiogenesis and neuroprotection (7, 16).

Experimental gliomas induced by alkylating agents have proven useful to study many aspects of tumorigenesis, neoangiogenesis, etc. (10). Using this model, we have previously described the progression of the tumor malignancy process associated with alterations in vascular morphology and blood–brain-barrier function (4, 5).

In the present study, we have examined the co-expression of eNOS and VEGF along with BBB markers in experimental glioma.

J.V. Lafuente (✉), S. Bulnes, E.G. Argandoña, H. Bengoetxea, O. Leis, and N. Ortuzar
Department of Neuroscience, LaNCE; Clinical and Experimental Neuroscience Laboratory, University of Basque Country, Leioa, Spain
e-mail: josevicente.lafuente@ehu.es; www.ehu.es/LaNCE

Material and Methods

Animals and Tumor Screening

Eight Sprague-Dawley rats were injected intraperitoneally (i.p.) with a single dose (80 mg/kg b.w.) of N-nitroso-N-ethylurea (ENU, Sigma-Aldrich) on day 15 of pregnancy (E15) as previously described (4). Fifty-five offspring were selected for the study. All experiments were performed in accordance with the European Community Council Directive of November 24, 1986 (86/609/EEC).

Tumor screening was performed by magnetic resonance imaging (MRI, Biospec BMT 47/40, Bruker). To aid in tumor visualization, animals were injected i.p. with 1.5 ml/kg b.w. of gadolinium (Gd-DTPA) (Magnevist, Schering) (13). Thirty minutes before the autopsy, 28.5 mg/Kg b.w. of Evans blue (EB) (Sigma Aldrich) or rose Bengal (RB) (Sigma Aldrich) solutions were administered intravenously for macroscopic identification of vascular permeability. Following transcerebral perfusion with 2% PFA, brains were removed and immersed overnight in the same solution at 4°C. Tumors were detected by intravital dyes or using stereoscopic microscopy (Lan Optics). Individual coronal sections including the tumor were embedded in paraffin wax (Histosec® Merck), and others were stored in 30% sucrose until the tissues sank.

Histology and Immunohistochemistry

For the histopathological study, hematoxylin-eosin (H&E) staining was carried out on 4 µm sections. Sections were observed for the presence of histological features, such as cellular anaplasia, atypical mitosis, microvascular proliferation, hemorrhages, necrosis or cysts.

Immunohistochemistry for occludin was performed on 4 µm paraffin slices after removing wax through xylene immersion and rehydrating. Endogenous peroxidase activity was blocked by incubation in 4% H₂O₂/methanol for 20 min. Sections were then boiled for 5 min in antigen retrieval solution (Vector Laboratories). Slices were washed in 0.1 M phosphate-buffered saline (PBS), pH 7.4, containing 0.5% bovine serum albumin and 0.1% Triton X-100 and then incubated overnight at 4°C in a moist chamber with primary antibody against occludin (Zymed, 1:100). After washing in buffer solution, sections were incubated in biotinylated secondary antibody for 2 h, washed and incubated for another 2 h in peroxidase-avidin-biotin complex (ABC Kit Elite, Vector) at room temperature. Immunohistochemical reactions were revealed by immersion in diaminobenzidine-H₂O₂ solution. Finally, the sections were counterstained with hematoxylin, dehydrated and covered with DePeX (Fluka).

To assess the integrity of the BBB, double staining for tomato lectin (LEA) and eNOS, VEGF₁₆₅, EBA or GluT-1 was carried out on free-floating sections using the appropriate antibodies. Briefly, 40 µm free-floating sections were incubated with blocking solution (10% BSA, 3% Triton X-100 in 0.1 M PBS) for 2 h. They were then incubated overnight at room temperature in a cocktail of primary antibodies or primary antibody and LEA-FITC (Sigma-Aldrich, 1:200) in 1% BSA containing 0.1% Triton X-100. The primary antibodies were: anti-VEGF (Santa Cruz Biotechnology, 1:75), anti-eNOS (Neomarkers, 1:200), anti-EBA (Sternberger Monoclonals, 1:2,000) and anti-GluT-1 (Chemicon, 1:1,000). Subsequently, sections were incubated for 2 h in a cocktail of secondary fluorescent antibodies including Alexa Fluor 568 and 488 (Invitrogen, 1:400). Sections were then incubated in Hoechst solution for 10 min. Finally, sections were rinsed, mounted on gelatine-coated slides and cover-slipped in an aqueous medium (Vectashield Mounting Medium H-100). Primary antibodies were omitted for control samples. Images were acquired with an Olympus Fluoview FV 500 confocal fluorescence microscope using sequential acquisition to avoid overlap of fluorescence emission spectra. The image treatment program used was FV 10-ASW 1.6 Viewer.

Results

Sixty-seven cerebral gliomas from 55 rats were selected by magnetic resonance imaging. Thirty-four classic oligodendrogliomas (CO) showed a homogenous hyperintense signal on T2-weighted images, but they displayed neither gadolinium contrast enhancement on T1-weighted images nor intravital dye extravasation (Fig. 1a). By histopathology, these tumors showed an isomorphous cellular pattern, constituted by cells with rounded, homogenous nuclei and clear cytoplasm (honeycomb pattern). No histopathological features of malignancy were found.

Thirty-three anaplastic oligodendroglioma (AO) displayed mild to high heterogeneous signals on T2-weighted images showing intratumor areas with both hyper- and hypointense signals. These masses also displayed either mild homogenous or highly heterogeneous gadolinium enhancement on T1-weighted images, and intravital dyes showed from light extravasation to strong staining of tumor and peritumoral regions (Fig. 1b, c). These malignant tumors displayed cellular anaplasia with atypical mitosis, endothelial proliferations, hemorrhagic areas, macrocysts and necrosis with pseudopallisading.

LEA glycoprotein was homogeneously present on all microvessels of normal and tumor tissue. According to the malignancy, we observed three vascular patterns: (a) vessels

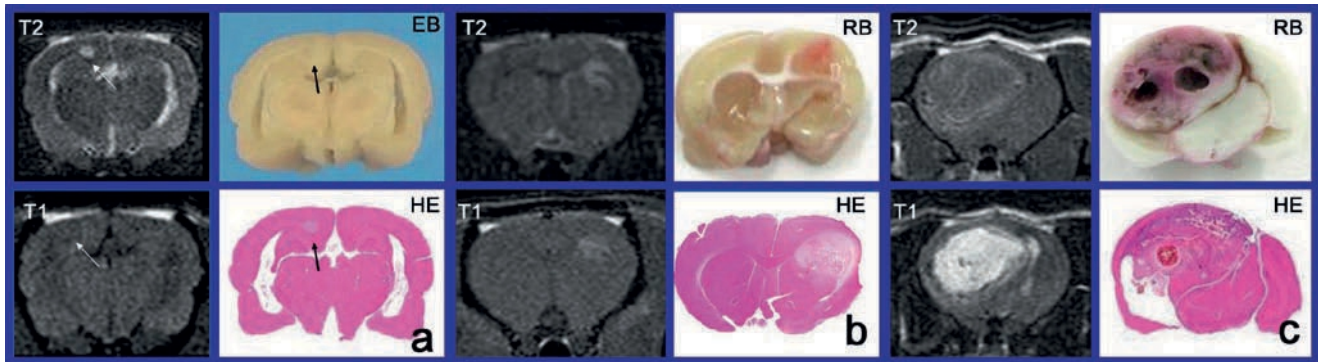


Fig. 1 Brain coronal sections of rats exposed to ENU showing classic oligodendroglioma (CO) (a) and anaplastic oligodendroglioma (AO) in the early (b) and advanced stages of development (c). T1- and T2-weighted MRIs. Evans blue (EB), rose Bengal (RB), Hematoxylin-eosin stain (HE)

similar to the normal ones (Fig. 2a), including homogenous angioarchitecture in low-grade tumors; (b) dilated, tortuous and branched vessels (Fig. 2b) in the early stage of AO; and (c) abundant aberrant vessels distributed in an anarchic and irregular network in the advanced stage of AO. Malignant oligodendrogliomas in the advanced stage showed mainly big glomeruloid formations on the neoplastic border, small glomeruloid vessels surrounding necrosis or cyst areas (Fig. 2c) and scarce huge dilated vessels inside the tumor (Fig. 2d).

Mild eNOS immunorexpression was observed in most capillaries (Fig. 2e, i), with strong staining in some dilated vessels of anaplastic gliomas. Distribution of this enzyme was heterogeneous and predominated in aberrant vessels, such as dilated and tortuous vessels corresponding to early stages of AO (Fig. 2f, j). In the advanced stage, endothelia of huge caliber vessels overexpressed eNOS in a patchy pattern (Fig. 2h, l). On the other hand, glomeruloid vessels from the tumor border and those surrounding intratumoral necrosis and cysts showed random immunopositivity in some vascular sections (Fig. 2g, k).

VEGF immunofluorescence demonstrated that only the astroglial structures (soma and end-feet) were positive for this growth factor. VEGF distribution in CO was similar to that observed in the normal neuropil (Fig. 2m). Tissues from early and advanced AO showed numerous reactive astrocytes on the border of the neoplasia and astrogliosis within the tumor. VEGF positive astrocytes were observed surrounding neoplastic and control blood vessels (Fig. 2n). Astrocytes around glomeruloid vessels on the borders of tumors showed light staining for VEGF, whereas astrocytes adjacent to perinecrotic glomeruloid lacked VEGF immunostaining (Fig. 2ñ). Intratumoral huge dilated vessels showed positive end-feet adjacent to endothelia and profuse glial fibers around the vessels bordering a gap between both structures (Fig. 2o).

Occludin was expressed in the intimae of cerebral capillaries (Fig. 3a). Endothelia of classic oligodendrogliomas

showed occludin immunopositivity on every vascular section (Fig. 3e). In contrast, anaplastic tumors showed irregular staining with positive and negative sections of vessels on the border of tumors as well as inside them (Fig. 3i).

Vascular profiles from the normal brain were intensely and ubiquitously labeled for the BBB markers, EBA and GluT-1. Labeling distribution varied according to the degree of malignancy. Both antigens were shown in every vascular section of normal brain (Fig. 3b–d) and CO (Fig. 3f–h), but in advanced AO, the most aberrant vessels showed irregular staining. Huge dilated and intratumoral glomeruloid vessels partially lacked the reactivity for EBA but maintained the positivity for GluT-1 (Fig. 3j–l).

Discussion

Evidence has shown that eNOS and VEGF overexpression mediated angiogenesis and vascular permeability increase in malignant gliomas (17). eNOS has been reported to be involved in vasodilation and in hypoxia-induced BBB permeability changes. In addition, the use of NOS inhibitors, such as L-NNA and L-NMMA, in pathological conditions attenuates BBB permeability and restores cerebral blood flow (20). However, the role of eNOS and VEGF in tumor-induced brain edema is still a matter of debate. The present study demonstrates that eNOS overexpression in the microvasculature of gliomas correlates with the loss of immunostaining for primary BBB markers.

The mild positivity for eNOS on the endothelium of normal brain vessels is due to basal concentrations of this enzyme. Constitutively, eNOS plays a crucial role in the regulation of vascular tone, vascular remodeling and neuroprotection. Relative tissue hypoxia in malignant gliomas due to irregular blood flow induces VEGF synthesis by reactive astrocytes located adjacent to blood vessels. This angiogenic cytokine activates the protein kinase Akt, which directly

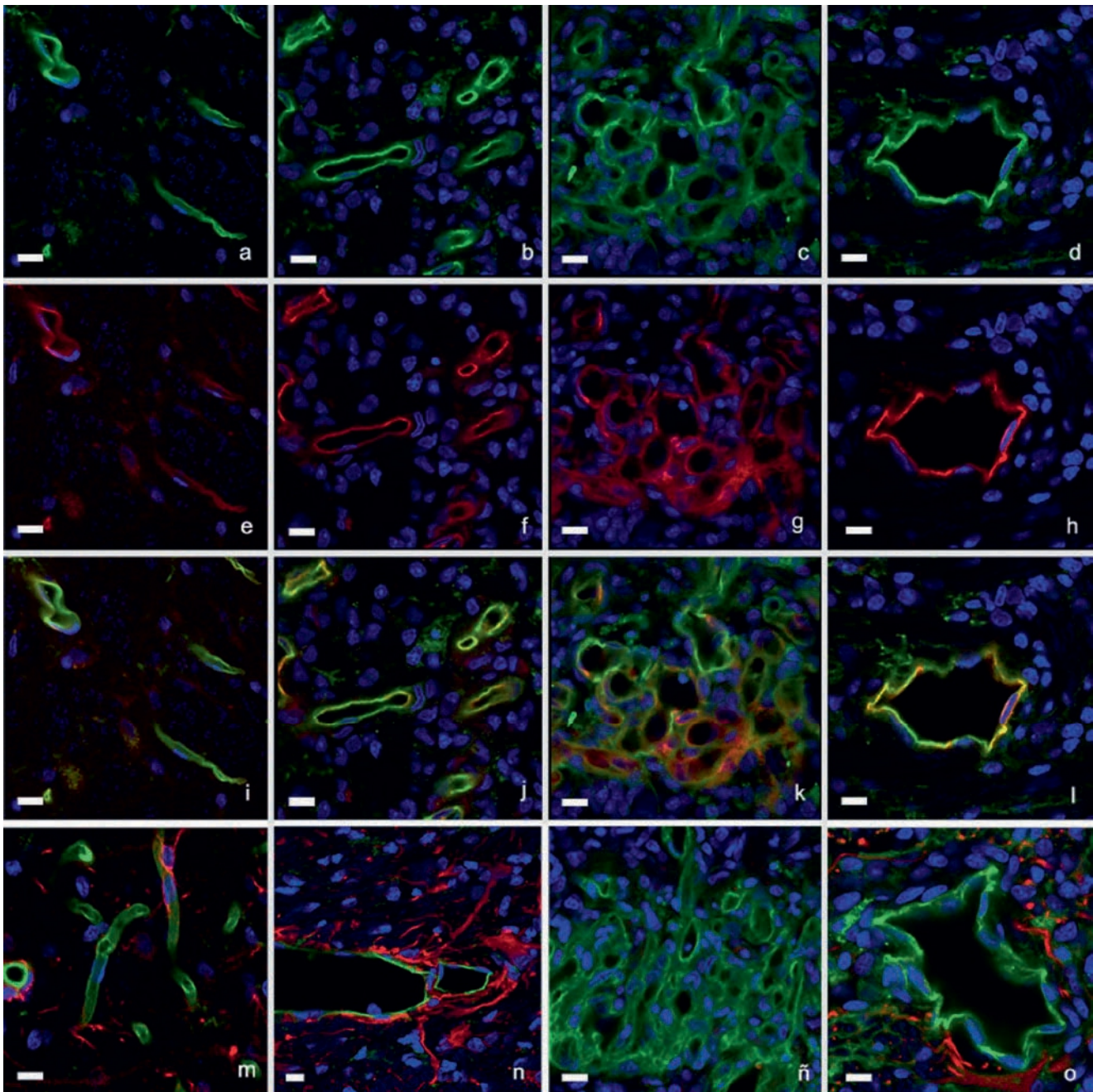


Fig. 2 Vascular sections viewed by confocal microscopy. Immunofluorescence for LEA (green, **a–d**), eNOS (red, **e–h**), LEA-eNOS co-expression (**i–l**) and LEA-VEGF₁₆₅ co-expression (**m–o**). Sections were counterstained with Hoechst (blue nuclei). Bar 10 μ m

phosphorylates eNOS on Ser¹⁷⁷, thereby increasing eNOS activity (16). According to the present model, aberrant vessels of malignant gliomas overexpressed eNOS, and adjacent astrocyte end-feet showed strong staining for VEGF. These findings support the role of eNOS, cooperating with VEGF, in vascular adaptation in gliomas.

Brain edema, defined as increased water content in brain, is a major complication in several central nervous system pathologies in which the integrity of the blood–brain–barrier

is altered (8). In addition to astrocytic processes and pericytes that loosely attached to endothelial cells of tumor vessels without forming a continuous layer (2), defective tight junctions (TJs) also lead to edema associated with brain tumors (18). Several studies have focused on occludin, a transmembrane protein located in the interendothelial tight junction, for the study of BBB breakdown. In our model, the capillary network of classic oligodendrogliomas shows this protein on every vascular section. In contrast, aberrant

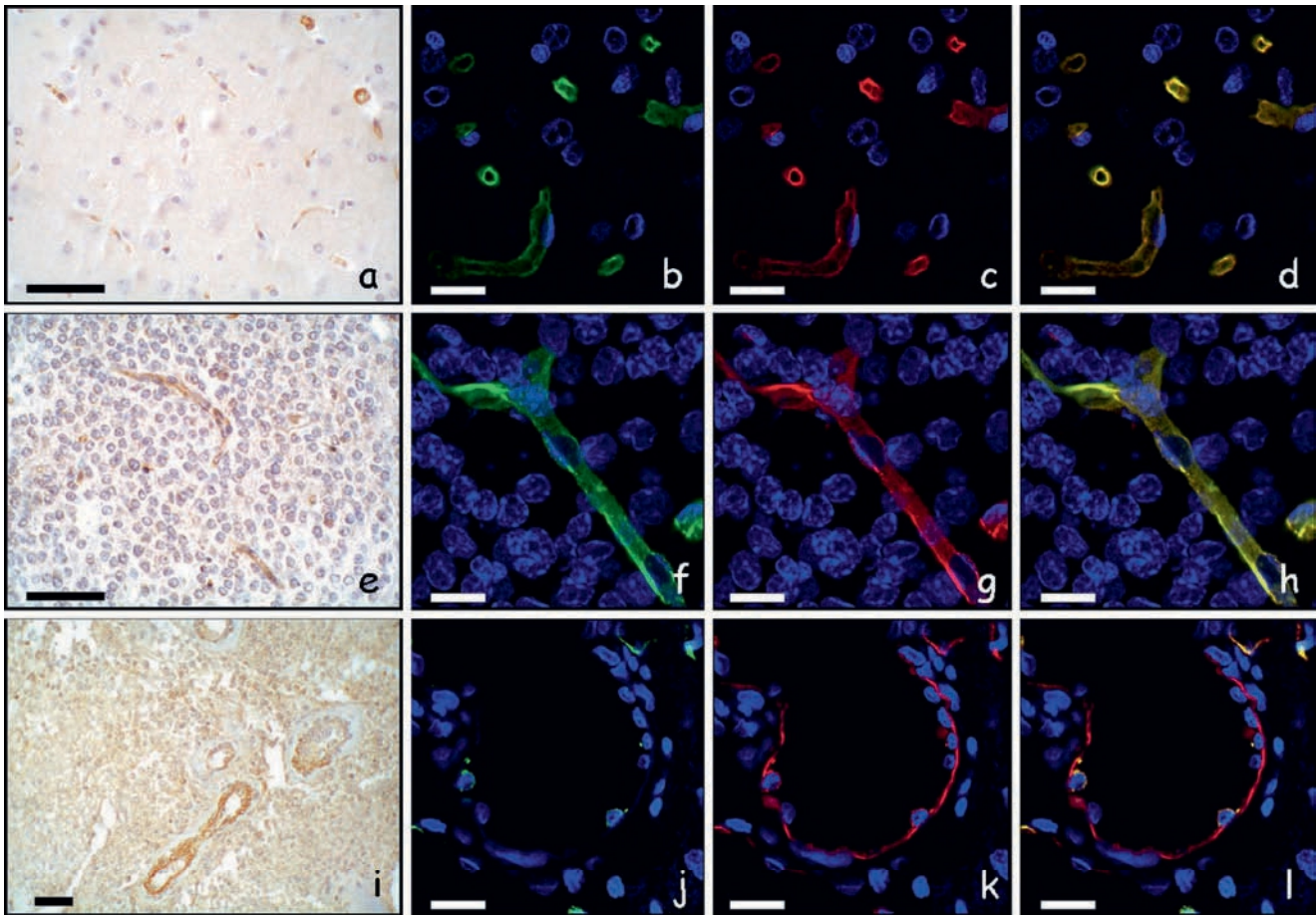


Fig. 3 Study of BBB markers in normal brain (a-d), classic oligodendrogliomas (e-h) and anaplastic oligodendrogliomas (i-l). Expression for EBA (green, b, f, j), GluT-1 (red, c, g, k) and EBA-GluT-1 (d, h, l). Sections were counterstained with Hoechst (blue nuclei). Bar 20 μm . HRP-DAB immunohistochemistry for occluding (a, e, i). Bar 50 μm .

vessels of anaplastic tumors lose occludin immunoreactivity. We have also found that these aberrant vessels lack normal expression levels of other BBB markers (EBA, GluT-1). Labeling distributions were similar when stained for EBA, GluT-1 or occluding, and staining for all varied according to vascular changes (1). Although the labeling profile with these three BBB markers was continuous and intense in the normal brain, aberrant vessels showed irregular staining including positive and negative vessels. Within the malignant tumor, occludin staining was negative, and BBB markers were scarcely observed, in dilated or glomeruloid vessels. On the other hand, few vessels on the periphery of the tumor were immunopositive for occludin, EBA or GluT-1. However, staining for glucose transporter-1 remained positive even when pathological alterations of the BBB promoted changes in EBA expression.

BBB breakdown and eNOS activity is closely related to tissue oxygenation. In general, the huge dilated vessels from the intratumor hypoxic area were strongly positive for eNOS and lost the BBB mechanism, whereas on the oxygenated periphery some vessels, with irregular immunostaining,

maintained glucose transport activity. The same relationship was found for occludin. These findings support the hypothesis that hypoxia leads to calcium overload in endothelial cells. Taking into account that NO is produced constitutively by calcium-dependent eNOS, alterations in calcium levels may impact NO formation and other calcium-dependent mechanisms involved in disruption of the tight junction complex.

In addition, areas of BBB distortion were identified by intravital dyes and gadolinium contrast enhancement (6). The integrity of the BBB function was evaluated *in vivo* by gadolinium contrast on T1-weighted images and by leakage of Evans blue or rose Bengal *ex vivo*. Vascular permeability was mainly observed in AOs. Mild gadolinium contrast enhancement and homogenous intravital dye extravasation were observed in regions with dilated and tortuous vessels. In regions with huge dilated and glomeruloid vessels, we found widespread heterogeneous contrast enhancement (hypointense as well as hyperintense signals) on T1-weighted images and leakage of intravital dyes. According to Papadopoulos et al. (18), occludin was significantly down-regulated in

aberrant hyperplastic vessels with strong eNOS activity, correlating with the presence of contrast enhancement.

In summary, sequential expression of VEGF and eNOS seems to be relevant to understanding vascular permeability through the loss of immunostaining for BBB markers. In the hypoxic glioma core, eNOS promotes vascular dilation and increased permeability. On the periphery of the tumor, eNOS promotes vascular proliferation. Thus, eNOS plays a pivotal role in intra- and peritumoral brain edema in this model of experimental gliomas.

Conflict of interest statement We declare that we have no conflict of interest.

Acknowledgements Financially supported by Gangoiti Foundation, SAIOOTEK & IT/460/07 (Basque Government). Confocal microscopy analysis was performed at the “Servicio de Microscopia Analítica y de Alta Resolución en Biomedicina” (High Resolution Analytical Microscopy Service for Biomedicine) at the University of the Basque Country.

References

- Argandona EG, Bengoetxea H, Lafuente JV (2005) Lack of experience-mediated differences in the immunohistochemical expression of blood–brain-barrier markers (EBA and GluT-1) during the postnatal development of the rat visual cortex. *Brain Res Dev Brain Res* 156: 158–166
- Baluk P, Hashizume H, McDonald DM (2005) Cellular abnormalities of blood vessels as targets in cancer. *Curr Opin Genet Dev* 15:102–111
- Bengoetxea H, Argandona EG, Lafuente JV (2008) Effects of visual experience on vascular endothelial growth factor expression during the postnatal development of the rat visual cortex. *Cereb Cortex* 18(7):1630–1639
- Bulnes S, Lafuente JV (2007) VEGF immunopositivity related to malignancy degree, proliferative activity and angiogenesis in ENU-induced gliomas. *J Mol Neurosci* 33(2):163–172
- Bulnes-Sesma S, de Ullibarri-Ortiz ZN, Lafuente-Sanchez JV (2006) Tumour induction by ethylnitrosourea in the central nervous system. *Rev Neurol* 43:733–738
- Claes A, Gambarota G, Hamans B, Van TO, Wesseling P, Maass C, Heerschap A, Leenders W (2007) Magnetic resonance imaging-based detection of glial brain tumours in mice after antiangiogenic treatment. *Int J Cancer* 122(9):1981–1986
- Fukumura D, Gohongi T, Kadambi A, Izumi Y, Ang J, Yun CO, Buerk DG, Huang PL, Jain RK (2001) Predominant role of endothelial nitric oxide synthase in vascular endothelial growth factor-induced angiogenesis and vascular permeability. *Proc Natl Acad Sci USA* 98:2604–2609
- Huber JD, Egleton RD, Davis TP (2001) Molecular physiology and pathophysiology of tight junctions in the blood–brain-barrier. *Trends Neurosci* 24:719–725
- Jain RK, Di TE, Duda DG, Loeffler JS, Sorensen AG, Batchelor TT (2007) Angiogenesis in brain tumours. *Nat Rev Neurosci* 8:610–622
- Kokkinakis DM, Rushing EJ, Shareef MM, Ahmed MM, Yang S, Singha UK, Luo J (2004) Physiology and gene expression characteristics of carcinogen-initiated and tumor-transformed glial progenitor cells derived from the CNS of methylnitrosourea (MNU)-treated Sprague-Dawley rats. *J Neuropathol Exp Neurol* 63:1182–1199
- Lafuente JV, Adan B, Alkiza K, Garibi JM, Rossi M, Cruz-Sanchez FF (1999) Expression of vascular endothelial growth factor (VEGF) and platelet-derived growth factor receptor-beta (PDGFR-beta) in human gliomas. *J Mol Neurosci* 13:177–185
- Lafuente JV, Bulnes S, Mitre B, Riese HH (2002) Role of VEGF in an experimental model of cortical micronecrosis. *Amino Acids* 23:241–245
- Machein MR, Knedla A, Knoth R, Wagner S, Neuschl E, Plate KH (2004) Angiopoietin-1 promotes tumour angiogenesis in a rat glioma model. *Am J Pathol* 165:1557–1570
- Mark KS, Burroughs AR, Brown RC, Huber JD, Davis TP (2004) Nitric oxide mediates hypoxia-induced changes in paracellular permeability of cerebral microvasculature. *Am J Physiol Heart Circ Physiol* 286:H174–H180
- Nag S, Picard P, Stewart DJ (2001) Expression of nitric oxide synthases and nitrotyrosine during blood–brain barrier breakdown and repair after cold injury. *Lab Invest* 81:41–49
- Osuka K, Watanabe Y, Usuda N, Nakazawa A, Tokuda M, Yoshida J (2004) Modification of endothelial NO synthase through protein phosphorylation after forebrain cerebral ischemia/reperfusion. *Stroke* 35:2582–2586
- Pan JW, Zhan RY, Tong Y, Zhou YQ, Zhang M (2005) Expression of endothelial nitric oxide synthase and vascular endothelial growth factor in association with neovascularization in human primary astrocytoma. *J Zhejiang Univ Sci B* 6:693–698
- Papadopoulos MC, Saadoun S, Binder DK, Manley GT, Krishna S, Verkman AS (2004) Molecular mechanisms of brain tumour oedema. *Neuroscience* 129:1011–1020
- Semenza GL (2003) Targeting HIF-1 for cancer therapy. *Nat Rev Cancer* 3:721–732
- Sharma HS, Westman J (2004) Blood-Spinal Cord and brain barriers in health and disease. Elsevier Academic, London
- Ziche M, Morbidelli L (2000) Nitric oxide and angiogenesis. *J Neurooncol* 50:139–148

Potential Role of CT Perfusion Parameters in the Identification of Solitary Intra-axial Brain Tumor Grading

Enrico Fainardi, Francesco Di Biase, Massimo Borrelli, Andrea Saletti, Michele Cavallo, Silvio Sarubbo, Stefano Ceruti, Riccardo Tamarozzi, and Arturo Chierogato

Abstract In this study, neoplastic perfusion abnormalities were investigated by computed tomography perfusion (CTP) scanning in 38 patients with solitary intra-axial brain tumors (19 with high grade gliomas, 7 with low grade gliomas and 12 with brain metastasis). Regional cerebral blood flow (rCBF), cerebral blood volume (rCBV), mean transit time (rMTT) and permeability surface flow (rPSF) levels were measured in two different regions of interest: (1) enhancing or non-enhancing tumor tissue and (2) a mirror area of apparently normal brain tissue located in the contralateral hemisphere. rCBF mean levels were greater in tumoral tissue than in the contralateral area for high-grade gliomas ($p < 0.02$). rCBV and rPSF mean values were higher in tumoral tissue than in the contralateral area for high-grade gliomas ($p < 0.01$ and $p < 0.05$, respectively) and metastasis ($p < 0.05$ and $p < 0.001$, respectively). rCBV mean values of tumoral tissue were greater in high-grade than in low-grade gliomas ($p < 0.05$). rPSF mean levels of tumoral tissue were higher in metastasis than in low-grade gliomas ($p < 0.02$). These findings indicate that multi-parametric CTP mapping may contribute to differential diagnosis of solitary intra-axial brain tumors.

Keywords Intra-axial brain tumors • CT perfusion • perfusion parameters • differential diagnosis

Introduction

Conventional Magnetic Resonance Imaging (MRI) is used widely in the diagnosis and follow-up treatment of brain tumors due to its ability to describe morphological characteristics

F. Di Biase
Neurosurgery Unit, Department of Neurosciences and Rehabilitation, Azienda Ospedaliera-Universitaria, Arcispedale S. Anna, Ferrara, Italy
e-mail: henryfai@tin.it

M. Borrelli
Dipartimento di Neuroscienze e Riabilitazione, Unità Operativa di Neuroradiologia, Azienda Ospedaliera Universitaria, Corso della Giovecca 203, Arcispedale S. Anna, Ferrara 44100, Italy

and anatomic relationships (12). However, conventional MRI is often non-specific and is limited in the determination of tumor angiogenesis, which is strongly associated with malignant potential of intracranial neoplasms and patient survival (9). For these reasons, increasing attention has been focused on perfusion-weighted imaging (PWI), an advanced MRI technique that detects hemodynamic abnormalities associated with brain tumors (2). In particular, PWI can identify increased cerebral blood volume (CBV) and blood-brain barrier permeability, which reflect underlying tumor angiogenesis (2, 9). This methodological approach seems useful in predicting tumor grading and could assist in surgical, radiation and chemotherapeutic planning as well as monitoring response to treatment. Emerging evidence from clinical studies indicates that dynamic computed tomography perfusion (CTP) scanning is a rapid, feasible and readily available imaging modality that provides a quantitative assessment of cerebral hemodynamic disturbances in patients with acute ischemic stroke (11). More important, recently CTP imaging has been shown to provide information about the physiology of cerebral neoplasms; thus, this technology may be a promising tool for the analysis of brain tumor microcirculation. In fact, it has been reported that cerebral blood flow (CBF), CBV and Permeability Surface flow (PSF) indicated by CTP seem to correlate well with tumor grade (4) and can help to distinguish high-grade gliomas from tumor-mimicking lesions such as subacute infarction (7) as well as to identify isolated brain metastasis (10). In addition, CTP multi-parametric maps have proven helpful in differentiating between high-grade and low-grade gliomas (3, 5) and between tumor recurrence and radiation necrosis (6). As PWI is not always available, CTP could be an alternative method for assessing the hemodynamics of brain tumors with their extension, type and grade and for discriminating tumor from post-radiation enhancement. In this study, we investigated by CTP imaging perfusion disorders occurring in solitary intra-axial brain tumors in order to further understand the role of CTP in differentiation between high-grade and low-grade gliomas and between cerebral gliomas and metastasis.

Materials and Methods

Patients

Thirty-eight patients (25 male and 13 female; mean age \pm SD = 61.6 ± 12.1 years) with suspected solitary intra-axial brain tumor at admission CT and/or MRI and having a Karnofsky performance status (8) at entry ranging from 60% to 95% were prospectively included in the study. All patients underwent surgical biopsy or tumor removal within 7 days after CTP examination. The neoplasms were histopathologically classified as: glioblastoma multiforme ($n = 10$), anaplastic astrocytoma ($n = 9$), diffuse astrocytoma ($n = 5$), oligodendroglioma ($n = 2$) and brain metastasis ($n = 12$). According to the World Health Organization system, our series included 19 high-grade gliomas (WHO grade IV = 10; WHO grade III = 9) and 7 low-grade gliomas (WHO grade II). Moreover, cerebral metastases were secondary to lung carcinoma ($n = 6$), breast carcinoma ($n = 4$), renal carcinoma ($n = 1$) and colon carcinoma ($n = 1$).

CTP Technique

CTP studies were performed using a single-section CT scanner (CT Hispeed ZX/i; GE Medical System, Milwaukee, Wis.) equipped for CT perfusion imaging (CT Perfusion; GE Medical System, Milwaukee, Wis). The CT perfusion protocol consisted of a series of 45 CT scans acquired in a single slice (10 mm slice thickness, 80 kVp; 200 mAs; matrix 512×512 ; FOV 25 cm; total scan time 50 s) located at tumor level containing the largest volume of neoplastic tissue during the automatic injection of 50 mL of non-ionic contrast agent at the rate of 3.5 mL/s, starting 5 s before the initial

image. According to Cenic (1), perfusion maps were generated for CBF, CBV, mean transit time (MTT) and PSF for each patient with a deconvolution-based algorithm and a two-compartmental model by using an imaging workstation (Advantage Windows; GE Medical System, Milwaukee, Wis) with commercial dedicated software (CT Perfusion 2, GE Medical System, Milwaukee, Wis). To minimize inaccuracies in the measured perfusion parameter values, care was taken to exclude large blood vessels from perfusion parameter calculation. As depicted in Fig. 1, regional CBF (rCBF), CBV (rCBV) MTT (rMTT) and PSF (rPSF) levels were measured in two different regions of interest (ROI) larger than 1 cm^2 and manually outlined on the baseline diagnostic CT scan: (1) enhancing or non-enhancing tumor tissue and (2) an area of apparently normal brain tissue that mirrored the tumor region and was located in the contralateral hemisphere. More precisely, tumor ROI was drawn in the solid portion of the neoplastic mass by avoiding necrotic and cystic areas of the tumor. In case of limited visibility of the solid part of the lesion on CT scan, the corresponding T1-enhanced MRI imaging was utilized to correctly guide tumor ROI placement. CBF, CBV, MTT and PSF values were expressed in mL/100 g/min, mL/100 g, s and mL/100 g/min, respectively.

Statistical Analysis

After checking data for normality using the Kolmogorov–Smirnov test, statistical analysis was performed by t-test and Mann–Whitney U test with Bonferroni correction for multiple comparisons.

A value of $p < 0.05$ was considered statistically significant.

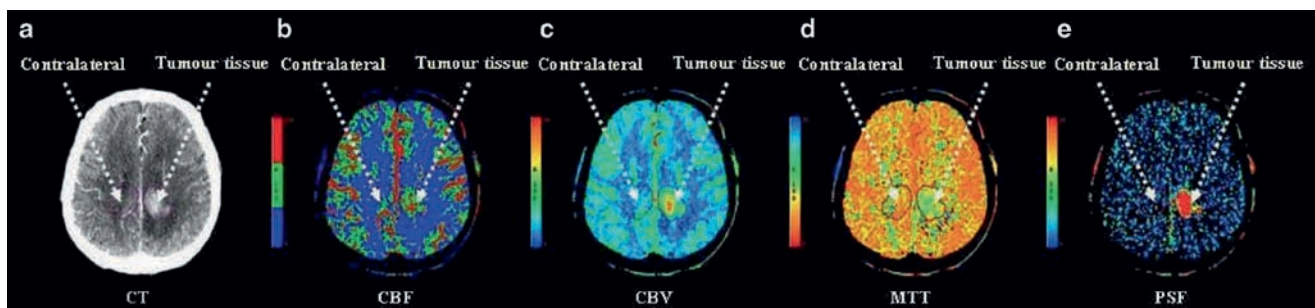


Fig. 1 Tumor location and perfusional mapping in patients with anaplastic astrocytoma located parasagittally in left parietal lobe. Image A shows tumor location on admission enhanced CT scan. Images B, C, D and E illustrate the corresponding maps of cerebral blood flow

(CBF), cerebral blood volume (CBV), mean transit time (MTT) and permeability surface flow (PSF). Hand-drawn regions of interest (ROIs) placed within tumor tissue and in the contralateral hemisphere are shown

Results

CTP Parameters Between Neoplastic Tissue and Contralateral Area in Each Tumor Subtype

As illustrated in Fig. 2, for high-grade gliomas, rCBF mean levels were significantly greater ($p < 0.02$) in tumor tissue (111.5 ± 52.9 mL/100 g/min) than in the contralateral area (71.2 ± 38.3 mL/100 g/min) whereas low-grade gliomas and metastases had similar rCBF values between tumor tissue (71.5 ± 32.9 and 106 ± 73.7 mL/100 g/min, respectively) and the contralateral area (69.5 ± 11.8 and 71.9 ± 28.9 mL/100 g/min, respectively). For high-grade gliomas, rCBV mean levels were significantly higher ($p < 0.01$) in tumor tissue (5.4 ± 2.3 mL/100) than in the contralateral area (3.2 ± 1.6 mL/100 g). For metastases, rCBV levels were

also significantly higher ($p < 0.05$) in tumor tissue (4.6 ± 2.2 mL/100 g) than in the contralateral area (3.0 ± 1.1 mL/100 g). Conversely, rCBV mean values were equivalent between tumor tissue (71.5 ± 32.9 mL/100 g) and the contralateral area (69.5 ± 11.8 mL/100 g) in low-grade gliomas. rPSF mean values were significantly increased ($p < 0.05$) in tumor tissue (6.9 ± 8.7 mL/100 g/min) compared to the contralateral area (1.7 ± 4.2 mL/100 g/min) for high-grade gliomas and were significantly more prominent in tumor tissue (9.9 ± 7.9 mL/100 g/min) than in the contralateral area (0.7 ± 0.5 mL/100 g/min) for metastases as well. On the contrary, comparable rPSF mean levels were observed between tumor tissue (2.5 ± 3.3 mL/100 g/min) and the contralateral area (0.8 ± 0.9 mL/100 g/min) in low-grade gliomas. No statistical difference was found for rMTT mean levels between tumor tissue and the contralateral area in the three tumor subtypes examined (data not shown).

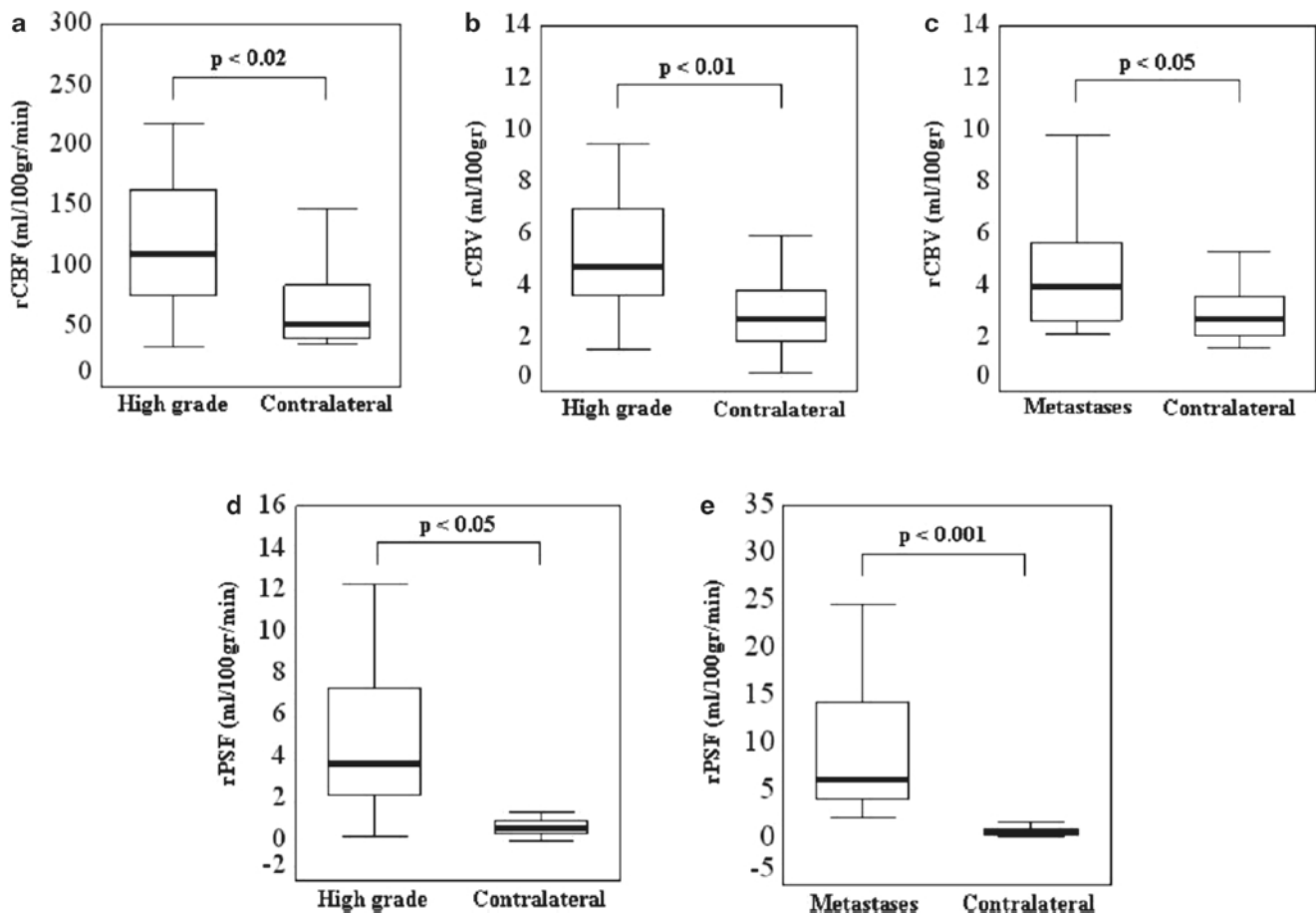


Fig. 2 Regional cerebral blood flow (rCBF), cerebral blood volume (rCBV) and permeability surface flow (rPSF) between neoplastic tissue and contralateral area in patients with high grade glioma ($n = 17$) and brain metastases ($n = 12$) expressed as median and interquartile range (IQR). rCBF mean levels were significantly greater ($p < 0.02$) in tumor tissue than in contralateral area for high grade gliomas (Panel A). rCBV mean values were higher in tumor tissue than in contralateral area for

high grade gliomas ($p < 0.01$; Panel B) and metastasis ($p < 0.05$; Panel C). rPSF mean levels were more elevated in tumor tissue than in contralateral area for high grade gliomas ($p < 0.05$; Panel D) and in metastasis ($p < 0.001$; Panel E). The boundaries of the box represent the 25th–75th quartile. The line within the box indicates the median. The whiskers above and below the box correspond to the highest and lowest values, excluding outliers

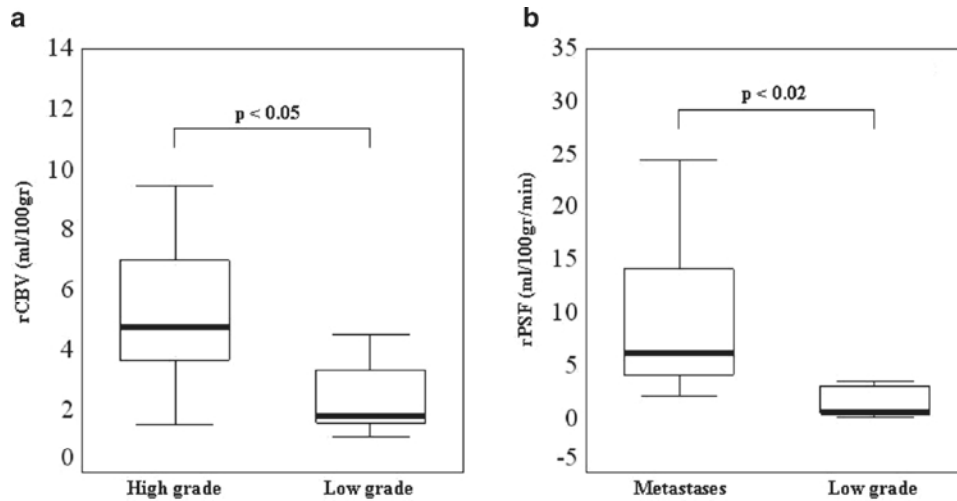


Fig. 3 Regional cerebral blood volume (rCBV) and permeability surface flow (rPSF) in neoplastic tissue from 28 patients with solitary intra-axial brain tumor (high grade gliomas = 17; low grade gliomas = 7; brain metastases = 12) expressed as median and interquartile range (IQR). Tumor tissue rCBV mean values were higher ($p < 0.05$) in high grade

than in low grade gliomas (Panel A). Tumor tissue rPSF mean levels were greater ($p < 0.02$) in metastases than in low grade gliomas (Panel B). The boundaries of the box represent the 25th–75th quartile. The line within the box indicates the median. The whiskers above and below the box correspond to the highest and lowest values, excluding outliers

CTP Parameters in Neoplastic Tissue Among the Different Tumor Subtypes

rCBF mean levels did not statistically differ among the three tumor subtypes analyzed. In contrast, as shown in Fig. 3, while tumor tissue rCBV mean levels were significantly higher in high-grade than in low-grade gliomas ($p < 0.05$), tumor tissue rPSF mean values were greater in metastases than in low-grade gliomas ($p < 0.02$). There was no additional statistical difference in tumor tissue rCBV and rPSF mean values between high-grade gliomas and metastases; in addition, there was no statistical difference in tumor tissue rMTT mean levels among the three tumor subtypes evaluated.

Discussion

It is generally assumed that tumor angiogenesis is related to the biological aggressiveness of intracranial neoplasms (2, 9). PWI is currently considered the most reliable imaging method in providing an accurate assessment of brain tumor microcirculation, as there is a strong correlation between tumor angiogenesis and an elevation in CBV and microvascular permeability (2, 9). However, the use of PWI technology is hampered by its limited availability, long scan-time, cost and patient tolerance. Thus, the identification of a faster and more easily accessible imaging modality for the recognition of perfusion changes associated with brain tumors would

be helpful. Recently, CTP has been proposed as an improved method for the detection of perfusion abnormalities associated with high-grade gliomas (4) and isolated brain metastasis (10), as well as in the discrimination between high-grade and low-grade gliomas (3, 5) and between recurrent tumor and radionecrosis (6). In this study we tested the multi-parametric CTP mapping in the determination of tumor grading in various neoplastic brain lesions. According to previous studies (3–5), high-grade gliomas had increased intralesional levels of rCBF, rCBV and rPSF compared to contralateral normal appearing brain tissue, whereas no difference was observed between tumor tissue and contralateral non-injured area in low-grade gliomas; for rMTT levels, no difference was observed in all neoplastic subtypes explored. In addition, rCBV levels obtained from the solid portion of the tumor were more elevated in high-grade than in low-grade gliomas. These findings confirm that CTP is a powerful tool in establishing tumor grade in brain neoplasms since it can reliably recognize perfusion alterations promoted by tumor angiogenesis. On the other hand, here we also show that intralesional rCBV and rPSF values were greater than those measured in the contralateral non-damaged tissue in brain metastases. Interestingly, tumor tissue rPSF levels, but not rCBV values, were more pronounced in metastases than in low-grade gliomas. These data were partially in agreement with a prior preliminary investigation (10) and suggest that, compared to low-grade gliomas, high-grade gliomas were characterized by an increase in rCBV levels, whereas metastases were marked by an elevation in rPSF values. Overall, our results indicate that increased vascularity and microvascular permeability, which are both consistent with

tumor angiogenesis, seem to be selectively restricted to high-grade brain tumors and brain metastases. Moreover, whereas a vascular proliferation may be associated with high-grade gliomas, in metastases a vascular leakage may predominate. Thus, rCBV and rPSF levels could serve to distinguish high-grade gliomas and metastases from low-grade gliomas, whereas rCBF values could be utilized to differentiate between high-grade gliomas and brain metastasis. Further studies with large numbers of patients are needed to explore the effectiveness of the multi-parametric analysis offered by dynamic CTP scanning in differential diagnosis of solitary intra-axial brain tumors.

Conflict of interest statement We declare that we have no conflict of interest.

References

1. Cenic A, Nabavi DG, Craen RA, Gelb AW, Lee T-Y (2000) A CT method to measure hemodynamics in brain tumors: validation and application of cerebral blood flow maps. *AJNR Am J Neuroradiol* 21:462–470
2. Cha S (2006) Update on brain tumor imaging: from anatomy to physiology. *AJNR Am J Neuroradiol* 27:475–487
3. Ding B, Ling HW, Chen KM, Jiang H, Zhu YB (2006) Comparison of cerebral blood volume and permeability in preoperative grading of intracranial glioma using CT perfusion imaging. *Neuroradiology* 48:773–781
4. Eastwood JD, Provenzale JM (2003) Cerebral blood flow, blood volume, and vascular permeability of cerebral glioma assessed with dynamic CT perfusion imaging. *Neuroradiology* 45:373–376
5. Ellika SK, Jain R, Patel SC, Scarpace L, Schultz LR, Rock JP, Mikkelsen T (2007) Role of perfusion CT in glioma grading and comparison with conventional MR imaging features. *AJNR Am J Neuroradiol* 28:1981–1987
6. Jain R, Scarpace L, Ellika S, Schultz LR, Rock JP, Rosenblum ML, Patel SC, Lee TY, Mikkelsen T (2007) First-pass perfusion computed tomography: initial experience in differentiating recurrent brain tumors from radiation effects and radiation necrosis. *Neurosurgery* 61:778–786
7. Lee R, Cheung RTF, Hung KN, Au-Yeung KM, Leong LLY, Chan FL, Lee TY (2004) Use of CT perfusion to differentiate between brain tumor and cerebral infarction. *Cerebrovasc Dis* 18:77–83
8. Mor V, Laliberte L, Morris JN, Wiemann N (1984) Karnofsky performance status scale. An examination of its reliability and validity in a research setting. *Cancer* 53:2002–2007
9. Provenzale JM, Mukundan S, Barboriak DP (2006) Diffusion-weighted and perfusion MR imaging for brain tumor characterization and assessment of treatment response. *Radiology* 239:632–649
10. Roberts HC, Roberts TPL, Lee T-Y, Dillon WP (2002) Dynamic, contrast-enhanced CT of human brain tumors: quantitative assessment of blood volume, blood flow, and microvascular permeability: report of two cases. *AJNR Am J Neuroradiol* 23:828–832
11. Wintermark M, Essay M, Barber E, Bodily K, Dillon WP, Eastwood JD, Glenn CT, Gradin CB, Pederast S, Susie JF, Maria T, Anarchic G, Camille JM, Doused V, Yonas H (2005) Comparative overview of brain perfusion imaging techniques. *Stroke* 36:e83–e99
12. Young RJ, Knopp EA (2006) Brain MRI: tumor evaluation. *J Magn Reson Imaging* 24:709–724

Part VIII
Treatment

Neuromodulation with Pleiotropic and Multimodal Drugs – Future Approaches to Treatment of Neurological Disorders

Dafin F. Muresanu

Abstract Neurologists are confronted with an ever-growing amount of new information regarding the intimate processes taking place in both normal and pathological brains. Concepts like neuroprotection, neurotrophicity, or anoikis and their clinical utility may be of dazzling complexity. This paper briefly reviews some of the mechanisms involved in the pathogenesis of neurological diseases and current therapies. Since it is becoming more and more clear that using neuroprotective molecule with only one mechanism of action in disease treatment is a utopist idea, the research and use of multimodal drugs should be encouraged.

It is not easy to find good therapeutic approaches to neurological disorders, especially if we do not have a deep understanding of all the basic endogenous biological processes, pathophysiological processes, and the links between them.

Basic Endogenous Biological Processes

Neurotrophicity, neuroprotection, neuroplasticity and neurogenesis are the most important biological processes that act together under genetic control to generate endogenous defense activity (EDA) which attempts to counteract pathophysiological processes (Table 1).

Neurotrophicity is a continuous process of cells to regulate gene expression in order to maintain the phenotype.

Neuroprotection denotes rescue of all the neuronal, glial and endothelial cell components in the CNS, against all the noxious stimuli or harmful factors. *Neuroplasticity*, on the other hand represents the continual adaptation of neurons to new functional horizons and responsibilities. It is the concept that describes the brain's ability to change in response to environmental stimuli such as learning or injury (1).

Neurogenesis is the process by which new nervous tissue cells (neurons, astrocytes, oligodendrocytes, etc.) are created from stem cells. In a strict sense, neurogenesis refers only to new neuron creation. These fundamental biological processes have no absolute boundaries. They overlap and share common mechanisms.

When studying neuroprotection, we have to distinguish between two different aspects, the so-called absolute and relative mechanisms. The *absolute* aspect refers to all mechanisms that determine the activation of DNA expression followed by protein synthesis induction. The *relative* aspect refers to all mechanisms that finally determine neuroprotective activities with preponderant expression in the membrane, the cytosol, and organelles. The absolute mechanisms are preponderantly controlled by neurotrophic factors and neurotrophic-like molecules while the relative mechanisms mainly utilize ion channel blockers, agonists, and antagonists of certain receptors, scavenger antioxidants, chelators of certain metals, and many others (2,3).

All of these biological mechanisms can be naturally or pharmacologically activated. If we want to fight successfully against pathophysiological processes, we have to pharmacologically enhance the effect of EDA. Sometimes the basic biological processes of EDAs share common mechanisms with pathophysiological processes. For example, excitotoxicity and neurotrophicity together with neuroplasticity have NMDAR activity as their common important driver. Inflammation is an important contributor to neuroregeneration, stimulating neuroplasticity via trophic factors.

Regulation disturbances in each of the four major players of EDA are themselves causes of some pathological conditions. A deficit of neurotrophicity will always increase the susceptibility for a lesion. So far no pathologies have been discovered that arise because of an excess of neurotrophicity or neuroprotection. For neuroplasticity, both up-regulation and down-regulation generates pathologies (down-regulation generates a deficit of recovery while up-regulation generates hundreds of neuropathological plasticities like in neuropathic pain, multiple sclerosis,

D.F. Muresanu (✉)
Department of Neurology, University of Medicine and Pharmacy
"Tuliu Hatieganu" Cluj-Napoca, Romania

Table 1 Endogenous fundamental biological processes and pathophysiological mechanisms

Fundamental biological processes	Pathophysiological mechanisms
Neurotrophicity	Excitotoxicity Free radicals
Neuroprotection	Metabolic dysfunction Inflammation
Neuroplasticity	Apoptosis like processes Protein misfolding
Neurogenesis ↓	↓
Endogenous defense activity	Genetic characteristics of the individual

movement disorders, tinnitus, and more). Regarding neurogenesis, both up-regulation and down-regulation generates pathological conditions (e.g. down-regulation in Alzheimer's disease) (4). Up-regulation of oligodendrogenesis and astrogenesis beyond normal neuron regeneration is responsible for neuroproliferative disorders.

Neuroprotection

Different pathophysiological mechanisms are triggered by different etiologic agents or biological events. Many neurological disorders with different evolutions (acute, chronic and hyper chronic) are generated. Blocking these pathogenic pathways is the aim of neuroprotective treatments.

These pathological cascades contain a limited number of pathophysiological processes (see Table 1) and have many similarities in various CNS diseases. Thus, in stroke there is excitotoxicity, oxidative stress, inflammation, and apoptotic-like processes. In neurodegenerative disorders we have excitotoxicity, inflammation, apoptotic-like processes, and protein misfoldings.

Controlling the common elements of neurodegenerative processes is the key to efficient neuroprotection. There is a relatively new concept on the horizon of neurophysiology known as the *neurovascular unit* (comprising endothelial cells and brain cells and matrix that function together using biochemical signaling) (5). This unit exists everywhere in the brain, in both grey and white matter and its malfunction can explain the occurrence and evolution of several brain diseases such as stroke, vascular dementia, migraine, trauma, multiple sclerosis, or even normal aging. Since the neurovascular unit is unique in the human body, the way cells die here is also unique. The lack of support coming from any component of the unit cells and the matrix causes a particular apoptosis-like phenomenon named anoikis (6).

Pathophysiological Processes

Excitotoxicity

Excitotoxicity is the pathological process by which nerve cells are damaged by excess glutamate and similar substances. NMDA receptor activation is one of the key features of excitotoxicity. Continuous activity of NMDAR is crucial for cell survival and the survival is achieved through regulation of neurotrophicity and neuroplasticity via calcium-controlled proteolytic systems (e.g. calpain system) (7). Physiological patterns of synaptic NMDAR activity actually promote neuronal survival by controlling the minimum calcium influx into the neuron. These very small quantities of calcium activate "high affinity calcium molecules" such as μ calpain which have the physiological roles of conducting proteolytic activity, an important factor in neurotrophicity and neuroplasticity. This process is highly regulated by neurotrophic factors (8).

The key pro-survival pathways involving NMDA receptors include some important aspects. The PI3K (phosphoinositide 3-kinase)–Akt cascade, is strongly activated by NMDARs in many, but not all neuronal types (9,10). Synaptic NMDAR signaling also activates the Ras–ERK1/2 (extra cellular-signal-regulated kinase 1/2) cascade, with pro-survival consequences including CREB, [CRE (cAMP-response element)-binding protein], activation, BAD inactivation, and antagonization of GSK3 β -induced apoptosis (9,11). Synaptic NMDAR-dependent calcium transients trigger a number of transcriptional changes that mediate long-lasting neuroprotection (via CRE-dependent gene expression) (11,12).

When NMDARs are overactivated by glutamate under pathological circumstances (such as stroke or trauma), large quantities of calcium enter the cells and activate "low affinity calcium molecules" such as m-calpain that have non-selective and uncontrolled proteolytic activities that lead to cell death. There are several fundamental mechanisms implicated in NMDAR dependent cell death (13–15). Cleavage of the plasma membrane Na⁺/Ca²⁺ exchanger by the Ca²⁺ dependent protease calpain leads to necrosis. Mitochondrial dysfunction brought about by excessive Ca²⁺ uptake through the uniporter also leads to apoptosis-like processes. Finally, overactivation of the Ca²⁺-dependent nNOS (neuronal nitric oxide synthase) by NMDAR activity has toxic downstream effects (p38 mitogen-activated protein kinase signaling, mitochondrial dysfunction and TRPM (transient receptor potential melastatin channel) activation) leading to apoptosis-like processes.

The next question that we will consider is what are the drivers for neurotrophicity, neuroplasticity or excitotoxicity? The first factor is the magnitude of activation of NMDAR (intensity or duration). Low levels are protective. Ca²⁺ effectors of

survival have considerably lower requirements for Ca^{2+} than the death effectors. Thus the $[\text{Ca}^{2+}]$ threshold for activating pro-survival signaling by PI3K, ERK1/2 and CaMKIV–CREB must be lower than that which triggers toxic levels of calpain activation, mitochondrial uptake or NO production. Certain potential death effectors, such as m-calpain and the mitochondrial uniporter have low Ca^{2+} affinity (16). The second important issue is NMDA receptor location (12,17). Extrasynaptic NMDAR activity promotes inactivation of CREB (by dephosphorylation) and early excitotoxic events such as mitochondrial depolarization concomitantly with inactivation of the ERK1/2 pathway, causing necrosis and apoptosis-like processes. On the other hand, synaptic NMDAR activity promotes activation of CREB and activation of the ERK1/2 pathway. It does not disturb mitochondrial function and offers overall neuroprotective activity and promotes neurotrophicity and neuroplasticity.

Inflammation

The pathological role of inflammation has been recognized in almost all neurological conditions. This well-orchestrated process situated on the borderline between physiology and pathology tends to become highly destructive when prolonged or insufficiently regulated. In normal conditions, however, inflammatory cells and mediators may also have beneficial functions and contribute to tissue repair processes (2).

There is evidence demonstrating that inflammation plays a positive role in neuroprotection and neuroplasticity. The major players in this process are neurotrophic factors. The neurotrophic factors produced by activated immune cells seem to participate in neuronal protection. They either bind directly to their receptors or act by modulating the local immune response (18–21). Even a very potent pro-inflammatory molecule when activates one receptor (e.g. like TNF- α) has a neuroprotective and neurotrophic effect (via trophic factors) when acting on a second receptor (22).

The very low permeability of the blood–brain barrier (BBB) extends to the immune cells and molecules. Usually, the resident cells in the central nervous system (CNS) (particularly astrocytes and microglia) are able to regulate immune reactivity within the CNS. Other alien immune entities enter the CNS only through highly regulated processes mediated by adhesion molecules, chemokines, cytokines and matrix metalloproteinases (23–27).

Apoptosis and Apoptosis Like Processes

Apoptosis is a positive process maintaining the number and the quality of cells. If a cell has a DNA lesion, it activates the p53 gene. Then the cell will either halt in the G1 phase of its

cycle (by bcl-2 activation), or repair its DNA and recommence the division. Alternatively, the altered DNA repair may cause the activation of “bax” leading to apoptotic death. If apoptosis is not effective, then a malignant clone formation will occur.

From the above highlights regarding the links between pathophysiological processes and endogenous defense activity, we can draw the following conclusions. 1) *NMDAR activity* might play a positive role during physiological activation or a deleterious role during pathological processes (stroke, trauma, neurodegenerative disorders) by facilitating excitotoxicity. 2) *Inflammation* is generally a negative phenomenon, but it can positively control neuroprotection and neuroplasticity via neurotrophic factors. 3) *Apoptosis* is a positive process whereas apoptotic-like processes are always negative. Apoptotic-like processes have to be endogenously and therapeutically controlled. *Therefore, the best approach for clinical neuroprotection is pleiotropic drug administration that inhibits excitotoxicity (via extrasynaptic NMDARs), decreases the “bad” effects of inflammation while increasing the “good” effects of inflammation, and prevents apoptotic-like processes.*

The EDA integrates all basic biological processes using complex genetic programs. These programs are able to switch from neuroprotective patterns to neuroplastic patterns using the same molecules by up and downregulation. There are hundreds of molecules (transcription factor, kinase network molecules, and neurotransmitter receptors, growth factors/receptors, growth-associated cytoskeletal molecules, synapse-related molecules, and adhesion molecules) to be regulated by immediate early genes and/or late activated genes. A large part of this regulation is managed by neurotrophic factors.

The search for clinical neuroprotection is complicated for several reasons. First, we are using translational synthetic molecules (which are not used by EDA) with only one mechanism of action against complex process with many mechanisms inside cascades. This leaves very few chances to create pharmacological neuroprotection. The design of clinical studies of neuroprotection must be more rigorous. Finally, despite a lack of consistent clinical results describing neuroprotection with simple mechanism molecules, there are several small trials that have had success (including erythropoietin, cerebrolysin, cytidicholine) (26). All of these successful molecules have a common pattern of action: they have *pleiotropic mechanisms* and are therefore able to control multiple processes in a biological cascade. Based on this pathophysiological assumption and these clinical facts, the best way to promote pharmacological neuroprotection is *pleiotropic drug* administration that can simulate mechanisms such as those in EDA.

Currently, there are no known molecules that simultaneously promote neuroprotection and an ability to switch to neuroplasticity at the same time except neurotrophic factors (Fig. 1). The capacity to switch to plasticity is crucial when considering the clinical effect on the patient. Drugs with this ability are called *multimodal drugs*. A multimodal drug is a

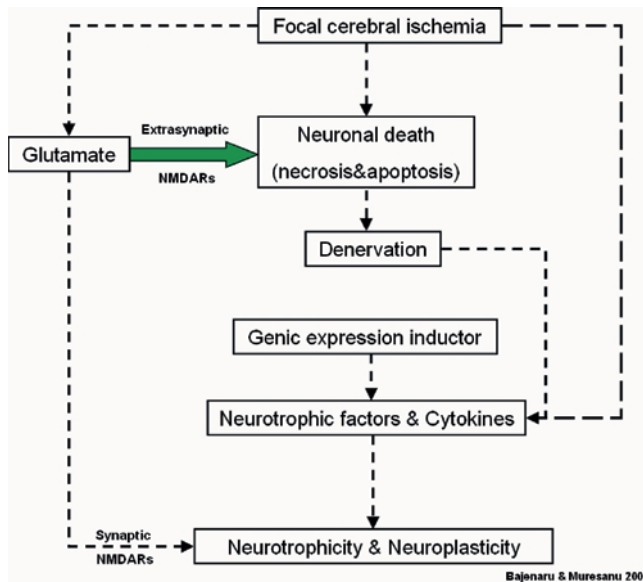


Fig. 1 The double game of glutamate makes it a potent and indispensable factor for neurotrophicity and neuroplasticity processes

drug that is able to regulate at the same time two or more basic biological processes from EDA.

A multimodal drug available for clinical use, Cerebrolysin, is based on active fragments of different neurotrophic factors (26). Taking stroke as an example (see Fig. 1) we see that glutamate is deleterious in the first minutes of exposure and for several hours after the event. However, after several hours, glutamate becomes the key player in controlling neurorecovery. Therefore, multimodal drugs are able to control the switch inside the continuous process of neuroprotection and neuroplasticity.

Conflict of interest statement We declare that we have no conflict of interest.

References

- Kalivas PW, Volkow ND (2005) The neural basis of addiction: a pathology of motivation and choice. *Am J Psychiatry* 162:1403–1413
- Muresanu FD (2007) Neuroprotection and neuroplasticity – a holistic approach and future perspectives. *J Neurol Sci* 257:38–43
- Muresanu FD (2003) Neurotrophic factors. Ed Libripres, Bucharest
- Teter B, Ashford JW (2002) Neuroplasticity in Alzheimer's disease. *J Neurosci Res*. Nov 1; 70(3):402–437
- Hawkins BT, Davis TP (2005) The blood-brain barrier/neurovascular unit in health and disease. *Pharmacol Rev* 57:173–185
- Frisch SM, Sreaton RA (2001) Anoikis mechanisms. *Curr Opin Cell Biol* 13(5):555–562
- Wu HY, Yuen EY, Lu YF, Matsushita M, Matsui H, Yan Z, Tomizawa K (2005) Regulation of N-Methyl-D-aspartate receptors by calpain in cortical neurons. *J Biol Chem* 280(22):21588–21593
- Hutter-Paier B, Grygar E, Fruhwirth M, Temmel I, Windisch M (1998) Further evidence that Cerebrolysin protects cortical neurons from neurodegeneration in vitro. *J Neural Transm Suppl* 53:363–372
- Hetman M, Kharebava G (2006) Survival signaling pathways activated by NMDA receptors. *Curr Top Med Chem* 6:787–799
- Brunet A, Datta SR, Greenberg (2001) M.E. Transcription-dependent and -independent control of neuronal survival by the PI3K-Akt signaling pathway. *Curr Opin Neurobiol* 11:297–305
- Hardingham GE, Arnold FJ, Bading H (2001) A calcium microdomain near NMDA receptors: on switch for ERK-dependent synapse-to-nucleus communication. *Nat Neurosci* 4:565–566
- Hardingham GE, Fukunaga Y, Bading H (2002) Extrasynaptic NMDARs oppose synaptic NMDARs by triggering CREB shut-off and cell death pathways. *Nat Neurosci* 5:405–414
- Arundine M, Tymianski M (2004) Molecular mechanisms of glutamate-dependent neurodegeneration in ischemia and traumatic brain injury. *Cell Mol Life Sci* 61:657–668
- Bano D, Young KW, Guerin CJ, Lefevre R, Rothwell NJ, Naldini L, Rizzuto R, Carafoli E, Nicotera P (2005) Calpain cleavage of the plasma membrane Na⁺/Ca²⁺ exchanger in excitotoxicity. *Cell* 120:275–285
- Stout AK, Raphael HM, Kanterewicz BI, Klann E, Reynolds IJ (1998) Glutamate-induced neuron death requires mitochondrial calcium uptake. *Nat Neurosci* 1:366–373
- Soriano FX, Papadia S, Hofmann F, Hardingham NR, Bading H, Hardingham GE (2006) Preconditioning doses of nmda promote neuroprotection by enhancing neuronal excitability. *J Neurosci* 26:4509–4518
- Ivanov A, Pellegrino C, Rama S, Dumalska I, Salyha Y, Ben-Ari Y, Medina I (2006) Opposing role of synaptic and extrasynaptic NMDA receptors in regulation of the extracellular signal-regulated kinases (ERK) activity in cultured rat hippocampal neurons. *J Physiol* 572:789–798
- Iseda T, Nishio T, Kawaguchi S, Yamamoto M, Kawasaki T, Wakisaka S (2004) Spontaneous regeneration of the corticospinal tract after transection in young rats: a key role of reactive astrocytes in making favourable and unfavourable conditions for regeneration. *Neuroscience* 126:365–374
- Kotter MR, Setzu A, Sim FJ, Van Rooi-jen N, Franklin RJM (2001) Macrophage depletion impairs oligodendrocyte remyelination following lysocleithin-induced demyelination. *Glia* 35:204–212
- Masson JL, Jones JJ, Taniike M, Morell P, Suzuki K, Matsushima GK (2000) Mature oligodendrocytes apoptosis precedes IGF-I production: an oligodendrocyte progenitor accumulation and differentiation during demyelination/remyelination. *J Neurosci Res* 61:251–262
- Arnett HA, Wang Y, Matsushima GK, Suzuki K, Ting JPY (2003) Functional genomic analysis of remyelination reveals importance of inflammation in oligodendrocytes regeneration. *J Neurosci* 23:9824–9832
- Marchetti L, Klein M, Schlett K, Pfizenmaier K, Eisel ULM (2004) Tumor necrosis factor (TNF)-mediated neuroprotection against glutamate-induced excitotoxicity is enhanced by N-methyl-D-aspartate receptor activation. *J Biol Chem* 279(31):32869–32881
- Becher B, Antel JP (1996) Comparison of phenotypic and functional properties of immediately ex vivo and cultured human adult microglia. *Glia* 18:1–10
- Windhangen A, Newcombe J, Dan-gond F, Strand C, Woodroffe MNB, Cuzner ML et al (1995) Expression of costimulatory molecules B7-1 (CD80), B7-2 (CD86), and interleukin 12 cytokine in multiple sclerosis lesions. *J Exp Med* 182:1985–1996
- Pachter JS, de Vries HE, Fabry Z (2003) The blood-brain barrier and its role in immune privilege in the central nervous system. *J Neuropathol Exp Neurol* 62:593–604
- Labiche LA, Grotta JC (2004) Clinical trials for cytoprotection in Stroke. *NeuroRx* 1:46–70
- Sharma HS, Ali SF (2008) Acute administration of 3,4-methylenedioxymethamphetamine induces profound hyperthermia, blood-brain barrier disruption, brain edema formation, and cell injury. *Ann NY Acad Sci* 1139:242–258

Selected Combination of Neurotrophins Potentiate Neuroprotection and Functional Recovery Following Spinal Cord Injury in the Rat

Hari Shanker Sharma

Abstract The possibility that a combination of neurotrophins induces long-lasting neuroprotection of the cord following spinal cord injury (SCI) was examined in a rat model. The SCI was performed by making a unilateral incision into the right dorsal horn of the T10–11 segments and the animals were allowed to survive 5 h after trauma. Different combination of neurotrophins, i.e., BDNF in combination with GDNF, NT-3, or NGF was applied topically over the traumatized spinal cord and motor dysfunction, blood-spinal cord barrier (BSCB) breakdown, edema formation, and cell injury were examined. Topical application of BDNF in combination with GDNF and NGF 30 min (but not 60 or 90 min) at high concentrations (0.5 μg each) after SCI significantly improved motor function and reduced BSCB breakdown, edema formation, and cell injury at 5 h. However, concurrent application of BDNF, IGF-1, and GDNF (but not with NT-3 or NGF) even 60 or 90 min after trauma induced a significant reduction in motor dysfunction and spinal cord pathology. These observations suggest that a combination of neurotrophins may have added therapeutic value in the treatment of SCI, not reported earlier.

Keywords Spinal cord injury • BDNF • IGF-1 • GDNF • blood–spinal cord barrier • edema • motor function • spinal cord pathology

Introduction

Spinal cord injury (SCI) is a serious clinical problem that induces lifelong disabilities for the victims and places a huge burden on society (see (5,6,11)). Although our knowledge

on the basic mechanisms of the pathophysiology of SCI has expanded tremendously in the last decades (2,3,5,6), suitable and effective therapeutic approaches to enhance neuroprotection and/or neurorepair are still not worked out. Thus, further studies in SCI are needed to enhance neurorepair mechanisms in order to improve the quality of life of trauma victims.

Experimental studies in SCI suggest that neurotrophins could play important roles in the repair mechanisms of the spinal cord following injury (2,3,5–10). Thus, dysregulation of neurotrophin receptors and/or altered expression of neurotrophins in spinal cord motoneurons following injury are quite common (see (12) for review). This indicates that therapeutic intervention using neurotrophic factors may influence recovery following SCI by enhancing neuroregeneration or neurorepair processes.

One of the important goals for the treatment of SCI with neurotrophins is to thwart the propagation of spinal cord pathology to the uninjured portion of the cord and to rescue damaged nerve cells and axons in order to improve functional outcome (10–15). Another therapeutic aim of SCI is to find a suitable combination of neurotrophins that can help to achieve neuroprotection and neurorepair even when applied at longer time intervals after the initial injury (7–10,12–15).

Keeping this in mind, our laboratory is engaged in exploring the possibility of enhancing functional recovery and enhancing neuroprotection using several neurotrophic factors, either alone or in combination, in experimental models of SCI (7–15). Considering modern day patient care, the time delay from the accident to the initiation of treatment can easily be reduced from 180 to 90 min (see (15)). Thus, any suitable combination of neurotrophins that can delay the propagation of cord pathology within 90 min after trauma will certainly be an added value to the current therapeutic strategies used in SCI.

This investigation is aimed at exploring the possibility of using a select combination of neurotrophins to improve functional outcome and reduce spinal cord edema formation and cell injury when applied 60 to 90 min after SCI in our rat model.

H.S. Sharma (✉)
Laboratory of Cerebrovascular Research, Department of Surgical Sciences, Anaesthesiology and Intensive Care Medicine, University Hospital, Frödingsgatan 12:28, Uppsala, SE-75421, Sweden
e-mail: Sharma@surgsci.uu.se

Materials and Methods

Animals

Experiments were carried out on Male Sprague Dawley rats (250 to 300 g) housed at controlled room temperature ($21 \pm 1^\circ\text{C}$) on a 12 h light and 12 h dark schedule. Food and tap water were supplied ad libitum before the experiments.

Spinal Cord Injury

Under equithesin anesthesia (0.3 mL/100 g, i.p.) a one segment laminectomy was made at the T10-11 segments. The SCI was inflicted using a longitudinal incision (4 mm long and 1.5 mm deep) on the right dorsal horn using a sterile scalpel blade (see Fig. 1). The deepest part of the incision was limited to Rexed's laminae VII or VIII (16). All experiments were carried out according to the National Institute of Health Guidelines for care of experimental animals and approved by Local Institutional Ethics Committee. Sham operated animals without SCI served as controls.

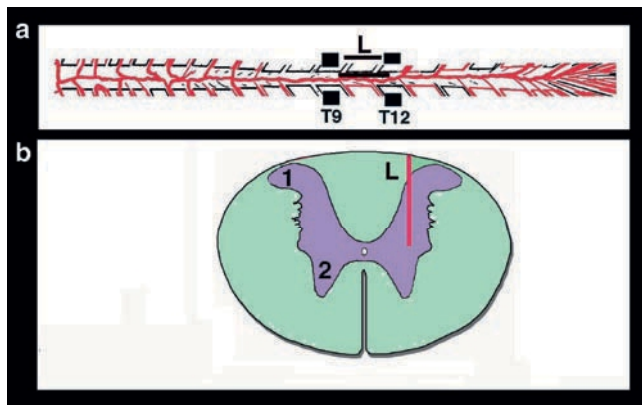


Fig. 1 The new model of rat spinal cord injury (SCI) and tissue sampling (see (11)). A focal incision to the right dorsal horn of the T10-11 segments was used to inflict SCI. (a) Longitudinal view of the lesion within the spinal cord. The focal incision is limited to the right dorsal horn of the T10-11 segment. Tissue pieces for morphological or biochemical studies are taken from the adjacent T9 (rostral) and T12 (caudal) segments. (b) Cross section of the spinal cord showing the extent of the lesion within the dorsal horn. The deepest part of the lesion is mainly present around Rexed's laminae VII or VIII. The white matter is largely intact. For high resolution light microscopy, tissue pieces were embedded in Epon, and approximately $1 \mu\text{m}$ thick whole spinal cord sections were cut and stained with toluidine blue. These sections were examined with light microscopy and photographed (see b). For immunohistochemistry or morphology, small areas from either the contralateral dorsal horn (1) or ventral horn (2) were selected to examine neuroprotection (modified after (11)). Bar: a ≈ 5 mm, b ≈ 2 mm (modified after 17)

Neurotrophin Treatment

Separate groups of animals were treated with various combination of neurotrophins, e.g., BDNF with GDNF, NGF, NT-3 or IGF-1, or GDNF. Neurotrophins were applied 30 to 90 min after SCI and the animals were allowed to survive 5 h after injury. The total dose of the neurotrophins was adjusted (0.5 μg each) in 30 μL (0.5 μg of BDNF + 0.5 μg of GDNF, or IGF-1, NGF or NT-3) and applied topically over the injured spinal cord with in 10 s (see (7-11)). The control group received 30 μL of 0.9% saline instead of neurotrophins (11-15).

Motor Functions

Tarlov scale and capacity angle were monitored in spinal cord injured animals in order to assess the functional outcome in neurotrophin- or saline-treated animals according to standard procedures (see (12-14)).

Blood-Spinal Cord Barrier Permeability

The blood-spinal cord barrier (BSCB) permeability to Evans blue albumin and radioiodine was examined in perifocal spinal cord segments (T9 and T12) according to standard protocol (see Fig. 1, Ref. 4,17).

Spinal Cord Edema

Spinal cord edema in T9 and T12 segments was assessed by measuring water content (1,16,18).

Spinal Cord Pathology

The spinal cord pathology in T9 and T12 segments (Fig. 1) was examined using Nissl or Hematoxylin and Eosin staining using standard histological techniques as described previously (17,18).

Statistical Evaluation of Data

ANOVA followed by Dunnet's test for multiple group comparison from one control was used to evaluate statistical

significance between control, injured, and neurotrophin treated groups. A p -value <0.05 was considered significant.

Results

Effects of Neurotrophins on Functional Outcome after SCI

Functional outcome was markedly improved when BDNF in combination with NT-3 or NGF (0.5 μ g each) was applied 30 min after SCI, as measured by the Tarlov scale or capacity angle test (Table 1). This effect was markedly absent when these neurotrophins were applied either 60 or 90 min after SCI. Interestingly, even a triple combination of these neurotrophins (BDNF+NT-3+NGF, 0.5 μ g each) did not induce significant improvement in motor function beyond 60 min SCI (results not shown). On the other hand, when BDNF was combined with IGF-1 and GDNF (0.5 μ g each), this triple combination was able to improve motor function even after 90 min of SCI (Table 1).

Effects of Neurotrophins on BSCB Permeability in SCI

Marked reduction in BSCB permeability to Evans blue and radioiodine was noted in traumatized animals that received BDNF in combination with NT-3 or NGF 30 min after SCI (Table 1). No apparent reduction in BSCB permeability was seen even when these neurotrophins were applied in a combination (BDNF+NT-3+NGF, 0.5 μ g each) beyond 60 min SCI (results not shown). However, a triple combination of BDNF with IGF-1 and GDNF (0.5 μ g each) significantly reduced BSCB leakage even after 90 min of SCI (Table 1).

Effects of Neurotrophins on Edema Formation in SCI

A combination of BDNF with NT-3 and/or NGF effectively reduced edema formation if applied at 30 min but not after 60 or 90 min SCI (Table 1). In contrast, a combination of BDNF with IGF-1 and GDNF remarkably reduced spinal cord edema formation when applied even 60 to 90 min after injury (Table 1).

Effects of Neurotrophins on Spinal Cord Pathology in SCI

The cell changes in the spinal cord were markedly reduced by the triple combination of BDNF, IGF-1, and GDNF treatment when these neurotrophins were administered 60 to 90 min after SCI (Table 1, Fig. 2). On the other hand, a combination of BDNF with NT-3 and/or NGF did not reduce cell changes in the spinal cord if applied 60 min after SCI (Table 1).

Discussion

The results presented here are the first to demonstrate that a select combination of triple neurotrophins enhance function outcome and spinal cord pathology if applied topically 30 to 90 min after SCI. This effect appears to be very specific to the specific combination of neurotrophins used and the time of their application at different post-trauma periods. Thus, a combination of BDNF with NT-3 and NGF remarkably reduced functional deficits and spinal cord pathology if administered 30 min after SCI. On the other hand, this combination of neurotrophins remained ineffective if applied 60 to 90 min after injury. This indicates that SCI induces a time-related deficit of specific neurotrophins that are normally required to maintain spinal cord functions.

Our observations further show that a triple combination of neurotrophins (BDNF, NT-3, and NGF) 30 min after SCI is far superior in inducing neuroprotection than a combination of the two of the neurotrophins (BDNF and NT-3 or BDNF and NGF). This suggests that exogenous supplements with the right kind of growth factors at the right time are needed to attenuate spinal cord pathology and to improve functional outcome following trauma (see 5,6,19).

We applied a dose of 0.5 μ g of each neurotrophin to the traumatized spinal cord in this investigation. However, there are reasons to believe that a specific combination of neurotrophins rather than the total amount of growth factors is responsible for the observed neuroprotection following the multiple combination of neurotrophins in SCI (2,6). This idea is further supported by the fact that no suitable neuroprotective effects on functional recovery or spinal cord pathology is seen in our experiments when the same amount of growth factors, i.e., BDNF, NT-3 and NGF (0.5 μ g each) were applied 60 or 90 min after injury. Thus, exogenous application of right kind of neurotrophins at different time intervals after SCI is needed to achieve neuroprotection and to improve functional outcome.

In SCI, all of the components of the spinal cord, i.e., neurons, glial, and endothelial cells are damaged progressively

Table 1 Effect of neurotrophins on functional outcome and spinal cord pathology following 5 h trauma. The spinal cord injury (SCI) was made by an incision into the right dorsal horn of the T10-11 segments and the animals were allowed to survive 5 h after injury

Type of experiment	Functional outcome		BSCB permeability		¹²⁵ Iodine %		Spinal cord edema		Spinal cord cell changes	
	Tarlov scale	Capacity Angle°	EBA mg%	T9	T12	T9	T12	Water content %	T9	T12
Normal control group (n = 6)										
Control	6	60	0.23 ± 0.05	0.23 ± 0.04	0.28 ± 0.06	0.30 ± 0.08	65.63 ± 0.21	65.68 ± 0.13	Nil	Nil
Untreated spinal cord injury 5 h (n = 8)										
5 h SCI	1.5 ± 0.05**	23 ± 3**	1.86 ± 0.23**	1.92 ± 0.11**	2.05 ± 0.13**	2.18 ± 0.09**	68.45 ± 0.42**	68.78 ± 0.21**	28 ± 2	34 ± 6
Topical application + 30 min after SCI (0.5 µg each; n = 6)										
BDNF + NT-3	3 ± 1**	34 ± 4**	0.80 ± 0.08**	0.78 ± 0.11**	0.90 ± 0.12**	0.92 ± 0.15**	66.34 ± 0.21**	66.56 ± 0.10**	18 ± 4**	22 ± 6**
BDNF + NT-3 + NGF	4 ± 2**	42 ± 3**	0.68 ± 0.12**	0.70 ± 0.09**	0.82 ± 0.08**	0.78 ± 0.07**	66.04 ± 0.08**	66.13 ± 0.09**	14 ± 3**	18 ± 2**
Topical application + 60 min after SCI (0.5 µg each; n = 6)										
BDNF + NT-3										
+NGF	2 ± 1**	24 ± 4**	1.60 ± 0.08**	1.68 ± 0.12**	1.98 ± 0.21**	2.05 ± 0.22**	67.87 ± 0.10**	68.08 ± 0.18**	26 ± 6	30 ± 6
BDNF + IGF-1	4 ± 1**	42 ± 4**	0.70 ± 0.08**	0.74 ± 0.12**	0.89 ± 0.08**	0.94 ± 0.11**	66.48 ± 0.21**	66.56 ± 0.23**	20 ± 5#	24 ± 4#
+GDNF										
Topical application + 90 min after SCI (0.5 µg each; n = 6)										
BDNF + IGF-1	3 ± 1**	38 ± 4**	0.76 ± 0.10**	0.83 ± 0.09**	0.86 ± 0.08**	0.90 ± 0.12**	66.58 ± 0.08**	66.78 ± 0.14**	20 ± 4#	22 ± 3#

Values are mean ± SD, ** = P < 0.05, # = P < 0.01, from SCI, ANOVA followed by Dunnet's test for multiple group comparison.

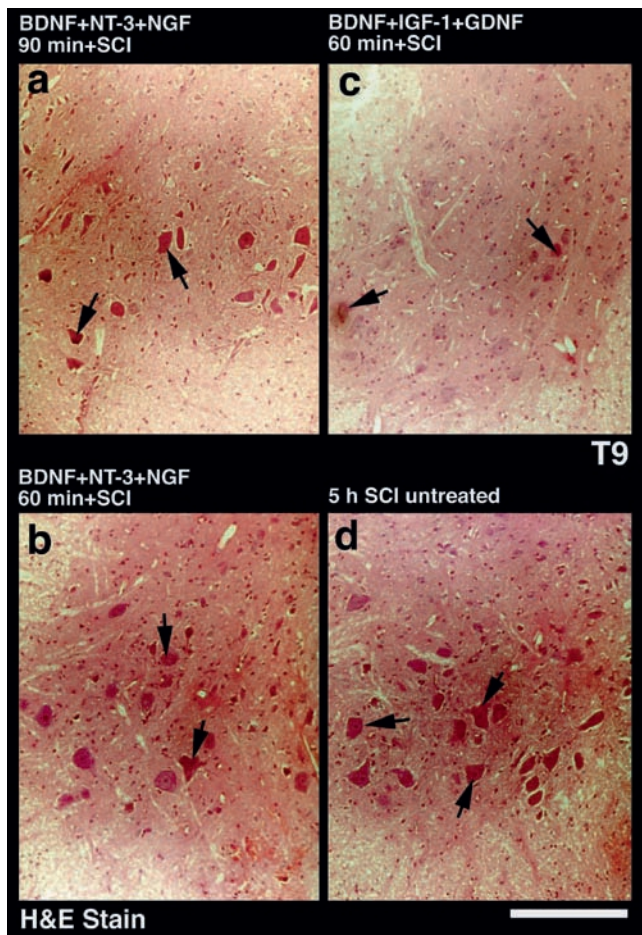


Fig. 2 Neuroprotective effects of combinations of neurotrophins 5 h after SCI. A combination of three neurotrophins, BDNF, IGF-1, and GDNF, almost completely attenuated nerve cell damage in the spinal cord when administered topically over the injured cord even 60 min after trauma (c). In contrast, other combinations of neurotrophins, i.e., BDNF, NT-3, and NGF, were not as effective in reducing nerve cell damage when applied either 60 (b) or 90 min (a) after injury as compared to the untreated injured rat (d). Several damaged nerve cells (arrows) are seen in the spinal cord following trauma in the untreated rat (d). Bar: 25 μ m

with time (11,12). Thus, maintenance of neuronal, glial, and endothelial cell functions after SCI is needed to achieve neuroprotection and improve functional outcome (see (14,15)). It appears that during the early phase of SCI, treatment with neurotrophins, (BDNF, NT-3 and NGF) is sufficient to thwart spinal cord pathology. However, later damage to glial cell function along with neuronal damage worsens the outcome of SCI induced cord pathology. Thus, a combination of neurotrophins acting on neuronal and glial cells is needed to improve spinal cord function during the later phases of SCI.

Keeping these views in consideration, we used a combination of BDNF with IGF-1 and GDNF and applied then at 60 to 90 min after SCI. Our results show that a combination

of neurotrophins acting on nerve cells (BDNF) and glial cells (GDNF), together with IGF-1 is effective in attenuating spinal cord pathology and improving functional outcome during later phases of SCI. These observations are in line with the idea that exogenous supplementation of neurotrophins supporting neural, glial, and endothelial cell functions after SCI could effectively induce neuroprotection and enhance functional recovery.

The possible mechanisms of neurotrophins-induced neuroprotection are not well understood. However, there are reasons to believe that neurotrophins may neutralize several neurotoxins released from neurons, glia, and endothelial cells following injury, which could adversely affect spinal cord functions (2,5,6,11,19). Thus, a suitable combination of neurotrophins that improves neural, glial, and endothelial cell functions will certainly improve the spinal cord cell and tissue structures and thus attenuate functional deficits. Obviously, a reduction in the breakdown of the BSCB by neurotrophins is in line with this idea (4). A reduction in BSCB permeability to proteins will attenuate vasogenic edema formation and thus reduce cell injury (16–18).

Further studies in our laboratory are in progress to identify the expression of various neurotrophin receptors in spinal cord injury at different time intervals after trauma that could shed additional light on the possible mechanisms of neurotrophins-induced neuroprotection in SCI.

Conflict of interest statement HSS has no conflict of interest with any organizations mentioned below.

Acknowledgements This investigation was supported by grants from Swedish Medical Research Council (2710 HSS), Stockholm, Sweden; Göran Gustafsson Foundation, Stockholm, Sweden; National Brain Research Centre, Sweden; Alexander von Humboldt Foundation, Bonn, Germany; Astra-Zeneca, Mölndal, Sweden; Acure Pharma, Sweden; IPSEN-Medical, Paris, France; The University Grants Commission, New Delhi, India; The Indian Medical Research Council, New Delhi, India; Ministry of Science & Technology, Govt. of India, New Delhi. The Secretarial help of Aruna Sharma and the Graphic assistance of Suraj Sharma are highly appreciated with thanks. The author (HSS) has no conflict of interest with any Granting authorities mentioned above.

References

1. Elliott KAC, Jasper H (1949) Measurement of experimentally induced brain swelling and shrinkage. *Am J Physiol* 157:122–129
2. Gibbons A, Wreford N, Pankhurst J, Bailey K (2005) Continuous supply of the neurotrophins BDNF and NT-3 improve chick motor neuron survival in vivo. *Int J Dev Neurosci* 23(4):389–396
3. Kaplan DR, Miller FD (2000) Neurotrophin signal transduction in the nervous system. *Curr Opin Neurobiol* 10:381–391
4. Rapoport SI (1976) Blood–brain barrier in physiology and medicine. Raven, New York, NY, pp 1–316

5. Schwab ME, Bartholdi D (1996) Degeneration and regeneration of axons in the lesioned spinal cord. *Physiol Rev* 76(2):319–370
6. Schwab JM, Breghtel K, Mueller CA, Failli V, Kaps HP, Tuli SK, Schluesener HJ (2006) Experimental strategies to promote spinal cord regeneration – an integrative perspective. *Prog Neurobiol* Feb 78(2):91–116. Review
7. Sharma HS (2005) Neuroprotective effects of neurotrophins and melanocortins in spinal cord injury: an experimental study in the rat using pharmacological and morphological approaches. *Ann N Y Acad Sci* Aug 1053:407–421
8. Sharma HS (2003) Neurotrophic factors attenuate microvascular permeability disturbances and axonal injury following trauma to the rat spinal cord. *Acta Neurochir Suppl* 86:383–388
9. Sharma HS (2005) Pathophysiology of blood–spinal cord barrier in traumatic injury and repair. *Curr Pharm Des* 11(11):1353–1389. Review
10. Sharma HS (2005) Neuroprotective effects of neurotrophins and melanocortins in spinal cord injury: an experimental study in the rat using pharmacological and morphological approaches. *Ann N Y Acad Sci* Aug 1053:407–421
11. Sharma HS (2004) Pathophysiology of the blood–spinal cord barrier in traumatic injury. In: Sharma HS, Westman J (eds) *The blood–spinal cord and brain barriers in health and disease*. Elsevier Academic, San Diego, pp 437–518
12. Sharma HS (2007) Neurotrophic factors in combination: a possible new therapeutic strategy to influence pathophysiology of spinal cord injury and repair mechanisms. *Curr Pharm Des* 13(18): 1841–1874
13. Sharma HS (2007) A select combination of neurotrophins enhances neuroprotection and functional recovery following spinal cord injury. *Ann NY Acad Sci* Dec 1122:95–111
14. Sharma HS (2006) Post-traumatic application of brain-derived neurotrophic factor and glia-derived neurotrophic factor on the rat spinal cord enhances neuroprotection and improves motor function. *Acta Neurochir Suppl* 96:329–334
15. Sharma HS, Olsson Y (1990) Edema formation and cellular alterations following spinal cord injury in the rat and their modification with p-chlorophenylalanine. *Acta Neuropathol (Berl)* 79(6):604–610
16. Sharma HS, Olsson Y, Pearsson S, Nyberg F (1995) Trauma induced opening of the blood–spinal cord barrier is reduced by indomethacin, an inhibitor of prostaglandin synthesis. Experimental observations in the rat using ¹³¹I-sodium, Evans blue and lanthanum as tracers. *Restor Neurol Neurosci* 7:207–215
17. Sharma HS, Olsson Y, Cervós-Navarro J (1993) Early perifocal cell changes and edema in traumatic injury of the spinal cord are reduced by indomethacin, an inhibitor of prostaglandin synthesis. Experimental study in the rat. *Acta Neuropathol* 85(2): 145–153
18. Sharma HS (2008) New perspectives for the treatment options in spinal cord injury. *Expert Opin Pharmacother* (16):2773–800. Review.
19. Tobias CA, Han SS, Shumsky JS, Kim D, Tumolo M, Dhoot NO, Wheatley MA, Fischer I, Tessler A, Murray M (2005) Alginate encapsulated BDNF-producing fibroblast grafts permit recovery of function after spinal cord injury in the absence of immune suppression. *J Neurotrauma* Jan 22(1):138–156

Antibodies to Dynorphin A (1–17) Attenuate Closed Head Injury Induced Blood–Brain Barrier Disruption, Brain Edema Formation and Brain Pathology in the Rat

H.S. Sharma, R. Patnaik, S. Patnaik, A. Sharma, S. Mohanty, and P. Vannemreddy

Abstract The potential neuroprotective efficacy of dynorphin A antiserum on BBB dysfunction, edema formation and brain pathology was examined in a closed head injury (CHI) model in the rat. The CHI was produced by an impact of 0.224 N on the right parietal bone under anesthesia by dropping a weight of 114.6 g on the skull from a height of 20 cm through a guide tube. This concussive brain injury resulted in profound BBB disruption as evidenced by leakage of Evans blue and radioiodine in the brain. Edema formation and swelling at 5 h were most pronounced in the contralateral cerebral hemisphere. Pretreatment with dynorphin A antiserum (1:20, monoclonal) infused into the left lateral cerebral ventricle (30 μ L in PBS) either 30 min before or 30 min after CHI significantly attenuated BBB dysfunction, brain edema formation, volume swelling and brain pathology. However, no reduction in brain edema, BBB permeability or improved brain pathology was seen when the antiserum was given 60 min post-CHI. These observations are the first to suggest that antiserum to dynorphin when administered into the CSF during early phase of CHI is neuroprotective. Our work further indicates that dynorphin is actively involved in the cellular and molecular mechanisms of edema formation and BBB breakdown in CHI.

Keywords Closed head injury • dynorphin A antiserum • blood–brain barrier • brain edema • brain pathology

H.S. Sharma (✉) and A. Sharma
Laboratory of Cerebrovascular Research, Department of Surgical Science, Anesthesiology and Intensive care Medicine, University Hospital, Frödingsgatan 12:28, Uppsala, SE-75421, Sweden
e-mail: Sharma@surgsci.uu.se

R. Patnaik, S. Patnaik
Department of Biomedical Engineering, Institute of Technology, Banaras Hindu University, Varanasi-221005, India

S. Mohanty
Department of Neurosurgery, Institute of Medical Sciences, Banaras Hindu University, Varanasi-221005, India

P. Vannemreddy
Department of Neurosurgery, LSUHSC-Shreveport, LA 71103, USA and Department of Surgical Science, Anesthesiology and Intensive care Medicine, University Hospital, Frödingsgatan 12:28, Uppsala, SE-75421, Sweden

Introduction

Closed head injury (CHI) is a serious life-threatening clinical situation that affects more than 50,000 victims worldwide every year (5,14). Most victims of CHI are males in their early 20 to 30s and their condition largely results from motor vehicle accidents, blunt head trauma or falls (2,5,8,14). To date no suitable therapy is available to reduce brain damage or death in CHI victims. Volume swelling of the brain in a closed cranium compartment resulting in depression of vital centers is the primary cause of death in CHI (see (2,8)). More often, a mild to severe concussive injury results in swelling of the whole brain, or otherwise counter-coup mechanisms result in damage to the contralateral side of the brain, leading to permanent disability causing huge burden on our society. Thus, exploration of suitable therapeutic measures to reduce brain damage and swelling is urgently needed to develop suitable clinical therapeutic strategies for CHI victims.

Our laboratory has developed a new model of CHI that simulates the clinical conditions of counter-coup injury and induces extensive brain damage to the contralateral side (2,8,12). Using this model, we have shown that serotonin and histamine play important roles in brain edema and blood–brain barrier (BBB) disturbances caused by CHI (2,12). Furthermore, neutralization of endogenous serotonin using intracerebroventricular administration of serotonin antiserum within 30 min of CHI induces neuroprotection (8). This indicates that antibodies to neurodestructive agents, e.g., serotonin, could induce profound beneficial effects in CHI and may have some therapeutic value (see (2,8)).

Since serotonin and dynorphin are both known neurotoxic agents and are released following CNS injuries (1,2,4,9,11), the possibility exists that dynorphin could also contribute to brain pathology following CHI (1,3,4). Topical application of antiserum to dynorphin on the spinal cord following trauma that results in neuroprotection (6,7,10) is in line with this idea. Interestingly, dynorphin antiserum also inhibits upregulation of neuronal nitric oxide synthase (nNOS) expression in spinal cord injury (6,7). These observations

suggest that neutralization of endogenous dynorphin activity is neuroprotective in nature.

Since the basic mechanisms of CNS injuries are very similar in nature, the present investigation examines the neuroprotective effects of dynorphin antiserum in CHI induced disturbances in BBB permeability, brain edema formation and brain pathology in our rat model (2,8,12).

Materials and Methods

Animals

Experiments were carried out on inbred male Charles Foster rats (200–250 g) housed in standard laboratory conditions ($21 \pm 1^\circ\text{C}$; 12 h light and 12 h dark schedule). Water and food were supplied ad libitum before the experiments.

Closed Head Injury

Under Equithesin anesthesia (0.3 mL/100 g, i.p.) the skull was exposed and a stainless steel weight of 114.6 g was dropped onto the right parietal bone from a 20 cm height through a guide tube (2, see Fig. 1). This resulted in an impact injury of 0.224 N at the level of the skull (8,12). Only those animals that did not develop a fracture in the skull bone were used in our investigation (8). The animals were allowed to survive 5 h after injury. Uninjured animals served as controls. This experimental design was approved by the local Institutional Ethics Committee.

Dynorphin Antibody Treatment

Dynorphin A 1-17 antiserum (Calbiochem, USA) was administered into the left cerebral ventricle (100 μL , 1:20) either 30 min before or 30 or 60 min after CHI through an indwelling stainless steel guide cannula implanted into the lateral ventricle (7,8,10). Control rats received saline infusions in an identical manner.

BBB Permeability and Brain Edema

The BBB permeability to Evans blue and ^{131}I iodine, and brain water content were measured using standard protocol as described earlier (8,11).

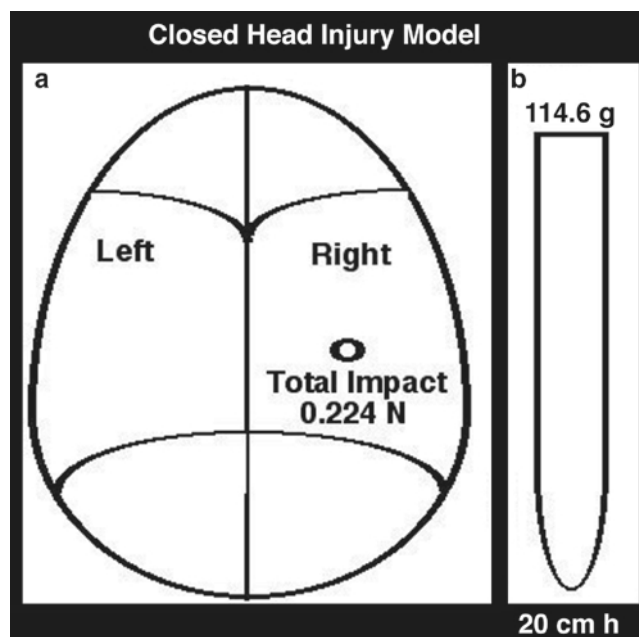


Fig. 1 The new model of closed head injury (CHI) in rats. Under Equithesin anesthesia, a silicon-coated iron bar weighing 114.6 g was dropped over the right parietal skull bone (o) from a height of 20 cm through an aluminum guide tube (see 2,8,12). This impact induced concussive injury in the animals and did not normally induce fracture of the skull. Following injury, the rats were allowed to survive under anesthesia for 5 h (modified after 12)

Brain Pathology

For histological studies, animals were perfused in situ with 4% paraformaldehyde preceded with a brief saline rinse (7,8,12). Selected coronal sections from the brain were cut and embedded in paraffin and 3 μm thick sections were obtained. These paraffin sections were stained with Nissl stain or Haematoxylin and Eosin to study brain pathology.

Statistical Analysis

ANOVA followed by Dunnet's test was used to evaluate statistical significance between the control and experimental rats. A p -value < 0.05 was considered significant.

Results

Effect of Dynorphin A Antiserum on BBB Permeability in CHI

CHI induces marked increases in BBB permeability to Evans blue and radioiodine, the intensity of which was most pronounced in the contralateral left hemisphere (Table 1).

Table 1 Effect of Dynorphin A antibodies (Dyn-A abs, 1:20) on 5 h CHI induced blood–brain barrier permeability, brain edema formation and brain pathology in the rat

Type of Experiment	BBB permeability			Brain edema formation			Nerve cell			Gital cell			Myelin	
	EBA mg%	¹²⁵ Iodine%	Water content%	% f	Distortion	Degeneration	Distortion	Degeneration	Distortion	Perivascular edema	Degeneration	Vesiculation		
A. Control														
Right half	0.28 ± 0.04	0.38 ± 0.08	77.89 ± 0.23	Nil	Nil	Nil	Nil	Nil	Nil	Nil	Nil	Nil	Nil	
Left half	0.26 ± 0.08	0.40 ± 0.06	77.83 ± 0.34	Nil	Nil	Nil	Nil	Nil	Nil	Nil	Nil	Nil	Nil	
B. 5 h CHI														
Right half§	1.34 ± 0.12**	1.86 ± 0.23**	81.67 ± 0.56**	+16	++++	++++	+++	+++	+++	+++	+++	+++	+++	
Left half	1.78 ± 0.23**#	2.34 ± 0.28**#	82.76 ± 0.44#a	+19	+++	+++	+++	+++	+++	+++	+++	+++	+++	
C. Dyn-A abs (1:20) + CHI (-30 min)														
Right half§	0.74 ± 0.09**a	0.84 ± 0.04**a	78.86 ± 0.13**a	+4	++	++	++	++	++	++	++	++	++	
Left half	0.80 ± 0.06**a#	0.90 ± 0.09**a#	79.04 ± 0.13**a	+5	+	+	+	+	+	+	+	+	+	
D. Dyn-A abs (1:20) + CHI (+30 min)														
Right half§	0.94 ± 0.08**a	1.07 ± 0.13**a	79.18 ± 0.13**a	+6	++	++	++	++	++	++	++	++	++	
Left half	0.99 ± 0.11**a#	1.18 ± 0.10**a#	80.09 ± 0.11**a	+6	++	++	++	++	++	++	++	++	++	
E. Dyn-A abs(1:20) + CHI (+60 min)														
Right half§	1.36 ± 0.13**	1.84 ± 0.10**	80.89 ± 0.24**	+13.5	+++	+++	+++	+++	+++	+++	+++	+++	+++	
Left half	1.44 ± 0.10**	2.04 ± 0.12**#	81.89 ± 0.20**	+18	++++	++++	+++	+++	+++	+++	+++	+++	++++	

Values are Mean ± SD of five to eight rats. § = injured, + = mild, ++ = moderate, +++ = severe, ++++ = extensive; %f = volume swelling, calculated according to Elliott and Jasper (1949). About 1% increase in water content represents +3% increase in volume swelling (Sharma et al. (2007) (8)). * = P < 0.05, ** = P < 0.01, *** = P < 0.001, compared from saline control, a = P < 0.05 compared from CHI, Student's unpaired t-test, # = P < 0.05 compared from right injured half, Student's paired t-test.

Intracerebroventricular administration of dynorphin A either 30 min before or 30 min after CHI significantly reduced the leakage of Evans blue and radioiodine into the brain, and the magnitude of this reduction was most pronounced in the uninjured left hemisphere (Table 1). However, dynorphin antiserum given 60 min after CHI was unable to reduce BBB permeability to protein tracers (Table 1).

Effect of Dynorphin A Antiserum on Brain Edema in CHI

A significant reduction in brain edema formation and volume swelling was seen in rats after CHI when the dynorphin antiserum was administered either 30 min before or 30 min after injury (Table 1). The most marked reduction in brain edema formation as a result of dynorphin antiserum was seen in the uninjured left cerebral hemisphere as compared to the injured right hemisphere (Table 1). However, no effect of dynorphin antiserum was seen on brain edema formation when the antiserum was given 60 min after CHI.

Effect of Dynorphin A Antiserum on Brain Pathology in CHI

Untreated traumatized rats showed several distorted neurons in the right and left hemispheres (Table 1, Fig. 2) that were largely located in the edematous regions. The incidence of damaged neurons was most pronounced in the left uninjured hemisphere, as compared with the right injured side (Table 1). Dynorphin antiserum was administered into the left cerebral ventricle either 30 min before or 30 min after injury markedly attenuated the neuronal damage and reduced the sponginess and edema in the neuropil (Fig. 2). This effect was most pronounced on the left side as compared with the right hemisphere (Table 1). On the other hand, dynorphin antiserum given 60 min after CHI was ineffective in reducing brain pathology (Table 1).

Discussion

The most important finding of this study is a marked neuroprotection following CHI that was achieved through intracerebroventricular infusion of dynorphin A within 30 min of injury. This suggests that the dynorphin peptide is actively involved in CHI-induced brain edema formation and brain pathology, not reported earlier. Our results further show that

dynorphin antiserum when administered either 30 min before trauma or 30 min after injury is neuroprotective. However, administration of the antiserum 60 min after CHI has no beneficial effects. This observation suggests that CHI induces an early release of dynorphin neuropeptide that is neurotoxic in nature. Thus, either neutralization of endogenous dynorphin before CHI or within 30 min of its release following trauma has beneficial effects. This suggests that early consequences of CHI induced BBB dysfunction, brain edema formation and development of brain pathology are somehow mediated through a dynorphin-related mechanisms.

Previously, topical application of dynorphin A antiserum over a traumatized spinal cord has been associated with profound neuroprotection if the antiserum is applied within 10 min after injury (7,9,10,13). Subsequent studies have shown that dynorphin antiserum can reduce upregulation of nNOS in the spinal cord following injury (6,7,9,10,13). This suggests that the dynorphin peptide may induce neurotoxicity via production of nitric oxide, a free radical that is injurious to the brain and spinal cord (see (6,7)). The failure of dynorphin A antiserum to improve brain pathology after 60 min suggests that late neutralization of dynorphin may not attenuate nitric oxide production. However, to further confirm this idea, additional investigations on nNOS immunoreactivity in CHI are needed.

Increased levels of dynorphins in the CNS are quite common following traumatic or hyperthermic brain injuries (6,7,9). Increased release of dynorphin could induce the release of amino acid neurotransmitters, e.g., glutamate and aspartate, to cause excitotoxicity (1,3,4,10,13). Thus, it is likely that dynorphin may stimulate NMDA receptors and thereby result in neurotoxicity (3,4). Neutralization of dynorphin by dynorphin antiserum attenuated the NMDA receptor activation much more effectively than did the NMDA receptor blocker MK-801 (see (3,4,7)). Thus, it appears that blocking the action of dynorphin in the CNS may attenuate neurotoxic events.

There are reasons to believe that, apart from excitotoxicity, dynorphin also activates the production and release of nitric oxide (7). This is evident from the fact that blocking NOS activity in heat stress can mitigate increased dynorphin expression in the brain (6). Furthermore, topical application of dynorphin antiserum reduced nNOS expression in the spinal cord after injury (7). Taken together, these observations suggest that dynorphin may affect brain pathology in CHI and that neutralization of dynorphin using its antiserum may induce neuroprotection.

Marked neuroprotection seen in the contralateral side in dynorphin antiserum treated rats following CHI appears to be unrelated to the high concentration and diffusion of antiserum in the injected side alone (see (2,8,12)). This is supported by the fact that significant improvement of brain pathology is also exhibited in the injured side, suggesting that the antiserum may affect the whole brain during the

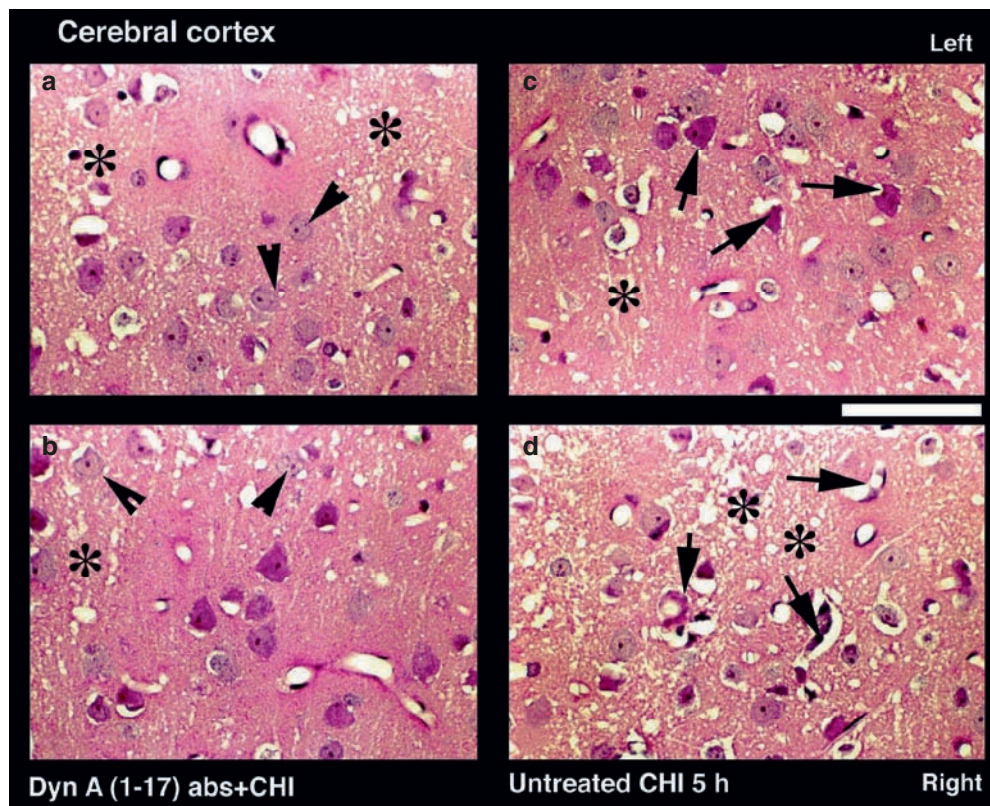


Fig. 2 Neuronal changes in the cerebral cortex following CHI and their modification with Dyn A antiserum treatment. Treatment with Dyn A antiserum 30 min after injury markedly attenuated nerve cell damage (a, b) that was most obvious in the left uninjured cortex (a) as compared to the untreated traumatized rat (c, d). Several almost healthy

neurons (arrowheads) are seen in the Dyn A antiserum treated rat in the cortex. In untreated rats, marked neuronal cell damage is seen in the contralateral left side (c) whereas loss of neurons and sponginess are most frequently observed in the injured side (d). Damaged nerve cells are clearly seen in the untreated injured rat (arrows, c, d). Bar: 25 μ m

short period of intracerebroventricular infusion. A reduction in BBB function and brain edema formation in both hemispheres following dynorphin antiserum treatment further supports this idea. A failure of neuroprotection following dynorphin antiserum given 60 min after injury also indicates that high concentrations and diffusion alone do not fully account for the beneficial effects of the antiserum.

It appears that CHI may induce a release of dynorphin in the brain that could stimulate the release of several neurotoxic elements, e.g., glutamate, nitric oxide, free radicals, lipid peroxidase, or various neurotoxic cytokines in the brain. All these elements could work together to induce BBB disruption and brain edema formation in CHI (1,3,4,6,8,10,13). Swelling of the brain in a closed cranium alone leads to profound compression of neuronal structures, and this in turn causes cell damage and eventually death following CHI (8,12,13). It appears that by neutralizing dynorphin using its antiserum we may have reduced the spread of these neurotoxic chemicals in the contralateral side. This resulted in a marked reduction in brain damage in the antiserum-treated animals as compared with the injured half. However to clarify this, immunostaining of various neurochemicals associated with CHI following dynorphin antiserum treatment is

needed. This is an important aspect of our current and future work plan in CHI.

In conclusion, our results clearly show that dynorphin antiserum has the ability to mitigate brain pathology in CHI if administered within 30 min following the insult. This indicates that dynorphin may play an active role in the early consequences of neuronal injury following CHI, a feature reported earlier in the literature.

Conflict of interest statement We have no conflict of interest with any organizations mentioned below.

Acknowledgements This research is supported by grants from Swedish Medical Research Council (2710 HSS), Göran Gustafsson Foundation, Stockholm (HSS), Astra-Zeneca, Mölndal, Sweden (HSS), Acure Pharma, Sweden (HSS); IPSEN Medical, Paris, France (HSS); Alexander von Humboldt Foundation, Germany (HSS/AS); The University Grants Commission, New Delhi, India (HSS); The Indian Medical Research Council, New Delhi, India (HSS); Ministry of Science and Technology, New Delhi, Govt. of India (HSS); Department of Science and Technology, UP Govt. (HSS); University of Shreveport, LA, USA (VP); Dept. of Science Technology, AP Govt., Hyderabad (VP); Banaras Hindu University, Varanasi (RP/SP). The technical assistance of Mohammad Siddiqui, Aftab Ahmed and Deep Chand Lal and the administrative assistance of Katherin Kern and Angela Jan are

greatly appreciated. There is no conflict of interest among any of the funding agencies listed above.

References

1. Bakshi R, Ni RX, Faden AI (1992) N-methyl-D-aspartate (NMDA) and opioid receptors mediate dynorphin-induced spinal cord injury: behavioral and histological studies. *Brain Res May* 15; 580(1–2): 255–264
2. Dey PK, Sharma HS (1984) Influence of ambient temperature and drug treatments on brain oedema induced by impact injury on skull in rats. *Indian J Physiol Pharmacol Jul–Sep*; 28(3):177–186
3. Faden AI (1990) Opioid and nonopioid mechanisms may contribute to dynorphin's pathophysiological actions in spinal cord injury. *Ann Neurol Jan*; 27(1):67–74
4. Faden AI (1992) Dynorphin increases extracellular levels of excitatory amino acids in the brain through a non-opioid mechanism. *J Neurosci Feb*; 12(2):425–429
5. Reddy CC, Collins MW, Gioia GA (2008) Adolescent sports concussion. *Phys Med Rehabil Clin N Am May*; 19(2):247–69, viii. Review
6. Sharma HS, Alm P (2002) Nitric oxide synthase inhibitors influence dynorphin A (1–17) immunoreactivity in the rat brain following hyperthermia. *Amino Acids* 23(1–3):247–259
7. Sharma HS, Nyberg F, Gordh T, Alm P (2006) Topical application of dynorphin A (1–17) antibodies attenuates neuronal nitric oxide synthase up-regulation, edema formation, and cell injury following focal trauma to the rat spinal cord. *Acta Neurochir Suppl* 96: 309–315
8. Sharma HS, Patnaik R, Patnaik S, Mohanty S, Sharma A, Vannemreddy P (2007) Antibodies to serotonin attenuate closed head injury induced blood brain barrier disruption and brain pathology. *Ann N Y Acad Sci Dec*; 1122:295–312
9. Sharma HS, Nyberg F, Olsson Y (1992) Dynorphin A content in the rat brain and spinal cord after a localized trauma to the spinal cord and its modification with p-chlorophenylalanine. An experimental study using radioimmunoassay technique. *Neurosci Res Aug*; 14(3):195–203
10. Sharma HS, Olsson Y, Nyberg F (1995) Influence of dynorphin A antibodies on the formation of edema and cell changes in spinal cord trauma. *Prog Brain Res* 104:401–416. Review
11. Sharma HS, Olsson Y, Dey PK (1990) Changes in blood–brain barrier and cerebral blood flow following elevation of circulating serotonin level in anesthetized rats. *Brain Res May* 28; 517(1–2): 215–223
12. Vannemreddy P, Ray AK, Patnaik R, Patnaik S, Mohanty S, Sharma HS (2006) Zinc protoporphyrin IX attenuates closed head injury-induced edema formation, blood–brain barrier disruption, and serotonin levels in the rat. *Acta Neurochir Suppl* 96:151–156
13. Winkler T, Sharma HS, Gordh T, Badgaiyan RD, Stålberg E, Westman J (2002) Topical application of dynorphin A (1–17) antiserum attenuates trauma induced alterations in spinal cord evoked potentials, microvascular permeability disturbances, edema formation and cell injury: an experimental study in the rat using electrophysiological and morphological approaches. *Amino Acids* 23(1–3):273–281
14. Xydakis MS, Robbins AS, Grant GA (2008) Mild traumatic brain injury in U.S. soldiers returning from Iraq. *N Engl J Med May* 15; 358(20):2177; author reply 2179

Serine Protease Inhibitor Attenuates Intracerebral Hemorrhage-Induced Brain Injury and Edema Formation in Rat

Takehiro Nakamura, Yasuhiro Kuroda, Naohisa Hosomi, Naohiko Okabe, Nobuyuki Kawai, Takashi Tamiya, Guohua Xi, Richard F. Keep, and Toshifumi Itano

Abstract Our previous studies have demonstrated that thrombin plays an important role in intracerebral hemorrhage (ICH)-induced brain injury and edema formation. We, therefore, examined whether nafamostat mesilate (FUT), a serine protease inhibitor, can reduce ICH-induced brain injury. Anesthetized male Sprague-Dawley rats received an infusion of autologous whole blood (100 μ L), thrombin (5U/50 μ L) or type VII collagenase (0.4 U/2 μ L) into the right basal ganglia, the three ICH models used in the present study. FUT (10 mg/kg) or vehicle was administered intraperitoneally 6 h after ICH (or immediately

after thrombin infusion) and then at 12-h intervals (six treatments in total, n = 5 in each group). All rats were sacrificed 72 h later. We also examined whether FUT promotes rebleeding in a model in which ICH was induced by intracerebral injection of collagenase. Systemic administration of FUT starting 6 h after ICH reduced brain water content in the ipsilateral basal ganglia 72 h after ICH compared with vehicle. FUT attenuated ICH-induced changes in 8-OHdG and thrombin-reduced brain edema. FUT did not increase collagenase-induced hematoma volume. FUT attenuates ICH-induced brain edema and DNA injury suggesting that serine protease inhibitor may be potential therapeutic agent for ICH.

T. Nakamura (✉)
Department of Neurobiology and Neurological Surgery, Kagawa University Faculty of Medicine, 1750-1, IkenobeMiki, Kita, Kagawa 761-0173, Japan
e-mail: tanakamu@kms.ac.jp

Y. Kuroda
Department of Emergency and Critical Care Medicine, Kagawa University Faculty of Medicine, 1750-1, IkenobeMiki, Kita, Kagawa, 761-0173, Japan

N. Hosomi
Department of Cardiorenal and Cerebrovascular Medicine, Kagawa University Faculty of Medicine, 1750-1, IkenobeMiki, Kita, Kagawa 761-0173, Japan

N. Okabe
Department of Neurobiology, Kagawa University Faculty of Medicine, 1750-1, IkenobeMiki, Kita, Kagawa 761-0173, Japan

N. Kawai and T. Tamiya
Department of Neurological Surgery, Kagawa University Faculty of Medicine, 1750-1, IkenobeMiki, Kita, Kagawa, 761-0173, Japan

G. Xi and R.F. Keep
R5018 Biomedical Science Research Building
Department of Neurosurgery
University of Michigan
109 Zina Pitcher Place
Ann Arbor, MI 48109-2200, USA

T. Itano
Department of Neurobiology, Kagawa University Faculty of Medicine, 1750-1, IkenobeMiki, Kita, Kagawa 761-0173, Japan

Keywords Intracerebral hemorrhage • thrombin • serine protease inhibitor • brain edema • rat

Introduction

Intracerebral hemorrhage (ICH) is a subtype of stroke with high morbidity. Our previous studies have demonstrated that toxic factors, including iron and thrombin, released from a blood clot may account for the formation of perihematomal edema in ICH (1,8). Thrombin is a serine protease and an essential component in the coagulation cascade. Previous study showed that nafamostat mesilate (FUT) inhibits complement factors thrombin and plasmin and suppresses the protease-based inflammation (2). FUT is a competitive serine protease inhibitor, widely used in Japan in the treatment of acute pancreatitis, disseminated intravascular coagulopathy, and as an anticoagulant for plasmapheresis. One of the purpose of the present study is to determine whether delayed systemic administration of FUT could reduce edema formation in a rat model of ICH involving injection of autologous blood into the basal ganglia. Another purpose is to examine whether FUT systemic administration would increase rebleeding in a collagenase-induced ICH model.

Materials and Methods

Animal Preparation and Intracerebral Infusion

Animal protocols were approved by the Animal Committee of the Kagawa University. Male Sprague-Dawley rats (CLEA, Tokyo, Japan), each weighing 300 to 400 g, were used for all experiments. Rats were allowed free access to food and water. The animals were anesthetized with pentobarbital (40 mg/kg i.p.) and the right femoral artery was catheterized to sample blood for intracerebral infusion. The rats were positioned in a stereotaxic frame (Narishige Instruments, Tokyo, Japan) and a cranial burr hole (1 mm) was drilled near the right coronal suture 3.5 mm lateral to the midline. A 27-gauge needle was inserted stereotaxically into the right basal ganglia (coordinates: 0.2 mm anterior, 5.5 mm ventral, and 3.5 mm lateral to the bregma). Autologous whole blood (100 μ L), 5U thrombin (50 μ L), or 0.4U type VII collagenase (2 μ L) were infused with the use of a microinfusion pump (Terumo, Tokyo, Japan).

Experimental Groups

There were four sets of experiments in this study. In the first two parts, all rats received an intracerebral injection of 100 μ L autologous whole blood (ICH). Part 1 examined the effect of FUT on ICH-induced brain injury by measuring brain edema 72 h after ICH ($n = 5$ each group). In the second set, 8-hydroxy-2'-deoxyguanosine (8-OHdG), hallmark of DNA damage, was examined by ELISA after treatment for ICH ($n = 3$ each group). Part 3 investigated the effect of FUT on thrombin-induced-brain edema ($n = 5$ each group). In this part, rats received an intracerebral injection of 5U thrombin (50 μ L). Part 4 examined whether FUT promotes rebleeding in a model in which ICH was induced by intracerebral injection of type VII collagenase (0.4U/2 μ L, $n = 5$ each group).

Brain Water Content

Animals were reanesthetized (pentobarbital 50 mg/kg i.p.) and decapitated 72 h after ICH for brain water content. The brains were removed, and a coronal brain slice (approximately 3 mm thick) 4 mm from the frontal pole was then cut with a blade. The brain slice was divided into two hemispheres along the midline, and each hemisphere was dissected into the basal ganglia. Two samples from each brain were obtained: the ipsilateral and the contralateral basal ganglia. Brain samples were immediately weighed on an electric analytical balance (R160P,

Sartorius, Goettingen, Germany) to obtain the wet weight. Brain samples were then dried at 100°C for 24 h to obtain the dry weight. The formula for calculation was as follows: $((\text{Wet Weight} - \text{Dry Weight})/\text{Wet Weight}) \times 100\%$.

Detection of 8-OHdG in DNA

DNA extraction was performed using a DNA isolation kit produced by Dojindo Molecular Technologies (Kumamoto, Japan). In this method, purified DNA (ratio of OD260/280 > 1.8) was isolated from brain tissues by guanidine method with Rnase A and proteinase K. This method avoided the use of phenol and the procedure of heating that may induce background. The brain tissue sampling was as for the brain edema measurements. The levels of 8-OHdG of the samples were determined using ELISA kit (Japan Institute for the Control of Aging, Shizuoka, Japan). The kit can measure extremely low levels of 8-OHdG, and the specificity of the monoclonal antibody has been established (7). The wells were subjected to OD measurement at 450 nm. 8-OHdG ELISA was triplicate and the means were calculated. The data, expressed as pg 8-OHdG per μ g DNA, were calculated based on the linear calibration curve generated for each experiment using 8-OHdG standard solutions.

Morphometric Measurement of Hemorrhage Volume

Animals were decapitated, and the brains were rapidly removed and sectioned coronally at 2-mm intervals. With the use of computerized image analysis system (NIH Image version 1.63), the hemorrhage area for each section was measured. The total hematoma volume was calculated by summing the clot area in each section and multiplying by the distance between sections.

Statistical Analysis

All data in this study are presented as mean \pm SD. Data were analyzed with Student's t-test. Significance levels were measured at $P < 0.05$.

Results

All physiologic variables were measured immediately before intracerebral infusions. Mean arterial blood pressure, pH, arterial oxygen and carbon dioxide tensions, hematocrit, and blood glucose were controlled with normal range.

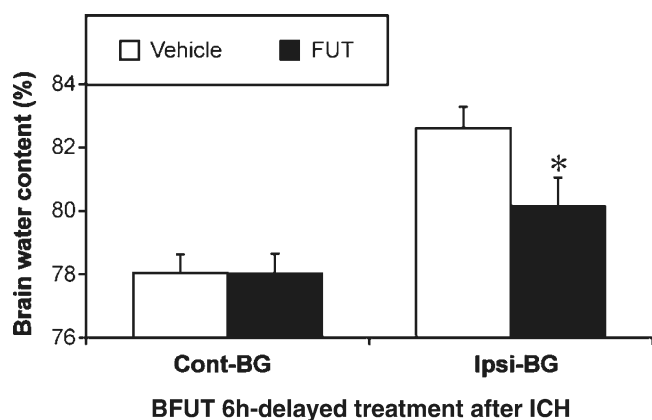


Fig. 1 Bar graphs depicting the effects of delayed nafamostat mesilate (FUT) treatment on water content in the brain 72 h after intracerebral hemorrhage (ICH). FUT (10 mg/kg) or vehicle was administered intraperitoneally 6 h after ICH and then at 12-h intervals (six treatments in total). Values are expressed as the means \pm SD; $n = 5$ each group, $*P < 0.05$. Cont: contralateral, Ipsi: ipsilateral, BG: basal ganglia

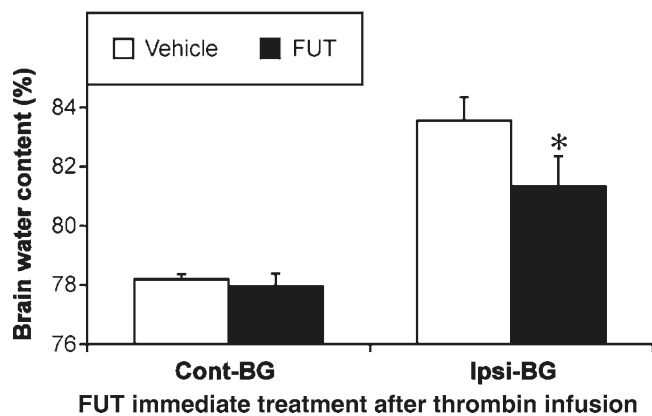


Fig. 2 Graphs showing the effects of immediate nafamostat mesilate (FUT) treatment on thrombin-induced brain edema 72 h after intracerebral thrombin infusion. FUT (10 mg/kg) or vehicle was administered intraperitoneally immediately after thrombin infusion and then at 12-h intervals (six treatments in total). Values are expressed as the means \pm SD; $n = 5$ each group, $*P < 0.05$. Cont: contralateral, Ipsi: ipsilateral, BG: basal ganglia

Systemic administration of FUT starting 6 h after ICH reduced brain water content in the ipsilateral basal ganglia 72 h after ICH compared with vehicle ($P < 0.05$, Fig. 1).

DNA oxidation marker, 8-OHdG, was increased in the ipsilateral basal ganglia compared with contralateral basal ganglia 72 h after ICH ($P < 0.05$, data not shown). Delayed FUT treatment significantly reduced the DNA oxidation marker ($P < 0.05$, data not shown).

FUT also had neuroprotective effects on brain edema after intracerebral infusion of thrombin when given immediately after the thrombin, compared with vehicle-treated rat 72 h later ($P < 0.05$, Fig. 2).

Hematoma volume was assessed morphometrically 72 h after collagenase-induced ICH. FUT did not increase collagenase-induced hematoma volume when given systemically at 6 h compared with vehicle.

Discussion

There are multiple mechanisms of perihematomal edema formation, but thrombin appears to be an important mediator (5). Thrombin is a serine protease and an essential component in the coagulation cascade. Thrombin can induce cytotoxic effects on brain parenchymal cells, blood brain barrier disruption and inflammatory response (1,8,9). Thrombin also could induce oxidative DNA injury (6). These effects may contribute to the edematogenic properties of thrombin. In the present study, FUT that is a serine protease inhibitor attenuated thrombin-induced brain edema in a model of intracerebral thrombin infusion. In previous experimental ICH studies, injection of anticoagulated blood dose did not cause perihematomal edema in rat (8). The systemic administration of high-dose argatroban (0.9 mg/h), thrombin inhibitor, starting 6 h after ICH also significantly reduced brain edema (4). Although thrombin is formed almost immediately after an ICH, there are potential reasons why delayed administration of a thrombin inhibitor would be effective. Thrombin can be bound within the clot and only gradually released into the surrounding parenchyma. There may also be sources of thrombin other than from hematoma (9). A long therapeutic time window for a thrombin inhibitor may exist. This is important because administration of thrombin inhibitor too soon after an ICH may lead to rebleeding and potentially devastating effects. Delayed systemic administration of FUT begun 6 h after ICH markedly reduced perihematomal edema and DNA damage in the present study.

The primary ICH model used in this study involved direct injection of autologous blood into the basal ganglia, and it did not have a disrupted vasculature as basis of the ICH. In order to assess whether FUT might induce rebleeding, the collagenase induced-ICH model was used. In the collagenase induced-ICH model there was no evidence of rebleeding after systemic FUT administration as assessed by measurement of hematoma volume. It is difficult to translate safety data between rats and humans. The rat collagenase induced-ICH model has a disrupted vasculature as the basis for ICH, but the form of that disruption is different from a normal human ICH. In the clinical setting FUT is a useful and safe anticoagulant for plasmapheresis in high bleeding risk patients (3). Great care would be needed in determining the safety window for FUT in humans.

Conclusions

FUT attenuates ICH- or thrombin-induced brain edema. In the rat, delayed FUT treatment was not associated with an increase in rebleeding after ICH. These results indicate that serine protease inhibitor may be a potential therapeutic agent for ICH.

Conflict of interest statement We declare that we have no conflict of interest.

Acknowledgments This study was supported by a Grant-in-Aid for Scientific Research from the Japanese Society for the Promotion of Science. Nafamostat mesilate was a kind gift from Torii Pharmaceutical Co. Ltd., Tokyo, Japan.

References

- Hua Y, Keep RF, Hoff JT, Xi G (2007) Brain injury after intracerebral hemorrhage: the role of thrombin and iron. *Stroke* 38(part II):759–762
- Ikari N, Sakai Y, Hitomi Y, Fujii S (1983) New synthetic inhibitor to the alternative complement pathway. *Immunology* 49:685–691
- Kinugasa E, Akizawa T, Nakashima Y, Wakasa M, Koshikawa S (1992) Nafamostat as anti-coagulant for membrane plasmapheresis in high bleeding risk patients. *Int J Artif Organs* 15:595–600
- Kitaoka T, Hua Y, Xi G, Hoff JT, Leep RF (2002) Delayed argatroban treatment reduces edema in a rat model of intracerebral hemorrhage. *Stroke* 33:3012–3018
- Lee KR, PColon G, Betz AL, Keep RF, Kim S, Hoff JT (1996) Edema from intracerebral hemorrhage: the role of thrombin. *J Neurosurg* 84:91–96
- Nakamura T, Kuroda Y, Yamashita S, Zhang X, Miyamoto O, Tamiya T, Nagao S, Xi G, Keep RF, Itano T (2008) Edaravone attenuates brain edema and neurologic deficits in a rat model of acute intracerebral hemorrhage. *Stroke* 39:463–469
- Saito S, Yamauchi H, Hasui Y, Kurashige J, Ochi H, Yoshida K (2000) Quantitative determination of urinary-8-hydroxydeoxyguanosine (8-OHdG) by using ELISA. *Res Commun Mol Pathol Pharmacol* 107:39–44
- Xi G, Wagner KR, Keep RF, Hua Y, de Courten-Myers GM, Broderick JP, Brott TG, Hoff JT, Muizelaar JP (1998) Role of clot formation on early edema development after experimental intracerebral hemorrhage. *Stroke* 29:2580–2586
- Yang GY, Betz AL, Chenevert TL, Brunberg JA, Hoff JT (1994) Experimental intracerebral hemorrhage: relationship between brain edema, blood flow, and blood brain barrier permeability in rats. *J Neurosurg* 81:93–102

State-of-the-Art management and Monitoring of Brain Edema and Intracranial Hypertension in Fulminant Hepatic Failure. A Proposed Algorithm

Jaime Gasco, Leonardo Rangel-Castilla, Brodus Franklin, Philip G. Thomas, and Joel T. Patterson

Abstract

Aim Develop an evidence-based clinical algorithm integrating clinical decision making on intracranial pressure (ICP) monitoring and intracranial hypertension (ICH) management in the setting of fulminant hepatic failure (FHF).

Material and Methods An English-language literature review was conducted using the PubMed database in November 2007. In compiling evidence on current management trends of ICP and FHF, the paired keywords: fulminant hepatic failure and either mannitol, hypertonic saline, hyperventilation, bioartificial liver, hypothermia, indomethacin, thiopental, or propofol were used. In compiling evidence on ICP monitoring in FHF, the terms “intracranial pressure monitoring” and “liver failure” were used. Excluded references were either pertinent to animal research or irrelevant to ICP monitoring and ICH management in the setting of FHF.

Results State-of-the-art management of ICH due to brain edema in FHF includes Class I therapies such as mannitol and hypertonic saline. Bioartificial liver, hypothermia and hyperventilation are supported by Class II evidence. Indomethacin and sedation remain Class III. Monitoring ICP is supported by Class II and III evidence. A clinical algorithm was created based on the existing therapeutic armamentarium and corresponding evidence support.

Keywords Brain edema • liver failure • intracranial hypertension • intracranial pressure monitoring

Introduction

Fulminant hepatic failure (FHF) is an infrequent but devastating condition. Encephalopathy manifests within 8 weeks after the onset of jaundice in patients without known chronic liver disease (38). Improvement in intensive care management of FHF has led to increased survival. Concerns arising in this scenario include brain edema, intracranial hypertension and cerebral herniation, which now are observed more frequently than in earlier decades (10). Incidence of cerebral edema in grade IV encephalopathy approximates 80% (3, 16, 26).

The pathophysiology of FHF-related brain edema and intracranial hypertension in summary results from a raise in serum ammonia (3, 9, 35), raised cerebral intracellular glutamine (40) and interference with cellular metabolism/energetics via inhibition of brain mitochondrial alpha-ketoglutarate dehydrogenase complex (KGDHC). These contribute to cellular swelling (24, 25), excess nitric oxide (32), altered reactivity to carbon dioxide, and loss of cerebral autoregulation, disrupting the blood–brain barrier and contributing to cerebral hyperemia (41).

Material and Methods

An English-language literature search was conducted in December 2007 summarized in Table 1. Excluded references were either pertinent to animal research or irrelevant to ICP monitoring and ICH management in the setting of FHF. Class evidence was then attributed following standard evidence criteria.

Results

A clinical algorithm was constructed aiming to serve as a guide on the standards of ICP management in a concise and practical manner.

J. Gasco (✉), L. Rangel-Castilla, B. Franklin,
and J. Patterson
Division of Neurological Surgery, University of Texas Medical
Branch, 301 University Boulevard, Galveston, TX 77555-0517, USA
e-mail: jagascot@utmb.edu

P.G. Thomas
Department of Surgery at University of Texas Medical Branch,
Galveston, TX

Table 1 Summary of systematic literature review of ICP management and monitoring in acute liver failure

Search methods	Keywords used	References found/discarded/analyzed
Mannitol	Mannitol, hepatic failure (HF), ICP	16 references found/13 discarded/3 analyzed (12, 17)
Hypertonic saline	Hypertonic saline, HF, cerebral edema	5 references found/3 discarded/2 analyzed (30)
Hyperventilation	Hyperventilation, HF, ICP	11 references found/10 discarded/1 analyzed (13)
Bioartificial liver (BAL)	BAL, HF, ICP	22 references found/20 discarded/2 analyzed (9)
Hypothermia	Hypothermia, acute liver failure, ICP	16 references found/15 discarded/3 analyzed (20)
Indomethacin	Indomethacin, HF, ICP	4 references found/3 discarded/1 analyzed (37)
Thiopental	Thiopental, HF, ICP	4 references found/3 discarded/1 analyzed (15)
Propofol	Propofol, HF, ICP	6 references found/5 discarded/1 analyzed (45)
ICP monitoring	ICP and liver failure	70 references found/52 discarded/18 analyzed 8 prospective (2, 14, 18, 27, 31, 34, 36, 42) 10 retrospective (1, 4, 6, 7, 11, 17, 21, 23, 28, 43) Class II evidence: (34, 42)

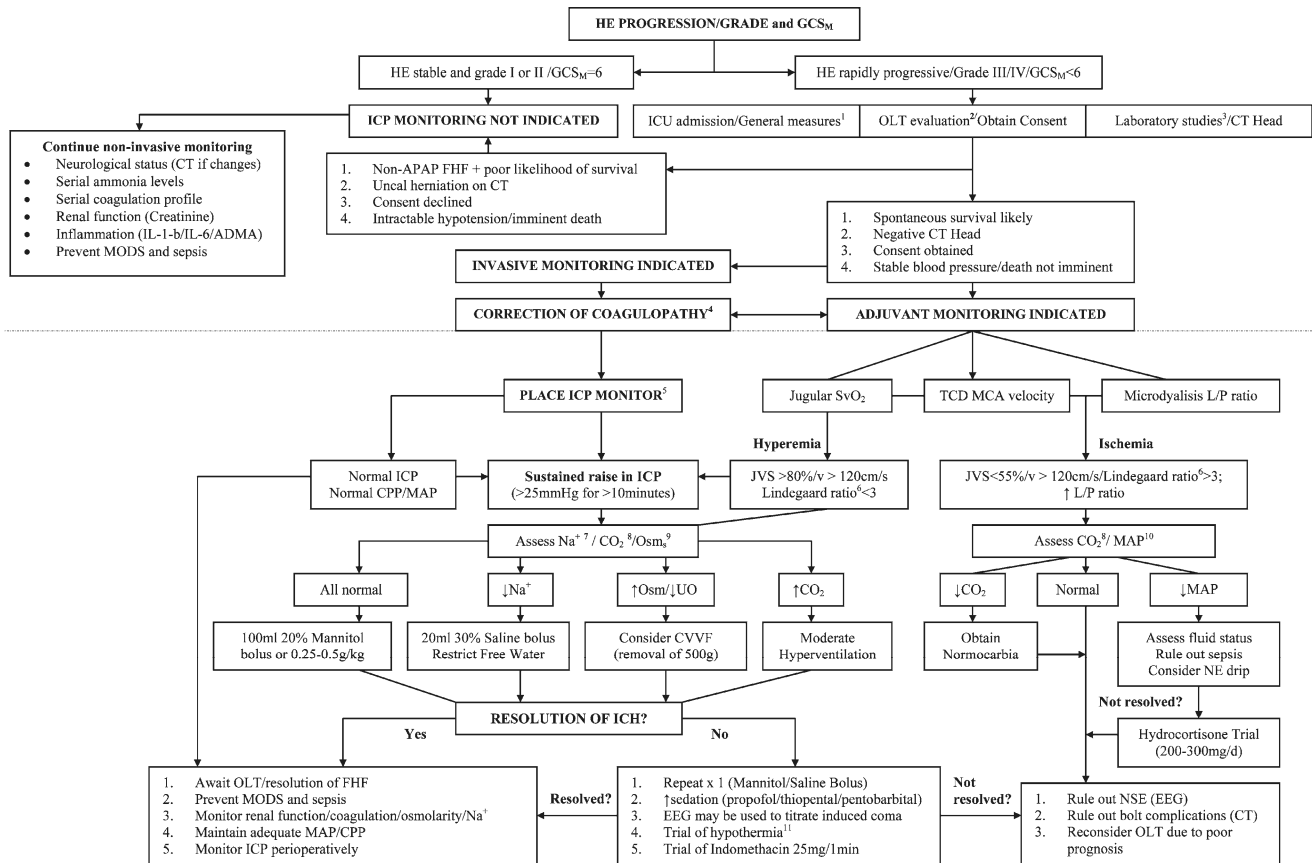


Fig. 1 ¹General measures: Induction/intubation, adequate sedation (e.g. propofol), arterial and central line placement, head-neck alignment at 30°, minimize endotracheal suctioning (may use local lidocaine), NAC administration¹², Prophylactic antibiotics¹³, adequate nutrition; ² OLT evaluation and classifications: Clichy, Model for End Stage Liver Disease, Kings College criteria; **OLT critical criteria:** Wilson's disease, age ≥ 18; life expectancy without OLT < 7 days; meets criteria for FHF; ICU patient with at least one of the following: ventilator dependence, INR > 2, requires renal replacement; ³ Laboratory studies: CMP, CBC, Coagulation profile (PT, PTT, INR), Type and cross match, ABG, Levels of: APAP, NAP-Q1, ADMA, Fibrinogen, Factors V/VII, Factor VIII/V ratio, Arterial ammonia (admission + serial); ⁴Coagulopathy correction: Target INR and Platelets 1.5 and 50,000; Administer 10 mg of vitamin K i.v.; If Fibrinogen < 100 mg/dL use CPT followed by 2 units of platelets, 2–4 units of FFP and rFVIIa (40 µg/kg). If Fibrinogen > 100 mg/dL, proceed the same way without CPT. Avoid rFVII in risk groups or doses beyond 90 µg/kg; ⁵ Monitor placement: Procedure to be performed within 30–60 min of rFVII; ⁶ Lindegaard ratio: MCA velocity/ICA velocity; ⁷ Target Na⁺ 145–155 mEq/L; ⁸ Target CO₂: 35 mmHg; ⁹ Target Osmolarity:

320 mOsm/L; ¹⁰ Target MAP: 75–80 mmHg; ¹¹ Temperature: 32–34°C for 10–14 h in OLT candidates and 8–10 h in other; ¹² NAC: 150 mg/kg for 15–60 min followed by 12.5 mg/kg/h for 4 h then 6.25 mg/kg/h (ALFSG recommends to start even if doubt of timing/dose of APAP intoxication); ¹³ Broad spectrum with third generation cephalosporin ± Vancomycin ± Antifungal (if no response). Abbreviations: **ABG:** Arterial Blood Gas; **APAP:** Acetaminophen; **ADMA:** Asymmetric dimethylarginine; **CBC:** Count blood cell; **CMP:** Comprehensive metabolic panel; **CPP:** Cerebral Perfusion Pressure; **CPT:** Cryoprecipitate; **CPFA:** Coupled Plasma Filtration Absorption; **CT:** Computerized tomography; **CVVF:** Continuous Venovenous Filtration; **EEG:** Electroencephalogram; **FFP:** Fresh Frozen Plasma; **rFVIIa:** recombinant Factor VII; **JVS:** Jugular Venous Saturation; **GCS_M:** Glasgow Coma Scale-Motor score; **HE:** Hepatic encephalopathy; **HRS:** Hepatorenal syndrome; **ICP:** Intracranial Pressure; **ICH:** Intracranial hypertension; **L/P:** Lactate/Pyruvate ratio; **MAP:** Mean Arterial Pressure; **MCA:** Middle cerebral artery; **MODS:** Multiorgan dysfunction syndrome; **NAC:** N-acetylcysteine; **NSE:** Non-convulsive Status Epilepticus; **OLT:** Orthotopic Liver Transplantation; **TCD:** Transcranial Doppler; **UO:** Urine output oliguric/anuric

The algorithm presented in Fig. 1 is based on previously suggested protocols (29), literature review (Table 1), and the data provided by the Acute Liver Failure Study Group (ALFSG) (34). Class I therapies directed at decreasing ICH in the setting of FHF include mannitol (5, 17) and hypertonic saline (30). Hyperventilation (13, 33), hypothermia (19, 20), and bioartificial liver (BAL) (8, 39) are supported by Class II evidence. On the other hand, use of indomethacin (35, 37), thiopental (15), and propofol (45) are supported by Class III evidence.

Discussion

A study of the available literature reveals that the use of ICP monitors in FHF remains controversial. As expressed by the ALFSG, the inclusion of ICP monitoring in the management of FHF may contribute to an improved neurologic recovery following liver transplantation (22, 34, 42). Also, ICP monitoring may prolong time to eventual death and increase the number of therapeutic interventions in monitored patients versus non-monitored patients, as observed by Keays in 1993 and Vaquero in 2005 (22, 42). Weldon and Larsen concluded that the therapeutic actions resulting from the analysis of the ICP values may change the disease progression, extending the available time to OLT and providing an objective neurological assessment thus strongly arguing in favor of ICP monitors (44).

Conclusion

The use of ICP monitoring in FHF is not currently supported by Class I evidence. It is indicated as an adjunct to therapy due to the outlined potential benefits, i.e. improved neurological outcome and increased number of therapeutic interventions in monitored patients. The algorithm proposed may provide a useful tool towards an evidence-based care for patients with brain edema in the setting of acute liver failure.

Conflict of interest statement We declare that we have no conflict of interest.

References

- Aggarwal S, Obrist W, Yonas H, Kramer D, Kang Y, Scott V, Planinsic R (2005) Cerebral hemodynamic and metabolic profiles in fulminant hepatic failure: relationship to outcome. *Liver Transpl* 11:1353–1360
- Ascher NL, Lake JR, Emond JC, Roberts JP (1993) Liver transplantation for fulminant hepatic failure. *Arch Surg* 128:677–682
- Blei AT (1991) Cerebral edema and intracranial hypertension in acute liver failure: distinct aspects of the same problem. *Hepatology* 13:376–379
- Blei AT, Olafsson S, Webster S, Levy R (1993) Complications of intracranial pressure monitoring in fulminant hepatic failure. *Lancet* 341:157–158
- Canalese J, Gimson AE, Davis C, Mellon PJ, Davis M, Williams R (1982) Controlled trial of dexamethasone and mannitol for the cerebral oedema of fulminant hepatic failure. *Gut* 23:625–629
- Cordoba J, Blei AT (1995) Cerebral edema and intracranial pressure monitoring. *Liver Transpl Surg* 1:187–194
- Daas M, Plevak DJ, Wijdicks EF, Rakela J, Wiesner RH, Piepgras DG, Dunn WF, Steers JL (1995) Acute liver failure: results of a 5-year clinical protocol. *Liver Transpl Surg* 1:210–219
- Demetriou AA, Brown RS, Jr., Busuttill RW, Fair J, McGuire BM, Rosenthal P, Am Esch JS, 2nd, Lerut J, Nyberg SL, Salizzoni M, Fagan EA, de Hemptinne B, Broelsch CE, Muraca M, Salmeron JM, Rabkin JM, Metselaar HJ, Pratt D, De La Mata M, McChesney LP, Everson GT, Lavin PT, Stevens AC, Pitkin Z, Solomon BA (2004) Prospective, randomized, multicenter, controlled trial of a bioartificial liver in treating acute liver failure. *Ann Surg* 239:660–667; discussion 667–670
- Detry O, Arkadopoulos N, Ting P, Kahaku E, Watanabe FD, Rozga J, Demetriou AA (1999) Clinical use of a bioartificial liver in the treatment of acetaminophen-induced fulminant hepatic failure. *Am Surg* 65:934–938
- Detry O, De Roover A, Honore P, Meurisse M (2006) Brain edema and intracranial hypertension in fulminant hepatic failure: pathophysiology and management. *World J Gastroenterol* 12:7405–7412
- Donovan JP, Schafer DF, Shaw BW Jr, Sorrell MF (1998) Cerebral oedema and increased intracranial pressure in chronic liver disease. *Lancet* 351:719–721
- Ede R, Gimson AE, Cannalese J, Williams R (1982) Cerebral oedema and monitoring of intracranial pressure in fulminant hepatic failure. *Gastroenterol Jpn* 17:163–176
- Ede RJ, Gimson AE, Bihari D, Williams R (1986) Controlled hyperventilation in the prevention of cerebral oedema in fulminant hepatic failure. *J Hepatol* 2:43–51
- Filho JA, Machado MA, Nani RS, Rocha JP, Figueira ER, Bacchella T, Rocha-e-Silva M, Auler JO Jr, Machado MC (2006) Hypertonic saline solution increases cerebral perfusion pressure during clinical orthotopic liver transplantation for fulminant hepatic failure: preliminary results. *Clinics* 61:231–238
- Forbes A, Alexander GJ, O'Grady JG, Keays R, Gullan R, Dawling S, Williams R (1989) Thiopental infusion in the treatment of intracranial hypertension complicating fulminant hepatic failure. *Hepatology* 10:306–310
- Gimson AE (1996) Fulminant and late onset hepatic failure. *Br J Anaesth* 77:90–98
- Hanid MA, Davies M, Mellon PJ, Silk DB, Strunin L, McCabe JJ, Williams R (1980) Clinical monitoring of intracranial pressure in fulminant hepatic failure. *Gut* 21:866–869
- Helmke K, Burdelski M, Hansen HC (2000) Detection and monitoring of intracranial pressure dysregulation in liver failure by ultrasound. *Transplantation* 70:392–395
- Jalan R, Olde Damink SW, Deutz NE, Davies NA, Garden OJ, Madhavan KK, Hayes PC, Lee A (2003) Moderate hypothermia prevents cerebral hyperemia and increase in intracranial pressure in patients undergoing liver transplantation for acute liver failure. *Transplantation* 75:2034–2039
- Jalan R, Olde Damink SW, Deutz NE, Hayes PC, Lee A (2004) Moderate hypothermia in patients with acute liver failure and uncontrolled intracranial hypertension. *Gastroenterology* 127:1338–1346
- Keays R, Potter D, O'Grady J, Peachey T, Alexander G, Williams R (1991) Intracranial and cerebral perfusion pressure changes before, during and immediately after orthotopic liver transplantation for fulminant hepatic failure. *Q J Med* 79:425–433
- Keays RT, Alexander GJ, Williams R (1993) The safety and value of extradural intracranial pressure monitors in fulminant hepatic failure. *J Hepatol* 18:205–209

23. Keays RT, Alexander GJM, Williams R (1993) The safety and value of extradural intracranial-pressure monitors in fulminant hepatic-failure. *J Hepatol* 18:205–209
24. Lai JC, Cooper AJ (1986) Brain alpha-ketoglutarate dehydrogenase complex: kinetic properties, regional distribution, and effects of inhibitors. *J Neurochem* 47:1376–1386
25. Lai JC, Cooper AJ (1991) Neurotoxicity of ammonia and fatty acids: differential inhibition of mitochondrial dehydrogenases by ammonia and fatty acyl coenzyme A derivatives. *Neurochem Res* 16:795–803
26. Larsen FS (2004) Optimal management of patients with fulminant hepatic failure: targeting the brain. *Hepatology* 39:299–301
27. LeRoux PD, Elliott JP, Perkins JD, Winn HR (1990) Intracranial pressure monitoring in fulminant hepatic failure and liver transplantation. *Lancet* 335:1291–1292
28. Munoz SJ, Robinson M, Northrup B, Bell R, Moritz M, Jarrell B, Martin P, Maddrey WC (1991) Elevated intracranial pressure and computed tomography of the brain in fulminant hepatocellular failure. *Hepatology* 13:209–212
29. Murphy N (2007) The pathology and management of intracranial hypertension in acute liver failure. In: Vincent J-L (ed) *Yearbook of intensive care and emergency medicine*. Springer, Berlin, Heidelberg, pp 678–690
30. Murphy N, Auzinger G, Bernel W, Wendon J (2004) The effect of hypertonic sodium chloride on intracranial pressure in patients with acute liver failure. *Hepatology* 39:464–470
31. Nakanishi K, Hirasawa H, Oda S, Shiga H, Matsuda K, Nakamura M, Hirano T, Hirayama Y, Moriguchi T, Watanabe E, Nitta M (2005) Intracranial pressure monitoring in patients with fulminant hepatic failure treated with plasma exchange and continuous hemodiafiltration. *Blood Purif* 23:113–118
32. Pugliese F, Ruberto F, Perrella SM, Cappannoli A, Bruno K, Martelli S, Celli P, Summonti D, D'Alio A, Tosi A, Novelli G, Morabito V, Poli L, Rossi M, Berloco PB, Pietropaoli P (2007) Modifications of intracranial pressure after molecular adsorbent recirculating system treatment in patients with acute liver failure: case reports. *Transplant Proc* 39:2042–2044
33. Strauss G, Hansen BA, Knudsen GM, Larsen FS (1998) Hyperventilation restores cerebral blood flow autoregulation in patients with acute liver failure. *J Hepatol* 28:199–203
34. Stravitz RT, Kramer AH, Davern T, Shaikh AO, Caldwell SH, Mehta RL, Blei AT, Fontana RJ, McGuire BM, Rossaro L, Smith AD, Lee WM (2007) Intensive care of patients with acute liver failure: recommendations of the US Acute Liver Failure Study Group. *Crit Care Med* 35:2498–2508
35. Taberner A, Schneider F, Potenza MA, Randriamboavonjy V, Chasserot S, Wolf P, Mitolo-Chieppa D, Stoclet JC, Andriantsitohaina R (2003) Cyclooxygenase-2 and inducible nitric oxide synthase in omental arteries harvested from patients with severe liver diseases: immuno-localization and influence on vascular tone. *Intensive Care Med* 29:262–270
36. Tofteng F, Jorgensen L, Hansen BA, Ott P, Kondrup J, Larsen FS (2002) Cerebral microdialysis in patients with fulminant hepatic failure. *Hepatology* 36:1333–1340
37. Tofteng F, Larsen FS (2004) The effect of indomethacin on intracranial pressure, cerebral perfusion and extracellular lactate and glutamate concentrations in patients with fulminant hepatic failure. *J Cereb Blood Flow Metab* 24:798–804
38. Trey C, Davidson CS (1970) The management of fulminant hepatic failure. *Prog Liver Dis* 3:282–298
39. van de Kerkhove MP, Di Florio E, Scuderi V, Mancini A, Belli A, Bracco A, Dauri M, Tisone G, Di Nicuolo G, Amoroso P, Spadari A, Lombardi G, Hoekstra R, Calise F, Chamuleau RA (2002) Phase I clinical trial with the AMC-bioartificial liver. *Int J Artif Organs* 25:950–959
40. Vaquero J, Butterworth RF (2006) The brain glutamate system in liver failure. *J Neurochem* 98:661–669
41. Vaquero J, Chung C, Blei AT (2004) Cerebral blood flow in acute liver failure: a finding in search of a mechanism. *Metab Brain Dis* 19:177–194
42. Vaquero J, Fontana RJ, Larson AM, Bass NM, Davern TJ, Shakil AO, Han S, Harrison ME, Stravitz TR, Munoz S, Brown R, Lee WM, Blei AT (2005) Complications and use of intracranial pressure monitoring in patients with acute liver failure and severe encephalopathy. *Liver Transpl* 11:1581–1589
43. Volk ML, Marrero JA (2006) Advances in critical care hepatology. *Minerva Anestesiol* 72:269–281
44. Wendon JA, Larsen FS (2006) Intracranial pressure monitoring in acute liver failure. A procedure with clear indications. *Hepatology* 44:504–506
45. Wijdicks EF, Nyberg SL (2002) Propofol to control intracranial pressure in fulminant hepatic failure. *Transplant Proc* 34:1220–1222

Novel Free Radical Monitoring in Patients with Neurological Emergency Diseases

Kenji Dohi, Kazue Satoh, Tomoya Nakamachi, Hirokazu Ohtaki, Sachiko Yofu, Shunsuke Nakamura, Seiji Shioda, and Tohru Aruga

Abstract Recent experimental studies have demonstrated that oxidative stress has important roles in various neuronal conditions. Stroke and traumatic brain injury are also related to oxidative stress. However few studies prove the existence of free radicals in humans because they are difficult to measure. We recently developed a technique for free radical and oxidative stress monitoring using the ex vivo electron spin resonance (ESR) spin trapping method in patients with neuroemergency. Blood samples were collected by catheterization of the internal jugular bulb. The alkoxy radical level was measured by ex vivo ESR spectrometry using 5,5-dimethyl-1-pyrroline-1-oxide (Dojin Chemical, Tokyo, Japan) as a spin trap. Electron spin response detection of the spin adduct was performed at room temperature using a JESREIX X-band spectrometer (JEOL, Tokyo, Japan). As a marker of reactive oxygen species, we also used the diacron-reactive oxygen metabolites test (d-ROM). This method is not invasive for patients, and it is technically easy to execute.

Oxidative stress monitoring is useful and may prove valuable for clarifying the pathophysiology of neuroemergency diseases, which has long been hampered by technical difficulties in measuring and monitoring oxidative stress.

Keywords Head injury • free radical • oxidative stress • human • alkoxy radical • monitoring • brain hypothermia • d-ROM test

Introduction

Reactive oxygen species (ROS) have been shown to play an important role in various neuroemergencies and neurodegenerative diseases (1, 3–7, 9, 16, 18). Several lines of evidence support the contention that it is important to control free radical production in the treatment of many of these conditions (5, 6), even though their mechanistic effects are difficult to quantify. The pathophysiological steps in neuronal injury have gradually been clarified with the technical development of molecular biology.

On the other hand, the brain is enriched with polyunsaturated fatty acids, rendering neuronal cells vulnerable to oxidative attack. In this regard, the control of radical formation has been shown to be very important for neuroprotection. In animal experiments, free radical scavengers and antioxidants have dramatically reduced cerebral damage (1–3, 5, 15, 20). However, clear corroboration of evidence from clinical studies has been somewhat slow in coming, and evidence obtained thus far is less than clear cut (10).

Recently, we have developed the ex vivo electron spin resonance (ESR) spin trapping method for detecting free radicals in blood (5, 7, 8, 14). In this report, we introduce free radical monitoring using this method. We also describe another novel and simple oxidative stress monitoring technique using the diacron-reactive oxygen metabolites (d-ROM) test in patients with a neuroemergency.

Methods

Ex Vivo Electron Spin Resonance Spin Trapping Method in Patients with Neuroemergency Diseases

Upon patient admission, blood samples were collected by immediate catheterization at the bulb of the internal jugular vein. Whole blood samples were immediately

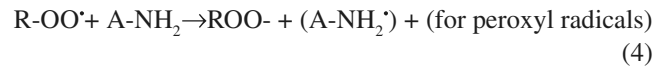
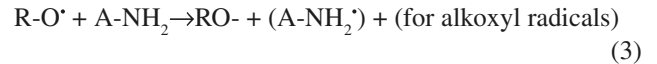
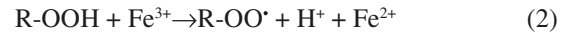
K. Dohi (✉), and T. Aruga
Department of Emergency and Critical Care Medicine, Showa University School of Medicine, Shinagawa-ku,
Tokyo 142-8555, Japan
e-mail: kdop@med.showa-u.ac.jp

T. Nakamachi, H. Ohtaki and S. Yofu
Department of Anatomy, Showa University School of Medicine,
Shinagawa-Ku, Tokyo 142-8555, Japan

mixed with the spin trap 5,5-dimethyl-1-pyrroline-1-oxide (DMPO) and analyzed within 1 h. ESR spectra were recorded at room temperature (23°C) with the following spectrometer settings: center field, 335.0 ± 5.0 mT; microwave power, 5 mW; modulation amplitude, 0.1 mT; gain, 200; time constant, 0.1 s; and scanning time, 2 min. Radical intensity (RI) was defined as the ratio of the signal intensity of the first peak of the alkoxy-DMPO spin adduct to that of MnO (Fig. 1B).

Diacron-Reactive Oxygen Metabolites Testing in Patients with Neuroemergency Diseases

The generation of free radicals was evaluated in each plasma sample by the colorimetric determination of reactive oxygen metabolites (i.e., the d-ROM test) using the free radical analytical system (FRAS, Diacron, Grosseto, Italy) (5). This method makes it possible to estimate the total amount of hydroperoxide present in a 20- μ L sample using a spectrophotometric procedure. In brief, the previously described samples were dissolved in acetate buffer (pH 4.8) with FeCl₂ at 37°C. They were then mixed gently, followed by the addition of 20 μ L of a chromogenic mixture including aromatic alkyl-amine. After incubation for 5 min at 37°C, the resultant pink aromatic derivative was measured at 546 nm according to the following reactions:



(R-OOH, hydroperoxides; R-O[·], alkoxy radicals; OH⁻, hydroxyl radical; A-NH₂, aromatic amine; (A-NH₂)^{·+}, pink aromatic derivative; ROO[·], peroxy radicals)

All results were expressed in conventional arbitrary units (Carr units). One Carr unit is equal to 0.08 mg/dL hydrogen peroxide. Within-run variations were <2.6% and between-run variations were <4.6%.

Results

Ex Vivo Electron Spin Resonance Spin Trapping Method in a Patient with Neurotrauma

Patient

The patient was a 55-year-old male who had a severe head injury caused by falling. Computed tomography (CT) imaging showed left acute subdural hematoma (Fig. 1A). Edaravone

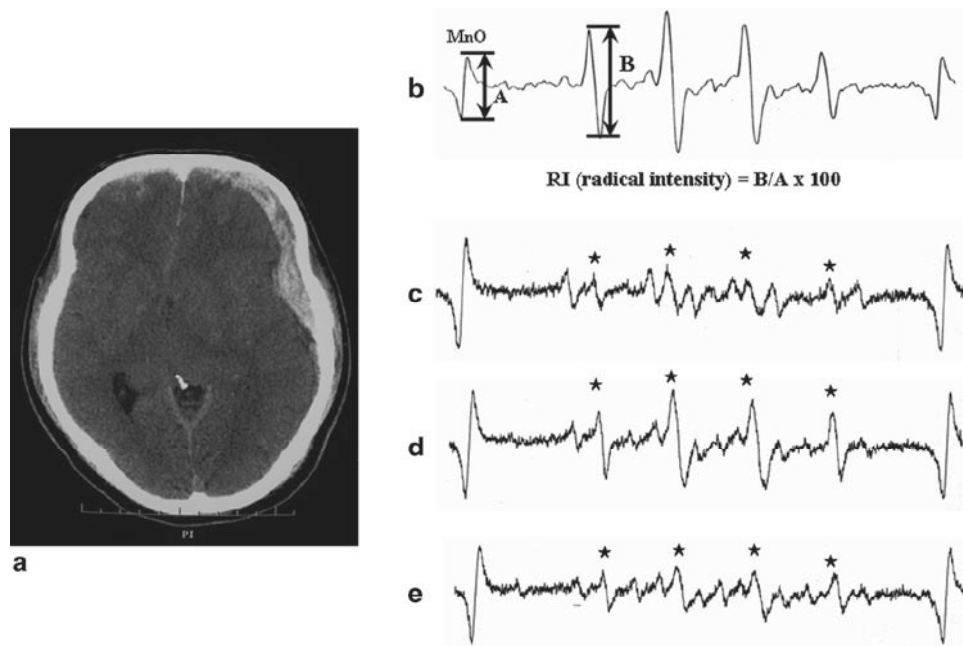


Fig. 1 Case: Computed tomography on admission (a) showing left acute subdural hematoma. Radical intensity was defined as the ratio of the signal intensity of the first peak of the alkoxy-DMPO spin adduct to that of MnO. B indicates signal intensity; A, marker intensity; and B/A \times 100, relative signal intensity. MnO was used as the external

standard (b). Free radical monitoring was performed on days 3 and 4, and 20 min after 30 mg of intravenous edaravone. On day 3, the alkoxy radical level of the blood sample collected from the internal jugular vein was measured (c). Alkoxy radical level increased on day 4 (d) and decreased after intravenous edaravone (E)

(60 mg/day) was administrated daily. Blood sampling and free radical monitoring were performed on days 3 and 4, and 20 min after 30 mg of intravenous edaravone. On day 3, radical intensity (RI) of the blood samples collected from the internal jugular vein was detectable (RI: 37.0) (Fig. 1C). RI increased on day 4 (RI: 66.7) and decreased 20 min after intravenous edaravone (RI: 45.8) (Fig. 1D and E). Administered edaravone scavenged 31.2% of RI in this patient.

Diacron-Reactive Oxygen Metabolites Test in a Patient with Cerebral Infarction

Patient

The patient was a 75-year-old female who complained of unconsciousness. CT imaging showed a large cerebral infarction in the posterior circulation area (Fig. 2a). Edaravone (60 mg/day), a free radical scavenger, was administrated daily. Blood sampling and oxidative stress monitoring were performed 1, 2, 3 and 4 days after ischemia. On day 1, the serum d-ROM level of the blood samples collected from the internal jugular vein was very high (394 Carr units), but gradually decreased (Fig. 2b). The normal level of d-ROM ranges between 250 and 300 Carr units.

Discussion

Neuroemergency Diseases and Free Radicals

Control of secondary brain damage plays an extremely important role in the treatment of neuroemergency diseases. One of the factors promoting secondary brain damage is excessive production of free radicals (3, 13). Free radicals produced in the injured brain are known to attack brain tissue and vascular

endothelial cells directly or indirectly and thereby promote brain damage and edema. Recently, some treatment methods aimed at controlling the production of free radicals in the acute phase have been developed; however, it has remained unclear how effective these treatment methods are in suppressing free radical production. Mihara et al. (14) have investigated the effect of brain hypothermia treatment on the suppression of free radicals in patients with traumatic brain injury using the ex vivo ESR method. They reported a gradual decrease in RI in blood collected from the internal jugular vein in patients with severe brain injury whose brain temperature was maintained at 33–35°C (n = 12): 74.5 ± 32.1 before brain hypothermia treatment, 64.9 ± 18.8 during the maintenance period, and 61.5 ± 20.7 after rewarming. In contrast, a gradual increase in RI was observed in blood collected from the radial artery, raising a concern about the systemic effect of brain hypothermia treatment (14).

In Japan, edaravone is an agent clinically applied for the treatment of cerebral infarction and acts as a free radical scavenger. It has recently been shown to directly eliminate hydroxyl radicals, nitric oxide (NO) and alkoxy radicals (7, 17), although its potential to scavenge free radicals has not been directly demonstrated to date in a clinical setting. Here we have measured the scavenging effect of edaravone on free radical production in patients with severe traumatic brain injury, and these effects have also been previously studied in rat models of traumatic brain injury using the ex-vivo ESR method (5, 7). In 17 patients with a traumatic brain injury, intravenous edaravone (30 mg/dL) has been shown to decrease the RI of alkoxy radicals in blood collected from the internal jugular vein by 24.6% (7).

As mentioned above, free radical monitoring using the ESR spin trapping method is useful for evaluating the efficacy of treatment for neuroemergency diseases involving free radicals and for designing treatment strategies. Methods for assessing oxidative stress within the body include measuring metabolites produced by oxidative stress and quantifying the antioxidant capacity of the body. In particular, 8-hydroxy-2'-deoxyguanosine (8-OHdG) has been well documented as a DNA oxidation marker. 8-OHdG is

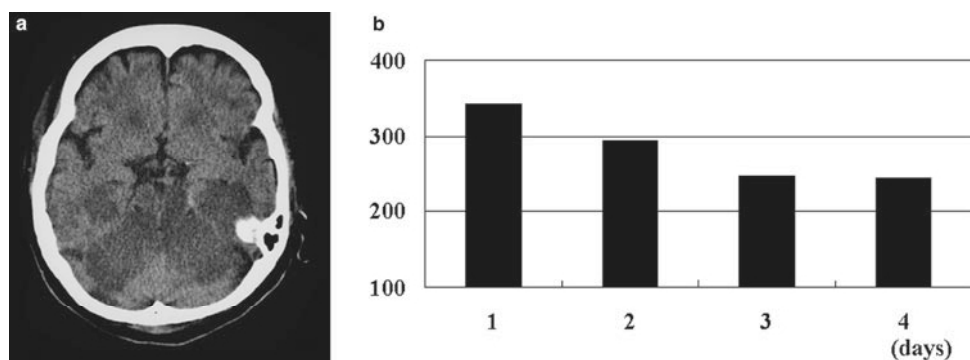


Fig. 2 Case: Computed tomography on admission (a) showing large cerebral infarction in the area of the basilar artery. Time courses of d-ROM level in (b). The d-ROM level of the blood sample collected from the jugular vein was high on day 1 and gradually decreased

expressed under various types of oxidative stress within the body and is therefore a highly sensitive marker of oxidative stress (11, 12, 19). With this marker, however, it is difficult to assess oxidative stress in particular organs and in certain types of disorders, and furthermore, a certain period of time is required to measure oxidative stress. For these reasons, this marker is not suitable for monitoring oxidative stress in many acute diseases in which the disease condition changes very rapidly.

On the other hand, the ESR spin trapping method allows for the easy measurement of free radicals in the blood and thereby makes it possible to capture free radicals produced at sites of injury by changing the site of blood collection. Moreover, this method only requires a very small amount of blood (100 μ L) for measurement and thus enables time-course monitoring. The radical species measured by this method is alkoxy radicals. Alkoxy radicals are derived from superoxide radicals, which are powerful reactive oxygen species (ROSs). Alkoxy radicals are produced by the Fenton reaction mediated by iron and are considered to be mainly involved in lipidperoxidation (7). As mentioned above, the brain contains a large amount of unsaturated fatty acids and iron, providing an environment favoring the production of alkoxy radicals. These facts also suggest that the ESR spin trapping method is suitable for assessing oxidative stress in brain damage. However, because ESR equipment is expensive and requires a special environment for installation, the method has not yet been adopted for clinical examinations. Thus, we have recently introduced FRAS, a simple oxidative stress analytical system. FRAS enables the measurement of oxidative stress by the d-ROM test, which is used for measuring the concentration of hydroperoxide in a biological substance and biological antioxidant potential. Measurement of oxidative stress by the d-ROM test using the cerebrospinal fluid of patients with neuroemergencies has also recently been performed (21). In our previous experimental study using the ESR spin trapping method and FRAS, both free radical production and hydroperoxide concentration in blood collected from the internal jugular vein increased after the induction of traumatic brain injury and were significantly higher in the non-treatment group than in the edaravone-treatment group (5). We are currently using the FRAS and ESR spin trapping methods for bedside free radical monitoring, as well as for estimating disease status and designing treatment strategies. Future studies will need to focus on the relationship between detailed conditions or classification of traumatic brain injury and oxidative stress, and between the level of free radical production and prognosis. Basic studies are also needed to identify the production sources of alkoxy radicals, to enable the analysis of the biological effects of these radicals.

Conflict of interest statement We declare that we have no conflict of interest.

Acknowledgements This project was mainly supported by a Showa University Grant-in-Aid for Innovative Collaborative Research Projects, a Special Research Grant-in-Aid for the Development of Characteristic Education, and a Grant-in-Aid for Scientific Research (C) 20592128, 2008 from the Japanese Ministry of Education, Culture, Sports, Science and Technology.

References

1. Alam ZI, Jenner A, Daniel SE, Lees AJ, Cairns N, Marsden CD, Jenner P (1997) Oxidative DNA damage in the Parkinsonian brain: An apparent selective increase in 8-hydroxy-guanine levels in substantia nigra. *J Neurochem* 69:1196–1203
2. Cernak I, O'Connor C, Vink R (2002) Inhibition of cyclooxygenase 2 by nimesulide improves cognitive outcome more than motor outcome following diffuse traumatic brain injury in rats. *Exp Brain Res* 147(2):193–199
3. Chan PH (1996) Role of oxidants in ischemic brain damage. *Stroke* 27:1124–1129
4. Dohi K, Ohtaki H, Inn R, Ikeda Y, Shioda HS, Aruga T (2003) Peroxynitrite and caspase-3 expression after ischemia/reperfusion in mouse cardiac arrest model. *Acta Neurochir Suppl* 86:87–91
5. Dohi K, Satoh K, Nakamachi T, Yofu S, Hiratsuka K, Nakamura S, Ohtaki H, Yoshikawa T, Shioda S, Aruga T (2007) Does edaravone (MCI-186) act as an antioxidant and a neuroprotector in experimental traumatic brain injury? *Antioxid Redox Signal* 9(2): 281–287
6. Dohi K, Satoh K, Ikeda Y, Ohtaki H, Shioda S, Aruga T (2003) Neuroprotective effect from ischemia and direct free radical scavenging activity of Choto-san (kampo medicine). *Acta Neurochir Suppl* 86:123–127
7. Dohi K, Satoh K, Mihara Y, Nakamura S, Miyake Y, Ohtaki H, Nakamachi T, Yoshikawa T, Shioda S, Aruga T (2006) Alkoxy radical-scavenging activity of edaravone in patients with traumatic brain injury. *J Neurotrauma* 23(11):1591–1599
8. Dohi K, Satoh K, Moriwaki H, Mihara Y, Miyake Y, Ohtaki H, Shioda S, Aruga T (2005) Levels of the alkoxy radical in patients with brain death. In: Shioda S, Hommma T (eds) *Breathing, feeding, and neuroprotection*. Springer, Tokyo
9. Dohi K, Satoh K, Ohtaki H, Shioda S, Miyake Y, Shindo M, Aruga T (2005) Elevated plasma levels of bilirubin in patients with neurotrauma reflect its pathophysiological role in free radical scavenging. *In Vivo* 19(5):855–860
10. Houkin K, Nakayama N, Kashiwada T (2003) Effect of a novel free radical scavenger, edaravone (MCI-186), on acute brain infarction. Randomized, placebo-controlled, double-blind study at multicenters. *Cerebrovasc Dis* 15(3):222–229
11. Jimbo H, Dohi K, Nakamura Y, Izumiyama H, Ikeda Y, Matsumoto K, Kushima M, Takaki A (2000) Fatal severe vasospasm due to rewarming following hypothermia – case report. *Neurol Med Chir* 40(9):463–466
12. Kasai H, Nishimura S (1984) Hydroxylation of deoxyguanosine at the C-8 position by ascorbic acid and other reducing agents. *Nucleic Acids Res* 12:2137–2145
13. Lewen A, Matz P, Chan PH (2000) Free radical pathways in CNS injury. *J Neurotrauma* 17:871–890
14. Mihara Y, Dohi K, Satoh K, Moriwaki H, Kuroki T, Miyake Y, Shioda S, Aruga T (2004) Mild brain hypothermia suppresses oxygen free radical in patients with neuroemergency: An ex vivo electron spin resonance study. In: Hayashi N, Bullock R, Dietrich DW, Maekawa T, Tamura A (eds) *Hypothermia for acute brain damage*. Springer, Tokyo

15. Ohtaki H, Funahashi H, Dohi K, Oguro T, Horai R, Asano M, Iwakura Y, Yin L, Matsunaga M, Goto N, Shioda S (2003) Suppression of oxidative neuronal damage after transient middle cerebral artery occlusion in mice lacking interleukin-1. *Neurosci Res* 45(3):313–324
16. Ohtaki H, Takeda T, Dohi K, Yofu S, Nakamachi T, Satoh K, Hiraizumi Y, Miyaoka H, Matsunaga M, Shioda S (2007) Increased mitochondrial DNA oxidative damage after transient middle cerebral artery occlusion in mice. *Neurosci Res* 58(4):349–355
17. Satoh K, Ikeda Y, Shioda S, Tobe T, Yoshikawa T (2002) Edaravone scavenges nitric oxide. *Redox Rep* 7(4):219–222
18. Smith MA, Rottkamp CA, Nunomura A, Raina AK, Perry G (2000) Oxidative stress in Alzheimer's disease. *Biochim Biophys Acta* 1502(1):139–144
19. Toyokuni S, Tanaka T, Hattori Y, Nishiyama Y, Yoshida A, Uchida K, Hiai H, Ochi H, Osawa T (1997) Quantitative immunohistochemical determination of 8-hydroxy-2'-deoxyguanosine by a monoclonal antibody N45.1: its application to ferric nitrilotriacetate-induced renal carcinogenesis model. *Lab Invest* 76(3):365–374.
20. Watanabe T, Yuki S, Egawa M, Nishi H (1994) Protective effects of MCI-186 on cerebral ischemia: possible involvement of free radical scavenging and antioxidant actions. *J Pharmacol Exp Ther* 268(3):1597–1604
21. Yamanaka G, Kawashima H, Suganami Y, Watanabe C, Watanabe Y, Miyajima T, Takekuma K, Oguchi S, Hoshika A (2006) Diagnostic and predictive value of CSF d-ROM level in influenza virus-associated encephalopathy. *J Neurol Sci* 15; 243(1–2):71–75

Cerebrolysin Attenuates Blood–Brain Barrier and Brain Pathology Following Whole Body Hyperthermia in the Rat

Hari Shanker Sharma, Sibilla Zimmermann-Meinzingen, Aruna Sharma, and Conrad E. Johanson

Abstract The possibility that Cerebrolysin, a mixture of several neurotrophic factors, has some neuroprotective effects on whole body hyperthermia (WBH) induced breakdown of the blood–brain barrier (BBB), blood–CSF barrier (BCSFB), brain edema formation and neuropathology were examined in a rat model. Rats subjected to a 4 h heat stress at 38°C in a biological oxygen demand (BOD) incubator exhibited profound increases in BBB and BCSFB permeability to Evans blue and radioiodine tracers compared to controls. Hippocampus, caudate nucleus, thalamus and hypothalamus exhibited pronounced increase in water content and brain pathology following 4 h heat stress. Pretreatment with Cerebrolysin (1, 2 or 5 mL/kg i.v.) 24 h before WBH significantly attenuated breakdown of the BBB or BCSFB and brain edema formation. This effect was dose dependent. Interestingly, the cell and tissue injury following WBH in cerebrolysin-treated groups were also considerably reduced. These novel observations suggest that cerebrolysin can attenuate WBH induced BBB and BCSFB damage resulting in neuroprotection.

Keywords Cerebrolysin • whole body hyperthermia • brain edema • blood–brain barrier • blood–CSF barrier • brain pathology • neuroprotection

H.S. Sharma (✉), and A. Sharma
Laboratory of Carebrovascular Research, Department of Surgical Science, Anesthesiology and Intensive Care Medicine, University Hospital, Frödingsgatan 12:28, Uppsala, SE-75421, Sweden and Neurochemistry Laboratory, Division of Neurotoxicology National Centre for Toxicological Research/FDA, Jefferson, AR, USA
e-mail: Sharma@surgsci.uu.se

S. Z. Meinzingen
EBEWE Neuro-Pharma, Mondseestrasse 11, Unterach A-4866, Austria

C. E. Johanson
Department of Clinical Neurosciences, Brown Medical School, Rhode Island Hospital, Providence, RI 02903, USA

Introduction

Heat stress either caused by external or internal factors affects brain functions particularly when the core body temperature reaches beyond 40.6°C in individuals (3, 6, 7, 11, 14). Thus, exposure to hot environment or exercise in high environmental heat, e.g., during summer months in many parts of the World as well as whole body hyperthermia (WBH) for tumor treatment is often associated with profound hyperthermia and brain damage (see (14, 16)). Likewise, bacterial or viral fever due to infection, intake of psychostimulant drugs, chemotherapy or radiotherapy for tumor treatment leads to high body temperature and abnormal brain functions (2, 17, 21).

Research carried out in our laboratory demonstrated that hyperthermia induced by external heat exposure or psychostimulants is associated with breakdown of the blood–brain barrier (BBB) to proteins in rats, which is instrumental in inducing brain edema formation and cell injury (19–22). Furthermore, pharmacological blockade of BBB disruption using several neurochemical receptor antagonists or synthesis inhibitor drugs attenuated brain edema formation and brain pathology (see (11, 12, 16)). This indicates that drugs reducing BBB damage in heat stress are able to thwart brain edema formation and cell injury.

Recent investigations in our laboratory clearly show that intracerebroventricular infusion of neurotrophins, i.e., brain derived neurotrophic factor (BDNF), glial cell line derived neurotrophic factor (GDNF) or insulin like growth factor-1 (IGF-1) reduces BBB dysfunction and brain pathology following WBH in a rat model (20). This suggests that neurotrophins are able to induce neuroprotection probably by attenuating the cellular stress response (24) or by replenishing an exhausted store of neurotrophic factors in the brain following hyperthermia (8–10, 13).

This investigation was focused on the possible neuroprotective efficacy of Cerebrolysin (Ebewe Neuro-Pharma, Austria), a mixture of several neurotrophic factors (13) on the pathophysiology of heat stress in our rat model.

Material and Methods

Animals

Experiments were carried out on male Wistar rats (age 9–12 weeks old, 150–200 g) maintained at standard laboratory conditions (room temperature $21 \pm 1^\circ\text{C}$) with 12 h dark and light schedule). Food and tap water were supplied ad libitum before the experiments.

Whole Body Hyperthermia

Animals were exposed to 4 h WBH at 38°C in a biological oxygen demand (BOD) incubator (relative humidity 45–47%, wind velocity 6–8 cm/s) (14). This experimental condition was approved by the local Institutional Ethics Committee and carried out according to the National Institute of Health guidelines for care of experimental animals. Rats kept at room temperature (21°C) were used as controls.

Cerebrolysin Treatment

Cerebrolysin (Ebewe Neuro-Pharma, Austria, 1, 2 or 5 mL/kg) was administered intravenously 24 h before heat stress through a jugular vein cannula implanted aseptically 1 week before experiment (14). The animals received a second dose of cerebrolysin 30 min before WBH.

Stress Symptoms and Physiological Variables

Rectal temperature and behavioral alterations, i.e., salivation and prostration in control or untreated and cerebrolysin treated rats subjected to WBH were recorded using standard procedures as described earlier (7, 11, 12). Gastric ulceration was examined at autopsy to assess individual stress reaction in animals (19).

BBB Permeability and Brain Edema

The BBB permeability to protein tracers, i.e., Evans blue and ^{131}I iodine normally bound to serum albumin when introduced into the systemic circulation was examined using standard procedures and expressing uptake of tracers as a volume distribution (brain/plasma) (19). After inspecting BBB leakage

to Evans blue albumin (EBA) visually, and analyzing the radioactivity in the brain tissues, the samples were placed in an oven maintained at 90°C for 72 h to obtain their dry weights. The difference between wet and dry weights was used to calculate brain water content as described earlier (17–19).

Histopathology

In a separate group of animals, immediately after WBH, the animals were anesthetized and perfused transcardially with saline followed by 4% paraformaldehyde (18, 22). After perfusion, the brains were removed and small pieces were embedded in paraffin and stained for hematoxylin and eosin or Nissl stain on 3- μm thick section as described earlier (20–22).

Statistical Treatment of Data

ANOVA followed by Dunnett's test for multiple group comparison was used using one control group to assess statistical significance of the data obtained. For semiquantitative evaluation of histological data, the non-parametric Chi Square test was used. A p-value of less than 0.05 was considered significant.

Results

Cerebrolysin Attenuates Hyperthermia and Stress Symptoms

Pretreatment with cerebrolysin markedly attenuated the WBH induced hyperthermia and behavioral symptoms (Table 1). Rats treated with cerebrolysin showed less salivation and prostration signs after WBH. The incidences of gastric ulcerations at post-mortem were also reduced by cerebrolysin treatment. This effect was most pronounced with the high dose of cerebrolysin (5 mL/Kg, i.v.) compared to lower doses of the compound.

Cerebrolysin Reduces BBB Permeability and Brain Edema Formation

Rats subjected to WBH showed profound increase in EBA and radioiodine leakage into the brain (Table 1). Cerebrolysin treatment in high doses significantly reduced these tracers' extravasation

Table 1 Effect of cerebrolysin on stress symptoms, BBB permeability, brain edema and cell changes following whole body hyperthermia

Parameters measured	Control n = 6	4 h WBH 38°C n = 8	Cerebrolysin + WBH n = 8
Rect T°C	36.8 ± 0.23	41.56 ± 0.34**	40.34 ± 0.22**a
Salivation	Nil	4+	3+
Prostration	Nil	4+	3+
Gastric haemorrhages	Nil	36 ± 6#	22 ± 6#b
Cortical EBA%	0.24 ± 0.08	1.90 ± 0.21**	0.89 ± 0.23**a
Cortical ¹³¹ Iodine%	0.35 ± 0.06	2.34 ± 0.34**	0.96 ± 0.44**a
CSF EBA%	0.18 ± 0.04	0.70 ± 0.11**	0.45 ± 0.08**a
CSF ¹³¹ Iodine%	0.25 ± 0.04	0.94 ± 0.14**	0.66 ± 0.06**a
Cortical water content%	76.34 ± 0.21	81.58 ± 0.43**	78.45 ± 0.21**a
Cortical cell damage	Nil	248 ± 23#	96 ± 18#b

Values are mean ± SD, EBA = Evans blue albumin, CSF = cerebrospinal fluid; ** = P < 0.01, from control, a = P < 0.05 from WBH, ANOVA followed by Dunnett’s test; # = P < 0.05 from control, b = P < 0.05 from WBH, Chi Square test.

in the brain after WBH (see Table 1; Fig. 1). Examination of regional BBB showed that cerebrolysin was able to significantly reduce the leakage of radioiodine in the cortex, hippocampus, thalamus and brain stem (see Fig. 1). WBH also induced marked breakdown of the blood–CSF-barrier (BCSFB, see Fig. 2). This is evident with blue staining of the ventricular walls and internal structures of the brain, i.e., dorsal surface of hippocampus, and caudate nucleus. Cerebrolysin treatment resulted in a considerably less staining of ventricular walls and internal structures of the brain.

Untreated rats exposed to WBH exhibited about 5% increases in brain water from the control value (Table 1). A significant reduction in brain water content is seen after WBH in animal treated with high dose of cerebrolysin compared to untreated rats following heat stress (Table 1). Cerebrolysin treatment also reduced regional brain edema formation significantly following WBH (Fig. 1).

Cerebrolysin Attenuates Brain Pathology

WBH markedly increased neuronal damage in several parts of the brain. Thus, nerve cells show profound swelling and distortion (Fig. 2) in rats subjected to WBH. These neuronal changes were considerably reduced by pre-treatment with cerebrolysin (Table 1, Fig. 2). This effect was most pronounced with high dose of cerebrolysin (5 mL/kg, i.v.).

Discussion

The present results are the first to show that cerebrolysin, a mixture of various neurotrophic factors is able to reduce WBH induced BBB dysfunction, brain edema formation and

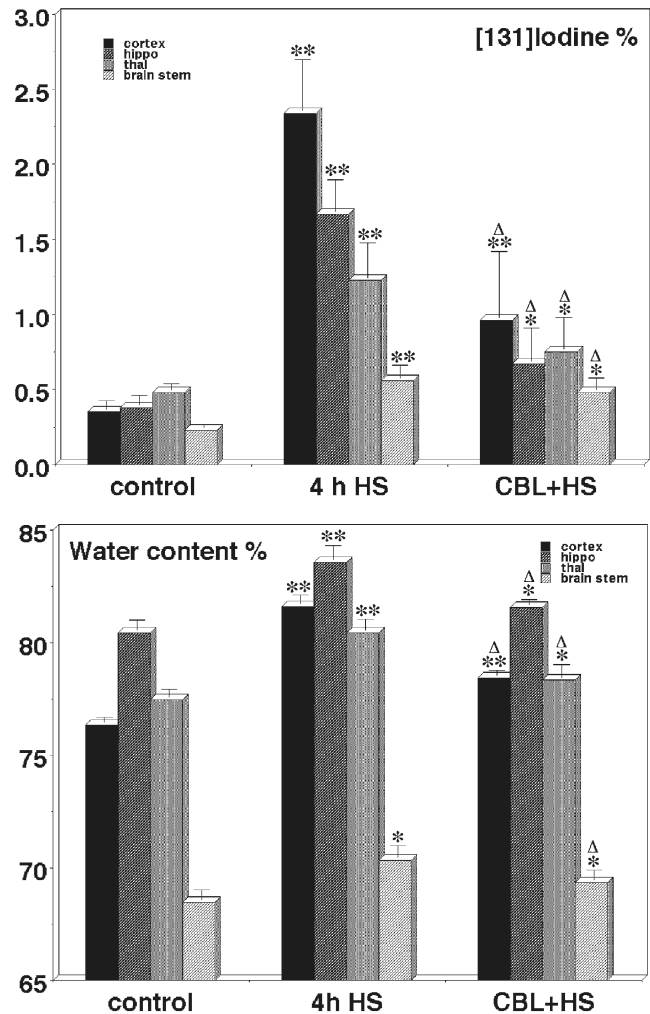


Fig. 1 Shows regional changes in the blood–brain barrier (rBBB) permeability (upper panel) and regional brain edema (lower panel) following 4 h WBH in rats and its modification with cerebrolysin. The most marked neuroprotective effects of cerebrolysin were seen in cerebral cortex, hippocampus and thalamus. Values are Mean ± SD, *P < 0.05, **P < 0.01 from controls, ΔP < 0.01 from 4 h WBH group, ANOVA followed by Dunnett’s test from one control group

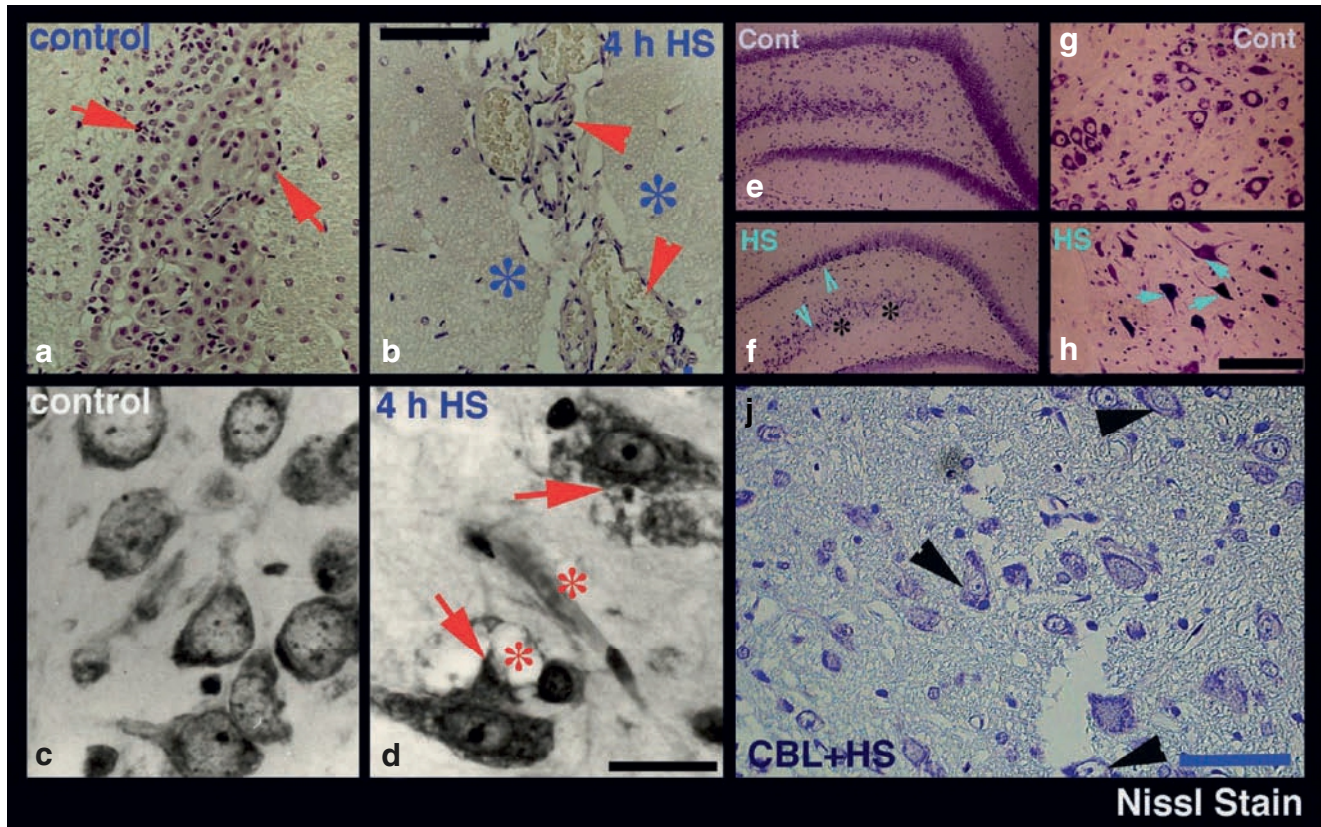


Fig. 2 Shows structural changes in choroidal epithelium, hippocampus and cerebral cortex following 4-h whole body hyperthermia at 38°C. Degeneration of choroidal epithelium (*arrowheads*) in the lateral ventricle of a 4-h heat stressed rat (**b**) is clearly seen compared to normal animal (**a**). Damage of nerve cells (*arrows*) and edema (*) is quite evident in the cerebral cortex (**d**), hippocampus CA4 region (**f**) and brain stem (**h**) in heat-stressed rat compared to controls (**c**, **e**, **g**). Marked neuroprotection by cerebrolysin in the cerebral cortical neurons following 4 h

WBH (**j**) compared to untreated heat stressed rat (**d**). Dark neurons with distortion of the cell body (*arrows*) were clearly evident in untreated heat stressed rat (**d**). A general sponginess and edematous swelling of the neuropil (*) were also seen (*arrows*, **d**). In cerebrolysin treated animal, WBH was not able to induce much damage in neurons (*arrowheads*) and the edematous swelling of the neuropil was largely absent (**j**). Paraffin sections 3 μ m, Nissl stain; Bar: **a**, **b**, **e**, **f** = 100 μ m, **c**, **d** = 30 μ m, **g**, **h** = 20 μ m, **j** = 40 μ m (modified after (6, 7, 12))

cell injury. Another important observation in this study is a remarkable reduction in hyperthermia and stress symptoms by cerebrolysin following WBH. This indicates that pretreatment of cerebrolysin attenuates WBH induced stress reaction. Obviously, a reduction in stress response by cerebrolysin is likely to least perturb the thermoregulatory system of animals following hyperthermia. Furthermore, cerebrolysin induced alterations of cytokines and other neurochemicals, for example serotonin or prostaglandins, could also influence body temperature regulation and heat stress symptoms (1, 3–5). Taken together, these observations suggest that cerebrolysin could be a possible candidate for the treatment of heat-related illnesses.

Several reports indicate that neurotrophins when administered in suitable combinations following brain or spinal cord injury reduced pathology and enhance repair mechanisms in the CNS (5–10, 13, 15). The probable mechanisms of neurotrophins-induced neuroprotection are unclear. However, it seems likely that trauma induces a decrease in the store of

neurotrophins within the cell, and thus replenishing of growth factors exogenously is likely to enhance neuroprotection following CNS insults (1, 3–5). It appears that heat stress may also deplete the stores of neurotrophins. Thus, exogenous supplements of neurotrophins markedly attenuated the brain pathology following hyperthermia (20). In the present study, cerebrolysin also significantly reduced brain pathology following WBH that is in line with this hypothesis.

Heat stress is associated with profound release of neurochemicals e.g., serotonin, prostaglandins, opioids, histamine and various neurotoxic cytokines (see (6, 7)). These neurochemical mediators are able to induce breakdown of the BBB (23–25) and enhance brain edema formation (6, 7, 12, 16). It is quite likely that cerebrolysin could modulate the action of these neurotransmitters and cytokines on cerebral microvessels leading to a significant reduction in the BBB breakdown (20–23). Obviously, a reduction in BBB permeability to large molecules, e.g. proteins will attenuate vasogenic edema formation (18, 22, 25). An

increased BBB dysfunction will allow leakage of several neurotoxic elements into the brain microenvironment leading to abnormal cell reaction and cell injury (22). Thus, blockade of BBB breakdown is associated with neuroprotection. Since cerebrolysin is able to attenuate BBB dysfunction in WBH, it is quite likely that this reduction in BBB leads to less edema formation and subsequently milder cell changes seen in drug-treated animals compared to untreated stressed groups.

Taken together, our results strongly indicate that cerebrolysin when administered before WBH is capable of inducing pronounced neuroprotection in animals and thus opens up the possibility to examine the role of cerebrolysin as a potential treatment option of heat-related disorders in future. This is a subject that is currently being examined in our laboratory.

Conflict of interest statement We have no conflict of interest with any organizations mentioned below.

Acknowledgements This study is supported by Grants from Swedish Medical Research Council, Stockholm (HSS 02710); National Institute of Health (R01 AG 027910, CEJ), USA; Alexander von Humboldt Foundation (HSS), Germany; Astra Zeneca Mölndal, Sweden (HSS); Society for the study on Neuroplasticity and Neuroprotection (SSNN), Romania and Ebewe Pharma, Austria (HSS). Technical assistance of Kärstin Flink, Ingmarie Olsson, Margareta Butler, Inga Hörte, Mari-Anne Carlsson and Ulla Nilsson as well as the secretarial assistance of Angela Ludwig and Nancy Johanson are highly appreciated.

References

- Guo S, Kim WJ, Lok J, Lee SR, Besancon E, Luo BH, Stins MF, Wang X, Dedhar S, Lo EH (2008) Neuroprotection via matrix-trophic coupling between cerebral endothelial cells and neurons. *Proc Natl Acad Sci USA*. May 27;105(21):7582–7587
- Kiyatkin EA, Brown PL, Sharma HS (2007) Brain edema and breakdown of the blood–brain barrier during methamphetamine intoxication: critical role of brain hyperthermia. *Eur J Neurosci*. Sep 26(5):1242–1253
- Milton AS (1989) Thermoregulatory actions of eicosanoids in the central nervous system with particular regard to the pathogenesis of fever. *Ann NY Acad Sci* 559:392–410. Review
- Mitrasinovic OM, Grattan A, Robinson CC, Lapustea NB, Poon C, Ryan H, Phong C, Murphy GM Jr. (2005) Microglia overexpressing the macrophage colony-stimulating factor receptor are neuroprotective in a microglial–hippocampal organotypic coculture system. *J Neurosci*. Apr 27; 25(17):4442–4451
- Schwab ME, Bartholdi D (1996) Degeneration and regeneration of axons in the lesioned spinal cord. *Physiol Rev*. Apr; 76(2):319–370. Review
- Sharma HS (2004) Blood–brain and spinal cord barriers in stress. In: Sharma HS, Westman J (eds) *The blood–spinal cord and brain barriers in health and disease*. Elsevier Academic, San Diego, pp 231–298
- Sharma H S. (1999) Pathophysiology of blood–brain barrier, brain edema and cell injury following hyperthermia: New role of heat shock protein, nitric oxide and carbon monoxide. an experimental study in the rat using light and electron microscopy, *Acta Universitatis Upsaliensis*. May 15; 830:1–94
- Sharma HS (2005) Pathophysiology of blood–spinal cord barrier in traumatic injury and repair. *Curr Pharm Des* 11(11):1353–1389. Review
- Sharma HS (2003) Neurotrophic factors attenuate microvascular permeability disturbances and axonal injury following trauma to the rat spinal cord. *Acta Neurochir Suppl* 86:383–388
- Sharma HS (2006) Post-traumatic application of brain-derived neurotrophic factor and glia-derived neurotrophic factor on the rat spinal cord enhances neuroprotection and improves motor function. *Acta Neurochir Suppl* 96:329–334
- Sharma HS (2006) Hyperthermia induced brain oedema: current status and future perspectives. *Indian J Med Res*. May 123(5):629–652. Review
- Sharma HS (2006) Hyperthermia influences excitatory and inhibitory amino acid neurotransmitters in the central nervous system. An experimental study in the rat using behavioural, biochemical, pharmacological, and morphological approaches. *J Neural Transm*. Apr 113(4):497–519
- Sharma HS (2007) Neurotrophic factors in combination: a possible new therapeutic strategy to influence pathophysiology of spinal cord injury and repair mechanisms. *Curr Pharm Des* 13(18):1841–1874. Review
- Sharma HS (2007) Methods to produce hyperthermia-induced brain dysfunction. *Prog Brain Res* 162:173–99. Review
- Sharma HS (2007) A select combination of neurotrophins enhances neuroprotection and functional recovery following spinal cord injury. *Ann NY Acad Sci* Dec 1122:95–111
- Sharma HS, Hoopes PJ (2003) Hyperthermia induced pathophysiology of the central nervous system. *Int J Hyperthermia*. May–Jun 19(3):325–354. Review
- Sharma HS, Ali SF (2006) Alterations in blood–brain barrier function by morphine and methamphetamine. *Ann NY Acad Sci*. Aug 1074:198–224
- Sharma HS, Cervós-Navarro J (1990) Brain oedema and cellular changes induced by acute heat stress in young rats. *Acta Neurochir Suppl (Wien)* 51:383–386
- Sharma HS, Dey PK (1986) Probable involvement of 5-hydroxytryptamine in increased permeability of blood–brain barrier under heat stress in young rats. *Neuropharmacology*. Feb 25(2): 161–167
- Sharma HS, Johanson CE (2007) Intracerebroventricularly administered neurotrophins attenuate blood cerebrospinal fluid barrier breakdown and brain pathology following whole-body hyperthermia: an experimental study in the rat using biochemical and morphological approaches. *Ann NY Acad Sci*. Dec 1122:112–129
- Sharma HS, Westman J (1998) Brain functions in hot environment, progress in brain research, 115. Elsevier, Amsterdam, pp 1–516
- Sharma HS, Westman J, Nyberg F (1998) Pathophysiology of brain edema and cell changes following hyperthermic brain injury. *Prog Brain Res* 115:351–412. Review
- Wahl M, Unterberg A, Baethmann A, Schilling L (1988) Mediators of blood–brain barrier dysfunction and formation of vasogenic brain edema. *J Cereb Blood Flow Metab*. Oct 8(5):621–634. Review
- Winkler T, Sharma HS, Stålberg E, Badgaiyan RD (2000) Neurotrophic factors attenuate alterations in spinal cord evoked potentials and edema formation following trauma to the rat spinal cord. *Acta Neurochir Suppl* 76:291–296
- Winkler T, Sharma HS, Stålberg E, Westman J (1998) Spinal cord bioelectrical activity, edema and cell injury following a focal trauma to the spinal cord. An experimental study using pharmacological and morphological approach. In: Stålberg E, Sharma HS, Olsson Y (eds) *Spinal cord monitoring*. Springer Wien, New York, pp 281–348

Chronic Hypertension Aggravates Heat Stress-Induced Brain Damage: Possible Neuroprotection by Cerebrolysin

Dafin Fior Muresanu, Sibilla Zimmermann-Meinzingen, and Hari Shanker Sharma

Abstract Whole body hyperthermia (WBH) aggravates brain edema formation and cell damage in chronic hypertensive rats compared with normotensive animals. In this investigation, we examined the influence of cerebrolysin on WBH-induced edema formation and brain pathology in hypertensive and normotensive rats. Rats subjected to 4 h WBH at 38°C in a biological oxygen demand (BOD) incubator showed breakdown of the blood–brain barrier (BBB), reduced cerebral blood flow (CBF), edema formation and cell injuries in several parts of the brain. These effects were further aggravated in chronic hypertensive rats (two-kidney one clip model (2K1C), for 4 weeks) subjected to WBH. Pretreatment with cerebrolysin (5 mL/kg, 24 h and 30 min before heat stress) markedly attenuated the BBB dysfunction and brain pathology in normal animals. However, in hypertensive animals, a high dose of cerebrolysin (10 mL/kg, 24 h and 30 min before heat stress) was needed to attenuate WBH-induced BBB dysfunction and brain pathology. These observations indicate that heat stress could affect differently in normal and hypertensive conditions. Furthermore, our results suggest that patients suffering from various chronic cardiovascular diseases may respond differently to hyperthermia and to neuroprotective drugs, e.g., cerebrolysin not reported earlier.

Keywords Cerebrolysin • whole body hyperthermia • hypertensive rats • brain edema • brain pathology • cerebral blood flow

Introduction

Heat stress is a serious clinical disorder that induces profound brain dysfunction and death in human populations (6–9). After sudden heat exposure, death can occur without any prior symptoms (11,14). Thus, further studies are required to understand the basic pathophysiology of heat-induced brain damage.

In recent years, several thousand people have died in Europe during summer months; although these deaths were linked to heat exposure, the exact mechanism underlying them remains unexplored (16–18). Heat stress has been suggested as the third largest cause of human mortality after cardiovascular and traumatic injuries of the CNS (see (8–11)). However, it is still uncertain whether heat exposure causes greater damage in persons suffering from cardiovascular or metabolic abnormalities (9).

Therefore, we investigated the possible effects of heat stress in populations suffering from chronic hypertension (2) or diabetes mellitus (3), the common diseases affecting many people worldwide. We have also shown that chronic hypertensive rats subjected to WBH exhibited exacerbation of BBB dysfunction, brain edema and brain pathology (2) and diabetic rats also showed marked aggravation of brain damage following heat stress (3). These observations suggest that cardiovascular or endocrine diseases can exacerbate the effects of heat in humans. It is also possible that drug effects are modified in humans suffering from cardiovascular and endocrine diseases.

In the present study, we examined the effects of the neuroprotective drug Cerebrolysin (see Ref. 20 in this volume) in hypertensive rats subjected to WBH as compared to normotensive rats.

H.S. Sharma (✉)

Laboratory of Cerebrovascular Research, Department of Surgical Science, Anaesthesiology and Intensive Care Medicine, University Hospital, Frödingsgatan 12:28, Uppsala, SE-75421, Sweden
e-mail: Sharma@surgsci.uu.se

D.F. Muresanu

Department of Neurology, University of Medicine and Pharmacy “Iuliu Hatieganu” Cluj-Napoca, Romania

S. Zimmermann-Meinzingen

EBEWE Neuro-Pharma, Mondseestrasse 11, Unterach A-4866, Austria

Materials and Methods

Animals

Experiments were carried out on Male Wistar rats (150–200 g) housed at controlled room temperature $21 \pm 1^\circ\text{C}$ with a 12 h light and 12 h dark schedule. Tap water and food were supplied ad libitum before the experiments. All experiments were carried out according to NIH guidelines for the care of experimental animals and approved by local Institutional Ethics Committee.

Chronic Hypertension

A two-kidney one clip (2K1C) model was used to induce chronic hypertension (2). Under Equithesin anesthesia (0.3 mL/100 g, i.p.), a U-shaped silver clip (0.23–0.25-mm internal diameter) was placed around the left renal artery and pressed slightly to induce partial occlusion of renal perfusion (2). After 4–6 weeks, these animals developed hypertension (40–50 torr greater than their basal value) (see (2)). Normal animals were used as controls.

Cerebrolysin Treatment

Cerebrolysin (Ebewe Neuro-Pharma, Austria) was administered intravenously (5 or 10 mL/kg) through a catheter implanted into the right jugular vein (5) 24 h before heat stress. A second dose of cerebrolysin was also administered 30 min before the onset of heat exposure (see Ref. 20 in this volume).

Whole Body Hyperthermia

Normal or hypertensive rats were placed in a biological oxygen demand (BOD) incubator maintained at 38°C (relative humidity 45–47%; wind velocity 18–22 cm/s) for 4 h (10–13). Control groups of normotensive and hypertensive rats were kept at room temperature (6).

Stress Symptoms and Physiological Variables

Rectal temperature, salivation, and prostration were monitored every hour during the 4 h period of heat exposure (6,10). The mean arterial blood pressure (MABP), arterial

pH and blood gases were analyzed using a radiometer apparatus (Copenhagen, Denmark) (see (5,10)).

Cognitive and Motor Functions

Rotarod performance (at 16 rpm for 120 s) and grid walking (elevated wire mesh, 1 mm^2 , at 30° for 60 s) tests were used to determine cognitive and motor functions after heat stress using standard procedures (8).

Blood–Brain Barrier Permeability

BBB permeability was measured using Evans blue and ^{131}I iodine tracers that bind to serum albumin when administered intravenously (4). These tracers were administered together at the end of heat exposure into the right jugular vein (Evans blue 0.3 mL/100 g and radioiodine $10\ \mu\text{Ci}/100\text{g}$) and allowed to circulate for 5 min (4–6). Animals were then perfused transcardially with saline followed by 4% paraformaldehyde and their brains were removed and analyzed for Evans blue staining and iodine radioactivity as described earlier (see (5)).

Cerebral Blood Flow

The cerebral blood flow (CNF) was measured using ^{125}I iodine-labeled carbonized microspheres as described previously (5,8).

Brain Edema

Brain edema was determined using brain water content calculated from differences between the wet and dry weights of the samples (12).

Brain Pathology

Neuronal damage following heat stress in normotensive and hypertensive rats and the effects of cerebrolysin treatment were examined using hematoxylin and eosin staining of $3\ \mu\text{m}$ -thick paraffin sections using standard procedures (8,10,12).

Statistical Analysis

A non-parametric Chi-Square test was used to evaluate significance of differences between control and experimental groups. $p < 0.05$ was considered significant.

Results

Stress Symptoms and Physiological Variables in Heat Stress

2K1C rats showed profound hypertension (150 torr) after 6 weeks compared with the normal group (102 torr) (Table 1). When subjected to 4 h heat stress, hypertensive rats showed profound hyperthermia compared with normotensive animals (Table 1) without exhibiting any differences in salivation and prostration (Table 1). The magnitude of hypotension was greater in hypertensive rats (-62 torr) as compared to normotensive animals (-23 torr). No marked differences in arterial pH or blood gases were seen between hypertensive and normotensive rats after heat stress (Table 1). Pretreatment with cerebrolysin (5 or 10 mL/kg) significantly attenuated heat stress-induced hyperthermia and behavioral symptoms in normotensive rats as compared to hypertensive animals (Table 1). No significant differences in hypotension, blood gases or pH were seen in cerebrolysin-treated normotensive or hypertensive animals following heat stress (Table 1). A mild but significant decrease in gastric ulceration by cere-

brolysin was seen in heat-stressed animals; this was more prominent in normotensive rats (Table 1).

Cognitive Function in Heat Stress

Hypertensive rats subjected to heat stress showed marked deficits on rotarod performance and grid walking tests as well as increased placement errors compared with normotensive animals (Table 1). Cerebrolysin (5 mL/kg) treatment significantly improved rotarod and grid walking performances and reduced placement errors after heat stress. These effects were far superior in normotensive animals than in hypertensive rats (Table 1). Interestingly, high doses of cerebrolysin (10 mL/kg) markedly improved the cognitive function of hypertensive animals quite comparable to that seen in normotensive animals which received only 5 mL/kg of cerebrolysin (results not shown).

BBB Permeability and CBF in Heat Stress

Hypertensive animals showed markedly increased permeability of the BBB to Evans blue and radioiodine, and exhibited slightly higher CBF at room temperature as compared to normal animals (Table 2). When hypertensive animals were subjected to heat stress, they showed significantly higher BBB permeability to Evans blue and radioiodine as compared to the normotensive groups (Table 2). The reduction of CBF in hypertensive rats following heat exposure

Table 1 Effect of hyperthermia on stress symptoms and cognitive dysfunction in control, sham and hypertensive rats and their modification with cerebrolysin treatment

Type of experiment	Control	4 h Heat stress (HS) at 38°C in BOD incubator			
		Sham n = 5	2K1C n = 6	CBL + Sham n = 5	CBL + 2K1C n = 6
Stress symptoms					
Rect T°C	37.0 ± 0.23	41.23 ± 0.33**	41.76 ± 0.21**	40.06 ± 0.11**a	40.18 ± 0.13**a
Salivation	Nil	++++	Nil	+++	++++
Prostration	Nil	++++	nil	+++	++++
Gastric ulceration	Nil	64 ± 8**	84 ± 4**	50 ± 8	62 ± 9
Cognitive functions					
Rotarod (performance sec)	120	62 ± 6**	56 ± 9*	88 ± 6**a	84 ± 4**a
Grid walking (total steps 60 s)	40	16 ± 8**	12 ± 8**	28 ± 4**a	24 ± 6**a
Placement errors (% in 60 s)	Nil	32 ± 6**	36 ± 4*	20 ± 4**a	22 ± 3**a

Values are Mean ± SD, CBL = cerebrolysin; * = $P < 0.05$, ** $P < 0.01$, compared from control, a = $P < 0.05$, compared from 4 h heat stress on Sham group, Chi-Square test

Table 2 Effect of hypertrehmia on physiological variables, BBB permeability, cerebral blood flow and Brain edema in control, sham or hypertensive rats and their modification with cerebrolysin treatment

Type of experiment	Rect T°C	Systolic BP (torr)	Arterial (pH)	PaO2 (torr)	PaCO2 (torr)	BBB leakage EBA (mg %)	¹³¹ Iodine %f	CBF (mL/g/min)	Brain Edema Water	%
At room temperature										
Control	36.86 ± 0.13	98 ± 4	7.4 ± 0.2	80.23 ± 0.21	33.35 ± 0.32	0.24 ± 0.04	0.38 ± 0.08	1.12 ± 0.06	76.34 ± 0.12	nil
Sham	37.08 ± 0.10	102 ± 5	7.4 ± 0.3	80.67 ± 0.34	34.21 ± 0.12	0.28 ± 0.10	0.40 ± 0.10	1.18 ± 0.10	76.69 ± 0.21	-
2K1C	37.06 ± 0.14	150 ± 8**	7.3 ± 0.2	81.56 ± 0.38	34.56 ± 0.67	0.37 ± 0.12*	0.52 ± 0.12*	1.21 ± 0.10*	76.76 ± 0.12*	<+1
CBL + Sham	37.08 ± 0.27	108 ± 2	7.4 ± 0.4	80.25 ± 0.16	33.22 ± 0.18	0.22 ± 0.08	0.28 ± 0.04	1.16 ± 0.04	75.94 ± 0.13	-
CBL + 2K1C	37.04 ± 0.14	144 ± 6	7.3 ± 0.4	80.37 ± 0.34	33.63 ± 0.11	0.30 ± 0.07	0.44 ± 0.08	1.19 ± 0.04	76.15 ± 0.12	-
4 h heat stress at 38° C										
Sham	41.56 ± 0.23**	75 ± 4	7.3 ± 0.2	81.78 ± 0.33	35.23 ± 0.41	1.89 ± 0.23**	2.67 ± 0.14**	0.78 ± 0.09**	81.34 ± 0.23**	+21
2K1C	41.88 ± 0.18**	88 ± 6*	7.3 ± 0.5	81.89 ± 0.23	34.67 ± 0.44	2.56 ± 0.23***	2.98 ± 0.12***	0.86 ± 0.08***	82.56 ± 0.13***	+25
CBL + Sham	40.38 ± 0.20***	74 ± 4*	7.3 ± 0.4	81.46 ± 0.44	34.56 ± 0.31	0.82 ± 0.14***	0.98 ± 0.11***	1.06 ± 0.06***	78.90 ± 0.10***	+8
CBL + 2K1C	40.61 ± 0.06***	84 ± 6*	7.3 ± 0.7	81.56 ± 0.40	34.64 ± 0.31	1.14 ± 0.14***	1.14 ± 0.13***	0.94 ± 0.05***	80.16 ± 0.23***	+16

CBL = cerebrolysin, ** P < 0.01, Student's unpaired t-test. Values are mean ± SD; CBL = cerebrolysin; * P < 0.05; ** P < 0.01, compared from control; a = P < 0.05 compared from heat stress; Student's unpaired t-test; %f = denotes volume swelling, about 1% increase in water content represents >4% increase in volume swelling (4)

was also greater than in normotensive animals (Table 2). Cerebrolysin treatment (5 mL/kg) markedly attenuated the decreased CBF and increased BBB permeability following heat stress (Table 2) that was most prominent in normotensive animals (Table 2). However, a higher dose of cerebrolysin (10 mL/kg) was able to considerably reduce the BBB dysfunction and CBF changes in hypertensive rats in heat stress (Table 2).

Brain Edema in Heat Stress

Hypertensive rats showed a mild but significant increase in brain water content at room temperature compared to controls (Table 2). When these animals were subjected to heat stress, they exhibited more brain edema formation and volume swelling as compared to normotensive animals (Table 2). Pretreatment with cerebrolysin (5 mL/kg) markedly reduced brain edema formation and volume swelling after heat stress that was most notable in normotensive animals (Table 2). However, pretreatment with 10 mL/kg cerebrolysin in the hypertensive group effectively reduced brain edema formation and volume swelling caused by heat stress (results not shown).

Brain Pathology in Heat Stress

Hypertensive animals at room temperature showed mild neuronal damage (results not shown). These neuronal changes were further aggravated following heat stress as compared to normotensive animals (Fig. 1, Table 2). Pretreatment with cerebrolysin (5 mL/kg) significantly reduced neuronal damage after heat stress in normotensive animals. However, 10 mL/kg cerebrolysin was needed to effectively reduce neuronal damage in hypertensive rats after heat stress (Table 2).

Discussion

The present results show that cerebrovascular reactions following heat stress were aggravated in hypertensive animals compared to the normotensive group. This suggests that hypertensive populations will suffer more from heat stress-induced brain dysfunction than normal healthy individuals following hyperthermia. These findings are in accordance with the increased stress response observed in hypertensive animals in heat stress as compared to normal animals. It

appears that hypertension induces alterations in the biochemical, physical and biological functions of microvessels that could play important roles in the hypersensitivity to heat in hypertensive animals (see 2).

Heat induced different biological reactions of microvessels to stress in hypertensive animals as compared to normotensive rats are further evident after cerebrolysin treatment (1). The neuroprotective effects of cerebrolysin in heat stress were most prominent in normotensive animals. This is apparent from the facts that in hypertensive rats, almost double the dose is required for similar effects. This suggests that hypertensive subjects might be less sensitive to drugs than normal healthy individuals. In clinical situations, drug therapy may therefore require adjustment for treatment of hypertensive patients suffering from various neurological diseases.

The basic mechanisms behind the different drug dosage requirements in normotensive and hypertensive animals are unclear. However, receptor functions and release of neurochemicals in stressful situations could be different in normotensive and hypertensive individuals (see (1,2)). Hypertension alone increases BBB permeability to proteins and leads to edema formation (1,4,9), as seen in the present investigation. Additional stress can further aggravate this situation, leading to worsening of brain damage. Thus, the hypertensive state itself may alter the physiological and pharmacological responses of cerebral microvessels (1,4,18,19) that could be instrumental for different responses to drugs or stress.

The increased edema formation in hypertensive rats following heat stress might have been due to enhanced tracer transfer into the brain compartments as compared to normal animals (15–18). Different patterns of neurochemical release in hypertensive rats following heat exposure might also account for enhanced sensitivity of cerebral microvessels, leading to aggravation of neurovascular responses (2,15,16,19). Hypertension itself results in the release of several neurotoxic cytokines and other vasomotor agents into the circulation (1,4). Additional heat stress might further worsen this situation, causing more damage in the hypertensive brain compared with normal controls (see (17)). The increased neuronal dysfunction, edema formation and brain damage seen in hypertensive rats following heat stress are in line with this hypothesis. It is likely that a large dose of cerebrolysin will be required to counteract the effects of cytokines and other neurotoxic agents in hypertensive animals. However, additional studies are required to evaluate this hypothesis.

Taken together, our results suggest that hypertensive animals are more susceptible to heat-induced brain damage, and that cerebrolysin exerts powerful neuroprotective effects against heat stress in normotensive animals and with higher doses similar neuroprotection could be achieved in, hypertensive animals.

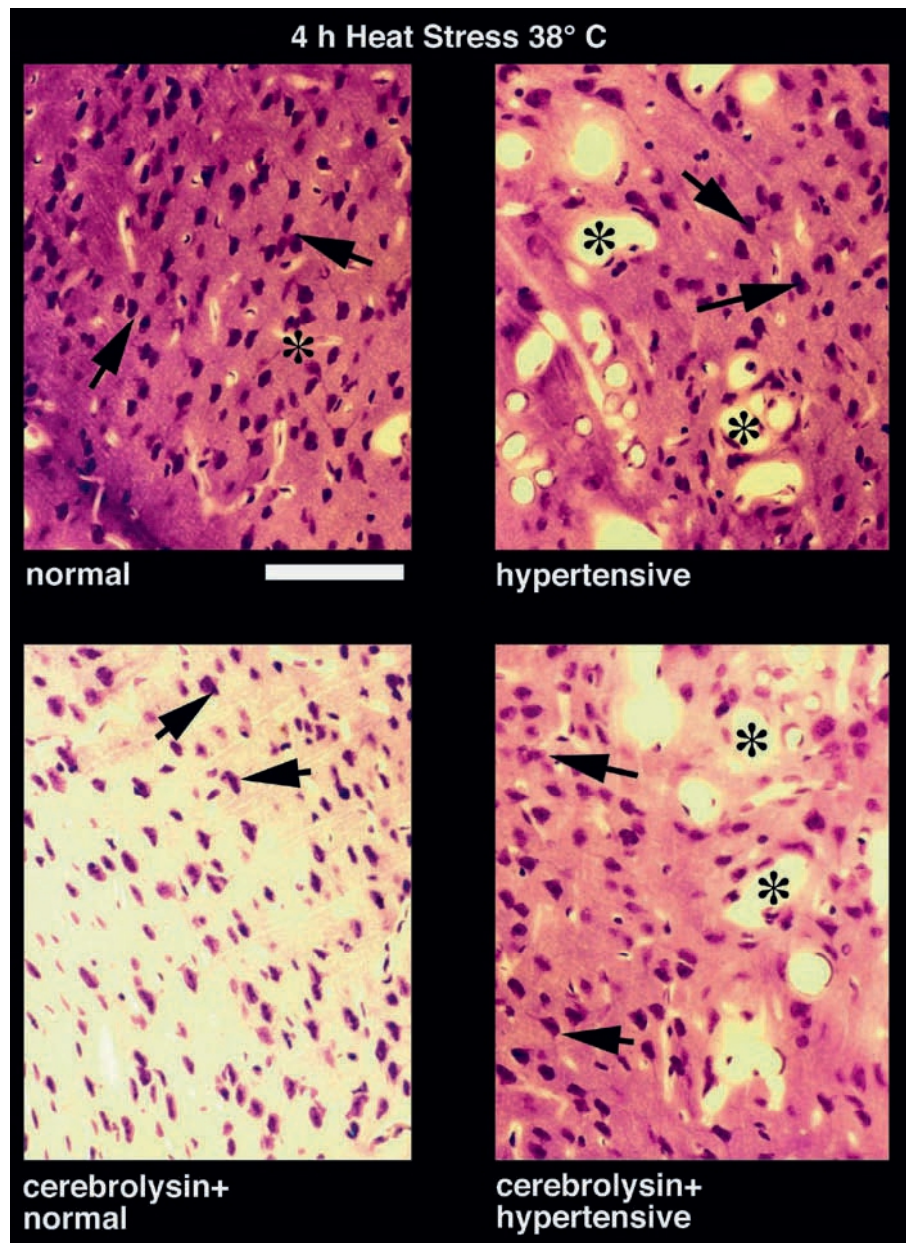


Fig. 1 Cortical nerve cell damage following whole body hyperthermia (WBH) in normal or hypertensive rats (*upper panel*) and its modulation with cerebrolysin pretreatment (*lower panel*). Hypertensive rats show much more damage to the neuropil and nerve cells after WBH as compared to normal animals. Damage to nerve cells (*arrows*) and general sponginess are most prominent in untreated hypertensive rat after WBH. Cerebrolysin treatment effectively attenuated the nerve cell damage; this effect was more prominent in normal rats as compared to hypertensive rats subjected to WBH. Bar: 20 μ m

Conflict of interest statement We have no conflict of interest with any organizations mentioned below.

Acknowledgements This study was supported by Grants from Swedish Medical Research Council, Stockholm (HSS 0217); Ebewe Neuro-Pharma, Austria (HSS); Alexander von Humboldt Foundation (HSS), Germany; Astra Zeneca Mölndal, Sweden (HSS); Society for study on Neuroplasticity and Neuroprotection (SSNN), Romania. We appreciate the technical assistance of Kärstin Flink, Ingmarie Olsson, Margareta Butler, Inga Hörte, Mari-Anne Carlsson and Ulla Nilsson as well as the secretarial assistance of Angela Ludwig and Siv Utterberg.

References

- Johansson BB (1983) The blood–brain barrier and cerebral blood flow in acute hypertension. *Acta Med Scand Suppl* 678:107–112
- Muresanu DF, Sharma HS (2007) Chronic hypertension aggravates heat stress induced cognitive dysfunction and brain pathology: an experimental study in the rat, using growth hormone therapy for possible neuroprotection. *Ann N Y Acad Sci*. Dec 1122:1–22
- Muresanu DF, Sharma A, Sharma HS (2008) Diabetes aggravates heat stress induced blood–brain barrier breakdown, edema formation and brain pathology. Possible neuroprotection with growth hormone. *Ann NY Acad Sci* (in press).

4. Rapoport SI (1976) Blood-brain barrier in physiology & medicine. Raven, New York
5. Sharma HS (1987) Effect of captopril (a converting enzyme inhibitor) on blood-brain barrier permeability and cerebral blood flow in normotensive rats. *Neuropharmacology*. Jan 26(1):85-92
6. Sharma HS (1999) Pathophysiology of blood-brain barrier, brain edema and cell injury following hyperthermia: new role of heat shock protein, nitric oxide and carbon monoxide. An experimental study in the rat using light and electron microscopy, *Acta Universitatis Upsaliensis* May 15;830:1-94
7. Sharma HS (2006) Hyperthermia induced brain oedema: current status and future perspectives. *Indian J Med Res*. May 123(5):629-652. Review
8. Sharma HS (2006) Hyperthermia influences excitatory and inhibitory amino acid neurotransmitters in the central nervous system. An experimental study in the rat using behavioural, biochemical, pharmacological, and morphological approaches. *J Neural Transm*. Apr 113(4):497-519
9. Sharma HS (2007) Neurobiology of hyperthermia. *Prog Brain Res* 162:1-617
10. Sharma HS (2007) Methods to produce hyperthermia-induced brain dysfunction. *Prog Brain Res* 162:173-199. Review
11. Sharma HS (2005) Heat-related deaths are largely due to brain damage. *Indian J Med Res* May 121(5):621-623
12. Sharma HS, Cervós-Navarro J (1990) Brain oedema and cellular changes induced by acute heat stress in young rats. *Acta Neurochir Suppl (Wien)* 51:383-386
13. Sharma HS, Dey PK (1986) Probable involvement of 5-hydroxytryptamine in increased permeability of blood-brain barrier under heat stress in young rats. *Neuropharmacology*. Feb; 25(2):161-167
14. Sharma HS, Hoopes PJ. (2003) Hyperthermia induced pathophysiology of the central nervous system. *Int J Hyperthermia*. May-Jun 19(3):325-354. Review
15. Sharma HS, Johanson CE (2007) Intracerebroventricularly administered neurotrophins attenuate blood cerebrospinal fluid barrier breakdown and brain pathology following whole-body hyperthermia: an experimental study in the rat using biochemical and morphological approaches. *Ann NY Acad Sci* Dec 1122:112-129
16. Sharma HS, Johanson CE (2007) Blood-cerebrospinal fluid barrier in hyperthermia. *Prog Brain Res* 162:459-478. Review
17. Sharma HS, Sharma A (2007) Nanoparticles aggravate heat stress induced cognitive deficits, blood-brain barrier disruption, edema formation and brain pathology. *Prog Brain Res* 162:245-273. Review
18. Sharma HS, Westman J, Nyberg F (1998) Pathophysiology of brain edema and cell changes following hyperthermic brain injury. *Prog Brain Res* 115:351-412. Review
19. Sharma HS, Westman J, Nyberg F, Cervós-Navarro J, Dey PK (1994) Role of serotonin and prostaglandins in brain edema induced by heat stress. An experimental study in the young rat. *Acta Neurochir Suppl (Wien)* 60:65-70
20. Sharma HS, Zimmermann-Meinzingen S, Sharma A, Johanson CE. Cerebrolysin attenuates blood-brain barrier and brain pathology following whole body hyperthermia in the rat. *Acta Neurochir Wien Suppl (in this volume)*.

Part IX
Nanoparticles and Brain Edema

Carbon Nanotubes in Neuroscience

Erik B. Malarkey and Vladimir Parpura

Abstract Carbon nanotubes have electrical, mechanical and chemical properties that make them one of the most promising materials for applications in neuroscience. Single-walled and multi-walled carbon nanotubes have been increasingly used as scaffolds for neuronal growth and more recently for neural stem cell growth and differentiation. They are also used in interfaces with neurons, where they can detect neuronal electrical activity and also deliver electrical stimulation to these cells. The emerging picture is that carbon nanotubes do not have obvious adverse effects on mammalian health. Thus in the near future they could be used in brain–machine interfaces.

Keywords Carbon nanotubes • modification • substrates/scaffolds • electrical interface • neurobiology

Introduction

The first evidence of nano-sized carbon tubes (Fig. 1a) is thought to have been shown by Radushkevich and Lukyanovich in 1952 (1). Several other groups observed similar carbon structures afterwards but it was the efforts of two groups in 1993 (2,3) that stirred the current interest in carbon nanotubes (reviewed in (4)).

Carbon nanotubes (CNTs) are composed of sheets of graphene formed into a cylinder, either a single cylinder, single-walled carbon nanotube (SWNT) or multiple concentric cylinders, multi-walled carbon nanotube (MWNT). Double-walled CNTs (DWNTs) are composed of two concentric graphene cylinders, and they represent an intermediate structure between MWNTs and SWNTs. The size of CNTs typically ranges from 0.4 to 2 nm in diameter for SWNTs and 2 to 100

nm for MWNTs while their length can vary from one to several hundred micrometers. The arrangement of the carbon atoms in the graphene sheet can take on several conformations, armchair, chiral or zigzag. These conformations of the nanotube determine its conductivity. Nanotubes are most commonly synthesized upon a catalyst by a variety of methods including, chemical vapor deposition, electric arc discharge and laser ablation.

After manufacture, CNTs are often modified to improve their biocompatibility or enable them to perform new functions by attaching various compounds to them. Lipids, DNA and various peptides can often be simply adsorbed to the CNT. If a more permanent attachment is desired, compounds may be covalently linked to nanotubes. This is most often done by incubating nanotubes with strong oxidizing agents like nitric acid, which add carboxyl groups to the ends of the tubes and any defect sites. Other groups can then be added, usually converting the carboxyl group to acyl chloride, which can then be reacted with the compound of interest. For review on CNT structure and modifications see (5,6).

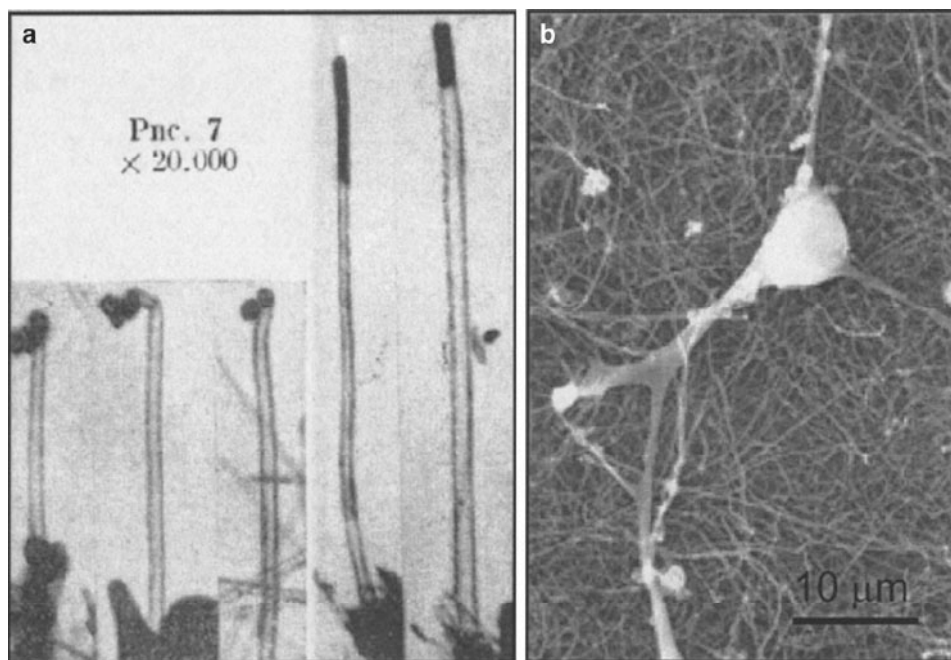
In this review we discuss the use of CNTs in neuroscience, focusing mainly on recent developments with regard to their use as scaffolds for neuronal growth and as electrical interfaces, with brief coverage of earlier studies. For review on the earlier applications of CNTs in neurobiology see (7).

Carbon Nanotubes as Substrates/Scaffolds for Neural Cell Growth

CNTs have been studied as substrates for neuronal growth. Their size and shape are similar to neuronal processes; they are strong yet flexible and can be made conductive. These are all qualities that are advantageous for creating scaffolds for neuronal growth. The first demonstration that nanotubes could be used as a substrate for neurons was provided by Mattson et al. (8) who grew hippocampal neurons on glass coverslips coated with the permissive substrate polyethyleneimine (PEI) and overcoated with MWNTs. They also

V. Parpura (✉)
Department of Neurobiology Center for Glial Biology in Medicine,
Atomic Force Microscopy and Nanotechnology Laboratories,
Civitan International Research Center, Evelyn F. McKnight
Brain Institute, University of Alabama 17196th Avenue South,
CIRC 429, Birmingham AL 35294, USA
e-mail: vlad@uab.edu

Fig. 1 (a) Transmission electron micrograph of carbon nanotubes displaying diameters in the range of 50 nm (modified Fig. 7 from (1); also see commentary in (4)). (b) Scanning electron micrograph of neurons grown on “as prepared” multi-walled carbon nanotubes. Scale bar: 10 μ m (modified Fig. 2 from (9))



discovered that they could improve the growth of neurons by modifying the MWNT with a biologically active compound, 4-hydroxynonenal; this modification was simply done by physisorption. This study was followed up by Hu et al. (9) who grew neurons on MWNT substrates with different charges to investigate whether nanotube substrates could be systematically modified in order to affect neurite outgrowth and branching. By imaging using the vital dye, calcein, they found that when compared to the commonly used substrate, PEI, neurons on as-prepared MWNT substrate (Fig. 1b) did not grow as well, although MWNTs did act as a permissive substrate. They next modified the charge of the MWNT substrate by functionalizing it with carboxyl groups, poly-m-aminobenzene sulfonic acid or ethylenediamine to create negatively, zwitterionic or positively charged nanotubes, respectively. They found that as the substrate became more positive the length and branching of neurites increased. In a subsequent study Hu et al. (10) found that culturing neurons on substrates made of a graft copolymer, where SWNTs were functionalized with branched PEI to “dilute” PEI’s positive charge, resulted in neurite outgrowth and branching intermediate to that of as-prepared MWNTs or PEI alone. Some modifications have been shown to decrease the biocompatibility of nanotubes. Liopo et al. (11) showed that 4-tertbutylphenyl or 4-benzoic acid functionalized SWNTs were less supportive of neural cell attachment and growth than unfunctionalized nanotubes.

Covalent modifications of CNTs, which increase the retention of an attached compound/group, can also be achieved with proteins that play a role in brain signaling. For

example, neurotrophins are protein growth factors that promote the survival and differentiation of neurons. Two such proteins, nerve growth factor (NGF) and brain-derived neurotrophic factor (BDNF), covalently bound to MWNTs, could be used to regulate the growth of neurons (12). Adding the MWNTs coated with NGF or BDNF to the culture medium of embryonic chick dorsal root ganglion cultures promoted neurite outgrowth similar to soluble NGF or BDNF. These results indicate that biologically active molecules like neurotrophin bound to CNTs can retain their activity and interact with cells to promote their function.

Beyond depositing nanotubes onto planar glass coverslips, freestanding films of a poly(N-cetyl-4-vinylpyridinium bromide-co-N-ethyl-4-vinylpyridinium bromide-co-4-vinylpyridine) SWNT copolymer have been created and used as a substrate for neural cell growth (13). Furthermore, Galvan-Garcia et al. (14) reported that directionally oriented MWNTs in the form of sheets or yarns offer an alternative presentation of CNTs to cells. These CNT forms promoted cell attachment, differentiation and cell growth. Additionally, when highly purified, these CNTs also allowed neurons to extend processes of which the number and length were comparable to those of neurons grown on a planar permissive substrate, represented by polyornithine pre-treated glass. Thus, the interaction between neurons and CNTs may be affected by the purity of CNTs as well as by the 3-dimensional organization of the CNT substrate/scaffold. Interestingly, using a particle coagulation spinning process, carbon threads and ribbons up to 30 cm in length can be made from SWNTs (15). These nanomaterials were also

compatible with neural cells as demonstrated by culturing hippocampal neurons and PC12 cells on them. After a week in culture, neurite outgrowth on the nanothread surface could be observed by immunolabeling against β III-tubulin, a neuron specific label. Soluble NGF that can induce neurite outgrowth from PC12 cells was able to exert such an action on PC12 cells grown on CNT threads. This demonstration of the biocompatibility of these nanothreads indicates that they may be suitable for the construction of electrodes or nanowires in implantable devices.

Gabay et al. (16) created a micropatterned array of CNT islands to study self-organization of neural networks. They used a poly (dimethyl siloxane) stamp to imprint a pattern of iron nanoparticle islands on quartz substrates and used chemical vapor deposition to grow CNTs on the iron catalyst islands. The neurons they cultured on these substrates had accumulated on the CNT islands within 4 days with neuronal processes seen to bridge across the non-permissive quartz to form connections between adjacent islands. Similarly, Sorkin et al. (17) created a SWNT patterned substrate by applying iron nitrate catalyst to coverslips with a polydimethylsiloxane stencil and then growing CNTs by chemical vapor deposition. Hippocampal neurons were cultured on these substrates and after 2 to 3 days spontaneously grew into islands with neurites connecting each island. These patterned networks could be used to study neuronal networking with CNT islands as electrical connections for sensing or stimulation.

Besides the above outlined studies on neurons, there have been some attempts to use CNTs in stem cell research. The growth and differentiation of neural stem cells on nanotube substrates was recently demonstrated (18). Coverslips coated with six layers of SWNTs dispersed in poly(sodium 4-styrene-sulfonate) and PEI were used to culture neural stem cells, along with coverslips coated with only poly-L-ornithine for comparison. Cells were bathed in epidermal growth factor (EGF)-depleted medium to induce differentiation. Cells adhered and differentiated into neurons, astrocytes and oligodendrocytes as shown by immunoreactivity of nestin, microtubule-associated protein 2 (anti-MAP2), glial fibrillary acidic protein (anti-GFAP), and oligodendrocyte marker O4 (anti-O4). These cells were just as viable on the CNT substrate as on poly-ornithine and differentiated and extended processes similarly. Since there was no adverse effect of growing on nanotube substrates these materials could readily be used for applications involving stem cells.

Carbon Nanotubes as Electrical Interfaces with Neurons

One of the most exciting developments at the crossroads of nanotechnology and neuroscience is that of designing neural interfaces. Such interfaces between CNTs and neurons have

been demonstrated, indeed. Wang et al. (19) patterned a microchip on a quartz substrate using plasma etching and photolithography. Iron pads were created in silicon dioxide and MWNTs were grown on them by chemical vapor deposition. The nanotubes were decorated with polyethylene glycol to make them more hydrophilic. Hippocampal neurons were cultured onto the microchips and allowed to grow for 4 days. Incubating the cells with fluo-4 allowed them to monitor Ca^{2+} activity during stimulation. Electrical stimulation of the neurons through the CNT microelectrodes on the chip caused rapid changes in fluo-4 fluorescence, indicating transient increases in intracellular Ca^{2+} concentration most likely due to Ca^{2+} influx after the stimulated neurons discharged action potentials. These changes in fluorescence were also seen upon application of glutamate. This demonstrates the feasibility of creating microchip arrays for studying neuronal networks. Liopo et al. (11) also used the conductive nature of CNT substrates to stimulate neurons cultured on them. They deposited SWNTs onto polyethylene terephthalate films and glued a ring in the middle of the film to contain dorsal root ganglion neurons. Electrodes attached to the CNT substrate outside of the ring were used to apply current through the nanotube substrate which resulted in an inward current in the neurons that resembled currents induced by depolarizing voltage steps.

Neuron–neuron signaling is mainly achieved by synaptic transmission. Initially, Lovat et al. (20) examined the effects that CNTs may exert on neuronal electrical activity. They cultured rat, postnatal, hippocampal cells on either uncoated glass coverslips or coverslips coated with unfunctionalized MWNT films. After 8 days of culturing, the neurons were probed for their electrical activity using single cell patch clamp recording. Neurons grown on MWNT films showed a sixfold greater frequency of spontaneous postsynaptic currents and spontaneous action potential generation when compared to those grown on plain glass. The authors proposed that the high conductivity of the CNT substrate might have affected voltage-dependent membrane processes resulting in the increased activity. If this is the case, then growing neurons on CNTs could be used as a platform for stimulation of neurons via CNTs to induce signaling through synaptic contacts. This was subsequently addressed by Mazzatenta et al. (21) who grew hippocampal neuronal cultures on glass coverslips coated with SWNT films. Scanning electron microscopy revealed that neurons grew on the nanotubes similarly to control glass surfaces; it also revealed tight interactions between the neuronal membranes and the SWNTs. Electrophysiological recordings indicated that neurons grown on SWNT substrates displayed spontaneous electrical activity. By applying current through the nanotube substrate they were able to induce action potentials in the cultured neurons. Also, after stimulation they could observe postsynaptic currents as an indication of neuron–neuron sig-

naling. Taken together, the above studies show that CNTs may provide a means for electrical coupling between devices and neurons.

During synaptic transmission at pre-synaptic terminals the vesicles fuse to the plasma membrane and release their cargo molecules in response to depolarization. Besides classical transmitters, such as dopamine, additional compounds such as chromogranin A (CgA), a protein located in dense core vesicles/granules, can be released. We briefly outline two studies that used CNTs to improve detection of dopamine and CgA.

Ali et al. (22) generated a non-oxidative method to detect dopamine, which can be otherwise detected oxidatively, albeit such detection has several disadvantages (see details in (22)). Briefly, they found that they could increase the sensitivity of electrochemical electrodes used in the detection of dopamine by coating them with conjugated SWNTs. The SWNTs were conjugated with poly(anilineboronic acid) (PABA) which acts as a selective dopamine reactant. The binding of dopamine forms a dopamineboronate ester complex which alters the conductivity of the polyaniline backbone without oxidizing dopamine itself. They used single stranded DNA to disperse SWNTs (23,24) and then attached PABA to them using electropolymerization. This composite was then applied to the electrodes. They also eliminated interference from ascorbic acid, the most common compound to interfere with the electrochemical detection of dopamine, without a loss in electrode sensitivity. This was accomplished by coating the composite with a thin layer of perfluorosulfonated ion-exchange polymer, Nafion. The large surface area of the nanotubes greatly increased the amount of borate groups that could detect dopamine. They were able to detect dopamine concentrations as low as 1 nM using cyclical voltametry and 40 pM using differential pulse voltametry. This was 1000× more sensitive than using only PABA coated electrodes.

Wang et al. (25) developed a SWNT based field-effect transistor (FET) to detect the release of CgA from cultured cortical neurons. The FET was created by photolithography and then coated with SWNTs. After baking, the nanotubes became connected to leads on the FET. A goat immunoglobulin G (IgG) antibody against CgA was immobilized on the SWNTs to enable detection of CgA. Upon application of CgA an increase in current in the FET could be detected. This FET could detect CgA at concentrations less than 1 nM. A coverslip containing cultured neurons was placed on the FET and the cells were stimulated by the application of glutamate. This stimulation caused the release of CgA as detected by an increase in current in the FET. This use of nanotubes in a FET provides another method for the real time detection of molecules released from neurons and presents a possible device for sensing neural activity.

Electrodes that have been used for brain implants are metal-based, have relatively high impedance and poor

charge delivery. Carbon nanotubes have several properties which could be employed to improve the performance of such microelectrodes; they have high mechanical strength to penetrate the tissue, and their ability to perform as ballistic conductors, aids in lowering the impedance and increasing the charge transfer compared to regular metal electrodes. Keefer et al. (26) successfully developed a deposition procedure for applying MWNTs to metal electrodes. They coated commercially available tungsten and stainless steel sharp electrodes with CNTs, which when tested in solution outperformed the bare metal electrodes by offering lower impedance and higher charge transfer. Two different animal models were used to test CNT-coated sharp electrodes: motor cortex of anesthetized rats and visual (V4) cortex of a trained monkey. In both in vivo experimental models, they used two parallel electrodes, one coated with CNTs and the other bare metal. CNT-coated electrodes outperformed their paired control electrodes in terms of reduced noise and increased sensitivity in the detection of spontaneous electrical neuronal activity. As one would predict from their mechanical strength, CNTs endured the advancement of electrodes through the dura mater. These hybrid electrodes could be now readily tested in the field of brain-machine interfaces (27).

Concluding Remarks

The intent of this review was to briefly discuss the use of CNTs in neuroscience, most notably as scaffolds for neuronal growth and as electrical interfaces with neurons.

It is apparent from the body of work detailed that there is already an impressive array of currently available CNT applications in neurobiology. As a result of their unique properties and the sophistication of the chemistries available for their modification, CNTs have immense potential in neuroscience. Indeed, further advances in nanotechnology will only provide greater opportunities to use these materials to expand our understanding of brain function and repair the loss of it. CNTs seem an excellent material for the construction of neuroprostheses for the repair of nerve injury, since they can be systematically modified to specifically modulate neurite outgrowth. The use of patterned arrays of CNTs to monitor neural network activity offers a possibility for bio-computing. When combined with their mechanical durability which makes CNTs well suited for use in implantable electrodes that can interact directly with the brain, it is tempting to speculate that the days of applications of CNTs in brain-machine interfaces are close. Although there have been concerns in respect to their toxicity (28,29), the experimental evidence indicates that mammalian exposure to nanotubes for several weeks seems to have no adverse health

effects (30). Of course, further studies are necessary before CNTs can be applied to human subjects, but at the present there is no indication that CNTs will be any more hazardous than other forms of carbon. Given their enormous potential in nanomedicine, it is imperative to continue the research on this unique nanomaterial using multifaceted approaches ranging from organic chemistry to translational medicine.

Conflict of interest statement We declare that we have no conflict of interest.

Acknowledgments The authors' work is supported by a grant from the National Institute of Mental Health (MH 069791). We dedicate this paper to Glenn I. Hatton, whose energy and creativity inspired new views of astrocyte-neuronal interactions.

References

- Radushkevich L, Lukyanovich V (1952) O strukture ugleroda, obrazujucesja pri termiceskom razlozenii oksii ugleroda na zeleznom kontakte. *Zurn Fisic Chim* 26:88–95
- Ijima S, Ichihashi T (1993) Single-shell carbon nanotubes of 1-nm diameter. *Nature* 363:603–605
- Bethune D, Kiang C, De Vries M, Gorman G, Savoy R (1993) Cobalt catalysed growth of carbon nanotubes with single-atomic-layer walls. *Nature* 363:605–607
- Monthieux M, Kuznetsov V (2006) Who should be given the credit for the discovery of carbon nanotubes? *Carbon* 44(9):1621–1623
- Bekyarova E, Haddon RC, Parpura V (2005) Biofunctionalization of carbon nanotubes. In: Kumar CSSR (ed) *Biofunctionalization of nanomaterials (nanotechnologies for the life sciences)*, vol 1. Wiley
- Bekyarova E, Ni Y, Malarkey EB, Montana V, McWilliams JL, Haddon RC, Parpura V (2005) Applications of carbon nanotubes in biotechnology and biomedicine. *J Biomed Nanotechnol* 1:3–17
- Malarkey EB, Parpura V (2007) Applications of carbon nanotubes in neurobiology. *Neurodegener Dis* 4:292–299
- Mattson MP, Haddon RC, Rao AM (2000) Molecular functionalization of carbon nanotubes and use as substrates for neuronal growth. *J Mol Neurosci* 14:175–182
- Hu H, Ni YC, Montana V, Haddon RC, Parpura V (2004) Chemically functionalized carbon nanotubes as substrates for neuronal growth. *Nano Lett* 4:507–511
- Hu H, Ni Y, Mandal SK, Montana V, Zhao B, Haddon RC, Parpura V (2005) Polyethyleneimine functionalized single-walled carbon nanotubes as a substrate for neuronal growth. *J Phys Chem B* 109:4285–4289
- Liopo AV, Stewart MP, Hudson J, Tour JM, Pappas TC (2006) Biocompatibility of native and functionalized single-walled carbon nanotubes for neuronal interface. *J Nanosci Nanotechnol* 6:1365–1374
- Matsumoto K, Sato C, Naka Y, Kitazawa A, Whitby RL, Shimizu N (2007) Neurite outgrowths of neurons with neurotrophin-coated carbon nanotubes. *J Biosci Bioeng* 103:216–220
- Gheith MK, Sinani VA, Wickstedt JP, Matts RL, Kotov NA (2005) Single-walled carbon nanotube polyelectrolyte multilayers and freestanding films as a biocompatible platform for neuroprosthetic implants. *Adv Mater* 17:2663–2670
- Galvan-Garcia P, Keefer EW, Yang F, Zhang M, Fang S, Zakhidov AA, Baughman RH, Romero MI (2007) Robust cell migration and neuronal growth on pristine carbon nanotube sheets and yarns. *J Biomater Sci Polym Ed* 18:1245–1261
- Dubin RA, Callegari G, Kohn J, Neimark A (2008) Carbon nanotube fibers are compatible with mammalian cells and neurons. *IEEE Trans Nanobioscience* 7:11–14
- Gabay T, Jakobs E, Ben-Jacob E, Hanein Y (2005) Engineered self-organization of neural networks using carbon nanotube clusters. *Phys a-Stat Mech Appl* 350:611–621
- Sorkin R, Gabay T, Blinder P, Baranes D, Ben-Jacob E, Hanein Y (2006) Compact self-wiring in cultured neural networks. *J Neural Eng* 3:95–101
- Jan E, Kotov NA (2007) Successful differentiation of mouse neural stem cells on layer-by-layer assembled single-walled carbon nanotube composite. *Nano Lett* 7:1123–1128
- Wang K, Fishman HA, Dai H, Harris JS (2006) Neural stimulation with a carbon nanotube microelectrode array. *Nano Lett* 6:2043–2048
- Lovat V, Pantarotto D, Lagostena L, Cacciari B, Grandolfo M, Righi M, Spalluto G, Prato M, Ballerini L (2005) Carbon nanotube substrates boost neuronal electrical signaling. *Nano Lett* 5:1107–1110
- Mazzatenta A, Giugliano M, Campidelli S, Gambazzi L, Businaro L, Markram H, Prato M, Ballerini L (2007) Interfacing neurons with carbon nanotubes: electrical signal transfer and synaptic stimulation in cultured brain circuits. *J Neurosci* 27:6931–6936
- Ali SR, Ma Y, Parajuli RR, Balogun Y, Lai WY, He H (2007) A nonoxidative sensor based on a self-doped polyaniline/carbon nanotube composite for sensitive and selective detection of the neurotransmitter dopamine. *Anal Chem* 79:2583–2587
- Zheng M, Jagota A, Semke ED, Diner BA, McLean RS, Lustig SR, Richardson RE, Tassi NG (2003) DNA-assisted dispersion and separation of carbon nanotubes. *Nature Mater* 2:338–342
- Zheng M, Jagota A, Strano MS, Santos AP, Barone P, Chou SG, Diner BA, Dresselhaus MS, Mclean RS, Onoa GB, Samsonidze GG, Semke ED, Usrey ML, Walls DJ (2003) Structure-based carbon nanotube sorting by sequence-dependent DNA assembly. *Science* 302:1545–1548
- Wang CW, Pan CY, Wu HC, Shih PY, Tsai CC, Liao KT, Lu LL, Hsieh WH, Chen CD, Chen YT (2007) In situ detection of chromogranin a released from living neurons with a single-walled carbon-nanotube field-effect transistor. *Small* 3:1350–1355
- Keefer EW, Botterman BR, Romero MI, Rossi AF, Gross GW (2008) Carbon nanotube coating improves neuronal recordings. *Nat Nanotechnol* 3:434–439
- Schwartz AB, Cui XT, Weber DJ, Moran DW (2006) Brain-controlled interfaces: movement restoration with neural prosthetics. *Neuron* 52:205–220
- Service RF (2003) Nanotechnology. Sorting technique may boost nanotube research. *Science* 300:2018
- Service RF (2004) Nanotoxicology. Nanotechnology grows up. *Science* 304:1732–1734
- Liu Z, Davis C, Cai W, He L, Chen X, Dai H (2008) Circulation and long-term fate of functionalized, biocompatible single-walled carbon nanotubes in mice probed by Raman spectroscopy. *Proc Natl Acad Sci U S A* 105:1410–1415

Nanowired-Drug Delivery Enhances Neuroprotective Efficacy of Compounds and Reduces Spinal Cord Edema Formation and Improves Functional Outcome Following Spinal Cord Injury in the Rat

Hari Shanker Sharma, Syed F. Ali, Z. Ryan Tian, R. Patnaik, S. Patnaik, Aruna Sharma, Arne Boman, Per Lek, Elisabeth Seifert, and Torbjörn Lundstedt

Abstract The possibility that drugs attached to nanowires enhance their therapeutic efficacy was examined in a rat model of spinal cord injury (SCI). Three Acure compounds AP-173, AP-713 and AP-364 were tagged with TiO₂-based nanowires (50–60 nm) and applied over the traumatized cord either 5 or 60 min after SCI in rats produced by a longitudinal incision into the right dorsal horn of the T10–11 segments under equithesin anaesthesia. Normal compounds were used for comparison. After 5 h SCI, behavioral outcome, blood–spinal cord barrier (BSCB) permeability, edema formation and cell injury were examined. Topical application of nanowired compound AP-713 (10 µg in 20 µL) when applied either 5 or 60 min after injury markedly attenuated behavioral dysfunction at 2–3 h after SCI and reduces BSCB disruption, edema formation and cord pathology at 5 h compared to other compounds. Whereas normal compounds applied at 5 min after injury (but not

after 60 min) had some significant but less beneficial effects compared to their nanowired combinations. On the other hand, nanowires alone did not influence spinal cord pathology or motor function after SCI. Taken together, our results indicate that the nanowired-drug-delivery enhances the neuroprotective efficacy of drugs in SCI and reduces functional outcome compared to normal compounds even applied at a later stage following trauma, not reported earlier.

Keywords Nanoparticles • nanowire • titanium dioxide • spinal cord injury • AP-713 • Blood–spinal cord barrier • spinal cord edema • Tarlov scale • motor function

Introduction

Recent advancement in nanotechnology has resulted in the development of nanowires that can be used to enhance drug delivery by coating them with suitable neuroprotective agents for enhanced drug delivery (2,6,8,9,20). About a decade ago, Kreuter (7) was the first to show the rapid analgesic effects of the peptide “dalargin” after its administration with polysorbate 80-coated polybutylcyanoacrylate (PBCA) nanoparticles into CNS. This suggests that drug-delivery to the brain or spinal cord can be enhanced using nanoparticles. Several in vitro models show that drugs attached to innocuous nanowires could enhance delivery within the CNS resulting in high therapeutic efficacy (see (1,3,4,23,25)). However, these novel aspects of therapeutic enhancement of drugs or compounds tagged with nanowires in vivo models are still lacking.

Our laboratory has initiated a series of investigations using in vivo models of CNS injuries and neuroprotection using various Acure compounds attached with the titanium nanowires (15,20). We use nanowire that is a TiO₂-based (hydrogen titanate) single crystalline ceramic biomaterial with a typical diameter ranging from 50 to 60 nm with a superb chemical stability that can enhance drug delivery within the CNS (4,15,20).

H.S. Sharma (✉) and A. Sharma

Laboratory of Cerebrovascular Research, Department of Surgical Sciences, Anaesthesiology and Intensive Care Medicine, University Hospital, Frödingsgatan 12:28, Uppsala, SE-75421, Sweden and Neurochemistry Laboratory, Division of Neurotoxicology, National Centre for Toxicological Research/FDA, Jefferson, AR, USA
e-mail: Sharma@surgsu.uu.se

S. F. Ali

Neurochemistry Laboratory, Division of Neurotoxicology, National Centre for Toxicological Research/FDA, Jefferson, AR, USA

Z. R. Tian

Department of Chemistry and Biochemistry, University of Arkansas Fayetteville, AR 72701, USA

R. Patnaik and S. Patnaik

Department of Biomedical Engineering, Institute of Technology, Banaras Hindu University, Varanasi-221 005, India

A. Boman, P. Lek and E. Seifert

AcurePharma AB, Ulleråkersv 38, Uppsala, Sweden

T. Lundstedt

Acure Pharma AB, Ulleråkersv 38, Uppsala, Sweden and Institutionen för läkemedelskemi, Avdelningen för Organisk farmaceutisk kemi, Uppsala University, Uppsala, Sweden

This investigation was undertaken to examine a few selected Acure compounds attached with nanowires applied over the traumatized spinal cord at different time intervals to see whether nanowired drug delivery even at a later stage may have some beneficial effects on the outcome of the spinal cord injury compared to the parent compound in our rat model.

Materials and Methods

Experiments were carried out on male Wistar rats (250–300 g) housed at controlled room temperature ($21 \pm 1^\circ\text{C}$) with 12 h light and 12 h dark schedule. Food and tap water were supplied ad libitum before the experiment. All animal experiments were conducted according to National Institute of Health (NIH), United States Government guidelines for care, handling and maintenance of animals and approved by Local Institutional Ethics Committee for Animal Care and Research.

Spinal Cord Injury

Under equithesin anaesthesia (0.3 mL/100 g, i.p.) one segment laminectomy was done over the T10–11 segments. A longitudinal incision (about 1.5 mm deep and 5 mm long) was made over the right dorsal horn using a sterile scalpel blade (10–12). The deepest part of the lesion was mainly limited to the Rexed's lamina VIII (see 13,14). No double brackets pl. The animals were allowed to survive 5 h after injury. Laminectomized rats without injury or intact animals served as controls.

Nanowired Drugs and Application

About 0.30 g of TiO_2 powder (Degussa P25) was introduced into 40 mL of 10 M alkali solution in a 150 mL Teflon-lined autoclave container. After a hydrothermal reaction in an oven for 7 days above 160°C , long nanowires were collected, washed with distilled water or dilute acid, fabricated into the white and flexible membrane on a Teflon template and then dried at room temperature, as described earlier (see (20), Fig. 1). The Acure compounds AP173, AP713 and AP364 (10 μg concentration) were tagged separately to nanowires (Fig. 1). For this purpose, the film was first sterilized in 70% ethanol, and then rinsed in sterile 0.9% saline. Subsequently, the membrane (1.0 cm \times 1.0 cm) was soaked in a 1.0 mL solution of 10 $\mu\text{g}/\text{L}$ AP173 or AP713 at room temperature for 12 h, then washed with deionized (DI) water before the use (4,20,25). These nanowired-compounds were adminis-

tered separately over the traumatized spinal cord 5 min after injury in identical manner. These animals were also allowed to survive 5 h after injury.

Functional Outcome

Functional outcome after SCI was measured using Tarlov scale and inclined-plane angle tests as described earlier (10–13). In brief, the Tarlov scale for hind limb function was assessed as 0 = total paraplegia; 1 = no spontaneous movement but responds to pinch; 2 = spontaneous movement; 3 = able to support weight but unable to walk; 4 = walk with gross deficits; 5 = walks with mild deficits; 6 = normal walk (16). For inclined plane test, the animals were placed on an inclined plane platform and the angle of the plane was adjusted as such that animals can stay on the platform for 5 s without falling (see 11–13).

Blood–Spinal Cord Barrier Permeability

The BSCB permeability was determined using Evans blue and ^{131}I Iodine tracers that bound to serum proteins in vivo as described earlier (17–19).

Spinal Cord Edema Formation

The spinal cord edema was determined using measurement of wet and dry weight of spinal cord samples in control, spinal cord injured and drug-treated groups (12,14). The volume swelling (% *f*) of the spinal cord was calculated from the differences between control and experimental spinal cord water content according to Elliott and Jasper (5).

Spinal Cord Morphology at Light and Electron Microscopy

Spinal cord morphology at light and transmission electron microscopy was examined using standard procedures (10–14).

Statistical Analyses

Quantitative data were analyzed using ANOVA followed by Dunnett's test for multiple group comparison from one control. A *p*-value of less than 0.05 was considered significant.

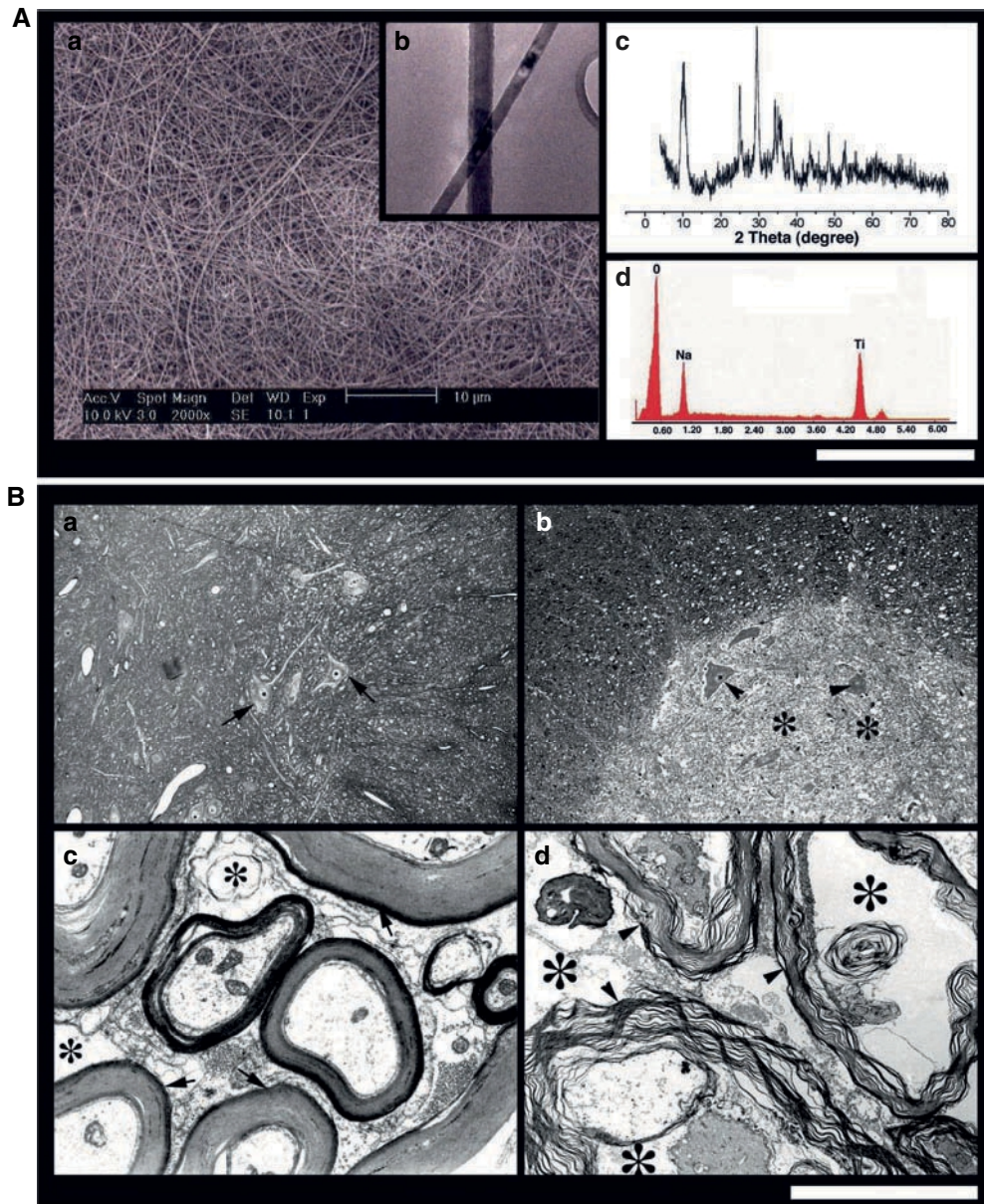


Fig. 1 (A) Nanowire characterizations. (a) Scanning electron microscope (SEM) and transmission electron microscope (TEM) characterizations of the nanowire film, showing an SEM photograph of the white, flexible, and assembled nanowire membrane, and a TEM picture (inset, b) for confirming the nanowire morphology (Scale bar: 50 nm). X-ray powder diffraction (XRD) pattern of titanate nanowire (c). An EDX spectrum of the titanate nanowire membrane is shown in (d). (B) Neuroprotective effects of nanowired compound AP713 on trauma induced spinal cord pathology at light (a) and electron microscopy (c). Low power light micrograph showed several dark and distorted neu-

rons (arrow heads) are seen in the untreated injured rat (b). Sponginess and edema (*) is clearly seen in the untreated animal after 5 h SCI (b). In nanowired AP713 treatment healthy neurons (arrows) are present in the ventral horn and signs of sponginess and edema are largely absent (a). Low power electronmicrograph showed myelin vesiculation (arrow heads) and edema (*) in the untreated injured rat (d). Nanowired AP713 treatment was not able to induce much damage to the myelin (arrows) and the signs of sponginess and edema (*) were much less frequent in the injured animal. Bars a,b = 80 μ m, c,d = 800 nm (modified after 20)

Results

Effects of Nanowired Compounds on Functional Outcome

Acure compound AP173, AP364 or AP713 when administered topically (10 μ g in 20 μ L) over the traumatized spinal cord markedly attenuated the functional outcome after SCI that was most marked around 2 to 3 h after trauma (see Table 1). This effect on Tarlov scale and capacity angle tests was most pronounced by AP713 compared to other AP compounds. This beneficial effect of AP713 was slightly but significantly reduced when the compound was administered 60 min after trauma compared to early intervention (5 min) (Table 1).

Interestingly, when these AP compounds were attached to nanowires and administered over the traumatized spinal cord 5 min after injury in identical manner, an enhanced effect on functional outcome was seen in these rats compared to animals that received AP compounds only (Table 1). However, the potential beneficial effects of nanowired AP713 at 5 min was significantly enhanced on the functional outcome compared to other nanowired compounds (Table 1). This effect of AP713 was still visible when the nanowired compound was administered 60 min after SCI compared to the normal AP713 compound given at this time period after injury (Table 1).

On the other hand, TiO₂ nanowire given without drugs either at 5 or 60 min after SCI did not influence the functional outcome of SCI (Table 1).

Effects of Nanowired Compounds on BSCB Permeability

Application of normal AP compounds significantly reduced the BSCB permeability to Evans blue and radioiodine when applied 5 min after SCI. This effect was most pronounced with AP713 compared to other compounds at this time period (Table 2). However, application of AP713 60 min after SCI resulted in a considerably less reduction in the BSCB permeability to protein tracers following trauma (Table 2).

When nanowired AP compounds were administered 5 min after injury, the reduction in BSCB permeability was much more enhanced than the normal compounds (Table 2). However, the most remarkable enhancement of BSCB permeability reduction was observed with nanowired AP713 compared to other nanowired compounds. On the other hand, application of nanowired AP713 at 60 min after injury showed a significantly less reduction in trauma induced

increased BSCB permeability to Evans blue and radioiodine (Table 2) compared to the nanowired compound applied at 5 min. However, this reduction in BSCB function by nanowired AP713 was much higher compared to normal AP713 applied at this time period (Table 2).

Whereas, TiO₂ nanowire given without drugs either at 5 or 60 min after SCI did not influence the BSCB function after SCI (Table 1).

Effects of Nanowired Compounds on Spinal Cord Edema

Normal AP compounds when applied over the traumatized spinal cord 5 min after injury significantly reduced spinal cord edema formation compared to untreated injury group (Table 2). This effect was most pronounced by AP713. On the other hand, topical application of AP713 after 60 min injury was less effective in reducing edema formation compared to this compound given at 5 min after trauma (Table 2).

When nanowired compounds were applied 5 min after SCI, the reduction in spinal cord edema was much more enhanced at 5 h compared to the normal compounds given at the same time period (Table 2). However, this reduction in edema formation was much more intense by nanowired AP713 compared to other nanowired AP compounds. Topical application of AP713 even at 60 min after SCI markedly reduced the edema formation that was significantly greater than the normal AP713 compound administered at the same time period (Table 2).

Administration of TiO₂ nanowire alone either at 5 min or 60 min after SCI did not alter spinal cord edema formation after injury (Table 2).

Effects of Nanowired Compounds on Spinal Cord Pathology

Normal AP compound 713 markedly attenuated spinal cord pathology and cell injury when applied 5 min after trauma compared to the other AP compounds (Table 2). However, this effect of AP713 was much reduced when the compound was administered 60 min after SCI (Table 2, Fig. 1).

On the other hand, topical application of nanowired AP713 was most effective in reducing spinal cord pathology and cell damage when applied after 5 min injury as compared to the same nanowired compound at 60 min after trauma (Table 2).

A representative example of spinal cord cell injury at light microscopy and myelin vesiculation at transmission electron

Table 1 Effect of nanowired Acure compounds on functional outcome in spinal cord injury in the rat. Spinal cord injury was made on the right dorsal horn of the T10-T11 segments and the animals were allowed to survive 5 h. Acure compounds AP173, AP364 or AP713 (10 µg) were applied over the traumatized cord topically in a volume of 20 µL 5 min after trauma. These compounds equivalent to 10 µg-nanowired were applied in identical manner. For details, see text

Experiment type	n	Functional outcome														
		Tarlov scale after spinal cord Injury						Capacity angle after spinal cord injury								
		-30 min	+1 h	+2 h	+3 h	+4 h	+5 h	-30 min	+1 h	+2 h	+3 h	+4 h	+5 h			
Control	5	6	6	6	6	6	6	6	6	6	6	6	6	6	6	6
Untreated SCI	6	6	3.5 ± 0.5	2.3 ± 1	2 ± 0.5	1.6 ± 0.5	1.3 ± 0.2	60	35 ± 2	31 ± 3	29 ± 2	26 ± 2	26 ± 2	26 ± 3	26 ± 3	26 ± 3
Acure compounds (10 µg in 20 µL)																
5 min after SCI																
AP173 + SCI	5	6	3.6 ± 0.4	2.8 ± 0.2*	2.2 ± 0.5	2.0 ± 0.3*	1.3 ± 0.4	60	35 ± 3	31 ± 3	30 ± 2	28 ± 2*	28 ± 2*	28 ± 3	28 ± 3	28 ± 3
AP364 + SCI	5	6	3.5 ± 0.4	2.5 ± 0.2	2.6 ± 0.3*	2.2 ± 0.3*	1.2 ± 0.2	60	36 ± 2	32 ± 3	30 ± 3	30 ± 2*	30 ± 2*	26 ± 3	26 ± 3	26 ± 3
AP713 + SCI	5	6	3.5 ± 0.6	3.6 ± 0.4*	2.8 ± 0.6*	2.6 ± 0.4*	1.3 ± 0.2	60	35 ± 2	34 ± 2a	34 ± 3**	30 ± 2*	30 ± 2*	27 ± 3	27 ± 3	27 ± 3
60 min after SCI																
AP713 + SCI	5	6	3.1 ± 0.4	3.1 ± 0.6*	2.0 ± 0.6*	1.6 ± 0.3*	1.0 ± 0.2	60	35 ± 3	31 ± 3a	31 ± 4**	30 ± 3*	30 ± 3*	26 ± 2	26 ± 2	26 ± 2
Acure compounds tagged with nanowires (equivalent to 10 µg in 20 µL)																
5 min after SCI																
AP173	5	6	3.4 ± 0.2	3.0 ± 1	2.6 ± 0.2a	2.4 ± 0.3a	1.6 ± 0.1a	60	34 ± 4	33 ± 2	33 ± 3a	30 ± 2a	30 ± 2a	28 ± 4	28 ± 4	28 ± 4
AP364	5	6	3.4 ± 0.3	2.8 ± 0.3a	2.6 ± 0.2*	2.4 ± 0.3*	1.5 ± 0.3*	60	35 ± 3	34 ± 4	32 ± 2a	32 ± 4	32 ± 4	30 ± 3a	30 ± 3a	30 ± 3a
AP713	5	6	3.6 ± 0.2	3.6 ± 0.2*	3.2 ± 0.2a	3.1 ± 0.2a	2.3 ± 0.2a	60	35 ± 4	36 ± 3	36 ± 4a	34 ± 3a	34 ± 3a	30 ± 3a	30 ± 3a	30 ± 3a
60 min after SCI																
AP713	5	6	3.4 ± 0.4	3.1 ± 0.3*	2.8 ± 0.4a	2.1 ± 0.3a	1.8 ± 0.4a	60	34 ± 6	35 ± 4	35 ± 3a	33 ± 4a	33 ± 4a	29 ± 5a	29 ± 5a	29 ± 5a
TiO₂-nanowires (<50 nm in 20 µL)																
5 min after SCI																
TiO ₂	5	6	3.5 ± 0.4	2.0 ± 0.2*	1.8 ± 0.2	1.4 ± 0.4	1.2 ± 0.2	60	35 ± 4	30 ± 3	27 ± 5	25 ± 5	25 ± 5	23 ± 4	23 ± 4	23 ± 4
60 min after SCI																
TiO ₂	5	6	3.6 ± 0.4	2.2 ± 0.4*	1.6 ± 0.3	1.6 ± 0.5	1.3 ± 0.3	60	35 ± 4	31 ± 3	28 ± 4	26 ± 4	26 ± 4	24 ± 3	24 ± 3	24 ± 3

Values are mean ± SD. * = P < 0.05, from untreated control, a = P < 0.05 from drug treated control, non-parametric Chi-Square test. + = faint, ++ = mild, +++ = moderate, ++++ = extensive.

Table 2 Effects of nanowired Acure compounds on blood–spinal cord barrier permeability and edema formation following spinal cord injury in the rat. Spinal cord injury was made on the right dorsal horn of the T10–11 segments and the animals were allowed to survive 5 h. Acure compounds AP173, AP713 or AP364 (10 µg) were applied over the traumatized cord topically in a volume of 20 µL 5 min after trauma. These compounds equivalent to 10 µg–nanowired were applied in identical manner

Experiment type	n	BSCB permeability ¹³¹ Iodine %		Spinal cord water content %		Cell injury	
		T9	T12	T9	T12	T9	T12
Control	5	0.34 ± 0.07	0.36 ± 0.08	65.23 ± 0.21	65.46 ± 0.17	Nil	Nil
Untreated SCI	6	1.96 ± 0.21**	2.04 ± 0.23**	68.56 ± 0.13**	68.76 ± 0.34**	++++	++++
Acure compounds (10 µg in 20 µL)							
5 min after SCI							
AP173 + SCI	5	1.08 ± 0.23aa	1.34 ± 0.31aa	66.98 ± 0.14aa	67.44 ± 0.22aa	+++	+++
AP364 + SCI	5	1.24 ± 0.23aa	1.67 ± 0.43aa	67.04 ± 0.11a	67.58 ± 0.38a	+++?	++++?
AP713 + SCI	5	0.96 ± 0.28aa	0.98 ± 0.54aa	66.78 ± 0.21aa	66.96 ± 0.42aa	++	++
60 min after SCI							
AP713 + SCI	5	1.16 ± 0.24aa	1.28 ± 0.34aa	67.08 ± 0.24aa	67.16 ± 0.22aa	+++	+++
Acure compounds tagged with nanowires (equivalent to 10 µg in 20 µL)							
5 min after SCI							
AP173	5	0.98 ± 0.21aa	0.96 ± 0.43aa	66.56 ± 0.12aa	67.02 ± 0.37a	+++	+++
AP364	5	0.94 ± 0.33aa	0.96 ± 0.45aa#	66.78 ± 0.34aa	67.04 ± 0.23aa	+++?	+++?
AP713	5	0.76 ± 0.23aa#	0.84 ± 0.41aa#	65.89 ± 0.32aa#	66.05 ± 0.21aa#	+	+
60 min after SCI							
AP713	5	0.96 ± 0.33aa#	1.04 ± 0.21aa#	66.09 ± 0.22aa#	66.14 ± 0.22aa#	++	++
TiO₂-nanowires (<50 nm in 20 µL)							
5 min after SCI							
TiO ₂	5	1.88 ± 0.32**	1.96 ± 0.54**	68.88 ± 0.54**	68.89 ± 0.34**	++++	++++
60 min after SCI							
TiO ₂	5	1.78 ± 0.22**	1.98 ± 0.44**	68.98 ± 0.64**	68.97 ± 0.54**	++++	++++

Values are mean ± SD. * = P < 0.05, ** = P < 0.01 from untreated control, a = P < 0.05 from drug treated control. # = P < 0.05, compared from same compound without Nanowiring. Non-parametric Chi-Square test. + = faint, ++ = mild, +++ = moderate, ++++ = extensive, ? = not clear.

microscopy after SI in untreated and nanowired AP713 treated rats is shown in 2. Nanowired AP713 markedly reduced cell damage and myelin vesiculation in the spinal cord when the compound was applied 5 min after trauma. The TiO₂ nanowire alone applied at 5 or 60 min after SCI did not influence the structural changes following SCI (Table 2).

Discussion

The salient new findings of the present investigation show that nanowired-compounds enhance the therapeutic efficacy of drugs and prolong their neuroprotective effects in spinal cord trauma even applied at a later stage. This finding has tremendous clinical scope as normally victims of SCI receive treatments between 1 and 3 h after the incident. Thus, if nanowired drugs are applied within 1 h after injury in clinical situations, the progression of spinal cord pathology may considerably be reduced and the sensory motor function can also be improved in such situations.

Our observations further show that the TiO₂ nanowires applied alone did not alter the spinal cord pathology or func-

tional outcome following SCI (see 3,4). This suggests that nanowires itself do not alter the spinal cord microenvironment and thus could be quite safe to be used in clinical situations. Furthermore, this observation clearly shows that a combination of drugs and nanowires are effective in inducing neuroprotection in SCI.

Another important finding of this study is that nanowiring of drugs although enhancing the potential effects of the parent compound, did not alter their function in the spinal cord. This is evident from the fact that AP713 was most effective in inducing neuroprotection in SCI even after nanowiring as compared to other nanowired compounds, i.e., AP173 or AP364. This suggests that nanowires do not induce any additional neuroprotective properties in normal compounds, but could only enhance their inherent neuroprotective effects.

Although the possible mechanisms behind enhancing the neuroprotective efficacy of drugs attached to nanowires are not well known, it appears that a slow and continuous release of the compounds due to nanowiring in the brain or spinal cord could play important roles (see 9,12,15,20). Furthermore, nanowiring could slow down the drug metabolism as well when introduced in the system (see 21,24). Thus, it appears that the nano-wired compounds may have

greater accessibility within the cord to exert their actions on neural cells and receptors compared to the parent compounds (20). Since nanowires alone did not induce any beneficial effects on motor function or spinal cord pathology following trauma, there are reasons to believe that an increased bioavailability (22), reduced biodegradation (1,23), long-term binding with receptors (1,24,25) and/or potentiation of receptor mediated intracellular signal transduction mechanisms (25) either alone or in combination could be responsible for such an enhanced beneficial effect of nanowired drugs (see 21,25).

Another possibility that nanowired-compounds penetrate faster, deeper and widespread into the spinal cord tissues to exert greater beneficial effects in spinal cord injury compared to the parent compounds is also likely (see 15,20). Thus, nociceptive effects of morphine following nasal delivery are markedly enhanced in a dose-dependent manner when administered with Biovetor nanoparticles (see 2,6). A direct and rapid increase in the nasal-brain transport of morphine in the presence of nanoparticles appears to be responsible for its prolonged antinociceptive activity in a dose-related manner.

An improvement in motor function following nanowired drug delivery was closely associated with a reduction in BSCB permeability and edema formation in our investigation (9–12). This suggests that functional outcome following SCI is related with spinal cord pathology (12,13). Thus, nanowired-drug delivery in the clinical situation immediately after injury may thwart the development of spinal cord pathology and/or improve the functional outcome. This strategy will certainly help to improve the quality of life of spinal cord injured victims.

Taken together our observations derive some hope that potential application of neuroprotective drugs using nanowiring techniques may improve clinical efficiency to treat spinal cord injured patients in future. However, further studies using different neuroprotective drugs are needed to see whether delayed application of these compounds, e.g., 3 to 5 h after injury using nanowire technology can still prevent cord pathology and improve functional outcome, a subject that is currently being examined in our laboratory.

Conflict of interest statement We have no conflict of interest with any organizations mentioned below.

Acknowledgements This investigation is partially supported by the Air Force Office of Scientific Research (London), Air Force Material Command, USAF, under grant number FA8655-05-1-3065. The U.S. Government is authorized to reproduce and distribute reprints for Government purpose notwithstanding any copyright notation thereon. The views and conclusions contained herein are those of the authors and should not be interpreted as necessarily representing the official policies or endorsements, either expressed or implied, of the Air Force Office of Scientific Research or the U.S. Government. We express sincere gratitude to several laboratories where a part of the work is

done or some data is recorded and evaluated. Financial support from Acure Pharma (Sweden); Astra-Zeneca, Mölndal, Sweden, Alexander von Humboldt Foundation (Germany); The University Grants Commission, New Delhi, India, Department of Science and Technology, Govt. of India, New Delhi is gratefully acknowledged. The authors have no conflict of interest with any financial agencies mentioned above. Technical assistance of Inga Hörte, Kerstin Flink, Madeleine Jarild, Mari-Anne Carlsson, Margareta Butler of Uppsala University are highly appreciated.

References

- Assie MB, Bardin L, Auclair A, Consul-Denjean N, Sautel F, Depoortere R, Newman-Tancredi A (2007) F15063, a potential antipsychotic with dopamine D(2)/D(3) antagonist, 5-HT (1A) agonist and D(4) partial agonist properties: (IV) duration of brain D2-like receptor occupancy and antipsychotic-like activity versus plasma concentration in mice. *Naunyn Schmiedeberg's Arch Pharmacol* Jun 375(4):241–250. Epub 2007 Apr 24
- Betbeder D, Sperandio S, Latapie JP, de Nadai J, Etienne A, Zajac JM, Frances B (2000) Biovector nanoparticles improve antinociceptive efficacy of nasal morphine. *Pharm Res* Jun 17(6):743–748
- Chi B, Victorio ES, Jin T (2007) Synthesis of TiO₂-based nanotube on Ti substrate by hydrothermal treatment. *J Nanosci Nanotechnol* Feb; 7(2):668–672
- Dong W, Zhang T, McDonald M, Padilla C, Epstein J, Tian ZR (2006) Biocompatible nanofiber scaffolds on metal for controlled release and cell colonization. *Nanomedicine* Dec; 2(4):248–52
- Elliott KAC, Jasper H (1949) Measurement of experimentally induced brain swelling and shrinkage. *Am J Physiol* 157:122–129
- Friese A, Seiller E, Quack G, Lorenz B, Kreuter J (2000) Increase of the duration of the anticonvulsive activity of a novel NMDA receptor antagonist using poly(butylcyanoacrylate) nanoparticles as a parenteral controlled release system. *Eur J Pharm Biopharm* Mar; 49(2):103–109
- Kreuter J (1995) Nanoparticulate systems in drug delivery and targeting. *J Drug Target* 3(3):171–173
- Olivier JC (2005) Drug transport to brain with targeted nanoparticles. *NeuroRx* Jan; 2(1):108–119
- Sharma HS (2007) Nanoneuroscience: emerging concepts on nanoneurotoxicity and nanoneuroprotection. *Nanomedicine* Dec; 2(6):753–758. Review
- Sharma HS (2005) Neuroprotective effects of neurotrophins and melanocortins in spinal cord injury: an experimental study in the rat using pharmacological and morphological approaches. *Ann N Y Acad Sci* Aug; 1053:407–1021
- Sharma HS (2005) Pathophysiology of blood–spinal cord barrier in traumatic injury and repair. *Curr Pharm Des* 11(11):1353–1389. Review
- Sharma HS (2004) Pathophysiology of the blood–spinal cord barrier in traumatic injury. In: Sharma HS, Westman J (eds) *The blood–spinal cord and brain barriers in health and disease*. Elsevier Academic, San Diego, pp 437–518
- Sharma HS (2008) New perspectives for the treatment options in spinal cord injury. *Expert Opin Pharmacother* (16):2773–2800. Review.
- Sharma HS, Olsson Y (1990) Edema formation and cellular alterations following spinal cord injury in the rat and their modification with p-chlorophenylalanine. *Acta Neuropathol (Berl)* 79(6):604–610
- Sharma HS, Sharma A (2007) Nanoparticles aggravate heat stress induced cognitive deficits, blood–brain barrier disruption, edema formation and brain pathology. *Prog Brain Res* 162:245–276

16. Sharma HS, Skottner A, Lundstedt T, Flardh M, Wiklund L (2006) Neuroprotective effects of melanocortins in experimental spinal cord injury. An experimental study in the rat using topical application of compounds with varying affinity to melanocortin receptors. *J Neural Transm Apr*; 113(4):463–476
17. Sharma HS, Olsson Y, Pearsson S, Nyberg F (1995) Trauma induced opening of the blood–spinal cord barrier is reduced by indomethacin, an inhibitor of prostaglandin synthesis. Experimental observations in the rat using ¹³¹I-sodium, Evans blue and lanthanum as tracers. *Restor Neurol Neurosci* 7:207–215
18. Sharma HS, Olsson Y, Cervós-Navarro J (1993) Early perifocal cell changes and edema in traumatic injury of the spinal cord are reduced by indomethacin, an inhibitor of prostaglandin synthesis. Experimental study in the rat. *Acta Neuropathol* 85(2):145–153
19. Sharma HS, Winkler T, Stalberg E, Olsson Y, Dey PK (1991) Evaluation of traumatic spinal cord edema using evoked potentials recorded from the spinal epidural space. An experimental study in the rat. *J Neurol Sci Apr*; 102(2):150–162
20. Sharma HS, Ali SF, Dong W, Tian ZR, Patnaik R, Patnaik S, Sharma A, Boman A, Lek P, Seifert E, Lundstedt T (2007) Drug delivery to the spinal cord tagged with nanowire enhances neuro-protective efficacy and functional recovery following trauma to the rat spinal cord. *Ann N Y Acad Sci Dec*; 1122:197–218
21. Silva GA, Czeisler C, Niece KL, Beniash E, Harrington DA, Kessler JA, Stupp SI (2004) Selective differentiation of neural progenitor cells by high-epitope density nanofibers. *Science Feb*; 27;303(5662): 1352–1355
22. Vyas TK, Tiwari SB, Amiji MM (2006) Formulation and physiological factors influencing CNS delivery upon intranasal administration. *Crit Rev Ther Drug Carrier Syst* 23(4):319–347
23. Wilson B, Samanta MK, Santhi K, Kumar KP, Paramakrishnan N, Suresh B (2008) Poly(n-butylcyanoacrylate) nanoparticles coated with polysorbate 80 for the targeted delivery of rivastigmine into the brain to treat Alzheimer's disease. *Brain Res Mar* 20; 1200: 159–168. Epub 2008 Jan 26
24. Yao C, Doose DR, Novak G, Bialer M (2006) Pharmacokinetics of the new antiepileptic and CNS drug RWJ-333369 following single and multiple dosing to humans. *Epilepsia Nov* 47(11): 1822–1829
25. Zhao D, Fei Z, Ang WH, Dyson PJ (2006) A strategy for the synthesis of transition-metal nanoparticles and their transfer between liquid phases. *Small Jul*; 2(7):879–883

A New Antioxidant Compound H-290/51 Attenuates Nanoparticle Induced Neurotoxicity and Enhances Neurorepair in Hyperthermia

Hari Shanker Sharma, Aruna Sharma, Saber Hussain, John Schlager, Per-Ove Sjöquist, and Daffin Muresanu

Abstract Previous reports from our laboratory show that animals treated with engineered nanoparticles derived from metals for 1 week and subjected to hyperthermia showed enhanced neurotoxicity in terms of blood–brain barrier (BBB) disruption, brain edema formation and cell injury. It appears that nanoparticle induced enhanced oxidative stress leads to increased lipid peroxidation and over-production of hydroxyl radicals are responsible for exacerbation of neurotoxicity in hyperthermia. Therefore, in this investigation, rats (after 1 week administration of Ag or Cu nanoparticles) were treated with a new antioxidant compound H-290/51 (an inhibitor of lipid peroxidation, 50 mg/kg, p.o.) before subjecting them to hyperthermia. One group of nanoparticle treated rat received H-290/51 and were kept at room temperature for comparison. Our results show that H-290/51 significantly attenuated heat stress induced BBB impairment, brain edema formation and neurotoxicity in nanoparticle treated rats. However, no significant diminution of nanoparticle induced BBB breakdown, or neurotoxicity was observed in H-290/51 treated rats kept at room temperature. These observations suggest that nanoparticles aggravate oxidative stress following hyperthermia leading to exacerbation of neurotoxicity through oxidative stress-related mechanisms, not reported earlier.

Keywords Nanoparticles • silver • copper • hyperthermia • blood–brain barrier • brain edema • oxidative stress • H-290/51 • neurotoxicity • neuroprotection

H.S. Sharma (✉), A. Sharma

Laboratory of Cerebrovascular Research, Department of Surgical Sciences, Anesthesiology and Intensive Care Medicine, University Hospital, Frödingsgatan 12:28, Uppsala, SE-75421, Sweden and Neurochemistry Laboratory, Division of Neurotoxicology, National Centre for Toxicological Research/FDA, Jefferson, AR, USA
e-mail: Sharma@surgsci.uu.se

S. Hussain and J. Schlager

Applied Biotechnology Branch, Human Effectiveness Directorate, Air Force Research Laboratory, Wright-Patterson Air Force Base, OH, USA

Per-Ove Sjöquist

Department of Integrative Pharmacology, Astra-Zeneca Mölndal, Mölndal, Sweden

D. Muresanu

Department of Neurology, University of Medicine and Pharmacy “Tuliu Hatieganu” Cluj-Napoca, Romania

Introduction

Effect of nanoparticles on brain function in normal conditions and following exposure to stress or trauma is still not well known (1,4–8). It appears that nanoparticles from the environment could enter into the body compartments and alter brain functions (10,17, see 21,23). Previous investigations from our laboratory show that the stress response and brain pathology following hyperthermia is aggravated in animals that received engineered nanoparticles from metals, i.e., Cu, Ag and Al prior to heat exposure (10,17). Although the physiological mechanisms of nanoparticle-induced exacerbation of brain pathology following hyperthermia are still unclear, it appears that nanoparticle-induced oxidative stress could play important roles (5–7).

Nanoparticles, e.g., Cobalt, carbon tubes, quantum dots, and ultrafine particles (20 to 80 nm) induce production of reactive oxygen species (ROS), especially following concomitant exposure to light, ultraviolet, or transition metals (7,8,17,23). Thus, it may be that nanoparticles could enhance production of ROS in animals when subjected to additional stress, e.g., heat exposure as well. Since hyperthermia alone induces profound oxidative stress (3), prior treatment with nanoparticles in animals before heat exposure may result in exacerbation of ROS production that could be instrumental in enhanced BBB disruption, brain edema formation and brain pathology.

In the present investigation, this hypothesis was examined using pretreatment with a potent chain-breaking antioxidant H-290/51 (24) on brain pathology in nanoparticle-treated normal animals as well as in rats subjected to heat exposure.

Materials and Methods

Experiments were carried out on Male Wistar rats (body weight 200–250 g) housed at controlled room temperature (21 ± 1°C) with 12 h light and 12 h dark schedule. Food

and tap water were supplied ad libitum. All animal experiments were conducted according to National Institute of Health (NIH), United States Government guidelines for care, handling and maintenance of animals and approved by Local Institutional Ethics Committee for Animal Care and Research.

Treatment with Nanoparticles

The metal nanoparticles (Cu, or Ag, \approx 50 to 60 nm in size, procured from IoLiTec Ionic Liquids Technologies, Denzlingen 79211, Germany) were suspended in Tween 80 and administered (50 mg/kg, i.p.) in separate groups of rats once daily for 7 days. The animals were observed for behavioral changes, if any, at every 24 h interval and their body weight and rectal temperatures were recorded daily (10,17,22).

Subjection to Whole Body Hyperthermia

Normal animals or rats treated with nanoparticles for 7 days were subjected to whole body hyperthermia (WBH) in a biological oxygen demand incubator (BOD) maintained at 38°C (relative humidity 45–47%, wind velocity 20–25 cm/s) for 4 h (11,12,14,15). Intact rats or nanoparticle-treated animals kept at room temperature were used as control.

Treatment with H-290/51

The compound H-290/51 (Astra-Zeneca, Mölndal, Sweden) was administered in a dose of 50 mg/kg, p.o. 30 min before the onset of heat exposure session (20). Rats kept at room temperature also received H-290/51 in identical manner for comparison (see 17).

Stress Symptoms and Physiological Variables

The mean arterial blood pressure (MABP), blood gases, heart rate and respiration were monitored using standard procedures (see (10,11); Table 1). In addition, several behavioral and functional parameters such as salivation, prostration and microhaemorrhages in the stomach wall were also determined (see 17).

Blood–Brain Barrier Permeability and Brain Edema Formation

The blood–brain barrier permeability was determined using intravascular Evans blue and radioiodine traces (13). The brain water content was used to determine from the differences between wet and dry weight of the brain samples brain edema formation (14–16). The volume swelling was measured according to the formula of Elliott and Jasper (2).

Brain Pathology

Brain pathology was examined on 3 μ m thick paraffin sections obtained from the cortical regions after staining with Nissl or Haematoxylin and Eosin using standard protocol (19,20).

Statistical Analysis

ANOVA followed by Dunnet's test for multiple group comparison was used to determine statistical significance of data obtained. A p-value less than 0.05 was considered significant.

Results

Effect of H-290/51 on Nanoparticles Induced Stress Symptoms and Physiological Variables

Treatment with Cu and Ag nanoparticles for 1 week in normal animals resulted in a slight decrease in body weight and arterial PaO₂ compared to intact animals (Table 1). On the other hand, a significant increase in heart rate and respiration together with PaCO₂ was noted in these nanoparticle-treated rats. Few microhaemorrhages were present in the stomach of nanoparticle-treated animals on the seventh day (Table 2). However, no significant differences between Cu and Ag treatment on physiological variables were seen (Table 1).

Subjection of these nanoparticle-treated animals to 4 h WBH resulted in marked aggravation of hyperthermia (Table 1) and stress symptoms (Table 2) compared to normal animals after heat stress (Tables 1 and 2). A significant decrease in MABP, heart rate and respiration was observed in nanoparticle-treated rats after WBH compared to normal animals (Table 1).

Table 1 Effect of H-290/51 on nanoparticles induced physiological variables in normal rats and in animals subjected to 4 h whole body hyperthermia (WBH) at 38°C

Experiment type	n	Temperature °C		Body weight (g)	MABP (torr)	Arterial pH	PaO ₂	PaCO ₂ (torr)	Heart rate (beats/min)	Respiration (cycles/min)	
		Rectal									
A. Normal animals											
Saline	6	37.41 ± 0.45		255 ± 12	120 ± 8	7.40 ± 0.02	81.34 ± 0.12	35.56 ± 0.21	315 ± 12	60 ± 4	
Cu	8	37.67 ± 0.23		242 ± 8*	132 ± 12*	7.30 ± 0.02	79.34 ± 0.89	37.34 ± 0.33*	345 ± 8*	68 ± 6*	
Ag	8	37.58 ± 0.23		248 ± 10*	134 ± 15*	7.20 ± 0.08	78.56 ± 0.22*	36.54 ± 0.34*	351 ± 7	70 ± 8*	
B. Heat stressed animals (38°C for 4 h)											
Saline	5	40.48 ± 0.15aa		248 ± 8aa	90 ± 6aa	7.30 ± 0.06a	83.24 ± 0.56a	34.48 ± 0.52	425 ± 11aa	74 ± 7a	
Cu	9	41.67 ± 0.13bb		242 ± 8b	82 ± 8b	7.33 ± 0.06*	82.44 ± 0.21*	33.16 ± 0.34b*	428 ± 11*	70 ± 8*	
Ag	7	41.27 ± 0.19b		238 ± 7b	70 ± 6bb*	7.21 ± 0.04b	83.18 ± 0.14*	32.43 ± 0.66b*	418 ± 12*	68 ± 6b*	
C. H-290/51 treated normal animal											
Cu	8	36.87 ± 0.33		248 ± 7	122 ± 8	7.32 ± 0.04	78.44 ± 0.39*	36.24 ± 0.13*	315 ± 12	64 ± 8	
Ag	8	38.46 ± 0.18		251 ± 6	124 ± 7	7.30 ± 0.06	78.46 ± 0.32*	36.43 ± 0.14*	320 ± 10	66 ± 7	
D. H-290/51 treated heat stressed animals											
Cu	9	41.04 ± 0.23b		240 ± 6b	86 ± 7	7.38 ± 0.08	81.74 ± 0.61	34.46 ± 0.14*	408 ± 10*	65 ± 6*	
Ag	7	41.07 ± 0.06b		230 ± 8b	80 ± 8b*	7.31 ± 0.06b	81.88 ± 0.84	33.93 ± 0.26*	410 ± 9*	67 ± 8*	

The nanoparticles were suspended in Tween 80 and administered separately intraperitoneally in rats daily once in a dose of 50 mg/kg (wt/vol).

Values are Mean ± SD from 5 to 9 animals at each data point. * = P < 0.05; ** = P < 0.01 compared from saline in normal animals, a = P < 0.05; aa = P < 0.01, compared from 4 h saline treatment in normal vs. heat stressed. b = P < 0.05, bb = P < 0.01 compared from saline treated heat stressed animals, ANOVA followed by Dunnett's test for multiple group comparison from one control group.

Table 2 Effect of H-290/51 on nanoparticles induced BBB permeability, brain edema formation and stress symptoms in normal rats and following 4 h whole body hyperthermia (WBH) at 38°C

Experiment type	n	BBB permeability		¹²⁵ Iodine %	Edema formation		Salivation		Prostration grade	Micro-hemorrhage in stomach (spots, nr)		Neural damage		Eccentric nucleolus
		Evens blue mg %	%		Brain Water %	%f	Saliva spread	Snout (mm)		Distortion Cell shape	Chromatolysis+ degeneration	Nuclear damage		
A. Normal animals														
Saline	6	0.28 ± 0.08		0.36 ± 0.06	74.23 ± 0.86	nil	nil	nil	nil	nil	nil	nil	nil	nil
Cu	8	0.56 ± 0.13**		0.68 ± 0.11**	75.14 ± 0.13*	3.53	nil	nil	nil	2 ± 4	+/-	++	+	+/-
Ag	8	0.64 ± 0.12**		0.74 ± 0.11**	75.04 ± 0.08*	3.14	nil	nil	nil	8 ± 4	+	+	+	+
B. Heat stressed animals (38°C for 4 h)														
Saline	5	2.06 ± 0.25aa		2.86 ± 0.24aa	81.34 ± 0.62aa	27.59	22 ± 6**	+++	+++	48 ± 12##**	++++	++++	+++	+++
Cu	6	2.68 ± 0.33b		3.17 ± 0.26b	83.12 ± 0.34b*	34.49	18 ± 6	+++	++++	55 ± 8#	++++	++++	++++	++++
Ag	8	2.64 ± 0.33b		3.14 ± 0.12bb	82.32 ± 0.26b*	31.39	20 ± 6	++++	++++	60 ± 12#a	++++	++++	++++	++++
C. H-290/51 treated normal animals														
Cu	8	0.58 ± 0.08**		0.62 ± 0.08**	74.94 ± 0.23	2.83	Nil	Nil	Nil	4 ± 4	+	+	+	+/-
Ag	8	0.66 ± 0.07**		0.68 ± 0.06**	74.89 ± 0.11*	2.62	Nil	Nil	Nil	6 ± 2	+	+	+	+
D. H-290/51 treated Heat stressed animals														
Cu	6	1.58 ± 0.23**b		1.87 ± 0.16**a,b	78.22 ± 0.24b**a,b	18.31	18 ± 8	+++	+++	50 ± 4#	++	++	++	++
Ag	8	1.64 ± 0.13**b		1.94 ± 0.10**a,bb	78.62 ± 0.22b**a,b	20.53	19 ± 7	+++	+++	48 ± 8#a	++	++	++	++

Nil = absent, +++++ = severe; +++ = moderate; ++ = mild; + = present; +/- = possible. %f = volume swelling calculated according to Elliott and Jasper (2). About 1% increase in water content corresponds to 3% increase in volume swelling.

The nanoparticles were suspended in Tween 80 and administered separately intraperitoneally in rats daily once in a dose of 50 mg/kg (wt/vol).

Values are Mean ± SD from 5 to 9 animals at each data point. * = P < 0.05; ** = P < 0.01 compared from saline in normal animals, a = P < 0.05; aa = P < 0.01, compared from 4 h saline treatment in normal vs. heat stressed. b = P < 0.05, bb = P < 0.01 compared from saline treated heat stressed animals, ANOVA followed by Dunnett's test for multiple group comparison from one control group.

Administration of H-290/51 in nanoparticle-treated animals did not significantly alter the stress symptoms or physiological variables in rats kept at room temperature. However, H-290/51 treatment, 30 min before WBH, in the nanoparticle-administered group markedly reduced the stress symptoms and physiological variables after 4 h heat stress (Tables 1 and 2).

Effect of H-290/51 on Nanoparticle-Induced BBB Permeability and Brain Edema Formation

Nanoparticle treatment in normal animals for 1 week slightly, but significantly increased the BBB permeability to Evans blue albumin and radioiodine along with a marked increase in brain water content compared to normal animals (Table 2). Subjection of nanoparticle-treated animals to 4 h WBH exacerbated the breakdown of the BBB and aggravated volume swelling and brain edema formation compared to intact animals exposed to heat stress (Table 2).

Interestingly, treatment with H-290/51 in nanoparticle-administered rats kept at room temperature did not reduce the BBB dysfunction and brain edema formation compared to the untreated group (Table 2). However, administration of H-290/51 in the nanoparticle-treated group 30 min before heat stress significantly attenuated the BBB permeability and brain edema formation as compared to nanoparticles alone treated rats after heat exposure (Table 2).

Effect of H-290/51 on Nanoparticle-Induced Brain Pathology

Nanoparticle treatment for 1 week in rats showed a mild but marked neuronal distortion, chromatolysis and nuclear damage (Table 2). When these nanoparticle-treated animals were subjected to 4 h heat stress, the neuronal damage were exacerbated compared to normal animals following similar heat stress (Fig. 1, Table 2).

Pretreatment with H-290/51 in nanoparticle-administered rats kept at room temperature did not induce any neuroprotection (Table 2). However, when H-290/51 was administered in these nanoparticle-treated animals 30 min prior to heat stress, a significant neuroprotection was observed in these animals as compared to nanoparticle-treated rats subjected to heat stress (Table 2).

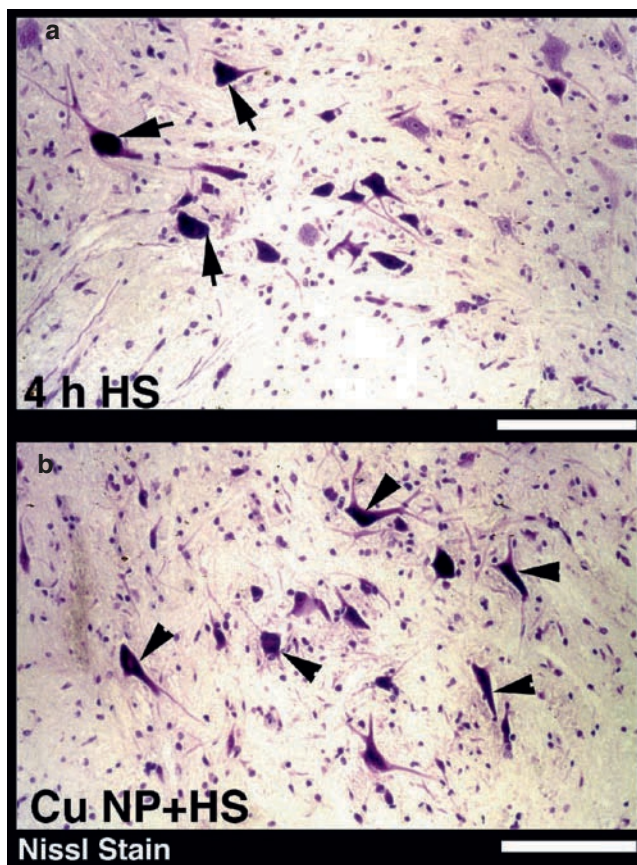


Fig. 1 Neuronal damage in heat stress (a) and its exacerbation with Cu nanoparticles (b). Many nerve cells (arrows) are dark and distorted in heat stressed rat (a) and sign of sponginess and edema are clearly seen. These cell changes appear to be more prominent in rat that received Cu nanoparticle treatment (for 1 week) before heat stress (b). The number of dark and distorted nerve cells (arrow heads) is much more pronounced in Cu nanoparticle treated rats after heat exposure (b) and saline treated rat (a). Bar = 100 μ m (modified after 17)

Discussion

The salient new findings of the present study clearly show that chronic nanoparticle treatment induces brain dysfunction probably by inducing breakdown of the BBB permeability. Furthermore, subjection of these nanoparticle-treated animals to additional stress, e.g., hyperthermia further aggravates the symptoms and brain damage. This indicates that nanoparticles enhance the stress perception and augment brain dysfunction under adverse or stressful circumstances (see (17)). These findings have immense strategic significance with regard to defense planning and military exercise, particularly in hot environments in various parts of the world (9). It appears that both military and non-military persons when exposed to nanoparticles from the ambient air either at

home or abroad are more vulnerable to additional environmental stress (7–10,17).

Another important finding from this investigation clearly shows an involvement of oxidative stress in nanoparticle-induced brain dysfunction. This becomes evident from the fact that antioxidant compound H-290/51, when administered in nanoparticle-treated rats before heat stress, significantly attenuated brain pathology caused by the combined effects of nanoparticles and heat stress. H-290/51 is a chain-breaking antioxidant and thus capable of inhibiting lipid peroxidation and formation of free radicals (20,23). Pretreatment with H-290/51 markedly reduces heat stress induced cellular stress, BBB dysfunction, and brain edema formation and brain pathology in normal animals (3,18–20). This suggests that hyperthermia alone induces profound oxidative stress and inhibition of free radical formation with H-290/51 is neuroprotective in animals or humans.

The present results further show that pretreatment with H-290/51 before heat stress is also able to attenuate brain pathology in nanoparticle-treated rats that already show brain dysfunction even before heat exposure. This finding has tremendous clinical significance. It appears that antioxidant may be able to attenuate brain dysfunction in human population and reduce the effects of additional stress on brain pathology even in subjects that are already exposed to nanoparticles from the environment.

Interestingly, H-290/51 is not very effective in reducing brain pathology in nanoparticle-treated rats kept at room temperature. This suggests that the timing of antioxidant treatment is an important factor in attenuating nanoparticle-induced oxidative stress and subsequent pathophysiological responses. Experiments carried out in our laboratory have shown that pretreatment with H-290/51 is able to thwart nanoparticle-induced oxidative stress in mice. However, if the drug is administered after few days of nanoparticle treatment, then the neuroprotective effects of the compound are lacking (Sharma HS unpublished observation). Obviously, late treatment with antioxidant could not neutralize the oxidative damage that has already occurred in the brain. However, additional generation of free radicals or lipid peroxidation, e.g. caused by heat exposure, may be thwarted by H-290/51 even given at a later stage or prior to heat stress.

Generation of free radicals will directly damage the cell membrane of neurons, glial cells and endothelial cells (19,20). Thus, nanoparticle treatment will induce either a direct or indirect effect on endothelial cell membrane permeability leading to BBB breakdown (11,12,14–16,18–20). Breakdown of the BBB will induce leakage of serum proteins into the brain compartment causing vasogenic edema formation (12). Entry of several unwanted substances from the blood to the brain into the fluid microenvironment of the brain will precipitate abnormal cell reactions causing cell death (11,12).

It appears that hyperthermia alone is not responsible for the BBB breakdown and brain pathology (11). This is supported by the facts that H-290/51 did not reduce the occurrence of hyperthermia although the compound was able to reduce BBB dysfunction and brain damage (20).

Taken together, our results clearly show that nanoparticles by inducing oxidative stress are able to induce BBB breakdown and brain edema formation. Furthermore, our results show that the antioxidant compounds are able to thwart brain damage caused by an additional heat exposure even in population suffering from nanoparticle stress, results that have not been reported earlier. It is quite likely that heat stress when given to nanoparticle-treated animals, a combination of two separate events, i.e. nanoparticle stress and heat exposure, would exacerbate oxidative stress and release free radicals that could together be instrumental in augmenting brain damage.

Conflict of interest statement We have no conflict of interest with any organizations mentioned below.

Acknowledgements This investigation is partially supported by the Air Force Office of Scientific Research (London), Air Force Material Command, USAF, under grant number FA8655-05-1-3065. The U.S. Government is authorized to reproduce and distribute reprints for Government purpose notwithstanding any copyright notation thereon. The views and conclusions contained herein are those of the authors and should not be interpreted as necessarily representing the official policies or endorsements, either expressed or implied, of the Air Force Office of Scientific Research or the U.S. Government. We express sincere gratitude to several laboratories where a part of the work is done or some data is recorded and evaluated. Financial support from Acure Pharma (Sweden); Astra-Zeneca, Mölndal, Sweden, Alexander von Humboldt Foundation (Germany); The University Grants Commission, New Delhi, India, Department of Science & technology, Govt. of India, New Delhi is gratefully acknowledged. The authors have no conflict of interest with any financial agencies mentioned above. Technical assistance of Inga Hörte, Kerstin Flink, Madeleine Jarild, Mari-Anne Carlsson, Margareta Butler of Uppsala University; and Mihaela Rusu and Sinziana Muresanu from Cluj Napoca are highly appreciated.

References

1. Elder A, Gelein R, Silva V, Feikert T, Opanashuk L, Carter J, Potter R, Maynard A, Ito Y, Finkelstein J, Oberdörster G (2006) Translocation of inhaled ultrafine manganese oxide particles to the central nervous system. *Environ Health Perspect* 114:1172–1178
2. Elliott KAC, Jasper H (1949) Measurement of experimentally induced brain swelling and shrinkage. *Am J Physiol* 157:122–129
3. Hedlund S, Sharma HS, Sjöquist P-O, Westman J (1999) A new antioxidant compound h-290/51 attenuates heat shock protein (HSP 72 kD) response, breakdown of the blood–brain barrier permeability, edema and cell injury following acute heat exposure. An experimental study using light and electron microscopy in the rat. *J Therm Biol* 24:409–414

4. Jin H, Chen WQ, Tang XW, Chiang LY, Yang CY, Schloss JV, Wu JY (2000) Polyhydroxylated C(60), fullerenols, as glutamate receptor antagonists and neuroprotective agents. *J Neurosci Res.* Nov 15 62(4):600–607
5. Kagan VE, Bayir H, Shvedova AA (2005) Nanomedicine and nanotoxicology: two sides of the same coin. *Nanomedicine.* Dec 1(4):313–316. Review
6. Long TC, Saleh N, Tilton RD, Lowry GV, Veronesi B (2006) Titanium dioxide (P25) produces reactive oxygen species in immortalized brain microglia (BV2): implications for nanoparticle neurotoxicity. *Environ Sci Technol.* Jul 15 40(14):4346–4352
7. Oberdörster E (2004) Manufactured nanomaterials (fullerenes, C60) induce oxidative stress in the brain of juvenile largemouth bass. *Environ Health Perspect.* Jul 112(10):1058–1062
8. Oberdörster G, Sharp Z, Atudorei V, Elder A, Gelein R, Kreyling W, Cox C (2004) Translocation of inhaled ultrafine particles to the brain. *Inhal Toxicol* 16:437–445
9. Porter AM (2003) Collapse from exertional heat illness: implications and subsequent decisions. *Mil Med.* Jan 168(1):76–81. Review
10. Sharma HS (2007) Nanoneuroscience: emerging concepts on nanoneurotoxicity and nanoneuroprotection. *Nanomedicine.* Dec 2(6):753–758. Editorial
11. Sharma HS (1999) Pathophysiology of blood–brain barrier, brain edema and cell injury following hyperthermia: New role of heat shock protein, nitric oxide and carbon monoxide. An experimental study in the rat using light and electron microscopy. *Acta Universitatis Upsaliensis* 830:1–94
12. Sharma HS (2004) Blood–brain and spinal cord barriers in stress. In: Sharma HS, Westman J (eds) *The blood–spinal cord and brain barriers in health and disease.* Elsevier Academic, San Diego, pp 231–298
13. Sharma HS (1987) Effect of captopril (a converting enzyme inhibitor) on blood–brain barrier permeability and cerebral blood flow in normotensive rats. *Neuropharmacology.* 26(1):85–92
14. Sharma HS, Cervós-Navarro J (1990) Brain oedema and cellular changes induced by acute heat stress in young rats. *Acta Neurochir Suppl (Wien)* 51:383–386
15. Sharma HS, Dey PK (1986) Influence of long-term immobilization stress on regional blood–brain barrier permeability, cerebral blood flow and 5-HT level in conscious normotensive young rats. *J Neurol Sci.* Jan 72(1):61–76
16. Sharma HS, Olsson Y (1990) Edema formation and cellular alterations following spinal cord injury in the rat and their modification with p-chlorophenylalanine. *Acta Neuropathol (Berl)* 79(6):604–610
17. Sharma HS, Sharma A (2007) Nanoparticles aggravate heat stress induced cognitive deficits, blood–brain barrier disruption, edema formation and brain pathology. *Prog Brain Res* 162:245–273. Review
18. Sharma HS, Westman J, Nyberg F (1998) Pathophysiology of brain edema and cell changes following hyperthermic brain injury. *Prog Brain Res* 115:351–412. Review
19. Sharma HS, Gordh T, Wiklund L, Mohanty S, Sjöquist PO. (2006) Spinal cord injury induced heat shock protein expression is reduced by an antioxidant compound H-290/51. An experimental study using light and electron microscopy in the rat. *J Neural Transm.* Apr 113(4):521–536
20. Sharma HS, Westman J, Alm P, Sjöquist PO, Cervós-Navarro J, Nyberg F (1997) Involvement of nitric oxide in the pathophysiology of acute heat stress in the rat. Influence of a new antioxidant compound H-290/51. *Ann NY Acad Sci.* 813:581–590
21. Sharma HS, Hussain S, Schlager J, Ali SF, Sharma A. Effect of nanoparticles on the blood–brain barrier permeability, brain edema formation in rats. *Acta Neurochir (Wien) Suppl.* (in this volume).
22. Sharma HS, Ali SF, Tian ZR, Hussain SM, Schlager JJ, Sjöquist P-O, Sharma A, Muresanu DF (2009) Chronic Treatment with Nanoparticles Exacerbate Hyperthermia Induced Blood-Brain Barrier Breakdown, Cognitive Dysfunction and Brain Pathology in the Rat. Neuroprotective Effects of Nanowired-Antioxidant Compound H-290/51. *J. Nanosci. Nanotechnol* 9:5073–5090.
23. Shvedova AA, Kisin ER, Mercer R, Murray AR, Johnson VJ, Potapovich AI, Tyurina YY, Gorelik O, Arepalli S, Schwegler-Berry D, Hubbs AF, Antonini J, Evans DE, Ku BK, Ramsey D, Maynard A, Kagan VE, Castranova V, Baron P (2005) Unusual inflammatory and fibrogenic pulmonary responses to single-walled carbon nanotubes in mice. *Am J Physiol Lung Cell Mol Physiol.* Nov 289(5):L698–L708
24. Westerlund C, Ostlund-Lindqvist AM, Sainsbury M, Shertzer HG, Sjöquist PO (1996) Characterization of novel indenolindoles. Part I. Structure–activity relationships in different model systems of lipid peroxidation. *Biochem Pharmacol.* May 17; 51(10):1397–1402

Influence of Nanoparticles on Blood–Brain Barrier Permeability and Brain Edema Formation in Rats

Hari Shanker Sharma, Saber Hussain, John Schlager, Syed F. Ali, and Aruna Sharma

Abstract Nanoparticles are small sized (1–100 nm) particles derived from transition metals, silver, copper, aluminum, silicon, carbon and metal oxides that can easily cross the blood–brain barrier (BBB) and/or produce damage to the barrier integrity by altering endothelial cell membrane permeability. However, the influence of nanoparticles on BBB integrity is still not well-known. In this investigation, effect of nanoparticles derived from Ag, Al and Cu (50–60 nm) on BBB permeability in relation to brain edema formation was examined in a rat model. Intravenous (30 mg/kg), intraperitoneal (50 mg/kg) or intracerebral (20 µg in 10 µL) administration of Ag, Cu or Al nanoparticles disrupted the BBB function to Evans blue albumin (EBA) and radioiodine in rats 24 h after administration and induced brain edema formation. The leakage of Evans blue dye was observed largely in the ventral surface of brain and in the proximal frontal cortex. The dorsal surfaces of cerebellum showed mild to moderate EBA staining. These effects were most pronounced in animals that received Ag or Cu nanoparticles compared to Al nanoparticles through intravenous routes. These observations are the first to suggest that nanoparticles can induce brain edema formation by influencing BBB breakdown in vivo.

Keywords Nanoparticles • silver • copper • aluminum • blood–brain barrier • brain edema • Evans blue • radioiodine

H.S. Sharma (✉) and A. Sharma

Laboratory of Cerebrovascular Research, Department of Surgical Science, Anesthesiology and Intensive Care Medicine, University Hospital, Frodingsgatan 12:28, Uppsala, SE-75421, Sweden and Neurochemistry Laboratory, Division of Neurotoxicology, National Centre for Toxicological Research/FDA, Jefferson, AR, USA
e-mail: Sharma@surgsci.uu.se

S. Hussain and J. Schlager

Applied Biotechnology Branch, Human Effectiveness Directorate, Air Force Research Laboratory, Wright-Patterson Air Force Base, OH, USA

S. F. Ali

Neurochemistry Laboratory, Division of Neurotoxicology, National Centre for Toxicological Research/FDA, Jefferson, AR, USA

Introduction

Recently there has been a surge to investigate the effects of nanoparticles on biological systems normally present in the environment (1–3). These small sized (1 to 100 nm) particles have novel properties, which can be highly desirable for applications within the commercial, medical and environmental fields (5,6). Most of these nanoparticles are formed from transition metals, e.g., silver, copper, aluminum, silicon, carbon and metal oxides (1,5). Due to their small sizes, these nanoparticles can either easily cross the blood–brain barrier (BBB) and/or produce damage to the barrier integrity by altering endothelial cell membrane function (5,6). Interestingly, in spite of our increased understanding of BBB function, influence of nanoparticles on BBB is still largely unknown (9,13,15).

It is quite likely that nanoparticles when reaching the CNS compartments may induce profound cellular and molecular stress (8) leading to BBB disruption and brain edema formation through a cascade of secondary cellular and molecular events (8,9,12,13). This investigation is focused on the influence of engineered nanoparticles from metals, e.g., Al, Cu and Ag (50–60 nm) on the BBB permeability to protein tracers, brain edema formation and cell injury in a rat model.

Materials and Methods

Animals

Experiments were carried out on Sprague Dawley rats (body weight 250 to 350 g) housed at controlled ambient temperature ($22 \pm 1^\circ\text{C}$) with 12 h light and 12 h dark schedule. Standard laboratory diet and tap water were supplied ad libitum before and after the experiments. All animal experiments described in this review were conducted according to National Institute of Health (NIH), United States Government guidelines for care, handling and maintenance of animals and approved by the Local Institutional Ethics Committee for Animal Care and Research.

Administration of Nanoparticles

Under equithesin anesthesia (3 mL/kg, i.p.), engineered nanoparticles from Copper (Cu), Aluminum (Al), or Silver (Ag) in the size range of 50 to 60 nm (obtained from US Air Force Research Laboratory from Dr Saber Hussain; and commercially procured from IoLiTec Ionic Liquids Technologies, 79211 Denzlingen, Germany). The nanoparticles were suspended in 0.05% Tween 80 in 0.7% NaCl solution (cf 10, 11, 13). This solution was administered intravenously (30 mg/kg), intraperitoneally (50 mg/kg) or used as cortical superfusion (c.s., 20 µg/10 µL). The Tween 80 solution alone when injected into the carotid artery does not produce any brain or spinal cord pathology (see 11,15). The animals were allowed to survive 24 h after the administration of nanoparticles.

Blood–Brain Barrier Permeability

The blood–brain barrier (BBB) permeability to Evans blue albumin (2% of a sterile solution, 0.3 mL/100 g body weight) and radioiodine tracer (¹³¹Iodine, either 100 µCi/Kg, or a minimum of 0.5 million CPM) given intravenously was determined as described earlier (10).

Morphological Investigations

For morphological investigations, the brains were perfused in situ with 4% paraformaldehyde preceded with a brief saline rinse (12–14), taken out and photographed. Then coronal sections passing through hippocampus, cerebellum and brain stem were embedded in paraffin. About 3 µm thick sections were cut and stained for standard histological stains, e.g., Nissl or Hematoxylin and Eosin and Luxol Fast Blue (13).

Brain Edema Formation and Electrolyte Content

Brain water content was measured from the differences in the wet and dry weight of the samples (10–14). Volume swelling from the differences between brain water content was calculated (see 13). Normally, an increase in 1% water content represents marked edema formation. After obtaining the dry weight, the tissue was processed to determine the Na⁺ and K⁺ content according to standard procedures (4).

Physiological Variables

In some group of animals mean arterial blood pressure (MABP) and blood gases including arterial pH were also examined using standard procedures (10).

Statistical Analysis

ANOVA followed by Dunnet's test was used to evaluate statistical significance of the data obtained from one control group. A p-value <0.05 was considered significant.

Results

Effects on Nanoparticles on the BBB Permeability

The Ag, Cu and Al nanoparticles altered the BBB to Evans blue albumin and radioiodine in the rats in a highly selective and specific manner. The leakage of Evans blue was seen on the ventral surface of the brain and in the proximal frontal cortex. The dorsal surfaces of cerebellum and the brain stem showed mild to moderate Evans blue staining (Fig. 1). The effect of Al nanoparticles on the BBB function was much less intense compared to Ag and Cu nanoparticles. Intraperitoneal administration of nanoparticles had least influence on BBB disruption (see Table 1).

Cortical superfusion with nanoparticles resulted in mild to moderate opening of the BBB to protein tracers largely to be seen on the ipsilateral side. However, the cerebellum and dorsal parts of the brain stem showed leakage of Evans blue albumin as well. This effect was most pronounced with Ag and Cu nanoparticles. The Al nanoparticles showed only faint to mild blue staining (Table 1). Intravenous administration of Al, Cu and Ag nanoparticles induced extravasation of Evans blue and radioiodine tracer in different brain areas (Table 1). There was no difference in radiotracer extravasation when the nanoparticles were administered as a suspension in water or mixed with Tween 80 (results not shown). Tween 80 or NaCl given in equimolar concentration did not induce radiotracer extravasation in any brain regions compared to control group.

Nanoparticles and Edema Formation

Intravenous administration of Cu nanoparticle resulted in mild but significant edema formation in different parts of the

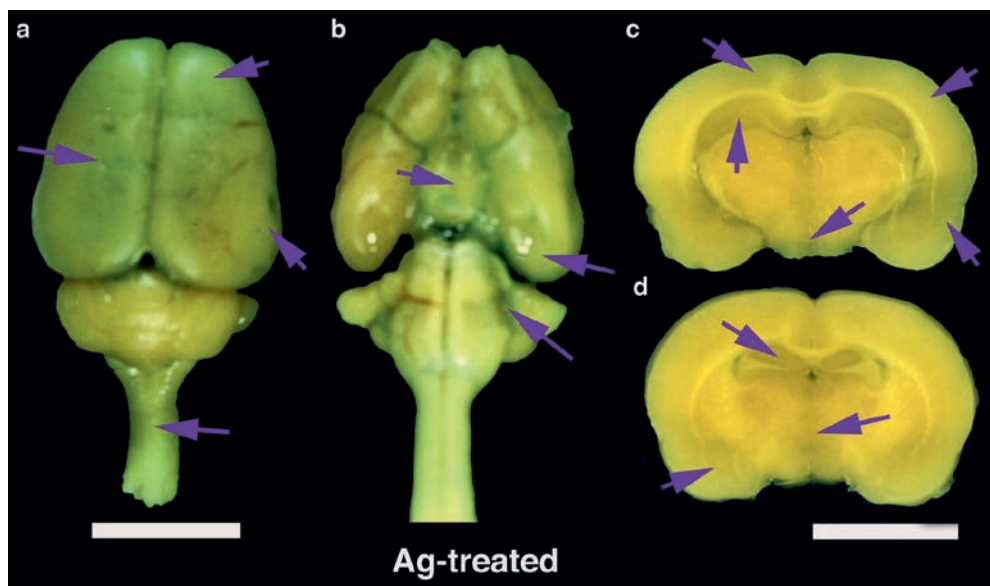


Fig. 1 Shows extravasation of Evans blue on the dorsal (a) and ventral (b) surfaces of rat brain after Ag nanoparticle treatment. The Ag nanoparticle was administered intravenously (35 mg/kg) and the rat is allowed to survive 24 h after injection. Coronal sections of the brain passing through hippocampus (c) and caudate nucleus (d) are also shown. Leakage of Evans blue dye can be seen in various brain

regions (arrows). The deeper parts of the brain, e.g. hippocampus, caudate nucleus, thalamus, hypothalamus, cortical layers including pyriform, cingulate, parietal and temporal cortices, showed moderate blue staining. This indicates widespread leakage of Evans blue albumin within the brain after Ag treatment. Bar = 3 mm (modified after 9 and 15)

cortex compared to the control group. Thus, about 0.5% to 1.2% increase in brain water content was noted in the cingulate, pyriform and temporal cortices. Administration of Al nanoparticle induced mild increase in water content compared to the controls (see Table 1).

Our data further show that Cu treatment increased Na^+ content in the sample with a slight decrease in K^+ content (Table 1). Ag treatment also altered ion content in the brain in a similar way. Al treatment showed minimum changes in Na^+ and K^+ contents in the brain compared to the control groups (Table 1).

Nanoparticles and Physiological Variables

Administration of nanoparticles either into the jugular vein or into the femoral artery slowed the heart rate immediately and the respiratory rate was temporarily increased. This effect lasted for about 10 min. However, none of the animals showed gasping. The effect of Cu and Ag nanoparticles were most pronounced on heart rate and respiration compared to Al nanoparticles (Table 1).

At the onset of nanoparticle (Cu and Ag) administration, the mean arterial blood pressure (MABP) was decreased by 20 to 30 torr for about 5 to 8 min that recovered partially, but remained depressed from the pre-injection value even 90 min after the nanoparticle injection. The decline in MABP following Al nanoparticle was least pronounced (Table 1). Arterial PaO_2 increased slightly after nanoparticle adminis-

tration whereas PaCO_2 was either unchanged or decreased slightly in some animals. The arterial pH was not affected significantly (Table 1).

Nanoparticles and Morphological Changes in the Brain

Nerve cell damage in several brain regions showing Evans blue extravasation (Fig. 2) was seen following administration of Ag and Cu nanoparticles (Fig. 2). Alterations in glial cell and myelin also occurred (Fig. 2). These neuropathological changes were least affected by Al nanoparticles (Table 1). Normal animals that received saline or Tween 80 did not show any cell changes in the brain (see Table 1).

Discussion

The present results are the first to suggest that engineered nanoparticles from metals when administered systemically are able to induce breakdown of the BBB permeability, depending on the route of administration and the type of nanoparticles. Thus, administration of Ag and Cu nanoparticles intravenously or superfused over the cortical surface profoundly induced the breakdown of the BBB to protein tracers compared to Al nanoparticles. On the other hand, intraperitoneal administration of nanoparticles was least effective in BBB disruption. These observations suggest that

Table 1 Effect of nanoparticles on Blood–Brain Barrier (BBB) permeability, brain edema formation and cell changes in rats and mice at 24 h after administration

Type of experiment	BBB permeability			Brain edema			Cell injury variables			Physiological variables		
	Evans blue (mg%)	¹³¹ Iodine %	Water content %	%f	Na ⁺ (mM/Kg dry wt)	K ⁺ (mM/Kg dry wt)	Neuron Nissl	MABP (torr)	Artrial	PaO ₂ (torr)	PaCO ₂ (torr)	
A. Control Group (saline treatment equimolar concentration)												
i.v.	0.23 ± 0.08	0.34 ± 0.03	76.34 ± 0.28	316 ± 8	218 ± 10	Nil	120 ± 8	7.38 ± 0.04	80.34 ± 0.12	34.56 ± 0.21		
i.p.	0.24 ± 0.08	0.30 ± 0.08	76.12 ± 0.32	310 ± 9	220 ± 12	Nil	123 ± 7	7.38 ± 0.06	80.54 ± 0.23	34.53 ± 0.22		
c.s.	0.28 ± 0.03	0.34 ± 0.06	76.10 ± 0.21	312 ± 12	224 ± 08	Nil	124 ± 9	7.36 ± 0.04	80.61 ± 0.12	34.45 ± 0.12		
B. Nanoparticles intraperitoneal (50 mg/kg)												
Ag	0.23 ± 0.05	0.32 ± 0.07	76.23 ± 0.12	320 ± 11	210 ± 12	+/-	118 ± 8	7.34 ± 0.06	80.56 ± 0.17	34.45 ± 0.23		
Cu	0.24 ± 0.12	0.37 ± 0.17	76.45 ± 0.43	317 ± 10	220 ± 15	+	120 ± 6	7.34 ± 0.04	80.59 ± 0.19	34.57 ± 0.26		
Al	0.28 ± 0.23	0.38 ± 0.21	76.78 ± 0.44	289 ± 12	209 ± 12	+/-	108 ± 12	7.34 ± 0.06	80.38 ± 0.29	34.52 ± 0.31		
C. Nanoparticles intravenous (30 mg/kg)												
Ag	0.67 ± 0.12**	0.89 ± 0.11**	77.34 ± 0.21**	+4	350 ± 18*	160 ± 21**	+++	90 ± 8**	7.34 ± 0.08	81.56 ± 0.67	33.45 ± 1.23	
Cu	0.60 ± 0.19**	0.76 ± 0.08**	77.18 ± 0.08**	+4	328 ± 12**	174 ± 10**	++	89 ± 6**	7.30 ± 0.08	81.89 ± 0.89	32.67 ± 0.56	
Al	0.54 ± 0.12*	0.60 ± 0.12*	76.89 ± 0.12*	+2	330 ± 16*	195 ± 12*	+	96 ± 8**	7.32 ± 0.05	81.34 ± 0.89	33.58 ± 0.41	
D. Nanoparticles Cortical superfusion (20 µg/10 µL)												
Ag	0.78 ± 0.20**	0.98 ± 0.12**	77.68 ± 0.11**	+15	328 ± 14**	144 ± 12**	++++	97 ± 10*	7.30 ± 0.04	82.46 ± 0.94	32.66 ± 0.67	
Cu	0.69 ± 0.11**	0.78 ± 0.14**	76.80 ± 0.14**	+12	308 ± 9**	150 ± 7**	+++	106 ± 4*	7.30 ± 0.08	82.13 ± 0.45	32.36 ± 0.41	
Al	0.46 ± 0.10*	0.56 ± 0.10*	75.21 ± 0.23*	+3	282 ± 6*	181 ± 10	+	98 ± 10*	7.33 ± 0.06	81.48 ± 0.36	33.27 ± 0.35	

Values are Mean ± SD of 5 to 8 animals. * P < 0.05; ** P < 0.01, ANOVA followed by Dunnett's test for multiple group comparison from one control group. c.s. = cortical superfusion, Nil = absent, Na = sodium, K = potassium; %f = volume swelling calculated from changes in water content (for details see text). + = faint, ++ = mild, +++ = moderate, ++++ = extensive, +/- = unclear, ? = border line.

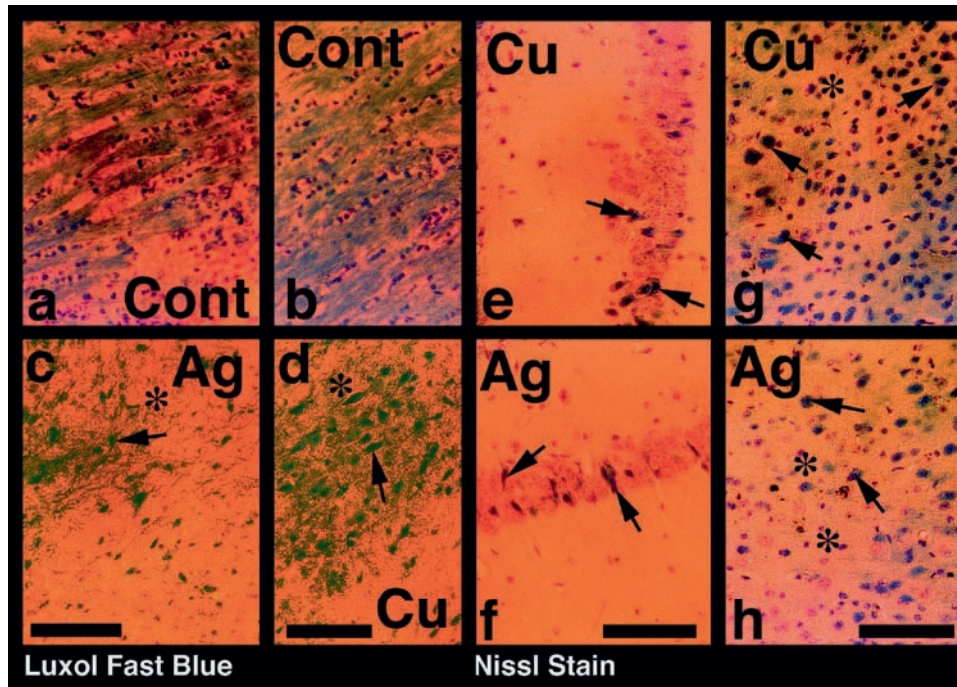


Fig. 2 Shows loss of myelin and nerve cell damage in rats treated with Ag (**c**, **f**, **h**) or Cu (**e**, **g**, **d**) nanoparticles. Luxol fast blue staining was done to check myelin loss in nanoparticle treated rats compared to controls (Cont **a**, **b**). Significant loss of myelin was seen in loss of blue-green staining following Ag[®] and Cu (**d**) treatment (*arrows*). The areas devoid of luxol fast blue (*) are clearly seen (**c**, **d**). Nissl staining

(**e**, **f**, **g**, **h**) shows dark and distorted neurons in the hippocampus following Cu (**e**) or Ag (**f**) treatment. In the cerebral cortex (**g**, **h**) Nissl stain showed many dark and distorted neurons following Cu (**g**) or Ag (**h**) treatment. Dark neurons (*arrows*), and loss of nerve cells (*) are clearly seen in the neuropil. Bar = 60 μm (after Sharma et al., 2009, Ref. 15)

the amount of nanoparticles reaching the cerebral circulation is largely determining their effects on BBB permeability. Obviously, intravenous administration or cortical superfusion exposes the brain microvessels to these nanoparticles more effectively compared to their administration through intraperitoneal route.

Although, the mechanisms by which nanoparticles influence the BBB function are still unclear, it appears that nanoparticles depending on their characteristics may induce cellular or oxidative stress within the brain microvessels (1, 8, 15). Cellular or oxidative stress is known to induce release of various neurochemicals, cytokines and other neurodestructive factors, e.g., lipid peroxidation, generation of free radicals and nitric oxide (see (9–14)). These neurodestructive elements may then act on the cerebral microvessels either from lumen (when the nanoparticles are administered intravenously) or on the abluminal side (in case of cortical superfusion with nanoparticles) to disrupt the endothelial cell membrane permeability allowing intravascular tracers to leak within the brain microfluid environment (13, 15). Our investigation thus further suggested that nanoparticles are able to disrupt both the blood–brain and brain–blood barriers, not reported earlier.

This breakdown of BBB caused by nanoparticles is unrelated to the possible hyperosmotic effects of Al, Ag or

Cu in saline or Tween 80 solution (7, 9, 10). This is apparent from the fact that Tween 80 alone or NaCl solution of equimolar concentration did not affect the BBB function. Moreover, selective effects of nanoparticles with least BBB breakdown by Al nanoparticles compared to Ag and Cu also rule out hyperosmotic effects of solutions per se on BBB dysfunction (7).

Breakdown of the BBB to protein tracers, e.g., Evans blue and radioiodine, leads to vasogenic edema formation and subsequent brain damage (12–14). Significant increase in brain water and volume swelling in the areas showing Evans blue leakage induced by nanoparticles is in line with this idea. Alterations in Na^+ and K^+ content following nanoparticle treatment further support the development of vasogenic edema formation (4). When the brain fluid microenvironment is altered, then various biochemicals, immunological agents, and neurodestructive factors can easily be transported from blood to brain. Entry of these restricted elements into the fluid microenvironment of the brain will thus initiate serious immunological, biochemical, and cellular or molecular stress leading to nerve cell, glial cell and myelin injury (Sharma HS unpublished observation). Obviously, leakage of BBB and exposure of neurons, glial cells and myelin to exogenous serum factors will induce cell reaction in the brain.

Conclusion

In conclusion, our observations suggest that engineered nanoparticles when administered systemically are capable to induce BBB disruption, brain edema formation and lead to abnormal cell reactions. These effects of nanoparticles on brain function are most pronounced with Cu and Ag nanoparticles, compared to Al. It remains to be seen whether nanoparticle-induced brain dysfunction is related to dose and size of the nanoparticles. Furthermore, whether this acute exposure of nanoparticles will further enhance early neurodegenerative changes leading to various brain diseases is unclear and currently being investigated in our laboratory.

Conflict of interest statement We have no conflict of interest with any organizations mentioned below.

Acknowledgements This investigation is partially supported by the Air Force Office of Scientific Research (London), Air Force Material Command, USAF, under grant number FA8655-05-1-3065. The U.S. Government is authorized to reproduce and distribute reprints for Government purpose notwithstanding any copyright notation thereon. The views and conclusions contained herein are those of the authors and should not be interpreted as necessarily representing the official policies or endorsements, either expressed or implied, of the Air Force Office of Scientific Research or the U.S. Government. We express sincere gratitude to several laboratories where a part of the work is done or some data is recorded and evaluated. Financial support from Acure Pharma (Sweden); Astra-Zeneca, Mölndal, Sweden, Alexander von Humboldt Foundation (Germany); The University Grants Commission, New Delhi, India, Department of Science and Technology, Govt. of India, New Delhi is gratefully acknowledged. The authors have no conflict of interest with any financial agencies mentioned above. Technical assistance of Inga Hörte, Kerstin Flink, Madeleine Jarild, Mari-Anne Carlsson, Margareta Butler of Uppsala University are highly appreciated.

References

- Crüts B, van Etten L, Törnqvist H, Blomberg A, Sandström T, Mills NL, Borm PJ (2008) Exposure to diesel exhaust induces changes in EEG in human volunteers. *Part Fibre Toxicol* Mar 11; 5:4
- Elder A, Gelein R, Silva V, Feikert T, Opanashuk L, Carter J, Potter R, Maynard A, Ito Y, Finkelstein J, Oberdörster G (2006) Translocation of inhaled ultrafine manganese oxide particles to the central nervous system. *Environ Health Perspect* 114:1172–1178
- Kim JS, Yoon TJ, Yu KN, Kim BG, Park SJ, Kim HW, Lee KH, Park SB, Lee JK, Cho MH (2006) Toxicity and tissue distribution of magnetic nanoparticles in mice. *Toxicol Sci Jan*; 89(1):338–347. Epub 2005 Oct 19. Erratum in: *Toxicol Sci. Mar* 2006; 90(1):267
- Kiyatkin EA, Brown PL, Sharma HS (2007) Brain edema and breakdown of the blood–brain barrier during methamphetamine intoxication: critical role of brain hyperthermia. *Eur J Neurosci Sep* 26(5):1242–1253
- Kreuter J (2007) Nanoparticles – a historical perspective. *Int J Pharm Feb* 22; 331(1):1–10
- Oberdörster G, Sharp Z, Atudorei V, Elder A, Gelein R, Kreyling W, Cox C (2004) Translocation of inhaled ultrafine particles to the brain. *Inhal Toxicol* 16:437–445
- Rapoport SI, Hori M, Klatzo I (1971) Reversible osmotic opening of the blood–brain barrier. *Science Sep* 10; 173(4001):1026–1028
- Rogers EJ, Bello D, Hsieh S (2008) Oxidative stress as a screening metric of potential toxicity by nanoparticles and airborne particulate matter. *Inhal Toxicol Jul*; 20(9):895
- Sharma HS (2007) Nanoneuroscience: emerging concepts on nanoneurotoxicity and nanoneuroprotection. *Nanomed Dec*; 2(6): 753–758. Editorial
- Sharma HS (1987) Effect of captopril (a converting enzyme inhibitor) on blood–brain barrier permeability and cerebral blood flow in normotensive rats. *Neuropharmacology* 6(1):85–92
- Sharma HS, Dey PK (1986) Influence of long-term immobilization stress on regional blood–brain barrier permeability, cerebral blood flow and 5-HT level in conscious normotensive young rats. *J Neurol Sci* 72(1):61–76
- Sharma HS, Sjöquist PO (2002) A new antioxidant compound H-290/51 modulates glutamate and GABA immunoreactivity in the rat spinal cord following trauma. *Amino Acids* 23(1–3):261–272
- Sharma HS, Sharma A (2007) Nanoparticles aggravate heat stress induced cognitive deficits, blood–brain barrier disruption, edema formation and brain pathology. *Prog Brain Res* 162:245–273. Review
- Sharma HS, Westman J, Cervós-Navarro J, Nyberg F (1997) Role of neurochemicals in brain edema and cell changes following hyperthermic brain injury in the rat. *Acta Neurochir Suppl* 70:269–274
- Sharma S, Ali SF, Hussain SM, Schlager JJ, Sharma A (2009) Influence of Engineered Nanoparticles from Metals on the Blood-Brain Barrier Permeability, Cerebral Blood Flow, Brain Edema and Neurotoxicity. An Experimental Study in the Rat and Mice Using Biochemical and Morphological Approaches. *J Nanosci Nanotechnol* 9:5055–5072
- Weiss CK, Kohnle MV, Landfester K, Hauk T, Fischer D, Schmitz-Wienke J, Mailänder V (2008) The first step into the brain: uptake of NIO-PBCA nanoparticles by endothelial cells in vitro and in vivo, and direct evidence for their blood–brain barrier permeation. *Chem Med Chem* 9:1395–1403

Author Index

A

- Aarabi, B., 228, 261, 262
Aarsen, F.K., 183
Aarseth, J., 33
Aaslid, R., 7
Abe, H., 91
Abilleira, S., 137, 140
Abrey, L.E., 51
Aburakawa, Y., 33
Acikbas, C., 91
Ackil, A.A., Jr., 228
Adamo, M., 10
Adams, H.P., 138, 142
Adams, J.H., 244
Adamson, P.C., 183
Adams, R.L., 183
Adan, B., 277, 283
Adegbite, A.B., 95
Adlbrecht, C., 97, 98
Agelink, M.W., 250
Aggarwal, S., 312
Agha, A., 221
Ahmadi, S., 231–233
Ahmed, M.M., 277
Ahn, E.S., 228, 233, 261, 262
Ahrens, M., 217
Aihara, Y., 133
Aikin, A.A., 183
Aiyagari, V., 152
Aizawa, H., 33
Aizawa, Y., 43, 45
Akabani, G., 10
Akamuma, Y., 251
Akbasack, A., 11
Akins, E.J., 121, 125
Akizawa, T., 309
Akyuz, M., 268
Alafuzoff, I., 78
Alam, Z.I., 315
Albanese, J., 261, 262
Albeck, M.J., 95, 199, 201
Albert, P.S., 184
Albert, R., 235, 265
Albrecht, R., 244
Albright, A.L., 207, 274
Albright, L.A., 271
Alexander, G.E., 177
Alexander, G.J.M., 312, 313
Alexander, J.S., 40, 45, 47
Alexander, M.J., 134, 151
Algra, A., 134
Ali, S.F., 61, 62, 65, 66, 293, 321, 322, 343–345, 348, 349, 351
Ali, S.R., 340
Alkiza, K., 277, 283
Alksne, J.F., 118
Allan, S.M., 33, 34
Allen, C.V., 5
Allen, D., 193
Allen, G.A., 201, 202
Allen, K.L., 165
Alliez, J.R., 261, 262
Allin, D.M., 114
Allt, G., 55, 211
Alm, P., 65, 301, 302, 304, 305, 352, 356
Alonso, C., 222
Alonso, D.F., 49
Alvarez-Sabín, J., 137, 140
Alwan, W., 33
Ameenuddin, S., 149
Am Esch, J.S., 2nd, 313
Amiji, M.M., 349
Amini, A., 228
Amoroso, P., 313
Anarchic, G., 283
Anbai, A., 187, 189
Anderson, H.E., 149
Anderson, N.E., 51
Anderson, R.C., 75
Anderson, S., 161
Andjelkovic, A.V., 32
Andrade-Gordon, P., 149
Andrews, P.J.D., 239
Andriantsitohaina, R., 311, 313
Andrich, J., 250
Ang, B.T., 228
Ang, J., 277
Ang, W.H., 343, 344, 349
Anile, C., 265, 268
Ansari, M.A., 29
Antel, J.P., 293
Anthony, D.C., 33, 183
Antonini, J., 351, 356
Anttia, H., 172
Antunes, J.L., 30
Arabi, B., 233
Arai, H., 121, 125
Arata, S., 43, 45
Araujo, J.C., 133
Archer, N.H., 118
Arenillas, J., 137, 140
Arepalli, S., 351, 356
Aresco, C., 228, 233

- Argandona, E.G., 277, 281
 Argandoña, E.G., 55, 58
 Arikan, F., 237
 Arimura, A., 13, 43, 45
 Arista, A., 9, 10
 Arita, K., 228
 Arkadopoulos, N., 311, 312
 Armstrong, C.L., 51
 Armstrong, D., 239, 244
 Armstrong, F.D., 171
 Armstrong, R.A., 177
 Arnett, H.A., 293
 Arnold, F.J., 292
 Arnold, T.C., 47
 Arntz, H.R., 223
 Arolt, V., 247
 Aronowski, J., 148, 161
 Arts, W.F., 183
 Aruga, T., 45, 260, 315–318
 Arumugam, T.V., 32
 Arundine, M., 292
 Arus, C., 171
 Asahi, M., 33
 Asai, J., 15
 Asano, M., 315
 Ascher, N.L., 312
 Aschoff, A., 81
 Asher, A.L., 11
 Asher, R.A., 251, 252
 Ashford, J.W., 292
 Ashhurst, D.E., 251, 252
 Ashley, D., 191
 Ashraf, W., 81
 Assie, M.B., 343, 349
 Astrakas, L.G., 183
 Atay, Y., 97
 Athanasoulis, C.A., 98
 Atudorei, V., 351, 359
 Atzori, M.G., 212
 Auclair, A., 343, 349
 Augustijn, P., 78, 101, 104
 Augustinus, A., 196
 Auler, J.O., Jr., 312
 Au-Yeung, K.M., 283
 Auzinger, G., 312, 313
 Avezaat, C.J.J., 69, 72, 78, 107, 111, 113
 Ayala, R., 255
 Ayasolla, K., 29
 Azcoitia, I., 161
 Azmitia, E.C., 247
 Azzam, N., 26
- B**
- Baba, A., 43, 45
 Bacchella, T., 312
 Bachert, P., 171, 183
 Bacic, F., 18
 Backer, J.M., 251
 Back, W., 32
 Badaut, J., 26, 45
 Badgaiyan, R.D., 304, 305, 321, 324
 Bading, H., 292, 293
 Baethmann, A., 5, 6, 228, 324
 Baggiolini, M., 33
 Bailes, J.E., 152
 Bailey, K., 295–297, 299
 Bailey, M., 118, 171
 Baker, E.H., 184
 Baker, F.J., 257
 Bakshi, R., 301, 304
 Baldi, E., 142, 144
 Baldwin, M., 228
 Balestreri, M., 225
 Balis, F.M., 183
 Ballabh, P., 21, 22, 40
 Ballantyne, C.M., 32
 Ballerini, E., 272
 Ballerini, L., 339
 Balogun, Y., 340
 Balsom, W., 196
 Baluk, P., 280
 Bamberg, M., 193
 Bankiewicz, K.S., 11
 Banks, W.A., 43
 Bano, D., 292
 Baranes, D., 339
 Barberan, E.M., 33
 Barber, E., 283
 Barboriak, D.P., 283, 286
 Barcikowska, M., 37, 38
 Bardin, L., 343, 349
 Bardt, T., 228, 265, 267, 268
 Bardutzky, J., 228
 Bargiel, P., 166
 Baricordi, O.R., 141, 142, 144
 Barnett, A.S., 184
 Barnett, P., 228
 Baroldi, G., 152
 Barone, P., 340
 Baron, P., 351, 356
 Barsan, W.G., 138, 142
 Bartholdi, D., 295, 299, 324
 Barucco, M., 212, 214
 Barzillai, B., 152
 Basbaum, A.I., 212
 Bassetti, C.L., 39
 Bass, N.M., 312, 313
 Bastianello S., 165
 Batchelor, T.T., 51, 277
 Bateman, G.A., 69, 71
 Bath, P., 30
 Battaglia, G., 247
 Bauer, P., 199
 Baughman, R.H., 338
 Bayard, R., 98
 Bayir, H., 351
 Bayston, R., 81
 Beal, M.F., 179
 Beaulieu, C., 227
 Bech-Azeddine, R., 72, 73
 Becher, B., 293
 Bech, R.A., 129
 Becker, D., 235
 Becker, D.P., 201, 202
 Becker, K., 18
 Becker, L.E., 125
 Beebe, D.W., 171
 Behan, M., 161
 Behar, K.L., 181
 Beiler, S., 40
 Beitzel, M., 11

- Bekyarova, E., 337
 Belayev, L., 52
 B eliveau, R., 23
 Belka, C., 193
 Belli, A., 313
 Bellini, T., 138
 Bellner, J., 107, 111
 Bello, D., 359, 363
 Bell, R., 312
 Belzil, C., 255
 Bemby, J., 24–26
 Ben-Ari, Y., 293
 Bendig, L., 97
 Bendszus, M., 165, 166
 Benedict, C.R., 152
 Bengoetxea, H., 55, 58, 277, 281
 Benhamou, D., 199, 202
 Beni-Adani, L., 203, 207
 Beniash, E., 348, 349
 Ben-Jacob, E., 338, 339
 Benjamin, M.V., 235
 Benjamin, V., 233
 Bennett, C.J., 40, 45, 211, 212, 214
 Bennett, M., 193
 Ben-Shabat, S., 26
 Ben-Shachar, D., 161
 Benveniste, E.N., 64
 Berardi, N., 55, 58
 Beray-Berthat, V., 32
 Berberich, S.N., 97
 Berber, P., 195
 Berdyga, J., 201, 202
 Berger, M., 11
 Berger, M.S., 95
 Bergeron, C., 179
 Bergmann, A., 222
 Bergmann, A.G., 30
 Bergmeister, H., 97, 98
 Bergsneider, M., 75, 76, 114, 269
 Berloco, P.B., 311
 Bernel, W., 312, 313
 Berry, M., 251, 252
 Bertsch, T., 32
 Besancon, E., 324
 Betbeder, D., 343, 349
 Bethune, D., 337
 Betz, A.L., 33, 309
 Beynon, C., 47, 48
 Bhardwaj, A., 225
 Bhende, S., 89
 Bhundia, C., 81
 Bialer, M., 348, 349
 Bieber, K., 47, 48, 217
 Bigner, D.D., 10
 Bigner, S.H., 10
 Bihari, D., 312, 313
 Biller, J., 138, 142
 Binder, D.K., 280, 281
 Binning, M.J., 95
 Biron, K.E., 40
 Biro, M., 228
 Bise, K., 8
 Bisnaire, D., 151
 Bjorkman-Burtscher, I., 171
 Bj ornstig, U., 200
 Black, J.L., 183
 Black, P.H., 211
 Black, P.M., 75, 76, 78, 114, 183
 Blackwell, T.S., 30
 Blamek, S., 183
 Bland, L., 30
 Blasberg, R.G., 4, 6, 7
 Blei, A.T., 311–313
 Bleier, R., 244
 Blessing, R., 134
 Bleyer, W., 196
 Blinder, P., 339
 Bliss, T.V., 250
 Blomberg, A., 359, 363
 Blumberg, P.M., 30
 Blumbergs, P.C., 211–215
 Bobo, R.H., 11
 Bocchicchio, B., 267
 Boch, A.L., 91, 93
 Bockhorst, K., 5
 Bodily, K., 283
 Bodzin, G., 32
 Boehmer, C.G., 212
 Boet, R., 133
 Bogaev, C.A., 267
 Bogeskov, L., 111
 Bogeskov, S.E., 111
 Bogousslavsky, J., 26
 Boillat, C.A., 121, 125
 Boksay, I., 129
 Boldshauser, E., 273
 Boman, A., 61, 62, 66, 343–345, 348, 349
 Bonderman, D., 97, 98
 Bond, M., 235
 Boon, A.J., 72, 73, 78, 105, 107, 111, 113, 129
 Boop, F., 107
 Booth, R., 193
 Bopp, A.C., 64
 Borel, C., 152
 Borgbjerg, B.M., 95
 Borgesen, S.E., 69, 72, 129, 199, 201
 Borgesen, S.V., 95
 Borlongan, C.V., 39
 Borm, P.J., 359, 363
 Borremans, J.J., 78
 Bor-Seng-Shu, E., 263
 Boscardin, W.J., 269
 Boschert, J., 111
 Botterman, B.R., 340
 Bottner, M., 159, 161
 Boughner, D.R., 151
 Boulis, N., 144
 Boulton, M., 239, 244
 Bounameaux, H., 98, 99
 Bowen, D.M., 179
 Bowman, C.C., 33
 Boyett, J.M., 274
 Bozzao, L., 165
 Braakman, R., 267
 Brabant, G., 221–223
 Bracci, P., 32
 Bracco, A., 313
 Brain, S.D., 211
 Brand, A., 185
 Brandt-Zawadzki, M., 196
 Brass, L.M., 161
 Braun, A., 21, 22, 40

- Braunwald, E., 152
 Braverman, A.C., 152
 Bravo, T., 217–219
 Brechbiel, M.W., 11
 Brecher, M.R., 195
 Brechtel, K., 295, 297, 299
 Bredesen, D.E., 212
 Brekelmans, G.J., 199
 Brene, S., 212
 Bret, P., 69
 Brettler, D.B., 30
 Breuer, A., 26
 Breu, V., 134
 Briegel, J., 133
 Brière, M.E., 183
 Brightman, M.W., 239, 243
 Brillman, J., 152
 Brimijoin, S., 214
 Bringas, J.R., 11
 Brisson, C., 125
 Brockmeyer, D.L., 75, 228
 Brodaty, H., 193
 Broderick, J.P., 138, 142, 307, 309
 Brodin, E., 214
 Broelsch, C.E., 313
 Bromberg, J.E., 51
 Brott, T., 138, 142
 Brott, T.G., 307, 309
 Brouwer, S., 33
 Brown, C., 47
 Brown, J.L., 212
 Brown, M.T., 10
 Brown, P.D., 239
 Brown, P.L., 61, 66, 321, 360, 363
 Brown, R., 312, 313
 Brown, R.C., 277
 Brown, R.S., Jr., 313
 Brownstein, M.J., 43
 Brown, T.R., 193
 Bruce, D.A., 4, 6
 Brunberg, J.A., 309
 Brundage, B.H., 98
 Brunet, A., 292
 Brunet, J.F., 45
 Brunet, L., 193
 Bruno, A., 212, 214
 Bruno, G., 212, 214
 Bruno, K., 311
 Bruno, V., 247
 Bruns, J., Jr., 225
 Bryan, D.W., 40
 Brydon, H.L., 81
 Brzeziński, J., 171, 184
 Buchanan, G.M., 191
 Buchfelder, M., 221–223
 Büchner, C., 190
 Budach, W., 193
 Buerk, D.G., 277
 Buket, S., 97
 Bullock, M.R., 233, 236, 250, 261, 262
 Bullock, R., 236, 267
 Bullock, R.M., 257, 260
 Bulnes-Sesma, S., 277, 278
 Bulsara, K.R., 152
 Bulski, T., 166
 Bungeroth, M., 26
 Burdelski, M., 312
 Burgess, J.H., 98
 Burke, D.G., 133
 Burke, J.M., 214
 Burroughs, A.R., 277
 Busija, D.W., 55
 Businaro, L., 339
 Buslei, R., 183
 Busto, R., 52
 Busuttill, R.W., 313
 Butchart, A.G., 33
 Butterworth, R.F., 311
 Butt, W., 228
 Buvanendran, A., 202
 Buxton, N., 207
 Buzzi, M.G., 211
- C**
- Cacciari, B., 339
 Caciagli, F., 247
 Cai, N., 58
 Cairns, C., 89
 Cairns, N., 315
 Cai, W., 254, 341
 Cai, X., 124
 Calabrese, P., 51
 Caldwell, S.H., 312, 313
 Calinisan, J.B., 52
 Calise, F., 313
 Callegari, G., 338
 Calvert, J.W., 47
 Camille, J.M., 283
 Campanella, R., 261, 262
 Campbell, A.B., 171
 Campbell, J., 240
 Campbell, S.J., 33
 Campidelli, S., 339
 Campisi, J., 64
 Canalese, J., 312, 313
 Cancedda, L., 58
 Candes, E.J., 167
 Caniatti, M.L., 142, 144
 Cannon, A., 152
 Cannon, J.L., 177
 Cao, R., 28, 125
 Cappannoli, A., 311
 Carafoli, E., 292
 Carcenac, C., 239
 Carden, D.L., 47
 Carlberg, B., 271
 Carlos, T.M., 32
 Carlson, S., 52
 Caroli, M., 261, 262
 Carosella, E.D., 141, 144
 Carrell, R.W., 84
 Carrion, E., 76
 Carroll, J., 39
 Carstensen, H., 274
 Carter, B.J., 121, 122, 124, 125
 Carter, J., 351, 359
 Caruso, R., 105
 Casey, R., 30
 Casi, M., 9, 10
 Caso, J.R., 30, 33
 Castellanos, M., 137

- Castellazzi, M., 138, 141, 142, 144
 Castillo, J., 137, 140
 Castranova, V., 351, 356
 Castro-Obregon, S., 212
 Catsman-Berrevoets, C.E., 183
 Catton, M.D., 212
 Caviness, W.F., 51
 Cecchelli, R., 23
 Celli, P., 311
 Cenic, A., 283, 284
 Cernak, L., 40, 45, 211, 212, 214, 315
 Cervoni, L., 105
 Cervós-Navarro, J., 65, 251, 252, 296, 299, 321, 322, 324, 328, 331, 344, 352, 356, 360, 363
 Cesaer, P., 272
 Chalela, J., 165
 Chamuleau, R.A., 313
 Chan, F.L., 283
 Chang, C., 217–219
 Chang, C.M., 33
 Chang, C.N., 187, 190
 Changc, S.M., 173
 Chang, L., 193
 Chang, R.C.C., 5, 6
 Chang, S., 185
 Chan, K.H., 119
 Chan, L., 196
 Chan, L.L., 171
 Chan, M.T., 133, 199
 Chan, P.H., 32, 33, 315, 317
 Chan, Y.L., 171, 174, 196
 Chan, Y.S., 125
 Cha, S., 173, 283, 284, 286
 Chasserot, S., 311, 313
 Chazal, J., 69
 Checchia De Ambrosio, C., 33
 Chehab, S., 73, 89, 98, 107, 108
 Chen, A.F., 155, 156
 Chen, C.J., 30
 Chenevert, T.L., 309
 Cheng, C., 39
 Chen, G.F., 121, 125
 Cheng, T., 151, 152
 Cheng-Yu, Ch., 196
 Chen, H., 32
 Chen, I.B., 133
 Chen, K., 228
 Chen, K.M., 283, 286
 Chen, L.W., 125
 Chen, M., 43, 155
 Chen, Q., 32
 Chen, R.Y.Z., 30
 Chen, S., 217
 Chen, S.F., 212
 Chen, T., 247
 Chen, W.Q., 351
 Chen, W.Y., 30
 Chen, X., 341
 Chen, Y., 26, 43, 225
 Chertoff, M., 33
 Chesnut, R., 261, 262
 Chesnut, R.M., 233, 236, 257, 260, 267
 Chetty, V.K., 185, 193
 Cheung, R.T.F., 283
 Cheung, W.C., 211
 Chhabra, R., 265
 Chiang, L.Y., 351
 Chi, B., 343, 348
 Chiba, Y., 114
 Chidlow, J.H., 32
 Chien, S., 30
 Chik, Ch., 196
 Chik, K.W., 171, 174
 Chinookoswong, N., 121, 124, 125
 Chintagumpala, M., 191
 Chi-Ping Ng, S., 235–237
 Chiu, J., 47, 217–219
 Choe, W.J., 190
 Choi, S., 235
 Cho, M.H., 359
 Chong, C., 235–237
 Chong Chong, V.F.H., 171
 Chopp, M., 32
 Chouaf-Lakhdar, L., 125
 Chou, S.G., 340
 Chou, S.M., 121, 124, 125
 Choux, M., 207
 Christ-Crain, M., 221
 Christman, J.W., 30
 Chumas, P., 111
 Chung, C., 311
 Chung, H.T., 190
 Chu, W.C., 171, 174, 196
 Ciccarelli, R., 247
 Cinalli, G., 107, 111, 193
 Cioffi Daggar, R.P., 33
 Cirafici, P., 98, 99
 Citron, B.A., 149
 Claes, A., 281
 Clark, D.L., 228
 Clarke, D.B., 55
 Clarke, J.A., 84
 Clarke, M., 195
 Clark, G.H., 247
 Clark, J.D., 223
 Clark, W.K., 228
 Clasen, R.A., 228
 Claudio, L., 37, 40
 Clavel, B., 239
 Clayton, F.C., 152
 Clifton, G.L., 228, 233, 257, 260, 267
 Cochrane, D.D., 107, 111, 118
 Cohadon, F., 267
 Cohen, M.E., 272
 Cohen, S.R., 207
 Cokgor, I., 10
 Colbourne, F., 228
 Coleman, M., 271, 272
 Coleman, R.E., 10, 11
 Collins, M.W., 301
 Collins, P., 244
 Collmann, H., 95
 Colohan, A., 48
 Condon, B., 236
 Connolly, E.S., Jr., 32
 Conrad, S.A., 47
 Constantini, S., 203, 207, 225
 Consul-Denjeau, N., 343, 349
 Contantinae, L.S., 196
 Convert, J., 263
 Cooke, S., 114
 Cook, G., 81

Coon, A.L., 134
 Cooper, A.J., 311
 Cooper, P.R., 228
 Copeland, B.R., 33
 Copeland, D., 196
 Copin, J.C., 33
 Corbett, D., 147
 Cordeiro, J.G., 133
 Cordoba, J., 312
 Cordobes, F., 261, 262
 Corelli, F., 212, 214
 Corleone, D., 47, 217–219
 Corn, C., 25
 Cornford, M., 193
 Correa, D.D., 51
 Corteen, E., 237
 Corwin, F.D., 250
 Costabile, G., 69, 72
 Costerton, J.W., 87
 Costerton, W., 81
 Couldwell, W.T., 93, 95
 Coull, B.M., 33
 Cowan, J.A., 261, 262
 Cox, C., 351, 359
 Coy, D.H., 43
 Coyle, J.T., 181
 Craen, R.A., 283, 284
 Crapo, J.D., 64, 65
 Crawford, F., 173
 Cremer, O.L., 199
 Cremonini, A.M., 9, 10
 Croci, N., 32
 Croll, S.D., 58
 Crome, L., 97
 Cronin-Golomb, A., 271–273
 Croteau, D., 11
 Crowell, R.M., 17
 Cruce, J.A.F., 244
 Crüts, B., 359, 363
 Cruz-Sanchez, F.F., 277, 283
 Csonka, C., 48
 Csont, T., 48
 Cui, X.T., 340
 Cujec, B., 152
 Culler, M.D., 43
 Culmsee, C., 212, 214
 Cummins, R., 52
 Cunha, B.A., 147
 Curran, W., 193
 Currie, R.W., 55
 Curry, D.J., 133
 Cusimano, M.D., 72, 73, 78, 101, 104, 107, 111, 129
 Cuzner, M.L., 293
 Czech, T., 118
 Czeisler, C., 348, 349
 Czernicki, Z., 81–84, 199, 201, 202
 Czigner, A., 40
 Czosnyka, M., 114, 134, 199, 201, 225, 228, 237
 Czosnyka, Z.H., 114
 Czuba, Z., 30

D

Daas, M., 312
 Dacey, R., 152
 Dach, N., 47, 217–219

Daffertshofer, M., 33
 Dahlborn, K., 55
 Dahl, R.R., 43
 Dai, H., 339, 341
 Dai, Z., 228
 D'Alimonte, I., 247
 D'Alio, A., 311
 Dallochio, F., 138
 Dally, M., 171
 Dalton, H.J., 76
 Damasio, A.R., 179
 Dan-gond, F., 293
 Daniel, S.E., 315
 Dascombe, M.J., 33
 Datas, L., 239
 Datta, S.R., 292
 Dauch, W.A., 78, 101, 104, 107, 111
 Dauri, M., 313
 Dauser, R.C., 207
 Dávalos, A., 137, 140
 Davern, T.J., 312, 313
 Davet, J., 239
 Davidson, C.S., 311
 Davidson, R.I., 95
 Davies, K.R., 151
 Davies, L.M., 228
 Davies, M., 312, 313
 Davies, N.A., 313
 Davis, C., 313, 341
 Davis, L.E., 81
 Davis, M., 313
 Davis, P.C., 171, 174, 184
 Davis, T.P., 277, 280, 292
 Dawling, S., 312, 313
 Dawson, A., 98, 99
 Dawson, D.A., 32
 Dean, C., 40
 Dearden, M., 267
 De Bonis, P., 268
 Debus, J., 51, 183, 187, 190
 de Castro Ribeiro, M., 26
 Decker, M., 10
 de Courten-Myers, G.M., 40, 307, 309
 de Crespigny, A., 227
 Dedhar, S., 324
 Dedrick, R.L., 11
 De Girolami, U., 183
 de Graaf, R.A., 181
 de Hemptinne, B., 313
 Deibert, E., 152
 de Jong, D.A., 69, 72, 78, 107, 111, 113
 De La Mata, M., 313
 de la Monte, S.M., 177, 178
 Del Bigio, M.R., 147
 Del Biagio, M.R., 91
 Del Fiacco, M., 212
 Delgado, P., 137, 140
 Del Rio, G., 212
 Delwel, E.J., 69, 72, 73, 78, 105, 107, 111, 113, 129
 del Zoppo, G.J., 24, 26, 33
 Demanet, L., 167
 Demetriadou, K., 240
 Demetriou, A.A., 311–313
 Demeule, M., 23
 de Moerloose, P., 98, 99
 Dempster, R., 33

- de Nadai, J., 343, 349
 Depelteau, J.S., 121, 122, 124, 125
 Depoortere, R., 343, 349
 Derdeyn, C.P., 161
 De Roover, A., 311
 DeSanctis, R.W., 98
 Dessi, M.L., 212
 Detry, O., 311, 312
 Deutz, N.E., 312, 313
 Deveikis, J., 152
 Devos, A., 171
 DeVries, A.C., 48
 de Vries, H.E., 293
 De Vries, M., 337
 Dey, P.K., 61–66, 301, 302, 321, 322, 328, 331, 344, 352, 360
 De Zeeuw, C.I., 247
 Dhallu, M.S., 23
 Dhoot, N.O., 299
 Diamond, D.L., 257, 260
 Dianzumba, S., 152
 Diaz-Arrastia, R., 199
 Di Betta, A.M., 271
 Di Chirico, A., 265, 268
 Dickstein, D.L., 40
 Didier-Bazés, M., 124
 Dietz, H., 233
 Di Florio, E., 313
 Di Iorio, P., 247
 Dillon-Carter, O., 39
 Dillon, W.P., 185, 283, 286
 Dimitriadou, V., 211
 Dimitrijevic, O.B., 32
 Dimopoulos, V.G., 199
 Diner, B.A., 340
 Ding, B., 283, 286
 Ding, S., 217, 219
 Di Nicuolo, G., 313
 Di Rienzo, F., 33
 Diringier, M.N., 161
 Dirnagl, U., 217
 Di Rocco, C., 91, 207
 Dirven, C., 78, 101, 104
 Ditchfield, M., 228
 Di, T.E., 277
 Dito, M., 89
 Dobo, E., 40
 Dodson, R.F., 25
 Doerfler, A., 226–228
 Dogrul, A., 64
 Dohi, K., 43, 45, 315–318
 Doi, K., 165
 Doiron, K., 178
 Dolanski-Aghamanoukjan, L., 199
 Dolara, P., 211
 Dollman, M., 33
 Dolphin, A.C., 250
 Domanska-Janik, K., 47, 48
 Domenici, L., 55
 Donaldson, M.H., 98
 Donato, R., 247
 DonCarlos, L.L., 161
 Dong, W., 343–345, 348, 349
 Donkin, J.J., 211, 212, 214
 D'Onofrio, M., 247
 Donoho, D., 167
 Donovan, J.P., 312
 Doose, D.R., 348, 349
 Dore-Duffy, P., 24, 26
 Doré, S., 137, 141, 144
 Douglas, L., 174
 Doused, V., 283
 Drake, J., 207
 Drake, J.M., 89, 107
 Dresselhaus, M.S., 340
 Droste, D.W., 78
 Dubal, D.B., 159, 161
 Dubin, R.A., 338
 Dublin, A.B., 223
 Dubowitz, M., 151, 152
 Ducker, T.B., 91, 97
 Duda, D.G., 277
 Duffner, P.K., 272
 Du, J., 49
 Duldner, J., 138, 142
 Dumalska, I., 293
 Duncan, J.A., 65
 Dunn, W.F., 312
 Duranteau, J., 199, 202
 Du, X.X., 179
 Duyn, J.H., 183
 Dyson, P.J., 343, 344, 349

E
 Eastwood, J.D., 283, 286
 Eberle, R., 138, 142
 Echizenya, K., 91
 Eckstein, H.B., 97
 Eder, H., 111
 Ede, R.J., 312, 313
 Edwards, D.F., 152
 Edwards, O.M., 223
 Egawa, M., 315
 Egeler-Peerdeman, S.M., 72, 73, 78, 105, 107, 111, 113, 129
 Egleton, R.D., 280
 Ehrenfels, S., 274
 Eichler, L., 93
 Eiden, L.E., 43
 Eisel, U.L.M., 293
 Eisenberg, H.M., 228, 233
 Ejlersen, T., 118
 Ekholm, S., 196
 Ekman, G., 212
 Ekstedt, J., 69, 72
 Elango, C., 29
 Elango Singh, A.K., 29
 Elder, A., 351, 359
 Elfverson, J., 69, 72
 Eliot, R.S., 152
 Ellika, S.K., 283, 286
 Elliott, J.P., 312
 Elliott, K.A.C., 65, 296, 344, 352, 354
 Ellis, E.F., 247
 Elrifai, A.M., 152
 Els, T., 228
 Emery, J.L., 97
 Emond, J.C., 312
 Emoto, K., 152
 Emsley, H.C., 3, 33
 Endo, S., 45
 Endresz, V., 40
 Engel, D., 228

- Engelhorn, T., 227, 228
 Enger, P., 87
 Eng, L.F., 212
 Enomoto, H., 33
 Enzan, H., 125
 Epstein, F., 207, 235
 Epstein, J., 343, 344, 348
 Erdohazi, M., 97
 Ergul, A., 30
 Ericson, K., 187, 190
 Eriksson, L., 172
 Ernst, T., 193
 Eros, C., 228
 Errington, M.L., 250
 Ertürk, Ü., 97
 Eskenazi, A.E., 171
 Eslava, R., 97
 Esmonde, T., 114
 Essay, M., 283
 Essig, M., 51, 187, 190
 Etienne, A., 343, 349
 Evans, A.E., 98
 Evans, D.E., 351, 356
 Evans, S., 193
 Evelhoch, J.L., 193
 Evera-Preesman, M., 183
 Everson, G.T., 313
 Eymann, R., 69–73, 75–78, 87–89, 91–93, 95, 98, 101, 102, 104, 105, 107, 108, 111, 114, 121, 122, 125, 128, 129
 Ezaki, O., 251
- F**
- Faber, J.A., 111
 Fabry, Z., 293
 Faden, A.I., 301, 304, 305
 Fagan, E.A., 313
 Fagan, S.C., 30
 Fagerlund, M., 69, 72, 271
 Fagiolini, M., 55
 Fahlbusch, R., 223
 Failli, V., 295, 297, 299
 Fainardi, E., 138, 141, 142, 144
 Fair, J., 313
 Falini, A., 193
 Fang, S., 338
 Faraci, F.M., 227
 Fareh, J., 239
 Farkas, E., 40
 Farkas, I.G., 40
 Farmer, S., 23
 Farro, S., 196
 Faso, L., 38
 Fassbender, K., 32, 33
 Fatar, M., 32
 Fatouros, P., 250
 Fattal-Valevski, A., 203, 207
 Fawcett, J.W., 251, 252
 Fayed, N., 196
 Fazeli, M.S., 250
 Fearn, S., 39
 Fedele, P., 171
 Feign, V.L., 134
 Feikert, T., 351, 359
 Fei, Z., 343, 344, 349
 Felberg, R.A., 148, 161
 Feltes, C.H., 199
 Fenart, L., 23
 Fenske, A., 4, 5
 Fenstermacher, J.D., 4, 6, 7
 Fenstermacher, J.P., 4, 6
 Ferdinandy, P., 48
 Ferguson, A.R., 64
 Fernández-Cadenas, I., 137
 Fernell, E., 95
 Festoff, B.W., 149
 Feuerstein, G.Z., 33
 Fèvre-Montange, M., 125
 Fiebich, B.L., 147
 Fieschi, C., 165
 Figueira, E.R., 312
 Filho, J.A., 312
 Filippini, V., 271
 Fingas, M.S., 228
 Fini, M.E., 33
 Finkelstein, J., 351, 359
 Fink, M.E., 151, 152
 Finn, T.M., 55
 Fischer, D., 359–361, 363
 Fischer, I., 299
 Fischer, S., 55
 Fisher, M., 30
 Fishman, H.A., 339
 Fishman, M.A., 199
 Fishman, R.A., 207
 Fitz, C., 274
 Flardh, M., 344
 Fleshner, M., 64
 Flessner, M., 239, 244
 Flickinger, J.C., 53, 187–190
 Flora, R.E., 201, 202
 Floyd, J., 134
 Foda, M.A., 240
 Follett, P.L., 33
 Fontana, R.J., 312, 313
 Fontanesi, J., 171
 Foote, R.L., 187, 190
 Forbes, A., 312, 313
 Forsting, M., 226–228
 Fortunati, M., 133
 Fossati Belani, F., 274
 Fouladi, M., 191
 Foulkes, M.A., 233
 Fountas, K.N., 199
 Frances, B., 343, 349
 Franceschi, G., 9, 10
 Francis, D., 196
 Francis, P.T., 179
 Frank, J.A., 183
 Franklin, R.J.M., 293
 Franklin, T.B., 55
 Frank, M.G., 64
 Frankowski, H., 212
 Franz, K., 9
 Frattarelli, M., 9, 10
 Freeman, A.I., 195
 Freeman, C.R., 271
 Friedman, A.H., 10, 134
 Friedman, H.S., 10
 Friese, A., 343, 349
 Frisch, S.M., 292
 Fritsch, C., 8

- Fritsch, M.J., 233
 Fritz, G., 247
 Frontczak-Baniewicz, M., 251, 252
 Fruhwirth, M., 292
 Fujii, S., 307
 Fujimoto, T., 45
 Fujita, T., 84
 Fujiwara, K., 33
 Fuke, N., 265, 267
 Fukumura, D., 277
 Fukunaga, Y., 292, 293
 Fukuyama, H., 177
 Funahashi, H., 315
 Furey, M.L., 177
 Furuno, M., 223
 Furuya, S., 185, 193
 Fuss, M., 193
- G**
- Gaab, M.R., 233
 Gabay, T., 338, 339
 Gabrion, J., 239, 243, 244
 Gabry, J., 30
 Gage, E.L., 235
 Gajjar, A., 51, 191, 193
 Gajkowska, B., 81–84
 Galasko, G.I.W., 151, 152
 Galvan-Garcia, P., 338
 Gambarota, G., 281
 Gambazzi, L., 339
 Gamrani, H., 124
 Garces, Y.I., 187, 190
 Garcia, J.H., 52, 156
 Garcia-Segura, L.M., 161
 Garden, O.J., 313
 Gardner, F.H., 98
 Garibi, J.M., 277, 283
 Garmestani, K., 11
 Garton, H.J., 118
 Gasche, Y.G., 33
 Gautille, T., 233
 Gavin, C.M., 33
 Gaynon, P., 195
 Gazendam, I., 4, 6
 Geeraerts, T., 199, 202
 Gelb, A.W., 151, 283, 284
 Gelein, R., 351, 359
 Gennarelli, T.A., 244
 Gentilello, L., 199
 George, A.P., 171
 Georgiadis, D., 228
 Georgieff, M., 223
 Georgiou, R.F., 33
 Georgopoulos, A., 97, 98
 Geppetti, P., 211
 Gerber, N., 155
 Gerhold, L.M., 161
 Gerlach, M., 161
 Germanson, T., 267
 Gerner-Smidt, P., 118
 Gertz, K., 217
 Ge, S., 23
 Geyer, J.R., 95
 Ghabriel, M.N., 58, 211, 240
 Ghajar, D., 261, 262
 Ghajar, J., 233, 236, 267
 Gharib, C., 239
 Gheith, M.K., 338
 Ghirnikar, R.S., 212
 Ghristina, A.G., 87
 Giaconelli, R., 81
 Gibbons, A., 295–297, 299
 Gibson, C., 30
 Gibson III, D.G., 30
 Gibson, J.S., 124
 Gidday, J.M., 33
 Gilberg, C., 271, 272
 Gildehaus, F.-G., 10
 Gildehaus, F.-J., 10
 Gilg, A.G., 29
 Gilsbach, J.M., 95
 Gimson, A.E., 311–313
 Ginis, I., 33
 Ginsberg, M.D., 52, 58
 Gin, T., 133
 Gioia, G.A., 301
 Giorgi, C., 271, 272
 Giricz, Z., 48
 Giri, S., 29
 Gisvold, S.E., 269
 Giugliano, M., 339
 Giuliani, G., 9, 10
 Giza, C.C., 58
 Gjerris, F., 69, 72, 73, 95, 129, 199, 201
 Glass, J.O., 191
 Glenn, C.T., 283
 Glenn, T.C., 269
 Goddard-Finegold, J., 199
 Godersky, J.C., 78
 Goedhart, Z.D., 78, 101, 104
 Goetz, A., 8
 Goetz, C., 7, 8, 10
 Goffin, J., 272
 Gohongi, T., 277
 Go, K.G., 17, 25
 Golabek, A.A., 38
 Goldsteins, G., 147
 Goldwein, J., 274
 Gold, W.M., 98
 Golech, S., 26
 Golomb, J., 129
 Gomez, D.E., 49
 Gong, C., 144, 147, 149
 Gong, Y., 147, 149
 Gonzalez, R.G., 137
 Goodrich, J.T., 91
 Gooskens, R.H., 78, 107, 111, 113
 Goplen, G., 152
 Gordh, T., 301, 302, 304, 305, 352, 356
 Gordon, D., 236
 Gorelik, O., 351, 356
 Gorman, G., 337
 Goto, N., 45, 315
 Gotsis E.D., 193
 Gottfried, O.N., 95
 Govoni, V., 141, 142, 144
 G&\$\$\$<owacki, M., 199, 202
 Graber, S., 6
 Grabiec, S., 30
 Gradilone, S.A., 24, 26
 Gradin, C.B., 283

- Graffagnino, C., 134
 Graff-Radford, N.R., 78
 Graf, U., 212, 214
 Graham, D., 147
 Graham, D.I., 244
 Graham, R., 3, 5
 Grandolfo, M., 339
 Granger, D.N., 32
 Granholm, A.C., 55
 Granieri, E., 138, 141, 142, 144
 Granstom, L., 212
 Grant, G.A., 301
 Gräslund, A., 174
 Grattan, A., 324
 Grau, J.W., 64
 Graupner, G., 47, 217–219
 Graves, E.E., 173, 185
 Graves, W., 129
 Gräwe, A., 233
 Gray, L., 52
 Greenberg, B.M., 75
 Greenberg, M., 196
 Greenberg, M.E., 292
 Greenberg, R., 235
 Green, P., 64
 Greitz, D., 69, 71, 104
 Grieb, P., 166, 171, 184
 Griesbach, G.S., 58
 Griggs, J.R., 199
 Grigorian, A.A., 199
 Grimm, C., 165
 Grochowski, W., 202
 Gröger, U., 7
 Gröhn, O.H., 29
 Grollmund, L., 45
 Groothuis, D.R., 4–7, 9
 Groothuis, E.N., 5
 Grosse-Wilde, H., 141
 Gross, G.W., 340
 Grossman, R.I., 193
 Grotta, J.C., 148, 161, 293, 294
 Gruetter, R., 178
 Grumme, T., 107
 Grünblatt, E., 178
 Grygar, E., 292
 Guan, Y., 217, 219
 Guell, A., 239
 Guérette, D., 125
 Guerin, C.J., 292
 Guerra, W.K., 233
 Gu, G.J., 217, 219
 Gujar, S.K., 171
 Gul, H., 64
 Gullan, R., 312, 313
 Guo, S., 324
 Gupta, A., 228
 Gupta, R., 265
 Gupta, S.K., 265
 Gupta, Y.K., 179
 Gurkoff, G.G., 58
 Gurney, J.G., 51
 Gutierrez-Ramos, J.C., 32
 Gwózdź, B., 30
 Haberkorn, U., 177
 Hacke, W., 165, 226, 227
 Haddon, R.C., 337, 338
 Hadman, M., 39
 Haerich, P., 51
 Haga, C., 40
 Haga, S., 40
 Hagler, H., 228
 Hahn, K., 10
 Haidri, N.H., 105
 Haines, S., 107
 Hakamata, Y., 17
 Hallenbeck, J., 18
 Hallenbeck, J.M., 32, 33, 43
 Hall, W.A., 11
 Halperin, M., 89
 Hamans, B., 281
 Hamelink, C.R., 43
 Hamilton, R.L., 228
 Hamou, M.F., 45
 Hampl, J.A., 81
 Hamprecht, F.A., 171
 Han, D.H., 190
 Hanein, Y., 339
 Hanid, M.A., 312, 313
 Hanlo, P.W., 72, 73, 78, 105, 107, 111, 113, 129
 Hann, I., 195
 Han, S., 312, 313
 Hansen, B.A., 312, 313
 Hansen, H.C., 312
 Hansen, K., 228
 Hansen, S., 179
 Han, S.S., 299
 Han, S.W., 24, 26
 Hanus, L., 26
 Hanyu, S., 17
 Haorah, J., 21
 Hara, M., 189
 Harder, H., 51
 Hardingham, G.E., 292, 293
 Hardingham, N.R., 293
 Hardy, I.G., 244
 Hargens, A.R., 199
 Harkness, W., 81
 Harms, C., 217
 Harrington, D.A., 348, 349
 Harris, J.S., 339
 Harris, M., 257, 260
 Harrison, M.E., 312, 313
 Harris, W.H., 98
 Hartl, R., 236
 Hartyanski, I., 97
 Hasan, D., 119
 Hasebe, N., 33
 Hasegawa, T., 187, 190
 Hashimoto, H., 43, 45
 Hashimoto, M., 91
 Hashizume, H., 280
 Hassan, A., 7
 Hassan, I., 211, 212, 214
 Hass, G.M., 228
 Hasui, Y., 308
 Hattori, A., 84
 Hattori, K., 48
 Hattori, Y., 156, 318
 Hauck, E.F., 33

H

- Hauerberg, J., 95
Haughton, V., 185, 193
Hauk, T., 359–361, 363
Hauser, G.J., 76
Hauser, S.L., 214
Hauser, W.A., 225
Hawkins, B.T., 292
Hawrylewicz, L., 174, 183
Hayakawa, H., 156
Hayashi, D., 13, 45
Hayashi, H., 7
Hayashi, N., 185, 193, 228
Hayashi, Y., 125
Hayes, P.C., 312, 313
Hay, J., 239, 244
Hayward, R., 81
Hayward, R.H., 51
Heath, D.L., 40, 45, 211, 212, 214
Hebb, A.O., 72, 73, 78, 101, 104, 107, 111, 129
Hedlund, S., 351, 356
Hedqvist, P., 211
Heegaard, W., 228
Heerschap, A., 193, 281
He, H., 340
Heideman, R.L., 271
Heiland, S., 217, 226–228
Heimann, A., 7, 33
Heissler, H.E., 233
Heizmann, C.W., 247
He, L., 341
Helmke, K., 312
Helps, S.C., 211, 214
Hemmer, R., 93
Hendryk, S., 30, 33
Hennerici, M., 32, 33
Henning, R., 228
Henry, S., 147
Henze, M., 177, 183
Heo, J.H., 24, 26
Herbuté, S., 239
Herfarth, K.K., 183
Hermann, D.M., 17, 39
Hermans, J., 72, 73, 78, 105, 107, 111, 113, 129
Herman, Z.S., 30
Hermelin, E., 91, 93
Herndon, J.E., 10
Herrmann, M., 51
Hertzberg, V., 138, 142
Hertzog, J.H., 76
Hesdorffer, D.C., 228, 233, 261, 262
Hess, D.C., 30, 39
Hetman, M., 292
Hetzl, A., 228
Heuer, G.G., 263
He, Y., 149
Hey, O., 7
Hiai, H., 318
Higgins, C.F., 23
Hildebrandt, G., 51
Hiler, M., 225
Hillered, L., 269
Hill-Felberg, S.J., 148, 161
Hillinger, S., 156
Hill, R.S., 183
Hilton, H.B., 97
Hinds, W., 239
Hiraizumi, Y., 315
Hirano, T., 312
Hirasawa, H., 312
Hirata, Y., 156
Hiratsuka, K., 315–318
Hirayama, Y., 312
Hiroi, T., 156
Hirose, M., 43
Hirsch, H.F., 89
Hirsch, J.F., 107, 193
Hirsch, R., 263
Hirt, L., 26
Hitomi, Y., 307
Hobgood, C.D., 87
Hochmuth, A., 165
Hochwald, G.M., 5, 6, 11, 244
Hockley, A.D., 107, 207
Ho, C.L., 228
Hodoyama, K., 43, 45
Hoehn-Berlage, M., 5
Hoekstra, R., 313
Hoff, J.T., 137, 140, 141, 144, 147–149, 159–161, 217, 307, 309
Hoffman, H.J., 97, 98, 107
Hoffmann, J.F., 33
Hoffmann, T.T., 228
Hof, H., 51, 187, 190
Hofmann, F., 293
Hogg, N., 155
Hogh, P., 72, 73
Hohnadel, E.J., 30
Hokfelt, T., 214
Hollanda, M., 121
Holleran, R., 138, 142
Holmes, E., 171
Holmin, S., 58
Homma, S., 151, 152
Honegger, J., 223
Hong, H., 155, 156
Honore, P., 311
Hook, M.A., 64
Hoopes, P.J., 321, 324, 327
Hopewell, J.W., 51
Hopkins, S.J., 33
Hoppe-Hirsch, E., 193
Horai, R., 315
Hori, M., 363
Horm, J.W., 271
Horn, P., 267
Horwitz, B., 177
Hoshika, A., 318
Hossmann, K.-A., 5
Houkin, K., 315
Hovda, D.A., 58, 269
Hovind, K.H., 97
Howard, R.G., 171, 174
Howe, F.A., 171
Hoyer, S., 177, 178
Hsieh, L., 32
Hsieh, S., 359, 363
Hsu, F.P., 217, 218
Hsu, P.W., 187, 190
Huang, P.L., 277
Huang, Y.C., 187, 190
Hua, Y., 147–149, 159–161, 217, 307, 309
Hubbs, A.F., 351, 356
Huber, J.D., 277, 280

Huber, P., 6, 7
 Hudson, J., 338, 339
 Huffer, W., 89
 Hug, E.B., 193
 Hu, H., 338
 Huie, J.R., 64
 Humphrey, J.A.C., 11
 Hung, K.N., 283
 Hung, S., 24, 26
 Hung, Y.W., 235–237
 Hunt, A., 177
 Huppertz, H.J., 165
 Hurn, P.D., 48, 159, 161
 Hurskainen, H., 78
 Husain, K., 61
 Hussain, S., 351
 Hutchinson, P.J., 225, 228, 237
 Hutrado, O., 33
 Hutrdo, O., 30, 33
 Hutter-Paier, B., 292
 Hu, X., 40, 45, 211, 212, 214
 Hu, X.J., 52, 156
 Hyman, B.T., 179
 Hynne, H., 269

I

Iadecola, C., 30, 33
 Iannotti, F., 267
 Ibáñez, V., 177
 Ichihashi, T., 337
 Ide, M., 185, 189, 193
 Iida, K., 228
 Ijima, S., 337
 Ikari, N., 307
 Ikeda, Y., 121, 125, 315, 317, 318
 Ikenaka, K., 45
 Imai, Y., 147
 Imfeld, S., 273
 Inaba, Y., 5, 17
 Inn, R., 315
 Intiso, D., 33
 Ippolito, S., 118
 Iseda, T., 293
 Ishida, A., 125
 Ishii, M., 156
 Ishii, Y., 185, 193
 Ishikawa, K., 40
 Ishimaru, H., 40
 Isimer, A., 64
 Islekel, S., 97
 Itabashi, K., 45
 Itano, T., 309
 Itoh, S., 185, 193
 Itokawa, H., 45
 Ito, U., 6, 7, 17
 Ito, Y., 351, 359
 Itoyama, Y., 33
 Ivankovich, A.D., 202
 Ivanov, A., 293
 Iwai, A., 228
 Iwakura, Y., 43, 45, 315
 Iwamoto, I., 211
 Izumi, J., 187, 189
 Izumi, Y., 277
 Izumiyama, H., 318

J

Jackson, R.G., 247
 Jadhav, V., 217–219
 Jaeger, M., 263
 Jagota, A., 340
 Jahromi, B.S., 133
 Jain, H., 107, 207
 Jain, R., 152, 283, 286
 Jain, R.K., 277
 Jakobs, E., 339
 Jakowitsch, J., 97, 98
 Jakubowska-Sadowska, K., 37
 Jalan, R., 312, 313
 Jan, E., 339
 Jane, J.A., 233, 267
 Janeway, C.A., Jr., 33
 Jansen, B., 81
 Januszewski, S., 37–40
 Jarrell, B., 312
 Jarvet, J., 174
 Jarvi, J., 239
 Jarz&aogonek;b, B., 33
 Jasmine, J.F., 23
 Jasper, H., 65, 296, 352, 344, 354
 Jatana, M., 29
 J&eogonek;drzejowska-Szypułka, H., 29
 Jefferies, W.A., 40
 Jeffries, A.R., 40
 Jenden, D.J., 193
 Jenkins, A., 147
 Jenkins, L.W., 228
 Jenner, A., 315
 Jenner, P., 315
 Jennett, B., 222, 235, 237
 Jennings, F.W., 214
 Jensen, F.E., 33
 Jetzki, S., 69, 73, 102
 Jiang, H., 283, 286
 Jiang, J.Y., 228, 261, 262
 Jiang, L., 43
 Jiang, Y., 160
 Jieyong, B., 228
 Jimbo, H., 318
 Jimbo, M., 189
 Jimenez, D.F., 91
 Jin, H., 351
 Jin, T., 343, 348
 Jodoin, J., 23
 Johansen, J., 185, 193
 Johanson, C.E., 65, 321, 322, 324, 327, 331
 Johansson, O., 212
 Johansson, R., 184, 192, 193
 Johnsen, J.I., 174
 Johnson, D., 152
 Johnson, D.J., 212
 Johnson, V.J., 351, 356
 Johnston, I.N., 64
 Johnston, M., 239, 244
 Johnston, S., 89
 Jones, H.C., 121, 122, 124, 125
 Jones, J.J., 293
 Jones, K., 179
 Jones, M.P., 78
 Jones, T.W., 121, 122, 124, 125
 Jones-Wallace, D., 274
 Joó, F., 17

Jorgensen, L., 312
 Josko, J., 30, 33
 Jourdan, C., 263
 Juhler, M., 72, 73
 Jung, G., 10
 Jung, J.C., 33
 Jun, S.S., 228
 Jurkiewicz, J., 199, 201, 202
 Juul, N., 268
 Juurlink, B.H., 30

K

Kaalund, J., 69, 72
 Kadambi, A., 277
 Kadar, K., 97
 Kadowaki, T., 251
 Kagan, V.E., 351, 356
 Kahaku, E., 311, 312
 Kahlon, B., 69, 72
 Kahn, C.R., 251
 Kaiser, G., 4, 6
 Kaiser, G.L., 121, 125
 Kajita, H., 239
 Kakoki, M., 156
 Kalend, A.M., 187, 189
 Kaliva, K., 33
 Kalivas, P.W., 291
 Kalkman, C.J., 199
 Kalyanaraman, B., 155, 156
 Kamada, K., 193
 Kammer, T., 33
 Kanamatsu, T., 181
 Kang, J.K., 228
 Kang, Y., 312
 Kang, Z., 49
 Kang, Z.M., 217, 219
 Kanmogne, G.D., 21
 Kanno, T., 228
 Kan, P., 75, 228
 Kanterewicz, B.I., 292
 Kapasi, M.Z., 228
 Kapinya, K., 217
 Kaplan, D.R., 295
 Kapsalaki, E.Z., 199
 Kaps, H.P., 295, 297, 299
 Karimi, A., 267
 Karlsson, B., 187, 190
 Karlsson, T., 69, 72, 271
 Karoui, H., 155
 Kasaga, M., 251
 Kasai, H., 318
 Kashiwada, T., 315
 Kashiwagi, A., 156
 Kassam, M., 199
 Kassubek, J., 228
 Kaste, M., 165
 Kastrup, A., 227
 Katan, M., 221
 Katayama, H., 265, 267
 Katayama, T., 33
 Kato, K., 125
 Kato, Y., 228
 Katsumori, H., 212
 Katyare, S.S., 252
 Kaufman, D.I., 155, 156

Kaufman, H.H., 221
 Kaufmann, F., 273
 Kaufman, S., 156
 Kauppinen, R., 184, 192, 193
 Kauppinen, R.A., 29
 Kaur, C., 239, 244
 Kawaguchi, S., 293
 Kawahara, N., 17
 Kawai, K., 17
 Kawai, N., 228
 Kawamura, Y., 185, 193
 Kawasaki, T., 293
 Kawashima, H., 318
 Kazan, S., 91, 268
 Keating, R., 91
 Keays, R.T., 312, 313
 Keefer, E.W., 338, 340
 Keene, D.L., 171
 Keep, R.F., 32, 137, 140, 141, 144, 147–149, 159–161, 217, 307, 309
 Keilholz, L., 51
 Keinanen, R., 147
 Keir, G., 81
 Keller, E., 133
 Kellie, S.J., 191
 Kelly, D.F., 269
 Kelm, B.M., 171
 Kemper, T.L., 51
 Kempski, O., 7, 24, 33
 Kennedy, K., 195
 Kennedy, P.G., 214
 Kennington, E.A., 30
 Kessler, J.A., 348, 349
 Kestle, J., 107
 Kestle, J.R., 75, 111, 228
 Kestle, J.R.W., 118
 Keucher, T.R., 95
 Kevil, C.G., 32
 Khan, M., 29, 95
 Khanna, R.K., 118
 Khan, P.A., 125
 Kharebava, G., 292
 Kharkar, S., 104
 Khoo, J.B.K., 171
 Khosla, V.K., 265
 Khoury, J., 138, 142
 Kiang, C., 337
 Kida, E., 38
 Kidd, G.A., 155, 156
 Kiefer, M., 69–73, 75–78, 87–89, 91–93, 95, 98, 101, 102, 104, 105, 107, 108, 111, 113, 114, 121, 122, 125, 128, 129
 Kiefmann, R., 8
 Kiehna, E.N., 193
 Kihlström, L., 187, 190
 Kikkawa, R., 156
 Kikuchi, K., 33
 Kikuyama, S., 43, 45
 Kilic, E., 39
 Kilic, U., 39
 Kim, B.G., 359
 Kim, D., 299
 Kim, D.G., 190
 Kimelberg, H.K., 45
 Kim, H.W., 359
 Kim, I.H., 190
 Kim, J.S., 359
 Kim, M.C., 228

- Kim, S., 309
 Kim, S.W., 228
 Kim, T.A., 185, 193
 Kimura, H., 185, 193
 Kimura, J., 177
 Kimura, T., 33
 Kim, W.J., 324
 Kim, Y.J., 228
 King, R.B., 161
 Kinoshita, K., 228
 Kintzel, D., 129
 Kinugasa, E., 309
 Kiraly, L., 97
 Kirkpatrick, 134
 Kirkpatrick, P.J., 225, 228, 237
 Kisin, E.R., 351, 356
 Kita, H., 240
 Kitamura, S., 43
 Kitamura, Y., 43
 Kitaoka, T., 309
 Kitazawa, A., 338
 Kiuchi, K., 156
 Kiuchi, Y., 156
 Kiyatkin, E.A., 61, 66, 321, 360, 363
 Kiyoku, M., 125
 Kizu, O., 185, 193
 Kjallquest, A., 118
 Klann, E., 292
 Klason, T., 174
 Klassen, H., 39
 Klatzo, I., 3, 5, 17, 18, 25, 228, 363
 Klauber, M.R., 233
 Kleffner, I., 26
 Klegeris, A., 149
 Kleindienst, A., 247, 250
 Klein, M., 51, 293
 Klein, N.C., 147
 Klepetko, W., 97, 98
 Klepstad, P., 269
 Klieman, C., 97
 Klimo, P., 75
 Klinge, P., 75, 76, 114
 Klisch, J., 228
 Kloner, R.A., 152
 Klotz, P., 250
 Kluger, A., 129
 Kluger, M.J., 33
 Klug, G., 228
 Knapp, F., 217
 Knedla, A., 278
 Kneussl, M., 97, 98
 Knopp, E.A., 283
 Knoth, R., 278
 Knudsen, G.M., 313
 Kocak, M., 191
 Kocan, M.J., 118
 Kochanek, P.M., 32, 228
 Kocher, E.T., 265
 Kocher, M., 190
 Kock-Jensen, C., 118
 Kockro, R.A., 81, 84
 Kodama, Y., 152
 Koenig, H.M., 161
 Kofler, J., 48
 Koga, K., 43
 Kogner, P., 174
 Kogure, K., 33
 Kohn, D.F., 121, 124, 125
 Kohn, J., 338
 Kohnle, M.V., 359–361, 363
 Koistinaho, J.E., 147
 Koizumi, J., 30
 Kojima, H., 156
 Kojima, T., 223, 235
 Kokkinakis, D.M., 277
 Kollmar, R., 228
 Kolodziejczyk, D., 107
 Komai, T., 91
 Komenda, Y., 114
 Kondrup, J., 312
 Kondziolka, D., 187–190
 Konishi, J., 177
 Koo, J.S., 228
 Kopeä N., 30
 Kopf, M., 43, 45
 Korinth, M.C., 95
 Kornfeld, M., 155
 Korpatchev, W.G., 17
 Kortmann, R.D., 193
 Koshikawa, S., 309
 Koskinen, L.O., 265, 268
 Kosteljanetz, M., 69, 72, 201
 Kostyk, S.K., 214
 Kotani, T., 125
 Kothari, R.U., 138, 142
 Kotov, N.A., 338, 339
 Kotter, M.R., 293
 Kowall, N.W., 214
 Koyama, S., 33
 Kozicz, T., 43
 Krakenes, J., 33
 Kramer, A.H., 312, 313
 Kramer, D., 312
 Kramer, J.H., 196
 Krasnov, I., 239
 Krause, G.S., 121, 125
 Krauss, J.K., 78, 105
 Kreisel, S., 32
 Kremastinos, D.T., 33
 Kremer, L.C., 51
 Kreuter, J., 343, 349, 359
 Kreyling, W., 351, 359
 Kreysch, H.G., 3, 4
 Krieglstein, J., 212, 214
 Krishna, S., 280, 281
 Krismer, A.C., 223
 Kristensen, B., 69, 72, 271
 Kroin, J.S., 202
 Krouwer, H., 185, 193
 Król, W., 30
 Krull, K., 191
 Krum, J.M., 55
 Krupska, T., 171, 174, 184, 193
 Ku, B.K., 351, 356
 Kubota, T., 185, 193
 Kuchta, J., 190
 Kudo, Y., 45
 Kuehn, S.M., 171
 Kuhlenbäumer, G., 26
 Kuhl, S., 32
 Kulkarni, A.V., 89
 Kumar, A., 61

- Kumar, K.P., 343, 349
 Kumar, R., 121, 125
 Kumthekar, M.M., 252
 Kunis, D., 32
 Kunkel, S.L., 33
 Kun, L.E., 51, 191
 Kunugi, A., 43
 Kunze, S., 81
 Kunz, M., 133
 Kuo, J.S., 30
 Kuramoto, S., 235
 Kurashige, J., 308
 Kurisu, K., 228
 Kuroda, K., 33
 Kuroda, Y., 309
 Kuroiwa, T., 17
 Kuroki, T., 315, 317
 Kusaka, G., 47
 Kuschinsky, W., 55
 Kushima, M., 318
 Kuwamura, M., 125
 Kuznetsov, V., 337, 338
 Kwok-Chu, G., 235–237
 Kwok, R., 133
- L**
- Labiche, L.A., 293, 294
 Lachance, C., 33
 Laemmli, V.K., 252
 Lafuente, J.V., 55, 58
 Lafuente-Sanchez, J.V., 251, 252, 277, 278, 281, 283
 Lagioia, G., 33
 Lagostena, L., 339
 Lai, J.C., 311
 Lainez, J.M., 137, 140
 Lai, W.Y., 340
 Lake, J.R., 312
 Laliberte, L., 284
 Lalu, M.M., 48
 Lamberti-Pasculli, M., 89
 Lamb, V.A., 118
 Landfester, K., 359–361, 363
 Langer, S., 64
 Lang, I.M., 97, 98
 Langmoen, I.A., 97
 Langston, J.W., 191
 Laniewski, P., 199, 201
 Laningham, F.H., 191
 Lanksch, W.R., 114, 228, 265, 267, 268
 Lannert, H., 178
 Lao, N., 217
 Lapierre, F., 267
 Lapras, C., 207
 Lapustea, N.B., 324
 Laroussinie, F., 193
 Larsen, F.S., 311–313
 Larsen, P.H., 147
 Larson, A.M., 312, 313
 Larson, D., 185
 Laske, D.W., 11
 Laskowitz, D.T., 134
 Laskowski, E.J., 228
 Latapie, J.P., 343, 349
 Laurent, J.P., 199
 Lavinio, A., 228
 Lavin, P.T., 313
 Lawrence, B., 196
 Lawrenson, J.G., 55
 Lazarewicz, J.W., 37
 Le Discorde, M., 141, 144
 Lee, A., 312, 313
 Lee, B.C., 193
 Lee, J.K., 359
 Lee, J.Y.K., 187, 190
 Lee, K.H., 359
 Lee, K.K., 228
 Lee, K.R., 309
 Lee, K.W., 89
 Leeman, S.E., 214
 Leenders, W., 281
 Leenen, L.P., 199
 Leep, R.F., 309
 Lee, R., 283
 Lees, A.J., 315
 Lee, S.K., 24, 26
 Lees, K.R., 33
 Lee, S.R., 324
 Lee, T.Y., 283, 284, 286
 Lee, W.M., 312, 313
 Lee, Y.L., 212
 Lefebvre, S., 33
 Lefevre, R., 292
 Le Gall, J.R., 222
 Leggio, M.G., 271
 Lehmann, G.L., 24, 26
 Lehnardt, S., 33
 Lehrke, R., 190
 Leibfritz, D., 185
 Leigh, C., 58, 211
 Leinwand, L., 64
 Leira, R., 137, 140
 Leiter, E.H., 251
 Leito de Morais, A., 133
 Lek, P., 61, 62, 66, 343–345, 348, 349
 LeMaoult, J., 141, 144
 LeMay, D.R., 93
 Lemcke, J., 73, 101, 104, 113, 114, 231–233
 Lemeshow, S., 222
 Lenkinski, R.E., 193
 Lennihan, L., 151, 152
 Lenz, F.A., 26
 Leone, M., 261, 262
 Leong, L.L.Y., 283
 Leonhardt, S., 69, 73, 102
 LeRoux, P.D., 312
 Lerut, J., 313
 Lester-Coll, N., 178
 Levanti, M.C., 212
 Levegrun, S., 51
 Levegrün, S., 187, 190
 Levi, C.R., 69, 71
 Levisohn, L., 271–273
 Levy, M.L., 89
 Levy, R., 312
 Levy, R.M., 5
 Lewen, A., 317
 Lewis, B.K., 183
 Lewis, E., 228
 Leza, J.C., 33
 Lian, Q., 49
 Liao, C.C., 187, 190

- Liao, H., 32
 Liao, L., 152
 Liao, S.L., 30
 Liao, W., 217
 Li, C., 193
 Lichy, M.P., 171
 Li, C.K., 171, 174
 Lienhart, H.G., 223
 Li, J., 217, 219
 LiMandri, G., 151, 152
 Lim, M.K., 239, 244
 Lin, B., 52
 Lin, B.W., 58
 Lindbom, L., 211
 Lindefors, N., 212
 Lindgrenb, F., 172
 Lind, J.G., 39
 Lindner, I.M., 223
 Lindner, K.H., 223
 Lindquist, C., 187, 190
 Lindskog, M., 174
 Ling, E.A., 239, 244
 Ling, H.W., 283, 286
 Lin, J., 254
 Linke, M.J., 40
 Link, M.J., 187, 190
 Lin, R.C., 212
 Linton, K.J., 23
 Liopo, A.V., 338, 339
 Lipkowski, A.W., 37, 38
 Lippoldt, A., 21
 Liptak, G.S., 95
 Lisanti, M.P., 23
 Liu, C.Y., 89
 Liu, G.T., 64
 Liu, H., 212
 Liu, K.F., 52, 156
 Liu, W., 217, 219, 228
 Liu, Y., 49
 Liu, Z., 341
 Li, W.P., 261, 262
 Li, X., 173
 Li, Y.P., 217, 219
 Lizasoain, I., 30, 33, 137
 Ł&aogonek;tka, D., 30
 Loach, A.B., 152
 Lobato, R.D., 261, 262
 Locatelli, M., 261, 262
 Lo, C.H., 118
 Loeffler, J.S., 277
 Lo, E.H., 33, 137, 138, 140, 324
 Lo, E.H.18, 24, 26
 Löfgren, J., 202
 Logan, A., 251, 252
 Lohr, J.M., 17
 Lohr, M., 263
 Lok, J., 324
 Lombardi, G., 313
 Lomber, S.G., 58
 Longa, E.Z., 52
 Long, N.C., 33
 Longridge, N.S., 223
 Long, T.C., 351
 Loppman, B.A., 121, 122, 124, 125
 Lorenz, B., 343, 349
 Lorenz, M., 233
 Lorenzo, P., 30, 33
 Lossinsky, A.S., 38–40
 Losy, J., 32
 Louis, P.T., 199
 Lovat, V., 339
 Lovblad, K.O., 273
 Lovett, E.C., 69, 71
 Lo, W., 217–219
 Lowe, S.L., 179
 Lowry, G.V., 351
 Lozier, A.P., 118
 Lsoasso, T.J., 97
 Luerssen, T.G., 233
 Luheshi, G.N., 33
 Lukas, L., 171
 Lukyanovich, V., 337, 338
 Lämätäinen, T., 29
 Lu, M.X., 211
 Lundar, T., 97
 Lundberg, J.M., 214
 Lundberg, N., 118
 Lundstedt, T., 61, 62, 66, 343–345, 348, 349
 Lunsford, L.D., 187–190
 Luo, B.H., 324
 Luo, J., 277
 Lurie, K.G., 223
 Lustig, S.R., 340
 Lu, Y.F., 292
 Lyeth, B.G., 228
 Lyke, K.E., 118
 Lynch, J.R., 134
 Lysenkov, S.P., 17
 Lyubimova, N., 51
- M**
 Maas, A.I., 267
 Maass, C., 281
 Mabbot, D., 196
 Macdonald, R.L., 133
 Machado, M.A., 312
 Machado, M.C., 312
 Machein, M.R., 278
 Macias, B.R., 199
 Maciejewski, B., 171, 173, 174, 184, 185, 192, 193
 MacLellan, C.L., 228
 Mac Neil, N., 107
 Macrae, I.M., 159
 Madden, C., 199
 Maddrey, W.C., 312
 Madhavan, K.K., 313
 Maeda, T., 185, 193
 Maegawa, H., 156
 Maffei, L., 55, 58
 Maggi, C.A., 211
 Maggio, J.E., 212
 Magistretti, P.J., 45
 Maheshwari, S., 171
 Mahgrefte, B., 97
 Maier, C.M., 32
 Maier, S.F., 64
 Mailänder, V., 359–361, 363
 Maitz, A.H., 187, 189
 Majid, A., 155, 156, 239
 Majos, C., 171
 Makita, Y., 33

- Malarkey, E.B., 337
 Maldjian, J.A., 165
 Malek, A.M., 228
 Malhotra, S., 23
 Malik, A.B., 39
 Malm, J., 69, 72, 271
 Manavis, J., 211–215
 Mancini, A., 313
 Mandal, S.K., 338
 Manfrinato, M.C., 138
 Mani-Ponset, L., 239
 Manley, G.T., 45, 280, 281
 Manninen, P.H., 151
 Mann, K.S., 119
 Mansfield, R.T., 228
 Mantyh, P.W., 212
 Marchetti, L., 293
 Marcus, K.J., 183
 Margail, I., 32
 Maria, T., 283
 Marinelli, R.A., 24, 26
 Marion, D.W., 233, 267
 Markgraf, C.G., 228
 Mark, K.S., 277
 Mark, L., 185, 193
 Markram, H., 339
 Marler, J.R., 138, 142
 Marmarou, A., 5, 6, 10, 11, 75, 76, 114, 233, 240, 250
 Maron, L., 51
 Marrero, J.A., 312
 Marriott, I., 33
 Marrocco, A., 133
 Marsden, C.D., 315
 Marshall, L.F., 233, 268
 Marshall, S.B., 268
 Martásek, P., 155, 156
 Martelli, S., 311
 Marti, H.H., 39, 47, 48, 55, 217
 Martin, D., 64
 Martinez, H., 17
 Martin, F.J., 58
 Martin, L.J., 48
 Martin, N.A., 188, 269
 Martin, P., 312
 Martin, R.D., 52
 Martin-Villalba, A., 30
 Maruyama, J., 33
 Maruyama, Y., 40
 Marzola, A., 141, 142, 144
 Masada, M., 156
 Masaoka, H., 7
 Masiulis, B.S., 95
 Mason, G.F., 181
 Maseguin, C., 239
 Masson, J.L., 293
 Masters, B.S.S., 155
 Matchett, G., 217, 218
 Matchett, G.A., 52
 Matchett, G.C., 52
 Mathew, P., 236
 Mathewson, A., 251, 252
 Mathew, T.C., 243, 244
 Matsler, E.J., 247
 Matsuda, K., 43, 45, 312
 Matsuda, T., 43
 Matsui, H., 292
 Matsumoto, K., 121, 125, 318, 338
 Matsunaga, A., 45
 Matsunaga, M., 315
 Matsuno, A., 265, 267
 Matsuno, R., 43, 45
 Matsuo, Y., 33
 Matsushima, G.K., 293
 Matsushita, M., 292
 Matsuura, N., 33
 Matta, B.F., 228
 Mattson, M.P., 337
 Matts, R.L., 338
 Matulewicz, Ł., 174, 183
 Matus, B., 217–219
 Matz, P., 317
 Maurel, D., 239
 Mauritz, W., 199
 Mautes, A.E., 225–228
 Maxwell, W., 147
 Maxwell, W.L., 244, 251, 252
 Ma, Y., 340
 Mayer, S.A., 151, 152
 Mayhall, C.G., 118
 Maynard, A., 351, 356, 359
 Mayr, V.D., 223
 Mazarati, A.M., 212
 Mazzatenta, A., 339
 Mazze, M., 195
 McAdory, B.S., 250
 McAllister, II J.P., 121, 125
 McArthur, D.L., 269
 McBride, D., 193
 McCabe, J.J., 312, 313
 McCarron, R.M., 18, 26
 McCarthy, R.J., 202
 McChesney, L.P., 313
 McCluggage, C.W., 191
 McCluskey, J., 141, 144
 Mc Coll, B.W., 33, 34
 McComb, J.G., 89, 93
 McConnell, P., 251, 252
 McDermott, M., 185
 McDonagh, P.F., 33
 McDonald, D.M., 280
 McDonald, J.V., 95
 McDonald, M., 343, 344, 348
 Mc Donald, S., 196
 McGadey, J., 244
 McGeer, P.L., 149
 McGirt, M.J., 134, 152
 McGrail, K.M., 97
 McGraw, G., 124
 McGuire, B.M., 312, 313
 McInerney, J., 187, 190
 McLean, A.J., 212
 McLean, C.A., 171
 McLean, R.S., 340
 McLendon, R.E., 10
 Mc Lone, D.G., 89, 91
 McNall-Knapp, R.Y., 183
 McWilliams, J.L., 337
 Mealey, J., 95
 Mechoulam, R., 26
 Medina, I., 293
 Medlock, M.D., 76
 Medzhitov, R., 33

- Megow, D., 217
 Mehta, R.L., 312, 313
 Meier, U., 70, 73, 78, 91–93, 101, 102, 104, 107, 108, 111, 113, 114, 129, 231–233
 Meinel, T., 8, 9
 Meixensberger, J., 263
 Melchiorri, L., 141, 142, 144
 Mellon, P.J., 312, 313
 Mendelow, A.D., 237
 Mengeot, M.M., 193
 Menier, C., 141, 144
 Menon, D., 228
 Menon, D.K., 237
 Menze, B.H., 171
 Merceron, S., 199, 202
 Mercer, R., 351, 356
 Merchant, T.E., 51, 191, 193
 Mercier, I., 23
 Merkel, N., 24
 Merrill, J.E., 64
 Metellus, P., 104
 Metnitz, P., 199
 Metreweli, C., 171, 174
 Metselaar, H.J., 313
 Meurisse, M., 311
 Meyer, B., 134, 165, 166
 Meyer, F.B., 97
 Meyer, G., 185, 193
 Meyerovitch, J., 251
 Meyerson, B., 214
 Micic, D., 25
 Mielke, O., 165
 Mierzejewski, M., 199, 202
 Mies, G., 17
 Miethke, C., 114
 Mihal, A., 40
 Mihara, Y., 315, 317, 318
 Mii, K., 260
 Mikkelsen, T., 283, 286
 Milani, N., 272, 274
 Miller, A.J., 33
 Miller, B.L., 184, 193
 Miller, D.C., 129
 Miller, F.D., 295
 Miller, J., 235
 Miller, J.D., 201, 202
 Miller, J.M., 121, 125
 Miller, R.W., 271
 Milligan, E.D., 64
 Mills, N.L., 359, 363
 Milner, R., 24, 26, 107
 Milton, A.S., 321, 324
 Minagar, A., 40, 45
 Minami, N., 39
 Minamino, N., 43
 Mintzopoulos, D., 183
 Misicka, A., 37, 38
 Mischczyk, L., 174, 193
 Mitchell, G.S., 161
 Mitchell, P., 237
 Mitolo-Chieppa, D., 311, 313
 Mitrasinovic, O.M., 324
 Mitre, B., 55, 277
 Mitsias, P.D., 133
 Mittler, M.A., 89
 Miyajima, M., 121, 125
 Miyajima, T., 318
 Miyake, Y., 315, 317, 318
 Miyamoto, O., 309
 Miyaoka, H., 315
 Miyata, A., 43
 Miyazaki, J., 43
 Miyazawa, T., 47, 121, 125, 217
 Mizoi, K., 187, 189
 Mlynarek, M., 133
 Modri, S.M., 105
 Mohammed, A.H., 55
 Mohanty, S., 301, 302, 304, 305, 352, 356
 Mohindra, S., 265
 Molfetta, R., 212, 214
 Molina, C.A., 137, 140
 Molinari, M., 271
 Monasterio, J., 137, 140
 Montana, V., 337, 338
 Montaner, J., 137, 140
 Monthieux, M., 337, 338
 Moody, M.R., 228
 Moomaw, C.J., 138, 142
 Moons, K.G., 199
 Mooradian A.D., 251, 254
 Moore, B., 196
 Morabito, V., 311
 Morales, H., 196
 Moran, D.W., 340
 Morbidelli, L., 211, 277
 Mordego, P., 196
 Moreau, P., 141, 144
 Morel, L., 121, 122, 124, 125
 Morell, P., 293
 Moreno-Torres, A., 171
 Morgenthaler, N.G., 221–223
 Mori, E., 33
 Moriguchi, T., 312
 Mori, K., 125
 Morikawa, K., 265, 267
 Morikawa, T., 125
 Morimoto, T., 152
 Morishita, H., 185, 193
 Mori, T., 33
 Moritz, M., 312
 Mori, W., 43
 Moriwaki, H., 315, 317
 Moriya, T., 228
 Moro, M.A., 30, 33
 Morris, G.F., 268
 Morris, J.N., 284
 Morrison, P.F., 11
 Morris, R., 171, 174, 184
 Morriss, G.M., 244
 Mortensen, E.L., 274
 Mor, V., 284
 Moseley, M.E., 227
 Moser, E., 193
 Moskowitz, M.A., 33, 211, 217
 Mossakowski, M.J., 37–40
 Mottolose, C., 263
 Mrsulja, B.B., 25
 Mueller, C.A., 295, 297, 299
 Mueller, J.U., 233
 Mueller, W., 185, 193
 Mühlbauer, M., 118
 Muir, J.K., 247

Muir, K.W., 33
 Muizelaar, J.P., 307, 309
 Mukherjee, K.K., 265
 Mukundan, S., 283, 286
 Mulhern, R.K., 51, 171, 191, 193, 195, 274
 Muller, A., 121, 125
 Muller, B., 221
 Muller, C., 247, 250
 Muller, J., 274
 Müller, R.P., 190
 Mun-Bryce, S., 155
 Munch, E., 267
 Munoz, S., 312, 313
 Munoz, S.J., 312
 Muraca, M., 313
 Murai, H., 91
 Murakami, M., 265, 267
 Muraszko, K., 207
 Muresanu, D.F., 327, 328, 331
 Muresanu, F.D., 291, 293
 Muroi, C., 133
 Murphy, G.M., Jr., 324
 Murphy, J.A., 55
 Murphy, N., 312, 313
 Murphy, R., 247
 Murphy, S., 30, 98
 Murray, A.R., 351, 356
 Murray, G., 237, 267
 Murray, M., 214, 299
 Muzzi, D.A., 97
 Myers, T.L., 55
 Myhr, K.M., 33

N

Nabavi, D.G., 283, 284
 Nadel, J.A., 98
 Nagalla, S.K., 202
 Nagano, T., 156
 Nagao, S., 228, 309
 Nagashima, G., 17, 45
 Nagashima, T., 7, 265, 267
 Nagata, D., 156
 Nagel, S., 217
 Nag, S., 25, 277
 Nakagawa, H., 4, 6, 7
 Nakagawa, N., 211
 Nakajo, S., 43, 45
 Nakamachi, T., 43, 45, 315–318
 Nakamura, M., 33, 43, 312
 Nakamura, N., 121, 125
 Nakamura, S., 315–318
 Nakamura, T., 5, 6, 11, 149, 159, 161, 228, 309
 Nakamura, Y., 318
 Nakanishi, K., 312
 Nakanishi, N., 156
 Nakashima, Y., 309
 Nakatani-Enomoto, S., 33
 Naka, Y., 32, 338
 Nakayama, H., 125
 Nakayama, K., 235
 Nakayama, N., 315
 Nakazawa, A., 277, 280
 Nakazawa, T., 30
 Naldini, L., 292
 Nani, R.S., 312

Narayana, P., 148, 161
 Narayan, R.K., 233, 267
 Narayan, R.R., 199
 Naredi, S., 265, 268
 Naruse, S., 185, 193
 Nathan, P.C., 51
 Navalitloha, Y., 5
 Nawashiro, H., 47, 217
 Nawata, S., 156
 Neary, D., 179
 Nedergaard, M., 21, 22, 40
 Neely, T.R., 177
 Negendank, W.G., 193
 Nehen, A.M., 69, 72
 Nehring, V., 5, 6
 Neimark, A., 338
 Nelson, S.J., 173, 185
 Nerurkar, M.A., 252
 Ness, K.K., 51
 Neumann, U., 73, 101, 104, 113
 Neumayer, G., 255
 Neuschl, E., 278
 Newbold, P., 211
 Newcombe, J., 293
 Newell, D.W., 233, 236, 267
 Newman, M.H., 207
 Newman-Tancredi, A., 343, 349
 Ng, B.L., 239, 244
 Ng, I., 228
 Ng, S.C., 199
 Nguyen, M.D., 255
 Nguyen, T.T., 11
 Nicholls, D.G., 212
 Nichols, V., 133
 Nicoletti, F., 247
 Nicotera, P., 292
 Niece, K.L., 348, 349
 Nie, H., 217
 Nikas, D., 193
 Nilsson, G., 214
 Nimmo, A.J., 40, 45, 211, 212, 214
 Ni, R.X., 301, 304
 Nishida, C., 155
 Nishi, H., 315
 Nishimatsu, H., 156
 Nishimura, S., 318
 Nishio, T., 293
 Nishio, Y., 156
 Nishiyama, Y., 318
 Nitecka, L., 17
 Nitta, M., 312
 Niwa, H., 43
 Ni, Y.C., 337, 338
 Noel, R.J., Jr., 61
 Nojima, Y., 125
 Nomikos, P., 223
 Nomura, N., 47, 217
 Nonaka, N., 45
 Nordell, B., 174
 Norden, J.J., 250
 Nordström, C.H., 118
 Norman, D., 196
 Northrup, B., 312
 Nortje, J., 228
 Novak, G., 348, 349
 Novelli, G., 311

Nowak, T.S., Jr., 17
 Nowotny, A., 8
 Nunomura, A., 315
 Nyberg, F., 62, 65, 256, 296, 299, 301, 302, 304, 305, 321, 322, 324,
 325, 327, 331, 344, 352, 356, 360, 363
 Nyberg, S.L., 312, 313

O

Obasanjo, O.O., 118
 Obenaus, A., 52, 217, 218
 Oberdörster, E., 351, 356
 Oberdörster, G., 351, 359
 O'Brien, R., 193
 Obrist, W., 312
 Ochi, H., 308, 318
 O'Connor, C., 315
 Oda, S., 312
 Oeffinger, K.C., 51
 Oehm, E., 228
 Oertel, M., 269
 Ogata, T., 235
 Ogawa, M., 177
 Ogino, I., 121, 125
 O'Grady, J.G., 312, 313
 Oguchi, S., 318
 Oguro, T., 315
 Ohansson, B.B., 331
 Ohara, Y., 26
 Ohe, Y., 40
 Ohlen, A., 211
 Ohman, J., 268
 Öhman, J., 172
 Ohno, K., 17
 Öhrström, J.K., 118
 Ohtaki, H., 43, 45, 315–318
 Ohtani, M., 228
 Ojemann, R.G., 78, 114
 Okada, Y., 5
 Okamura, T., 156
 Okauchi, M., 228
 O'Kelly, P., 221
 Okuda, H., 43
 Okuda, M., 45
 Olafsson, S., 311
 Olde Damink, S.W., 312, 313
 Oldfield, E.H., 11
 Olinger, C.P., 138, 142
 Olin, M.S., 223
 Olivecrona, M., 265, 268
 Oliver, J.C., 343
 Olsson, I.A.S., 55
 Olsson, T., 271
 Olsson, Y., 17, 295, 296, 299, 301, 302, 304, 305, 344, 352, 356
 Oluoch-Olunya, D., 236
 Omachi, K., 187, 189
 O'Mara, K., 239
 Omata, M., 156
 Ommaya, A., 17
 Onda, J., 152
 O'Neill, R.R., 51
 Onley, D., 32
 Onoa, G.B., 340
 Onodera, H., 33
 Ono, Y., 189
 Ooneda, G., 30

Opanashuk, L., 351, 359
 Oppel, F., 9
 Orozco, J.A., 33
 Orszagh, M., 78
 Orte, C., 55
 Ortega-Aznar, A., 137
 Ortega, F.J., 223
 Ortiz de Montellano, P.R., 155
 Osawa, T., 318
 Osborn, A.G., 165
 Oski, F.A., 98
 Osmanovic, J., 178
 Ostlund-Lindqvist, A.M., 61, 351
 Ostrowski, R.P., 47, 48, 156, 217–219
 Osuka, K., 277, 280
 Otani, T., 187, 189
 Otterness, I., 33
 Ott, P., 312
 Outtrim, J., 228
 Owens, E.S., 4, 6, 7
 Özerkan, F., 97

P

Paakko, E., 195, 196
 Pachter, J.S., 23, 293
 Packard, B.A., 40
 Packer, R.J., 271, 274
 Padavic-Shaller, K.A., 193
 Padgett, C.A., 171, 174, 184
 Padilla, C., 343, 344, 348
 Paek, S.H., 190
 Pait, T.G., 221
 Pakos, P., 263
 Paleologos, N., 10
 Paljarvi, L., 78, 129
 Palma, P., 91
 Palmer, S.L., 191, 195
 Panagiotakos, D.B., 33
 Pancani, S., 91
 Pan, C.Y., 340
 Pandolfi, S., 228
 Panikashvili, D., 26
 Pan, J.W., 279
 Pankhurst, J., 295–297, 299
 Panner, A., 11
 Pannu, Y.S., 11
 Pantaleoni, C., 272, 274
 Pantarotto, D., 339
 Panzenböck, H., 97, 98
 Paolino, E., 141, 142, 144
 Papadia, S., 293
 Papadopoulos, M.C., 24, 26, 45, 280, 281
 Pappalardo, P., 118
 Pappas, T.C., 338, 339
 Paquier, P.F., 183
 Parajuli, R.R., 340
 Paramakrishnan, N., 343, 349
 Paramore, C.G., 118
 Park, C.K., 228
 Park, J.W., 159, 161
 Park, P., 118
 Park, S.B., 359
 Park, S.J., 359
 Park, T.S., 33
 Parlow, S.E., 171

- Parpura, V., 337, 338
 Parry-Jones, A.R., 29
 Parsch, H., 221–223
 Pascual, J.M.S., 97, 98
 Passani, L.A., 181
 Pastan, I., 11
 Patel, A.B., 181
 Patel, S.C., 283, 286
 Patlak, C.S., 4, 6, 7
 Patnaik, R., 61–66, 301, 302, 304, 305, 343–345, 348, 349
 Patnaik, S., 301, 302, 304, 305, 343–345, 348, 349
 Patrizi, S., 33
 Pattisapu, J.V., 124
 Paul, T., 267
 Paung, S.L., 30
 Payne, B.R., 58
 PColon, G., 309
 Peachey, T., 312
 Pearlstein, R.D., 51
 Pearsson, S., 296, 299, 344
 Pedain, C., 11
 Pederast, S., 283
 Peeling, J., 147
 Pegram, C.N., 10
 Pellegrino, C., 293
 Pelligrino, D.A., 161
 Peng, Z., 49
 Peng, Z.Y., 217, 219
 Penke, B., 40
 Pennell, N.A., 147, 149, 150
 Penny, W.J., 98, 99
 Pérez-Casanova, A., 61
 Perez, R.S., 33
 Perkins, J.D., 312
 Pernow, B., 214
 Perrella, S.M., 311
 Perring, W., 273
 Perry, G., 315
 Perry, T.L., 179
 Perry, V.H., 33, 39
 Persidsky, Y., 21
 Persson, L., 268
 Persson, M.G., 211
 Peters, G., 81
 Peters, M., 247
 Petrella, G., 265, 268
 Pettorini, B., 268
 Pfeifer, C.G., 40
 Pfenninger, E.G., 223
 Pfeuffer J., 178
 Pfisterer, W., 118
 Pfizenmaier, K., 293
 Pham, T.M., 55
 Phillips, J., 221
 Phong, C., 324
 Piatt, J., 107
 Piatt, J.H., Jr., 97, 98
 Picard, P., 277
 Pichlmeier, U., 8, 9
 Pickard, J.D., 114, 134, 199, 225, 228, 237
 Pieck, J., 233
 Pieni&aogonek;æk, P., 171, 174, 184, 193
 Pieper, G.M., 152
 Pieper, R.O., 11
 Piepgras, A., 267
 Piepgras, D.G., 312
 Pierre-Kahn, A., 89, 193
 Pietrini, P., 177
 Pietropaoli, P., 311
 Pietsch, T., 9
 Pine, D.S., 152
 Pinsky, D.J., 32
 Pitkin, Z., 313
 Pitossi, F.J., 33
 Pitts, L.H., 267
 Piva, S., 30
 Pizzorusso, T., 55
 Planinsic R., 312
 Plate, K.H., 278
 Plesnila, N., 228
 Plets, C., 272
 Plevak, D.J., 312
 Plotkine, M., 32
 Pluta, R., 37–40
 PMcL, B., 78
 Poell, W., 10
 Poepperl, G., 10
 Poirier, V.C., 223
 Poli, L., 311
 Polinko, P., 274
 Polin, R.S., 267
 Poljanc, K., 193
 Pollack, I.F., 274
 Pollock, B.E., 187–190
 Pollock, D.M., 30
 Poll, W., 5, 6
 Pompucci, A., 268
 Ponten, U., 118
 Ponthan, F., 174
 Poon, C., 324
 Poon, W.-S., 133, 199, 235–237
 Pople, I.K., 111
 Porter, A.M., 355
 Port, J.D., 261, 262
 Postert, T., 250
 Potapovich, A.I., 351, 356
 Potenza, M.A., 311, 313
 Potter, D., 312
 Potter, R., 351, 359
 Potthoff, P.C., 93
 Poussaint, T.Y., 183
 Pouvles, P., 196
 Povlishock, J.T., 228
 Power, C., 147
 Powers, W.J., 161
 Pradillo, J.M., 30, 33
 Prados, M.D., 185
 Prakash, U.B.S., 97, 98
 Prass, K., 217
 Prato, M., 339
 Pratt, D., 313
 Predescu, D., 39
 Prehn, J.H., 247
 Prengel, A.W., 223
 Preston-Hurlburt, P., 33
 Prevedello, D.M., 133
 Price, C.P., 247
 Price, J.L., 87
 Prioleau, G.R., 5
 Pritchard, K.A., Jr., 155
 Probst, C., 69, 72
 Prost, P., 185, 193

Provencher, S.W., 178
 Provenzale, C.J., 10
 Provenzale, J.M., 11, 283, 286
 Prueckner, S., 133
 Przelaskowski, A., 166
 Przuntek, H., 250
 Pugliese, F., 311
 Pujari, S., 104
 Pumar, J.M., 137
 Punt, J., 207
 Puri, R.K., 11
 Putignano, E., 58
 Pyhitnen, J., 195, 196

Q

Qin, Z., 217
 Qiu, W., 228
 Quack, G., 343, 349
 Quian, J., 144
 Quintana, M., 137, 140

R

Raabe, A., 134
 Rabkin, J.M., 313
 Rachinger, W., 10
 Radcliffe, J., 247
 Radushkevich, L., 337, 338
 Ragauskas, A., 199
 Raghavan, R., 11
 Ragoschke, A., 32
 Rahat, Ö., 91
 Rahimi-Movaghar, V., 53
 Rahner-Welsch, S., 55
 Raina, A.K., 315
 Rainer, T., 235–237
 Rajapakse, J.C., 177
 Rakela, J., 312
 Rallidis, L.S., 33
 Rama, S., 293
 Ramirez, S.H., 21
 Ramsey, D., 351, 356
 Randriamboavonjy, V., 311, 313
 Rand, S.D., 185, 193
 Ranshoff, J., 235
 Ranshoff, J., 233
 Ranshoff, R.M., 58
 Rao, A.M., 337
 Rao R.V., 212
 Raphael, H.M., 292
 Rapoport, S.I., 65, 177, 299, 328, 331, 363
 Raslan, A., 225
 Rasley, A., 33
 Rau, S.W., 159, 161
 Ray, A.K., 61–66, 301, 302, 304, 305
 Raymond-Spenden, E., 196
 Reardon, D.A., 11
 Reber, G., 98, 99
 Rebmann, V., 141
 Reddick, W.E., 51, 191
 Reddingius, R.E., 183
 Reddy, C.C., 301
 Reddy, P.H., 179
 Redwan, B., 97, 98
 Redzic, Z.B., 239

Reeves, C.B., 191
 Regan, R.F., 155
 Regel, J.P., 78, 105
 Regli, L., 26, 45
 Reglodi, D., 43
 Rehnrona, S., 69, 72
 Reiche, W., 121
 Reid, A.R., 55
 Reilly, P.L., 211
 Reimers, T.S., 274
 Reinprecht, A., 118
 Reithmeier, T., 263
 Reith, W., 226, 227
 Rekate, H.L., 203, 207
 Relkin, N., 75, 76, 114
 Rem, J.A., 78
 Renier, D., 89
 Rénier, D., 193
 Renner, M.K., 97, 98
 Ren, P., 49
 Reulen, H.-J., 3–10
 Reyer, T., 233
 Reynolds, I.J., 292
 Ribó, M., 137, 140
 Richards, H., 134
 Richards, H.K., 114
 Richardson, R.E., 340
 Richards, P.M.P., 171
 Rich, S., 98
 Richter-Landsberg, C., 185
 Rickels, E., 237
 Ridolfi Luthy, A., 273
 Riederer, P., 161, 178
 Riese, H.H., 277
 Ries, L.G., 271
 Rigamonti, D., 104
 Righi, M., 339
 Rilliet, B., 91
 Ringel, F., 134
 Ringelstein, E.B., 26
 Rinkel, G.J., 134
 Risling, M., 58
 Ris, M.D., 171, 274
 Ritter, L.S., 33
 Rittierodt, M., 233
 Riva, D., 271, 272, 274
 Riva, N., 9, 10
 Riva, P., 9, 10
 Rivas, J.J., 261, 262
 Rivera-Amill, V., 61
 Rivera, E.J., 177, 178
 Rizos, I., 33
 Rizzo, R., 141, 142, 144
 Rizzuto, R., 292
 Robbins, A.S., 301
 Roberts, H.C., 283, 286
 Roberts, J.P., 312
 Roberts, T.P.L., 283, 286
 Robinson, C.C., 324
 Robinson, J.S., 199
 Robinson, L., 196
 Robinson, M., 312
 Rocha-e-Silva, M., 312
 Rocha, J.P., 312
 Rock, J.P., 118, 283, 286
 Rodel, F., 51

- Rodgers, J., 214
 Rodgers, K.M., 211, 214
 Rodling-Wahlstrom, M., 265, 268
 Rodriguez-Crespo, I., 155
 Rodríguez Ponce, I., 11
 Roebuck, D.J., 171, 174
 Roebuck, T., 196
 Rogers, E.J., 359, 363
 Rogove, A.D., 150
 Rohde, V., 9, 95
 Roitberg, B.Z., 89, 91
 Romagnoli, M.F., 118
 Roman, M., 121, 124, 125
 Romero, M.I., 338, 340
 Romner, B., 107, 111
 Ropper, A.H., 161
 Rorick, M., 138, 142
 Rorke, L.B., 271
 Rosell, A., 24, 26, 137
 Rosenbaum, D.M., 23
 Rosenberg, G.A., 21, 24, 26, 155
 Rosenberg, P.A., 33
 Rosenblum, M.L., 118, 283, 286
 Rosenblum, W.I., 33
 Rosenfeld, J., 228
 Rosenstein, J.M., 55
 Rosenthal, P., 313
 Rosewell, K.L., 159
 Rosner, M.J., 267
 Ross, A.J., 193
 Rossaro, L., 312, 313
 Ross Bullock, M., 247
 Rossi, A.F., 340
 Rossi, M., 277, 283, 311
 Ross, M.E., 30
 Rossol, S., 33
 Rothenburger, S., 89
 Rothermundt, M., 247
 Rothman, D.L., 181
 Rothoerl, R.D., 235, 265
 Rothwell, N.J., 29, 33, 34, 292
 Rottkamp, C.A., 315
 Rouas-Freiss, N., 141, 144
 Rozga, J., 311, 312
 Ruben, J.D., 171
 Ruberto, F., 311
 Ruetzler, C.A., 17, 18, 32
 Rumpel, H., 171
 Rusche, J.R., 32
 Rushing, E.J., 277
 Russell, J., 228
 Rustamzadeh, E., 11
 Rutka, J.T., 125
 Rutkowski, T., 173, 184, 185, 192, 193
 Ryan, H., 324
- S**
 Saadoun, S., 45, 280, 281
 Sachdev, P.S., 193
 Sachs, C., 214
 Sadowski, M., 37
 Sahar, A., 244
 Sahuquillo, J., 237
 Saïdo, T.C., 39
 Sainsbury, M., 61, 351
 Sainte-Rose, C., 89, 91, 93, 107, 193, 207
 Saito, I., 189
 Saito, N., 17
 Saito, R., 11
 Saito, S., 308
 Sakai, Y., 307
 Sakamoto, T., 260
 Sakaue, M., 43
 Sakuma, I., 187, 189
 Sakuma, S., 125
 Sakurai, A., 228
 Sale, A., 58
 Saleh, N., 351
 Salizzoni, M., 313
 Salkovic-Petrisic, M., 178
 Saller, B., 221
 Salmeron, J.M., 313
 Salsbury, A.J., 84
 Salter, J.W., 32
 Salton, J., 129
 Salvati, M., 105
 Salyha, Y., 293
 Salzman, E.W., 98
 Samal, B., 43
 Samanta, M.K., 343, 349
 Samii, M., 7
 Sampson, J.H., 11
 Samra, G.S., 247
 Samsonidze, G.G., 340
 Samuels, B.A., 255
 Sanders, J.A., 193
 Sandström, T., 359, 363
 Sankar, R., 212
 Sano, H., 211, 228
 Santamarina, E., 137, 140
 Santhi, K., 343, 349
 Santimaria, M., 10
 Santizo, R.A., 161
 Santos, A.P., 340
 Sarnowska, A., 47, 48
 Sartor, K., 226, 227
 Sarvestani, G.T., 211–215
 Sasaki, A., 40
 Satav, J.G., 252
 Sato, C., 338
 Satoh, K., 315–318
 Satoh, M., 91
 Sato, K., 121, 125
 Saucedo, N.S., 133
 Sauerbeck, L., 138, 142
 Sauerbeck, L.R., 138, 142
 Sauer, R., 51
 Saul, I., 52
 Saulnier, F., 222
 Sautel, F., 343, 349
 Sauter, R., 193
 Savard, P.E., 125
 Savolainen, S., 78, 129
 Savoy, R., 337
 Sawada, M., 48
 Scalea, T.M., 228, 233
 Scarpace, L., 283, 286
 Schabitz, W.R., 226–228
 Schäbitz, W.R., 26
 Schade, R.P., 118
 Schafer, B.W., 247

- Schafer, D.F., 312
 Schafer, M.K., 212, 214
 Schaffner, A., 156
 Schallert, T., 148, 159, 161
 Schapiro, M.B., 177
 Schebesch, K.M., 235, 265
 Scheiling, M., 81
 Scheller, S., 30
 Schellinger, P.D., 228
 Schiding, J.K., 228
 Schielke, G.P., 33
 Schiffbauer, H., 26
 Schiff, D., 51
 Schiff, S.J., 107
 Schilling, L., 324
 Schinkel, J., 118
 Schirmer, C.M., 228
 Schirmer-Mikalsen, K., 269
 Schlager, J., 351
 Schlegel, W., 51, 187, 190
 Schlemmer, H.P., 171, 183
 Schlett, K., 293
 Schlichter, L.C., 147
 Schloss, J.V., 351
 Schluessener, H.J., 295, 297, 299
 Schmahmann, J.D., 271–274
 Schmidek, H.H., 223
 Schmid-Elsaesser, R., 133
 Schmid, R.A., 156
 Schmid-Schonbein, G.W., 33
 Schmiedek, P., 267
 Schmiegelow, M., 274
 Schmitz-Wienke, J., 359–361, 363
 Schnall, M., 193
 Schneider, A., 30
 Schneider, F., 311, 313
 Schneider, G.H., 228, 265, 267, 268
 Schneider, H.J., 221
 Schneider, J., 121
 Schneider, M., 221
 Schneider, P.A., 98, 99
 Schnell, L., 39
 Schniedek, P., 134
 Schoch, H.J., 55
 Schoedon, G., 156
 Schofield, P., 69, 71
 Schomberg, P.J., 187, 190
 Schönknecht, P., 177
 Schrader, H., 202
 Schröder, J., 177
 Schultheiss, R., 165, 166
 Schultz, L.R., 283, 286
 Schulz, R., 48
 Schumann, P., 217
 Schurer, L., 267
 Schwab, J.M., 295, 297, 299
 Schwab, M.E., 39, 295, 299, 324
 Schwab, S., 217, 228
 Schwaninger, M., 30, 47, 48, 217
 Schwartz, A.B., 340
 Schwartz, E.S., 5
 Schwegler-Berry, D., 351, 356
 Schwerdtfeger, K., 225–228
 Sciacca, R.R., 118
 Scott, G., 212
 Scott, J.G., 183
 Scott, V., 312
 Scream, R.A., 292
 Scuderi, V., 313
 Seegers, W., 78
 Seelig, J., 235
 Segal, M.B., 239
 Seidl, U., 177
 Seifert, E., 61, 62, 66, 343–345, 348, 349
 Seiller, E., 343, 349
 Seitelberger, F., 17
 Sekhon, B., 29
 Sekhon, C., 29
 Semenza, G.L., 277
 Semke, E.D., 340
 Sengupta, S., 193
 Senior, R., 151, 152
 Sennstrom, M., 212
 Serena, J., 137
 Serlo, W., 111
 Servadei, F., 236, 237, 268
 Service, R.F., 340
 Setzu, A., 293
 Seyfried, D., 133
 Sgouros, S., 91, 93, 107, 207
 Shaffrey, M.E., 267
 Shafi, S., 199
 Shah, A.R., 33
 Shaikh, A.O., 312, 313
 Shakil, A.O., 312, 313
 Shani, J., 30
 Shanklin, D.R., 91
 Shann, F., 228
 Shapiro, K., 5, 6, 10
 Shapiro, M.B., 171, 174, 184
 Shapiro, S.D., 33
 Shareef, M.M., 277
 Sharma, A., 301, 302, 305, 327, 331, 343–345, 348, 349, 51, 352, 355, 356, 359, 360, 363
 Sharma, H.S., 22, 61–66, 279, 293, 295, 296, 299, 301, 302, 304, 305, 321, 322, 324, 325, 327, 328, 331, 343–345, 348, 349, 351, 352, 355, 356, 359, 360, 363
 Sharma, M., 179
 Sharp, Z., 351, 359
 Shaw, B.W., Jr., 312
 Sheng, H., 228
 Shen, X.Q., 121, 125
 Sherman, D., 151, 152
 Sherman, J.C., 271
 Sherr, G., 95
 Shertzer, H.G., 61, 351
 Sherwin, T., 89
 Shiga, H., 312
 Shigemori, M., 235, 260
 Shih, P.Y., 340
 Shih, S.R., 152
 Shi, M., 125
 Shima, K., 47, 217
 Shiming, Z., 228
 Shimizu, N., 338
 Shimizu, S., 156
 Shimoda, K.C., 184
 Shimono, M., 91
 Shim, S.Y., 255
 Shindo, M., 315
 Shinozaki, K., 156
 Shintani, N., 43, 45

- Shioda, H.S., 315–318
 Shioda, S., 43, 45
 Shiozaki, T., 228
 Shirzadi, A.L., 148, 161
 Shishido, T., 7
 Shi, Y., 255
 Shmiegelow, K., 274
 Shnderkaer, S., 274
 Shohami, E., 26, 225
 Shoji, M., 40
 Shozuhara, H., 33
 Shuck, J., 104
 Shukla, H., 193
 Shulman, K., 10
 Shulman, R.G., 181
 Shumsky, J.S., 299
 Shvedova, A.A., 351, 356
 Siebing, D.A., 217
 Siebing, D.A., 47, 48
 Siesjo, P., 107, 111
 Silbergleit, R., 217
 Silk, D.B., 312, 313
 Silva, G.A., 348, 349
 Silva, V., 351, 359
 Silva, Y., 137, 140
 Silverberg, E., 271
 Silveri, M.C., 271
 Simeonidou, C., 26
 Sim, F.J., 293
 Simone, P., 33
 Simpson, D.A., 212
 Sims, N.R., 211, 214
 Sinani, V.A., 338
 Singer, A.J., 89
 Singh, A.K., 29
 Singha, U.K., 277
 Singh, I., 29
 Singh, J., 239, 244
 Sinha, R.P., 91, 97
 Sitkauskas, A., 199
 Sjöquist, P.O., 61, 62, 65, 351, 352, 356, 359, 360, 363
 Sjostrom, M., 172
 Skandsen, T., 269
 Sklina, K., 166
 Skold, M.K., 58
 Skottner, A., 344
 Skou, J.K., 118
 Skroba&\$\$\$äki, P., 32
 Sleight, G., 98, 99
 Slemmer, J.E., 247
 Slosman, D., 98, 99
 Smalley, D.L., 91
 Smielewski, P., 225, 228
 Smith, A.D., 312, 313
 Smith, C.J., 33
 Smith, J.S., 11
 Smith, M.A., 315
 Smith, M.J., 263
 Smith, R., 171
 Smith, R.W., 118
 Smulian, A.G., 40
 Soggi, D.J., 124
 Söderström, S., 118
 Soehle, M., 263
 Soimakallio, S., 184, 192, 193
 Sojka, P., 200
 Sokół, M., 171, 173, 174, 183–185, 192, 193
 Solaroglu, I., 217, 218
 Solomon, B.A., 313
 Solomon, R.A., 30, 32
 Solymosi, L., 165, 166
 Somera, K.C., 121, 125
 Somogyvari-Vigh, A., 43
 Song, L., 23
 Song, S., 217
 Soos, K., 40
 Sorensen, A.G., 277
 Soriano, F.X., 293
 Soriano, S.G., 30
 Sorkin, R., 339
 Sorrell, M.F., 312
 Soscia, S.J., 178
 Sowers, L.C., 156
 Spadari, A., 313
 Spalluto, G., 339
 Spangler, D.J., 89
 Sparks, D.L., 149
 Spatz, M., 3, 5, 17, 18, 21, 24–26
 Speake, T., 239
 Speich, R., 156
 Spelman, D., 118
 Spenger, C., 174
 Sperandio, S., 343
 Sperduto, P.W., 53
 Spetzler, R.F., 188
 Spiegler, B., 195, 196
 Spilker, J., 138, 142
 Spisacka, S., 37, 38
 Spraggins, T.A., 193
 Springer, M.F., 257
 Springer, T.A., 32
 Sprung, C., 107, 114, 129
 Squire, I.B., 33
 Staar, S., 190
 Stadlbauer, K.H., 223
 Staff, C., 226, 227
 Stafford, S.L., 187, 190
 Stainer, J., 185, 193
 Ståhlberg, E., 304, 305, 321, 324, 344
 Stalla, G.K., 221
 Stålnacke, B.M., 200
 Stamatovic, S.M., 32
 Stammberger, U., 156
 Steen, E., 177
 Steers, J.L., 312
 Steffen-Smith, E.A., 184
 Steiger, H.J., 133
 Steinberg, G.K., 32
 Steinbok, P., 107, 118
 Steiner, L., 187, 190
 Steiner, L.A., 225, 239
 Stein, F., 199
 Steinlin, M., 273
 Steltzer, H., 199
 Stenager, E., 118
 Stepińska, G., 201, 202
 Stepp, H., 8
 Sternbach, G., 75
 Stern, D.M., 32
 Studel, W.I., 69, 73, 76, 78, 89, 95, 98, 101, 102, 104, 105,
 107, 108, 114, 121, 122, 125, 128, 129, 225–228
 Stevens, A.C., 313

Stewart, D.J., 25, 277
 Stewart, M.P., 338, 339
 Stiefel, M.F., 263
 Stignani, M., 142, 144
 Stillman, A.E., 193
 Stins, M.F., 324
 Stjernholm, Y., 212
 Stocchetti, N., 268
 Stocker, S., 8, 10
 Stoclet, J.C., 311, 313
 Stoffel, M., 228
 Stoka, V., 212
 Stolke, D., 114
 Stout, A.K., 292
 Strand, C., 293
 Strano, M.S., 340
 Strasser, A., 26
 Strauss, G., 313
 Stravitz, R.T., 312, 313
 Stravitz, T.R., 312, 313
 Strazielle, N., 125
 Streit, W.J., 147, 149, 150
 Streng, I.C., 183
 Strohmenger, H.U., 223
 Stromblad, L.G., 107, 111
 Strong, R., 148, 161
 Strowitzki, M., 73, 89, 95, 98, 101, 104, 107, 108
 Struck, J., 222
 Strunin, L., 312, 313
 Strzałkowski, R., 81–84
 Stuart, D., 228
 Stuart, M.J., 98
 Stummer, W., 7–9
 Stumm, R., 212, 214
 Stupp, S.I., 348, 349
 Sturm, V., 190
 Styрке, J., 200
 Suetake, S., 43
 Suganami, Y., 318
 Sugimoto, H., 228
 Sugimoto, T., 228
 Sullivan, H.G., 201, 202
 Sumii, T., 33
 Sumitomo, K., 33
 Summonti, D., 311
 Sundbärg, G., 69, 72, 118
 Sundgren, P.C., 171
 Sung, C., 11
 Sun, G.H., 32
 Sun, L., 217
 Sun, X., 49
 Sun, X.J., 217, 219
 Suo, Z., 149
 Suresh, B., 343, 349
 Susie, J.F., 283
 Suykensa, J.A.K., 171
 Suzuki, A., 187, 189
 Suzuki, E., 156
 Suzuki, K., 293
 Suzuki, R., 45
 Suzuki, S., 114
 Suzuki, T., 45
 Suzuki, Y., 33
 Svendsen, F., 87
 Swanson, R.A., 212
 Syojima, K., 235

Szabo, K., 32
 Szakacs, J.E., 152
 Szalai, J.P., 239, 244
 Szczygielski, J., 225–228

T

Tabernero, A., 311, 313
 Tack, A., 5
 Tada, Y., 7
 Takada, M., 7
 Takahashi, A., 40
 Takahashi, S., 187, 189
 Takaki, A., 43, 45, 318
 Takaku, F., 251
 Takano, K., 30
 Takano, T., 125
 Takeda, H., 18
 Takeda, T., 315
 Takekuma, K., 318
 Takenoya, F., 43
 Talvessari, K., 195, 196
 Tamaki, N., 7
 Tamas, M., 11
 Tamborino, C., 138
 Tamiya, T., 309
 Tanaka, H., 265, 267
 Tanaka, K., 43, 265, 267
 Tanaka, T., 318
 Tanak, K., 5, 6, 11
 Taneda, M., 228
 Tang, J., 47, 156, 217–219
 Tang, K., 133
 Tang, X.W., 351
 Tani, E., 39
 Taniike, M., 293
 Tans, J.T.J., 72, 73, 78, 105, 107, 111, 113, 129
 Tan, W.F., 78, 101, 104
 Tao, H.Y., 217, 219
 Tarbell, N.J., 183
 Tarnawski, M., 37
 Tarnawski, R., 171, 173, 174, 183–185, 192, 193
 Tashiro, F., 43
 Tassi, N.G., 340
 Tate, A.R., 171
 Tatlisumak, T., 30
 Tatsch, K., 10
 Tauber, A.I., 30
 Tavares, R., 177
 Taylor, A., 228
 Teasdale, G.M., 222, 237, 267
 Tega, F., 212, 214
 Teichberg, D., 177
 Teixeira, M.J., 263
 Tejada, J., 137, 140
 Tejima, E., 137, 138, 140
 Temmel, I., 292
 Tenhunen, M., 184, 192, 193
 Terry, B.M., 177
 Ter Weeme, C., 4, 6
 Terwey, B., 193
 Terzic, A., 133
 Tessler, A., 299
 Teter, B., 292
 Theoharides, T.C., 211
 Thieliz, P.S., 17

- Thode, H.C., 89
 Thomas, A., 240
 Thomas, A.J., 133
 Thomas, G.H., 251, 252
 Thomassen, L., 33
 Thome, C., 134
 Thompson, B.G., 118, 152
 Thompson, C.J., 221
 Thompson, E.J., 81
 Thorgeirsson, U.P., 49
 Thornton, E., 221
 Thorstad, W.L., 10
 Thureson-Klein, A., 211
 Tian, Q., 179
 Tian, Z.R., 343–345, 348, 349
 Tibballs, J., 228
 Tierney, L., 152
 Tietz, A., 78
 Tikka, T.M., 147
 Tilton, R.D., 351
 Timberlake, G., 221
 Timofeev, I., 225, 228, 237
 Ting, J.P.Y., 293
 Ting, P., 17, 311, 312
 Tisdale, N., 267
 Tisone, G., 313
 Titova, E., 47, 156, 217–219
 Tiwari, S.B., 349
 Tixier-Vidal, A., 239
 Tkàè, I., 178
 Tobe, T., 317
 Tobias, C.A., 299
 Toda, N., 156
 Todd, G.L., 152
 Todd, R.F., 32
 Tofteng, F., 312, 313
 Tojo, A., 156
 Tokoro, K., 114
 Tokuda, M., 277, 280
 Tokunaga, J., 84
 Tokutomi, T., 260
 Tola, M.R., 141, 142, 144
 Tolia, C.M., 250
 Tolxdorff, T., 5
 Tomida, S., 17
 Tomimoto, S., 43
 Tominaga, B., 7
 Tomita, H., 7
 Tomita, T., 89, 91
 Tomizawa, K., 292
 Tomoi, M., 185, 193
 Tomsick, T., 138, 142
 Tomura, N., 165, 166, 187, 189
 Tonali, P., 33
 Tone, O., 7
 Tong, W., 217–219
 Tong, Y., 279
 Tonn, J.-C., 9, 10
 Too, H.P., 212
 Tordo, P., 155
 Toretsky, J.A., 171
 Tormey, W., 221
 Törnqvist, H., 359, 363
 Tosi, A., 311
 Tour, J.M., 338, 339
 Towbin, R., 274
 Toyokuni, S., 318
 Tranguch, S.L., 33
 Traystman, R.J., 48
 Trembovler, V., 225
 Trendelenburg, G., 217
 Treuer, H., 190
 Trey, C., 311
 Tripp, G., 196
 Trost, H.A., 114
 Tsai, C.C., 340
 Tsai, L.H., 255
 Tseng, C.K., 187, 190
 Tseng, M.Y., 134
 Tsirka, A.E., 150
 Tsirka, S.E., 147, 150
 Tsubokawa, T., 48
 Tsuda, M., 114
 Tsudzuki, M., 125
 Tsujigami, S., 91
 Tsuji, K., 137
 Tsuyumu, M., 5
 Tsuzuki, N., 47, 217
 Tulberg, M., 129
 Tuli, S.K., 295, 297, 299
 Tuman, K.J., 202
 Tumolo, M., 299
 Tuncer, R., 91, 268
 Turner, D.A., 118
 Turner, D.E., 144
 Turner, R., 51
 Turner, R.J., 211, 212, 214
 Turner, S., 32
 Turowski, B., 9
 Tychmanowicz, K., 199
 Tyler-Kabara, E., 207
 Tymianski, M., 292
 Tyrrell, P.J., 33
 Tyurina, Y.Y., 351, 356
 Tzika, A.A., 183
 Tzouras, A., 78, 114
- U**
 Ułamek, M., 37, 39, 40
 Ucar, T., 268
 Uchida, D., 43
 Uchida, K., 318
 Ueda, S., 185, 193
 Uehara, A., 43
 Uematsu, S., 18
 Uemo, M., 23
 Uemura, K., 165, 166
 Ueno, H., 91
 Ueno, T., 199
 Uhl, E., 5, 6
 Ujite, M., 40
 Ulitovskaia, I.I., 51
 Ulitovskii, D.A., 51
 Ullibarrí-Ortiz de, Z.N., 277
 Ulvestad, E., 33
 Unger, P.F., 98, 99
 Unterberg, A., 228, 237, 265, 267, 268, 324
 Uozumi, T., 152
 Urasaki, E., 91
 Urbach, H., 165, 166
 Usenius, J.P., 184, 192, 193

Usenius, T., 184, 192, 193
 Usrey, M.L., 340
 Usuda, N., 277, 280
 Utagawa, A., 228

V

Vach, W., 78, 105
 Vaghi, L., 141, 142, 144
 Vail, A., 33
 Vainio, P., 184, 192, 193
 Vajkoczy, P., 134
 Valenzuela, M.J., 193
 Van Calenbergh, F., 272
 van de Kerkhove, M.P., 313
 Van de Laar, A., 272
 Van den Berghe, G., 223
 van den Bergh, W.M., 133, 134
 Van Den Brink, W., 240
 Vander, A.J., 33
 van der Graaf, M., 171
 Vandertop, W.P., 111
 van Dijk, G.W., 199
 Van Eldik, L.J., 250
 van Etten, L., 359, 363
 van Gijn, J., 134
 Vanhamme, L., 171
 Van Hoesen, G.W., 179
 Vanhorebeek, I., 223
 Van Huffel, S., 171
 van Kaick, G., 183
 van Leyen, K., 137
 Vannemreddy, P., 301, 302, 304, 305
 Vanneste, J.A., 78, 101, 104, 129
 Van Rooi-jen, N., 293
 van, T.O., 281
 van Wensen, E., 199
 Vapalahti, M., 78, 129
 Vaquero, J., 311–313
 Vartanian, T., 33
 Vásquez-Vivar, J., 155, 156
 Vassilyadi, M., 171
 Vass, K., 17
 Vaudry, D., 43
 Vedeler, C.A., 33
 Velardi, F., 91
 Veltkamp, C., 47, 48
 Veltkamp, R., 47, 48, 217
 Ventureyra, E.C.G., 171
 Venugopalan, R., 25
 Verhey, L., 185
 Verkman, A.S., 24, 26, 45, 280, 281
 Vermeulen, M., 119, 134
 Vernet, O., 91
 Veronesi, B., 351
 Verrelli, D.M., 51
 Vesce, S., 212
 Vespa, P., 269
 Veyna, R.S., 133
 Vick, N.A., 10
 Victorio, E.S., 343, 348
 Victorov, I.V., 217
 Vieg, A., 58
 Vigdorichik, A., 52
 Vigh, S., 43
 Vigna, S.R., 212

Vignerón, D.B., 173, 185
 Vigué, B., 199, 202
 Vik, A., 269
 Vikelis, M., 33
 Villacara, A., 25
 Villavicencio, A.T., 152
 Villemure, J.G., 45
 Vincent, M., 125
 Vink, R., 40, 45, 51, 211–215, 240, 315
 Vinters, H.V., 212
 Viso, M., 239
 Visser, L.G., 118
 Vitale, A.M., 105
 Vitzthum, E., 111
 Voelker, J., 221
 Vogel, J., 30, 55
 Vogel, S.M., 39
 Voges, J., 190
 Vogl, T.J., 193
 Voigt, S., 228
 Volk, M.L., 312
 Volkow, N.D., 291
 Volpe, J.J., 33
 von Kalm, L., 124
 von Kummer, R., 226, 227
 von Kummer R., 165, 166
 von Rosen, F., 221
 Vonsattel, J.P., 181
 von Tiling, S., 121, 125
 Voorn, P., 196
 Vyas, T.K., 349

W

Wada, H., 265, 267
 Wada, K., 47, 217
 Wada, M., 121, 124, 125
 Waga, S., 223
 Wagner, K.R., 40, 307, 309
 Wagner, S., 8, 47, 48, 52, 156, 278
 Wahl, M., 324
 Wainwright, H., 212
 Waje-Andreassen, U., 33
 Wajima, T., 156
 Wakasa, M., 309
 Wakisaka, S., 51, 293
 Walasek, N., 81–84, 199, 202
 Walbridge, S., 11
 Waldemar, G., 72, 73, 129
 Waldrop, S.M., 174, 184
 Walecki, J., 166, 171, 174, 183, 193, 199, 201, 202
 Walker, J.T., Jr., 17
 Walker, M., 138, 142, 207
 Walker, M.L., 75, 228
 Wallace, D., 228
 Walls, D.J., 340
 Walsh, A.R., 107, 207
 Walski, M., 39, 40, 251, 252
 Walter, M., 69, 73, 102
 Walter, R., 156
 Walter, S.A., 147, 149, 150
 Walters, B.C., 236
 Waltman, A.C., 98
 Wands, J.R., 177, 178
 Wang, C.M., 228
 Wang, C.W., 340

- Wang, H., 134
Wang, J., 255
Wang, J.Z., 137, 141, 144, 147, 150, 179
Wang, K., 339
Wang, M.Y., 89
Wang, W., 228
Wang, X., 24, 26, 33, 324
Wang, X.C., 137, 179
Wang, Y., 39, 69, 71, 293
Ward, J., 235
Wardlaw, J.M., 165
Warner, D.S., 134
Warren, K.E., 183, 184
Washburn, S.N., 64
Wasserman, J.K., 147
Wasterlain, C.G., 212
Watanabe, C., 318
Watanabe, E., 312
Watanabe, F.D., 311, 312
Watanabe, H., 45
Watanabe, J., 43, 45
Watanabe, M., 235
Watanabe, T., 315
Watanabe, Y., 277, 280, 318
Watarai, J., 187, 189
Waters, S., 33
Watkins, L.R., 64
Watson, L., 32
Watt, C., 244
Webb, L.X., 87
Weber, B., 39
Weber, D.J., 340
Weber, J.T., 247
Webster, S., 311
Weder, W., 156
Wehrli, S.L., 193
Weidauer, S., 134
Weihe, E., 212, 214
Weih, F., 30
Wei, K.C., 187, 190
Wei, L.C., 125
Weiner, H., 129
Weinstein, P.R., 52
Weinstock, M., 225
Weinzierl, M.R., 95
Weir, C.J., 33
Weiss, C.K., 359–361, 363
Wei, T., 58
Wells, C., 152
Wendon, J.A., 312, 313
Wendt, L., 95
Wen, W., 193
Wenzel, V., 223
Wesley, M., 155
Wesseling, P., 281
Westergaard, E., 25
Westergaard, L., 69, 72
Wester, K., 87
Westerlund, C., 61, 351
West, G.A., 95
Westman, J., 61, 62, 65, 279, 304, 305, 321, 322, 324, 325, 327, 331, 351, 352, 356, 360, 363
Wheatley, M.A., 299
Whitaker-Azmitia, P.M., 247
Whitaker, S., 32
Whitby, R.L., 338
White, G.L., Jr., 228
Whitten, C., 51
Whitwell, C., 239
Wicklow, K., 193
Wicksted, J.P., 338
Wiegand, F., 217
Wiemann, N., 284
Wiendl, H., 141, 144
Wieseler-Frank, J., 64
Wiesner, R.H., 312
Wiestler, O.D., 8
Wijdicks, E.F., 312, 313
Wijdicks, E.F.M., 119
Wiklund, L., 61, 62, 66, 344, 352, 356
Wikstrand, C.J., 10
Wilberger, J.E., 236, 257, 260
Wilberger, J.W., 267
Williams, M.A., 75, 104, 118
Williamson, D., 84
Williams, R., 312, 313
Willingham, S., 124
Willmot, M., 30
Willoughby, K.A., 247
Wilson, B., 343, 349
Wilson, G.L., 251
Wilson, M.E., 159
Winblad, B., 55
Windhagen, A., 293
Windisch, M., 292
Winfree, C.J., 32
Winkler, T., 304, 305, 321, 324, 344
Winn, H.R., 312
Wintermark, M., 283
Wirth, S., 33
Wirth, T., 30
Wise, P.M., 159, 161
Wisniewski, H.M., 37–40
Wisoff, J., 129
Wisoff, J.H., 171, 207
Woertgen, C., 235, 265
Woiciechowsky, C., 9
Wolburg, H., 21
Wold, S., 172
Wolf, J., 93
Wolf, P., 311, 313
Wolpin, L.C., 121, 125
Wolters, P.L., 184
Won, D.J., 89
Wong, C.W., 236
Wong, G.K.-C., 133
Woodroffe, M.N.B., 293
Woo, S., 191
Wrba, E., 5, 6
Wreford, N., 295–297, 299
Wroblewska, B., 24
Wu, C., 52
Wu, H.C., 340
Wu, H.Y., 292
Wu, J., 148, 159, 160
Wu, J.Y., 351
Wu, M., 149
Wurzer, H.A.L., 72, 73, 78, 105, 107, 111, 113, 129
Wurzinger, U., 250
Wu, S., 191
Wydmański, J., 171, 174, 183, 184

X

Xiang, C.C., 43
 Xiang, J., 160
 Xiao, F., 47
 Xi, G., 137, 140, 141, 144, 147, 149, 159–161, 217, 307, 309
 Xiong, L., 217
 Xiong, X., 191, 193
 Xu, J.J., 217, 219
 Xu, N., 217
 Xu, S., 30
 Xu, W., 217, 219, 261, 262
 Xu, W.G., 217, 219
 Xu, X.J., 177
 Xu, Z., 228
 Xydakis, M.S., 301

Y

Yahara, O., 33
 Yakota, M., 39
 Yamada, H., 107
 Yamaguchi, M., 47
 Yamaguchi, S., 177
 Yamakami, I., 228
 Yamamoto, F., 260
 Yamamoto, K., 43, 185, 193
 Yamamoto, M., 189
 Yamamoto, T., 156
 Yamanaka, G., 318
 Yamanoto, M., 293
 Yamasaki, Y., 33
 Yamashita, S., 309
 Yamate, J., 125
 Yamauchi, H., 177, 308
 Yamaura, A., 228
 Yamaura, I., 39
 Yan, D., 45
 Yang, C.Y., 351
 Yang, F., 338
 Yang, G.-Y., 33
 Yang, G.Y., 309
 Yang, S., 149, 277
 Yang, Y., 21, 24, 26
 Yan, S.D., 32
 Yan, Z., 292
 Yao, C., 348, 349
 Yap, E.P., 239, 244
 Yaron, M., 89
 Yassari, R., 133
 Yassouridis, A., 221
 Yatsushige, H., 48
 Yavuzgil, O., 97
 Yehia, B.R., 121, 125
 Yenari, M.A., 32
 Ye, S., 161
 Yesilyurt, O., 64
 Yeung, D.K., 171, 174
 Yeung, J., 235–237
 Yildiz, O., 64
 Ying, L., 167
 Yin, L., 315
 Yofu, S., 45, 315–318
 Yokota, A., 91
 Yonas, H., 283, 312
 Yonekawa, Y., 133

Yonekura, Y., 177
 Yong, V.W., 137, 147, 179
 Yoon, B.W., 228
 Yoon, T.J., 359
 Yordanov, A.T., 11
 Yoshida, A., 318
 Yoshida, H., 228
 Yoshida, J., 277, 280
 Yoshida, K., 308
 Yoshida, M., 185, 193
 Yoshida, T., 125
 Yoshida, Y., 30, 156
 Yoshiji, H., 49
 Yoshikawa, T., 315–318
 Yoshioka, T., 228
 Yost, W.T., 199
 Youdim, M.B., 161
 Younger, J.G., 149
 Young G., 171
 Young, H.A., 223
 Young, J., 271
 Young, K.W., 292
 Young, R.J., 283
 Yousem, D.M., 193
 Yuen, E.Y., 292
 Yuen, M., 196
 Yu, F., 32
 Yu, G., 39
 Yuki, K., 152
 Yuki, S., 315
 Yu, K.N., 359
 Yun, C.O., 277

Z

Zabka, A.G., 161
 Zacest, A.C., 211–215
 Zachrisson, O., 212
 Zager, J., 97
 Zagorski, J., 33
 Zajac, J.M., 343, 349
 Zakhidov, A.A., 338
 Zalewska, T., 47, 48
 Zalutzky, M.R., 10
 Zanella, F., 8
 Zapata, V., 64
 Zaremba, J., 32
 Zarifi, M.K., 183
 Zarrelli, M.M., 33
 Zausinger, S., 133
 Zazulia, A.R., 161
 Zeilinger, F.S., 129
 Zeit, T., 250
 Zemack, G., 107, 111
 Zhang, F., 30
 Zhang, J., 47
 Zhang, J.H., 47–49, 52, 156, 217–219, 228
 Zhang, M., 279, 338
 Zhang, P., 125
 Zhang, Q., 58
 Zhang, R.L., 32
 Zhang, S., 47
 Zhang, T., 343, 344, 348
 Zhang, X., 309
 Zhang, Y., 228
 Zhang, Z.D., 133

- Zhan, R.Y., 279
Zhao, B., 338
Zhao, B-Q., 137, 138, 140
Zhao, D., 343, 344, 349
Zhao, W., 52
Zhao, X.G., 10
Zheng, M., 340
Zhong, W., 228
Zhou, J., 228
Zhou, Y.Q., 279
Zhu, C., 58
Zhu, Y.B., 283, 286
Zhu, Z., 217
Ziai, W.C., 261, 262
Ziche, M., 211, 277
Ziemka-Nalecz, M., 47, 48
Zimmerman, C., 133
Zimmermann-Meinzingen, S., 327
Zimmermann, R., 78, 101, 104, 107, 111, 228
Zimmerman, R.A., 193, 196
Zingale, A., 118
Zink, J., 228
Zolindaki, M.G., 33
Zollinger, A., 156
Zoloty, J.E., 149
Zuccarello, M., 138, 142
Zulau, P., 273
Zurakowski, D., 183
Zweckberger, K., 228
Zwetnow, N.N., 202

Subject Index

A

Acute lymphoblastic leukemia (ALL)
 children treatment, 195
 CNS treatment, 196
 cranial irradiation (CRT), 195
 intrathecal methotrexate (ITMTX), 195, 196
 magnetic resonance spectroscopy (MRS), 195, 196
 materials and methods, 195–196
 prophylactic treatment, 195
 results, 196
Acute subdural hematoma (ASDH)
 brain edema, 257
 conservative treatment, 260
 Glasgow Outcome Scale (GOS), 257
 patients and methods, 257–258
 results, 258–260
Alkoxyl radical. *See* Reactive oxygen species (ROS)
ALL. *See* Acute lymphoblastic leukemia
Alzheimer's disease, 177
5-Aminolevulinic acid (5-ALA), 8, 9
Amyloid precursor protein (APP), 37–39
Anaplastic oligodendroglioma (AO), 278, 279, 281
Aneurysmal subarachnoid hemorrhage, 133
Antioxidant H-290/51, 61
Aquaporins (AQPs), 24
Aquaporin-4 (AQP4) water channel, 45
Argatroban, 309
Arteriovenous malformations (AVMs), 51, 187
ASDH. *See* Acute subdural hematoma
Astrocytes, 22, 24

B

BDNF. *See* Brain-derived neurotrophic factor
Bilateral decompressive craniectomy
 guidelines of, 267
 head trauma, 265
 ICP and CPP, 268
 materials and methods, 266–267
 National Hospital Organization Disaster Medical Center, 265
 pre and post-operative factors, 267–269
Biological processes vs. pathophysiological mechanisms, 292
Blood brain barrier (BBB)
 basement membrane components
 dystroglycan, 24
 extracellular matrix (ECM), 22, 24, 25
 integrins, 24
 matrix adhesion receptors, 24
 matrix metalloproteinase's (MMP), 24

 cellular components
 astrocytes, 22, 24
 caveolae and caveolin, 23
 endothelium, 22
 neurons, 25
 pericytes, 24
 smooth muscle, 24
 endothelial barrier antigen (EBA), 55–57
 eNOS and VEGF, co-expression, 277, 279, 281
 function and brain pathology
 antioxidant H-290/51, 61
 morphine, 61–64
 luminal membrane
 caveolae and caveolin, 23
 glycocalyx, 23
 P-glycoprotein (P-gp), 23
 markers, 281
 nanoparticles, 363
 pathophysiology
 AQP4 null mice, 26
 cerebral ischemia and trauma, 25
 2-DG uptake, 25
 marker of, 25
 post-ischemic hypoperfusion, 26
 radical species, 26
 tight junctions (TJ)
 adherens junction (AJ), 23
 claudin-1, 2 and 3, 22, 25
 cytoplasmic accessory proteins, 23
 junctional adhesion molecules (JAM), 22, 23
 occludin, 22–23
Blood-barrier integrity, CSF, 247, 249
Blood-spinal cord barrier (BSCB), 296, 297, 299
Brain-derived neurotrophic factor (BDNF), 296, 297, 299
Brain hypothermia and decompressive craniectomy (DC)
 cooling effect and evaluation of edema, 226
 methods
 analysis of variance (ANOVA), 226
 male CD-1 mice, experimental groups, 225
 middle cerebral artery (MCA) occlusion model, 227
 optimal time point, 228
 traumatic brain injury and intracranial pressure, 225
Brain metabolic changes, rat
 Alzheimer's disease, 177
 glucose metabolism, 181
 gross brain weights, 179
 ¹HMR spectroscopy, 178
 metabolites quantification and concentration, 179
 MRS quantification and statistics, 178–179
 streptozotocin, intracerebroventricular injections of, 178

- Brain tissue
 damage
 histopathologic findings, 184
 proton magnetic resonance spectroscopy (MRS), 183
 supratentorial tumor, 184
 metabolism
 craniospinal radiotherapy, 192
 Lip/Cr ratio, 193
 magnetic resonance spectroscopy (MRS), 191
 NAA/Cr ratio, 192–193
 ophthalmologic examination, 192
 short-term memory, 192
- Bulk flow and diffusion
 clinical applications
 5-aminolevulinic acid (5-ALA), 8, 9
 antibody-isotope-complex, 9, 10
 convection-enhanced delivery, 11
 intracavitary radioimmunotherapy, 9–11
 Kaplan-Meier curve, 9
 malignant gliomas, fluorescence-guided surgery, 7–9
 cold-induced edema model, 3
 vasogenic brain edema
 vs. calculated theoretical distances, 4
 edema fluid formation, 5–6
 edema fluid, resolution of, 5–6
 peritumoural edema, clinical studies in, 6–7
 RISA and C-14 sucrose appearance, 5
 sodium-fluorescein and Texas-red albumin, 5
 spreading of, 3–5
 white matter, CT-numbers, 6
- C**
- Carbon nanotubes (CNTs), neuroscience
 composed of, 337
 electrical interfaces
 dopamine and CgA detection, 340
 field effect transistor (FET), 340
 metal electrodes, 340
 microchip, 339
 non-oxidative method, 340
 modifications, 337
 substrates/scaffolds for
 micropatterned array, 339
 multi-walled carbon nanotube (MWNT), 338
 nanothreads, 339
 neurotrophins, 338
- Cranial irradiation (CRT), 195
 Caveolae and caveolin, 22–23
 CCMs. *See* Cerebral cavernous malformations
 Central nervous system (CNS), 121, 125
 Cerebral arteriovenous malformations (AVMs), 187
 Cerebral blood flow (CBF)
 Doppler perfusion imaging system, 44
 measurement, 44
 Cerebral cavernous malformations (CCMs), 187
 Cerebral ischemia
 blood-brain barrier (BBB), 17
 NIH, 17, 18
 pathoclinic theory, 18
 Cerebrolysin
 heat stress
 BBB permeability and cerebral blood flow, 329–330
 brain edema and pathology, 331
 cognitive function, 329
 cortical nerve cell damage, 332
 microvessels reactions, 331
 neurochemical release, 331
 normotensive and hypertensive animals, 331
 stress symptoms and physiological variables, 329
 neuroprotective effects
 animals, 322
 BBB permeability and brain edema formation, 322–323
 brain pathology, 323
 histopathology, 322
 hyperthermia and stress symptoms, 322
 statistical data, 322
 stress symptoms and physiological variables, 322
 treatment, 322
 whole body hyperthermia (WBH), 322
 Cerebrospinal fluid (CSF), 87, 200–201, 247, 248
 Chemoattractant receptor (CCR2), 32
 Choroidal epithelial cells (CEC), TBI
 materials and methods
 animal perfusion and tissue preparation, 240
 induction and animals, 239–240
 microvilli (MV), 241
 scanningelectron microscopy (SEM), 240
 transmission electron microscopy (TEM), 240
 Chromogranin A (CgA), 340
 Chronic hydrocephalus
 co-morbidity-index (CMI), 76, 77
 idiopathic normal pressure hydrocephalus (iNPH), 75
 materials and methods, 75–76
 results, 76–78
 secondary normal pressure hydrocephalus (sNPH), 75, 76
 Classic oligodendrogliomas (CO), 278–280
 Closed head injury (CHI)
 dynorphin A antiserum effects
 on BBB permeability and brain edema, 302–304
 on brain pathology, 304
 materials and methods
 animals, 302
 brain pathology, 302
 dynorphin antibody treatment, 302
 statistical analysis, 302
 serotonin, 301
 Codman-Hakim and Shunt-Assistant (CHSA), 108–110
 Co-morbidity index (CMI), 128–129
 Computed tomography perfusion (CTP)
 perfusion parameters, 285–286
 technique, 284
 Convection-enhanced delivery (CED), 11
 Copeptin, AVP prohormone
 fractures of, 223
 injury severity, 221
 methods
 Glasgow Coma Score (GCS (15)), 222, 223
 osmolality measurement, 222
 osmoregulation, 221, 223
 Creepy delayed neuronal death, hippocampus and Alzheimer disease, 37
 amyloid precursor protein (APP), 37–39
 blood-brain barrier, 39
 CA1 area, 38–39
 HRP immunoreactivity, 38
 immunoreactivity, APP, 38
 materials and methods, 38
 mechanisms, 38, 39
 neuronal pathology, 38–39
 CSF. *See* Cerebral spinal fluid (CSF); Cerebrospinal fluid

D

- Decompressive craniectomy, surgical outcome
 - acute epidural hematomas (AEDH), 261
 - cerebral tissue oxygenation, 263
 - computed tomography (CT) scans, 261
 - Glasgow Outcome Scale (GOS), 261
 - Mann-Whitney U test, 262
 - patients and methods, 261–262
 - results, 262
- Diacron-reactive oxygen metabolites (d-ROM)
 - testing, 316, 317
- Dopamine, 340
- Doppler perfusion imaging system, 44
- Dual-Switch-(DSV) valves, 111
- Dynorphin A antiserum
 - failure of, 304
 - neuroprotective effects
 - on BBB permeability and brain edema, 302–304
 - on brain pathology, 304
 - neutralization, 304

E

- Endogenous defense activity (EDA)
 - neurodegenerative processes, 292
 - neuroprotection, 291
 - neurotrophicity, 291
 - regulation disturbances, 291
- Endothelial barrier antigen (EBA)
 - animals and surgical procedures, 56
 - fixation and tissue processing, 56
 - histopathological analysis, 56–57
 - immunohistochemistry, 56–57
 - results, 57–58
- Endothelial nitric oxide synthase (eNOS) role,
 - vascular permeability
 - anaplastic oligodendroglioma (AO), 278
 - blood-brain-barrier (BBB), 280
 - cerebral gliomas, 278
 - classic oligodendrogliomas (CO), 278
 - intravital dyes, 281
 - material and methods, 278
 - occludin, 279
 - tight junctions, 280
 - vascular endothelial growth (VEGF)
 - immunofluorescence, 279
- Enzyme-linked immunosorbent assay (ELISA), 142
- Estrogen, iron-mediated brain edema and neuronal death
 - deferroxamine, iron chelator, 161
 - materials and methods
 - animal preparation and intracerebral injection, 159–160
 - brain water and ion content measurements, 160
 - experimental groups, 159
 - live/dead cell assay and statistical analysis, 160
 - measurement of lactate dehydrogenase (LDH), 160
 - primary cortical neuronal culture, 160
- EVD. *See* External ventricular drainage
- External ventricular drainage (EVD)
 - cerebrospinal fluid (CSF), 117
 - GRAEB classification, 118
 - parallel shunt system, 117, 118
 - phase-II trial, 117
- Ex vivo electron spin resonance spin trapping method
 - alkoxyl radical, 318
 - 5,5-dimethyl-1-pyrroline-1-oxide (DMPO), 316

F

- Fisher CT grade, magnesium sulfate infusion effects, 134
- Focal cerebral ischemia and reperfusion. *See* Neutrophils and proinflammatory mediators
- Free radical monitoring, neurological emergency
 - edaravone, 317
 - 8-hydroxy-2'-deoxyguanosine (8-OHdG), 317
 - methods
 - diacron-reactive oxygen metabolites (d-ROM) testing, 316
 - ex vivo electron spin resonance spin trapping method, 315–316
 - results, 316–317
- Fulminant hepatic failure (FHF)
 - acute liver failure, 311–312
 - clinical algorithm, 311
 - ICP monitoring, 312, 313
 - material and methods, 311
 - pathophysiology, 311

G

- Gel zymography, 48
- Glasgow Outcome Scale (GOS), 257
- Glial cell derived neurotrophic factor (GDNF), 296, 297, 299
- Glial scar formation, diabetic rats
 - apoptosis morphological features of, 253
 - glial fibrillary acidic protein (GFAP) and vimentin, 252, 253
 - immunohistochemical and immunochemical pathways, 251
 - immunoreactivity (IR), 254
 - ultrastructural studies, 252
- Glioma, 277, 279
- Global cerebral ischemia, 47, 48
- Gravitational shunt complications
 - chronic hydrocephalus, 108
 - Dual-Switch valve (DSV), 108
 - performance and failures, 107
 - statistics, 108
 - survival rate, 111
 - ventriculo-peritoneal (VP), 108

H

- H-290/51 antioxidant
 - brain pathology, 356
 - hyperthermia, 355
 - materials and methods
 - blood-brain barrier permeability and brain edema formation, 352
 - brain pathology, 352
 - statistical analysis, 352
 - stress symptoms and physiological variables, 352
 - treatment, 352
 - whole body hyperthermia (WBH), 352
 - nanoparticles
 - BBB permeability and brain edema, 355
 - brain pathology, 355
 - stress symptoms and physiological variables, 352–355
 - neuronal damage, 355
 - reactive oxygen species (ROS), 351
- Heat stress. *See also* Cerebrolysin
 - BBB permeability and cerebral blood flow, 329–330
 - brain edema, 331
 - brain pathology, 331
 - cerebrolysin, 321
 - cognitive function, 329
 - stress symptoms and physiological variables, 329

- Human leukocyte antigen-G molecules
 (sHLA-G1/HLA-G5) antigens
 anti-inflammatory functions, 144
 CT evaluation, 142
 hematoma and edema volumes, 143
 immunoassay methods and statistics, 142
 patient selection, 142
 vs. relationships, 143–144
 spontaneous intracerebral hemorrhage, 141
 time course, 142–143
- Human malignant gliomas, CED, 11
- Human traumatic brain injury
 ischaemic brain injury, 214
 materials and methods
 archival post mortem material, 212
 confocal microscopy, 213
 immunohistochemistry, 212
 tissue analysis, 212–213
 neurogenic inflammation, 212, 214
 SP immunoreactivity
 changes in, 214
 in control cases, 213–214
- Hydrocephalus, intracranial abnormalities
 anesthesia, 122
 cerebellar cyst, 123–124
 cerebellar vermis defect (CVD), 125
 colonies, comparison, 124–125
 hydrocephalic animals, 122
 magnetic resonance imaging (MRI), 122
 midline cyst, 123
 subcommissural organ (SCO), 125
 unilateral enlarged ventricle, 123
 ventriculo-peritoneal shunting and postoperative
 monitoring, 122
- Hydrocephalus pathophysiology
 CSF hydrodynamic parameters, 71
 idiopathic normal pressure hydrocephalus (i-NPH), 69
 intracranial pressure (ICP), 69, 70
 magnetic resonance imaging (MRI), 69, 71
 materials and methods
 patients, indication policy and documentation, 69–70
 shunt hardware, 70
 statistics, 70
 pressure volume index (PVI), 71, 72
 resistance to outflow (Rout), 71
 Windkessel effects, 71
- 8-Hydroxyl-2'-deoxyguanosine (8-OHdG), in DNA, 308, 309
- Hyperacute ischemic stroke, CT examinations
 computer aided diagnosis (CAD), 165–166
 conventional-windowed image, 168
 distinct hypodensity extraction (DHE) algorithm
 extraction and visualization, 167
 image conditioning and ROI segmentation, 167
 focal hypodense changes, 166
 stroke monitor, 166–169
- Hyperbaric oxygen precondition (HBO-PC)
 Evan's blue dye extravasation, 218
 materials and methods
 blood brain barrier permeability, 218
 brain water content, 218
 neurological assessment of, 218
 statistical analysis, 218
 surgical brain injury modeling, 217–218
 treatment groups, 218
 wire hang and beam balance tests, 218
 surgical brain injury, 217
- Hyperthermia and stress symptoms, 322
- I**
- Idiopathic normal pressure hydrocephalus (i-NPH), 69, 75
 clinical data results, 102
 clinical grading (KI), 102
 co-morbidity index (CMI), 103
 diagnosis, material and methods
 endoscopic third ventriculostomy (ETV), 101–102
 policy and group allocation, 102
 shunt hardware, 102
 statistics, 102
 materials and methods
 clinical grading, 128
 co-morbidity index (CMI), 128–129
 diagnosis, 127–128
 non-iNPH comparison, 103–104
- Immunoreactivity (IR), 254, 255
- i-NPH. *See* Idiopathic normal pressure hydrocephalus
- Insulin-like growth factor 1 (IGF-1), 296, 297, 299
- Intracavitary radioimmunotherapy
 clinical studies, 10–11
 diffusion, 9
 experimental studies, 10
 tenascin antibody, 9, 10
- Intracerebral hemorrhage (ICH)-induced brain injury
 materials and methods
 animal preparation and intracerebral infusion, 308
 brain water content, 308
 detection of 8-OHdG in DNA, 308
 experimental groups, 308
 morphometric measurement of hemorrhage volume, 308
 statistical analysis, 308
 nafamostat mesilate (FUT), 307
 thrombin, 307
- Intracranial hypertension syndrome (IHS)
 acetazolamide and dexamethasone, 206
 CSF hypertension, 206
 intraventricular catheter and reimplantation, 204
 MRI examination, 205
 neuroradiology, 203
 pathological findings, 203
 slit ventricle syndrome (SVS), 203, 207
- Intracranial pressure (ICP). *See* Fulminant hepatic failure (FHF)
- Intracranial volume (ICV) reserve assessment
 cerebrospinal fluid (CSF), 200–201
 CT imaging, 200
 drawback, 202
 results, 200–201
 traumatic brain injury (TBI), 199–201
- J**
- Junctional adhesion molecules (JAM), 22, 23
- K**
- Kiefer-index, 102
 Kruskal-Wallis test, 148, 149
- L**
- Luria neuropsychological test, 272
- M**
- Magnesium sulfate infusion effects
 aneurysmal subarachnoid hemorrhage, 133
 Fisher CT grade, 134

- mean transit times, 134
 - methods and materials, 133–134
 - pilot studies, 133
 - Malignant gliomas, fluorescence-guided surgery
 - 5-aminolevulinic acid (5-ALA), 8
 - Kaplan-Meier curve, 9
 - survival in, 9, 11
 - Matrix metalloproteinase (MMP), 24, 26
 - Matrix metalloproteinase-9 (MMP-9)
 - activity, 47–49
 - experimental results, 48
 - gel zymography, 48
 - tissue inhibitor of metalloproteinases-1 (TIMP-1), 49
 - Mean arterial blood pressure (MABP), 148
 - Minocycline inhibitor
 - Kruskal-Wallis test, 148, 149
 - materials and methods
 - animal preparation and intracerebral injection, 147–148
 - behavioral tests and statistical analysis, 148
 - brain atrophy examination, 148
 - brain water and ion content measurements, 148
 - experimental groups, 148
 - mean arterial blood pressure (MABP), 148
 - microglia cells, 147
 - Morphine
 - materials and methods
 - administration and development of dependence, 62
 - animals, 62
 - blood-brain barrier permeability and brain edema formation, 62–64
 - H-290/51 treatment, 64
 - pathology, 62
 - physiological variables, 62
 - statistical analysis, 64
 - withdrawal, 62
 - results
 - cell changes, 64
 - permeability and edema formation, 62
 - symptoms and physiological variable, 64
 - Multimodal drugs, 293
 - Multi-walled carbon nanotube (MWNT), 338
 - Myocardial dysfunction
 - hypothalamic ischemia, 152
 - intracranial hemorrhage, 152
 - materials and methods, 151
 - population study, 152
 - regional wall motion abnormalities (RWMA), 152–153
 - sub-arachnoid hemorrhage (SAH), 151, 152
- N**
- Nafamostat mesilate (FUT), 307, 309
 - Nanoparticles
 - Ag and Cu nanoparticles, 363
 - brain morphological changes, 361
 - cell changes, 362
 - cellular/oxidative stress, 363
 - and edema formation, 360–361
 - Evans blue extravasation, 361
 - materials and methods
 - administration, 360
 - animals, 359
 - BBB permeability, 360
 - brain edema formation and electrolyte content, 360
 - morphological investigations, 360
 - physiological variables and statistical analysis, 360
 - physiological variables, 361
 - vasogenic edema formation, 363
 - Nanowired-drug delivery
 - application, 344
 - blood-spinal cord barrier (BSCB) permeability, 344
 - characterizations, 345
 - effects of
 - BSCB permeability, 346
 - functional outcome, 346
 - spinal cord edema, 346
 - spinal cord pathology, 346–348
 - functional outcome, 344
 - motor function improvement, 349
 - neuroprotection, 348
 - spinal cord edema formation, 344
 - spinal cord injury, 344
 - statistical analyses, 344
 - National Institutes of Health (NIH), 17, 18
 - Nerve growth factor (NGF), 296, 297, 299
 - Neuroimaging (T2WI), 52
 - Neurological function, 52
 - Neurological recovery, 247
 - Neuroplasticity processes, 294
 - Neuroprotection
 - neurodegenerative processes, 292
 - pathophysiological processes
 - apoptosis, 293–294
 - excitotoxicity, 292–293
 - inflammation, 293
 - pleiotropic drug administration, 293
 - Neurotrophicity, 291
 - Neurotrophins 3 (NT-3), 296, 297, 299
 - Neutrophils and proinflammatory mediators
 - chemoattractant receptor (CCR2), 32
 - CSF stimulation, 29
 - ET-1
 - leukocyte activation, 33
 - plasma concentration, 31, 32
 - IL-1 β expression, 32
 - LPS, 33
 - materials and methods
 - animals, 30
 - chemiluminescence, 30, 31
 - cisterna magna (CM), 30
 - lymphocyte culture, IL-1 α and TNF α measurement, 31
 - statistical analysis, 31
 - PMNs
 - invasion of, 32, 33
 - oxidative activity, 30
 - therapeutic targets, 30
 - TLR4 signaling, 30
- O**
- Occludin, 22–23, 279
 - Octylcyanoacrylate tissue adhesive (OTA), 88, 89
 - OTA. *See* Octylcyanoacrylate tissue adhesive (OTA)
 - Overdrainage complication
 - idiopathic normal-pressure hydrocephalus (iNPH), 113–114
 - primary hypothesis, 114
 - secondary outcomes, 114
 - trial flow, documentation, and follow-up, 114
- P**
- PAI. *See* Platelet aggregation inhibitors (PAI)
 - Partial least squares discriminant analysis (PLS-DA), 171, 172

- Pattern recognition (PR) methods
 Perceptual reasoning (PRI), 272
 Permanent middle cerebral artery occlusion (pMCAO), 43–44
 P-glycoprotein (P-gp), 23
 Pituitary adenylate cyclase activating polypeptide (PACAP)
 animals, 43
 brain swelling calculation, 44
 cerebral blood flow measurement, 44
 permanent cerebral ischemia model, 44
 results, 44–45
 Platelet aggregation inhibitors (PAI), 98
 PLS-DA. *See* Partial least squares discriminant analysis (PLS-DA)
 Polymorphonuclear cells (PMNs)
 IL-1 β , 33
 invasion of, 32, 33
 oxidative activity, 30
 Posterior fossa brain tissue injury
 behavioral disorders, 271
 deficits in, 274
 indices in, 272
 linguistic processes and emotional traits, 274
 materials and methods, 272–273
 neurobehavioral changes, 273
 tumor location, 271
 tumors, histopathological diagnoses of, 272
 WAIS-R and WISC-R (III Edition) tests, 272
 Posterior fossa tumors, cerebellar tissue
 chemotherapy treatment, influence of, 172
 ¹H NMR *in vivo*, 172
 Lip and Lac signals, 173–174
 MRS and PR methods, 171
 multivariate analyses, 172
 normal appearing tissue
 chemotherapy influences, 172
 surgical influences, 172–173
 tumor state, 172
 PLS-DA scores plot, 173
 Postirradiation imaging changes incidence, AVM and CCM
 computed tomography (CT), 188
 magnetic resonance imaging (MRI), 188
 Preconditioning with hyperbaric oxygen (HBO-PC)
 experimental results, 48
 ischemic induction, 48
 laminin degradation, 48
 Primary decompressive craniectomies
 Glasgow coma scale (GCS), 235, 236
 mortality rates, 236
 neurological outcomes, 236
 traumatic acute subdural hematomas, 236
 Proton magnetic resonance spectroscopy (MRS), 171
- R**
- Radiotherapy
 inflammation, 51
 methods, 52
 results, 52–53
 risk factors, 51
 treatment, 53
 Reactive oxygen species (ROS), 315
 Regional cerebral blood flow (rCBF), 285, 286
 Regional wall motion abnormalities (RWMA), 152–153
- S**
- S100B release, CSF and blood
 Glasgow Coma Score, 248
 subarachnoid hemorrhage, 248
 traumatic brain injury (TBI), 247–249
 Scanning electron microscopy (SEM), 81, 83, 84, 92
 Secondary normal pressure hydrocephalus (sNPH), 108
 Serine protease inhibitor, 307, 309
 Serum active matrix metalloproteinase (MMP-9, MMP-2 levels)
 perihematomal edema development and hematoma
 expansion, 140
 spontaneous intracerebral hemorrhage
 blood-brain barrier (BBB), 137
 hematoma and edema volumes, 139
 materials and methods, 138
 serum relationships, 139–140
 time course, 138–139
 tissue inhibitors of metalloproteinases (TIMP), 137
 zinc and calcein endopeptidases, 137
 Severe head injury, decompressive craniectomy
 Glasgow Outcome Scale (GOS), 231
 outcome
 vs. age, 232
 discharge, 231, 232
 epidural and subdural hematomas, 232
 vs. isocoria, 232
 long-term, 232
 midline shift predicts, degree of, 232
 trauma to surgery, time duration, 232
 patients and methods, 231
 Shunt catheters
 biodegradation and mineralization, 91
 calcifications, 92, 93
 fractures and cracks, 93
 inner surfaces, 82–83
 materials and methods, 81–82
 methods, 92
 potential consecutive biological reactions, 91–92
 red blood cells, 82–84
 results, 82–83, 92–93
 scanning electron microscopy (SEM), 81, 83, 84, 92
 thalassaemic phenotype, 83
 thin fibrin fibers, 82, 83
 types, 83
 Shunt infections
 cerebral spinal fluid (CSF), 87
 materials and methods
 octylcyanoacrylate tissue adhesive (OTA), 88, 89
 patient population and study design, 87, 88
 results, 88–89
 statistics, 88
 techniques, 88
 2-octylcyanoacrylate, 87
 Shunt operation, 129
 Solitary intra-axial brain tumor
 computed tomography perfusion (CTP), 283
 CTP technique, 284
 patients, 284
 regional cerebral blood flow (rCBF), 285, 286
 statistical analysis, 284
 Spinal cord injury (SCI)
 materials and methods
 animals, 296
 BSCB permeability, 296
 edema, 296
 motor functions, 296
 neurotrophin treatment, 296
 pathology, 296
 spinal cord injury, 296
 statistical evaluation of data, 296–297

neurotrophin effects
 on BSCB permeability, 297
 on edema formation, 297
 on functional outcome after SCI, 297
 on spinal cord pathology, 297
 Spontaneous intracerebral hemorrhage (SICH), 141
 blood-brain barrier (BBB), 137
 hematoma and edema volumes, 139
 materials and methods, 138
 serum relationships, 139–140
 time course, 138–139
 tissue inhibitors of metalloproteinases, 137
 zinc and calcium endopeptidases, 137
 SPSS® and Statistica® v 6.0 software, 273
 Streptozotocin, intracerebroventricular injection, 178
 Surgical brain injury (SBI), 217, 218
 SVASONA trial, 113, 114

T

Terminal deoxynucleotidyl transferase-mediated dUTP nick end
 labeling (TUNEL), 48, 49
 Tetrahydrobiopterin (BH4)
 aromatic amino acid hydroxylases, 156
 collagenase-induced hemorrhage, 156
 intracerebral hemorrhage (ICH), 155, 156
 materials and methods
 animal preparation and brain water content, 155
 brain water content, 156
 neurological deficits and mortality, 156–157
 Thalassemic phenotype, 83
 Thin fibrin fibers, 82, 83
 Thrombin, 307, 309
 Toll-like receptor 4 (TLR4), 30
 Traumatic brain injury (TBI), 212, 214, 239, 240, 242

TUNEL staining, 52–53
 T1-weighted 3D-gradient-echo sequence, 122
 T2-weighted, 2D-RARE sequence, 122
 T2-weighted 3D-Turbo-RARE sequence, 122

V

Vascular endothelial growth factor (VEGF),
 55–58
 immunofluorescence, 279, 280, 282
 Vasogenic brain edema, bulk flow and diffusion
 vs. calculated theoretical distances, 4
 edema fluid formation, 5–6
 edema fluid, resolution of, 5–6
 peritumoural edema, clinical studies in, 6–7
 RISA and C-14 sucrose appearance, 5
 sodium-fluorescein and Texas-red albumin, 5
 spreading of, 3–5
 white matter, CT-numbers, 6
 VEGF. *See* Vascular endothelial growth factor
 Ventriculo-atrial (VA) shunt
 contraindications, 98
 dyspnea and venous congestion, 95
 frequency, 97
 heart failure, 96
 pathophysiology, 97–98
 prophylaxis and therapy, 98
 screening and follow-up examination, 98–99
 venae jugularis, and subclavia, 97
 Verbal comprehension index (VCI), 272

W

Whole body hyperthermia (WBH), 322–323
 Working memory index (WMI), 272